UNCLASSIFIED

AD NUMBER

AD824697

NEW LIMITATION CHANGE

TO

Approved for public release, distribution unlimited

FROM

Distribution authorized to U.S. Gov't. agencies and their contractors; Administrative/Operational Use; NOV 1967. Other requests shall be referred to Air Force Materials Lab., Wright-Patterson AFB, OH 45433.

AUTHORITY

AFML ltr, 26 May 1972

THIS PAGE IS UNCLASSIFIED

Air Force Materials Laboratory
Research and Technology Division
Air Force Systems Command
Wright-Patterson Air Force Base, Ohio



AFLC
RECEIVED
JAN 8 1963
RESEARCH
A

AD 824 997

DEVELOPMENT OF MANUFACTURING METHODS FOR PRODUCING PYROLYTIC GRAPHITE IN VARIOUS SHAPES AND STRUCTURES

Thomas J. Clark

This document is subject to special export controls and each transmittal to foreign governments or foreign nationals may be made only with prior approval of the Air Force Materials Laboratory (MATC) Wright-Patterson Air Force Base, Ohio 45433.

Best
Available
Copy

FOREWORD

This final Technical Report covers all the work performed under Contract AF33(615)-3136 from 1 July 1965 to 29 September 1967. The manuscript was released by the author on 6 October 1967 for publication.

The contract with General Electric Company, Metallurgical Products Department, Detroit, Michigan, was initiated under MATC Project 8-349, "Development of Manufacturing Methods for Producing Pyrolytic Graphite in Various Shapes and Structures." It was accomplished under the technical direction of Mr. Lawrence Kopell of the Chemical Processing Branch (MATC) Manufacturing Technology Division, Air Force Materials Laboratory, Wright-Patterson Air Force Base, Ohio.

Mr. George R. Hemmeter was the Program Manager. Others working on the project were Dr. Thomas J. Clark, Technical Program Director, and Mr. Bruce L. Ettinger, Engineer, Dr. Paul Gorsuch, Dr. Edward Stover, Mr. Phillip Bolinger, Mr. S. Davis, Miss G. McKinley, Mr. W. Mueller and Mr. J. Zlupko, Subcontract Engineers; and Dr. T. McDonough and Dr. D. Nestler, Subcontract Consultants at General Electric Re-Entry Systems Department; Dr. James Pappis, Dr. William Kotlensky and Mr. L. Hagen, Subcontract Engineers at Raytheon Company; and Dr. R. J. Diefendorf and Mr. Barry Butler, Scientists at Rensselaer Polytechnic Institute.

This project has been accomplished as a part of the Air Force Manufacturing Methods Program, the primary objective of which is to develop, on a timely basis, manufacturing processes, techniques and equipment for use in economical production of USAF materials and components. The program encompasses the following technical areas:

Metallurgy -- Rolling, Forging, Extruding, Casting, Fiber, Powder.
Chemical -- Propellant, Coating, Ceramic, Graphite, Nonmetallics.
Electronic -- Solid State, Materials & Special Techniques, Thermionics.
Fabrication -- Forming, Material Removal, Joining, Components.

Suggestions concerning additional Manufacturing Methods development required on this or other subjects will be appreciated.

This Technical Report has been reviewed and is approved.

Frank J. Harsacky

FRANK J. HARSACKY, Acting Chief
Chemical Processing Branch
Manufacturing Technology Division
Air Force Materials Laboratory

ABSTRACT

DEVELOPMENT OF MANUFACTURING METHODS FOR PRODUCING PYROLYTIC GRAPHITE IN VARIOUS SHAPES AND STRUCTURES

George R. Hennator
General Electric Company
Metallurgical Products Department

The objective of this program is the development of a manufacturing technology which will enable the prediction and specification of manufacturing process parameters for producing, with a high degree of reliability, pyrolytic graphites in specific sizes, shapes, and quality beyond the present state of the art and suitable for re-entry vehicles and rocket nozzles.

Although pyrolytic graphites for aerospace applications were being made for five years prior to this contract, the technical depth of related knowledge was exceedingly shallow compared to more familiar design materials. This fact coupled with the unique properties of the pyrolytic graphitics for aerospace systems created a need for documenting the current state of the art and also advancing it specifically in those areas related to its manufacturability. The following pages of this document satisfy these needs by presenting the most current state of the art including the new knowledge developed under this program.

The major events and conclusions resulting from this program are as follows:

Pyrohydrolysis has proven to be the most reliable and accurate technique for determining the boron percent in pyrolytic graphites deposits.

Mandrel graphites were evaluated and rated. Correction factors for graphite mandrel dimensions should be -1.0% to -1.5% of the finished part dimension to allow for thermal expansions and changes in deposit dimensions. Mandrel thickness to deposit thickness ratio of 1:1 to 1.5:1 is satisfactory.

A new and unique mandrel separator has been developed which allows the separation of highly stressed shapes from adjacent deposits. The reversed curvature shape of the separator provides a beneficial stress reversal allowing the separation of the part.

Mandrel precoats should preferably be 0.0005" or less to achieve best parting of part from mandrel.

The use of baffles to achieve uniform deposition profiles in frustums and cylinders is not recommended for circular sections less than six inches. Baffles for larger sections are recommended.

Boron gradation during the deposition process produced the most favorable delamination pattern in nose cones. The gradation that was most effective was an initial BCl_3: CH_4 ratio of 1% and grading down to 0.1%.

Acetylene as an alternate source gas in place of methane has not been as satisfactory as methane because of poor profile reproducibility and the formation of large growths on the gas injector.

The use of a diffuser cap in promoting improved profile and material quality in BPG nose cones has not been successful.

Although graphitization as a function of boron percent in pyrolytic graphite can be specified and controlled, it was concluded that graphitization is detrimental to the manufacture of shapes.

It was demonstrated that thin deposits of BPG introduced during normal deposition of PG will allow controlled delaminations to form. These delaminations lower residual stress and allow production of crack-free parts having a thickness to radius(t/r)ratio greater than .1.

A new process control method based on photoresistance is discussed which measures gas maturity by the sooting characteristic in the hot zone.

A complete process specification for producing 10° half angle, 1/4" nose radius, 1.00" stagnation thickness and 0.180" wall thickness nose cones is shown in the appendix.

TABLE OF CONTENTS

		Page No.
SECTION I	INTRODUCTION	1
	A. Prior History	1
	B. The Need for a Manufacturing Technology Program	1
	C. Scope of this Program	1
	D. Discussion	2
SECTION II	SUMMARY	
	A. Introduction	5
	B. Preliminary Studies - State of the Art for Nose Cones	5
	C. Mandrel-Related Studies	6
	1. Graphite Grade Evaluation	6
	2. Mandrel Design	6
	3. Mandrel Surface Treatment	7
	4. Mandrel Termination Design	7
	D. Process Studies for Straight-Through Flow Systems	7
	E. Profile Studies for Straight-Through Flow Systems	8
	F. Advanced Studies for Straight-Through Flow Systems	8
	G. Process and Profile Studies for Reflex Flow Systems	9
	H. Special Studies	10
	1. Turbulent Nozzle Studies	10
	2. Deposition from Acetylene	10
	3. Interrupted Deposition	10
	4. Additive and Impurity Studies	11
	5. Hafnium Alloy Deposition Studies	11
	I. Advanced Studies for Reflex Flow Systems	12
	1. Delamination Control Studies	12
	2. Process Optimization for Nose Cones	12
SECTION III	ESTABLISHMENT OF STATE OF THE ART FOR NOSE CONES (TASK 3.5.1)	15
	A. Process Parameters for Task 3.5.1	15
	B. Process Details	15
	Background	15
	Nozzle Position	15
	Exhaust Area	16
	Hydrocarbon Gas Flow	16
	Boron Trichloride Flow	16
	Deposition Time	16

		Page No.
	C. Results	17
	D. Summary and Conclusions	19
	E. Process Recommendations	20
SECTION IV	MANDREL-RELATED STUDIES	21
	A. Graphite Grade Selection for Mandrels (Task 3.3.5)	21
	Mandrel Property Requirements	21
	Prior Mandrel Experience	21
	Standard Grade Selection	22
	Selection of Evaluation Grades	22
	Graphite Grade Evaluation	23
	Results	23
	Summary and Conclusions	24
	Grade Recommendations	24
	B. Mandrel Design (Task 3.3.3)	24
	Background	24
	Initial Mandrel Design	25
	Mandrel Design Evaluation for Cylinders	25
	Results for Cylinders	26
	Extension of Work to Frustums	27
	Results for Frustums	27
	Summary and Conclusions	27
	Mandrel Design Recommendations	28
	C. Mandrel Surface Treatments (Task 3.3.4)	28
	Background	28
	Techniques Selected for Evaluation	29
	Results	30
	Summary and Conclusions	31
	Mandrel Treatment and Recommendations	31
	D. Mandrel Termination Design (Tasks 3.3.1 and 3.3.2)	32
	Background	32
	Termination Designs	33
	Results	33
	Summary and Conclusions	34
	Recommendations	34
SECTION V	PROCESS STUDIES FOR STRAIGHT-THROUGH FLOW SYSTEMS	37
	A. Constant Level Boron-Alloyed Material	37
	Background	37
	Experimental Conditions Selected	37
	Results	38

Page No.

B. Graded Level Boron-Alloyed Material (Task 3.4.1.3)---- 38
Background---- 39
Experimental Conditions Selected---- 39
Results---- 39
C. Unalloyed Material (Task 3.4.1.1)---- 40
Background---- 40
Experimental Conditions Selected---- 40
Results---- 40
D. Best Process Selection---- 41
E. Discussion of Task Results---- 41
Processing Difficulties---- 42
Microstructures---- 43
Density and Boron Analysis---- 43
Thermal Expansion---- 44
Mechanical Properties---- 45
Annealing and Graphitization---- 48
F. Summary and Conclusions---- 51
G. Process Recommendations---- 52

SECTION VI PROFILE CONTROL STUDIES FOR STRAIGHT-THROUGH FLOW SYSTEMS---- 53

A. Flow Control Studies (Task 3.2.2.1)---- 53
Background---- 54
Experimental Conditions Selected---- 54
Results---- 55
Summary and Conclusions---- 55
Recommendations---- 56
B. Hydrocarbon Replenishment Studies (Task 3.2.2.2)---- 56
Background---- 56
Experimental Conditions Selected---- 56
Results---- 57
Summary and Conclusions---- 57
Recommendations---- 57
C. Hydrogen Dilution Studies (Task 3.2.2.3)---- 57
Background---- 57
Experimental Conditions Selected---- 58
Results---- 58
Summary and Conclusions---- 60
Recommendations---- 60
D. Optimization---- 60

SECTION		Page No.
VII	ADVANCED STUDIES FOR STRAIGHT-THROUGH FLOW SYSTEMS---	63
	A. Boron Alloy-Deposition Studies (Task 3.4.6)------	63
	Background----------	63
	Experimental Conditions Selected----------	64
	Results----------	64
	Profile----------	65
	Microstructure----------	65
	Bulk Density----------	65
	Boron Assay----------	65
	Residual Stress----------	65
	Analysis of Results----------	66
	Temperature Influence on Boron Incorporation----------	66
	Pressure Influence on Boron Incorporation----------	67
	Boron Trichloride Influence on Boron Incorporation----------	67
	Pressure Influence on Deposition Rates----------	68
	Temperature Influence on Deposition Rates----------	68
	Summary and Conclusions----------	68
	Recommendations----------	68
	B. Boron Alloy-Assay Studies (Task 3.4.7)----------	69
	Background----------	69
	Survey of Assay Techniques----------	71
	Layer Separation After a Stablization Anneal----------	72
	Fast Neutron Activation Analysis-------	72
	Electron Microbeam Probe----------	73
	Spark Source and Laser-Probe Mass Spectrography----------	73
	Ion-Beam Probe Mass Spectrometry-------	73
	Experimental Procedures and Results----------	74
	Sample Preparation----------	74
	Impurities----------	74
	Pyrohydrolysis and Titration of Large Samples----------	75
	Emission Spectroscopy with External Standards----------	76
	Emission Spectroscopy with an Internal Standards----------	77
	Pyrohydrolysis of Small Samples and Spectrophotometry----------	78
	Summary and Conclusions----------	79
	Recommendations----------	80

		Page No.
	C. Graphitization Studies (Task 3.4.1.5)----------	81
	Background----------	81
	Experimental Conditions Selected----------	83
	Results----------	84
	Phase 1 (Deposits)----------	84
	Phase 2 (Appealing Tests and Results)--	84
	Phase 3 (Analysis and Deposits)--------	86
	Summary and Conclusions----------	88
	Recommendations----------	90
SECTION VIII	PROCESS AND PROFILE STUDIES FOR REFLEX FLOW SYSTEMS--	91
	A. Effects of Process Variables (Tasks 3.2.1.1 and 3.4.2.1)----------	92
	Experimental Conditions Selected----------	92
	Results----------	93
	Nozzle Orifice Size Studies----------	94
	Base-Line Run----------	94
	Nozzle Withdrawal and Temperature Variation Studies----------	94
	Graded and Higher Boron Level Studies-------	95
	Nitrogen Dilution Study----------	96
	Other Processing Variables----------	96
	Characterization and Evaluation----------	96
	Thickness Profile----------	96
	Tip Growth and Closure----------	97
	Number and Tightness of Delaminations-------	98
	Boron and Density Analysis----------	98
	Normalization of Deposition Rates----------	99
	Summary and Conclusions----------	100
	Recommendations----------	101
SECTION IX	SPECIAL STUDIES----------	103
	A. Turbulent Nozzle Studies (Task 3.2.1.3)----------	103
	Background----------	103
	Experimental Conditions Selected----------	105
	Results----------	108
	Summary and Conclusions----------	110
	Recommendations----------	111
	B. Turbulent Nozzle Studies for LPG (Task 3.2.1.4)--	112
	Background----------	112
	Experimental Conditions Selected----------	112
	Results----------	112
	Summary and Conclusions----------	114
	Recommendations----------	115

Page No.

C. Deposition from Acetylene (Task 3.4.2.3)---------- 115
Background for Task 3.4.2.3a---------- 115
Experimental Conditions Selected - Phase 1---------- 115
Results - Phase 1---------- 116
Summary and Conclusions - Phase 1---------- 118
Experimental Conditions Selected - Phase 2---------- 118
Results - Phase 2---------- 118
Summary and Conclusions - Phase 2---------- 119
Background for Task 3.4.2.3B---------- 120
Experimental Conditions Selected---------- 120
Results---------- 121
Summary and Conclusions - Task 3.4.2.3b----- 122
Recommendations---------- 123
D. Interrupted Deposition (Task 3.3.6)---------- 123
Background---------- 124
Experimental Conditions Selected---------- 124
Results---------- 125
Summary and Conclusions---------- 128
Recommendations---------- 129
E. Additive and impurity studies (Task 3.2.1.2)----- 129
Background---------- 130
Experimental Conditions Selected---------- 130
Results---------- 132
Summary and Conclusions---------- 134
Recommendations---------- 135
F. Hafnium Alloy Deposition Studies (Task 3.4.2.4)-- 135
Background---------- 135
Description of $HfCl_4$ Feed System---------- 136
Component Specifications---------- 138
Status---------- 140

SECTION X ADVANCED STUDIES FOR REFLEX FLOW SYSTEMS---------- 141

A. Delamination Control Studies (Task 3.3.7)-------- 141
Background---------- 141
Experimental Conditions Selected---------- 142
Results---------- 144
Summary---------- 153
Recommendations---------- 154
B. Process Optimization for Nose Cones (Task 3.5.2)- 155
Background---------- 155
Experimental Conditions Selected---------- 156
Results---------- 157
Recommendations---------- 158

SECTION XI AUXILIARY TASKS---------- 161

BIBLIOGRAPHY---------- 163

		Page No.
TABLES		
I.	Cross-Reference Chart-Revised Work Statement	171
II.	Task 3.5.1., Summary of Runs	172
III.	Graphite Grades, Summary of Properties	175
IV.	Rating Factors for Graphite Grade Evaluations	176
V.	Processing Characterization for Cylinder Deposits	177
VI.	Density and Boron Analysis for Cylinders	179
VII.	Measured Tangential Residual Stress (o.d.) for Cylinders	180
VIII.	Mechanical Property Data for Cylinders	181
IX.	Effect of Annealing on Mechanical Property Data for Cylinders	182
X.	Effect of Time on the Graphitization of BPG	183
XI.	Process Conditions for Frustums Deposited in Task 3.2.2.1.	184
XII.	Process Conditions for Cylinders Deposited in Task 3.2.2.2.	185
XIII.	Process Conditions for Cylinders Deposited in Task 3.2.2.3	186
XIV.	Deposition Conditions for Task 3.4.6	187
XV.	Calculated Linear Velocities for Task 3.4.6.	188
XVI.	Deposition Conditions for Task 3.4.6.	189
XVII.	Test Results for Task 3.4.6.	190
XVIII.	Reproducibility of Standards in Semi-Quantitative Spectroscopic Method for Boron Assay	192
XIX.	Reproducibility of Boron Assay by Comparison with External Standards in Light Emission Spectroscopy	193
XX.	Comparison of Boron Assay by Pyrohydrolysis and Light Emission Spectroscopy	194
XXI.	Boron Assay by Pyrohydrolysis followed by Titration or Spectrophotometry	198
XXII.	Reproducibility of Results on Small Samples by Pyrohydrolysis and Spectrophotometry	198
XXIII.	Processing Characteristics for Cylinder Deposits	199
XXIV.	Property Measurements on As-Deposited Material	200
XXV.	Property Measurements on Rings Annealed at 2000°C for 5 Hours	201
XXVI.	Property Measurements on Rings Annealed at 2000°C for 15 Hours	201
XXVII.	Relative Structural Integrity	202
XXVIII.	Dimensional Changes after Annealing at 2000°C	202
XXIX.	Unit Cell Height (C_o) for Cylinder Deposits	203
XXX.	Effect of Annealing at 2000°C on Unit Cell Height (C_o) Å	204
XXXI.	Coefficient of Thermal Expansion from 0-1000°C	204
XXXII.	Boron Assay and C_o Characterization for Cylinder GEDC-9R	205
XXXIII.	Processing Characteristics for Cylinders GEDC-10R 13R	205
XXXIV.	Processing Characterization for Cone Deposits	206
XXXV.	Boron Analysis for Cones	208

TABLES		Page No.
XXXVI.	Summary of Process Parameters	209
XXXVII.	Summary of Results	210
XXXVIII.	Operating Conditions - Task 3.2.1.4	211
XXXIX.	Process Conditions - Task 3.4.2.3a - Phase 1	212
XL.	Experimental Results Phase I - 3" Diameter Tubes	213
XLI.	Process Conditions - Task 3.4.2.3a - Phase 2	214
XLII.	Deposition Thickness Profiles - Task 3.4.2.3a Phase 2	215
XLIII.	Process Conditions - Task 3.4.2.3b	216
XLIV.	Summary of Results - Task 3.4.2.3b	217
XLV.	Processing Matrix	218
XLVI.	Processing Parameters	219
XLVII.	Results	220
XLVIII.	Deposit Thickness	221
XLIX.	Composition of Natural Gas	222
L.	Levels of Impurities	223
LI.	Effects of Impurities on the Deposition Rate	224
LII.	Composition of Synthesized Gas for Filament Runs	225
LIII.	Task 3.3.7-1 Summary of Operating Conditions and Results	226
LIV.	Task 3.3.7-2 Summary of Operating Conditions and Results	227
LV.	Task 3.3.7-3 Summary of Operating Conditions and Results	228
LVI.	Task 3.3.7-4 Summary of Operating Conditions and Results	229
LVII.	Task 3.3.7-5 Summary of Operating Conditions and Results	230
LVIII.	Task 3.3.7-6 Summary of Operating Conditions and Results	232
LIX.	Task 3.5.2 Summary of Operating Conditions and Results	233

ILLUSTRATIONS		Page No.
1.	Flow Chart AF33(615)-3136	235
2.	Flow Chart (Revised) AF33(615)-3136	236
3.	PIM Shield Cone	237
4.	As-Deposited Nose Cone	238
5.	Task 3.5.1 Radiograph of Nose Cone No. 1	239
6.	Summary of Nose Cone Thickness Data. Task 3.5.1	240
7.	Polished Surface, Grade B Graphite	241
8.	Polished Surface, Grade C Graphite	241
9.	Polished Surface, Grade A Graphite	242
10.	Polished Surface, Grade D Graphite	242
11.	Single Spiral Undercut Mandrel	243
12.	Spiral Undercut Mandrel After Failure	243
13.	Typical Mandrel Failure Patterns	244
14.	Typical Failure of Spirally Undercut Mandrel	245
15.	Shield Frustum "G"	246
16.	Task 3.3.3 Spalled Surface of Frustum Deposited in in Tapered Thickness Mandrel	247
17.	Nose Cone Cool-Down without Mandrel Failure	248

Page No.

ILLUSTRATIONS

18a	Deposition Surface Resulting from Mandrel Polished with 600 Grit Paper followed by .0003" Precoat	249
18b	Deposition Surface Resulting from Mandrel oxidized 1 hour at 1050°F with no subsequent Precoat	249
19a	Deposition Surface Resulting from Mandrel Oxidized 1 hour at 1050°F followed by .0003" Precoat	250
19b	Deposition Surface Resulting from Mandrel Oxidized 1 hour at 1150°F followed by .0003" Precoat	250
20.	Deposition of Pyrolytic Graphite at Mandrel Juncture	251
21.	Category A Terminations	252
22.	Category B Terminations	252
23.	Category C Terminations	253
24.	Schematic Arrangement of Parts in Multiple Tube Deposition Assembly for Evaluation of Termination Design	254
25.	Mandrel Separator	255
26.	Characteristic Deposit with Separator 344013 Attached	256
27.	Separator 344013 Before and After Axial Cut	257
28.	Shield Frustum "G"	258
29.	Photograph of Mandrel Assembly and Typical Tube Deposited	259
30.	Deposition Profile for Cylinders	260
31.	Deposition Profile for Cylinders	261
32.	Deposition Profile for Cylinders	262
33.	Deposition Profile for Cylinders	263
34.	Micrographs for PG Cylinder Deposits, Deposition Rate variable.	264
35.	Micrographs for Boron PG Cylinder Deposits, Boron Content Variable from Trimethyl Borate and Methane	265
36.	Micrographs for Boron PG Cylinder Deposits, Boron Content Variable from Trimethyl Borate and Methane	266
37.	Micrographs for Cylinder Deposits	267
38.	Micrographs for Cylinder Deposits	268
39.	Correlation bwtween Unit Cell Height and Percent Boron	269
40.	Thermal Expansion A-Direction	270
41.	Thermal Expansion C-Direction	271
42.	Coefficient of Thermal Expansion for BPG from 0° to 1000°C as a Function of Boron Content	272
43.	Photograph of Diametral Ring Compression Apparatus	273
44.	Photograph of Close Up of Diametral Ring Compression Assembly	274
45.	Modulus of Elasticity and Poisson's Ratio for BPG as a Function of Boron Content	275

Page No.

ILLUSTRATIONS

46. Comparison of Calculated (Lines) and Measured (Circles) Residual Stress---------- 276
47. Characteristics of Hydrocarbon Gas Flowing Inside Heated Tube and Deposition Profile which Results-- 277
48. Equilibrium Mol Fractions of Various Gas Species in C-H System at 0.1 Atmosphere Pressure and C/H Ratio of 1/4---------- 278
49. Baffling Technique for Frustum Deposition ---------- 279
50. Plug Technique for Frustum Deposition---------- 280
51. Frustum Plug and Baffle Designs---------- 281
52. Frustum Mandrel for Task 3.2.2.1---------- 282
53. Thickness Profiles for Task 3.2.2.1---------- 283
54. Microstructure from Exhaust End of Frustums deposited in Task 3.2.2.1---------- 284
55. Schematic Representation of a possible Gas-Replenishment Technique for Achieving Uniform Wall Thicknesses in Long Frustums---------- 285
56. Deposition Assembly for Replenishment Experiment----- 286
57. Replenishment Nozzle Assembly including Graphite Nozzle Gas Feed---------- 287
58. Deposition Thickness Profiles---------- 288
59. Task 3.2.2.3 Initial Deposition Thickness Profiles--- 289
60. Task 3.2.2.3 Deposition Thickness Profiles---------- 290
61. Effects of Hydrogen Dilution in Boron-Alloyed and Unalloyed PG Deposition---------- 291
62. Microstructure and Density-Run 8043---------- 292
63. Task 3.2.2.3 Comparison of Characteristic Slopes----- 293
64. Frustum Deposits-Simple Baffle Control---------- 294
65. Deposition Assembly for Task 3.4.6---------- 295
66. Typical Cylinders Prior to Mandrel Removal---------- 296
67. Sampling Plan---------- 297
68. Typical Deposit, Cut for Sampling---------- 298
69. Task 3.4.6 Deposition Profile for Cylinders---------- 299
70. Task 3.4.6 Deposition Profile for Cylinders---------- 300
71. Task 3.4.6 Deposition Profile for Cylinders---------- 301
72. Task 3.4.6 Deposition Profile for Cylinders---------- 302
73. Task 3.4.6 Deposition Profile for Cylinders---------- 303
74. Task 3.4.6 Deposition Profile for Cylinders---------- 304
75. Task 3.4.6 Deposition Profile for Cylinders---------- 305
76. Microstructures of Tube Deposits, Task 3.4.6--------- 306
77. Microstructures of Tube Deposits, Task 3.4.6--------- 307
78. Microstructures of Tube Deposits, Task 3.4.6--------- 308
79. Microstructures of Tube Deposits, Task 3.4.6--------- 309
80. Microstructures of Tube Deposits, Task 3.4.6--------- 310
81. Microstructures of Tube Deposits, Task 3.4.6--------- 311
82. Microstructures of Tube Deposits, Task 3.4.6--------- 312
83. Microstructures of Tube Deposits, Task 3.4.6--------- 313
84. Microstructures of Tube Deposits, Task 3.4.6--------- 314
85. Microstructures of Tube Deposits, Task 3.4.6--------- 315
86. Microstructures of Tube Deposits, Task 3.4.6--------- 316

Page No.

ILLUSTRATIONS

87. Task 3.4.6 Deposit 8059-1B---------- 317
88. Task 3.4.6 % Boron in Solid vs. Temperature---------- 318
89. Task 3.4.6 % Boron in Solid vs. Temperature---------- 319
90. Task 3.4.6 % Boron in Solid vs. Temperature---------- 320
91. Task 3.4.6 % Boron in Solid vs. Temperature---------- 321
92. Task 3.4.6 Soot Deposit as Exposed at Inlet End Cylinder 8059-2---------- 322
93. Task 3.4.6 Boron in Solid vs. Pressure for 3800°F---- 323
94. Task 3.4.6 Boron in Solid vs. Pressure for 3640°F---- 324
95. Boron in Solid vs. Pressure for 3450°F---------- 325
96. Task 3.4.6 Boron in Solid vs Boron Trichloride Concentration in Reactant---------- 326
97. Task 3.4.6 Smoothed Calibration Curve - Ring "B" Values---------- 327
98. Task 3.4.6 Deposition Rate vs. $(P)^{\frac{1}{2}}$ - Temp. 3800°F--- 328
99. Task 3.4.6 Deposition Rate vs. $(P)^{\frac{1}{2}}$ - Temp. 3640°F--- 329
100. Task 3.4.6 Deposition Rate vs. $(P)^{\frac{1}{2}}$ - Temp. 3450°F--- 330
101. Task 3.4.6 Deposition Rate vs. Temperature---------- 331
102. Unit Cell Height as a Funtion of Boron Content in Pyrolytic Graphite As-Deposited and after Annealing; Scatter in Data is due in part to Inaccuracies in Boron Assay by Spectroscopy.------ 332
103. Comparison of Data on the Same Sample by Pyrohydrolysis and Titration (1.4 Gram Samples) with Data by Emission Spectroscopy with an Internal Standard (0.01 Gram Samples)---------- 333
104. Standard Curves for Boron determination by the Spectrophotometric Method as a Function of Time of Reaction between H_3BO_3 and HF. Azure C - Tetrafluoborate Complex is extracted with 25% CCl_4 in Dichloroethane---------- 334
105. Typical Microstructures of Cylinders Polarized Light, 100X Magnification---------- 335
106. Photograph of Mandrel Assembly and Typical Cone Deposited---------- 336
107. Deposition Thickness Profile for Cones---------- 337
108. Deposition Thickness Profile for Cones---------- 338
109. Deposition Thickness Profile for Cones---------- 339
110. Deposition thickness profile for cones---------- 340
111. Deposition thickness profile for cones---------- 341
112. Photographs of Polished Tip Sections. Magnifications from 1½ to 2X---------- 342
113. Photographs of Polished Tip Sections. Magnification 1½X---------- 343
114. Photographs of Polished Tip Sections. Magnifications 1 to 1½X---------- 344
115. Photographs of Polished Tip Sections. Magnification 1X---------- 345
116. Photograph of GEDP-2---------- 346
117. Wall Delamination Profile for Cone GEDP-1---------- 347

Page No.

ILLUSTRATIONS

118. Wall Delamination Profile for Cone GEDP-3---------- 348
119. Wall Delamination Profile for Cone GEDP-4---------- 349
120. Wall Delamination Profile for Cone GEDP-5---------- 350
121. Wall Delamination Profile for Cone GEDP-6---------- 351
122. Wall Delamination Profile for Cone GEDP-7---------- 352
123. Wall Delamination Profile for Cone GEDP-8---------- 353
124. Wall Delamination Profile for Cone GEDP-9---------- 354
125. Wall Delamination Profile for Cone GEDP-11---------- 355
126. Wall Delamination Profile for Cone GEDP-12---------- 356
127. Wall Delamination Profile for Cone GEDP-13---------- 357
128. Wall Delamination Profile for Cone GEDP-15---------- 358
129. Photograph of Polished Sections of Cone GEDP-7 at a - 3 in. and b - 7 in. from tip showing Circumferential Delaminations.---------- 359
130. Schematic Diagrams of State-of-Art and Desired Growth Profiles---------- 360
131. Schematic Diagram of Fluid Mechanics Model of Pyrolytic Graphite Deposition---------- 361
132. Local Wall Jet Flow Regimes---------- 362
133. Schematic Diagram of Boron Catalytic Effects on Pyrolytic Graphite Deposition---------- 363
134. Furnace Set-up for all Nose Cone Tip Deposition Experiments---------- 364
135. Photograph of Nose Cone Tip 3213-1---------- 365
136. Radiographic Positive Nose Cone Tip 3213-1 Base Line Run No. 1 Nozzle Orifice 0.069"---------- 366
137. Deposit Profile Nose Cone Tip 3213-1 Base Line Run No. 1 Orifice 0.069"---------- 367
138. Photograph of Nose Cone Tip 3213-2---------- 368
139. Radiographic Positive Nose Cone Tip 3213-2 Base Line Run No. 2 Nozzle Orifice 0.250"---------- 369
140. Deposit Profile Nose Cone Tip 3213-2 Base Line Run No. 2 Orifice 0.250"---------- 370
141. Nozzle Diffuser Cap No. 3---------- 371
142. Photograph of Diffuser Cap - Side View---------- 372
143. Photograph of Diffuser Cap - Bottom View---------- 372
144. Photograph Nose Cone Tip 3213-3---------- 373
145. Radiographic Positive Nose Cone Tip 3213-3 Turbulent Diffuser Cap No. 3---------- 374
146. Deposit Profile Nose Cone Tip 3213-3 (Diffuser Cap)-- 375
147. Photograph of Nose Cone Tip 3213-4---------- 376
148. Radiographic Positive Nose Cone Tip 3213-4---------- 377
149. Deposit Profile Nose Cone Tip 3213-4 (Nose Cone Tip 3213-4 with additional 15 hours deposit)---------- 378
150. Radiographic Positive Nose Tip 3213-6---------- 379
151. Deposit Profile Nose Cone Tip 3213-6---------- 380
152. Photograph of Orifice Inset---------- 381
153. Photograph of Nose Cone Tip 3213-5---------- 382
154. X-ray Positive Nose Cone Tip 3213-5---------- 383
155. Deposit Profile Nose Cone Tip 3213-5---------- 384

Page No.

ILLUSTRATIONS

156. Deposition Assembly for Nose Cones---------- 385
157. 304012 Nozzle Cap---------- 386
158. Nozzle Cap Before Deposition---------- 387
159. Nozzle Cap After Deposition---------- 387
160. Run 6048 - Nozzle Cap Close-up of Discharge Holes After Deposition---------- 388
161. Run 6048 - Nozzle Cap Cross Section After Deposition- 388
162. Task 3.2.1.4 PG-6048 - Run #1---------- 389
163. Run 6048 - Nose Region Cross Section -- 5X---------- 390
164. Run 6049 - Nozzle Cap Cross Section After Deposition- 391
165. 304013 Nozzle Cap---------- 392
166. Run 6052 - Nozzle Cap Cross Section After Deposition- 393
167. Run 6052 - Nozzle Cap Close-up of Discharge Holes After Deposition---------- 393
168. Task 3.2.1.4 PG-6052 - Run #4---------- 394
169. Run 6052 - Nose Region Cross Section --5X---------- 395
170. Run 4064 - Nozzle Cap Side View After Deposition----- 396
171. Run 4064 - Nozzle Cap Discharge Holes After Deposition---------- 396
172. Task 3.2.1.4 PG-4064 - Run #5---------- 397
173. Run 4064 - Nose Region Cross Section -- 5X---------- 398
174. Task 3.2.1.4 PG-4065 - Run #6---------- 399
175. Run 4065 - Nose Region Cross Section -- 5X---------- 400
176. 304015 Nozzle Cap---------- 401
177. Task 3.2.1.4 Deposition Profile Summary---------- 402
178. Schematic Diagram Illustrating Phase 1 Furnace Assembly---------- 403
179. Effect of Deposition Pressure on Deposit Thickness Profile---------- 404
180. Effect of Deposition Pressure on Deposit Thickness Profile---------- 405
181. Effect of Deposition Pressure on Deposit Thickness Profile---------- 406
182. Effect of Deposition Temperature on Deposit Thickness Profile---------- 407
183. Effect of Methane/Acetylene Ratio on Deposition Rate at Various Deposition Pressures---------- 408
184. Photograph of Cylinder 1-42 Illustrating the Inner Surface Condition and Overall Appearance---------- 409
185. Photograph of Cylinder No. 2-43 Illustrating the Inner Surface Condition and Overall Appearance---- 410
186. Photograph of Cylinder 1-39 Illustrating the Inner Surface Condition and Overall Appearance---------- 411
187. Photograph of Cylinder 1-38 Illustrating the Inner Surface Condition and Overall Appearance---------- 412
188. Photograph of Cylinder 1-36 Illustrating the Inner Surface Condition and Overall Appearance---------- 413
189. Photograph of Cylinder 1-35 Illustrating the Inner Surface Condition and Overall Appearance---------- 414

Page No.

ILLUSTRATIONS

190. Photograph of Cylinder 2-42 Illustrating the Inner Surface Condition and Overall Appearance---------- 415
191. Photograph of Cylinder 1-40 Illustrating the Inner Surface Condition and Overall Appearance---------- 416
192. Photograph of Cylinder 1-41 Illustrating the Inner Surface Condition and Overall Appearance---------- 417
193. Photograph of Cylinder 2-41 Illustrating the Inner Surface Condition and Overall Appearance---------- 418
194. Photograph of Cylinder 2-40 Illustrating the Inner Surface Condition and Overall Appearance---------- 419
195. Photomicrographs through deposit thickness showing Microstructure of these Tubes---------- 420
196. Photomicrographs through deposit thickness showing Microstructure of these Tubes---------- 421
197. Photomicrographs through deposit thickness showing Microstructure of these Tubes---------- 422
198. Photomicrographs through deposit thickness showing Microstructure of these Tubes---------- 423
199. Radiographic Positive Nose Cone 1-43 Illustrating the General Growth Pattern---------- 424
200. Radiographic Positive Nose Cone 2-46 Illustrating the General Growth Pattern---------- 425
201. Radiographic Positive Nose Cone 1-48 Illustrating the General Growth Pattern---------- 426
202. Deposition Thickness Profile - Nose Cones 1-43, 2-46 and 1-48---------- 427
203. Photograph of Nose Cone 1-43 Illustrating Surface Condition and Overall Appearance---------- 428
204. Photograph of Nose Cone 2-46 Illustrating Surface Condition and Overall Appearance. Note Extremely Heavy Spallation due to Residual Stresses Introduced by Process Fluctuations---------- 429
205. Photograph of Nose Cone 1-48 Illustrating Surface Condition and Overall Appearance---------- 430
206. Task 3.4.2.3b PG-5051 - 3800°F---------- 431
207. Task 3.4.2.3b Radiograph of 5051---------- 432
208. Task 3.4.2.3b PG-5058 - 3640°F---------- 433
209. Task 3.4.2.3b Radiograph of 5058---------- 434
210. Task 3.4.2.3b PG-5060 - 3450°F---------- 435
211. Task 3.4.2.3b Radiograph of 5060---------- 436
212. Task 3.4.2.3b PG-5053---------- 437
213. Task 3.4.2.3b Radiograph of 5053---------- 438
214. Task 3.4.2.3b PG-5054---------- 439
215. Task 3.4.2.3b Radiograph of 5054---------- 440
216. Frustum---------- 441
217. Schematic Diagram Illustrating Furnace Assembly Used for the Fabrication of the Frustums---------- 442
218. Photographs of Fabricated Part No. 1-77---------- 443
219. Deposition Thickness Profile for Frustum No. 1-77---- 444

Page No.

ILLUSTRATIONS

220. Photomicrographs Through the Deposit Thickness Showing Microstructure of Material from Top and Bottom of Frustum 1-77---------- 445
221. Photographs of Fabricated Part Run No. 2-88---------- 446
222. Deposition Thickness Profile for Frustum No. 2-88---- 447
223. Photomicrographs through Deposit Thickness showing Microstructure of Material from the Top and Bottom of Frustum 2-88---------- 448
224. Photographs of Fabricated Part---------- 449
225. Deposition Thickness Profile for Frustum No. 2-90---- 450
226. Photomicrographs through Deposit Thickness showing Microstructure of Material from the Top and Bottom of Frustum---------- 451
227. Deposition Thickness Profile for Frustum No. 1-82---- 452
228. Photograph of Fabricated Part---------- 453
229. Photomicrographs through Deposit Thickness showing Microstructure of Material from Top and Bottom of Frustum 1-82---------- 454
230. Photographs of Fabricated Part No. 2-105---------- 455
231. Deposit Thickness Profile for Frustum No. 2-105------ 456
232. Photomicrographs through Deposit Thickness showing Microstructure of material from Top and Bottom of Frustum 2-105---------- 457
233. Deposit Thickness Profile for Frustum No. 2-108 458
234. Photographs of Fabricated Part 2-108---------- 459
235. Photomicrographs Through the Deposit Thickness Showing Microstructure of Material from Top and Bottom of Frustum No. 2-108---------- 460
236. Deposition Furnace ---------- 461
237. Optical Systems---------- 462
238. Impurity Effects on Pure CH_4 at 1500°C---------- 463
239. Deposit on Filaments Near Tops of Tubes Gas Composition as Shown---------- 464
240. Hafnium Feed System Schematic---------- 465
241. Typical Nose Cone Setup---------- 466
242. Task 3.3.7-1 PG-6050 - Run #1---------- 467
243. Task 3.3.7-1 Radiograph of 6050---------- 468
244. Run 6050 - Nose Region Cross Section - 5X---------- 469
245. Run 4063 - Nozzle Growth---------- 470
246. Task 3.3.7-1 PG-6053 - Run #3---------- 471
247. Task 3.3.7-1 Radiograph of 6053---------- 472
248. Run 6053 - Nose Region Cross Section - 5X---------- 473
249. Task 3.3.7-1 PG-6056 - Run #4---------- 474
250. Task 3.3.7-1 Radiograph of 6056---------- 475
251. Run 6056 - Nose Region Cross Section - 5X---------- 476
252. Task 3.3.7-2 PG-6054 - Run #1---------- 477
253. Task 3.3.7-2 Radiograph of 6054---------- 478
254. Run 6054 - Nose Region Cross Section - 5X---------- 479
255. Task 3.3.7-2 PG-6055 - Run #2---------- 480

Page No.

ILLUSTRATIONS

256. Task 3.3.7-2 Radiograph of 6055---------- 481
257. Run 6055 - Nose Region Cross Section - 5X---------- 482
258. Task 3.3.7-2 PG-6057 - Run #3---------- 483
259. Task 3.3.7-2 Radiograph of 6057---------- 484
260. Run 6057 - Nose Region Cross Section - 5X---------- 485
261. Task 3.3.7-3 PG-5061 - Run #1---------- 486
262. Task 3.3.7-3 Radiograph of 5061---------- 487
263. Run 5061 - Nose Region Cross Section - 5X---------- 488
264. Task 3.3.7-3 PG-5062 - Run #2---------- 489
265. Task 3.3.7-3 Radiograph of 5062---------- 490
266. Run 5062 - Nose Region Cross Section - 5X---------- 491
267. Task 3.3.7-3 PG 5064-Run #3---------- 492
268. Task 3.3.7-3 Radiograph of 5064---------- 493
269. Run 5064 - Nose Region Cross Section - 5X---------- 494
270. Task 3.3.7-3 PG-5068-Run #4---------- 495
271. Task 3.3.7-3 Radiograph of 5068---------- 496
272. Run 5068 - Nose Region Cross Section - 5X---------- 497
273. Task 3.3.7-4 Summary of Deposition Thickness Profiles 498
274. 304014 Nozzle Cap---------- 499
275. Task 3.3.7-4 PG-5057 - Run #2---------- 500
276. Task 3.3.7-4 Radiograph of 5057---------- 501
277. Run 5057 - Nose Region Cross Section - 5X---------- 502
278. 304016 Nozzle Cap---------- 503
279. Task 3.3.7-4 PG-4067 - Run #3---------- 504
280. Task 3.3.7-4 Radiograph of 4067---------- 505
281. Run 4067 - Nose Region Cross Section - 5X---------- 506
282. Task 3.3.7-5 Radiograph of 5065---------- 507
283. Task 3.3.7-5 Radiograph of 4071---------- 508
284. Task 3.3.7-5 Radiograph of 6060---------- 509
285. Task 3.3.7-5 Radiograph of 5066---------- 510
286. Task 3.3.7-5 Radiograph of 5071---------- 511
287. Run 5065 - Nose Region Cross Section - 5X---------- 512
288. Run 4071 - Nose Region Cross Section - 5X---------- 513
289. Run 6060 - Nose Region Cross Section - 5X---------- 514
290. Run 5066 - Nose Region Cross Section - 5X---------- 515
291. Run 5071 - Nose Region Cross Section - 5X---------- 516
292. Task 337-5 Profile Summary---------- 517
293. Task 337-5 Nose Deposition Rate---------- 518
294. Task 3.3.7-5 PG 4072---------- 519
295. Task 3.3.7-5 Radiograph of 4072---------- 520
296. Run 4072 - Nose Region Cross Section - 5X---------- 521
297. Task 3.3.7-5 PG 6061---------- 522
298. Task 3.3.7-5 Radiograph of 6061---------- 523
299. Run 6061 - Nose Region Cross Section - 5X---------- 524
300. Task 3.3.7-5 PG 4074---------- 525
301. Task 3.3.7-5 Radiograph of 4074---------- 526
302. Run 4074 - Nose Region Cross Section - 5X---------- 527
303. Task 3.3.7-5 PG 4075---------- 528
304. Task 3.3.7-5 Radiograph of 4075---------- 529

Page No.

ILLUSTRATIONS

305. Run 4075 - Nose Region Cross Section - 5X---------- 530
306. Task 3.3.7-5 PG 4076---------- 531
307. Task 3.3.7-5 Radiograph of 4076---------- 532
308. Run 4076 - Nose Region Cross Section - 5X---------- 533
309. Task 3.3.7-5 PG 6065---------- 534
310. Task 3.3.7-5 Radiograph of 6065---------- 535
311. Run 6065 - Nose Region Cross Section - 5X---------- 536
312. Task 3.3.7-5 PG 6068---------- 537
313. Task 3.3.7-5 Radiograph of 6068---------- 538
314. Run 6068 - Nose Region Cross Section - 5X---------- 539
315. Nose Region Thickness Patterns---------- 540
316. Task 3.3.7-6 PG 6067---------- 541
317. Task 3.3.7-6 Radiograph of 6067---------- 542
318. Run 6067 - Nose Region Cross Section - 5X---------- 543
319. Task 3.3.7-6 PG 7082---------- 544
320. Task 3.3.7-6 Radiograph of 7082---------- 545
321. Run 7082 - Nose Region Cross Section - 5X---------- 546
322. Task 3.3.7-6 PG 5074---------- 547
323. Task 3.3.7-6 Radiograph of 5074---------- 548
324. Run 5074 - Nose Region Cross Section - 5X---------- 549
325. Task 3.5.2 Specification Deposits---------- 550
326. Task 3.5.2 PG 6069---------- 551
327. Task 3.5.2 Radiograph of 6069---------- 552
328. Task 3.5.2 PG 4083---------- 553
329. Task 3.5.2 Radiograph of 4083---------- 554
330. Task 3.5.2 PG 6072---------- 555
331. Task 3.5.2 Radiograph of 6072---------- 556
332. Task 3.5.2 Radiograph of 6070---------- 557
333. Task 3.5.2 Radiograph of 4084---------- 558
334. Task 3.5.2 Radiograph of 6071---------- 559
335. Task 3.5.2 Radiograph of 5078---------- 560
336. Task 3.5.2 Radiograph of 4085---------- 561
337. Task 3.5.2 Radiograph of 5079---------- 562

APPENDIX I MATERIAL SPECIFICATION---------- 563

APPENDIX II PROCESS SPECIFICATION FOR BORON-ALLOYED PYROLYTIC GRAPHITE NOSE CONES---------- 569

APPENDIX III STRESS EQUATION FOR CUT RINGS---------- 573

APPENDIX IV RESIDUAL STRESS PREDICTIONS---------- 575

I. INTRODUCTION

A. PRIOR HISTORY. Pyrolytic graphite is produced by the thermal decomposition of a hydrocarbon gas on a heated substrate.

At the time work began in this contract, General Electric Company and others had carried out basic studies relating characteristics of deposits to conditions used in the deposition process. Process conditions could be specified for production of desired structural types. Equations had been developed for the tangential, radial and axial stresses which result on post-deposition cool-down of simple shapes of an anisotropic material. These equations had been modified to account for structural differences across the thickness of a given deposit and for the effects of annealing at deposition temperature.

B. THE NEED FOR A MANUFACTURING TECHNOLOGY PROGRAM. The biggest problem area was the application of this research-scale knowledge to the production of full-scale aerospace hardware. Some progress had been made in this area of hardware production, but certain difficulties were frequently encountered. These difficulties included.

1. Non-uniformity in dimensions--particularly thickness --for a given hardware shape and size.

2. Presence of cracks or delaminations and high non-uniform residual stresses.

3. Non-uniformities of composition, density and microstructure from point to point, both along the length and through the thickness of a deposit.

4. Practical problems; such as best means for removing the desired portion of a deposit from unwanted portions and machining to final dimensions without creating new stresses or allowing catastrophic release of existing stresses.

Clearly, a systematic study was needed to improve the manufacturing technology of this desirable aerospace material, so that it could be applied on advanced re-entry vehicles.

C. SCOPE OF THIS PROGRAM. The stated objective of this program was "... the development of a manufacturing technology which will enable the prediction and specification of manufacturing process parameters for producing, with a high degree of reliability, pyrolytic graphites in specific sizes, shapes and quality beyond the present state of the art and suitable for re-entry vehicles and rocket nozzles."

It was agreed that full use would be made of background data and that every effort would be made to avoid duplication of new and prior studies outside this contract.

A two-year program of effort was outlined to meet the stated objective and an initial Work Statement for this effort was written.

When this statement of work was agreed upon, the Program Plan was written. It detailed the experimental program as envisioned at the outset of this work.

In order to accomplish this effort in the time allowed, to extend technical capabilities and to increase the available equipment and facilities, certain tasks were subcontracted by the Metallurgical Products Department of General Electric Company to the Re-Entry Systems Department of G.E., the Raytheon Company, and Rennsselaer Polytechnic Institute.

After further planning, the tasks were arranged in a logical chronological order, and a PERT diagram was prepared for use in project scheduling and monitoring. The Flow Chart in Figure 1 is an abbreviated form of the PERT diagram, which shows the sequence of tasks and the grouping of related tasks. Subcontract effort is identified.

About midway through the two-year program, efforts were redirected and a new Work Statement was issued. A modified Flow Chart is shown in Figure 2, and a cross-reference chart of tasks is shown in Table 1. Three additional months were approved for addition to the program schedule.

The new tasks--based on prior knowledge and the knowledge developed in this contract--were aimed at solving the most important residual problems. Briefly, these were:

1. Lack of ability to incorporate precisely the desired or "nominal" concentrations of boron in deposits of boron-alloyed pyrolytic graphite.

2. Inability to determine accurately, reliably and conveniently the boron concentration in deposits of boron-alloyed pyrolytic graphite.

3. The need for assessment of the effects of graphitization on residual stress levels and patterns in deposits of boron-alloyed and unalloyed pyrolytic graphite.

4. Lack of experimental data required to evaluate the use of turbulent nozzles and of acetylene addition in the production of boron-alloyed pyrolytic graphite deposits.

5. The need for control of delamination patterns in nose cones.

6. The need to optimize nose cone deposition by combining prior results with those obtained in this contract.

D. DISCUSSION. During the course of this work, several successful

applications have been made--using boron-alloyed pyrolytic graphite nose cones on test vehicles.

There is strong and continuing interest in the fabrication of such nose cones, using the process concepts developed in this contract. Further improvements can be expected but the basic manufacturing technology will be influenced by the results of these systematic studies for some time to come.

II. SUMMARY

A. INTRODUCTION

The purpose of this program was ..."the development of a manufacturing technology which will enable the prediction and specification of manufacturing process parameters for producing, with a high degree of reliability, pyrolytic graphites in specific sizes, shapes and quality beyond the present state of the art and suitable for re-entry vehicles and rocket nozzles."

In order to accomplish this goal, to avoid duplication with earlier studies, and to schedule work in an orderly fashion, a program plan and PERT diagram were prepared and submitted for approval.

The work was divided into a number of categories, including:

1. Mandrel-related studies.
2. Straight-through flow system studies.
3. Reflex flow system studies.
4. Special studies.

Each category was sub-divided into individual tasks. Some tasks were carried out by General Electric Company, Metallurgical Products Department and some were sub-contracted to G.E., Re-Entry Systems Department, Raytheon Company and Rensselaer Polytechnic Institute. In addition, some funding of tasks was provided by GE-RSD. These tasks were:
Task 3.3.6 (Interrupted deposition), Task 3.4.2.3a (Deposition from Acetylene), Task 3.4.2.4 (Hafnium alloy deposition studies), and Task 3.4.5 (Non-destructive test techniques).

A detailed description, task by task, is given in Sections III through XI for the results of these studies. Recommendations are also presented in these sections, for use by those skilled in the art, for production of aerospace hardware.

In this section the results are highlighted and summarized for those who may be less familiar with this field.

B. PRELIMINARY STUDIES - STATE OF THE ART FOR NOSE CONES

This work was done at the beginning of the contract while planning was carried out for the other tasks. Its purpose was to show the existing state of the art for producing 10° half-angle, 1/4 inch radius nose cones of graded, boron-alloyed pyrolytic graphite. A total of 27 nose cones were deposited, using conditions judged best at the time. Two modifications were made to the process during the course of this work. The first modification was an increase in pressure in an attempt to attain higher deposition rates and a shorter process cycle. At the higher pressure, voids formed in the nose tip region, so the process was modified again to an intermediate value. A process specification was written and

recommended as the basis for further work in the contract. The nose cones were evaluated separately under another Air Force Contract by G.E., Re-Entry Systems Department.

C. MANDREL-RELATED STUDIES

1. Graphite Grade Evaluation

The mandrels upon which pyrolytic graphite is deposited are made from commercial graphite. Mandrel grades are selected on the basis of mechanical and thermal properties, chemical purity, machinability, cost and availability. Not many grades are available which meet the requirements in all these categories. Grade ATJ, a product of the Carbon Products Division, Union Carbide Corporation was in use by all producers of pyrolytic graphite aerospace hardware at the time this study was carried out. Other grades were commonly used for non-critical auxiliary parts of deposition assemblies.

From these studies it was concluded that of the best candidate grades:* A and C were preferred, B was better than acceptable but less than preferred, and grade E was unacceptable for mandrel use.

2. Mandrel Design

A mandrel must be of proper size to allow for expansion when heated and then produce a deposit which will be of desired dimensions when it cools. At some point in time the mandrel fails in tension, either as a result of deposit growth which can occur at deposition temperature if the mandrel is too thin or as a result of shrinking onto the deposit during cooldown because of the difference in thermal expansion coefficients.

For the graphites recommended in 1, dimensional correction factors were determined. Mandrels of Grade A used to deposit pyrolytic graphite within, should be made 1± 0.25 percent smaller than the final deposit dimensions required. For Grade C the factor is about 1.5 percent and for Grade B the value is about 1.2 percent, based on limited experience.

Correct thickness for mandrel graphites are 1, 1, and 1.4 times deposit thickness for grades A, C, and B, respectively. A better technique, however, is to machine the mandrels to twice the deposit thickness required, and then to put in spiral grooves on the outside surface. These grooves, which predetermine the failure patterns in the mandrels, should be cut deep enough so that the remaining thickness is that specified for ungrooved mandrels.

---

*For graphite identification, contact MATC, Air Force Materials Laboratory, WPAFB.

3. Mandrel Surface Treatments

Production of deposits with smooth surfaces and minimum spalling (where a portion of the deposit surface is carried away by the mandrel) requires deposition on a carefully prepared surface. Even the best mandrel graphites are porous and the initial deposit can lock into the pores at the exposed surface.

A number of techniques were evaluated for preparing deposition surfaces. The best practical system involved hand polishing of the surface with 600 grit paper, washing with volatile organic solvents, and then depositing an ultra-thin pre-coat (0.00025 to 0.0005 inches) which subsequently becomes the surface on which the aerospace hardware is deposited.

4. Mandrel Termination Designs

Cracks and delaminations often originate in poor quality regions of deposit outside the mandrel, on auxiliary parts such as supports or exhaust stacks. Such defects can propagate easily into the deposit on the mandrel if not prevented from doing so.

A number of termination designs were developed for: a) deposition of crack-and delamination-free parts, b) deposition of crack-free, delaminated parts, and c) preservation of roundness in deposits of circular cross-section.

D. PROCESS STUDIES FOR STRAIGHT-THROUGH FLOW SYSTEMS

This nomenclature describes the gas flow path through the deposition assembly, entering at one end and flowing unidirectionally toward the other end. Depending on conditions, pyrolytic graphite (PG) or boron-alloyed pyrolytic graphite (BPG) can be deposited. Boron trichloride, added to the inlet flow of methane (or natural gas), provides a ready source of available boron.

Trimethylborate can also be used. The flow ratio can be controlled to give constant level or graded level boron concentration through the thickness of a deposit. In these studies PG at graded deposition rates, constant level BPG and graded level BPG cylinders were deposited and evaluated for use in production of aerospace hardware. All these methods had potential for favorable alteration of residual stress levels in the deposits.

From the results a number of conclusions were made. For unalloyed PG, grading the deposition rate from 15 mils/hr to 5 mils/hr was good from the standpoints of density, tangential residual stress and ring-crushing strength. For constant level PBG deposits, in the range from 0.1 to 1.9 weight percent, low levels (0.2 - 0.3 percent) were best on the basis of strength, cracking tendency and the balance between tangential and axial residual stresses. For graded level BPG deposits, of the varieties included in this study, 0.1 to 0.4 weight percent grading

was best, but not as good as 0.2 percent constant level.

Two tentative process specifications were detailed.

E. PROFILE STUDIES FOR STRAIGHT-THROUGH FLOW SYSTEMS

Deposition thickness at any point in a deposition assembly is determined by total deposition time and the localized deposition rate. The deposition rate at a given point depends on many factors including: surface temperature, gas pressure, active species concentration and the degree to which thermal and chemical equilibria are attained in the gas phase. The active species concentrations at the point are determined by the prior history and thus depend on such things as the degree to which carbon stripping has occurred in previous contact with mandrel surfaces, linear velocity and residence time of the gas within the heated zone, the presence (or absence) of soot particles within the gas stream, and the presence of diluents including by-product hydrogen.

The studies in this work were directed toward alteration of deposition thickness profiles by the use of baffles and plugs in the gas stream, replenishment of partially depleted gas by use of a second inlet nozzle, and the use of hydrogen as a diluent.

While all results showed some alteration in deposition thickness profiles, the best improvements were obtained with simple baffles, especially in deposition of frustums larger than 8 inches in base diameter. Such baffles divert the incoming gas stream toward the frustum wall and also provide some surface for preheating the gas.

F. ADVANCED STUDIES FOR STRAIGHT-THROUGH FLOW SYSTEMS.

When revised, the Work Statement included tasks related to three important problems:

1) the lack of ability to incorporate precisely the desired, or "nominal", concentrations of boron in deposits of boron-alloyed pyrolytic graphite.

2) The inability to determine accurately, reliably and conveniently the boron concentration in deposits of boron-alloyed pyrolytic graphite.

3) the need for assessment of the effects of graphitization on residual stress levels and patterns in deposits of boron-alloyed and unalloyed pyrolytic graphite.

A systematic series of deposits were made at controlled temperatures (3800, 3640 and 3450°F or approximately 2100, 2000 and 1900°C), controlled pressures (3, 5 and 7 mm. Hg.) and controlled inlet flow ratios of methane to BCl_3 (30/1, 60/1, 120/1 and 240/1). Samples from these deposits were analyzed by various methods, the best of which was large

sample pyrohydrolysis. Other analytical techniques, including emission spectroscopy with internal and external standards, gave less reliable or reproducible results. The values from pyrohydrolysis were used to prepare curves relating temperature, pressure and boron trichloride concentration to the weight percentage of boron deposited in the solid. Additionally the data provided information enough to obtain deposition rates as functions of temperature and pressure.

The results from the studies on the effects of graphitization showed that while the degree of graphitization could be specified and controlled it could not be used to advantage in depositing aerospace hardware at 2000°C. Post-deposition graphitization was also deleterious to the structural integrity of constant level and graded level BPG. Lower temperature deposits and lower level boron concentrations appeared to be better solutions to the problem.

G. PROCESS AND PROFILE STUDIES FOR REFLEX FLOW SYSTEMS

The reflex flow system used in nose cone deposition involves injection of the inlet gas mixture along the central axis of a cone toward the nose tip where the flow is reversed. The gas is heated, partially decomposed and is exhausted as an annular flow around the inlet nozzle. It is a complex system and one which does not easily adapt to in-process measurements of process variables. Experience was, of necessity, largely empirical. Moreover, very little investigation of process variables had been carried out because of the pressing need for aerospace research hardware pieces. These studies were directed toward establishing the effects of variables, the useful ranges of variables, and the formulation of preliminary process specifications for 10° half-angle, 1/4 inch nose radius cones.

The results showed that:

a) nozzle orifices from 0.075 inch to 0.150 inch diameter were usable, but 0.100 inch was preferred.

b) programmed nozzle withdrawals and low-level boron grading gave the most favorable deposition thickness profiles.

c) high levels of boron introduced heavy sooting and exhaust clogging. The high levels also enhanced graphitization and caused delaminations.

d) programmed temperature variations (1950°C to 2150°C) appeared to give cones with slightly tighter delaminations.

e) nitrogen dilution reduced deposition rates but did not give better deposition thickness profiles.

f) smaller exhaust opening areas (which offered some choking of the flow) gave better deposition thickness profiles. If

the openings were made too small, of course, deposition might close them off prematurely.

g) unshielded, water-cooled inlet nozzles showed some influence on the wall thickness profile outside the nose tip region.

Preliminary process specifications were made for graded and constant level boron-alloyed nose cones (10° half-angle, 1/4 inch nose radius).

H. SPECIAL STUDIES

Special studies were carried out to investigate: process modifications (turbulent nozzles, unsaturated hydrocarbons), interrupted deposition, additive studies, and hafnium-alloyed nose cone deposition.

1. Turbulent Nozzle Studies

Metal caps, designed for breaking up the inlet gas stream and introducing turbulence into the flow, were fitted onto ordinary water-cooled inlet nozzles and used successfully to produce thicker nose tip regions in pyrolytic graphite nose cones.

Similar caps made of a graphite were used for the deposition of BPG nose cones. These were not so successful because of sooting problems and because the maximum deposition rate occurred downstream from the nose tip where it was desired. The technique would be useful for any future nose cones where boron is specifically excluded in the specifications.

2. Deposition from Acetylene

Unsaturated hydrocarbons are produced as intermediate species in the deposition of carbon from methane or natural gas. If unsaturated hydrocarbons could be used directly under conditions where heavy sooting were prevented, this technique might allow more efficient use of thermal energy.

After preliminary experiments with cylinders, PG nose cones were deposited from acetylene/methane mixtures (1:3). At 4 mm Hg. or higher pressure, nose cones with good thickness profiles can be deposited but the material has lower than normal density.

No BPG cones could be deposited, using boron trichloride as the boron source, because of rapid side reactions which clog the inlet nozzle and gas lines.

3. Interrupted Deposition

If residual stress exceeds material strength in a given deposit it will crack or delaminate (or both) to relieve stress. This may render the part useless as aerospace hardware. This situation arises when thickness is too great for the radius of curvature. If parts were made as a series of shells, each with allowable thickness to radius of curva-

ture ratios, thicker parts should be allowable.

This technique produced good quality frustums with thickness more than twice the normally allowed value. Separation is not complete between shells unless BPG is deposited in an ultra-thin layer between PG shells. Simply interrupting deposition by shutting off methane flow for a short period of time does not isolate one shell deposit from another with certainty.

This technique has general applicability for all future thick PG deposits, regardless of shape.

4. Additive and Impurity Studies

A special technique was devised using soot particle nucleation and growth in the gas phase as an indication of wall deposition rate of pyrolytic graphite. A lab-scale furnace was modified to allow adaptation of a photoresistor which sensed light from the particles against a black background.

The experiments, all at low-temperature, indicated that:

a) boron trichloride, ethane and propane increase the deposition rate of carbon from methane.

b) hydrogen decreases the deposition rate of carbon from methane.

c) The effect of the higher hydrocarbons appears to saturate at the higher concentrations.

d) boron trichloride increases the deposition rate of carbon more with the higher hydrocarbons than with methane.

e) hydrogen decreases the deposition rate of carbon less with the higher hydrocarbons than with methane.

f) all the effects are multiplicative.

These results may be valid, or only slightly modified, at temperatures in the normal range used for aerospace hardware deposition. However, this has yet to be experimentally verified.

5. Hafnium Alloy Deposition Studies

Hafnium-alloyed pyrolytic graphite has a number of potentially useful characteristics for use in aerospace hardware if a process can be developed for producing it to required specifications.

The halides of hafnium are available in relatively pure form but are not so volatile as the halides of boron. Hafnium tetrachloride is a

solid at room temperature. In order to use it with methane to deposit hafnium-alloyed pyrolytic graphite, the entire gas inlet system must be heated to prevent condensation.

Equipment has been assembled for this purpose and will be ready for future use. The system is a sophisticated one, even allowing flow rate measurement of the heated vapor. Its design represents a large improvement in the field of chemical vapor deposition.

I. ADVANCED STUDIES FOR REFLEX FLOW SYSTEMS

The revised Work Statement included tasks designed to study methods for improving delamination patterns in cones with half-angles of 10° or less and to optimize processes for the deposition of such cones.

1. Delamination Control Studies

Most nose cones used as aerospace hardware require nose tip thicknesses of one inch or greater and uniform wall thicknesses of 0.180 to 0.200 inches. It is difficult to deposit such a deposition thickness profile without getting a thin spot just outside the nose tip region. Near the thin spot, delaminations are generally not parallel to the outside surface as desired by aerospace design engineers. Studies were carried out to modify and improve the delamination patterns in cones with 10° or 6° half-angles.

Of the many techniques investigated, the best approach for 10° half-angle cones was to first deposit a uniform thickness, by using nozzle positions further from the nose tip than usual in combination with than usual gas flow rates, and then to move the nozzle to a more normal position and continue deposition with higher gas flow rate. This two phase deposition process displaces the outer delamination inward and allows it to form parallel to the outer surface. Great care must be exercised to prevent air leaks as a result of moving the nozzle through a sliding seal.

None of the 6° half angle cones were successfully deposited without voids in the nose tip region. The results indicated that nozzle position 6" or closer to the nose tip would be required. The cross-sectional area available for the inlet nozzle is small for narrow angle cones.

2. Process Optimization for Nose Cones

Using the results of all other tasks in this contract, a new process specification was written for 10° half-angle, 1/4 inch nose radius cones. Three deposits were made to demonstrate this process. Equipment trouble prevented the inclusion of one important portion of the process - the two phase deposition developed in the task preceding. The cones were of good quality but would have been even better if the two phase deposition could have been used.

Void-free 6° half-angle cones were deposited at close nozzle positions. Exhaust port modifications might be required, to allow longer deposition periods, if greater thicknesses were specified. It now appears possible to specify a process for narrow angle cones with small nose radii for advanced aerospace hardware requirements.

III. ESTABLISHMENT OF STATE OF THE ART FOR NOSE CONES (TASK 3.5.1)

Task 3.5.1 was authorized to proceed while planning was still being carried out for the other tasks of this contract. According to the Work Statement for Task 3.5.1, "A characterization of the current state of the art will be made by performing thirty (30) full scale runs on a nose cone whose specifications are in advance of current specifications for the part. The advanced specifications will be mutually agreed upon by the contractor and MATC. The nose cones produced by these runs will be fully characterized to determine conformance with the advanced specifications."

It was mutually agreed by General Electric and MATC that work in this task would cease when twenty (20) machined cones had been transferred to GE-RSD for characterization. The cone dimensions are shown in Figure 3, and the advanced specifications are shown in Appendix I.

Nose cones of graded boron pyrolytic graphite had been deposited for Re-Entry Systems Department in earlier development work. Eight nose cones had been deposited in mandrels with one-quarter inch nose radii. Of these eight, six had the required one inch nose thickness or better. The average thickness was 1.380 inches with a standard deviation of 0.420. This work and other work with nose cones of different radii formed the experimental background for Task 3.5.1.

A. PROCESS PARAMETERS FOR TASK 3.5.1

On the basis of the prior experience, a process was chosen with a temperature of 3750°F., a pressure of 2mm. Hg., methane flow of 10 CFH and BCl_3 flow varying from 0.109 down to 0.015 CFH during the run. The rotating water-cooled inlet nozzle was positioned eight and one-half inches from the nose, centered and fitted with a graphite shield. Fifty-three hours were scheduled for each deposition.

After 10 runs, the pressure was raised from 2 mm. Hg. to 3.6 mm. Hg. to shorten the process cycle, and 50-hour runs were scheduled. After run #14, pressure was reduced to 3.0 mm. Hg. and 55-hour runs were scheduled. The process changes will be discussed in the Results section of this task report.

B. PROCESS DETAILS

Background

The setup and process design variables considered critical for the deposition of a satisfactory nose cone included nozzle position, exhaust area, hydrocarbon gas flow, boron trichloride flow and deposition time. The selection of values for these variables was based upon (a) MPD Process Instructions and (b) GE Re-Entry Systems Department Process Specification No. 8157-001 Revision B.

Nozzle Position

Positions 7" from the nose to 9" from the nose had been found to be satisfactory for 1/4" radius nose cones. The 7" nozzle position

tended to reduce the deposition rate in the nose but also reduced differences in deposition rate along the wall. The 9" position maximized the nose deposition rate but also tended to increase the difference in rates along the wall. The 8-1/2" position selected was a compromise between the above factors. This position allowed acceptable nose thickness and wall thickness to be developed in the shortest time.

Exhaust Area

This area is generally expressed as a percent obtained from the quotient of the exhaust area and cone base area. Values as high as 100% and as low as 20% had been used with success. Generally speaking, the higher the percent, the more sensitive the system was to nozzle position and transient operating conditions. The deposition rate in the unrestricted system was measurably less than in restricted ones. The lower limit of restriction was set not by deposition character or quality but by other practical limits. One such practical limit resulted from gas flow channel restriction resulting from the deposit itself. In extreme cases, total closure could result which would terminate the furnace run. Another case resulted from the need to subdivide exhaust area to allow symmetrical gas flow. Individual exhaust holes could not be too small or deposition would close them, terminating the furnace run early. The 21.4% value selected for this work was the minimum based on the closure and symmetry limits.

Hydrocarbon Gas Flow

Although gas flow was considered a critical variable, all earlier work on this type of nose cone at MPD had been done at 10 SCFH and had yielded satisfactory results for the nozzle positions indicated.

Boron Trichloride Flow

Boron addition has a catalytic effect on deposition rate and can favorably alter the residual stress characteristics of the deposited piece. Experiments had been conducted to determine the best boron addition technique. Results were evaluated on the basis of cracks, delamination patterns and delamination separations. A grading technique, holding the BCl_3 flow constant at a gas-to-BCl_3 ratio of 90:1 for roughly one-third of the run time, then grading the ratio from 90:1 to 650:1 over the next one-third, and holding a constant ratio at 650:1 for the last one-third had been determined to give the best results.

Deposition Time

When all the conditions stated above were used for nose cone depcsition at 3750°F. and 2.0 mm. Hg., 53 hours were required to deposit an acceptable part.

C. RESULTS

Twenty-seven furnace runs were completed under Task 3.5.1. A summary of thickness data is shown in Table II, along with process data and remarks. A review of individual runs follows. It should be kept in mind while reading these reviews that successive runs were often overlapping in time. Troubles observed in one run could not necessarily be corrected in the next. This schedule was necessary in order to provide nose cones for use as test models for another contract.

Runs #1 (5019) and #2 (7027) progressed normally with no variations observed. The surface finish of both parts was considered good with the exception of a pit approximately 1/8" diameter representing the site of a nodule in the second run. X-ray examination indicated that there was a high density inclusion in the nodule. This was concluded to be due to a metallic impurity which boiled out of the mandrel during heat-up and was subsequently trapped by the deposit. Such impurities are rarely encountered with ATJ graphite as mandrels. No other nodules were found in this series of runs. The conditions used for these two runs has been designated Process #1. This same process was used through #10. An exterior and X-radiographic view of run #1 are attached as Figures 4 and 5, respectively.

Run #3 (5021) was carried out using Process #1 with the nozzle position altered to 8-1/4". This adjustment was an attempt to reduce stagnation thickness and improve wall profile. The run was terminated at 40.5 hours when gas flow could not be maintained. Upon subsequent examination of the deposited part it was determined that the nozzle shield had broken, either during heat-up or in the early part of the run, and was pushed by the rotating nozzle into a position which reduced the shield-to-part clearance. As normal deposition continued, the gap between the part and shield closed, blocking the exit path of the gas. The surface condition of the part was considered to be only fair due to light spalling. It is important to understand that the specification does not allow machining of the exterior surface. By the rating system used in this report, "poor" represents visible spalling which is, nevertheless, acceptable in terms of the specification and drawing.

Run #4 (7028) progressed normally with no variation observed. The surface finish was rated poor.

Run #5 (7029) was a repeat of run #3 which had terminated without providing sufficient information to evaluate the altered nozzle position. The run progressed without any variations being observed. The results indicated that there was no advantage to the 8-1/4" nozzle position. In light of later results, there is little difference between the 8-1/4" and the 8-1/2" positions; therefore, 8-1/2" was used as the position for the balance of the runs. The surface finish was rated fair.

Runs #6 (4022), #7 (4023), #8 (7030), #9 (5024), and #10 (7031) progressed normally with no variations observed. In run #6, the nozzle shield was inadvertently left out. In runs #7 and #9, the shield was improperly centered. The deposit of run #6 was thinner than expected. The deposits in Runs #7 and #9 were not symmetric. The values shown in Table II are not the average at the positions indicated. They represent the circumferential minima as well as the axial. The combined results in these runs indicate the influence of the nozzle shield on deposition profile and rate. The deposit of run #8 was thinner than expected. The surface finishes of runs #6 and #9 were rated good, #7 fair and #8 and #10 poor.

Run #11 (7032) was carried out at a higher pressure, 3.6 mm. Hg., and a shorter period of time, 50 hours. With this change the process was designated Process #2. A review of data from runs #1 through #10 indicated the desirability of increasing deposition rate. The pressure adjustment to 3.6 mm. Hg., was used to accomplish this. A new nozzle shield design was used to eliminate the centering problem. A malfunction of the boron trichloride metering system caused the first one-half hour of deposit to be made without the boron addition. It was observed that pressure regulation was more difficult at this higher pressure. Results indicated that the new nozzle shield design was satisfactory. The surface finish was rated fair.

Runs #12 (5025) and #13 (7033) were also carried out using Process #2. The high pressure continued to give problems in pressure regulation. During run #12, a temporary decrease in gas flow was observed. The problem cleared itself and the gas flow returned to normal. A malfunction of the boron trichloride metering system on run #13 caused the first 2-1/2 hours of deposit to be made without the boron addition. The X-radiographs indicated that there were low density inclusions or voids in the stagnation thickness of these cones, as shown in Figure 5. It was concluded that these defects were related to the pressure difficulties. The surface finishes were rated poor and fair, respectively.

Runs #14 (5026), #15 (4026) and #16 (5027) were carried out at 3.0 mm. Hg. and the process was designated Process #3. This value represents a compromise between the higher pressure and its problems of regulation and the low pressure with unsatisfactory rates. A different control valve for boron trichloride was used to prevent the problems experienced in runs #11 and #13. During the first few hours of run #15, liquid boron trichloride (instead of vapor) was carried from the cylinder into the gas feed system. The pressure regulation was poor on run #14 despite the decreased pressure. Run #15 was made with a modified pressure adjusting system which was still not satisfactory. The boron trichloride flowmeter on run #15 developed a leak at 2-1/2 hours, requiring replacement. This run should have been terminated at this time. Run #16 was

made with a new pressure adjusting system which provided excellent pressure regulation. Also, a heated inlet feed system was used for the boron trichloride to prevent liquid carry-over. The X-radiograph of run #14 indicated that there was a low density inclusion or void in the stagnation thickness. The defect was again related to poor pressure regulation. The surface finish of #14 was completely unsatisfactory. Pitted regions on the surface of this cone, resulting from whisker growth, are attributed to the liquid boron trichloride carry-over. The surface finish of run #16 was rated good.

Runs #17 through #27 were carried out at the conditions designated as Process #3. These eleven runs were completed with a minimum of processing difficulty except for isolated mechanical problems associated with the gas feed system which caused three premature shutdowns. The scheduled time for each deposition was 55 hours. The results are also shown in Table II. In those cases where no remarks are made, the deposition was terminated by excessive deposit thickness in the exhaust or gas flow path.

Twenty-one cones were machined whereas only twenty were required. The twenty-first cone was to replace an early run which showed a void or low density region in the nose tip when X-radiographed.

All twenty-one machined cones were shipped to the Re-Entry Systems Department of General Electric Company for characterization, against specifications which were in advance of the state of the art.

D. SUMMARY AND CONCLUSIONS

Statistical analysis shows that the average nose thickness for the 27 cones was 1.150 inches with a standard deviation of 0.46. If the three aborted runs--#15, 19 and 21--are omitted, the average is 1.270 with a standard deviation of 0.310. These results summarize the entire series of runs in this task.

To indicate the learning process involved, results have been shown as a function of time by plotting nose thickness in each of the consecutive runs in Figure 6. Bar heights in this plot indicate nose thickness actually deposited. A horizontal line shows the minimum acceptable one-inch thickness for comparison. Those bars which are cross-hatched represent deposits having minimum wall thicknesses of 0.180 inches or better, as required.

Most of the troubles encountered in work with Process #1 were related to the graphite shield around the water-cooled nozzle. Four of the first ten (40%) were machinable to tolerance. The process was altered by raising pressure from 2 mm. Hg. to 3.6 mm. Hg. to alter the deposition profile and to shorten the deposition cycle. Pressure regulation was a problem and also an unfavorable deposition profile led to voids in the nose tip region of runs #12 and 13.

The process was then altered for the third and last time by reducing pressure to 3 mm. Hg. and increasing the deposition time to 55 hours. During this phase of work, equipment trouble accounted for the only unsuccessful runs. A ruptured gas-regulator diaphragm let air into the inlet gas flow in runs #19 and #21. Air leaks at fittings on the boron trichloride flowmeters accounted for the other two thin deposits. Ten of the fourteen runs made with Process #3 had satisfactory nose and wall thicknesses (71.5%). For these runs, the average nose thickness was 0.99 inches with a standard deviation of 0.54--but, if the three aborted runs are ignored, the average is 1.26 with a standard deviation of 0.30. This latter set of values represented the state of the art for nose cones of this type, using Process #3.

From a processing standpoint, the conditions used in Process #3 were the best for depositing these nose cones. Particular attention must be paid to the elimination of air leaks in the inlet gas-flow manifolds.

E. PROCESS RECOMMENDATIONS

For future depositions of nose cones of this type, the following conditions were recommended for those skilled in the art:

MANDREL:	Grade "A" graphite or equivalent, machined, polished and lightly precoated with pyrolytic graphite.
INLET NOZZLE:	Water-cooled, preferably rotating, fitted with a graphite shield, having a gas orifice of .060-.090 inches diameter, positioned 8-1/2 inches from the nose tip.
TEMPERATURE:	3750°F. measured with an optical pyrometer.
PRESSURE:	3.0 mm. Hg. measured in the deposition furnace.
GAS FLOW RATES:	a) Methane or dry natural gas at 10 CFH measured with any calibrated flowmeter.
	b) Boron trichloride, technical grade or better (Matheson or equivalent) at flow rates varied from an initial value of 0.109 CFH to a final value of 0.015 CFH, measured with any calibrated flowmeter.
DEPOSITION TIME:	55 hours, or adjusted as experience dictates.

Special attention should be paid to eliminate air leaks in the furnace or associated inlet gas lines. Boron trichloride is particularly sensitive to the presence of air and lines carrying this gas will plug with B_2O_3 if allowed to react with moist air.

IV. MANDREL-RELATED STUDIES

A. GRAPHITE GRADE SELECTION FOR MANDRELS (TASKS 3.3.5)

This work was carried out early in order to standardize mandrel material for all subsequent tasks. According to the Work Statement for this task, "Grades of graphite will be evaluated for use as mandrels considering availability, cost, strength, porosity and machinability."

MANDREL PROPERTY REQUIREMENTS

The graphite mandrel on which pyrolytic graphite is deposited is a major factor affecting the quality of the deposited shape. Purity of the graphite must be high to prevent boil-out of metallic impurities onto the deposition surface. Strength of the graphite must be adequate to maintain shape integrity during the deposition but allow mandrel breakage during subsequent cool-down. Thermal expansion characteristics must be known since the mandrel will be used at high temperature. A low thermal expansion anisotropy ratio is desirable so that different design factors need not be used to compensate for with-grain and across-grain orientations. The graphite must have excellent machinability, giving a good finish with close tolerance. The macropore sizes should be adequate to allow bonding of the deposit to the mandrel during the early phase of deposition but the bond should fail during subsequent cool-down. In addition to having the foregoing properties, the material should be readily available in sizes up to 30" diameter. The cost of mandrel materials was not considered as a measurement criterion for these studies.

PRIOR MANDREL EXPERIENCE

It was originally intended, within the bounds of propriety, to determine the current mandrel grades used by the industry. This was not found necessary, however, since the Marquardt Corporation had already carried out such a study and made the results available. Marquardt's report indicated that ATJ (Union Carbide Corporation, Carbon Products Division) was the "standard" mandrel material used by most producers. ATJ presented size limitations since the largest billets which were available were blocks 9" X 20" X 24" and solid cylinders $16\frac{1}{2}$"diameter X 14" long. The study showed that larger parts were generally prepared using mandrels of one of the following grades:

HLM--Great Lakes Carbon Corporation
CS --Unior Carbide Corporation, Carbon Products Division
AUC--Union Carbide Corporation, Carbon Products Division

It should also be noted that while Grades K, L, and M had been used as special mandrel materials,* size limitations prevented their general usage.

STANDARD GRADE SELECTION

It became necessary to select a mandrel grade for use in other tasks in this contract prior to the completion of this task. The selection allowed work in other tasks to be accomplished by their programmed dates. Grade A was selected. It met requirements better than the other grades already in use. Grade A was also chosen as the "Standard" material in Task 3.3.5 for comparing results with other grades selected for evaluation.

Previous experience with D, H, and N grades indicated that they did not meet all the desired requirements, Macropore sizes and distributions as indicated indirectly by post-deposition adhesion between mandrel and deposit were not acceptable for these grades. Chemical purities, although generally acceptable, presented some problems. Lack of uniformity from billet to billet and the presence of localized impurities within billets sometimes caused the formation of large nodules in the deposits which rendered them unacceptable.

Experience with Grade J indicated that the material was sufficiently pure to provide satisfactory deposits but that mandrel treatment techniques were not adequate to satisfactorily overcome adhesion between mandrel and part during cool-down.

SELECTION OF EVALUATION GRADES

Graphite vendors were contacted for grade recommendations and current property data. The grades considered as possible candidates for mandrel material are summarized in Table III. With the exception of B, G, and C, all other materials shown in the table had been used as mandrels with some success. As requirements with respect to surface finish, nodule size and thickness-to-radius ratios become more demanding the mandrel characteristics for successful or satisfactory performance became more critical.

The grades selected for further investigation were B, E, and C. The B, and E materials were selected with a known compromise. The grain size was relatively large, indicating a less desirable macropore size distribution than Grade A but it was felt that a mandrel material available in larger sizes than A should be evaluated.

---

* For graphite identification contact MATC, Air Force Materials Laboratory, WPAFB.

GRAPHITE GRADE EVALUATION

For the evaluations, mandrels of each material were fabricated using two designs:

A. 0.188" thick wall, spirally grooved to 0.120" thick, and

B. Constant 0.120" thickness.

This allowed direct comparison to experiments conducted in the other tasks with Grade A mandrels of similar designs. All mandrels were prepared on the same lathe, using the same turning speeds and tool feed rates. The machine operator reported that the materials acted essentially the same, except Grade C which was noticeably harder. The mandrels were subsequently polished with 600 grit paper. Samples of these grades similarly prepared are shown for comparative purposes in Figures 7 through 10 .

RESULTS

On the basis of the data indicated in Table III and experimental results, the following rating system has been established for comparing graphite grades:

$$\text{Rating Factor} = K_a \cdot K_{sf} \cdot K_{ms}$$

where K_a = an arbitrary constant denoting quality with respect to ash content

K_{sf} = an arbitrary constant denoting quality with respect to surface finish

K_{ms} = an arbitrary constant denoting quality with respect to mandrel separation.

The scale, used in this work for values of the constant, was

2 = preferred

1 = acceptable

0 = unacceptable*

The rating factors which were then derived are shown in Table IV. Rating factors of 4 or greater are preferred, 2 is acceptable and 0 is unacceptable.

*A rating of zero for any of the constants will lead to a rating factor of zero (unacceptable) since the factors are to be multiplied.

Two of the grades shown in Table III which were not eliminated on the basis of properties were G and F. Both of these materials appeared to have at least acceptable ratings, excluding the mandrel separation rating which would have to be obtained experimentally. However, the mandrel grade recommendations for this program are limited to those evaluated. None of the grades determined as acceptable were available in sufficient sizes to make the mandrel for the large frustum required in the original Work Statement. This would require a billet approximately 32" diameter and even Grade B was available only to 30".

SUMMARY AND CONCLUSIONS

Evaluation of graphite grades for mandrel use has been carried out experimentally, using Grade A graphite as a standard for comparison. The primary factors evaluated were ash content (or purity), surface finish (or machinability) and mandrel separation (or post-deposition release). As such evaluations are apt to be subjective, a relationship was developed which provided an overall rating factor from the primary factors. The results of the evaluation showed that Grade A and C graphites were preferred, B graphite was better than acceptable but less than preferred, and E was unacceptable.

GRADE RECOMMENDATIONS

Of the grades considered, three had properties consistent with the requirements in other tasks of this contract: A, C and B. These grades were specified for use as mandrels and associated assembly parts where post-deposition release, surface finish and nodules are design considerations.

B. MANDREL DESIGN (TASK 3.3.3)

According to the Work Statement for this task, "Mandrels with controlled thickness variations will be evaluated for controlling the breakage patterns during post-deposition cool-downs. This will reduce cracking by providing restraint or stress relief, depending on which is required for a given portion of a deposited shape"

BACKGROUND

The proper design of graphite mandrels to produce pyrolytic graphite parts within dimensional tolerance requires consideration of a number of factors. The outside dimensions of a deposit are determined at deposition temperature initially by the mandrel size at that temperature. Thus the room temperature dimensions of the mandrel must be adjusted to allow for thermal expansion of the mandrel.

Normal design procedures use graphite mandrels which fail in tension on cool-down, while shrinking onto the deposit as a result of the difference in thermal expansion coefficients. Thus, the outside

dimensions of the deposit at room temperature are determined by the final outside deposit dimensions at deposition temperature in the normal case. This factor must be incorporated into the initial mandrel size, also.

Another factor to be considered is the dimensional instability (growth of deposit by annealing) at deposition temperature. The mandrel must not be too thin or it will break early, during deposition, allowing out-of- roundness to develop. The mandrel must be thick enough to resist creep during deposition but a mandrel which is too thick will not fail early enough during post-deposition cool-down, and may impose loads on the deposit which cause it to crack or delaminate.

INITIAL MANDREL DESIGN

Since this task was scheduled in parallel with others in this group, a cylindrical mandrel design was selected for the other tasks which would provide additional information for this task. Grade A graphite was specified, with a mandrel thickness-to-deposit thickness ratio of 1.4:1. Past experience with breakage patterns had not always been favorable for this proportion, however. Often the only breakage was in one or two axial cracks rather than in the desired random crazing pattern. Usually when a mandrel failed in axial cracking alone, not only did out-of- roundness occur but also serious surface spalling of the deposit.

In order to correct this situation, a mandrel thickness was selected which gave a 2:1 ratio and then it was undercut spirally (one inch lead) back to the 1.4:1 ratio. This design favored the release of circumferential mandrel stresses by initial failure of the reduced section which had some axial component. Subsequent axial cracking was through the full cross-section. Long, continous axial cracks were prevented this way. Figures 11 and 12 show schematically such a mandrel before and after failure. In Figure 12, notice the large number and relatively small size of each fragment after failure. This pattern provided the desired symmetrical breakage, deposit roundness and reduction of spalling.

MANDREL DESIGN EVALUATION FOR CYLINDERS

The experiments in the cylinder deposition run in this task used three isothickness mandrels (no undercutting) with mandrel-to-part thickness ratios from 0.7 to 2.8: 1 and two spirally undercut thickness-to-part ratios of 0.7:1 and 2:1. In addition, another mandrel was undercut axially at 120° intervals to evaluate the effects on deposit roundness of straight, axial mandrel cracks. The mandrel was otherwise proportioned like the mandrels used for the other tasks in this group (3.3.1, 3.3.2, 3.3.4 and 3.3.5).

RESULTS FOR CYLINDERS

The results of the cylinder experiment conducted in this task and the related information generated by using the mandrel design indicated for the other tasks in this group were as follows: all the mandrel designs were thin enough to fail during cool-down. The isothickness mandrels all broke in a desirable random pattern typified by the lower mandrel in Figure 13 (this mandrel was a 0.7:1 isothickness design). The mandrel shown as the upper piece in Figure 13 was the 1.4:1 axially undercut mandrel. In this particular case, note that the only mandrel failure occurred along the axial slots. Figure 14 typifies the mandrel breakage pattern experienced with the spiral undercut design. Although it is not clear in this figure, the undercut area failed along its length. The mandrel design shown utilized a 1.4:1 ration with a 1" lead spiral undercut. The total mandrel thickness was approximately twice the intended deposit thickness.

The results of the experiments indicated that for isothickness mandrels, a mandrel thickness-to-deposit thickness ratio of 0.7:1 produced parts whose out-of-roundness was satisfactory. The axial undercut was unacceptable on the same basis. Mandrel-to-deposit thickness ratios of 1.4:1 to 2.8:1 were found to be acceptable whether undercut or not.

As a result of these observations, a 1.4:1 spiral undercut mandrel was designed for use in deposition run #3 of Task 3.3.1/3.3.2 with a thicker deposit than had previously been planned, thus increasing the absolute mandrel thickness. The mandrel performance was determined to be good but the mandrel was somewhat thicker than required if judged by the type, number and distribution of mandrel cracks generated on cool-down.

Since the initially recommended Grade A mandrel was used for several tasks, sufficient data was collected to indicate that Grade A mandrel (for internal deposits) should have dimensions 1% ± 0.25% smaller than the desired deposit dimensions (both diameter and length). This design value corrected for the dimensional changes in the mandrel during heat-up and the dimensional changes in the deposit during subsequent cool-down to room temperature. It produced cylinders of the desired size. On the basis of more limited data, the mandrel size correction factors for Grade C and B graphites were determined to be about 1.5% and 1.2% respectively. However, the factor shown for Grace C was a result of only two observations and for B was based on a single observation.

Mandrel thickness sepecifications for materials other than Grade A were based on manufacturer's strength data as found in references 1,2,3 and 4; and observations recorded when conducting the experiments in Task 3.3.5. On the basis of strength, mandrel thickness should be corrected by multiplying the thickness determined for Grade A by the following factors:

A -- 1

C -- 1

B -- 1.4

These factors were determined from comparisons of published values for transverse (flexural) strengths Mandrel failure occcurs in tension but tensile strengths for these graphites are directly proportional to flexural strengths for graphite, the accepted factor being about 60% (reference 4).

EXTENSION OF WORK TO FRUSTUMS

The final experiment of Task 3.3.3 was the deposition of two frustums of the type shown in Figure 15, using mandrels of two different designs. One design was based on the results for cylinders and used a thick mandrel spirally undercut to a ratio of 1.35: 1 for undercut mandrel-to-deposit thickness. Actually, two opposed spirals were used to increase the number of breakage lines. The uncut mandrel- to-deposit thickness ratio was 1.9:1. The second design was a tapered mandrel with a variable mandrel thickness along the length, adjusted for deposit diameter and thickness. The mandrel thickness-to -deposit thickness varied from 1.9:1 at the large end to 1.35:1 at the small end.

RESULTS FOR FRUSTUMS

The undercut mandrel provided a round deposit with satisfactory unmachined surface finish. The 1% correction value for mandrel size applied to frustums as well as it did for cylinders. The mandrel breakage pattern, along the spiral undercuts, was as satisfactory as that shown in Figure 14 for cylinders.

In contrast, the tapered mandrel did not produce a satisfactory surface. The outer surface of deposit spalled as shown in Figure 16. Although the breakage pattern was random, as desired, and the average fragment was small, breakage occurred catastrophically. Mandrel parts were found over an unexpectedly wide area of the furnace floor. Some had portions of the deposit still adhering.

SUMMARY AND CONCLUSIONS

It is possible to design mandrels of proper thickness to provide strength during deposition and yet allow failure during post-deposition cool-down. Mandrels of grade A, C or B (the grades recommended from Task 3.3.5) should be 1 to 1.5 times as thick as the intended deposit.

Mandrel breakage must not be purely by axial cracking or roundness will not be preserved. The best way to prevent this is to provide spiral undercut grooves which fail early. Heavier mandrels with undercut spirals having the 1 to 1.5 times deposit thickness have been found to be satisfactory for cylinders and frustums.

It should be pointed out that nose cone mandrels were not covered in this work. A number of factors, peculiar to nose cones, might alter the application of the principles developed for cylinders and frustums. For instance:

1. A nose cone mandrel is usually free at one end and restrained at the other.

2. A point of symmetry exists at the nose. At or near this point, cool-down stresses may be accommodated without mandrel failure.

3. The deposit in the nose area may be different with respect to anisotropy, orientation and delamination patterns than elsewhere in the deposit.

From these considerations, mandrel failure in nose cones could be expected to be different than mandrel failure in cylinders and frustums. For the 27 nose cones deposited in Task 3.5.1, only one mandrel failed in the nose region and seven mandrels did not break at all. When this occurred, the deposit extended below the mandrel after cool-down, as shown in Figure 17.

MANDREL DESIGN RECOMMENDATIONS

Mandrels for deposition of cylinders or frustums should be made by the spirally undercut technique. If an increase in the number of breakage pieces is desirable (as in the case of larger deposits) this is best accomplished by the use of opposed spirals. Undercut mandrel thickness-to-deposit thickness ratios should be in the range of 1:1 (for A or C graphites) to 1.5:1 (for B graphite).

C. MANDREL SURFACE TREATMENTS (TASK 3.3.4)

According to the Work Statement for this task, "Further technique development will be conducted relative to the treatment of mandrel surfaces for providing easy release during post-deposition cool-down. This will reduce spallation from the surface of the deposits at the mandrel-deposit interface, due to high shear stresses."

BACKGROUND

Producing parts with smooth surfaces and minimum spalling is frequently difficult since the mandrel graphite is porous and can become mechanically locked to the pyrolytic graphite deposit at its surface. During cool-down, this mechanical bond is broken by shearing at the interface. A bond at the mandrel-deposit interface is desirable since the initial deposit is not self-supporting and must depend on the mandrel for

integrity and shape. A good mandrel- deposit bond is one which provides the necessary support during deposition but shears during subsequent cool-down (i.e., on cool-down the interface has a significantly lower shear strength than the deposit). A common technique for aiding the separation between mandrel and deposit is to precoat the mandrel with from .001 to .010 inches of pyrolytic graphite, discontinue the deposition process temporarily and then deposit the required component. In theory, this provides a locked coating on the mandrel onto which the part will be deposited with the interface between the coating and component having the lowest shear strength of the system. This technique is, at best, only partially successful. The interface between coating and component is not always the site of failure. Some portions of a surface may have failed at the mandrel-coating interface, some at the coating-component interface, and still other portions may have failed within the deposited component material itself.

TECHNIQUES SELECTED FOR EVALUATION

The following techniques were considered in this task:

A. Surface finishes.

1. Polished surface.
2. As-machined surface (lathe).
3. Roughened surface.
   a) Abrasion with coarse paper.
   b) Controlled oxidation.

B. Deposition variations

1. No precoat, using the surface finishes in A.
2. .002 inch precoat, using the surface finishes in A.
3. Thick precoat (.04")

C. Surface contaiminants.

1. Tungsten Carbide powder.
2. Pyrolytic graphite soot.

The experiments of A & B, with the exception of B-3, were designed to evaluate mandrel-to-coating, coating-to-deposit and mandrel-to-deposit separation characteristics. The experiments conducted in Part C evaluated the bond strength between mandrel and deposit when particulate matter was introduced at their interface. B-3 was the equivalent of a single level evaluation of a pyrolytic graphite mandrel. The relatively heavy precoat thickness was selected to insure that it would be stronger than the mandrel and thus be the controlling influence.

RESULTS

A number of deposits were made evaluating the techniques outlined. The pyrolytic mandrel or thick precoat was unacceptable, as there was no clear demarcation between precoat and deposit. It was impossible to remove the precoat except by machining. Other techniques, although better than the pyrolytic graphite mandrel, still were not completely acceptable. The sooted precoat, although very effective in the first attempt, was unsuccessful when tried in a different furnace. The difficulty of controlling the degree of sooting makes the use of this technique difficult. The tungsten carbide powder rubbed into the mandrel surface gave satisfactory results but was not recommended because of the difficulty of obtaining uniformity and the possibility of contamination of the deposit.

Mandrels left in the as-machined condition or roughened by a controlled method produced parts which were generally rated as having better mandrel release than those mandrels which had been intentionally polished. In some cases, the roughened mandrels altered the macrostructure of the material by increasing the average grain size in the deposit. Also, patterns such as the circumferential marks left by lathe tools were visible in the deposit. The increased grain size in itself was not deleterious unless carried to extremes. It could even be advantageous by reducing the effects of an isolated nodule (large grain) caused by a serious mandrel surface discontinuity. Cylinders of extremely fine grain material with an isolated nodule at near maximum thickness-to-radius ratio usually failed axially through the nodule during cool-down. A structure which had a fine grain size was more susceptible to isolated imperfections. A nodule-forming imperfection was less deleterious when the average grain size was larger. The nodule was then restricted by growth interference from the adjoining structure and, even if not inhibited by interference, represented a smaller stress concentration than the same size nodule in fine grained material.

Polishing of the mandrels had the disadvantage that adjacent shear areas between mandrel and precoat or mandrel and deposit were increased in size by the removal of peaks and valleys on the mandrel surface. If the precoat-mandrel bond did not break, the resulting surface spall of the part was over a relatively large area. Where the precoat-mandrel bond did fail with a polished mandrel, it did so over a large area. In neither case, however, was the surface condition as good as with a roughened mandrel

Of the techniques used for roughening mandrels, oxidation gave the best results and seemed to offer a convenient, reproducible technique. However, there was a noticeable variation in surface appearance for samples oxidized at nominal temperatures of 1000° or 1150°F. for periods of one hour. These differences were attributed to :

1. Variations in air circulation within the ovens.
2. Temperature gradients within the ovens.
3. Geometrical differences in mandrels.

a) As they affect the surface/weight ratio.
b) As they affect air circulation across the surface.

It became apparent in these studies that the oxidation technique was not so easily reproduced as anticipated, and would be difficult to control on larger pieces. In view of this concern, the other techniques were reviewed for possible further contribution. The review indicated that one of the major difficulties with the precoat techniques was the spall left on the surface of the deposit when the interface between precoat and component was not the failure site. This difficulty could be minimized by making the precoat exceptionally thin (less than .0005").

Four experiments were conducted. In the first, the mandrels were oxidized. In the second, the mandrels were simply polished with 600 grit paper. In the third and fourth, the oxidized and polished surfaces were coated with .0003" of pyrolytic graphite prior to component deposition. The results of the experiments clearly indicate the advantage of a thin precoat. Figure 18 shows the good surface obtained by the oxidation technique compared with the better surface obtained when the mandrel is polished and then lightly precoated. Figure 19 shows the surface obtained with oxidized precoated mandrels. When compared with the unoxidized precoated mandrel of Figure 18a, it is evident that there is no advantage to oxidizing the mandrel prior to a thin precoat.

SUMMARY AND CONCLUSIONS

The factors which allow a good mandrel-deposit bond followed by uniform shear failure during post-deposition cool-down are not limited to the treatment of the mandrel surface. Mandrel design as related to failure characteristics and mandrel material properties are also significant. The recommended design of Task 3.3.3, the materials recommended in Task 3.3.5 and the surface treatment recommendation given here consider the inter-relationship. This combination of recommendations has been applied outside this contract to full scale re-entry hardware, with results equivalent to those shown in Figure 18a.

MANDREL TREATMENT AND RECOMMENDATIONS

The following mandrel surface treatment should be used when depositing pyrolytic graphite or boron alloyed pyrolytic graphite components:

A. The mandrel to be used should have been designed and the material selected on the basis of the recommendations of Tasks 3.3.3 and 3.3.5, respectively.

B. The mandrel should be polished with 600 grit paper until all machining marks are removed.

C. After polishing, the mandrel should be washed thoroughly

with acetone or any other appropriate volatile organic cleaning agent.

D. The mandrel should then be installed in the deposition assembly, exercising care that the deposition surface is not touched by hands or implements.

E. After heating the assembly to the deposition temperature, the precoat should be deposited using appropriate pyrolytic graphite processing parameters. The deposition should be conducted for a period of time corresponding to a deposit thickness of 0.0002" to .0005.

F. After this period the deposition process should be interrupted for a period of at least 15 minutes and then restarted at the parameters selected for the desired deposit.

D. MANDREL TERMINATION DESIGN (TASK 3.3.1 AND 3.3.2.)

According to the Work Statement for Task 3.3.1, "Mandrel termination techniques will be further developed for minimizing the loss of otherwise acceptable nose tips and frustums due to cracks or delaminations propagating from material deposited in other sections of the furnace." The Work Statement for Task 3.3.2 reads, "Mandrel termination techniques will be further developed for retaining roundness of deposits during cool-down from deposition temperatures to room temperature."

These two tasks were combined when it was found possible to incorporate both types of terminations in combined deposition runs in the furnaces.

BACKGROUND

A primary problem in crack and delamination control is associated with the manner in which the component being deposited is separated from other regions (exhaust and inlet structures) where material has deposited which is apt to be cracked or delaminated. Terminations which act as effective crack and delamination isolaters between such a component and its associated structures may also be useful in isolating multiple parts where it is necessary to connect them together. Although it is not intended that any of the multiple parts crack, the possibility does exist that a nodule, for instance, might cause a crack. Effective terminations between several parts can prevent the propagation of the crack from the failed part into others. Separators or end termination on mandrels should ideally allow disassembly without generation of additional stress which might crack or delaminate deposited components. Terminations have been designed to stop cracks and delaminations; also to allow or even promote delaminations while stopping crack propagation. The second type of termination is required when a curved deposit has a thickness-to-radius of curvature ratio

exceeding that for crack and delamination-free fabrication. In this particular case special efforts must be made to insure that the excessive residual stress is relieved by delaminations since axial cracks generally render a part unacceptable. In certain conditions, termination design can influence the roundness of a deposited part.

Early efforts at termination design were concerned with the first type. If the included angle is proper, pyrolytic graphite deposited at the juncture of two mandrel surfaces can be made to establish a plane of weakness. This is shown in Figure 20, for a right-angle juncture. Cracks or delaminations originating in either section of the pyrolytic graphite deposit do not usually propagate across a plane of weakness. This simple type represented the state of art at the beginning of this contract.

TERMINATION DESIGNS

For these tasks, a number of experiments were planned to determine the most effective termination design for:

A. Crack and delamination-free deposits.
B. Crack-free deposits.
C. Preservation of roundness.

For cylinders, eight different designs were evaluated in category A, seven in category B, and two in C. The geometry and proportions of the designs are shown in Figures 21, 22 and 23, respectively. To effectively evaluate each design, it was necessary that the deposition assembly provide a component adjacent to each termination which would be crack- and delamination-free (for categories A and C) or crack-free (for B). On the other side of the termination a region was required which would crack and delaminate. For this purpose, high stress regions were placed adjacent to the conventional tubes as shown in Figure 24. The top end of the top tube and bottom of the bottom tube were adjacent to the sharp radius at the retainer lid and bottom. The other ends of the top and bottom tube and both ends of the middle tube were adjacent to a separator (Figure 25) which, by its design, exceeded the allowable thickness-to-radius ratio.

RESULTS

All category A terminations developed well defined plans of weakness and effectively stopped delaminations. Several cracks were generated in bottom tubes at the retainer ends which propagated into the tube sections. Despite the higher thickness to radius-of-curvature ratios in the separators, it was necessary to induce axial cracks in them by sawing. Only then could the effectiveness of adjacent terminations be determined. The plane of weakness between the tube end and separator failed when the induced crack propagated to the plane. The failure at this shear line isolated the separator from the tube and stopped the crack propagation. Subsequent stress measurements indicated inner fiber tensile stress in the tube section but, unexpectedly,

compressive inner fiber stress in the separator section. A part similar to those fabricated in this task is shown in Figure 26 with the separators still attached. Figure 27 is a separator before and after axial cutting for stress measurement. The opening of the cut demonstrated the inner fiber compressive residual stress. This separator design was then incorporated into experiments conducted for several tasks with essentially 100% success. It effectively isolated a sound part from any cracks formed during cool-down or in subsequent setup disassembly. A theoretical analysis (Task 3.4.4) was given for the separator configuration by Dr. T. Mc Donough, GE-RSD. Details are presented in Appendix IV of this report.

Category B terminations are not generally required to stop stress generated cracks since a portion of the stress will have been relieved by delaminations. The Type VII termination was the most effective in inducing delaminations. The separators used in the category A experiments were again effective in crack stopping with the "B" configurations. The need for category C terminations is minimized with good mandrel design. Also, the combination of separator and category A and B terminations was found to provide and maintain roundness in deposits. As a result, Task 3.3.2 was de-emphasized and the effort reassigned in other tasks (including 3.3.1). The mandrel design selected as standard for this work produced all parts with better than average roundness. It was thus difficult to identify any contributions from the two roundness terminations used.

Additional work was carried out for cylinders in Tasks 3.3.3 and 3.3.4, in which type III, category A terminations, were used with separators. The results indicated that the type III proportions are still satisfactory when scaled for thicker or thinner deposits.

Separator design was varied and, with constant tube diameters of 3 inches, throat radii from 3/16 to 3/8 inches all showed the stress reversal effect. No direct correlation between radii and measured stress values could be found.

A frustum, as shown in Figure 28, was deposited using a separator 6 inches in diameter. A 1/4-inch throat radius performed successfully. Cracks, formed in the lower support structure, were isolated from the frustum by the separator and type III termination.

SUMMARY AND CONCLUSIONS

Terminations have been designed and evaluated for use in cylinder deposition which are effective in producing: a) crack-and delamination-free deposits, b) crack-free deposits; and c) round deposits. When used in conjunction with a separator as shown in Figure 24, these terminations provide easy disassembly after deposition.

RECOMMENDATIONS

The type III termination in category A is judged the best for

future work since it is the easiest to fabricate and provides a well-defined plane of weakness. It does not protrude into the gas stream so far as to cast a large shadow on the mandrel surface or to induce turbulence.

Type III category B is judged the best termination for most work, unless the part curvature does not clearly indicate that delaminations will be formed and thus residual stress might abe relieved catastrophically by axial cracking. If the latter is true, then the type VII termination should be used to promote delaminations.

A separator of the type shown in Figure 25 should be used in conjunction with the termination recommended for category A and whenever crack propagation appears to be a problem in conjunction with the category B terminations.

A 1/4-inch throat radius was satisfactory for cylindrical mandrels of 2 inch to 6 inch inside diameter. It might be satisfactory beyond that range, but this has not been experimentally verified. (Separator height is not known to be critical but should probably be scaled from geometric considerations. If the separator were too high, stress reversal might not be realized at the separator-termination interface. If the separator were not high enough, its geometry would be altered appreciably as deposition thickness built up.

V. PROCESS STUDIES FOR STRAIGHT-THROUGH FLOW SYSTEMS

When the mandrel-related studies were complete, attention was turned to process development in straight-through flow systems. This terminology describes the unidirectional flow patterns of the hydrocarbon source gas through the deposition assembly during deposition of cylinders, frustums, free-standing rocket nozzles and other related shapes. This type of flow is less complex than the reflex flow systems used in nose cone deposition (which is described later in this report). Studies were made in this contract on process optimization in straight-through flow systems for deposition of boron-alloyed and unalloyed pyrolytic graphite. Cylinders were deposited with about 3-inch outside diameter and about .10 to 0.11 inch wall thicknesses. The work was carried out on subcontract by the Raytheon Company, Waltham, Massachusetts.

A. CONSTANT LEVEL BORON-ALLOYED MATERIAL (Task 3.4.1.2)

According to the Work Statement for this task, "Boron pyrolytic graphite cylinders or frustums will be deposited at three boron levels to investigate strengthening of deposit by alloying."

BACKGROUND

Previous experimental work at Raytheon had indicated not only that boron increased the strength of pyrolytic graphite, but that the magnitude of effect was a function of the boron content. Such strengthening would be desirable if it could be used to increase the allowable thickness-to-radius of curvature ratio for a given deposit.

In the boron alloying of pyrolytic graphite, Raytheon had used trimethylborate as the source gas while General Electric and others had used boron trichloride. It was not known whether any differences in deposit characteristics could be related to this difference in process conditions. Accordingly, both source gases were included in this study.

EXPERIMENTAL CONDITIONS SELECTED

Using the results of the mandrel-related work, spirally grooved cylindrical mandrels were prepared from grade A graphite. The mandrels were 9 inches long, 3 inches inside diameter, with 180 mils wall thickness. Opposed spirals, 60 mils wide and deep were cut on the mandrel exterior with a 1-inch lead. The inside surface was cleaned, polished with 600-grit paper, and wiped dry with acetone-moistened lintless paper. Terminations and separators were used at both ends of the mandrel. Figure 29 shows a typical deposition assembly and a typical deposited cylinder.

The three boron levels were selected to cover the range of greatest interest in aerospace hardware. With boron trichloride source gas, nominal levels of 3/8, 3/4 and 1-1/2 percent were chosen. With trimethylborate, these same levels were chosen, but in addition 3 percent was also selected since no problems with excessive sooting had previously been observed at this level.

RESULTS

Each deposited cylinder was profiled for wall thickness uniformity and the ends were polished for microstructure examination. Density and boron assay were obtained from samples obtained at several locations. Selected, sound cylinders were used to obtain thermal expansion and mechanical property data. All these data and the processing conditions are presented in Tables V to VIII, which also contain the information for the next two tasks of this group (Tasks 3.4.1.3 and 3.4.1.1). The deposition thickness profiles are given in Figures 30 through 33 and photomicrographs are shown in Figures 34 through 38 for all the cylinders in this group of tasks.

Preliminary visual examinations were given each cylinder after removal from the deposition assembly with the following results:

GEDC-1 (nominal 3/8% B from TMB)--heavily nodulated, cracked axially due to high t/r and circumferential asymmetry in wall thickness.

GEDC-4B (nominal 3/4% B from TMB)--structurally sound cylinder, nodules 1/32 inch in diameter at surface.

GEDC-6A (nominal 1-1/2% B from TMB)--structurally sound cylinder, nodules 1/32 inch in diameter at surface.

GEDC-7A (nominal 3% B from TMB)--axially cracked, one delamination.

GEDC-8A (Nominal 3/4% B from BCl_3)--structurally sound until removal of termination when axial cracking occurred. Nodules 1/32 inch in diameter at surface.

GEDC-10A (nominal 1-1/2% B from BCl_3)--structurally sound until removal of termination when axial cracking occurred.

GEDC-11A (nominal 3/8% B from BCl_3)--structurally sound until removal of termination when small axial crack occurred. Small crack section removed leaving remainder sound; nodules 1/32 inch in diameter at surface.

GEDC-13A (repeat of GEDC-10A)--several delaminations, no cracks, nodules 1/32 inch in diameter at surface.

GEDC-14A (repeat of GEDC-1)--structurally sound deposit.

B. GRADED LEVEL BORON-ALLOYED MATERIAL (Task 3.4.1.3)

According to the Work Statement for this task, "Graded boron pyrolytic graphite cylinders or frustums will be deposited to obtain increased deposit strength while favorably altering residual stress patterns."

BACKGROUND

State of the art, current at the beginning of work in this contract, had indicated that residual stress levels and patterns could be altered in a deposit by grading the amount of boron in the deposit through the thickness. While the exact mechanism of this alteration is still not certain, it probably involves the grading of thermal expansion coefficients and the grading of other properties including strength. The important thing is that proper use of this technique allows thicker deposits of anisotropic material for a given radius of curvature.

Certain gradings had been successful but optimum grading had not been investigated.

EXPERIMENTAL CONDITIONS SELECTED

Previous Ratheon Company data had shown that maximum thermal expansion anisotropy occurred at boron levels of about 0.75 percent, where maximum tangential residual stress had been observed. This suggested two graded boron regimes: a) low boron to 0.75 percent; and b) high boron to 0.75 percent. The early work at General Electric had been similar to type b, but at lower absolute levels. On the basis of these experiences, the two grading techniques selected were nominal 0.1 to 0.75 percent and nominal 1.5 to 0.75 percent.

The mandrel and assembly details were the same as those selected for Task 3.4.1.2 of this task group.

RESULTS

Evaluation of these cylinders was similar to that for the cylinders of Task 3.4.1.2. The test data and processing conditions are found in Tables V to VIII and again the thickness profiles and photomicrographs are contained within Figures 30 through 38.

Preliminary visual examinations of each cylinder gave the following results:

GEDC-16A (graded boron 0.1 to 0.75% B from BCl_3)--
three small delaminations, no cracks,
nodules 1/32 inch in diameter at surface.
GEDC-17A (graded boron 0.1 to 0.75% B from BCl_3)--
axial cracks, appreciable delamination.
GEDC-18A (graded boron 1.5 to 0.75% B from TMB)--
structurally sound deposit, nodules 1/32
inch in diameter at surface.
GEDC-20A (graded boron 0.1 to 0.75% B from BCl_3)--
structurally sound deposit, nodules 1/32
inch in diameter at surface.
GEDC-21A (graded boron 0.1 to 0.75% B from TMB)--
several microdelaminations, no cracks, some
nodules 1/16 inch in diameter at surface.

C. UNALLOYED MATERIAL (Task 3.4.1.1)

According to the Work Statement for this task, "Secondary anisotropy will be evaluated as a means of residual stress control in high thickness-to-radius frustums. The method of achieving this property variation will be programmed variations in deposition rate "

This work was carried out in parallel with that of Tasks 3.4.1.2 and 3.4.1.3. The aim was to achieve the same goals without the addition of any alloying element by varying the deposition rates to produce a material of varying anisotropy.

BACKGROUND

The anisotropy in thermal expansion coefficients of pyrolytic graphite deposits had been found to be a function of deposition conditions. Those conditions which favored well-oriented deposits (e.g., high temperature, low pressure, low deposition rates) gave rise to the lowest tangential and highest radial expansion coefficients in cylindrical deposits. A programmed variation in deposition conditions could thus give rise to a variation in tangential and radial expansion coefficients through the thickness of a deposit. This, in turn, could give rise to an alteration in residual stress levels on cool-down from deposition temperatures.

EXPERIMENTAL CONDITIONS SELECTED

Deposition of "normal" pyrolytic graphite aerospace hardware is at a rate within the range of 5 to 20 thousandths of an inch per hour (5-20 mils/hr.). For the studies in this task, nominal deposition rates of 15, 10 and 5 mils/hr. were selected for constant rate deposition and a graded rate from 15 to 5 mils/hr. was chosen for the graded rate deposition. The constant rate deposits were made to establish thermal expansion coefficients and to see if adjustments were required for the process parameters.

The mandrel and assembly details were the same as those selected for Task 3.4.1.2 of this task group.

RESULTS

Evaluation of these cylinders was similar to that for the cylinders in the other two tasks of this group. The test data and processing conditions are found in Tables V through VIII and the thickness profiles and photomicrographs are shown within Figures 30 through 38.

Preliminary visual examinations of each cylinder gave the following results:

GEDC-2 (nominal 15 mils/hr, rate)--uniform surface texture, cracked axially in two locations due to non-uniform wall thickness circumferentially.
GEDC-3A (nominal 10 mils/hr, rate)--structurally sound, thin, low density.
GEDC-5A (nominal 5 mils /hr, rate)--three axial cracks 120° apart, delaminated, nodules 1/16 inch in diameter at surface.
GEDC-9A (graded rate, 15 to 5 mils/hr.)--structurally sound.
GEDC-15A (repeat of GEDC-2)--structurally sound.

D. BEST PROCESS SELECTION

Based upon visual examinations, photomicrographs, and the test data for all the cylinders described in the three tasks of this group, two processes were specified for best predicted results and one deposit was made with each.

Process number one, for producing a 0.3 weight percent, constant level boron-alloyed cylinder called for 2000°C., 20 torr, with 7 lpm flow of CH_4, 1.6 lpm flow of N_2 diluent and trimethylborate as required.

Process number two, for producing an unalloyed deposit at a graded rate from 15 to 5 mils/hr. called for 2000°C., 20 torr, with CH_4 flows from 9 down to 4.5 lpm and N_2 diluent at 0 up to 4.5 lpm.

The average deposition rates to be expected were 20 mils per hour for Process 1 and 10 mils per hour for Process 2.

The results of post-deposition visual examination were as follows:

GEDC-19A (Process No. 1, 0.3% B from TMB)--structurally sound deposit, nodules 1/64 inch in diameter at surface.
GEDC-22A (Process No. 2, graded rate unalloyed PG, 15 to 5 mils/hr.)--structurally sound deposit.

The same characterization was given these cylinders as for the previous ones. Processing conditions and test data are shown in Tables V through VIII.

E. DISCUSSION OF TASK RESULTS

It is convenient to discuss the results from all three tasks together because the comparison brings out a number of observations.

PROCESSING DIFFICULTIES

The chronological order of the depositions can be deduced from the identification numbers for the cylinders, although in certain cases more than one cylinder was being deposited simultaneously.

In the early stages, some difficulties were experienced in transferring technology and techniques between the contractor and subcontractor. For instance, when conditions for mandrel oxidation as a pretreatment were prescribed, the results were not as expected. Although the conditions were faithfully used, the mandrels were overoxidized which prejudiced the quality of the deposits. It was then mutually agreed that this technique would be abandoned for these tasks. Instead, a 5 mil precoat was used for the remainder of the work.

Asymmetry in wall thickness was traced to misalignment between the nozzle and cylinder mandrel and to the nozzle itself. It was decided that this could be minimized by the use of a baffled system. The baffle system has an additional advantage since this is the type of arrangement that must be used to produce full-scale deposits.

Two different baffled arrangements were used to deposit cylinders GEDC-3A through GEDC-18A. In the first arrangement, which was used to deposit cylinders GEDC-3A through GEDC-12A, a large baffled system was employed. The baffle was 3-1/4 inches in diameter by 1/2 inch thick. The preheat chamber was a graphite tube 8 inches in length by 6 inches I.D. The deposits were symmetrical in wall thickness but the deposition reates were low. In order to reduce the amount of carbon stripping by the large preheat chamber, and to increase the deposition rates, a smaller, modified baffled system was used to deposit cylinders GEDC-13A through GEDC-18A. In this arrangement, the baffle was made 2 inches in diameter. The preheat chamber was 4 inches I.D. by 6 inches in length. As seen in Table V, the deposition rates for the cylinders deposited using the smaller baffle and preheat chamber were appreciably higher than the cylinders deposited using the large baffle and preheat chamber.

The circumferential wall thickness was quite uniform for the cylinders deposited using the baffle arrangement. The thickness along the length for some cylinders, however, was non-uniform. A number of the cylinders cracked because of the great unevenness in wall thickness along the length. This was a more severe problem for the BCl_3 deposits than for the straight PG or TMB deposits. Cylinders GEDC-19A through GEDC-22A were deposited using a carefully aligned throughflow system in order to improve the uniformity in wall thickness along the length. Figure 33 shows that these cylinders had good circumferential uniformity in wall thickness and that the axial uniformity was significantly improved over the deposits made with the baffled system.

MICROSTRUCTURES

Figures 34 through 38 show the microstructures at the gas inlet (bottom) and gas exit (top) ends at approximately 100X magnification. Except for the bottom end of GEDC-7A which showed a continuously nucleated microstructure all of the cylinders had a substrate nucleated microstructure with the shape of the growth cones varying from fine to medium. No significant difference was seen between the top and bottom ends. The difference in microstructure for GEDC-7A appeared to be inconsistent with the boron analysis (1.9% B at the top and 1.0% at the bottom). It seems probable that the boron samples were interchanged, since continuously nucleated microstructure is generally associated with high boron level deposits.

DENSITY AND BORON ANALYSIS

Density and boron analysis data are given in Table VI. A number of generalizations were made concerning the density and boron data. High boron (> 0.5%B) deposits had densities around 2.23 g/cc and low boron (< 0.5%B) had densities around 2.20 g/cc. Density values were around 2.00 g/cc for unalloyed pyrolytic graphite deposited in the baffled flow assembly (GEDC-3A, 5A and 12A). The densities were remeasured on several cylinders and the low values were found again. The reason for the low density was not clearly understood. One possible explanation is that the actual deposition temperature was appreciably lower than the nominal value and may have been within the 1700° to 1800°C. range where low density PG is normally deposited. The graded rate, unalloyed PG deposit GEDC-9A, on the other hand, was deposited under similar conditions and yet the density was higher (2.14 g/cc). This suggests that deposition rate as well as temperature may have been responsible for the low density, since the first layers for GEDC-9A were deposited at about 15 mils/hr., and the density for GEDC-15A was 2.19 g/cc. The latter tube was deposited at an average deposition rate of 15 mils/hr using the baffled flow system.

A comparison of the nominal, constant weight percent boron levels selected and the measured boron levels obtained is summarized below:

Nominal boron selected, %	0.375	0.75	1.5	3.0
Obtained from TMB	0.1	1-1.3	0.7-1.2	1-1.9
Obtained from BCl_3	0.11	0.14 a)	.19-.25	--
		b)	1	

The nominal 3/4, 1-1/2 and 3% boron deposits from TMB were considered within the current Raytheon state of the art. The nominal 3/8% boron from TMB was low. All boron levels from BCl_3 were low and were attributed to the difficulty of applying previous processing data for a through-flow system to a baffled flow system. The repeat of the nominal 1-1/2% boron from BCl_3 (b) however, was somewhat better. The fact that the levels obtained were so far from the desired

values was an indication of the need for calibration curves for the BPG processes. It was this difficulty that led to the proposal of Task 3.4.6 for the revised Work Statement.

The boron results for the graded boron deposits were also considered within the current state of the art. The initial boron data for several of the graded tubes were somewhat perplexing. After rechecking several samples, it was concluded that the sampling technique of taking material from regions several mils from the surface was responsible for the high non-typical boron results which had been obtained. High boron levels in samples taken from a few mils at the surface may be associated with a boron diffusion effect. In subsequent samples, material from at least the first 10 to 15 mils was taken for boron analysis. The results for the graded deposits reported in Table VI thus represented the preferred boron levels measured. Uncertainties in the emission spectroscopic techniques of analysis as used in this and other tasks led to the inclusion of Task 3.4.7 in the revised Work Statement. In that task, pyrohydrolysis was developed and compared to this technique for boron assay.

Previous Raytheon Company data, as well as data reported by others, had shown that the unit cell height for BPG over a range of boron 0.7 to 1.6% was lower than that for unalloyed PG deposited under similar conditions. This suggested a qualitative method for estimating boron by measurement of the unit cell height, if a suitable correlation could be found between boron percent and unit cell height. The results of such a correlation are shown in Figure 39. Except for the 0.6 to 1.2% boron range, the correlation was deemed quite good. It was also interesting to note that the unit cell height goes through a minimum in this range. Other properties (CTE, resistivity, modulus, etc.) had also shown maximum or minimum values in this same boron range. The increased graphitic character for BPG containing 0.6 to 1.2% boron appeared to be associated with a catalytic graphitization effect caused by the boron. The increasing unit cell height with higher boron might be associated with a second phase (B_4C). A more detailed study was felt necessary on the relationship between boron content and time at temperature (the one point in Figure 11 after 25 hours indicated that this was important). This led to the formulation of Task 3.4.1.5 in the revised Work Statement.

THERMAL EXPANSION

Previous Raytheon Company data from flat plates deposited at 2000°C. had shown that the maximum thermal expansion anisotropy occurred for BPG containing about 1/2% boron. Thermal expansion data parallel (a-direction) and perpendicular (c-direction) to the deposition surface were obtained for six structurally sound cylinders (boron levels 0 to 1%) for comparison with previous data for plate stock. The thermal expansion data shown in Figures 40 and 41 were obtained with a Leitz dilatometer.* The shapes of the curves were similar to those obtained from plate stock. The error in measuring the coefficient of thermal expansion was ±5% for the range 0° to 1000°C.

*Ernst Leitz, Wetzlar, Germany

The coefficients of thermal expansion [illegible] in these two figures. Figure 42 shows a comparison [illegible] (circles) with previous data (solid curves) reported [illegible] c-direction data, except for the 0.2% boron point, were [illegible] to be in fair agreement with the flat plate data.

The a-direction data, on the other hand, were somewhat lower than what might be expected. The difference, although not too significant, could be associated with the different geometries, cylinder vs. flat plate, or could reflect differences in the processing temperatures, gas flow rates, pressure, etc.

MECHANICAL PROPERTIES

A diametral ring compression test was developed during this program and used to measure modulus of elasticity, Poisson's ratio, and ultimate strength. Bortz and Lund (Ref. 6) had shown this method to be applicable for graphite. Pyrolytic materials can be tested in this manner if no circumferential stiffness variation is assumed. Outer tangential surface, residual stress was measured on the same ring.

A photograph of the apparatus is shown in Figure 43 and a close-up of the ring assembly in Figure 44. The load was applied and recorded with an Instron model TTC-M-1, tensile tester. Strain gage output from rosette gages mounted on the outer surface drove the x-axis of the Instron recorder. The resulting load vs. strain curve yielded the elastic constants. The ring was loaded to failure after at least three tests were performed on each strain gage. The limiting load used for the elastic constant determinations was approximately 1/3 of the ultimate load.

Failure occurred at either the top or the bottom of the ring and was due to tension on the inner surface. The residual stress measured on the inner surface could be algebraically added to the crushing strength to determine the apparent tensile strength of the material. It should be noted, however, that the ring crushing strength should be used (for the particular size cylinders deposited) when using the strength data for engineering design. Strain readings after complete failure determined the outer surface residual stress.

The equations used for calculating the elastic constants, ultimate strength and residual stress for a radius of 1.5 inches were:

$$E = \frac{\sigma}{e} = \frac{P}{e} \frac{(2.22-h)}{2bh^2}$$

$$\mu = \frac{e_{0^\circ}}{e_{90^\circ}}$$

$$\sigma \text{ ult} = 1.94 \frac{PR}{bh^2}$$

$$\sigma \text{ res} = \frac{E}{1 - \mu^2} \quad (e_t + \mu e_a)$$

where E = modulus of elasticity

σ = stress

e = strain

P = load (negative)

b = width

h = thickness

μ = Poisson's ratio

0° = the direction of load

90° = perpendicular to load

ult = ultimate

res = residual

t = transverse
a = axial
R = Radius

This type of test had several advantages. The elastic constants and the ultimate strength could be determined easily and inexpensively. In addition, the residual stress was obtained from the same material, negating any errors due to variation in material properties with location.

Calculations showed that variations in material stiffness could cause serious errors in the measured elastic constants and ultimate strength. Circumferential thickness gradients of approximately $\pm$ 3% was the upper limit for the application of this technique. The circumferential gradients for rings tested in this study were lower than this upper limit. Circumferential variation in boron content might also cause variations in the property measured; however, this effect was likely

to be small. Machining of a non-uniform ring to constant wall thickness, on the other hand, could introduce errors due to variations in modulus of elasticity along the circumference.

A disadvantage of this technique was that the maximum stress was realized only on a small area at the load points. This same disadvantage had been previously noted by proponents of the four-point flexure test as opposed to the three-point test.

Tangential residual stress data measured by the above technique as well as by the gapping technique are given in Table VII. Table VII gives the measured modulus and Poisson ratio values and the ring-crushing strength. The mechanical property data by the strain gauge technique were obtained only on structurally sound rings which were crack- and delamination-free. The modulus and Poisson's ratio values (symbols) as a function of boron level are compared in Figure 45 with previous Raytheon Company data (Reference 5) obtained for flat plate deposits. The modulus data was seen to be somewhat higher and the Poisson's ratio data lower than the values obtained for flat plate stock. The modulus values for high boron level deposits (6 to 9 million psi) were significantly higher than the flat plate stock data. The reason for these high modulus values was thought to be associated with stress-induced graphitization which occurred during deposition.

The measured tangential residual stress data are plotted as a function of t/r in Figure 46. Also included in this figure as solid and dashed curves are tangential residual stress calculated as a function of boron percent and t/r. These curves were calculated by means of the following equation:

$$\sigma_T = 1/2 \frac{Et}{1-\mu^2} \left(\frac{1}{R}\right) \Delta \alpha \Delta T$$

where σ_T = tangential residual stress, E = modulus, t = thickness, μ = Poisson's ratio, R = radius, $\Delta \alpha$ = difference in CTE, and ΔT = temperature range. Thermal expansion, modulus and Poisson's ratio data were taken from Figures 42 and 45 for flat plate stock. The residual stress data in Figure 46 can be grouped into three regions:

1) -500 to -1500 psi
2) -2800 to -4500 psi
3) -5600 to -8500 psi

In region 1, all three samples (GEDC-3A, 9A, 12A) were unalloyed PG deposits with low apparent densities. From a structural standpoint, these deposits were undesirable because of the low densities and also because a low tangential residual stress was associated with a high axial residual stress which would cause failure by a spiral type of crack. In region 2, the measured residual stress for deposits containing 0 to 0.9% boron was approximately one-half the calculated residual stress. In this region growth had occurred (as is described

in Ref. 7) which, along with the graphitization effect during deposition, had offset one-half of the residual stress due to primary thermal expansion anisotropy. In region 3, which included the rings tested containing 1% boron or greater as well as the graded boron deposits, the measured residual stress was approximately equal to the calculated residual stress. Based upon the effect of growth on the measured residual stress as described in Ref. 7, this meant that the net growth was less in region 3 then in region 2. From a structural application standpoint, the deposits in region 2 were most desirable since the tangential residual stress was not too high and the axial residual stress was approximately the same as the tangential residual stress. In region 2, the graded rate unalloyed PG (GEDC-22A) and 0.2% boron (GEDC-19A) deposits were seen to have the lowest tangential residual stresses.

Another criterion for selecting a particular process for structural application could be based upon its ring-crushing strength. These data for structurally sound deposits are given in the last column in Table VIII. The lowest values (GEDC-3A, 15A, 22A) were seen to come from the unalloyed PG deposits. This was not too surprising since it was generally recognized that BPG had a higher strength than PG. On the other hand, the two highest values, 28,300 and 28,700 psi, were seen to be associated with the graded rate, unalloyed PG deposit (GEDC-9A) and a graded boron deposit (GEDC-20A). The next highest strength values were for GEDC-12A (27,000 psi) and GEDC-20A (25,700 psi). The unalloyed PG deposit GEDC-12A was unsatisfactory since the axial residual stress was high (low tangential residual stress and low density). The analysis was complicated by the fact that the two unalloyed PG graded rate deposits, GEDC-9A and GEDC-22A, had the highest and lowest crush strengths. The difference in strength for these two deposits may have been due to the difference in deposition temperatures, 1900° vs 2000°C; however, this hypothesis was not experimentally verified.

These results show that from a strength standpoint, the two most desirable materials were:

1) Constant boron level BPG at about 0.2 weight percent.
2) Graded rate unalloyed PG, 15 to 5 mils/hr.

ANNEALING AND GRAPHITIZATION

Tangential residual stresses, measured for cylinders GEDC-18A and 20A, did not agree with values which had been calculated for them. The calculations were based on a rigid mandrel, ignoring any possible growth or any plastic deformation occurring at the deposition temperature.

Heat treating was considered as a test which would indicate whether or not growth had occurred. Accordingly, rings from these two deposits were heat-treated at 2000°C. for 20 hours in an inert atmosphere. A ring from the constant 0.2% boron deposit (GEDC-19A) was also heat-

treated at the same time to serve as a control sample. The 1.7/0.6 graded sample (18A) cracked and delaminated as a result of the heat treatment. The 0.2/0.4 graded sample (20A) and the 0.2% boron sample were both structurally sound after heat treating--neither cracked nor delaminated. Strain gauges were applied to these rings and the residual stress, modulus, and crushing strengths were measured. These data and the dimensional changes after heat treatment, along with the values for the as-deposited cylinders are given in Table IX. Both tested rings showed an increase in residual stress and a decrease in crushing strength. The modulus increased with heat treatment as did the degree of graphitization, as measured by a decrease in unit cell height (C_o). The 1.70/0.6% boron graded deposit showed the greatest growth in the a-direction (2.8%) and greatest shrinkage in the c-direction (-5.2%). The dimensional changes for the 0.2/0.4 and 0.2% boron deposits were the same, about 1% growth and 1% shrinkage. These results show that graphitization can be a very important factor in affecting the structural integrity of cylinder deposits. They also suggest that the shrink-fit ring model was not adequate, since they show that for cylinders deposited for long periods of time, the grading technique should be reversed from what had been previously thought. Considering Figure 39, it was postulated that by grading from 0.5 to 0.1% boron or from 0.6 to 1.5% boron, the outer fiber would be graphitized most, the inner fiber least, and that structurally sound deposits with higher t/r ought to be able to be produced.

The unit cell height (C_o) is a useful parameter which can be used to characterize the structure of pyrolytic graphite. For PG deposits produced within the temperature range 2000° to 2200°C, the C_o value has been found to lie between 6.84 and 6.86$\mathring{A}$. Annealing of PG for long periods of time (~ 50 to 100 hrs) at these deposition temperatures would cause no significant changes in these C_o values. Annealing at higher temperatures for much shorter periods of time, however, caused a marked decrease in C_o to occur. Annealing of a substrate-nucleated PG at 3000°C for one hour, for example, lowered the C_o value to that approaching the graphite single crystal value of 6.709$\mathring{A}$. The 3000°C annealed PG, however, was still polycrystalline. The change in the C_o value from that for PG to that of the graphite single crystal was one recognized way of defining graphitization. The particular C_o value which was measured for PG, as-deposited or annealed, could be used to specify the degree of graphitization. Franklin (Ref. 8) established a simple correlation between the degree of graphitization and layer stacking as related to the C_o value. The degree of graphitization according to this correlation was 0% for a C_o value of 6.88$\mathring{A}$ (turbostratic structure) and 100% for a C_o value of 6.709$\mathring{A}$ (completely ordered structure). It should be noted that other structural changes, besides a decrease in C_o, accompany the graphitization of PG. A marked increase in layer stacking, crystallite growth, and preferred orientation accompanies a high degree of graphitization. In addition, the mechanical, thermal, and electrical properties for PG become more anisotropic.

Referring to Figure 39, it is seen that for the same deposition time (3 to 6 hrs) and temperature (2000°C), the degree of graphitization would be greater for deposits containing 0.6 to 1.2% boron than 0.1 or 1.9% boron. It is interesting to note also that the degree of graphitization for BPG containing 0.6 to 1.2% boron is equivalent to PG annealed at about 2600°C (Ref. 9) for the same length of time. This means that the threshold temperature for this degree of graphitization is lowered about 600°C in BPG by this range of boron content.

In Ref. 9, three stages of graphitization had been defined which were based upon the temperature and time dependency for C_o to change and upon other structural changes accompanying a decrease in C_o. In the first stage of graphitization, C_o was reduced from the as-deposited value to a value of about 6.74Å. This was accompanied by a slight increase in preferred orientation with little or no crystallite growth. The second stage corresponded to a decrease in C_o from 6.74 to 6.72Å. Here, a marked increase in preferred orientation and crystallite growth occurred. In the third stage, the C_o value approached the graphite single crystal value.

Figure 39 shows the limiting C_o value is about 6.74Å for as-deposited BPG; therefore, it seemed reasonable to conclude that this represented the first stage of graphitization for BPG. As a consequence, a slight increase in preferred orientation would be expected, with little or no crystallite growth.

Some indication of the rate of graphitization as a function of boron content was provided by the data shown in Table X. Again, the uncertainties in boron assay prevented any precise correlation.

At this stage of the work, a number of factors were identified which were deemed important in assessing the effect of graphitization on the soundness of BPG. These would apply during deposition, after cool-down, and during subsequent use in high heat flux environments. The factors were:

1) Degree of graphitization.
2) Rate of graphitization.
3) Dimensional changes (growth in the a-direction and shrinkage in the c-direction).
4) Fluctuations in boron content across the thickness and along the length of the deposit and loss by boron diffusion.
5) How the above factors affect the modulus, Poisson's ratio, and the coefficient of thermal expansion in the a- and c-directions.

Furthermore, stresses would accompany the graphitization of BPG. If the degree and rate of graphitization were low (low boron levels and high deposition rates), these stresses could be kept low. If high, delaminations and/or cracks could be expected to occur. The dimensional changes should be adequately controlled so that the room

temperature tangential residual stress and the axial residual stress would be approximately the same (as in deposit GEDC-19A). The boron content should be held constant or graded in such a way to offset the graphitization stresses (for instance, by boron grading from 0.5 weight percent on the o.d. to 0.2 percent on the i.d.). If large changes or fluctuations in the BCl_3 flow occurred during deposition, graphitization stresses between the layers might be sufficiently high to produce a delamination. If large gradients in boron level occurred in a deposit causing high differential graphitization, the resulting stresses might be sufficiently high to cause cracks or delaminations. Considering the stress equations shown in the discussion on mechanical properties, a high modulus, high Poisson's ratio, and high anisotropy in a- and c-direction CTE would all result in a high tangential residual stress. The values for these properties could be kept moderately low with a low degree of graphitization.

The importance of the results in this annealing and graphitization work led to Task 3.4.1.5 in the revised Work Statement.

F. SUMMARY AND CONCLUSIONS

Considering the variables investigated in the cylinder study (unalloyed PG at constant deposition rates and at a graded deposition rate, BPG at different levels from BCl_3 and TMB, graded boron BPG from BCl_3 and TMB) and the property data obtained for the cylinder deposits, the following conclusions were reached:

1. For unalloyed PG deposits, a graded rate tube is best from the standpoints of density and satisfactory tangential residual stress and ring-crushing strength.

2. In a baffled system of the type used in this study, BPG from TMB is favored over BPG from BCl_3 because of the greater uniformity obtained in wall thickness along the length of the cylinder. In a through-flow system and for cylinders with similar profiles, no difference would be expected between deposits made from TMB and BCl_3.

3. For constant boron level deposits produced over the range of boron 0.1 to 1.9%, a BPG deposit of about 0.2% is best because of its good mechanical strength, nearly equal tangential and axial residual stresses and less tendency to crack than higher boron level deposits.

4. Of the graded boron deposits made in this work, the 0.1 to 0.4% boron grade is better than the 1.7 to 0.6% boron grade from a consideration of strength, residual stress, and graphitization characteristics. The constant 0.2% boron deposit was found to have greater structural integrity than either of the two graded boron deposits.

5. The degree and rate of graphitization markedly affect the structural soundness of BPG deposits.

G. PROCESS RECOMMENDATIONS

Based on the results of this group of tasks, the Raytheon Company made two recommendations for processes in straight-through flow systems.

For production of boron-alloyed pyrolytic graphite:

Temperature	2000°C.	
Pressure	20 torr	
CH_4 flow rate	9 lpm	(~ 19 CFH)
BCl_3 flow rate	0.02 lpm	(~ 0.04 CFH)

which should give a deposit of 0.3 weight percent material at a deposition rate of 20 mils/hr.

For production of unalloyed pyrolytic graphite:

Temperature	2000°C.
Pressure	20 torr
CH_4 flow rate	9--4.5 lpm (19-9.5 CFH)
N_2 flow rate	0--4.5 lpm (0-9.5 CFH)

which should give a deposit at a graded rate from 15 to 5 mils/hr.

VI. PROFILE CONTROL STUDIES FOR STRAIGHT-THROUGH FLOW SYSTEMS

The thickness of deposit at a given position on a mandrel is obviously a function of total deposition time in the process cycle; however, many factors interact to determine the deposition rate at such a point.

A number of factors were considered by Diefendorf (Reference 10) for the simple case of straight-through flow in a right-circular cylinder. Figure 47 shows the case in a schematic form. As the cool inlet gas flows from the cold to hot portion of the cylinder, heat is transferred by conduction as the gas contacts the wall surface. For an infinitely long cylinder, thermal equilibrium might eventually be established if composition of the gas remained or became constant.

Chemical reactions occur in the gas phase as the temperature increases. The tendency is toward equilibria of the type discussed by Duff and Bauer (Reference 11) and shown for one case in Figure 48. During gas flow through the cylinder, reactive species are removed from the gas by diffusion to the wall. As a result, composition of the gas varies with distance from the wall. For an infinitely long cylinder chemical equilibria might eventually be established for gas phase species in the presence of carbon walls.

The net result of changes in these factors and others is a non-uniform deposit thickness along the length of a cylinder. The figure illustrates a typical thickness profile. A profile of this type is not satisfactory for an anisotropic deposit of pyrolytic graphite. Residual stress levels are altered too far from those for an ideal, uniform thickness deposit, which leads to cracking and delamination during post-deposition cool-down.

Some aerospace hardware of pyrolytic graphite is made by straight-through flow in mandrels more complex than cylinders. The next simplest case is that of a frustum of circular cross-section, where cross-sectional area changes regularly along the length. The linear velocity of a constant volume flow of gas thus varies along the length of the mandrel. This factor must be accounted for to avoid undesirable deposition thickness profiles.

An even more complex case is that of a free-standing rocket nozzle. Here the gas flow is conducted through a region of diminishing cross-sectional area to the throat region and then through a region of increasing cross-sectional area.

The work in this group of tasks was directed toward techniques which could be used to control deposition thickness profiles in all such mandrels for straight-through flow systems.

A. FLOW CONTROL STUDIES (Task 3.2.2.1)

According to the Work Statement, "The magnitude of the changes which can be made through modification in gas flow patterns will be established. Techniques which will be evaluated include baffles,

plugs, and preheater zones with diffuser plates."

BACKGROUND

The general ideas for baffles and plugs were conceived before the beginning of this contract. Some baffling was used in the process studies at Raytheon in Tasks 3.4.1.1 through 3.4.1.3, where cylinders were deposited. Some plugs had been used at General Electric in work outside this contract.

The use of a baffle in the deposition of a frustum is shown in idealized form in Figure 49. The baffle is so contoured as to deflect the inlet gas stream toward the mandrel walls. Successful baffling would result in laminar flow over the entire mandrel wall, eliminating the need for long distance diffusion from the injected core of gas.

The use of a plug in the deposition of a frustum is shown in idealized form in Figure 50. A plug reduces the cross-sectional area for gas flow. Successful plugging would lead to high efficiency deposition from a relatively high velocity flow of gas in intimate contact with the deposition surface. While it might appear that a secondary frustum could be obtained from deposition on the plug, experience has shown that this material is generally of low quality and with unfavorable residual stresses.

EXPERIMENTAL CONDITIONS SELECTED

Three baffle systems were investigated in this task. In the first, a simple baffle was used as shown in Figure 51a. In this case, the baffle was not intended to control the cross sectional area but to act as a gas preheater (rather than using the mandrel surfaces) and also to prevent the formation of a wasteful core of unusable, unreacted hydrocarbons along the flow axis.

The second baffle was designed to maintain a constant gap between the mandrel deposition surface and the baffle. This design is shown in Figure 51b and for the same gas flow as in the first design it increased the linear velocity significantly. Linear velocity increases in a plugged frustum for two reasons. Less cross-sectional area is available for the given volume flow. Also, by the geometry of a frustum, cross sectional area decreases along the length toward the small end.

The third baffle was designed to maintain a flow cross section which was essentially constant over the length of the part deposited. In this case, the relatively uniform velocity eliminated any variation in deposition rates as a result of changes in velocity and allowed much of the information developed for simple cylinders to be applied to this frustum configuration. This baffle is shown as Figure 51c, and, like 51b, it allowed a very high linear velocity as compared to Figure 51a.

The mandrel used for this task is shown in Figure 52. It was designed to approximate closely the size and shape of interest for use in aerospace re-entry vehicles.

Processing conditions for these depositions are shown in Table XI. The deposit was alloyed with boron at a nominal level of 0.3 weight percent. The linear velocities shown in the table are not measured, but calculated values. Inlet flow volumes were corrected for thermal expansion and for estimated changes in the volumes which resulted from partial degradation of methane, formation of hydrogen, and carbon removal.

RESULTS

It was expected a priori that the plugged runs would yield a better deposition thickness profile than the baffled run and that the uniform gap design would give the best of all.

From the results, as shown in Figure 53, it can be seen that the constant gap plug gave a more uniform deposition profile than the constant area plug. The surprising thing was that the simple baffle gave the best profile and, in addition, produced a thicker frustum for the same process conditions, including deposition time. Preheaters with diffuser plates were not investigated, as adequate gas heating was provided by the use of a simple cylinder attached to the bottom end of the mandrel.

Some differences were found in microstructures for materials deposited near the gas exhaust (small) ends of the three frustums. The photomicrographs in Figure 54 show the onset of a regenerative microstructure in the plugged runs.

SUMMARY AND CONCLUSIONS

The primary difference between a frustum mandrel and a cylinder mandrel is the changing cross-sectional area with length for the former and the constant cross-sectional area of the latter. When steps were taken to make a frustum like a cylinder by the use of a plug which altered its flow cross-section to a constant value, the resultant deposition thickness profile became equivalent to that for a cylinder. Unfortunately, as the curve for run 9033 indicated, the deposition profile for the cylinder equivalent was not uniform for the conditions used.

The non-uniform cross-sectional areas available to the gas flows in the simple baffle and the constant gap plug cases, gave more uniform deposition thickness profiles. Apparently, these cases gave a better balance among factors such as linear velocities, Reynold's numbers, active species concentrations, gas heating rates, gas-phase reaction rates and carbon depletion rates for a frustum this size.

Since the curve for the simple baffle case lies above the curve for the constant gap plug case, it might appear that carbon stripping from the gas was more efficient in the baffle case. This was not so, however, if

the additional pyrolytic graphite deposited on the surface of the plug were considered. Carbon deposited on the plug is not useful product, though, and represents a wasteful competition for the carbon content of the incoming gas.

RECOMMENDATIONS

For frustums of current interest as aerospace hardware, simple baffles should be used for gas flow control. These will provide uniform deposition thickness profiles, while offering little in the way of surface which competes with the mandrel for the carbon content of the gas.

In very large frustums, where the cross-sectional area must be limited to restrict the total required gas flows in the deposition furnace, plugs may be necessary. If so, plugs contoured so as to provide constant gaps are preferred to plugs which provide constant cross-sectional areas.

B. HYDROCARBON REPLENISHMENT STUDIES (Task 3.2.2.2)

According to the Work Statement, "The magnitude of change in deposit thickness profile and deposition rate through gas replenishment techniques will be evaluated."

BACKGROUND

A portion of the decrease in deposition thickness along the length of a deposit, as shown in Figure 47, can be ascribed to carbon depletion from the core of reactant gas. For very efficient carbon stripping, this depletion effect would be significant. Even for relatively inefficient carbon stripping, this effect must be considered when the gas flow path is a long one.

If fresh hydrocarbon gas could be injected properly, it should be possible to make up for some or all of the carbon depletion in the primary inlet flow.

EXPERIMENTAL CONDITIONS SELECTED

For this work, cylinderical mandrels of 5-inch inside diameter and 20-inch length were chosen. These were identical to those chosen for the hydrogen dilution task of this group (Task 3.2.2.3) so that results could be compared directly.

A deposition temperature of 3800°F. was used at 5.0 mm. Hg. pressure with 36 CFH of methane as the gas flow. These conditions were identical with those of run 8036W from the hydrogen dilution task, except that the inlet flow was divided for this task. In one case, half of the gas was put through the inlet nozzle and half through the extended replenishment nozzle. In another case, two-thirds of the gas was put through the inlet nozzle and one-third through the replenishment nozzle. These conditions are shown in Table XII.

Figure 55 shows, in schematic form, the concept as it might be reduced to practice for the deposition of a long frustum. Figure 56, which is not to scale, shows the method as reduced to practice with modifications to existing equipment for the deposition of cylinders. Figure 57 is a photograph of the actual nozzle showing the central water-cooled replenishment nozzle with its provisions for water inlet and outlet and gas inlet. The figure also shows the dual uncooled inlet tubes which formed the inlet system for the gas entering the base of the mandrel assembly. The o-ringed flange separated the vacuum portion of the deposition furnace from the atmospheric pressure portion.

RESULTS

The deposition thickness profiles for the two runs are shown in Figure 58. They are compared with a normal deposit prepared at the same temperature, pressure and total flow. For an exact comparison the normal deposit curve would have to be adjusted downward to account for the two extra hours deposition time.

SUMMARY AND CONCLUSIONS

From the shapes of the deposition thickness profile curves, it could be seen that an improvement (flattening of the curve) was obtained when a portion of the inlet flow of methane was used as a replenishment about halfway down the length of a cylinder of the dimensions used. The best (flattest) profile was obtained when half the total gas flow was used for replenishment.

RECOMMENDATIONS

While this technique offers an improvement in deposition thickness profile, its implementation is more difficult than that of simple baffles or hydrogen dilution. All the difficulties and potential hazards associated with long water-cooled nozzle systems in operation in high temperature, low pressure environments must be taken into account. Routine pre-deposition leak checks are a must.

Properly used, this technique could be adapted to a wide variety of sizes and shapes and would be equally useful in resistance-heated or induction-heated furnaces.

C. HYDROGEN DILUTION STUDIES (Task 3.2.2.3)

According to the Work Statement, "Chemical techniques for modifying deposition rates and deposition thickness profile will be evaluated using hydrogen as a diluent."

BACKGROUND

An overall reaction equation of the form:

$$CH_4 \xrightarrow{\Delta} C + 2H_2 \uparrow$$

offers a convenient means of expressing the deposition of carbon from a hydrocarbon source gas. Such an equation, however, is not adequate to indicate the complex set of reactions, consecutive reactions, competing reactions and back reactions which actually occur and whose individual importance depends on temperature, pressure and other conditions which prevail in the flowing mixture of species and at the mandrel surface.

Fortunately, an exact knowledge of the mechanism or an identification of intermediate species is not required to deposit pyrolytic graphite from a hydrocarbon gas, nor to develop a manufacturing technology. Enough experience with empirical relationships is at hand to assure reasonable success for most depositions.

The overall equation is useful to the extent that it indicates hydrogen is a product of the overall reaction and how much hydrogen would be obtained if the reaction were carried to completion. It seemed reasonable to assume that hydrogen might be effective in modifying the rate (or rates) at which completion would be attained.

In addition to its possible action as a chemical back-reactant, hydrogen could be expected to exert influences in other ways. For instance, the presence of hydrogen should influence the rate at which the gas becomes heated near the inlet to the hot mandrel system. Hydrogen might also compete for active sites at the mandrel surface and thus influence the rate at which carbon precursors were added to the surface.

Thus, for many reasons hydrogen showed promise as a "diluent" in the inlet hydrocarbon gas stream. Finally, its influence should be greatest near the inlet end since hydrogen (as a product of reaction) would already be expected near the outlet end.

EXPERIMENTAL CONDITIONS SELECTED

The results provided by Raytheon from their studies in Tasks 3.4.1.1-3.4.1.3 showed the advisability of producing boron-alloyed pyrolytic graphite cylinders with about 0.3 weight percent of boron. It was decided to deposit that material in the work in this task.

Calculations showed that for 5-inch diameter deposits flows of 36 cfh methane and 0.19 cfh BCl_3 would provide a linear gas velocity similar to that used by Raytheon for their 3-inch cylinders. Then, addition of 7 and 14 cfh hydrogen would give the desired 20 and 40 percent dilution for the initial runs in this task. All deposits were made at 3800°F. and 5 mm. Hg. Process conditions are shown in Table XIII.

RESULTS

The first experimental results were those shown in Figure 59. These results were exactly reversed from those which had been predicted. Although the trouble was eventually proved to be an error in labeling the two cylinders made simultaneously in deposition run 8035, this could not

be stated with certainty at the time these curves were plotted. Consequently, it was necessary to allow that the results might be correct as shown, to devise plausible reasons which could explain such results and to test the reasoning.

For these results to be correct, the decreased concentration of active species near a given point along the mandrel surface which resulted from dilution (and/or back reaction) would have to be overshadowed by a concentration increase as a result of increased linear velocity of the total gas flow. No past experience would justify a flow velocity dependence of this magnitude in this range of linear velocities.

A new cylinder (4041) was deposited at such conditions that linear flow rate was identical to that for the no dilution case (8035W) but with a diluted composition equivalent to 4040. Presumably, the curve would fall on or slightly below that of 8035W since velocities were identical but 4041 was diluted. Instead, the curve for 4041, as seen in Figure 60, was nearly identical with the curve for 8035E. This suggested strongly that the labels had been reversed on 8035E and 8035W. If so, the upper curve would be for no dilution as had been originally predicted and the lower curve would be for the case of most dilution.

Further proof that hydrogen dilution decreased the deposition rate as expected was obtained in two ways:

a) A set of unalloyed pyrolytic graphite cylinders was deposited, again with and without dilution (8036E and 8036W). The curve for the undiluted flow lies above the curve for diluted flow as seen in Figure 61. Thus, at least for systems without BCl_3, dilution decreased deposition rates as would be predicted.

b) Another set of cylinders (8043E and 8043W) of boron-alloyed pyrolytic graphite was deposited with and without dilution. The runs were scaled down in such a way as to give high linear velocities but with decreased volume flows in smaller cylinders (4.5 inches diameter instead of 5.0 inches). Due to an error in instructions, the run was carried out at a higher volume flow than planned, as indicated in Table XIII. However, as seen in Figure 61, the curve for the undiluted run lies above the curve for the diluted run as would have been predicted originally (before the trouble in 8035E and W). Not only did this reaffirm the mislabeling of the 8035 cylinders, but it also eliminated the need to consider any model based on possible catalytic effects associated with hydrogen in the presence of BCl_3. Such a catalytic effect model was given some consideration because of the unknown effects of side reactions (possibly borane formations) on the deposition rates in the alloyed system. The relatively flat initial portions of the curves for 8043E

and W are a consequence of an assembly redesign to eliminate the gas inlet baffles which had been used for all other cylinder depositions in this task.

At this point in time, the Work Statement was being revised and no further work was carried out in Task 3.2.2.3.

Microstructures of material deposited in the 8043 cylinders are shown in Figure 62. No great differences are observed between the diluted and undiluted system materials.

SUMMARY AND CONCLUSIONS

For the range of dilution conditions used in these studies, hydrogen dilution was effective in reducing deposition rates of both boron alloyed and unalloyed pyrolytic graphite. It had been predicted, however, that the influence of hydrogen would be greatest near the inlet end. Such a change would lead to a relative flattening of the deposition thickness profile since the high initial portion of the curve would be lowered most. No such flattening was observed in these studies.

Figure 63 is a plot of the logarithms of the apparent deposition rates (total thickness divided by total time) against lengths along the cylinders. Assuming that an exponential decay in deposition rates of the form $R = R_{max}e^{-kl}$ could be used to describe the case for these cylinders, such a plot would give straight lines with slopes of characteristic value (-k). There are end effects seen in these plots but they are indicative of thermal-gradient end effects in the deposition assemblies. In this plot, however, the linear portions of the curves are all of identical slope whether for boron alloyed or unalloyed pyrolytic graphite. This unexpected result reaffirms the statement that hydrogen addition did not alter the basic shapes of the deposition thickness profiles.

This result is in apparent contradiction to other work done outside this contract in deposition assemblies for other geometrical shapes. It may be that the effect of hydrogen is more pronounced at lower linear flow velocities (longer residence times for active species) and at much higher velocities (where heating of the inlet gas stream is a limiting factor).

RECOMMENDATIONS

On the basis of the results from this task, hydrogen dilution alone is not recommended as a technique for control of deposition thickness profile in straight-through flow systems. It might, however, be useful in certain cases such as those where very high or very low gas flows are required. It might also be useful when combined with other control techniques such as baffles and plugs.

D. OPTIMIZATION

The results from all three tasks of this group were considered for combination into a series of optimization runs. Only one deposit was made

at the time the revised Work Statement went into effect. This deposit was a frustum of the same type used in Task 3.2.2.1.

The new deposition run (9034) was carried out with the same deposition assembly design, including a simple baffle, as the best run (9031) from Task 3.2.2.1. All deposition conditions were identical to those for 9031 as shown in Table XI, except for the addition of 20 cfh hydrogen in the inlet gas flow. This 30 percent dilution lowered the deposition rate somewhat, as seen in Figure 64, but did very little to improve an already acceptable thickness profile.

On the basis of these results, it was decided that the next task (3.4.6) would be carried out without hydrogen dilution.

VII. ADVANCED STUDIES FOR STRAIGHT-THROUGH FLOW SYSTEMS

A portion of the revised Work Statement was directed towards residual problems in straight-through flow systems. The results, of course, would also be applicable to reflex flow systems but the work was more conveniently carried out in cylinder deposition.

The problems which led to the formulation of these elements of the revised Work Statement were:

1. Lack of ability to incorporate precisely the desired or "nominal" concentrations of boron in deposits of boron-alloyed pyrolytic graphite.

2. Inability to determine accurately, reliably and conveniently the boron concentration in deposits of boron-alloyed pyrolytic graphite.

3. The need for assessment of the effects of graphitization on residual stress levels and patterns in deposits of boron-alloyed and unalloyed pyrolytic graphite.

The first two problems were intimately related. Part of the uncertainty in depositing material with the desired boron content resulted from the uncertainty involved in boron assay of the material. Part of the difficulty with the development of an adequate boron assay technique resulted from the fact that no series of samples were available which had been prepared in a systematic way. To overcome these problems, cylinders of boron-alloyed pyrolytic graphite were prepared at General Electric, Metallurgical Products Department using a matrix of preselected conditions. Assay was carried out on samples of these deposits at General Electric, Re-Entry Systems Department on subcontract.

A. BORON ALLOY--DEPOSITION STUDIES (Task 3.4.6)

According to the Work Statement "Calibration curves will be prepared for incorporation of controlled weight percentages of boron in vapor deposits by controlling volume percentages of boron trichloride vapor in the inlet gas streams. No simple correspondence is expected because of competing gas phase reactions which remove boron in soot".

BACKGROUND

Boron-alloyed pyrolytic graphite had been prepared and characterized before work began in this contract. No firm specifications, requiring boron at a definite weight percent level within very narrow limits had yet been imposed for the production of any specific aerospace hardware. As a result, each producer had developed capabilities for supplying material of "about X weight percent boron ± y percent" or "nominal X weight percent" where X varied between zero and 2 and y was about 0.1 to 0.2. Process conditions were modified slightly if the first run of a series was nearly correct when assayed. Actually the results were better than might be expected for such an

empirical situation. The primary variable in most systems was the inlet flow ratio of hydrocarbon-to-boron source gases. Some work had also been done to investigate the effects of temperature and pressure.

EXPERIMENTAL CONDITIONS SELECTED

Cylinders, 4-1/2" diameter by 20" long, were selected for deposition in this work. A deposition assembly was designed which permitted two such cylinders to be made simultaneously. It was necessary that a common temperature and pressure be used, but the methane-to-boron trichloride ratios could be varied independently. A drawing of the deposition assembly (not to scale) is shown in Figure 65. All the design practices recommended from the mandrel-related studies were incorporated.

A matrix of 26 deposition conditions was devised which would cover the range of temperature, pressures and boron concentrations most likely to be useful for fabricating aerospace hardware. These conditions are shown in Table XIV.

In addition to this matrix, other runs were made either to extend the range of conditions or to repeat runs whose results might have been influenced by excessive sooting. For instance, the additional conditions were: a) 3640°F., 5 MM and 450/1 flow ratio; b) 3450°F., 7 MM and 240/1 ratio; and c) 3450°F., 7 MM and 120/1 ratio.

Detroit natural gas (greater than 95 percent methane) was substituted for pure methane in these studies in accordance with normal manufacturing practice. Its flow rate was fixed at 36 cfh on the basis of the previous experience in Task 3.2.2.3, and boron trichloride flow was varied to obtain the desired inlet flow ratios. Approximate linear flow velocities were calculated, allowing for heat-up and dissociation of the inlet gas. These values are shown in Table XV and should be used as the starting point for any independent studies. Pressure and temperature effects were estimated using ideal gas law relationships. If methane completely dissociated, two mols of gas (molecular hydrogen) would be formed for each dissociated mol of methane. Since total dissociation does not occur, a factor of 1.5 was used to adjust the inlet methane flow.

RESULTS

A summary of the operating conditions and test data are shown in Tables XVI and XVII, respectively.

Figure 66 shows a typical set of cylinders before mandrel removal. Although it is not obvious in this figure, the mandrel had failed in two ways: Along the circumferential grooves and axially. The sampling was done in accordance with the drawing in Figure 67 as seen for a typical case in Figure 68.

Residual stress, bulk density and microstructure were determined on rings "B" and "D". After material was removed for this characterization, the balance of material from these rings was shipped to General Electric, Re-Entry Systems Department for boron assay in Task 3.4.7.

The primary objective of this task was to provide enough data so that processing conditions could be selected to yield desired weight percentages of boron in deposits. In the course of this work, however, other data were gathered which supplement the boron studies. It is convenient to discuss the results in a number of separate categories.

Profile Figures 69 through 75 show the deposition thickness profiles of the cylinders. The plotted values are actually each averages of four readings taken at 90° increments around the circumference. The average circumferential profile variation was about 10 percent. The shapes of the profile curves were, for the most part, simply reflections of the concentration gradients of active species in the gas as the gas flowed along the lengths of the cylinders. In some profiles, the initial rates were lower than the maximum rates. This was attributed to the fact that the "0" position of the deposit (along the cylinder length) was close to the furnace floor and, therefore, often in a zone where the gas was not yet at temperature.

Microstructure Figures 76 through 86 show the microstructures of rings "B" and "D" for all deposits at an approximate magnification of 50X. No significant difference in structures between the two rings were observed for any cylinder.

"Pepper-like" specks in 8059-1B were examined at higher magnifications, as shown in Figure 87. The particles were attributed to excessive soot development in the gas stream, and not to extraneous foreign matter introduced into the system. There is a possibility that the specks might contain a new phase, B_4C, but no further work was done to identify them and no such specks were found in other samples of similar boron content.

Bulk Density. Apparent bulk densities were obtained by the displacement of freshly-boiled distilled water.

Boron Assay. All boron values in Table XVII were obtained in Task 3.4.7.

Residual Stress. Residual stress values are shown in Table XVII only for the cases where crack-and delamination-free deposits were obtained. The stress values were obtained from cut rings by the technique detailed in Appendix III.

ANALYSIS OF RESULTS

The results from this task can be used to show the influences of temperature, pressure and boron trichloride concentration in determining the weight percentage of boron deposited in boron-alloyed pyrolytic graphite. In addition, the results can be used to show how deposition rate of this material varies with pressure and with temperature. These influences are best discussed separately.

Temperature Influence on Boron Incorporation Figures 88 through 91 indicate the effect of temperature variations on the weight percent of boron incorporated in the solid for methane-to-boron trichloride ratios of 30/1, 60/1, 120/1 and 240/1.

Although the absolute values of boron decreased with an increase in the flow ratio, as would be expected, the increase with respect to decreasing temperature was relatively independent of the flow ratio. Most of the data agree fairly well with an increase in boron content of 0.2 percent for a decrease in deposition temperature of about 100°F.

Some data points appeared to be lower than would be expected from the general nature of the curves. For example, the points for 3640°F., 5 MM. and 30/1 flow ratio in Figure 88; and 3640°F., 5 MM. and 240/1 ratio in Figure 91 were definitely below what might have been predicted. These two cylinders were one set deposited simultaneously. Severe sooting had been noted during this run, as judged by the appearance of many particles in the exhaust stream. Large growths were deposited within the cylinders, of a type shown in Figure 92 for another cylinder in this task.

Since some gas phase nucleation occurred at all conditions used in this task, it is important to describe the condition referred to as "sooting." In the absence of measured particle distributions, the concept was described in terms of two regimes:

a) A low concentration of ultra-fine particles in the effluent gas stream.

b) A high concentration of large particles in the effluent gas stream.

The results of deposition in regime B are dramatic. Large compacts of low density material are laid down in the exhaust stack region of the deposition assembly. In extreme cases, coating of the furnace walls and pump line occurs. The material within the hot zone can vary in nature from piles of individual particles to strong compacts of well-bonded carbon of low quality. Some soot structures become coated with pyrolytic graphite as was the case shown in Figure 92. The compacts can cause partial or complete choking of the gas flow path.

Normal deposition takes place within regime A and it is for this condition that calibration curves are valid.

When boron trichloride is present, soot formation removes part of the boron which otherwise would have been incorporated in the normal deposit on the mandrel wall. Thus, boron assay would give abnormally low results for such deposits.

Returning to the case of the two cylinders with low boron content, it was decided to make a new run repeating the 240/1 ratio but substituting a 450/1 ratio for the 30/1 ratio. The sooting had originated in the 30/1 ratio cylinder, closed the common exhaust stack and influenced the 240/1 ratio cylinder. The new set was deposited successfully without sooting in regime B, and the data points fell where they were predicted on the curves.

Pressure Influence on Boron Incorporation. The weight percent of boron in boron-alloyed pyrolytic graphite increases with increasing deposition pressure. This effect is illustrated in Figures 93, 94 and 95 for deposition at 3800°F, 3640°F, and 3450°F, respectively. There is more scatter in these data than was the case for the temperature influence studies. Pressure was measured at a point beyond the exhaust stack in the deposition assembly. Thus the pressure measurement was not a reliable indication of the true pressure within the deposition assembly for those where sooting led to growths in the exhaust stack. The error would vary, depending on the degree of stack closure.

Nevertheless, if allowance is made for those points associated with sooted runs, it can be stated that the boron content in the deposit increased with an increased deposition pressure. The average slopes for the curves at the three temperatures were 0.10 weight percent per MM. for 3800°F., 0.07 for 3640°F, and 0.14 for 3450°F. In view of the scatter in data, it is probably best to assume an average slope of 0.10 for future process selection or modification within this temperature range.

Boron Trichloride Concentration Influence on Boron Incorporation. The calibration curves, relating the relative amount of boron introduced as BCl_3 in the inlet gas stream to the concentration incorporated in solid deposit, are shown in Figure 96. This figure is confusing, not only because there are so many data points but also because none of the data have been corrected in any way for the effects of sooting.

For convenience, the smoothed curves in Figure 97 may be found more useful. This curve was prepared by transferring ring "B" (bottom) points from the temperature influence curves (Figures 88 through 91) after first replacing them on their respective

curves if they were not already so. While such a correction technique is bound to admit errors of judgment, the smoothed calibration curves are believed to be reasonably accurate. The curves may be used to specify conditions for production of a given weight percent alloy or to modify conditions when a trial run has been nearly successful. The boron values are for ring "B" positions which would be about average values over the lengths of the cylinders.

Pressure Influence on Deposition Rates. Deposition rate was found to be proportional to the square root of the deposition pressure, as can be seen in Figures 98, 99 and 100. This relationship was true over the temperature range studied. The dashed lines indicate the average slope for each set of curves.

Temperature Influence on Deposition Rates. The deposition rates were found to increase at about 0.86 mils/hour per 100°F, regardless of pressure, over the range of temperature studied. The data points are shown in Figure 101. The "ideal" straight lines also shown for comparison were prepared from values taken from the dashed, average lines of Figures 98, 99 and 100.

SUMMARY AND CONCLUSIONS

The results from this task provide the necessary information for predicting boron concentrations in boron-alloyed pyrolytic graphite deposits. The separate influences of temperature, pressure and inlet flow ratios of hydrocarbon to boron source gases on the ultimate concentration have been determined. In addition, the influences of temperature and pressure on deposition rates has been determined.

RECOMMENDATIONS

The results of these studies allow selection of boron trichloride concentration for incorporation of about 0.3% to 1.0 percent at deposition temperatures of 3640 and 3800°F. Any attempt to exceed the percent level at these deposition temperatures is not advised, since excessive sooting will occur. Boron levels in excess of 1 percent can, however, be obtained without too much difficulty if the processing temperature is reduced to 3450°F. The material deposited at this lower temperature appears to be "normal" with respect to density and the observed microstructure. At 3450°F. the boron incorporated in the solid can be varied up to about 1.5 percent. Beyond this point sooting occurs in regime B and results are not predictable from these studies.

A temperature of 3800°F. with pressures of 3 MM to 5 MM would appear to be the best deposition conditions for obtaining boron levels below 0.5 percent. The methane to BCl_3 flow ratio could be determined from Figure 97. An alternate method for obtaining lower boron levels would be to increase the deposition temperature but this

approach assumes that the deposit would have satisfactory properties. With this approach, a 0.2 percent boron content might be obtained in a deposit by using 240/1, 3 MM and 3900°F, as the deposition conditions.

It must be emphasized that the experiments reported here were for a single volumetric flow value for methane and this parameter, as well as temperature and pressure, can influence the boron concentration in the solid. However, this flow is representative of that which would be used for a piece of aerospace hardware such as the frustums now in demand. A reasonable change in methane flow is not likely to change the general nature of the curves but could have a profound influence on the point where sooting becomes an important factor. The deposition assembly design is also an important factor. For instance, decreased exhaust stack area or sudden changes in flow direction (for example, the 180° change in direction required in reflex flow systems, as for nose cone deposition) might cause sooting at much lower boron trichloride flows or pressures than observed for straight-through flow systems.

The calibration curves for methane-to-boron trichloride flow ratios versus weight percent boron in the solid (Figure 97) might need to be modified for other assembly designs or in different equipment

B. BORON ALLOY--ASSAY STUDIES (Task 3.4.7)

According to the Work Statement, "Newer methods of boron assay will be evaluated for use with boron-alloyed pyrolytic graphite. These will include the use of electron beam microprobe techniques and X-ray crystallite parameters of fully-annealed specimens."

BACKGROUND

During the early part of this manufacturing development program, it was found that a critical problem was the inability to determine accurately, reliably, and conveniently the concentration of boron in the deposits. A need existed to investigate possible new methods of assay. There was also a need to evaluate the actual reproducibility of the methods used most often with an adequate number of measurements on a consistent series of deposits. These studies were undertaken as a subcontract at General Electric Company, Re-Entry Systems Department, and were intended to provide accurate assays of the cylinders produced under Task 3.4.6 at the Metallurgical Products Department. The nose cones produced under Task 3.3.7 were also analyzed. The results were also relevant to studies of graphitization at the Raytheon Company under Task 3.4.1.5. In all of these tasks, boron content was an important variable.

In general, the significance of boron content in pyrolytic graphite is twofold. It has a direct influence on certain characteristics and properties of the deposit. In addition, the presence of boron

in the vapor species from which deposition occurs and in the changing structure on the surface immediately after deposition influences the characteristics and properties of the carbon which is produced.

The effect of boron as a direct (or intrinsic) material variable results primarily from its ability to substitute for carbon atoms in the graphite lattice. The solubility in perfect graphite (Ref. 11) varies from 2.35 atomic percent at 2350°C, which is close to the B_4C + C eutectic at 2375°C (Ref. 12) to 1.0 atomic percent at 1800°C. The lattice is expanded slightly in the plane of the atomic layers and the separation between planes is reduced by the addition with a net increase in lattice volume. In graphite formed by solidification from the melt, boron atoms may also be occluded between the layer planes, and this produces a thermally unstable expansion of the layer separation (Ref. 13). It is possible that both substitutional and interlayer boron atoms result from chemical vapor deposition, but x-ray measurements of layer separation are also influenced by the interlayer expansion due to misalignment of successively stacked, parallel planes, so that the position of the boron has not been completely determined. An additional source of lattice strain due to boron can be the diffusion of boron out of the lattice at high temperatures leaving concentrations of lattice vacancies (Ref. 14, 15, 16). All of these strain-producing mechanisms may contribute to mechanical hardening of graphite containing boron, as a result of heat treatments.

A second direct effect of boron is its influence on the electronic band structure of carbon and graphite. Magnetic susceptibility decreases to a minimum over the range 0.01 percent boron to about 0.2 percent boron due to a decrease in the Fermi level (Ref. 17, 18, 19, 20). As a consequence, PG/BPG thermocouples can be made, although the effects of other imperfections in graphite on the electronic structure, and possibly atmospheric effects, have limited their stability range to about 2000°C. (Ref. 19).

The most important influence of boron in pyrolytic graphite, however, is the lowering of the temperature range for annealing due to graphitization (decreasing layer separation by orientation of parallel planes). Several studies have shown the effect of increasing boron on increasing graphitization at constant temperature (Ref. 20, 21, 22) up to about 0.8 percent boron. High temperature tensile tests also indicate that boron reduces the temperature at which strain-induced straightening of layers, with associated graphitization, takes place (Ref. 23). BPG nose cones are often partially annealed when deposited in the 2000°-2100° C. range, and the studies at Raytheon under Task 3.4.1.5 were based on an attempt to utilize this transformation immediately after deposition to control residual stress. Consequently, the effect of boron on graphitization may be regarded as both a direct influence on properties (stability during subsequent heating) and an indirect or process variable which affects the kind of material produced.

The composition of the gas stream also affects the structure which is deposited in certain ranges of the process variables. The mechanical and thermal properties which have been reported for BPG (Ref. 23, 24, 25, 26, 27, 28) have been influenced not only by the higher degree of graphitization in many deposits, which results in higher preferred orientation and fewer voids, but by the creation of many small, uniformly distributed growth cones. Deposits containing the "highly regenerative" or "fine-grain continuously nucleated" stratigraphy have a lower preferred orientation (for the same degree of annealing) and consequently have higher thermal expansion coefficients in the AB plane and higher strengths in shear or flexure. Such cones, which are nucleated by "whiskers" growing as a conical spiral (Ref. 29) appear to result from conditions of higher pressure which are not quite sufficient to cause extensive gas-phase nucleation of large soot particles. The boron content in the gas stream, which tends to increase the deposition rate, can influence the creation of this structure, which has a significant effect on properties; however, it does not occur under most conditions of BPG deposition used for nose cones.

The significance of boron content in pyrolytic graphite is thus a function of the product application (whether electronic or mechanical properties are of interest) and of the conditions of deposition which are selected. The density (in terms of the proportion of voids and average layer separation), the preferred orientation of atomic planes, the "degree of graphitization" and the microstructural aspects of the layer stacking are the principal intrinsic material characteristics, as they are in all pyrolytic graphites. The significant mechanical properties, particularly thermal expansion coefficients in the two directions and the elastic constants, are a function of these characteristics and should be determined directly wherever possible. The boron content is particularly important in the range 0.2 percent to 0.8 percent where it affects the degree of graphitization and preferred orientation of as-deposited material and will influence its stability during subsequent heating.

SURVEY OF ASSAY TECHNIQUES

The principal methods for boron assay, which have been used in the past, are light emission spectroscopy and several chemical techniques. The simplest procedure, weight of ash after oxidation, has usually produced erratic results, due primarily to uncontrolled hydrolysis and volatilization of the oxide. Fusion in sodium carbonate had been used for borides (Ref. 30) but this is also subject to losses of the sample. A more reliable method of sample preparation had proved to be pyrohydrolysis, or complete volatilization of all boric oxide by reaction with steam, followed by condensation and dissolution of the vapor in a closed system (Refs. 31 and 32). Comparison of this latter procedure with the spectroscopic methods were the primary subject of the experimental studies.

In addition, the available information about several other techniques was reviewed. Methods which were not applicable to pyrolytic graphite, such as the counting of etch pits in annealed single crystals (Refs. 14 and 16) were not considered. Following are brief discussions of these other techniques.

Layer Separation After a Stabilization Anneal. The subcontract work at the Raytheon Company led to the suggestion that measurements of unit cell height, Co, (twice the average layer separation) would provide a method of boron assay. Figure 102 illustrates the data reported by Raytheon, including the results for Task 3.4.1.5. Additional data reported by Tombrel (Ref. 21) and data obtained at the Re-Entry Systems Department on samples as-deposited are included for comparison.

X-ray diffraction measurements can be competitive in time and cost of analysis with chemical assay methods if relatively simple, calibrated comparisons are used instead of the more elaborate procedures necessary for maximum precision. The Raytheon method, used in Task 3.4.1.5, is similar to methods used in other studies of graphitization. (Ref. 33). Pyrolytic graphite powder is mixed with aluminum powder and the (004) diffraction peak is compared with two aluminum lines using a 57.3 mm diameter Debye-Scherrer camera with cobalt radiation. The error limit of 0.01 Angstrom at the Co of 6.80 Angstrom, and 0.004 Angstrom at 6.75 Angstrom, corresponds to about 0.04 percent boron, as shown in Figure 102.

The method thus provides a means of comparing the boron content in the range (0.2%B to 0.8%B) which is relevant to the effect on kinetics of graphitization. Measurements of lattice parameter should first be made as a function of distance across the thickness of the deposit after deposition in order to determine the effects of time at deposition temperature. Subsequent measurements after annealing for about 20 hours at 2000°C. indicate the relative tendency to graphitize, which is a function of boron content, provided that the microstructural characteristics which affect annealing are similar. The procedure is a measure of fundamental characteristics of the material, but it is not necessarily a boron assay method of general applicability.

Fast Neutron Activation Analysis. In April, 1965, 29 samples containing 0.2-1.2 percent boron were evaluated by triplicate determinations at the General Atomic Division of General Dynamics Corporation for the Re-Entry Systems Department, General Electric Company (Ref. 34). Large samples (2 to 7 grams) were required. Each specimen was irradiated for 20 seconds in a 14 Mev neutron flux of approximately 10^8 n/cm^2-sec during each determination. After a 10 second delay, the 11.5 and 9.2 Mev Beta activities from the $B^{11}(n,p)\ Be^{11}$ reaction were

measured as a function of the boron present and compared with known samples. The standard deviation estimated from counting statistics was ±0.04% B or better (maximum spread was ±0.08% B). However, comparison of the data on certain samples with colorimetric analysis of oxidation products indicated a poor correlation and suggested that accuracy might be poor.

A possible source of absolute error in this method is variation in the boron isotope ratio in the BCl_3 used to prepare the boronated pyrolytic graphite. If this procedure were to be adopted, a portion of the BCl_3 from each cylinder used in depositions would have to be retained for standardization. Other difficulties with the method are the large sample size required for precision and the fact that only one laboratory source for such measurements has been identified.

Electron Microbeam Probe. Although precision in the range below 1 percent boron was questionable, the evaluation of feasibility of this device for assay was planned as part of the task. Micropolished samples having 0.2 percent to about 1 percent boron, assayed by pyrohydrolysis, were mounted in a conducting medium and examined by tracing the specimen current and electron backscatter current with an ARO electron probe. It was anticipated that differences in electrical properties in regions containing low boron might be observable. However, no such differences could be seen. Slight variations in specimen current were seen where large differences in deposit orientation occurred (around growth cones) and delaminations were detected. Attempts to obtain boron assay directly were unsuccessful due to repeated failure of the 200 Angstrom thick collodian windows which are required for low element analysis with the gas-flow proportional counters used for analyzing the X-ray emission. Such difficulties are common in electron probe work, suggesting that this device has limited utility for assay at the present time (Ref. 35).

Spark Source and Laser-Probe Mass Spectrography. Differences in boron content in different regions of graphite crystals have been reported by mass spectrography of the material emitted from a spark (Refs. 14 and 36) and the laser beam probe can be used in a similar manner. At present, however, these methods should be regarded as semi-quantitative procedures for detecting differences in boron, due to variability in the amount of material removed. Boron content might, however, be compared to the amount of an impurity or other additive if this were constant.

Ion-Beam Probe Mass Spectrometry. An ion microprobe mass spectrometer (Ref. 37) has recently been used to analyze trace amounts of boron in silicon, SiO_2, and many other materials. Graphite has also been analyzed for other elements.

A primary ion source, usually argon, is used to sputter ions from the specimen which are then analyzed by a high resolution mass spectrometer. The rate of sputtering is controlled between 1 and 100 microns per hour by varying beam density, and the sputtered area can be varied between 0.1 mm^2 and 75 $mm.^2$. This instrument should be considered in future studies where gradients in boron content through the thickness in specific regions of a graded deposit must be evaluated, since it appears at present to be the most promising of the microprobe techniques for boron assay. Lack of availability of the instrument may be a deterrent to its use for routine assay, however, for some time to come.

EXPERIMENTAL PROCEDURES AND RESULTS

Sample Preparation. Since a primary objective of this task was to obtain reliable boron assays of the cylinders produced in Task 3.4.6, these cylinders were used in most of the comparisons. As a standard procedure, 1.5-inch rings were cut from positions 4 inches and 12 inches from the bottom of the tube. After measurements of residual stress, density and microstructure at G.E., Metallurgical Products Department, the rings were shipped to Re-Entry Systems Department for analysis. A 1-inch to 2-inch long section was removed, the substrate surface was separated by cleaving or by polishing, and powder was obtained from the remainder by filing. Large flakes were eliminated from this powder by passing it through a 200 mesh screen.

Additional stock samples, prepared in the same manner, were obtained from rings cut from 2-1/2 inch diameter tubes deposited at G.E., Re-Entry Systems Department and from a plate deposit prepared at the Metallurgical Products Department. The former deposits were made at 2100°C, 3 mm Hg. pressure for 5 hours. One, deposited from a 1/1000 ratio of BCl_3/CH_4, was 0.03-inch thick; the other, deposited from a 1/250 ratio, was 0.06-inch thick. The plate had been made at 1800°C, 2 mm Hg pressure, from a 1/70 ratio over a 70 hour period and was 0.11-inch thick; this material, unlike all of the others examined, had regions of large fiber-nucleated growth cones originating from specific layers in the cross section. Three regions were analyzed.

All of the samples described above were prepared as 5 gram blends of the powder. Samples of each lot of powder were then removed for comparative analysis. In addition, a limited number of comparative analyses by a procedure utilizing small specimens were made from deposits prepared in Task 3.3.7 (nose cone configurations).

Impurities. In order to insure that impurities did not interfere with the analysis, three samples (Task 3.4.6 deposits

8044-1B and 8044-2B and D) were examined by qualitative spectroscopic analysis. In addition to boron, the following were found in all three:

0.001-0.01%:	Sn
0.0001-0.001%:	Mg, Si, Fe, Cu
< 0.0001%:	Al, Cr, Mn, Ag, Pb, Ca

The following elements were not detected: Li, Be, Na, K, Ti, V, Co, Ni, Zn, Ga, Ge, As, Rb, Sr, Zr, Nb, Mo, Ru, Rh, Pd, Cd, In, Sb, Te, Cs, Ba, Hf, Ta, W, Re, Os, Ir, Pt, Au, Hg, Tl, Bi, P. During oxidation yellow and white oxides formed on the surface, but these were the result of some residual mounting compound (a Pb-Sn-Bi-Cd alloy) which had adhered to the last-deposited surface after the cylinders were sectioned.

Pyrohydrolysis and Titration of Large Samples. Procedures developed at the Aerospace Corporation (Ref. 32) similar to those used for the analysis of borides (Ref. 31) had shown excellent reproducibility in duplicate determinations (Ref. 38). In the studies conducted here, a 1 to 1-1/2 gram sample of powder was reacted at 1150°C in a fused silica tube with O_2 saturated with H_2O, and the evolved gases were passed through an all-silica system into 300 ml of distilled water. It was found that 1 hour was required for complete reaction at this temperature. To decrease the time and cost of analysis, the temperature was increased to 1200°C and time reduced to 25 minutes when small (0.1 gram) samples were analyzed by colorimetry (as described later). This procedure was successful, although it was found that the furnace must be maintained at temperature continuously, since the tubes always cracked on cooling from 1200°C.

The large sample analysis was found to be the most reliable method of analyzing the deposits from Task 3.4.6, since good reproducibility was obtained. After boiling the boric acid solution to remove CO_2, the percent boron was obtained by titration with a standardized NaOH solution. Duplicate determinations on sixteen collections of powder from 3.4.6 deposits showed the following results:

Difference between 2 values wt. percent B:	0.00	0.01	0.02	0.03	0.05	0.10
Number of samples with this difference:	2	6	5	1	1	1

Of these, the two deposits having 0.05 or 0.1 percent differences had been prepared from relatively small samples, in which only 4 or 5 mg of boron were available. In previous studies, differences of 0.05 to 0.11 wt. percent B between duplicate samples had been observed when less than 3 to 5 mg of boron

were in the solution. Consequently, the present results confirmed that reproducibility was good only when the sample size is relatively large. Although this was the case for the 3.4.6 series, some effort was devoted to procedures for small sample analysis, of importance in the assay of most aerospace hardware deposits.

Emission Spectroscopy with External Standards. Many past determinations had involved comparison of the intensities of two spectral emission lines from boron-alloyed pyrolytic graphite with those of a series of standards exposed on the same photographic plate. Usually two samples were "shot" by consumption in the arc, and a single set of standards was used.

In the present study, the "stock" samples were compared with two sets of standards, using the same photographic plate to record all spectra. Two 0.004 gram samples of each unknown were obtained from the same powder filings used for pyrohydrolysis. The standards were obtained from 0.150 g batches of -200 mesh pyrolytic graphite filings mixed with boron powder in a "Wig-L-Bug" for 30 one-minute cycles. Samples of 0.5, 2.0, and 8.0 wt. percent mixtures were "shot" in 0.004 gram amounts, and 0.002 gram samples of the same mixtures were burned to provide standard line intensities for 0.25, 1.0 and 4.0 wt. percent B compositions.

Reading the line intensities themselves was not a significant source of error. Repeated measurements with a microphotometer, which was calibrated soon after the measurements, showed that 98% of readings were within ±1% of the average transmittance, corresponding to less than 0.05 percent at the 1% B level.

A principal source of error results from inadequate reproducibility of shots on the standard powder mixtures. Table XVIII illustrates percent transmittance readings of the duplicate standard samples exposed on the plate. Possible reasons for the difference in line intensities between samples from the same powder mixture are insufficient mixing, variations in weight of specimens in the graphite cup of the electrode, or non-reproducible events within the arc itself. The latter possibility may have been responsible for difficulties with the spectrochemical determination of boron in graphite reported by Feldman and Ellenburg (Ref. 39) who concluded that boron carbide failed to volatilize completely, even when finely divided. Although boron rather than carbide powder was used for just this reason, reactions and interactions within the arc may have affected the results.

The average of the two readings for each composition in Table XVIII was used in constructing a calibration curve for each of the two lines. The line intensities of the unknowns were

compared with these curves and the results were reported as the boron assay. Since human judgment is required in such a procedure, the process of reading, plotting the curve and making the comparison was repeated three times for the "stock" samples in order to assess the reproducibility of this phase of the analysis. The results, shown in Table XIX, indicate that the human error can contribute significantly to the lack of reproducibility of the methods; repeated measurement, which can reduce this cause of variability, adds to the time and cost of the assay.

In addition to the variability inherent in the semiquantitative spectroscopic method, an error resulted from an attempt to extrapolate the calibration curve to compositions below 0.25 wt. percent B. Thus, it was reported that sample 2-48 in Table XIX contained 0.18 wt. percent B (or 0.15 wt. percent B in a previous determination) although the true analysis by both pyrohydrolysis and spectroscopy using an internal standard was 0.06 wt. percent boron.

Because of these results, use of this spectrochemical procedure was abandoned for any precise determination of boron in pyrolytic graphite. Previous analyses obtained in this manner may be in error by 0.1-0.2 wt. percent boron.

Emission Spectroscopy with an Internal Standard. The procedure developed by G.M. Bonini in the testing laboratory of the Jarrell-Ash Corporation (Ref. 40) had been used for many previous determinations of boron in pyrolytic graphite. Of the first nine samples from Task 3.4.6 which were submitted, eight agreed within 0.03 wt. percent boron with results of pyrohydrolysis. Consequently, all Task 3.4.6 deposits were analyzed in this way, in addition to the "stock" samples. A portion of each batch of filings used in pyrohydrolysis (0.1 g or more) was shipped in bottles to Jarrell-Ash. In several cases, samples of the same powder were shipped separately with separate identification.

Results of the comparisons with pyrohydrolysis are presented in Table XX. A 0.01 gm sample was diluted with SP-2 graphite powder in 1:9 ratio and mixed with 0.05 gm SnO_2. From this mixture four 0.01 gm samples were "shot." In some cases, the average of these four determinations differed significantly from results of pyrohydrolysis, so a second portion of the powder was mixed with SnO_2 and the process was repeated. These second determinations of the powder in the bottle differed significantly from the first (indicated by brackets in Table XX). In some cases, the samples of the same deposits which were delivered separately agreed with each other, and in some cases they did not. In the final series of samples submitted to Jarrell-Ash, the samples in the bottles were mixed in their

entirety with SnO_2 in order to eliminate any de-mixing in the bottle during transit. However, these results (shown in Table XX as photographic plates k through q) did not show any difference in the variability.

The origin of this variability was not identified. As shown by the data, there were no consistent trends and no step in the procedure, either at Jarrell-Ash or at the Spacecraft Department of General Electric, where the samples were prepared, could be identified as a source of error. The scatter in data compared with the large sample analysis by pyrohydrolysis is illustrated in Figure 103. Each point represents the average of four separate spectroscopic samples from the same powder batch, and an even wider distribution is obtained when all of the data points in Table XX are compared. Since powder mixtures were used, variations with location in the deposit itself must be large to explain the results, and the very finely dispersed location of the boron and similarity of densities with small boron variations should eliminate the possibility of powder segregation as the cause.

Pyrohydrolysis of Small Samples and Spectrophotometry. The procedure developed for small sample analysis following pyrohydrolysis is based on the colormetric method developed by Pastor and Bode using monomethylthionine ("Azure C") (Ref. 41,42). This is one of the more sensitive of a wide variety of reagents which can be used, including "Curcurmin" (Ref. 43), "Methylene Blue" (Ref. 44) and 1,1'-bis(6-chloroanthraquinonyl) amine (Ref. 45). The method described here was developed for the comparative analyses of later samples from GE, Metallurgical Products Department, in this contract.

In each analysis, a 0.1000 gram sample was weighed into platinum boats. These were then supported on "Vitreosil" (fused silica) boats and pushed into the heated region of the fused silica system. The samples were allowed to react for 25 minutes at 1200°C while oxygen was passed through water in a steam flask at 45 ml per minute; the steam flow rate was 2 to 3 ml per minute. The condensate was collected at the end of the fused silica system in a plastic beaker which was supported in an ice bath. For efficient trapping of the condensate, 25 ml of distilled water was added to the beaker before pyrohydrolysis.

The condensate was diluted to 100 ml volume and transferred to a plastic bottle. A 10 ml volume of hydrofluoric acid solution (40:100) was added to the condensate and the solution was allowed to stand for at least 18-24 hours. A 10 ml aliquot was transferred to a 250 ml plastic bottle, and the pH was adjusted to the range 2.8-3.2 using NaOH solution (100 gm/liter) and pH paper. After pH adjustment the sample was diluted to 50 ml volume, and the following additions were made:

5 ml of 0.01 molar solution of monomethylthionine (Azure C) and 25 ml of a mixture of dichloroethane and chloroform (75:25). The bottle was tightly capped and the solution was shaken for one minute. The two layers were allowed to separate and a portion of the organic layer on the bottom was transferred to a 1-cm cell of a Beckman DK-1 spectrophotometer. The transmittance of the solution in the cell at 638 millimicrons was then read; the instrument was nulled using a reagent blank solution. The standard curve shown in Figure 104 was prepared using aliquots of standard boric acid solution (10 micrograms/ml of boron) which had been carried through the entire procedure. The standard curve covered the 0 to 100 microgram range (0.1 wt. percent to 1.0 wt. percent B). The samples which were expected to have more than 1 wt. percent boron were diluted by twice the amount of the others.

It was necessary to run a set of standards with every set of samples. The formation of the HBF_4 complex is slow and does not reach completion for about 100 hours. The time interval in which the hydrofluoric acid is reacting with the boron must be the same for both samples and standards.

Table XXI presents results of a comparison of three separate pyrohydrolysis and photometric determinations on each of several samples which were also analyzed by the large sample pyrohydrolysis technique used for the assays in Table XX. The variability is intermediate between the large sample analyses and the spectroscopic results. Table XXII shows a similar comparison on samples which had been previously assayed by single analyses in the Task 3.3.7 series. These results suggest a trend of decreasing reproducibility with decreasing sample size (from 1 g to 0.1 g to 0.01 g) regardless of the method used. However, the accuracy is sufficient for determination in the range of boron contents relevant to the annealing behavior of pyrolytic graphite.

SUMMARY AND CONCLUSIONS

The most reliable and reproducible procedure for analysis of boron in pyrolytic graphite, based on the results of this study, is pyrohydrolysis of a large sample, dissolution of the condensate, removal of CO_2 and titration of the boric acid. The sample should contain at least 4 mg of boron for reproducibility within ± 0.2 percent boron, or about 1 gram of powder. This technique has provided reproducible assays of the boron in the deposits produced in Task 3.4.6.

When only small samples (about 0.1 gram) are available, careful calibration and repetitive analysis is necessary. The methods studied here, in order of decreasing reproducibility, are as follows:

1) Pyrohydrolysis, reaction of dissolved oxide with HF for

a period of several days, reaction of the HBF_4 with Azure C, and comparison of the color with those of standards prepared under identical conditions by spectrophotometry.

2) Light emission spectroscopy using an internal standard.

3) Light emission spectroscopy and comparison with standard mixtures.

Since many past analyses of pyrolytic graphite have been based on only one or a few determinations by spectroscopic techniques, these may have been in error by as much as 20 to 30 percent.

The low precision, small sample methods for boron assay may be adequate where only a check on the approximate amount of boron is sufficient for process control. Once a reproducible manufacturing procedure is established, boron has importance primarily as it affects degree of graphitization during the deposition heat treatment and during subsequent heating in service. The direct determination of the change in C_o by X-ray diffraction, which is a "small sample" technique, may be more meaningful than boron assay under these circumstances. In general, boron content is not, as far as is known at present, a fundamental material variable which determines the properties of pyrolytic graphite; it is an important process parameter which affects the structure of the material, and hence the properties indirectly. Consequently, the effort devoted to boron assay should be balanced with an appropriate effort on characterizing the structure of the material by X-ray diffraction and microscopy.

RECOMMENDATIONS

Future boron assays of small samples by pyrohydrolysis and spectrophotometry should include sufficient standardization and multiple analyses which will establish further the reproducibility of this procedure. Spectroscopic analysis with an internal standard is probably adequate for a general check on approximate boron level and is the most economical procedure encountered in this study. Pyrohydrolysis and titration, which takes about 1 man hour per sample longer than the small sample method, should always be used where accuracy is required and where there is sufficient homogenous material for the method.

The series of deposits produced in Task 3.4.6. should be carefully saved, since they have been partially characterized and their process conditions are well documented. Since property data on pyrolytic graphite of the type produced in nose cones is inadequate at present, the following measurements on selected samples could provide information necessary for the accurate prediction of thermal stresses:

1) Thermal expansion coefficients (AB and C directions).

2) Tensile elastic modulus and Poisson's ratio (AB plane, parallel to cylinder axis).

3) Adiabatic elastic constants (from sound velocity and density) through the thickness.

4) Tensile or flexure strength (AB plane and C direction by bonding to blocks).

5) C_o on first and last deposits before and after heat treatment at 2000°C.

6) Change in dimensions, density, and C_o as a function of time at 2400-2800°C.

C. GRAPHITIZATION STUDIES (Task 3.4.1.5)

According to the Work Statement, "Controlled graphitization will be evaluated as a technique for reducing the levels of residual stress in deposits of boron-alloyed pyrolytic graphite. Boron levels and annealing times and temperatures are variables to be investigated." This work was carried out on a subcontract at Raytheon Company, Waltham, Massachusetts.

BACKGROUND

Residual stress limits the manufacture of boron pyrolytic graphite (BPG) Closed-shape deposits which have a thickness-to-radius ratio (t/r) greater than about 0.1. A number of advances in the understanding of residual stress have been made over the past few years. The theory and equations (Ref. 46, 47 and 48) for predicting the tangential, axial, and radial residual stress behavior of cylindrical, thin-shell deposits of anisotropic materials have been fairly well worked out. However, theory and experimental results have not always been found to be in agreement.

The disagreement between measured residual stress values and values calculated from theory have been accounted for on the basis of growth* stresses (Refs. 49 and 50) and secondary anisotropy (Ref. 51). According to the growth stress concept, BPG is considered to be deposited in thin layers which are laid down stress free at the deposition temperature. Growth in the layers is time dependent and the rate of growth is a nonlinear function of time. This means that growth in a particular layer is partially inhibited by adjacent layers which results in a bi-axial stress condition established between layers. If a flexible mandrel is used, the layers deposited on the mandrel surface grow to a greater extent than the last deposited layers on the i.d. surface. In this manner, a differential in growth occurs in the layers across the thickness of a deposit. Upon cooling to room temperature, residual stresses arise in the cylindrical deposit due to the primary anisotropy. According to

* As used here, growth refers to an increase in dimension in the a-direction and a decrease in dimension in the c-direction during deposition.

this concept, growth stresses have partially offset the residual stresses due to primary anisotropy, and they cause the difference between the measured residual stress and the residual stress calculated from theory.

The secondary anisotropy concept considers that there are microstructure variations through the thickness which cause variations in material properties, particularly coefficients of thermal expansion. Variation in thermal expansion across the thickness causes the cool-down stresses to be different from what would be calculated on the basis of constant thermal expansion across the thickness. Besides microstructure variations, a gradient in the degree of graphitization can also cause property variation to occur across the thickness of a deposit.

Some insight into the structural features associated with growth and secondary anisotropy in BPG was evolved from earlier tasks in this contract. It had been found that the degree of graphitization for BPG, as measured by the unit cell height parameter, C_o, was both temperature and time dependent as well as dependent upon the boron level. For deposits made under similar conditions, the degree of graphitization was found to show a maximum at approximately 0.8 percent boron. Other investigators (Refs. 52 and 53) had reported that the properties of plate stock BPG, such as coefficient of thermal expansion, modulus, thermal conductivity, etc., showed maximum or minimum values as a function of boron near this same boron level. It would seem possible, therefore, that growth and secondary anisotropy, both of which are related to the degree of graphitization, could be used to improve the structural soundness of BPG closed-shaped deposits by controlling the degree of graphitization across the thickness.

It was known that boron atoms could enter the graphite lattice in polycrystalline graphite (Ref. 54 and 55) or in graphite single crystals (Ref. 56, 57 and 58) by either substituting for carbon at the trigonal sites or as interstitials in the lattice. The presence of boron accelerates the graphitization of boron pyrolytic graphite (Ref. 59 and 60) and bodies made from coal tar and coke (Ref. 54 and 61) doped with boron. The mechanism by which substituted and interstitial boron atoms affect graphitization, however, was not well understood, nor had the effect of time and temperature on graphitization been clearly established. The separate effects of boron atoms and of the degree of graphitization on the properties of boron pyrolytic graphite, likewise, had not been clearly established. Both the presence of boron atoms and the increase in degree of graphitization also contribute to the electrical and thermal conductivity behavior of boron pyrolytic graphite (Ref. 62) at very low (0.1 weight percent) boron levels, it is the boron atoms which have the strongest influence on these properties.

In the previous subcontract work at Raytheon, it had been concluded that the following factors would need to be considered in any comprehensive program aimed at evaluating the effect of graphitization on the mechanical soundness of boron-alloyed pyrolytic graphite cylindrical deposits:

1) Degree of graphitization.

2) Rate of graphitization.

3) Dimensional changes (growth in the a-direction and shrinkage in the c-direction).

4) How factors 1, 2 and 3 above affect the modulus, Poisson's ratio, and coefficient of thermal expansion in the a- and c-directions.

EXPERIMENTAL CONDITIONS SELECTED

The work planned for this task was divided into three phases:

Phase 1. Deposit six cylinders (four constant boron level deposits and two graded boron deposits and characterize the properties of the deposits.

Phase 2. Anneal free and restrained rings cut from the above six deposits and characterize the properties of the annealed rings.

Phase 3. Evaluate data from Phases 1 and 2 and deposit cylinders with a t/r of approximately 0.1 and a cylinder with a t/r of approximately 0.2.

The mandrel assembly and the procedure used to deposit the cylinders were the same as employed by Raytheon in Tasks 3.4.1.1. to 3.4.1.3. Boron trichloride was used as the source of boron. A through-flow system without baffling was used in making all of the deposits. As before, the cylinders were deposited inside graphite mandrels which were 3 inches in diameter and 9 inches in length.

The C_o lattice spacings were obtained from powder diffraction patterns with a 57.3 mm diameter Debye-Scherrer camera using cobalt radiation. Aluminum powder was used as an internal standard. Good quality film patterns were obtained with (typically) 3-hour exposures. In the combined pattern, the graphite (004) line was bracketed by the (200) and (220) aluminum reflections. These latter reflections were used to determine the angular corrections which were applied to the (004) graphite line. The error limit in measuring C_o values was about 0.01 Å for C_o values of the order of 6.8 Å, at 6.75 Å the error limit was about 0.004 Å .

RESULTS

Phase 1 (Deposits)

Processing characteristics for cylinders deposited in Phase 1 are given in Table XXIII. These cylinders were all deposited nominally at 2000°C, at a pressure of 15 torr, and, except for GEDC-1R, were deposited over a 4- to 6-hour time period.

With the exception of cylinder GEDC-1R which terminated prematurely due to equipment failure and cylinder GEDC-2R which cracked due to a high t/r (0.07) all cylinders under this task were satisfactory for property measurements. Typical microstructures of these deposits are shown in Figure 105.

Six rings, 1/2 inch in width, were carefully cut from the central 4-inch section of each cylinder. Two rings from near the base were annealed for 5 hours and two rings from near the top were annealed for 15 hours. One ring from the center was used to obtain property measurements (Table XXIV) and the other ring from the center was used for boron assay. Samples for boron assay (Table XXIII) were taken from regions approximately 20 mils in from the substrate (o.d.) and the deposition (i.d.) surfaces. An analysis and comparison of the property data for the as-deposited material with the annealed material are given in the next section.

Phase 2 (Annealing Tests and Results)

Property measurements on rings annealed at 2000°C for 5 and 15 hours are given in Tables XXV and XXVI. It was originally planned to make the annealing tests at 10 and 20 hours; however, this was modified in favor of the 5- and 15-hour annealing schedule so that the data would be more compatible with the expected deposition times required to deposit cylinders with t/r values of about 0.1 and 0.2

A number of generalizations were made by comparing these data with the property data for the as-deposited materials given in Table XXIV. These generalizations are as follows:

1. The modulus increased with boron level and annealing, the largest increase occurring after the 5-hour anneal. For example, the 0.13 percent boron deposit (GEDC-4R) had values of 4.4, 6.0, and 6.9 X 10^6 psi respectively for the as-deposited, 5-hour annealed, and 15-hour annealed specimens. Comparable values for the 0.74 percent boron deposit (GEDC-5R) were 7.6, 9.5 and 10.2 X 10^6 psi.

2. There did not appear to be any clear-cut, systematic trend between failure stress and boron level for the as-deposited cylinders or after annealing; however, the two strongest as-deposited cylinders were GEDC-4R (0.13 percent boron)

24,500 psi and GEDC-8R (graded 0.40 o.d. to 0.24 percent boron i.d.) 25,100 psi. These results were in general agreement with previous findings in Tasks 3.4.1.2 and 3.4.1.3--that the strongest cylinders were those containing low boron levels.

The strongest rings after the 5- and 15-hour anneal were from deposit GEDC-7R (graded 0.67 o.d. to 0.24 percent boron i.d.) with strengths of 19,500 and 18,900 psi, respectively. The two rings from deposit GEDC-8R delaminated prior to failure. The failure stresses, therefore, were lower than what normally would be expected.

3. The residual stress increased after annealing, the largest increase occurring after the 5-hour anneal. If one used the ratio of t/r to residual stress multiplied by the failure stress as an indication of structural soundness (Table XXVII) it was found that deposit GEDC-4R (0.13 percent boron) ranked the highest, with the two graded boron deposits GEDC-8R (0.40/0.24) and GEDC-7R (0.067/0.24) ranking next in order. Annealing was seen to cause a marked reduction in the structural integrity for all these deposits. From this it was concluded that post-deposition graphitization was undesirable.

4. No systematic trend was found in Poisson's ratio which could be related to either boron level or annealing time.

5. With respect to the ultimate stress, which is the sum of the failure stress and residual stress, deposits GEDC-5R and GEDC-7R were the highest after annealing 5 hours, and deposits GEDC-7R and GEDC-3R were the highest after annealing 15 hours.

Dimensional changes after annealing are given in Table XXVIII. No real difference in dimensional changes was found between the cut and uncut rings. The data in this table are averages for both sets of rings. The largest dimensional changes after annealing were seen to occur for deposits GEDC-3R (0.29 percent boron) and GEDC-6R (0.48 percent boron) and the smallest dimensional changes were for deposits GEDC-4R (0.13 percent boron) and GEDC-7R (graded 0.67/0.24 percent boron). Dimensional changes were a function of both boron level and time at temperature. The higher the boron level, the higher the dimensional changes. The data for GEDC-5R were low because of a high degree of graphitization for the as-deposited material. This deposit contained a high boron level (0.74 percent) and would be expected to have the highest dimensional changes during deposition. An indication of this is seen in Table XXIX. The as-deposited cylinder had a C_o value of 6.75 Å for the first deposited layers and 6.78 Å for the last deposited layers. Table XXX gives the unit cell height data for three deposits after annealing.

There appears to be a correlation between dimensional changes and degree of graphitization (Ref. 63). Growth in the a-direction of approximately 2 percent and shrinkage in the c-direction of approximately 4 percent corresponds to the end of Stage 1 graphitization (unit cell height 6.74 Å) for pyrolytic graphite. The correlation gives about 0.5 percent growth and 1 percent shrinkage for a degree of graphitization corresponding to a unit cell height of 6.79 Å. Assuming that there are negligible dimensional changes corresponding to a unit cell height of 6.86 Å and that the graphitization of boron pyrolytic graphite is similar to pyrolytic graphite, except for the presence of boron which catalyzes graphitization, then from Tables XXVIII and XXIX it can be concluded that the dimensional changes for cylinder GEDC-5R during deposition were approximately 1 percent growth and 2 percent shrinkage. For cylinder GEDC-4R, there would be negligible dimensional changes for the as-deposited condition and about 0.5 percent growth and 1 percent shrinkage after annealing 15 hours. The expected dimensional changes were in good agreement with measured values. Unit cell data were not available for annealed specimens from deposits GEDC-3R and GEDC-6R. The expected C_o values would be 6.74 Å after annealing 15 hours and 6.77 Å after 5 hours annealing.

A very significant point for this study may be drawn from the data in Table XXX. Cut and uncut rings were annealed to study the effects of stressed and unstressed conditions on graphitization. The available data did not show any real difference. The cut rings (unstressed) show the same degree of graphitization as the uncut (stressed) rings. This indicates that the stresses present during annealing were too small to cause any stress-induced graphitization.

Table XXXI gives the coefficient of thermal expansion data in the a- and c-direction as a function of boron, as well as c-direction data after heat-treating. As reported in the earlier Raytheon subcontract work, the a-direction coefficient, within the accuracy of our equipment, was independent of boron level and the c-direction coefficient increased with boron level and was in fair agreement with results for boron-alloyed pyrolytic graphite flat plate deposits. After annealing, the coefficient increased for the 0.13 and 0.29 percent boron deposits and apparently decreased for the 0.48 and 0.74 percent boron deposits.

Phase 3 (Analysis and Deposits)

When pyrolytic graphite is deposited under normal conditions (2000°C) the C_o value is found to lie between 6.84 and 6.86 Å. The C_o value for boron-alloyed pyrolytic graphite deposited under similar conditions decreases (increasing degree of graphitization) with increasing boron level up to about 0.8 percent boron for a constant boron level deposit. It is lower at the substrate surface than at the deposition surface. This is because graphitization is time dependent, and since the substrate is at temperature for a longer period of time than the deposition surface, it shows a higher degree of graphitiza-

tion. A differential in the degree of graphitization thus exists across the thickness of a deposit. This differential is dependent upon boron level, time, and temperature. Thermal expansion and dimensional changes are also dependent upon the degree of graphitization. These relationships, however, are not well defined.

The deposits made under Phase 1 of this task can be grouped into three graphitization ranges:

1. For low boron level deposits (0.1 percent boron) the differential in graphitization across the thickness was low because of the initial low degree of graphitization. Deposits in this range, such as GEDC-4R (Table XXIV) had high failure stresses and low residual stresses. With annealing, the failure stress decreased rapidly and the residual stress increased rapidly (Tables XXV and XXVI) and the differential in graphitization across the thickness remained constant (Table XXX).

2. A higher degree of graphitization was present across the thickness for higher constant boron level deposits (0.3 to 0.7 percent). With annealing, the failure stress decreased and the residual stress increased markedly (Tables XXV and XXVI).

3. The third range of graphitization was obtained in the graded boron deposits. A high differential in the degree of graphitization across the thickness (C_o = 6.74 Å for substrate surface and 6.84 Å for deposition surface) was obtained in deposit GEDC-7R. The rate of failure stress and residual stress change with annealing was less for this deposit than any other deposit made under this study (Tables XXIV, XXV and XXVI). Annealed rings from deposit GEDC-8R delaminated when tested to failure and, therefore, the failure stress was difficult to evaluate. The differential in degree of graphitization across the thickness for this deposit (C_o = 6.78 Å for substrate surface and 6.81 Å for deposition surface) was the same as measured for deposit GEDC-6R. The failure stress, however, for the as-deposited cylinder (GEDC-8R) was higher and the residual stress lower (Table XXIV) than for deposit GEDC-6R.

Considering these three graphitization ranges, it was tentatively concluded that for the boron range investigated and for the deposition conditions employed, differential graphitization during deposition had merit for controlling residual stresses. Of course, it was not possible to establish a mathematical model based upon this limited data.

Based upon the data available, a differential graphitization of C_o - 0.1 was selected as a prerequisite for depositing the first cylinder in Phase 3. A boron grade from 0.5 to 0.15 weight percent

(of many possible grades) was selected to satisfy this ΔC_o in depositing a cylinder with a t/r of 0.1. This cylinder (GEDC-9R) was deposited crack-free and varied in t/r from 0.095 to 0.115; however, it was delaminated in two places. The cylinder was highly stressed and during handling it cracked on the inner fiber across a thickness of about 50 mils. The crack propagated across the thickness during the machining of 1/2-inch wide rings. Characterization data for this deposit are given in Table XXXII. Agreement between the measured and expected boron and C_o values is excellent. However, the cylinder was not satisfactory for residual stress and strength measurements.

This area of work was reviewed with the technical program director, and it was mutually agreed to attempt to deposit the next series of cylinders with t/r values $\leq$ 0.085 for comparison with previous deposits. Four cylinders were deposited at a t/r $<$ 0.085. Processing characteristics for these deposits are given in Table XXXIII. Cylinder GEDC-10R was deposited with the same nominal boron grade as GEDC-9R, but for a shorter deposition time. The cylinder showed two delaminations and was cracked on the i.d. surface. Cylinder GEDC-11R was deposited with the same nominal boron level on the o.d. surface as GEDC-9R and -10R, but with a higher boron level (0.3 percent boron) on the i.d. surface. This deposit was made to study the effect of a lower differential degree of graphitization in a graded boron cylinder. The cylinder was uncracked and had a sound ring to it, despite the appearance of a single, tight delamination. Cylinders GEDC-12R and -13R were deposited with the same nominal boron grade (0.4 to 0.2) as GEDC-8R, but with a higher t/r ratio. Both of these cylinders were delaminated as well as cracked axially across the thickness in several places.

SUMMARY AND CONCLUSIONS

Under the deposition conditions employed in this study, satisfactory BPG cylinders could be deposited crack- and delamination-free with a t/r of $<$ 0.065. A t/r $\sim$ 0.065 appeared to be the borderline for success or failure, sometimes the cylinders were satisfactory and sometimes they cracked. At t/r values $>$ 0.07, the cylinders invariably cracked.

In view of the current data, the relationship between strength, boron level, and deposition temperature for closed shape and plate stock BPG deposits now becomes a little clearer. At any given deposition temperature the flexural strength increases with boron level for plate deposits. Typical values for plates deposited at 2000°C would be 26,000 psi for 0.1 percent boron and 29,000 psi for 1.2 percent boron. At a constant boron level, the flexural strength is higher for a deposit made at 1850°C than at 2000°C. A typical flexural strength for BPG plate stock deposited at 1850°C and containing 1.4 percent boron is 36,000 psi. The same trend in flexural strength with deposition temperature is also found for unalloyed pyrolytic graphite (plate material). For example, a typical flexural strength

for a deposit made at 1700°C is 36,000 psi. For a 2000°C deposit, the flexural strength is about 26,000 psi.

The total stress (residual plus failure stress) for closed shapes deposited at 2000°C appears to be independent of boron level, as measured by the ring compression test. Graphitization raises the residual stress and lowers the failure stress. The strengthening effect caused by alloying with boron (noted in flat plate deposits) appears to be offset by the graphitization which occurs in closed shapes deposited at 2000°C, at least for deposits containing up to 0.7 percent boron. This is thought to be due to graphitization stresses (Ref. 64) and Mrozowski cracks (Ref. 65) caused by the graphitization. If graphitization were minimized by depositing at very high deposition rates or at lower temperatures, a positive strengthening effect with boron might be attained.

Conclusions From These Studies Can Be Enumerated:

1. Differential graphitization across the thickness of a deposit was found to have some merit in improving the structural soundness of BPG cylinders for t/r values < 0.065. Above a t/r value of 0.07, differential graphitization did not appear to be helpful.

2. High boron levels at low deposition temperatures (1800°C with little or no graphitization) and low boron levels at high deposition temperatures ($\sim$ 2000°C) as well as high deposition rates, appear to be useful areas for attempting to deposit BPG cylinders with t/r capabilities beyond the current state-of-the-art.

3. An increase in graphitization, either associated with an increase in boron level or with annealing, results in an increase in modulus. Values as high as 10×10^6 psi were obtained for a sample containing 0.7 percent boron.

4. Unlike the case of BPG plate stock, there does not appear to be any strengthening effect caused by the presence of boron for cylindrical BPG deposits containing up to 0.7 percent boron.

5. Residual stress increases with increasing boron level and with graphitization.

6. No systematic trend was found in Poisson's ratio which could be related to either boron level or annealing time.

7. No relationship between boron level (0.1 to 0.7 percent) and a-direction coefficient of thermal expansion was found a constant CTE value (0 - 1000°C) of $0.8 \pm 0.2 \times 10^{-6}$ was obtained. The c-direction CTE for the as-deposited cylinders, on the other hand, was found to increase from 24×10^{-6} to 28×10^{-6} for this same boron range.

8. No evidence of any stress-induced graphitization at 2000°C was found in this study.

RECOMMENDATIONS

It appears that for the deposition conditions employed, differential graphitization across the thickness has some merit in improving the structural soundness of BPG cylinders for values of $t/r < 0.065$. Above this t/r value, differential graphitization did not appear helpful in attempting to deposit structurally sound cylinders with higher thickness-to-radius ratio (beyond the current state of the art). Some control of residual stress can be achieved by means of differential graphitization; however, this technique does not offer any improvements over lower temperature and lower boron level deposition techniques which are currently used for depositing crack- and delamination-free cylinders with t/r values of ~ 0.1. The extent of graphitization can be specified and controlled; however, it cannot be used to advantage in depositing closed shapes at 2000°C. Post-deposition graphitization is also deleterious to the structural integrity of constant boron level and graded BPG deposits, and should be avoided.

VIII. PROCESS AND PROFILE STUDIES FOR REFLEX FLOW SYSTEMS

All the studies reported in Sections V, VI and VII of this report were based on straight-through flow systems. While it might be possible to deposit a pyrolytic graphite nose cone on the exterior surface of a properly shaped graphite plug using a straight-through flow system, there are a number of reasons why this is not a good technique. One reason is the difficulty in keeping the plug (or deposition) surface hot, since in most deposition assemblies the plug is not a heated piece. Another reason is that most nose cones require a thicker deposit in the nose region than along the remainder of the walls and that is not easily accomplished on a plug. The most important reason, however, is that residual stresses on such a deposit exceed the material strength with the result that the deposit is cracked, delaminated and out of round when removed from the mandrel. For all these reasons, a reflex flow system is used to deposit nose cones.

In a reflex flow system, the inlet gas mixture is injected into the interior of a closed and heated mandrel along its central axis. The gas is heated, partially decomposed and is exhausted as an annular flow, returning around the incoming flow along the mandrel wall. Thus, in addition to the many complexities found in straight-through systems, new problems are created which are unique to reflex flow systems.

Some of the unique problems are:

1) The need to inject gases at a point well within the assembly. A water-cooled inlet nozzle is required to prevent clogging from premature deposition, but the available cross-section within the mandrel is small. The nozzle is effectively a cold plug, influencing the linear velocity of the gas on its return path. The nozzle also acts as a heat sink within the assembly.

2) The difficulties associated with in-process measurements within a heated graphite mandrel in gases at low pressure and high linear velocity. For instance, it would be desirable to know what actual pressure exists at each point in the flow path. It would also be desirable to know how much turbulent mixing occurs at the incoming-outgoing flow interface and whether the gas flow is laminar or turbulent at each point.

3) The difficulties imposed by typical material specifications, based on the end use as aerospace hardware. For instance, post-deposition machining of the exterior cannot be allowed for fear of contamination of the otherwise ultrapure carbon surface and also for fear of cutting into delaminations which might not be precisely parallel to the exterior. This requires accurate mandrel design and proper mandrel pretreatments. The deposit must have at least the minimum thermal and mechanical properties specified in order to perform satisfactorily in use. None of these deposit requirements can be met without a reliable, reproducible reflex flow process.

Obviously the reflex flow system is a complex one. At the time these studies began, an empirical apprcach had been devised which allowed occasional success in the deposition of nose cones of about 10 degree half angles with about 0.250 inch nose radii using graded boron-alloyed pyrolytic graphite. Each material supplier had certain successes, not all suppliers performed equally well in the production of any given nose cone, and none had had the time or opportunity to examine the effects of variables in any controlled studies because the need for hardware pieces was too great.

This program of studies represents the first extensive, systematic set of experiments aimed at understanding the effects of variables (and their interactions) in the process. Task 3.5.1 had established the state of the art for production of one typical nose cone. The state of the art was surprisingly good in view of the complex nature of reflex flow systems. It represented a combination of "best estimates" by experienced process engineers.

A. EFFECTS OF PROCESS VARIABLES (Tasks 3.2.1.1 and 3.4.2.1)

According to the Work Statements, "The magnitude of the changes in deposit thickness profile and deposition rate which can be made through modification in gas flow patterns will be established. Techniques which will be evaluated include baffles and chokes." and "The number, uniformity and tightness of delaminations will be evaluated in deposits made using: a) Variations in deposition temperature and variations in deposition rate, and b) Variations in boron content and distribution (axial and radial), effects of diluent gases, changes in setup design, and variations in nozzle size and position."

The work in Task 3.4.2.1 was started first, on subcontract to Raytheon Company. The revised Work Statement eliminated most of the planned effort in Task 3.2.1.1.

EXPERIMENTAL CONDITIONS SELECTED

The processing conditions used to deposit cones at Raytheon Company and General Electric-Metallurgical Products Department differed somewhat. Therefore, it was mutually agreed that Raytheon Company would initially use GE-MPD conditions. The only important difference in the deposition assemblies at the two facilities was that at Raytheon Company the work piece was rotated, whereas at GE-MPD the gas nozzle was rotated. In either method, a relative motion was obtained which was intended to eliminate any problems arising from possible inlet nozzle misalignment.

A typical mandrel assembly and cone deposit is shown in Figure 106. The exhaust holes, however, were located at the base of the mandrel sleeve rather than at the top as shown in this figure.

The inside mandrel surface was polished with 600 grit paper, wiped dry with acetone-moistened, lintless paper, sprayed with Dr-Glide* dried and again wiped with lintless paper. The Dri-Glide step was eliminated in the last five cone runs since its benefit was concluded to be marginal. The mandrel assembly consisted of a 3-1/3 inch i.d. by 8 inches long graphite sleeve pinned to the mandrel, a graphite disk pinned at the base of the graphite sleeve, and a 1-1/2 inch diameter graphite rod screwed and pinned to the top of the mandrel. The upper end of the graphite support rod was fastened to a metal rod which was connected to a gear driven rotating shaft. The water-cooled nozzle, insulated by a graphite sleeve, was positioned inside the mandrel sleeve at the appropriate distance from the cone tip. A flash precoat of PG 5 to 10 mils thick was applied over a 30 minute period. This was followed by 15 minutes of evacuation prior to the start of deposition. The rotation of the cone at 3 rpm was generally very smooth during the first few hours of deposition; however, before the end of deposition in the early runs, the support rod would break due to a thick buildup of EPG "clinkers" and binding between the nozzle sleeve and mandrel sleeve plate. The fact that the mandrel was stationary for part of the deposition at the end did not detract from the variable under investigation. For the most part, it only accentuated the asymmetry in wall thickness.

Two changes were made in the mandrel assembly after about half the cones were deposited. 1) Improvement in the rotating assembly and support rod. 2) Attaching the nozzle sleeve directly to the mandrel end plate and rotating the assembly around the water-cooled nozzle. These improvements reduced the binding problem due to the build-up of EPG clinkers and made it possible for the cone to be rotated for the entire run duration. In addition, the redesign resulted in a better control over the exhaust area.

After cool-down, the thickness of the cone was profiled and four to six radiographs were taken at various orientations. The cone was than cut longitudinally and a 3-inch tip section was polished and photographed for a study of deposition and closure characteristics at the tip. Samples were taken at various locations for boron analysis and density measurement.

RESULTS

Data on the processing and characterization of the cones deposited are given in Tables XXXIV and XXXV, and in Figures 107 through 129. Details on the processing of individual deposits and the variable under investigation are given in the following sections:

---

*Magnus Chemical Co., Inc., Garwood, N.J.

NOZZLE ORIFICE SIZE STUDIES. Three cones were deposited under essentially the same conditions to investigate the effect of nozzle orifice size before deposition of a standard.

Run GEDP-1 (75 mil nozzle orifice) was set up to deposit for 47 hours After about 10 hours, the support rod broke and the mandrel fell, thereby reducing the nozzle to cone tip distance to approximately 6-1/2 inches. The run was terminated after 45-3/4 hours because of increased pressure in the gas flow lines caused by plugging of the exhaust holes. The inner surface of the cone was rough and showed nodular growth attributed to the increased pressure.

Run GEDP-2 (150 mil nozzle orifice) was terminated after 6 hours of deposition due to pressurization of the gas flow meters. Figure 116 shows a photograph of the cone after cutting. The center of the cone above the nozzle was filled with a hard, gray, sooty pyrolytic coke. The maximum wall thickness was 2 inches below the tip. The sequence of events which led to the formation of this coke is believed to have been:

a) Closing of exhaust holes due to rapid deposition there.

b) Increase in pressure and turbulence inside the cone.

c) Gas phase formation of aromatic hydrocarbons and soot.

d) Formation of pyrolytic coke (or hard soot compact).

Run GEDP-3 (100 mil nozzle orifice) was a normal deposit except that the rotation ceased after 7-1/2 hours.

BASE-LINE RUN. In order to have a "standard" deposit with which to compare later deposits, a base-line run was made. A nozzle orifice size of 89 mils was selected for the base-line run, based upon a careful examination of the deposition characteristics for deposits GEDP-1 and GEDP-3. This run, GEDP-4, was made under the same conditions as the first three runs. The inner cone surface at the base contained some large nodules and the wall thickness was asymmetric around the circumference.

NOZZLE WITHDRAWAL AND TEMPERATURE VARIATION STUDIES. The nozzle withdrawal experiments were aimed at assessing the effect of maintaining a constant and increasing nozzle to cone tip distance on the deposition characteristics. These runs were made early in the program so that nozzle withdrawal could be assessed and included as a standard processing item if the results warranted it.

Because of problems associated with rotating the mandrel, the preliminary nozzle withdrawal experiment (GEDP-5) was made with a fixed base support. The nozzle was withdrawn at the rate of 1/4 inch per each five hours of

The second nozzle withdrawal experiment (GEDP-6) was accompanied by an increase in deposition temperature over the range 1950° to 2100° C. Temperature variation was selected as a processing variable in an attempt to produce a tighter delamination pattern by offsetting secondary residual stresses. The deposit was rotated and the nozzle was withdrawn at a rate of 1/8 inch after 5 and 10 hours, 1/4 inch after 15 and 20 hours and 1/2 inch after 25 hours. The cone rotated satisfactorily for the first 15 hours of deposition.

Run GEDP-7 was made with an increase in temperature over the range 1950° to 2100°C with a stationary nozzle. The hole in the mandrel base plate was enlarged to provide additional clearance between the rotating base plate and the deposit build-up on the o.d. of the stationary nozzle sleeve. The mandrel rotated satisfactorily for 25 hours. This deposit was similar to GEDP-6.

GRADED AND HIGHER BORON LEVEL STUDIES. The BCl_3 flow rate for all previous runs had been held constant at 0.04 lpm. In the graded and higher boron level experiments, the BCl_3 flow rate was varied as follows:

GEDP-8 Decreased from 0.04 to 0.01 lpm as a function of time.

GEDP-9 Constant at 0.08 lpm.

GEDP-11 Decreased from 0.08 to 0.04 lpm as a function of time.

GEDP-14 Constant at 0.16 lpm.

An improvement in the design of the rotating assembly evolved during these runs which made it possible for the mandrel to be rotated more smoothly and with less binding tendency between the rotating and non-rotating parts. In addition, the redesign resulted in a better control over the exhaust area. A metal universal joint was added to the rotating support assembly after run GEDP-8 and a graphite universal joint after run GEDP-9. In GEDP-11 the nozzle sleeve was attached to the mandrel base plate and rotated with the mandrel around the nozzle. The mandrel rotated satisfactorily for the entire run. Run GEDP-14 was terminated after 7-1/4 hours due to "clinkers" depositing on the nozzle and binding between the nozzle and nozzle sleeve. This binding problem was associated with the very high BCl_3 flow and did not occur in any lower boron level experiments. A more or less uniform coating was deposited on the nozzle sleeve in the lower boron level experiments. All deposits except GEDP-14 exhibited a smooth inside surface texture with nodules 1/8 inch in diameter or less and were considered to be satisfactory deposits. The surface of GEDP-14 was very hard and had a soot-like appearance.

NITROGEN DILUTION STUDIES. This run (GEDP-15) was made using what was considered to be the best set of deposition conditions. The deposit was unusually thin (185 mils at the tip and 210 mils at the base) and was not considered to be a satisfactory deposit. The presence of nitrogen appeared to have retarded the deposition rate and was thus considered undesirable from a practical consideration.

OTHER PROCESSING VARIABLES. Two nozzle withdrawal runs (GEDP-10 and GEDP-12 were made to investigate the effect of an initial 7-1/2 inch nozzle-to-cone tip distance on the sooting tendency in the stagnation tip region. These modified nozzle withdrawal runs rotated satisfactorily during the entire deposition. The deposit, however, was considered thick enough for an evaluation of the 89 mil nozzle orifice size.

After a preliminary examination of the processing data, it was recognized that the exhaust area and the presence of a cold finger (unshielded 1-1/2 inch end section of the water-cooled nozzle) had a marked effect on the deposition rates. A Raytheon Company run (R-1) was made to investigate these two parameters in more detail and for comparison with previous runs. Run R-1 was deposited for 20 hours using a stationary mandrel support. The deposit was thin, as was expected, because of the exhaust area and nozzle position but the surface testure was smooth and free of large nodules.

CHARACTERIZATION AND EVALUATION

Characterization and evaluation of the cone deposits were made by examining the thickness profile, growth characteristics at the cone tip stagnation region, boron content, density, and delamination characteristics for number and tightness. The effects of a cold finger, exhaust area, temperature variation, nozzle to cone tip distance, and nozzle withdrawal were assessed with respect to the deposition rate in the stagnation tip region and the deposition rates at the maximum and minimum cone wall thickness.

THICKNESS PROFILE. The wall thickness for each cone was carefully measured along the length of the cone wall at four locations 90° apart. Figures 107 through 111 show the maximum and minimum wall thickness profiles and the tip stagnation regions. Except for GEDP-2, the minimum wall thickness is seen to occur generally in the region from 1 to 3 inches from the cone tip and the maximum from 7 to 8 inches from the cone tip. A tabulation of the tip thickness and spread in the maximum and minimum wall thickness for each deposit is given in Table XXXIV. The early deposits are seen to show appreciable circumferential asymmetry. As better control of the processing evolved (alignment, rotation of mandrel for entire run, etc.) this asymmetry was reduced to $\pm$ 10 mils (runs GEDP-13 through GEDP-15).

The presence of the minimum wall thickness and sooting characteristic in run GEDP-2 can be explained from a consideration of the gas flow profile. The gas is assumed to spread in the shape of a plume as it leaves the nozzle. In the cone tip region, gas turbulence may exist and deposition there is probably controlled by gas-phase diffusion. In run GEDP-2,

because of the 150 mil nozzle and low center line velocity, the gas plume may have spread quickly, striking the cone wall about 4 inches from the tip producing a larger turbulent region which, because of the reverse gas flow and long residence time of active species formed, probably caused appreciable sooting to occur. Because of the higher center line velocity in the 75 to 100 mil nozzle runs, less turbulence would exist. The gas plume would spread and strike the wall in the region 1 to 3 inches from the tip, thereby causing a low rate of deposition. This correlation is valid only under the particular deposition conditions used in this study. That is, a set of deposition conditions could probably be specified under which a satisfactory cone could be deposited using a 150 mil nozzle.

TIP GROWTH AND CLOSURE. Three regions may be considered in characterizing the deposition at the tip of the cones deposited in these studies:

1. The initial 80 to 100 mils deposit thickness.
2. The region from 100 to 300 mils.
3. The region greater than 300 mils in thickness showing a line closure.

In region 1, normal deposition occurs with a decreasing radius and with a greater rate of deposition than at the minimum cone wall thickness. Delaminations are spaced from 10 to 20 mils apart and are associated with the high t/r. For a 1/4 inch radius, the upper limit between delaminations at the tip is about 25 mils. Nodules which occurred within this region were traced to a poor blend of the mandrel radius to the cone wall and to surface flaws at the mandrel tip. Such nodules could be eliminated by improved machining techniques and by proper conditioning of the mandrel surface.

Region 2 has two different aspects. One is a continuation of region 1 to a point closure at about 300 mils thickness. The second aspect is associated with gas growth in a "fish-tail" like shape caused by near sooting conditions. This phenomenon can be minimized by keeping the boron content low and by proper nozzle withdrawal during deposition.

Region 3 is characterized by a line closure along the central axis of the cone. This closure line is a function of the cone geometry at the tip and the way in which growth occurs.

Referring again to Figures 112 through 115 and neglecting the nodules in the regions 1 and 2 which are due to mandrel flaws, the best tip closures were concluded to be those of runs GEDP-6, 8, 11 and 12. The two most important processing parameters in these runs responsible for the favorable closure pattern were nozzle withdrawal and graded boron. Unfavorable processing parameters which should be avoided are nominal high boron content (GEDP-9) because of the sooting tendency and fast nozzle withdrawal (GEDP-5) because of the tendency to produce a void.

The growth and closure characteristics in the tip region will markedly affect the performance of a BPC nose cone during re-entry. Only the

outermost surface layers would be peeled away, thereby exposing new thermal barrier surfaces. Any flaws in the tip such as due to a void, large nodules, severe delaminations and cracks such as seen for some of these cones would have a deleterious effect on the performance of such nose cones if they were used as aerospace hardware.

NUMBER AND TIGHTNESS OF DELAMINATIONS. A visual comparison of the radiographs for number and tightness of delaminations at the tip and base revealed very little difference for all deposits produced. Actual differences may be present which were not clearly resolved subjectively from the radiographs. A simple procedure was devised for characterizing the number and tightness of delaminations. The radiograph for each cone which showed the best defined delamination pattern was marked off at 3 and 7 inches from the cone tip and the distance from the outer wall surface to each visible delamination was measured. A delamination profile was constructed by plotting this distance against the tightness of the delamination. Tightness was ranked into five categories according to the approximate width of each delamination: VVL-- very very loose (10 mils), VL---very loose (5 mils), L--loose (3 mils), t--tight (1 mil), and Vt--very tight (1 mil). Figures 117 through 128 show the delamination profiles constructed in this manner for all radiographed cones. Close examination revealed no significant differences in the number of delaminations: however, cones GEDP-6, 7, 8 and 13 appear to have tighter delaminations toward the inner surface than the other cones. The favorable tightness rating for GEDP-13 is not considered to be very significant since the cone wall was thin. An increase in temperature during deposition might have some merit in improving the tightness of delaminations; however, the data suggest a trend rather then a definite effect. High nominal boron content, nitrogen dilution, nozzle size, as well as the other parameters studied were found to show no improvement in the number and tightness of delaminations. This is not to say that any real effects may not have been present, but if so, these were overshadowed by the stresses due to wall thickness asymmetry along the length. A uniform wall profile would be expected to show some real improvements in the delamination pattern.

Photographs of polished sections for cone GEDP-7 at 3 and 7 inches from the tip are shown in Figure 127. The delaminations are seen to be discontinuous. Good agreement was obtained in a comparison of the number of delaminations between this figure and Figure 122 for the same transverse regions.

BORON AND DENSITY ANALYSIS. Boron spectrographic analysis* reported as weight percent are given in Table XXXV. Selected samples were taken from the center, outer and inner regions at the tip and from the first and last deposited layers at the base. The samples were powdered and passed through a 200 mesh sieve prior to analysis. Duplicate analyses were made on each sample and the difference was generally within 10 percent of the measured boron level. The boron levels for cones GEDP-3, 6 and 7 were not

*Jarrell-Ash Co., Waltham, Mass.

markedly different and were considered typical for cones deposited with the processing conditions used. The boron levels at the base for all cones, except GEDP-1, 5 and 8, fell within the range of 1.1 to 2.2. percent boron, with the higher boron levels associated with the last deposited layers. This might be reasonable if boron diffusion occurred since the first deposited layers would be at temperature for a long period of time, thereby giving the boron a chance to diffuse. In run GEDP-1, the first deposited layers were at temperature for a longer period of time than in any of the other deposits and, therefore, the boron level on the outside surface would be low. Run GEDP-8 was a graded boron deposit (medium to low), and the boron content ratio between the first and last deposited layers are in good agreement with the BCl_3 flow rates. The reason for the low boron levels for GEDP-5 and in the tip for GEDP-4 is not understood. Depletion of boron by diffusion, if it occurred in these deposits, may have been accelerated by the presence of the void in the tip for GEDP-5 and the peculiar "Whisker-like" growth in the tip of GEDP-4. How these and other structural features might affect boron diffusion is not clearly understood.

Density data (by toluene displacement) were obtained only on a few specimens. The measured values varied from 2.20 to 2.24 g/cc with no obvious correlation with the boron analyses.

NORMALIZATION OF DEPOSITION RATES. An attempt was made to normalize the deposition rates in the stagnation tip region and the deposition rates at the maximum and minimum cone wall thickness for the effects of the following processing variables:

a) Cold finger (unshielded section of nozzle).

b) Exhaust area of 50%*.

c) Temperature variation.

d) Initial nozzle to cone tip distance of 7-1/2 inches.

e) Nozzle withdrawal.

It should be noted that with the number of variables looked at in the program and the number of runs made, it was impossible to assess the effects of these variables on the deposition rates unless it was assumed that they were independent of each other. To first approximation, this

*the exhaust area described in terms of the annular cross-section between the top of the inlet nozzle and the adjacent mandrel, which is the minimum flow area within the mandrel region. The values used in these studies were 23 percent and 50 percent.

is a reasonable assumption. By means of this analysis, the normalized deposition rates for almost all runs were observed to fall within the following ranges:

Stagnation tip	41 - 44.5 mils/hr
Max. wall	13.1 - 14.1 mils/hr
Min.	6.1 - 6.7 mils/hr

These normalized values apply only to deposits made with a 100 mil nozzle orifice size at a constant medium boron level. Differences from these normalized values can be accounted for on the basis of orifice size graded or high boron levels, fast rate of nozzle withdrawal and nitrogen dilution.

SUMMARY AND CONCLUSIONS

A number of processing variables were investigated in an attempt to improve the state of the art for depositing BPG cones and to advance the technology for depositing full-scale BPG components for re-entry applications. The effects of intended variables (nozzle orifice size, nozzle withdrawal, temperature variation, graded and high boron contents, nitrogen dilution) as well as several assembly features (unshielded nozzle end section, exhaust area initial nozzle to cone tip distance) were assessed with respect to tip growth characteristics, wall thickness profile, and delamination pattern. The conclusions reached during this investigation with regard to these variables are summarized as follows:

1. Considering the four nozzle orifice sizes investigated at Raytheon (150, 100, 89, 75 mils) and the conditions used to produce the cone deposits, the 100 mil nozzle was most satisfactory from the standpoints of deposition rate, tip closure characteristics and wall thickness profile. The 89 mil nozzle ranked second in this respect.

2. Nozzle withdrawal and graded low level boron were found to be the two most important variables in producing a favorable tip closure pattern and wall thickness profile.

3. Nominal high constant boron levels as well as nominal high graded boron levels should be avoided because of the sooting tendency and high degree of graphitization. The former would result in nodular growth and the latter would be expected to enhance the delamination tendency.

4. No marked improvement in delamination pattern was observed with any of the variables investigated, although a temperature variation during deposition (1950° to 2100° C) tended to give a slightly tighter delamination pattern toward the last deposited surface. It was felt, however, that the results were not enough

better to warrant using an increasing temperature during deposition.

5. Nitrogen dilution was found to reduce the deposition rate significantly, but not to better the deposition profile.

6. In comparing two initial exhaust areas (23 and 50%) and two initial nozzle-to-cone-tip distances (7-1/2 and 8-1/2in.) the 23 percent area and 8-1/2 inch tip distance were found to give the most favorable deposition rate and wall thickness profile.

7. An unshielded nozzle tip section (cold finger) appeared to improve the uniformity in wall thickness along the length of the cone.

RECOMMENDATIONS

Based on the results of these studies, the Raytheon Company made two recommendations for processes in reflex flow systems for the production of nose cones.

For production of graded boron-alloyed material:

Temperature	2000°C
Pressure	3 torr
CH_4 Flow Rate	4.7 lpm (~10 cfh)
BCl_3 Flow Rate	graded from 0.005 to 0.03 lpm
Nozzle orifice size	100 mils
Initial nozzle position	8-1/2 inches from tip
Withdrawal rate	1/8 inch each 5 hours
Exhaust area	23 percent
Cold finger	1-1/2 inch unshielded nozzle tip

which should give deposition rates of 15.5 mils/hr in the tip, 3.3 mils/hr at the maximum wall rate position (near the skirt) and 3.0 mils/hr at the minimum wall thickness position.

For production of constant level, boron-alloyed material:

Temperature	2000°C
Pressure	3 torr
CH_4 Flow Rate	4.7 lpm (~10cfh)
BCl_3 Flow Rate	0.04 lpm
Nozzle orifice size	100 mils
initial nozzle position	8-1/2 inches from tip
Withdrawal rate	1/8 inch each 5 hours
Exhaust area	23 percent
Cold finger	1-1/2 inch unshielded nozzle tip

which should give deposition rates of 30.6 mils/hr in the tip, 7.4 mils/hr.

at the maximum wall rate position (near the skirt), and 4.8 mils/hr at the minimum wall rate position.

Cone rotation with respect to the nozzle was recommended for both of these tentative processes.

IX SPECIAL STUDIES

While the primary studies were being carried out on straight-through and reflex flow systems, special studies were done to investigate.

1. Process modifications, such as the use of unsaturated hydrocarbons and the use of special nozzles designed to introduce turbulence in the gas flows.

2. Interrupted deposition, for the introduction of delaminations at will to allow thicker deposits for a given radius of curvature.

3. Development of a process and the manufacturing technology for production of hafnium-alloyed pyrolytic graphite.

4. Additive studies, for determining the effects of impurities in a hydrocarbon gas.

General Electric Company, Re-Entry Systems Department at King of Prussia, Pennsylvania, carried out the work in the first three areas on subcontract. The first area was then extended into studies for boron-alloyed pyrolytic graphite by the contractor, General Electric Company, Metallurgical Products Department, at Detroit.

The fourth area was carried out on subcontract at Rensselaer Polytechnic Institute, Troy, New York. The work subsequently provided the basis for the degree Master of Science for Mr. Barry Butler, under the direction of Dr. R. J. Diefendorf at R.P.I.

A. TURBULENT NOZZLE STUDIES (Task 3.2.1.3)

According to the Work Statement, "Controlling gas flow patterns in nose tips will be evaluated as a means of achieving proper axial thickness distributions and delamination patterns in the nose tips. The techniques to be used include nozzles which produce turbulent conditions particularly in the nose tip region. Comparison will then be made between the deposition rate and deposit characteristics for materials made under both laminar and turbulent gas flow conditions."

BACKGROUND

It can be shown analytically that residual stresses resulting from the anisotropy in thermal expansion characteristics may cause delaminations to develop in pyrolytic graphite when the radial stress exceeds 1500 psi. Once a delamination has developed, however, a radial stress of only 500 psi is sufficient to cause it to propagate. Nose cones with small nose radii and small half angles have a high t/r and thus high stresses are developed during cool-down from deposition temperatures of about 4000°F even with a relatively thin deposit thickness. This condition is aggravated as the deposit thickness is increased using "state of the art" techniques. These conventional

techniques produce nose cones where the deposition rate in the tip and the side walls near the tip are essentially equal. This results in a growth pattern in the nose tip region where the radius of curvature is continually decreasing as illustrated in Figure 130a.

This type of growth pattern causes a large number of delaminations to develop in the nose tip region and propagate into the skirt region of the cone to a point where the radial stresses are less than the "c" direction strength of the material. If the deposition rate in the nose tip can be substantially increased without increasing the deposition rate along the length of the cone, the radius of curvature on which new material is being deposited will be continually increasing. This would result in a decreasing t/r with its associated lower stresses. Thus fewer delaminations would develop during the cool-down portion of the fabrication cycle.

Another major advantage of increasing the deposition rate in the tip region is that an improved delamination pattern would result. Delaminations propagate along deposit thickness growth profiles. In early state of the art nose tips the delaminations as illustrated in Figure 130a almost come to a point about 1/4 inch behind the tip for 1/4" nose radius components. If any recession, caused by ablation or erosion during use occurred, the delaminations in the tip region would become almost parallel to the flow field around the tip. Thus high shear forces would act on both edge planes of the material and at delaminations. If, however, cones were deposited with the radius of curvature always increasing, any delaminations that did develop during the process would be essentially parallel to the outer contour of the nose tip. The flow field developed during re-entry would be essentially parallel to the outer contour of the nose cone. Therefore, as recession occurred, edge planes of the material and delaminations would not be exposed to the high shear forces encountered during re-entry and thus improved performance would result.

An understanding of the gas dynamics occurring within a reflex flow pyrolytic graphite deposition chamber is difficult to achieve. Some of the many factors which must be considered important to understanding these gas dynamics are (1) the mixing of gases passing through an orifice at an initial pressure of 40-500 mm Hg into a deposition chamber at a pressure of 2-6 mm Hg, (2) the heating and subsequent dissociation of the gases, (3) the gas interactions, and (4) the expansion of the gases as they are further heated. The non-reproducibility in the fabrication of state of the art pyrolytic graphite nose cones before this contract could be the result of operating under conditions that were border-line between turbulent and laminar flow. A review was made of empirical information concerning deposition processes in the fabrication of these nose cones. In this review, the qualitative effects of jet impingement fluid mechanics were utilized to aid in interpretation of results.

A schematic diagram of the fluid mechanics model of the pyrolytic graphite nose tip deposition process is shown in Figure 131. A

cold methane jet expands from the nozzle chamber pressure into the low ambient pressure within the pyrolytic graphite deposition chamber. Impingement of this jet in the tip region is followed by a reverse flow wall jet along the conical skirt. For typical inlet pressures (400 mm Hg absolute injector pressure, 5 mm Hg absolute chamber pressure) and nozzle exit diameter (.069) inches), the Reynolds Number of the jet based on fully expanded flow properties and jet diameter is approximately 10,000. This value of Reynolds number is well above the limit of 1000 to 2000 required for transition from laminar flow (Ref 66) hence, the jet is undoubtedly turbulent prior to impingement. The impingement region involves highly complex processes due to the rapid temperature increase of the gas caused by convective heat transfer from the hot mandrel surface. The state of the local wall jet flow in the impingement region (laminar or turbulent) is dependent upon a Reynolds number based on local flow properties and characteristic length such as momentum thickness of the wall jet boundary layer. A small region of laminar flow is possible in the stagnation region followed by transition to turbulent wall jet flow. Expansion from stagnation region pressure to the ambient pressure causes a decrease in gas density. Simultaneously, a decrease in gas velocity is caused by the mixing effects characteristic of wall jet flows. The resulting decrease in local Reynolds number with distance from the impingement region eventually may cause a return to laminar flow. These flow regimes are illustrated schematically in Figure 132, and appear to agree qualitatively with certain of the experimental deposition results.

Since the deposition rate is a function of local turbulence level, residence time, and gas temperature, the variations in local flow conditions will cause corresponding variations in deposition rate. Increased deposit thicknesses in the impingement region should result from increases in jet Reynolds number and jet turbulence level. Even if a small laminar flow region exists in the impingement region, it is well known that increased free stream turbulence causes increased laminar stagnation point heating (e.g., Ref. 67). Hence, devices for increasing the jet turbulence level should be beneficial towards increased stagnation point deposit thickness. An increase in mass flow rate would increase the Reynolds number, but would also require a longer distance from the stagnation point for the wall jet flow to be heated to a given temperature.

EXPERIMENTAL CONDITIONS SELECTED

Previous discussions with various investigators had ruled out the use of a device such as a smoke generator to study gas flow patterns in a pyrolytic graphite deposition chamber. The pressure differential and the driving force can be simulated but it is not possible to incorporate the effects of gas decomposition and subsequent 8-fold expansion on heating.

A meaningful demonstration model did not appear feasible and preliminary analytical techniques were not conclusive due to unknown parameters within the deposition chamber; therefore, the follo-i-.

experimental approach was evolved.

1. A nose tip was to be fabricated using conventional processing techniques without boron additions to provide base line data for evaluating the effectiveness of various turbulent creating devices.

2. A second nose tip was to be fabricated with a larger injector nozzle orifice size to evaluate the effect of gas stream Reynolds number on deposit thickness profile. The orifice size was to be chosen so as to produce a significant decrease in Reynolds number.

3. A diffuser cap was to be designed for creating turbulence as the gas is ejected from the nozzle. A third nose tip was to be subsequently fabricated to evaluate the effect of turbulence created in this manner.

4. If necessary, two additional nozzles were to be designed and fabricated to create turbulence by such means as a swirling action from the nozzle or a mixture of a high velocity and lower velocity gases in the nose tip region. As required, additional nose tips were to be fabricated with these nozzles and the results evaluated.

The results of previous pyrolytic graphite nose cone studies established general ground rules on which the parameters for this study were selected. For example, it was fairly well established that a restriction is required between the exit (open) end of the cone and the furnace chamber. This restriction does several things. First, it increases the residence time of the gas in the deposition chamber; secondly, it undoubtedly increases the local pressure within the deposition chamber; and finally, it alters the exhaust gas flow path. The results obtained with this type of restriction are (1) increased deposition rate in the tip, and (2) a more uniform wall thickness. Other factors such as mandrel thickness, deposition pressure, gas flow rates, and deposition time had been fairly well established.

Previous work with boron-alloyed pyrolytic graphites in nose cone configurations had demonstrated that boron has a catalytic effect on pyrolytic graphite deposition rates. The catalytic effect of boron additions has been used by various pyrolytic graphite producers to fabricate boron-alloyed pyrolytic graphite nose cones with a deposition rate in the tip up to 8 times greater than the deposition rate along the skirt region. This catalytic effect is graphically illustrated in Figure 133; however, this effect is somewhat difficult to use so that two cones made under supposedly identical conditions would often have greatly different stagnation thickness. This non-reproducibility could be due to several things. Boron-alloyed pyrolytic graphite tends to deposit in dendritic fashion when the temperature

is in the 1500-1600°C range. These dendritic deposits generally occur in the cooler zones of the deposition chamber. Two zones that are most effected are the exhaust stack from the chamber and the surface of the water-cooled injector nozzle. Dendritic growths can cause closures of the exhaust stack and build up a deposit on the injector nozzle so that gas flow is impeded. These growths were unpredictable and probably were the cause of a majority of variations.

Because of the unpredictable deposition characteristics of the boron pyrolytic graphite in the cooler regions of the furnace, boron additions were not used in this study. It was felt that boron catalytic effects and the variations that have been experienced would mask the induced turbulent effects. Hydrogen gas was used as a diluent. Hydrogen had been reported to lower the deposition rate but to give a deposit of good microstructure.

As previously discussed, analytical techniques cannot be used to determine exact changes required to the pyrolytic graphite process or to the injector nozzle design to induce a specific gas flow pattern. Furthermore, the degree of turbulence required to produce the desired deposit thickness profile is unknown.

Taylor and VonKaiman (in Ref. 68) described turbulence as follows: "Turbulence is an irregular motion which in general makes its appearance in fluids, gaseous or liquid, when they flow past solid surface or even when neighboring streams of the same fluid flow past or over one another." This definition indicates that turbulence can be generated by friction forces at fixed walls (flow through conduits, flow past bodies) or by the flow of layers of a fluid with different velocities past or over one another.

Using the implications of this definition, several concepts were considered to create and/or increase turbulent flow within the mandrel deposition chamber. These were (1) a diffuser cap (flow past a body) (2) a "Swirler" insert (a combination of flow past a body, and flow of layers of a fluid with different velocities past or over one another) and (3) a dual injector to introduce gas at different velocities (flow of layers of fluids with different velocities). Definition of the nozzle configuration required to obtain a specific cone geometry could only be obtained by conducting experiments with design concepts empirically selected on the basis of chemical engineering technology, and previous empirical data. To properly assess the effect of turbulence, however, it was necessary to establish a reference. Two base line runs were made using identical process parameters except for injector nozzle orifice. With these deposit thickness profiles for reference, the additional nose tips, which were fabricated using turbulent creating devices, could be evaluated. Table XXXVI shows the deposition conditions used in these studies.

RESULTS

The experimental results are summarized in Table XXXVII. For convenience, a detailed summary of the runs follows.

Base Line Experiment (Nose Cone 3213-1). This experiment was conducted using a conventional water-cooled injector nozzle with an orifice of 0.069 inches. Calculations for the process parameters used (see Table XXXVI) show the jet Reynolds number for this experiment to be about 10,000. This nose cone was deposited without any indications of process fluctuations.

Figure 134 shows the furnace setup used throughout these experiments. The process parameters are listed in Table XXXVI and except for modifications of the injector nozzle to change flow patterns of the gases, the same deposition parameters were used throughout this task.

Figure 135 is a photograph of the cone and Figure 136 is a radiographic positive illustrating the axial thickness profile. Figure 137 is a curve of the deposition thickness profile. The nose tip had a thickness of 0.280 inches and the minimum wall thickness was 0.050 inches. The minimum wall thickness occurred about 2-1/2 inches from the tip of the cone. The average deposition rate in the tip was 7 mils/hour and at the minimum wall thickness the deposition rate was only slightly greater than 1 mil/hour. This nose tip had a typical delamination pattern which followed the growth profile shown in Figure 137. The material was fine grained and free of axial cracks. The outer surface was spalled due to poor mandrel pretreatment, but this had no significant effect relative to deposit thickness profile.

Base Line Experiment (Nose Cone 3213-2). A second base line experiment was made to establish the effect of orifice size (Reynolds number) on deposit thickness profile for unalloyed pyrolytic graphite. Increasing the orifice size to 0.250 significantly reduced the jet Reynolds number for the gas as it exited from the nozzle. Using the same process conditions and furnace setup, the calculated jet Reynolds number was reduced from approximately 10,000 for the 0.069 inch orifice to about 750 for the 0.250 inch orifice. Figure 138 is a photograph, Figure 139 is a radiographic positive, and Figure 140 summarizes the deposit thickness profile for this cone. The results show that reducing the Reynolds number decreased the tip thickness from 280 mils to about 220 mils. The deposition rate at the base of the cone was also less than for nose cone 3213-1. The material was fine grained and free of cracks; however, the mandrel could not be easily removed from the tip and the cone was damaged during this operation as indicated in Figure 138.

First Diffuser Cap Experiment (Nose Cone 3213-3). With a reference established, a diffuser cap was designed and fabricated. The cap was designed to induce and/or increase turbulence in the nose tip region. The design of the cap is shown in Figure 141 and Figures 142 and 143 are photographs of the part. After several preliminary

experiments were completed to verify the design and attachment methods, a nose tip was fabricated using process parameters identical to those used in the base line experiments.

Figure 144 is a photograph, Figure 145 is a radiographic positive and Figure 146 summarizes the deposit thickness profile for this cone. The results show that the diffuser cap greatly enhanced the deposition rate in the nose tip region. The tip thickness was somewhat less than for the base line experiments but this was more than offset by the greatly increased deposit thickness from the region 1/2 inch behind the tip to about 3 inches from the tip and the fact that the wall thickness from station 3 to the base of the cone was very uniform. The deposit profile summarized in Figure 146 shows that the zone of low deposit thickness was eliminated which had been one of the major objectives of this task. The uniform wall thickness achieved in this experiment produced a favorable delamination pattern.

A review of the radiographs for this nose tip indicated that the stagnation thickness could be substantially increased if the deposition cycle had been longer. It was decided to adapt nose cone 3213-3 to allow processing for an additional 15 hours.

Nose Cone 3213-4 (Cone 3213-3 with an Additional 15 Hours Deposit).

The nose cone fabricated with the diffuser cap was placed back in the furnace for an additional fifteen hours of deposit. During the heat-up cycle, hydrogen gas continually swept the surface. Identical process parameters, furnace setup and nozzle configuration were used as for the earlier run. Figure 147 is a photograph, Figure 148 is a radiographic positive and Figure 149 summarizes the deposit thickness profile. The additional 15 hours gave favorable results; the tip thickness was increased to 400 mils and the rest of the deposit increased slightly. A void developed, starting at 400 mils behind the tip, but this was due to either some misalignment of the nozzle or to the selected parameters. This void could be eliminated with proper adjustments to the system. Neither the radiographic films nor a visual examination of the base of the nose tip indicated where the deposition cycle was interrupted. The cone was fine grained and free of cracks.

Nose Cone 3213-6 . Examination of the radiographs of the cones deposited with the diffuser cap indicated that the stagnation thickness might be greatly enhanced if the nozzle were moved closer to the tip. The maximum deposition rate on the previous cones occurred about 3/4" behind the tip. Therefore, another furnace run was made using identical process parameters, except the nozzle was placed 7-3/4" below the tip; whereas, on all previous cones, the nozzle position was at 8-1/2 inches. Figure 150 is a radiographic positive and Figure 151 summarizes the deposit thickness profile of this cone. Moving the nozzle 3/4" closer to the tip increased the tip thickness from 175 mils to 220 mils, and decreased the wall thickness from

about 150 mils to 80 mils. These results were very promising. The growth profile achieved in this experiment, as in the previous experiments with a diffuser cap would produce nose cones with a favorable delamination pattern. The relatively low deposition rate in the skirt region of the cone is not deleterious since for hardware the overall thickness requirement in both the tip and wall thickness would have to be increased.

Nozzle Orifice Insert (Nose Cone 3213-3). Another method of inducing turbulence or increasing turbulence level in the nose tip region is to cause the gas stream to have a rotating or "swirling" action as it leaves the injector nozzle orifice and enters the deposition chamber. This concept was implemented by machining a thin-walled copper insert open at one end and closed at the other end. The closed end had two slots, perpendicular to each other, machined through the wall to form four surface quadrants. The slots were 1/32" wide and 3/16" long and the four quadrant surfaces were contoured as shown in Figure 152. The contoured faces were shaped to induce a "swirling" effect so that the combination of orifice restriction and "swirling" action would create turbulence. The machined insert was then press-fitted into the orifice with the slotted end 1/2" down in the orifice.

An experiment using the same process setup as for previous nose cones was made with this assembly. Figure 153 is a photograph, Figure 154 is a radiographic positive, and Figure 155 summarizes the deposition profile of this nose tip. The stagnation thickness was only 105 mils and the average wall thickness was less than those obtained in the reference runs. The results of this run indicate that the effects of an insert in the nozzle orifice does not improve either the deposition rate or the deposit thickness profile.

SUMMARY AND CONCLUSIONS

Six nose cones were deposited using identical process parameters except for attachments to the injector nozzle or a change in nozzle orifice size to give various gas flow characteristics. The results showed that altering the nature of the gas flow materially changed the deposition rates and the deposit thickness profiles obtained in nose cone tips.

Two experiments were made to investigate the effect of jet Reynolds number on deposit thickness profile. In one experiment, the Reynolds number of the gas leaving the injector nozzle was about 10,000 which is well above the transition from laminar to turbulent flow while the other experiment had a Reynolds number about 750 which is well below the transition point. The experiment with the high Reynolds number had a slightly higher deposition rate in the nose tip thickness.

One of the two concepts investigated for creating turbulence in the tip region of nose cones did not increase the deposition rate. In fact, this concept, which was intended to give a swirling action to the gas stream as it left the nozzle, actually produced a cone with a tip thickness of

less than 105 mils and a very thin wall deposit.

The other concept investigated, a diffuser cap over the end of the nozzle to create turbulence, gave encouraging results. The cones fabricated with the diffuser cap had a uniform wall thickness, did not have a minimum deposit thickness region near the skirt and showed promise of producing cones with acceptable nose tip thicknesses. The actual cones deposited had relatively little thickness at the tip, but the deposition rates 3/8" from the tips were high. It appears entirely feasible to shift the maximum deposition rate from about 3/8" below the tip region into the tip region itself. Slight variations in nozzle position, gas flow rates, diffuser cap design and/or deposition pressure might lead to substantial improvements.

The following conclusions were drawn from the results of these studies by GE-RSD:

1) Deposit thickness profiles can be significantly altered by variations in gas flow patterns.

2) A diffuser cap attached to a standard injector nozzle can be utilized to create turbulence which leads to favorable deposit thickness profiles.

3) Cones fabricated with unalloyed pyrolytic graphite were fine grained and free of cracks as-deposited. Enhancement in nose tip deposition rate over skirt deposition rate was achieved.

4) Turbulence can be achieved in the gas stream as it leaves the injector nozzle.

5) Devices to create turbulence that are inserted into the nozzle do not appear effective in increasing deposition rate in the nose cone tip region.

6) A decrease in Reynolds number from 10,000 to 750 slightly reduces deposition rate in both the tip and skirt regions.

7) The tungsten alloy (85W-15Mo) used for caps will withstand vapor deposition conditions for at least 100 hours even when not water-cooled, if properly designed.

RECOMMENDATIONS

The following recommendations were made as the result of these studies in pyrolytic graphite deposition:

1) The results obtained in this task did not warrant a revision of the program plan at this time. That is, this alternate process technique was not favored to the exclusion of a normal process using boron-alloyed pyrolytic graphite.

2) The results obtained in this task could warrant further studies to optimize the improvement in growth patterns that was achieved with diffuser caps attached to the injector nozzle. The other process variables might be varied to obtain better results.

3) Boron-alloyed pyrolytic graphite nose tips should be fabricated and evaluated using the diffuser cap concept.

It was this last recommendation which led to the inclusion of the next task in the revised Work Statement.

B. TURBULENT NOZZLE STUDIES FOR BPG (Task 3.2.1.4)

According to the Work Statement, "Turbulent nozzles will be evaluated for use with inlet gas streams containing boron trichloride, for the production of boron-alloyed pyrolytic graphite nose cones with satisfactory deposition thickness profiles."

BACKGROUND

Work in Task 3.2.1.3 showed that turbulent nozzles of a "shower-head" design were able to provide some alteration in the deposition thickness profile when used in pyrolytic graphite nose cones. Although the results were not quite adequate for the production of flightworthy hardware, it appeared feasible to combine this effect with that of catalysis from boron trichloride to produce satisfactory nose cones of boron-alloyed pyrolytic graphite.

EXPERIMENTAL CONDITIONS SELECTED

Seven nose cones were deposited in this task. One was fabricated of pyrolytic graphite, using a "shower-head" type diffuser cap similar to the one recommended for continued study in Task 3.2.1.3. This deposit served as a base line for the balance of the experiments. The balance of the runs were to be boron-alloyed and were designed to evaluate nozzle caps and their effect on deposition profiles and delamination patterns.

Table XXXVIII shows the number of deposits made (7) and the deposition conditions for each one. Figure 156 shows the assembly used to carry out the deposition. The diffuser caps were bonded to a stainless steel nozzle using SermeTel Allen PBX ceramic cement and SermeTel Allen "P" solvent.

RESULTS

Run 6048 was the base line run for the task. Figure 157 shows the cap used in this run. This cap was identical in design to the cap judged most faborable in Task 3.2.1.3, but the material of construction was graphite instead of arc-cast tungsten alloy. Earlier work at GE-MPD had indicated that graphite was a suitable construction material for the cap and was more easily machined than the tungsten alloy.

This run was completed without difficulty. Figures 158 and 159 are pictures of the nozzle cap before and after deposition, and Figures 160 and 161 are more detailed views of the cap's o.d. and i.d. after deposition. All flow passages in the cap were open after the run. Figure 162 is the deposition profile for the deposit. Figure 163 is a cross-section of the nose region viewed at 5X. This view was prepared by potting both the i.d. and o.d. of the cone nose region in a self-hardening plastic. The nose was then cut off using an abrasive wheel. The resulting encased nose piece was cut slightly off axis but parallel to it, and then polished back by mechanical methods as close to on-axis as possible. Figure 163 indicates that the material in the nose was highly regenerative, delaminated about the same as the walls, and was cracked.

The second run (6049) was planned to be the same as 6048 but with boron trichloride added as a reactant. This run was terminated after 1-1/4 hours due to a plugged gas feed system. Subsequent examination indicated that the diffuser cap was plugged. Figure 164 is a picture of the cap after sectioning. The small chamber above the nozzle in the cap was filled with a low density pyrolytic deposit which blocked the flow path between the nozzle orifice and the nozzle cap holes. Apparently, the diffuser cap temperature was such that the deposition rate within the cap was sufficiently low to keep from plugging the holes in an unalloyed deposition system. This same temperature, however, caused sufficient sooting and deposit to clog the passage when boron trichloride was added.

The third run was then designed so as to correct the problems in 6049, by reducing the size of the gas preheat chamber in the diffuser cap. This modified design is shown as Figure 165. Reducing the size of the internal chamber also probably reduced the cap temperature since all surfaces were moved closer to the nozzle which acts as a heat sink. The gas feed in this run (6051) was terminated after 1-1/4 hours due to plugging. Post-run examination of the deposition assembly and diffuser cap indicated that the diffuser cap had not been seated properly when installed. Figure 166 is a cross-section of the cap. The top of the nozzle was at the base of the soot deposit but should have been at the point where the i.d. changes diameter. The gas did not have the reduced preheat planned for, nor was the cap temperature reduced as a result of the improper installation of this cap.

Run 6052 was made with the same modified cap as 6051 but special precautions were taken to insure that the cap was properly installed. This run was completed as scheduled and post-run examination indicated that all cap passages were clear. Figure 167 is an end view of the cap after deposition. Figure 168 is the profile of the deposit, and Figure 169 the nose region cross-section. Figure 168 indicated that the deposition profile, when boron trichloride was added, was modified as compared to the unalloyed profile. The maximum deposition rate occurred at the same position along the axis but was 40 percent greater than for the unalloyed deposit. Figure 169 indicated that there were three different types of material in the nose region. The material on the right appeared to be of normal density and microstructure, whereas the material in the nose was highly regenerative and contained soot. The material on the left

wall was similar to that on the right with respect to delaminations but appeared to be more regenerative. A misaligned nozzle may have been responsible for this difference.

The deposition conditions for the next run (4064) were similar to 6052 except that the diffuser cap position was moved one inch closer to the nose so the effect of cap position could be evaluated. The run was completed without difficulty and the side and end views of the diffuser cap are shown as Figures 170 and 171, respectively. Figure 172 is the profile of the deposit and Figure 173 a cross-section of the nose region. The profile indicated that the one inch forward change in the diffuser cap position increased the maximum deposition rate slightly but did not shift the position of the maximum rate. Figure 173 indicated that the quality of the deposit in the immediate nose area deteriorated. The material in this area appeared to have been formed by intermittent deposition of soot and normal pyrolytic graphite.

Run 4065 was deposited at conditions similar to 4064 and 6052 except that, in this case, the diffuser cap position was withdrawn one inch with respect to its position in 6052. No difficulties were experienced in completing the run as planned. The diffuser cap after deposition was similar in all respects to the cap used in 4064, shown as Figure 171. The profile of this deposit is shown in Figure 174, and indicated that its characteristics were just about the same as 6052. Figure 175 is a cross-section of the nose and shows evidence of sooting just as the two previous runs did.

The final run (4066) was deposited using deposition conditions similar to those in the earlier runs but with a modified nozzle cap design. This cap is shown in Figure 176. It was similar to the 304013 cap in that it had the reduced preheat chamber size but was different to the extent that a different hole pattern was used. This discharge pattern reduced the flow cross-section by 80%. The gas flow was terminated after 10 minutes due to a blocked gas feed system. Postrun examination indicated that the nozzle cap was plugged with pyrolytic coke. Indications were that the reduced exit cross-section of the cap caused a pressure increase in the preheat chamber between the top of the nozzle and the cap--resulting in the formation of excessive soot.

Profiles from these runs are compared with one from Task 3.2.1.3 in Figure 177. The peak in the deposition thickness curves did not occur at the zero position, as desired.

SUMMARY AND CONCLUSIONS

The use of boron trichloride with turbulent nozzles proved difficult because of the increased sooting tendency. Graphite diffuser caps must be designed with care or clogging will occur as a result of the formation of a sooty compact or deposit within the cap.

From these studies, it was concluded that a nozzle cap which generally increased the Reynolds number in the nose region did change the profile, broadening the region in which high deposition rates were experienced. This broader zone, however, was displaced back from the nose. Such a displaced peak deposition rate is undesirable. Nozzle caps appear to be useful but only if unalloyed deposits are to be prepared.

RECOMMENDATIONS

Unless further development work were carried out, the use of turbulent nozzle caps does not appear to offer a better alternative for the production of boron-alloyed pyrolytic graphite nose cones. Normal inlet nozzles are recommended.

C. DEPOSITION FROM ACETYLENE (Task 3.4.2.3)

According to the Work Statement, "(a) Chemical techniques for modifying deposit thickness profile will be evaluated for nose tips using acetylene as hydrocarbon gas for comparison to results for methane; and (b) Acetylene will also be used as the hydrocarbon gas, with boron trichloride for producing boron-alloyed pyrolytic graphite with modified deposit thickness profiles."

BACKGROUND FOR TASK 3.4.2.3a

When methane or other simple alkanes are used as the hydrocarbon gas in the deposition of pyrolytic graphite, unsaturated and aromatic hydrocarbons are produced during the course of the reactions that lead to carbon deposition. If unsaturated and aromatic hydrocarbons were used directly, under conditions where heavy sooting were prevented, then pyrolytic graphite might be deposited using less thermal energy.

Some preliminary investigations had been carried out, using acetylene as a carbon source gas, prior to these studies. Dr. R.J. Diefendorf (RPI) studied the deposition kinetics of the pyrolytic graphite process using actylene as a source gas while he was a staff member at the General Electric Research Laboratory. Discussions were held with Dr. Diefendorf, and his results were factored into the test matrix selected for these studies by General Electric Company, Re-Entry Systems Department.

This task was divided into two phases. The first phase was designed to investigate the effects of (1) the methane/acetylene ratio, (2) the deposition pressure and (3) the deposition temperature. The second phase used the results of Phase I to deposit nose cones.

EXPERIMENTAL CONDITIONS SELECTED--PHASE 1

The experiments in this phase were:

1) Methane/acetylene Ratio: 3 to 1

2) Methane/Acetylene Ratio: 1 to 1
3) Methane/Acetylene Ratio: 1 to 3
4) Deposition Temperature Series: 1750°C, 1925°C, 2100°C

To study these effects, 2-1/2 inch diameter tubes, 9 inches long, were deposited. In the first three types, the effects of deposition pressures of 2, 4 and 8 mm Hg were investigated and in the fourth type, the methane/acetylene ratio and the deposition pressure were held constant while only the deposition temperature was varied. Table XXXIX shows the process conditions.

A deposition assembly was designed at GE-RSD to insure a uniform deposit thickness profile along the length of the tube. Figure 178 is a schematic diagram of this setup. This design proved to be very effective.

RESULTS--PHASE 1

The results of Phase 1 are shown in Table XL and illustrated in Figures 179 through 198. The deposits obtained in these studies were for the most part of good quality. As shown in Table XL, the density in almost every experiment conducted at 2100°C was 2.16-2.18 gm/cm^3, which is representative of good unalloyed pyrolytic graphite. Two of the experiments did, however, have a somewhat lower density (2-43) and (1-41). No valid explanation could be found for the low density in experiment 2-43 (methane/acetylene ratio--3, pressure--4 mm Hg), but the low density may have been the result of some processing malfunction. Experiment 1-41 (methane/acetylene--1/3, pressure--8 mm Hg) had a normal density at the bottom (inlet) of the tube but a low density at the top (outlet) of the tube. The low density at the top of the tube was attributed to the extremely high deposition rate attained at this location (30 mils/hour).

The deposition rate increased with an increase in deposition pressure in all cases. In general, when identical conditions were used, the deposition rate increased proportional to the square root of the deposition pressure.

Density depends on temperature in the range used in these experiments. When the deposition temperature was lowered from 2100 to 1925°C the density decreased from $\sim$ 2.17 to $\sim$ 1.98 gm/cm^3. A further reduction in deposition temperature to 1750°C decreased the density to $\sim$ 1.1 gm/cm^3.

The deposit thickness profiles obtained in these experiments are shown in Figures 179, 180, 181 and 182. Thickness was quite uniform along the length of the tubes. The deposit thickness profiles for the 3 to 1 methane/acetylene ratio were very uniform at 2 and 4 mm Hg pressure, but decreased slightly along the length of the tube at 8 mm Hg deposition pressure, as seen in Figure 179. For a 1 to 1 methane to acetylene ratio the deposit thickness profiles were uniform at all three pressures, as seen in Figure 180. At a 1 to 3

methane to acetylene ratio, the deposit thickness slightly increased along the length of the cone at 2 and 4 mm Hg pressure and had an abrupt change at the center section of the tube deposited at 8 mm Hg pressure. It is interesting to note that at a 3 to 1 methane to acetylene ratio, the deposit thickness decreased along the length of the tube, and at a 1 to 3 methane to acetylene ratio, the deposit thickness increased along the length. The difference in the deposit profiles obtained at the different methane/acetylene ratios could be the result of the thermal conductivities of the gases. Methane has a higher thermal conductivity than acetylene and might be heated more readily and thus decompose more quickly.

Figure 181 shows the effect of deposition temperature on deposit thickness profile. The 1925°C deposition temperature experiment had an anomalous behavior for which no explanation could be devised. The density of the deposits at 1925° and 1750°C were too low for use as a material for aerospace hardware.

A summary of the effects of deposition pressure and methane/acetylene ratio on deposition rate, is shown in Figure 183. Notice that rate increases with both deposition pressure and acetylene addition.

Figures 184 and 194 are photographs of the deposits from these experiments. The mandrel material used for these experiments was as-machined Grade O, a material available at GE-RSD at the time. Since the object of Phase I was to establish deposition kinetics and not to evaluate the properties of the cylinders produced, it was not considered necessary to use much more expensive, treated mandrels. The effects of the "as-machined" surfaces of the mandrels on the appearance of the deposit is evident in these photographs. The nodules in some of the cylinders were also due to the mandrel surfaces. Such nodules could be eliminated if aerospace hardware were deposited by using the practices established in the mandrel-related studies of this contract.

Figure 192 shows the appearance of the cylinder made at 8 mm Hg pressure and at a methane/acetylene ratio of 1/3. The appearance of this material (deposition rate 30 mils/hour) indicates that these process conditions are about the upper limit in pressure and acetylene concentration which can be used to deposit acceptable material.

The microstructure of each tube was examined and a photomicrograph of each part was made. Figure 195 shows the microstructure of parts made at a methane/acetylene ratio of 3. The microstructure of 1-42 (2 mm Hg) and 1-39 (8 mm Hg) was typical for unalloyed pyrolytic graphite except the grain size was somewhat larger than normal for the 1-42 experiment. The microstructure of Experiment 2-43 (4 mm Hg) varied along the length of the tube as illustrated in the figure. The microstructure and low density of this part indicates some process fluctuation occurred during the deposition cycle.

Figure 196 illustrates the microstructures obtained at methane/acetylene ratio of 1 and at 2, 4, 8 mm Hg deposition pressure. All three structures were normal.

Figure 197 illustrates the microstructures obtained at a methane/acetylene ratio of 1/3 and a deposition pressure of 2, 4 and 8 mm Hg. The microstructures at 2 and 4 mm Hg pressure were normal; however, at 8 mm Hg deposition pressure, the structure varied along the length of the part. It was large grained at the bottom (inlet) of the tube but was fine grained at the top.

The effect of deposition temperature on microstructure is illustrated in Figure 198. At 2100°C, the structure was normal, at 1925°C the structure was large grained, and at 1750°C the structure had a "washed-out" appearance.

SUMMARY AND CONCLUSIONS--PHASE 1

The results of Phase 1 may be summarized as follows:

1. The deposition rate increased with the addition of acetylene in the range of methane/acetylene ratios studied (3/1 to 1/3).

2. The deposition rate increased with deposition pressure for the range investigated (2 to 8 mm Hg).

3. The densities obtained were normal for all deposits made at 2100°C except for the experiment conducted at 8 mm Hg pressure and at a methane/acetylene ratio of 1/3.

4. Deposition temperature greater than 1925°C was required to obtain good density.

5. The structure of the material generally appeared normal in all experiments that had normal densities.

EXPERIMENTAL CONDITIONS SELECTED--PHASE 2

Three nose cones were fabricated in this phase of the task. A review of Phase 1 results showed that the most favorable methane/acetylene ratio was 1/3 and the deposition pressure was selected at 4.0 mm Hg. The borderline results obtained at a deposition pressure of 8 mm Hg and at the high acetylene content did not appear favorable for this phase of the study. The other processing conditions were selected from results obtained in previous experiments. The process conditions are summarized in Table XLI.

RESULTS--PHASE 2

The results of Phase 2 of this task are listed in Table XLII, and illustrated in Figures 199 through 205.

The deposition thickness profiles for the first three nose cones are illustrated in Figures 199, 200 and 201.

The growth pattern achieved in the first experiment (1-43) was very good. The nose tip thickness was 0.96" in only 30 hours and the minimum wall thickness was 0.17. The wall thickness was very uniform and the growth pattern was good. This part had a somewhat lower density than was anticipated but the cause and extent of the low density were not determined. This cone did not contain any large delaminations but did contain more delaminations than a normal boron-alloyed pyrolytic graphite nose cone. Figure 203 is a photograph of this cone.

Figure 200 is a radiographic positive of the second nose cone. During this experiment, an electric storm occurred and caused a power outage for about 40 minutes. As the objective of this experiment was to study deposit thickness growth patterns and was not to deposit a usable piece of hardware, the experiment was continued. The loss of power and the subsequent cooling of the furnace caused destructive residual stresses to develop, which caused the part to badly spall as shown in Figure 204. The growth profile, delamination pattern and size, and the density were about the same as the first nose cone. The only difference in deposition conditions were (1) the hydrogen gas was omitted from the selected processing conditions, and (2) the inlet nozzle o.d. was reduced to 13/16" from 1".

In the third experiment (1-48) the same conditions were used as in experiment 1 (1-43) except the deposition pressure was reduced to 3.0 mm Hg. The growth pattern is shown in Table XLII and in Figure 201. Decreasing the deposition pressure 1 mm Hg reduced the deposition in the tip to 1/3 of the previous rate and the skirt deposition rate to 1/2 of the previous rate. Figure 205 is a photograph of the cone produced in the third experiment.

SUMMARY AND CONCLUSIONS--PHASE 2

Figure 202 summarizes the deposit thickness profiles. These results show that the hydrogen gas used in experiment 1-43 but not in 2-46 had little effect on deposition rate; however, the results for experiment 1-48 vividly illustrate the effect of deposition pressure on deposition rate in nose cone tips. The results were summarized by GE-RSD as follows:

1. Acetylene can be used as a carbon source to give good growth patterns in nose cones.

2. Deposition pressures of 4 mm Hg or higher were required to give reasonable deposition rates.

3. The cones fabricated in this phase had a lower density and more delaminations than was expected.

BACKGROUND FOR TASK 3.4.2.3b

The results from the first parts of Task 3.4.2.3 were not good enough to provide a better process for making nose cones than the usual graded, boron-alloyed pyrolytic graphite process; therefore, the revised Work Statement included this subtask b to extend the studies with acetylene to deposition of BPG nose cones. This subtask also called for deposition of unalloyed pyrolytic graphite nose cones at three temperatures to determine the effect, if any, this variable had on deposition thickness profile and deposit density.

EXPERIMENTAL CONDITIONS SELECTED

Three cones were deposited using acetylene as the carbon source. The cones were unalloyed deposits made at identical conditions except for temperature. The selected deposition temperatures were 2000°C, 1900°C, and 1800°C. The cones were evaluated on the basis of deposition profile, delamination patterns and unit cell height C_o as measured in the solid nose-tip region. The unit cell height measurement would provide some indication of anisotropy, assuming that lower anistropies would correspond with higher C_o values.

Three additional runs were to be made in which the problems associated with fabricating a boron-alloyed deposit were to be investigated.

Table XLIII is a summary of the deposition conditions. The acetylene used as the source gas was commercial grade material, primarily intended for industrial heating application. A typical analysis of this gas is (Ref. 69):

Component	Volume Percent
Acetylene	99.7
Phosphine	50 ppm
Hydrogen Sulphide	25 ppm
Oxygen	.05
Arsine	2 ppm
Moisture	-50°F Dew Point

In addition, acetone vapors are present in the acetylene since the packaging technique is to dissolve the acetylene in acetone within the cylinder to reduce shock sensitivity. Due to this shock sensitivity, acetylene is not normally available purified or commercial grade in other than acetone-filled cylinders. As a result of the acetone solvent used, acetylene withdrawn from the cylinder contains some acetone vapor. The concentration of acetone vapor depends on the amount of acetylene in the cylinder at time of usage and on the rate of withdrawal.

RESULTS

The deposition profile of the first acetylene deposit of unalloyed material (5051) is shown as Figure 206. Figure 207 is a radiograph of the as-deposited part. The nose thickness of 1.3 inches was that judged from the exposure on the x-ray film as normal density material. This and the wall thickness represented unusually high deposition rates for unalloyed pyrolytic graphite. It appeared that the last material deposited was of very poor quality, as indicated by the radiograph and by the low "last-deposit" density shown in Table XLIV. This change in characteristics towards the end of the deposition period is attributed to changes in the exit flow path which were caused by the nozzle growth (also shown in Figure 207).

The other two unalloyed deposits from acetylene were made later. These were runs 5058 at 3640°F, and 5060 at 3450°F. The deposit thickness profiles are shown in Figures 208 and 210. The nose thickness decreased with decreasing deposition temperature, as shown by a comparison of these two figures with Figure 206. Of the three unalloyed deposits, the best nose cone could be produced from the process used for 5058, as judged from Figures 207, 209 and 211. All these deposits were relatively disordered (not very anistropic) as seen by the high C_o values in Table XLIV.

The major problem with these runs was the deposition of large sooty compacts on the injector nozzle surfaces. Such deposits interfere with the gas flows and give non-reproducible effects. These growths are not as great a problem in deposits from methane.

Even greater problems were found in the attempts to produce boron-alloyed deposits. Run 5052 was the first of these. As indicated in Table XLIII, the run time was only 10 minutes. A post-run examination of the deposition assembly indicated a very thin coating of deposit which in every respect appeared normal. Examination of the gas feed line and injector revealed a solid residual clogging the line immediately downstream from a manifold where all the reactant gases were mixed. In this run the gases were: natural gas, cylinder acetylene and boron trichloride. Several subsequent attempts were made to mix the reactants, but the feed line plugged after very short term operation in each case. During the trial runs, careful attention was paid to insure a leak-tight system since boron oxide, produced by the reaction of boron trichloride and moist air, could cause gas line plugging in a system which had a leak. There was no evidence of boron oxide in any of the residues removed from the lines. Further investigation by experiments with acetone and boron trichloride indicated that a solid forms rapidly when the two vapors come in contact at room temperature. Apparently, a solid coordination complex forms at the oxygen in ketones with boron trichloride. Such a reaction had been reported with trifluorides. From these experiments, it was concluded that the acetone carryover from the storage cylinder was causing the feed line plugging. Thus, boron-alloyed pyrolytic graphite deposits cannot be made using boron trichloride and

cylinder acetylene without removing the acetone from the acetylene.

It is possible to reduce the vapor pressure of the acetone significantly by liquefying it in a dry-ice/acetone trap. Freezing the acetone out was not considered as acetone freezes at -93.5°C, lower than the -84°C freezing temperature of acetylene. It was also not certain that liquefying the acetone with available equipment would be efficient enough to eliminate the acetone--boron trichloride reaction.

Instead of pursuing the acetylene problem any further in the runs which were made to be boron alloyed, an alternate carbon source gas was selected. MAPP is the trade name of a gas developed by The Dow Chemical Company for industrial heating purposes. MAPP gas is a stabilized mixture of 68-70 percent methyl acetylene-propadiene and the balance propylene and other paraffinic and olefinic C_3 and C_4 hydrocarbons. (Refs. 70 and 71). MAPP gas was selected as an alternate to acetylene for the boron alloyed deposits since the methyl-acetylene with its triple bond would act chemically like acetylene, and MAPP gas is not shock sensitive and, therefore, need not be dissolved in acetone for handling. Some preliminary studies with a gas-manifold assembly were made to verify that boron trichloride and MAPP were compatible. These tests seemed to indicate that they were.

A base-line run (5053) of unalloyed material was made from MAPP gas to evaluate the parameters selected for deposition. This run was considered satisfactory and a deposit with MAPP and boron trichloride was made (5054). As Table XLIII indicates, this run was terminated after four hours. The premature termination was a result of plugging somewhere in the gas feed system. A second attempt was made (5055) and was also terminated due to a gas feed line plug. The gas distribution system was disassembled and a heavy black condensate was blocking the injector line. Apparently this condensate went unnoticed in the preliminary tests. These results indicate that even without acetone, there is a reaction between boron trichloride and unsaturated hydrocarbons such as acetylene and MAPP.

The deposition thickness profiles for runs 5053 and 5054 are shown in Figures 212 and 214. The boron-alloyed profile (5054) appeared to be promising but techniques would be required for preventing inlet line clogging before this process could be used. Radiographs are shown in Figures 213 and 215 for the same two cones.

SUMMARY AND CONCLUSIONS--TASK 3.4.2.3b

The work on unalloyed pyrolytic graphite nose cones deposited from acetylene can be summarized as follows:

1. Deposition rates of unalloyed deposits using acetylene as a carbon source were similar to alloyed deposits using boron trichloride and methane as the carbon source.

2. The material quality of acetylene deposits was similar to those deposited using methane.

3. The deposition profile of acetylene-deposited cones was similar to boron trichloride-methane deposited cones.

4. Deposition temperatures between 1800°C and 2000°C appeared to give similar results.

5. Deposition thickness profile reproducibility was poor due to effects of large growths formed on the injector during deposition.

The work on boron-alloyed pyrolytic graphite from acetylene and boron trichloride revealed a number of practical problems:

A successful boron-alloyed deposit was not made. Initial attempts with acetylene were not successful due to the acetone content of clylinder acetylene and an undesirable reaction between boron trichloride and this acetone.

Stabilized methyl acetylene-propadiene, containing an unsaturated hydrocarbon similar to acetylene, was also used as a carbon source gas. The formation of a heavy condensate at room temperature when this gas was mixed with boron trichloride prevented any useful deposits from being made. This room temperature reaction appeared to be a reaction between the unsaturated hydrocarbon and boron trichloride.

These difficulties indicated that making a boron-alloyed deposit using an unsaturated hydrocarbon such as acetylene presented problems which were beyond the scope of this task. No further attempts at making a boron-alloyed deposit were made.

RECOMMENDATIONS

Deposition from acetylene is feasible and can produce material of good quality; however, unwanted side reactions with BCl_3 prevent its use for production of boron-alloyed pyrolytic graphite. Even in the unalloyed case, there are problems with large sooty growths and compacts on the surface of water-cooled inlet nozzles. Such growths interfere with gas flows in the reflex flow systems used for nose cone fabrication.

For these reasons, the use of acetylene is not recommended as an alternative to the use of methane in aerospace nose cone production.

D. INTERRUPTED DEPOSITION (Task 3.3.6)

According to the Work Statement, "Deposition will be interrupted at calculated intervals for control of delamination patterns."

BACKGROUND

Boron-alloyed pyrolytic graphite in configurations where the thickness-of-deposit to radius-of-curvature ratio (t/r) exceeds about 0.08 has a tendency to build up destructive residual stresses during cool-down from the deposition temperature (about 3850°F) to room temperature. These residual stresses are produced by the thermal expansion anisotropy of pyrolytic graphite. The thermal expansion coefficient through-the-deposit thickness is about 14.0×10^{-6} in/in°F and in the circumferential direction of a shaped component the thermal expansion is 0.6×10^{-6} in/in°F. When a constrained shape such as a frustum cools from deposition temperature, the material wants to shrink through the deposit thickness but is restrained by the shape of the part and the low thermal shrinkage which occurs in the circumferential direction. The result is that stresses are produced in the part. If these residual stresses exceed the material strength, the fabricated component will crack or randomly delaminate, thus relieving the residual stresses but rendering the part useless. However, if the finished structure consists of a series of concentric rings or frustums, each of which has a t/r of less than 0.05, the residual stress in the total part should not exceed the material strength, since the stresses in each ring are not additive, and the component should be of good quality. Therefore, a finished structure consisting of a series of concentric frustums might be produced by interrupting the process during the fabrication cycle at predetermined material thicknesses. The interruption would cause a material separation and thus control both the delamination pattern and the residual stresses in the part.

EXPERIMENTAL CONDITIONS SELECTED

An experimental investigation was conducted to evolve the technology required to fabricate boron-alloyed pyrolytic graphite frustums having a t/r of at least 0.10, and yet free of cracks and random delaminations. A total of five (5) frustums, 3 inches o.d. at the small end and 4.5 inches o.d. at the large end (see Figure 216) were fabricated using an interrupted deposition technique. Table XLV lists the program plan employed in this task.

A preliminary part was fabricated to establish processing conditions such as deposition rate, gas flow, methane/hydrogen ratio, etc. This part (Run 1-77) established deposition rates for the selected processing conditions employed and these results were then used to select the processing conditions for the remainder of this task. The desired concentric rings or frustums for this part were achieved by interrupting the process for 30-minute intervals at predetermined material thicknesses to insure the formation of complete delaminations. Part 1-77 was evaluated and the following preliminary conclusions were made:

1. The design of the deposition chamber setup was acceptable.

2. The processing conditions selected (interruption technique) were adequate.

3. The deposition rate was greater than planned. Deposition time would have to be adjusted for future parts.

4. The selected methane/hydrogen ratio produced a good deposit thickness profile.

The five planned frustums were then fabricated, using the process matrix listed in Table XLVI, and the furnace setup illustrated in Figure 217. The results of previously deposited frustums were analyzed to select the most suitable processing parameters for each part.

A 13/16" o.d. stainless steel water-cooled gas injector nozzle with 0.069 inch orifice was used throughout this task. The nozzle orifice was placed 2-1/2 inches below the baffle as is illustrated in the furnace setup (Figure 217). The mandrel material used for the preliminary experiment (Run No. 1-77) and the first planned experiment (Run No. 2-88) was grade H. The last experiment (Run No. 2-108) used grade D graphite. Grade A graphite was used in the other three experiments: Run No. 2-90, Run No. 1-82, and Run No. 2-105.

RESULTS

The results of these processing experiments were evaluated to determine (1) residual strain in each concentric ring and in the total part, (2) density of each ring, (3) deposit thickness profile of each ring, and (4) microstructural analyses of the material through the deposit thickness. Table XLVII summarizes the results obtained and Table XLVIII shows the average deposit thickness profiles obtained for each part.

For convenience, the experiements are discussed separately.

Experiment No. 1-77. The first experiment was designed to yield five (5) equal thickness, concentric rings with a total deposit thickness of 0.150", which would result in a part t/r of 0.10. The five rings were separated by distinct delaminations as illustrated in Figure 218, and the average thickness for the rings was 41 mils. Figure 219 illustrates the planned and obtained thicknesses of each ring and the total deposition profile along the length of the part. The deposit thickness was greater than planned, which gave a maximum t/r for the part of 0.15 at the small end of the frustum. With this high t/r, destructive residual stresses developed on cool-down which resulted in an axial crack on the inner surface and in an interdelamination crack as illustrated in Figure 218. This experiment was planned to yield only processing information and no special precautions were taken during the separation of the frustum from its furnace supports. The axial crack on the inner surface

of the frustum formed during the removal of the furnace support parts from the frustum. Some spallation occurred on the outer surface of this frustum (Figure 218); however, this was to be expected since a porous grade graphite was used for the mandrel of this preliminary experiment.

The average density of the frustum material was high (about 2.23 gm/cc) which indicates that it was good boron-alloyed PG material. The results of all tests performed on this part are listed in Table XLVII. Figure 220 illustrates the microstructure of the material through the deposit thickness from both the small and large end of the frustum. This microstructure appears to be mainly substrate-nucleated. However, some additional nucleation also took place at each delamination location.

Experiment No. 2-88. Experiment 2-88 was designed to produce five (5) concentric frustum shells, each shell having a deposit thickness of about 30 mils and the total part having a thickness of 0.150 inches. The deposition rate established in Run 1-77 was used to plan this experiment.

The results of this run were considered good. There were five (5) concentric rings at the top and bottom of the frustum separated by distinct delaminations as illustrated (Figure 221) and the average thickness for the rings was 26 mils. Figure 222 illustrates the planned and obtained thicknesses of each ring and the total thickness profile for the part. The maximum t/r for any one ring was 0.02 and the maximum t/r for the part was 0.10 at the small end of the frustum.

This part was free of axial cracks, and the outer surface was free of spallation. The center ring at the large end of the frustum contained a crack as shown in Figure 221. This crack was attributed to incomplete material separation at the planned delamination site.

The density of this material was also about 2.23 gm/cc. The microstructure illustrated in Figure 223 appears to be basically substrate-nucleated but it is intermixed with new nucleation starting at each delamination.

A 1" ring was removed from both ends of the frustum and residual strain measurements were made in concentric rings. These results are listed in Table XLVII. It was interesting to note that the maximum hoop strain at the large end of the part occurred in the outer shell while the maximum strain at the small end of the part was in the inner rings.

Experiment No. 2-90. The mandrel material for this experiment was ATJ. The experiment was designed to produce three equal concentric rings, each 50 mils thick (see Table XLV). The results of this experiment were considered excellent. Three concentric frustum shells were produced which only varied in thickness in the axial direction between 47 to 54 mils and the average thickness for each of the three rings was 50 mils.

Figure 224 illustrates the overall appearance of this part. The outer surface was very good and the desired three shells were produced; however, it should be noted that an interdelamination crack developed in the outer ring at the small end of the part. Figure 225 illustrates the planned and obtained thicknesses of the rings. The maximum t/r for any one ring was 0.04 and the maximum t/r for the whole part was 0.10 at the small end of the frustum.

The average density of the material was again about 2.23 gm/cc. The microstructure appeared to be basically substrate-nucleated intermixed with new nucleation starting at each delamination. This structure is illustrated in Figure 226.

No axial cracks developed in this part. Residual strain determinations were made in each concentric ring. These results are shown in Table XLVII. The results of the residual strain measurements were similar to those obtained for Experiment 2-88 in that the maximum strain was in the outer shell at the small end of the frustum.

Experiment No. 1-82. The mandrel material used in this experiment was grade A graphite. The process conditions were adjusted to produce only two concentric rings. Each ring was to be about 75 mils thick (see Table XLV). The results of this experiment were considered very good. Two concentric frustum shells were produced, each being 75 mils thick. Figure 227 illustrates the planned and obtained thicknesses of these two rings. The maximum t/r for either ring was 0.06 and the maximum t/r for the whole part was 0.11 at the small end of the frustum.

The part was free of axial cracks and the mandrel separation was good. Residual strain determinations made on each concentric ring are listed in Table XLVII. It is interesting to note that even though the t/r of each ring was greater than in the earlier experiments, the residual strain in these rings were lower. Figure 228 illustrates the clean outer surface of the frustum and the general appearance of the material at the small and large end of the frustum. One of the photographs in this figure shows that some additional fine localized random delaminations are present in the material at the large end of the frustum.

The average density of this material was also about 2.23 gm/cc. Figure 229 illustrates the microstructure through the deposit thickness. The structure is mainly substrate-nucleated with some additional nucleation starting at each new delamination.

Experiment No. 2-105. The separation between the concentric frustum shells in the first three frustums fabricated were not as complete as was desired; therefore, a modified interrupted deposition technique was used to fabricate this frustum. The mandrel material used to deposit this frustum was grade A graphite.

This experiment was designed to yield a part with two separations. The outer shell was to be 0.070", the middle shell 0.050", and the inner shell 0.030". Instead of just interrupting the process for 1/2 hour,

a modified procedure was used in which a flash coat of BPG was sandwiched between each concentric frustum shell.

The results of this run were considered excellent. Total separation was achieved between the layers forming completely separate concentric frustum shells as illustrated in Figure 230. Figure 231 shows the planned and obtained thicknesses of each ring. The part was free of axial cracks, interdelaminational cracks, and random delaminations. The maximum t/r for any one ring was 0.05 and the maximum t/r for the part was 0.11 at the small end of the frustum.

The density of this material was 2.23 gm/cc, and the average residual strain for the individual rings was about 0.035 in/in. Figure 332 illustrates the microstructure through the deposit thickness. The structure nucleated at the substrate and at each delamination. This indicates good non-continuity in material growth caused by the flash coat of BPG, which was sandwiched between each concentric frustum shell.

Experiment No. 2-108. The mandrel material used for this part was grade D graphite. The same modified interruption cycle was used as in the last previous experiment.

The separation between the concentric frustum shells was not as distinct as in the previous experiment. In addition, the deposit thickness for the part was much thicker than planned (see Figure 233). The maximum t/r for the part was 0.17. Since the concentric shells did not separate cleanly, the residual stresses were not properly relieved. Two axial cracks developed in the part during the cool-down cycle. Figure 234 shows photographs of this part illustrating the axial cracks and some of the random delaminations which also developed.

The average density of the material was about 2.23 gm/cc. The test results are summarized in Table XLVII. Figure 235 illustrates the microstructure through the deposit thickness. The increased deposition rate and the lack of complete separation at the delamination sites resulted in the failure of this part. Some processing difficulty undoubtedly occurred but none could be identified.

SUMMARY AND CONCLUSIONS

A total of six BPG frustums were fabricated, using the interrupted deposition technique. The finished structures consisted of a series of concentric frustums separated by pre-planned delaminations.

The procedure used to achieve the necessary material separation between the concentric rings of the first four frustums seemed adequate. However, separation between the shells was not as complete as was desired. A modified interruption procedure was, therefore, developed and used in the fabrication of the last two frustums. The results were excellent in the first of these two frustums. Total separation was achieved between the layers forming completely separate concentric frustum shells.

Although the maximum t/r for the individual rings was 0.05 and the maximum t/r for the part was 0.11, the frustum was free of axial and interdelaminational cracks. Complete separation between concentric shells was not achieved on the final frustum and the thicknesses of the individual shells was much greater than planned. The result was that the part developed two axial cracks during the cool-down cycle. However, since a different grade graphite (D) was used for the mandrel material and the deposit thickness was much greater than planned, it is believed that the processing parameters may have been erroneously recorded.

The results of this interrupted deposition study demonstrated the feasibility of producing shaped components of BPG with t/r's up to 0.10. This study also revealed that if stresses are not to be transferred between shells, complete separation is required. The original idea that complete delaminations could be achieved by merely shutting off the gas flow for 1/2 hour was shown to be inadequate. In this study, a modified interruption technique was developed and was employed with excellent results.

RECOMMENDATIONS

Interrupted deposition is recommended as a technique for depositing PG or BPG aerospace hardware with unusually high thicknesses for given radii of curvature, regardless of the shape or its complexity. Simply interrupting the gas flows will not produce satisfactory isolation between neighboring segments of a deposit. A very thin coating of BPG between neighboring deposits of PG produced the desired results. Although not experimentally proven, a thin coating of PG between neighboring deposits of BPG might also be useful.

Consideration should be given to subsequent bonding between the isolated segments before use as aerospace hardware and to the requirements for joining such a bonded piece to the remainder of the body.

E. ADDITIVE AND IMPURITY STUDIES (Task 3.2.1.2)

According to the Work Statement, "The effects of chemical additives will be evaluated with respect to catalysis in gas phase reactions. Process specifications will be made, indicating the need to add or remove chemical species in the gas streams."

This work was carried out on subcontract at Rennselaer Polytechnic Institute, Troy, New York, under the direction of Dr. R. J. Diefendorf, a former General Electric Company employee at the Research and Development Center, Schenectady, New York. The work was altered somewhat in nature to provide a part of the requirements for the degree Master of Science for Mr. Barry Butler. Portions of the total work were carried out on other funds subsequent to this subcontract.

BACKGROUND

The deposition of pyrolytic graphite from methane gas has been found to be enhanced by small additions of boron trichloride. Although the magnitude of this catalysis is known to vary with deposition conditions, experiments performed under apparently identical conditions have often given different results. A possible explanation is the presence of varying amounts of impurities in the feed stock gases. Because of the value of boron trichloride in altering deposition profiles and in improving mechanical properties, this task was carried out to determine the effect of impurities on the boron trichloride-catalyzed deposition of pyrolytic graphite.

The deposition of pyrolytic graphite is a complicated process, where a number of competing reactions are occurring simultaneously. (Refs. 72 and 73). Any change in processing conditions will alter the relative importance of these reactions and a different pyrolytic graphite will be deposited (Refs. 74, 75, 76). A description of the system is also compounded by the large number of variables (Ref. 74). These include temperature, pressure, flow rate, geometry and composition. In the present study, there were an additional ten parameters necessary to describe composition. However, by holding temperature, flow and geometry constant and showing that the effects of nitrogen, argon, and other relatively inert gases had little or no first-order effect, the number of experiments was decreased to 2^5, or 32.

For this work, a new process monitoring technique was devised. It was based on the assumption that increases in deposition rate at the mandrel wall would be associated with an increased deposition rate on gas-phase soot particles. The technique was to measure the growth of the soot particles instead of the deposition at the wall (Refs. 77 and 78). This was done by monitoring the light emitted by the incandescent soot suspended in the gas phase.

This technique gave very reproducible results, so that in a short time a large number of data points could be obtained; hence, more interactions could be determined with good accuracy. The technique, along with the other simplifying factors, allowed the gas composition variables to be studied in greater detail.

EXPERIMENTAL CONDITIONS SELECTED

The apparatus necessary to carry out the described work consisted of gases, regulators, flow meters, a high temperature resistance heated furnace (Ref. 79) vacuum valves, and a high volume, rotary vacuum pump. The whole system shown in Figure 236 was designed to feed gases of various controlled compositions through a high temperature chamber, while being able to change the pressure and observe the effect on the sooting tendency. The apparatus was designed so that the flow rate, temperature and geometry could also be changed; however, they were

held constant during this work.

The gaseous components were purchased at very high purity levels from a commercial supplier. They were stored in their cylinders and fed through regulators at 5 psig. into calibrated flow meters. Then the gases were passed into a low pressure manifold (0.1-15 mm Hg) depending on the furnace pressure. The manifold had multiple inlet valves, so that only the desired gases were mixed.

When the gases left the manifold mixed, they flowed into the furnace, which was a resistance-heated cylinder approximately 8 inches long and 1 inch diameter. The furnace was kept at low pressure and the temperature was read with an optical pyrometer. The reacted gas passed out of the furnace through a large pressure regulating valve, and then through the vacuum pump.

A photo-electronic device was constructed which would have a much higher sensitivity than the human eye, and which would also make the sooting point reproducible as shown in Figure 237. The device consisted of a photoresistor, which was aimed down the axis of the furnace cylinder. The collimated optical system was designed such that light from the heated deposition surface would not impinge directly on the photoresistor. This resistor was used as one arm of an electrical bridge circuit. The bridge was first balanced at the temperature of the experiment, and I_o was noted with the gas of proper composition passing through at a given flow rate. The pressure was then increased rapidly at a rate of 30 mm/min. by partially closing the valve 1 (see Figure 236) and any bridge unbalance was determined by galvanometer G, and recorded at each mm pressure. There was one complicating factor which had to be overcome before reproducibility could be attained. The temperature and hence I_o would decrease rapidly as the pressure increased, because of increased thermal losses in the furnace. To counteract this, a precisely controlled power increase was applied to the furnace when the pressure was increased so that I_o remained more nearly constant. This was rechecked at the end of each experiment by rapidly lowering the pressure from 30 mm to 1 mm and recording I_o, to see if the temperature had changed. Unless I_o showed temperature constant within $\pm$ 2° C the data were disregarded, and the run was repeated. This technique yielded highly reproducible data. The control data varied very little at constant T compared to the variations caused by composition and flow rate. Hence, the temperature variable was eliminated.

At 1500°C all of the data were plotted as I versus P^3 as shown in Figure 238. A theoretical justification for this type of plot will be given in a paper to be published by Diefendorf and Butler. This plot yields a curve with two portions. The first portion is an indication of background scatter and of how stable the temperature is inside the furnace. The second portion is a straight line, with a slope that is directly proportional to the deposition rate. As the temperature is increased (or the flow rate decreased) the slope increases. However, temperature and flow were held very constant, so their effect on the data was very small. Any difference in slope, therefore, reflects changes in the

surface reaction rate constant.

A temperature correction was used to correct the I values, to I_o at 1500°C. These corrections were necessary to correct for small drifts in furnace temperature. Wien's Law was used to make the corrections.

Once the data had been corrected, the effects of the composition of the gas were determined. It might be added that while the results are reasonably valid with no corrections, the corrections decrease the standard deviation by correcting for small temperature drifts.

The sooting experiments were designed around the use of "ultra pure" methane which could be doped with various impurities to simulate natural gas. The composition of the natural gas delivered by Niagara Mohawk Power Corporation is shown in Table XLIX. Direct comparisons of similar data from other gas fields showed relatively minor differences in composition of the delivered gas over a period of six years. There was a seasonal variation in gas composition, however. The composition of the synthesized natural gas is shown in Table L. The impurity levels for this task were arbitrarily selected at about twice the values measured in natural gas. Then, any chance variation in natural gas composition would still be below the impurity level of the synthesized gas. Although the higher hydrocarbons were absent from the synthesized natural gas mixture, this synthesis gas behaved similarly to natural gas in comparison experiments.

RESULTS

A matrix of 32 sets of gas composition was investigated to determine which gases or combination of gases showed impurity effects. Typical results are shown in Figure 238. A positive effect is shown by an increase in slope. Since flow rate and temperature also alter the slopes, both were held constant in these experiments.

The results of these experiments are summarized in Table LI. The calculated values were computed from terms obtained by regression analysis, and the following equation:

$$1 = I_o\, k_o\, f_a\, f_b\, f_{ab}\, f_d\, f_{ad}\, f_{bd}\, f_e\, f_{ae}\, p^3$$

where I_o is the light emitted from a unit area of soot particles at a given temperature.

k_o = 1.65 is proportional to the base rate of deposition of pure methane on soot.

f_a = 1.65 is the factor for increased rate when ethane is present.

f_b = 1.26 is the factor for propane.

f_{ab} = 0.77 is the factor for the interaction of ethane and propane.

f_d = 0.69 is the factor for hydrogen.

f_{ad} = 1.16 is the factor for the interaction of hydrogen and ethane.

f_{bd} = 1.14 is the factor for the interaction of hydrogen and propane.

f_e = 2.12 is the factor for boron trichloride.

f_{ae} = 1.17 is the factor for the interaction of boron trichloride and ethane.

In the calculations, the values of the factors given above for unit concentration were used whenever the particular gases were present. The factors were set at unity for any gases which were not present in the flow for a given experiment. The agreement between the calculated and experimental values of the slopes is good considering the sensitivity to temperature and that a linear analysis was used. Even assuming a zero activation energy for the chemical reactions, a ten degree variation, run to run, would make a seven percent error in slope because of emitted light intensity variation.

There was some question whether the small observed shifts with CO_2 could be a simple dilution effect of the methane. Several runs with argon were made. Concentrations of argon below 25 volume percent showed no observable change in the sooting characteristics of methane. Hence the small changes in methane concentration in the different mixtures cannot be important.

Since the heavier hydrocarbons and boron trichloride appeared to give significant increases in rate of soot growth, a series of four deposition runs were made to see if corresponding increases in wall deposition rates would be observed. The conditions were 1500°C, 15 mm pressure, 1.9 cfh total flow, and 1 inch diameter tubes. The four compositions studied were: (See Table LII)

1) Ultra pure methane.

2) Ultra pure methane and ethane.

3) Ultra pure methane and boron trichloride.

4) Ultra pure methane, ethane and boron trichloride.

The one exception from an otherwise standard deposition run was that four 0.004" diameter carbon filaments were placed across the diameter of each tube at four points along the length. These filaments were used as a measure of wall deposition rate. The filaments provided several advantages because of their fine diameter and placement in the gas stream. The deposition rate on the fine diameter filament with a cross-flowing gas will be close to the surface reaction rate, while the deposition rate at the wall would be largely diffusion controlled.

Secondly, a thinner deposit thickness could be measured which is important at 1500°C, where deposition rates can be very low. Finally, the filament is out in the gas stream where the sooting measurements were made.

The results of these runs are shown in Figure 239, for the four filaments positioned near the tops of the tubes. The other filament positions showed similar effects but with less total buildup. The observed deposition rates on the filaments were in the order which would be predicted from the light intensity values.

SUMMARY AND CONCLUSIONS

Four primary effects were observed in the experiments. The addition of boron trichloride and the higher hydrocarbons, either ethane or propane, to methane increased the deposition rate. Hydrogen was observed to inhibit the deposition rate. Frazee and Anderson (Ref. 78) observed similar effects at lower temperatures. In addition, four second-order effects were found to be significant. Three of these interactions appear because the higher hydrocarbons show greater responses with other impurity gases than does methane. Hence, hydrogen reduces the deposition rate less with propane and ethane than with methane. Similarly, boron trichloride increases the deposition rate of carbon from ethane (or its products) more than it increases the deposition rate of carbon from methane. All these primary and secondary effects of the higher hydrocarbons can be explained by their greater reactivity.

There is also a secondary interaction between ethane and propane, which is the same magnitude as the primary propane effect but of opposite sign. The most probable explanation is a saturation of the effect of higher hydrocarbons on deposition rate at higher concentrations. Saturation of this type was observed in our preliminary experiments.

These experiments have shown that:

1) Boron trichloride, ethane and propane increase the deposition rate of carbon from methane.

2) Hydrogen decreases the deposition rate of carbon from methane.

3) The effect of higher hydrocarbons appears to saturate at the higher concentrations.

4) Boron trichloride increases the deposition rate of carbon more with the higher hydrocarbons than with methane.

5) Hydrogen decreases the deposition rate of carbon less with the higher hydrocarbons than with methane.

6) All the effects are multiplicative.

RECOMMENDATIONS

The results of this work have shown that primary interactions can and do occur in certain gas mixtures used for chemical vapor deposition of carbon. The results must be considered if impure methane is used or if additives (such as boron trichloride) are used.

It must be remembered, however, that these results were all obtained at low temperature (1500°C). The relative importance of the data at the higher temperatures usually used for deposition has not been determined. It is recommended that these results be used and extrapolated with caution until further studies at Rennselaer are published.

F. HAFNIUM ALLOY DEPOSITION STUDIES (Task 3.4.2.4)*

BACKGROUND

An investigation was conducted on an improved method of introducing and controlling the addition of hafnium to the vapor deposition process for producing hafnium-alloyed pyrolytic graphite. This investigation was conducted in order to evaluate the potential of hafnium-alloyed pyrolytic graphite as a material for the fabrication of nose cones, rocket nozzles and other high performance assemblies. The advantage of this material is that it exhibits simultaneously a number of desirable properties among which are high mechanical strength at elevated temperatures, good resistance to oxidation, outstanding resistance to erosion, and good thermal behavior.

Unfortunately, technical problems associated with the apparatus used to feed, control and record the hafnium flow to the furnaces (where attempts have been made to produce hafnium alloyed pyrolytic graphite) have curtailed the production of useful engineering shapes.

In the past, several schemes were evolved concerning the design of a hafnium feed system. These have included the vaporization of a static mass of $HfCl_4$ crystals to yield a supply of $HfCl_4$ vapor, the vaporization of a column of $HfCl_4$ fed continuously into a small heated chamber, and the reaction of Cl_2 gas with heated hafnium metal chips. None of these systems proved to be entirely satisfactory from the standpoint of yielding a steady, reliable flow of hafnium-bearing vapor.

The system which has been designed and is being assembled in this study is based on the controlled vaporization of a continuously agitated mass of $HFCl_4$ (Ref. 80). It is felt that this system will avoid the difficulties met within the other systems previously described and will allow precise control over the flow of hafnium bearing vapor to the furnace.

---

*This Task is still being carried out at General Electric Company expense under funding from Development Authorization 8157-Lo-34-003.

DESCRIPTION OF $HfCl_4$ FEED SYSTEM

Systems based on the vaporization of a static mass of $HfCl_4$ and also on the reaction of heated hafnium metal chips with Cl_2 gas suffer from a diminishing rate of reaction or vaporization with time, and require increasingly higher temperatures in order to secure a steady flow of hafnium. Presumably this behavior is due to some condition involving the surface of the $HfCl_4$ crystals or the hafnium metal chips; possibly the formation of a crust of HfO_2 or $HfOCl_2$, due to residual traces of oxygen, or the formation of very large perfect crystals of $HfCl_4$ having a low rate of vaporization. It would seem that the scheme involving the progressive vaporization of a column of $HfCl_4$ fed into a heated vaporizer would avoid this difficulty by supplying to the vaporizer a steady flow of fresh material in which surface changes had not yet occurred. Unfortunately this method does not yield a uniform flow of hafnium, probably due to difficulty in mechanically feeding the $HfCl_4$ powder to the vaporizer and in the inherent inhomogeneity of the powder in the column.

In order to circumvent the above mentioned difficulties, a system was devised based on the controlled vaporization of a continuously agitated mass of $HfCl_4$. Agitation is accomplished by means of a motor driven impeller and insures the continuous production of fresh crystal surface by mixing and abrasion of the $HfCl_4$ crystals. Vaporization rate is controlled by regulating the vaporizer temperature. A pressure transducer senses the vapor pressure of the $HfCl_4$ in the vaporizer and signals a proportional controller which, in turn, regulates the vaporizer temperature to maintain a steady pre-selected pressure in the chamber. Flow of $HfCl_4$ vapor is controlled by a micrometer handle metering valve and is monitored by a thermal conductivity type flow meter.

The vaporizer itself is of stainless steel, has a capacity of 1 cubic foot and contains up to 10 kg. of $HfCl_4$, sufficient material for 81 hours of operation at a flow rate of 145 s.c.c.p.m. (0.310 SCFH) The vaporizer is heated to temperatures of 200° to 300°C in order to provide $HfCl_4$ vapor at pressures up to 400 torr. A 6 r.p.m. stirrer, driven through a special carbon face rotary seal in order to agitate and abrade the powder was originally planned, but the design has been altered to a triple seal on the basis of troubles experienced by the subcontractor making the vaporizer.

The pressure transducer is a thin film, strain gauge type and monitors the vaporizer pressure at the ambient temperature of the vapor. A Honeywell recorder and controller accepts the pressure transducer signal and produces a proportional output to drive a silicon controlled rectifier, which supplies power to the vaporizer.

The vapor is throttled through a Nupro stainless steel, bellows-sealed metering valve with micrometer handle. Flow is monitored with a Hastings-Raydist mass flow meter. This instrument operates on a unique thermal conductivity principle enabling it to measure small flow rates, at high temperatures and low pressures in corrosive

environments, and has been used successfully in connection with such materials as WF_6 and UF_6. The $HfCl_4$ vapor is mixed with hydrocarbon gas and then fed through an electrically heated stainless steel nozzle into the carbon resistance furnace where the hafnium-alloyed pyrolytic graphite is to be deposited.

All lines are 316 stainless steel tubing and connections are made using stainless steel "Swagelock" fittings and adaptors. Components such as the flow meter and pressure transducer are of stainless steel or monel metal. All valves are bellows sealed of stainless steel construction and capable of operation at 600°F. The entire system is heated with nichrome resistance wire sheathed in fiberglas and monel metal, and thermally insulated with a woven, staple fiberglas tape. Temperatures of the feed lines, valves, sensing elements and vaporizer are measured by chromel-alumel thermocouples which are fed through a compensated switching arrangement to a galvanometer type pyrometer. A schematic diagram of the feed system and associated vacuum manifold is shown in Figure 240.

In order to prevent condensation (actually sublimation) of $HfCl_4$ in the injector nozzle gas conduit and orifice, this section must be maintained at an elevated temperature. Assuming that pure $HfCl_4$ vapor is to be injected through the nozzle, a temperature of approximately 575°F (300°C) must be maintained. Dilution of the $HfCl_4$ vapor with hydrocarbon gas reduces the required temperature considerably.

In order to satisfy the condition elevated temperature without unduly increasing the bulk of the .e (a large diameter nozzle introduces difficulty in the fabrication of small diameter, small half-angle nose cones) heating is accomplished by passing an electric current directly through the gas conduit. Since the low resistance of the stainless steel tube is only of the order of 0.1 ohm, a low impedance power source is required.

Using a 1-1/2 KVA filament transformer (120 volt primary/12 volt secondary) controlled by a 3 KVA variable transformer, and approximately 30 mils of polyimide-fiberglas sleeving as insulation, it was found possible to maintain a temperature of 600°F within the gas conduit while the exterior of the insulation was immersed in cold water. Only 0.5 KVA was required to heat an actual conduit removed from a damaged nozzle.

Mounting of the components of the above described system is subject to certain constraints. The nozzle must be capable of being raised and/or lowered during the course of a run as well as rotated through angles as great as 180°. Due to the necessity of using stainless steel, the only suitable material for the construction of this system, and the inherent stiffness of stainless steel hose, it would require an impractically long length of such hose in order to achieve the flexibility of motion outlined above. In addition, flexing of the hose in the presence of $HfCl_4$ at elevated temperatures might result in stress corrosion failure.

As an alternate procedure, it was decided to mount all the components of the system including the nozzle but excepting electrical equipment on a portable elevating table, giving the capability to raise or lower the nozzle as required. Rotation of the nozzle is achieved as required either through the use of a rotating carbon face seal, or by equipping the elevating table with a rotating platform on which all of the rigidly connected components were mounted. The vacuum pump is mounted on the lower shelf of the elevating table. The associated electrical equipment is mounted on a separate portable table.

COMPONENT SPECIFICATIONS

A list of the specialized components used in this system is given below. (Refer to Figure 240):

1. Vaporizing Oven: The final design of the oven has not yet been detailed. This design will conform to the following requirements:

Capacity:	1 cubic foot.
Ports:	Removable top or side for cleaning. Additional 4" diameter port for fill.
Static Seals:	Gold wire "O" rings or "V" seals.
Rotary Seal:	Originally a carbon face bellows type seal as shown in Drawing B FFD-918 Sealol Inc., Providence, R.I. It is now being redesigned as a triple seal.
Stirrer:	6 R.P.M. 1/2 H.P.
Drive Shaft:	Approximately 3/4" diameter. To engage mixing blade by means of dis-engageable spline.
Vacuum Connection:	1/2" o.d. with internal powder baffle.
Temperature Capability:	300° continuous.
Power:	208 volts A.C. single phase. 5KVA or less at maximum temperature.
Vacuum:	Ultimate vacuum of 10 microns with vaporizer empty.

2. Valves:

V1, V6:	"Nupro" SS-8BG sealed bellows valves with replaceable bellows. All S.S. 1/2" "Swagelock" connections.
V3, V4:	"Hoke" "roto-ball" 30134-1 bar stock valve. 303 S.S. with "teflon" "O" rings 1/2" N.P.T. female connections.

	V2:	"Hoke" 561B spring loaded toggle valve. Pressure relief range 45-55 psig Nickel plated Brass. 1/4" N.P.T. male connections.
	V5:	"Hoke" 458 toggle valve. Angle flow pattern. Brass. "Viton" seat and "O" ring. 1/4" N.P.T. male connections.
	V7, V8, V11, V12, V13, V14:	"Nupro" SS-4H sealed bellows valve. "All S.S. 1/4" "Swagelock" connections.
	V9, V10:	"Nupro" SS-4 BMG micrometer handle bellows sealed metering valve with replaceable bellows. All S.S. 1/4" "Swagelock" connections.
3.	Vacuum Pump:	Precision Scientific Model D-25 vacuum pump. 25 l.p.m. Two stage (compound model). Ultimate vacuum 0.1 micron.
4.	Flexible Hose ("U" Tube Freeze Out Trap):	"Swagelock" 810-6FH (34S)-316 flexible metal hose with "Swagelock" union end fittings, both ends. All S.S. Hose diameter 3/4". Live hose length 19".
4a.	Dewar Flask (Freeze Out Trap):	Fisher #10-197 flask, evacuated, pyrex brand glass, wide-mouth, 4 quart capacity, 6" i.d.
5.	Resistance Heating Wire:	"Tophet" c nichrome wire with fiberglas insulation and monel sheathing. Resistance 4.251 ± 5% ohms/ft. 28 gauge. (Haddam Mfg. Co., Haddam, Conn.)
6.	Thermal Insulation:	Style #2275 type ESS-13A Staple Fiber Glaspun (Fiberglas) Tape. 0.025" thick x 3/4" wide. (Atlas Asbestos Co., North Wales, Pa.)
7.	Tube Fittings:	316 Stainless Steel "Swagelock" fittings and adaptors as required.
8.	Thread Lubricant (High Temperature):	"Swagelock" "Silver-Goop"
9.	Pressure Transducer:	Statham Instruments model PA-732-TC-10-350 thin film strain gauge pressure transducer. All S.S. Bridge resistance 350 ohms. Temperature capability to 600°F. Pressure range 0-10 P.S.I.A. Complete with high temperature electrical mating plug.

10. Regulated D.C. Power Supply for Pressure Transducer: Sorensen QB6-2 transistorized low voltage D.C. Supply. 5-9 V.D.C. 2 amperes maximum output current.

11. Pressure Recorder and Controller: Honeywell 18301136-01-31-0-700-006-07-019-053. Electronik 18 Single Record Strip Chart Recorder with Integrally Mounted Electr-O-Volt Current Proportioning Control.

12. Flowmeter: Hastings-Raydist LF-100X Mass Flowmeter. Dial face scale 0-100 linear. Type 100 MX monel flow transducer modified for 600°F operation. Calibration curve of 0-150 s.c.c.p.m. $HfCl_4$ vs. 0-100 linear dial included. 8 ft. connecting cable with high temperature wire and connector.

13. Thermocouples: Chromel-Alumel type G/G-24-CT fiberglas insulation and sheathing. 24 gauge.

14. Silicon Controlled Rectifier: Barber-Colman 621A-20860-058 Silicon Controlled Rectifier Power Pack. 208 volts single phase. 5.8 KVA. Forced Air cooling. Solid state with power output meter, inrush protection, current limiting, bias control and line voltage compensation.

15. Power Transformer for Heated Nozzle: General Electric 9-10-51 Y-111 Filament Transformer. Primary 120-240 volts. Secondary 12-24 volts. 1-1/2 KVA.

16. Insulating Sleeving for Heated Nozzle: Bently-Harris 963 ML Grade B Polyimide-Fiberglas sleeving. Size 8.

STATUS

The assembly of the hafnium feed system was delayed because of procurement problems. The vendor who was subcontracted to construct the vaporizer experienced extreme difficulty in building a vacuum seal for the drive assembly which could be heated to 200-300°C, and still maintain the required partial pressure. This problem was solved by a redesign which replaced the original seal with a triple seal. The outer seal in the redesign unit is now unheated. The vaporizer is completed and has been shipped to General Electric Company, Re-Entry Systems Department. The hafnium feed system is assembled except for installing the vaporizer.

This equipment will now be available for conducting studies in the refractory metal alloying of pyrolytic graphite on future programs.

X. ADVANCED STUDIES FOR REFLEX FLOW SYSTEMS

A. DELAMINATION CONTROL STUDIES (TASK 3.3.7.)

According to the Work Statment for Task 3.3.7, "Controlled nozzle movement (insert and/or withdrawal), controlled pressure variation and gas preheating will be evaluated as techniques for removing the thin spot characteristic of the walls of state of the art nose cones. Removal of this thin spot will eliminate the associated delaminations which are not parallel to the outside deposition surface."

BACKGROUND

The nose cones of boron-alloyed pyrolytic graphite in general use require nose tip thicknesses of one inch or greater and with wall thicknesses of about 180 to 200 mils. Two closely related problems exist in producing such cones. At a position just outside the nose tip region, a thin spot often exists along the wall. Because of this thin spot, delaminations in the surrounding material are not parallel to the outer deposit surface. The delaminations approach the outer surface near the thin deposit.

The objective of this task was to evaluate several specific process modifications which might improve the delamination pattern in nose cones by reducing or eliminating the thin spot just outside the nose tip region, and/or by changing various properties of the material deposited in the nose tip region.

Some related work had already been done in other tasks and influenced the work planned for this task. Nozzle position, for instance, was shown (in Task 3.4.2.1) to have an effect on the profile. This suggested that a combination of nozzle positions, varied during the course of deposition, might provide a more favorable delamination pattern than could be obtained from any single position. This idea of "dynamic processing" could also be applied to other process variables.

Since there had been indications by end-users of nose cones that some reduction in anisotropy could be allowed in the nose tip region, increased deposition pressure appeared to be one process variation which might have several desirable effects. First, material with a somewhat lower anisotropy might be deposited at higher pressures and the deposit with its lower anisotropy would be delaminated to a lesser degree, due to lower residual stresses. Also, increased deposition pressure could have a desirable effect on thickness profile in the nose tip region. It was recognized, however, that the problems associated with undesired growths on the nozzle and in the downstream exhaust paths, are always more severe with increasing deposition pressure. For this reason, a better approach appeared to be a form of dynamic processing where high pressure was used only in the early stages of deposition to develop the desired characteristics in the nose region. This would then be followed by decreasing pressure to develop the desired material characteristics and thickness in the

cone outside the nose region.

Neither nozzle position nor pressure is an isolated, independent variable, so changes in either would have secondary effects. For instance, both variables influence the rate at which the inlet gases are heated, and thus influence the rates of chemical reactions in the gas. They also control the gas flow patterns within the mandrel. The nozzle is a flow barrier in the deposition system by virtue of its size and position in the reflex-flow gas stream. Pressure also affects the flow patterns and stream lines within the mandrel. Reaction rates vary with the square root of pressure in most systems.

Heating rates are obviously important since a high rate of deposition is required at the initial point where the gas stream meets the mandrel (in the nose tip region). Special modifications to the inlet nozzle were desired which could provide some preheating of the gas before its arrival at the nose tip.

EXPERIMENTAL CONDITIONS SELECTED

As initially planned, the work in this task would cover:

a) Nozzle position variations during the deposition cycle.
b) Pressure variations during the deposition cycle.
c) Preheating of the inlet gas.

in a series of subtasks. As actually carried out, two forms of a) were investigated, and another element d) was added: Deposition at various inlet flow rates

In all cases, the deposits were nose cones. Each was a 1/4" radius, 10° half-angle cone, similar to SA317A, shown as Figure 3. The deposition assembly is shown schematically as Figure 157. Figure 241 shows the graphite parts in the several stages of assembly. The mandrels were made from Grade A graphite and all other design considerations were consistent with recommendations developed in the mandrel-related tasks (3.3.1 through 3.3.5).

The inlet nozzles were water-cooled, stainless steel, with a 13/16" o.d. and a 0.069 inch diameter gas discharge orifice. In all cases, the nozzle was rotated electro-mechanically at 1 rpm during the deposition cycle to minimize the effects of any minor misalignments. In those cases where nozzle movements were required, they were carried out without interruption of reactant flows or injector rotation. rotation.

Detroit natural gas and technical grade cylinder boron trichloride were used as the reactants for all runs. The flows were metered and mixed prior to introduction into the nozzle.

The process parameters selected as standard, from which variations were to be made, were consistent with the recommendations from Task 3.5.1, except where noted. The deposition temperature in all cases

was 3750°F. A standard pressure of 2mm was used instead of the 3mm recommended in 3.5.1, since high deposition rates were not required in this work. The 2 mm pressure was considered a conservative approach which would allow the best execution of a large number of runs. In most of the cases, nozzle position was a variable but in those cases where it was not, a position 8-1/2" from the nose was used, as recommended in Task 3.5.1. A reactant flow of 10 cfh natural gas was standard, with some variations as indicated in the discussions. Boron trichloride was not graded as recommended in Task 3.5. 1, since there was some concern that there might be leakage at the stem of the control valve used to grade the flow. In view of this, constant boron flows were used although the results in each case might be bettered by boron grading.

Following the post deposition cool-down, the cone deposit was separated from the mandrel and supporting base, using conventional hand tools. The cone was then radiographed in two views, both with the longitudinal axis of the cone parallel to the film plane and one view right angles to the other. The deposition thickness profile was determined from the radiographs from which preliminary appraisals of the delamination patterns could also be made.

Delamination patterns in the nose region, back to the thin spot along the wall, were the primary concern in this task. To obtain a more precise view of the delamination pattern in the nose region, each was potted inside and out, in a self-hardening plastic. The nose was then cut off slightly off the longitudinal axis, but parallel to it using an abrasive wheel. It was then polished back as close to the axis as possible. A photographic enlargement of this section was made at approximately 5X. This photograph provided a detailed view of the nose region for comparison with other deposits.

In an attempt to make the analysis of the delamination pattern less subjective, the delaminations were located and classified according to gap width using a bench microscope equipped with a micrometer eyepiece. Tightness of delaminations was ranked in the fashion suggested by Raytheon in Task 3.4.2.1 work: that is: VVL--very,very loose (10 mils): VL--very loose (5 mils): L--loose (3mils); T--tight (1mil); and VT--very tight (< 1 mil). In most cases, though, the information was easier to interpret by visual examination of the polished sections or from photographs of them. Boron assay by the pyrohydrolysis (colormetric) method was conducted separately on the first and last half of the material deposited in each nose section, and the first and last half of the material deposited in each skirt at a point about 8 inches from the nose.

Unit cell height C_o was determined by X-ray diffraction on the first and last deposited material of each cone in the nose and skirt area.

RESULTS

The results of each subtask are discussed separately and at some length in order to show what had been expected, how the results were interpreted, and how each set of results influenced the next runs.

Subtask 3.3.7-1. Table LIII summarizes the processing conditions and characteristics of the deposits made in this subtask. These four runs were designed to evaluate the effect on the deposition profile of variations in nozzle position during the the deposition cycle. Hopefully, such processing would provide a nose tip about 1 inch thick, measured along the longitudinal axis of the part, and a uniform wall thickness of about 0.200 inch. Run 6050 was the first deposit and was started using a nozzle to nose distance of 7 inches. Experience had shown that this nozzle position would yield good deposition rates in the nose region but was not completely satisfactory because of a very low deposition rate immediately outside the nose region, causing a thin spot in the deposit. During the run the nozzle was withdrawn 1/4 inch every 5 hours so that after nine 5-hour periods, the nozzle had been moved to 9 inches from the nose. Positions from 8 inches to 9 inches were believed to be better with respect to a uniform wall profile but would not produce as thick a nose as the 7-inch position. Figure 242 is the actual profile of the deposit: Figure 243 the radiograph; and Figure 244 the 5X photograph of the polished nose section. The desired profile was not obtained. In this case, the minimum wall is somewhat thinner than what might be expected, even for a deposit whose full term has been at a 7-inch nozzle position.

The next run (4063) was the same as 6050 except the initial nozzle position was 6 inches from the nose and the incremental adjustments were 1/2 inch every 5 hours, instead of 1/4 inch. In this case, the run was terminated prematurely when it was observed that nozzle withdrawal was not occurring even though the withdrawal apparatus had been activated. Post-run examination revealed a pyrolytic growth on the nozzle, which interfered with withdrawal. Figure 245 is a picture of this growth.

Run 6053 was a repeat of 4063, and Figures 246, 247 and 248 are the profile, radiograph and photograph, respectively, of the cone. In this case, the overall deposition rate was abnormally low. The furnace and deposition assembly were examined for signs of oxidation which would be evidence of a leak. No evidence of oxidation was found. The profile of this run indicated that the deposition rate was definitely below what should be expected. Although there were no visible signs of excessive oxidation, it is thought that there was an oxidant being introduced along with the reactants, in a quantity sufficient to materially alter the observed deposition rates.

The last run in this subtask (6056) was a third attempt to deposit a cone, using the 6-inch to 10 -inch nozzle withdrawal. The characteristics of this cone as shown by the profile, radiograph and photograph (Figures through 251) are somewhat different from those of the first run (6050). It appears that the 6-through 10-inch withdrawal was not

as effective as the 7-through 9-inch withdrawal for developing the desired nose thickness. The wall thickness was not really altered much by the nozzle movements. The 0.110 inch wall for the 6050 deposit was considered to be at the low end of the normal variation of wall thickness. the 0.170 inch wall for 6056 is about average for previous results of cones run at fixed 8- inch nozzle positions.

None of the deposits exhibit any delamination patterns which could be classified excellent. The samples designated for boron assay in run 6050 were lost prior to analysis and not replaced. Boron contents are reported for the other deposits. Although the boron content varied from one cone to the other for no apparent reason, two other trends are evident: that is, a) for a constant boron trichloride flow the amount incorporated in the first half of the deposit was less than that in the last half and b) the boron incorporated in the skirt region exceeded that in the nose region for a given cone. Higher boron concentration in the last half of the deposit was attributed to an uncontrolled increase in deposition pressure associated with the closing of the exhaust ports as deposit thickness increased. This judgment was supported by the repetition of this effect in subsequent runs where the nozzle was not moved. The changes in cell height (C_o) from first to last deposited layers seem to be consistent with the increase in boron content from first to last deposit.

Subtask 3.3.7-2. In this subtask the goal was to deposit the initial material at a uniform thickness and then to deposit at conditions which would give a preferential deposition rate in the nose region. This type of processing could avoid the undesirable delamination pattern found in many cones, where the initial (or outer) delaminations approach and nearly intersect the exterior surface immediately behind the solid portion of the nose. A uniform coating would displace the first non-parallel delamination inward where it would not be exposed during use. The processing conditions and results for this subtask are summarized in Table LIV.

The first run (6054) used an initial nozzle position of 12 inches from the nose, at otherwise conventional deposition conditions. The 12-inch nozzle position was maintained for 12 hours and then a 7-inch position was used for the balance of the run. The 12 -inch position was considered the most favorable for obtaining the desired uniform profile for the first deposited material. Figure 252 is the profile of 6054, and Figure 253 and 254 the radiograph and photograph of the cross-section. Figure 254 clearly indicates that the delamination pattern was modified. The pattern is very favorable from the standpoint of the location of the first non-parallel delamination with respect to the wall. This type of thickness distribution, however, could cause voids in the nose tip region if continued in small half-angle cones because of the increasing rate with increasing distance from the nose. The anomaly in the nose of this deposit is not completely understood. It may have been the result of heavy soot buildup due to an unobserved process variation. There is an initial deposit of normal material which indicates that the 12-inch nozzle position

by itself was not the cause of sooting. The deposition rates of the initial deposit were between 2 and 5 mils per hour.

Run 6055 was another run to deposit an initial uniform coating followed by a conventional deposit. In this case, the 12-inch nozzle position was used again, but the gas flow during the initial period was modified by reducing the methane to 4 cfh instead of 10 cfh, and by adding a considerable amount of diluent. The profile, radiograph and photograph of this deposit are shown as Figures 255, 256 and 257 respectively. The photograph shows that the initial material had the desired profile in that it was parallel to the outside contour and the first delamination was not less than 30 mils from the outer surface, as compared to the 5 to 20 mils from the outer surface obtained in subtask 1 deposits.

The final deposit of the series was run 6057. This was a repeat of the first run (6054), except with reduced boron trichloride flow. This flow was reduced in an attempt to avoid the apparent sooting problems experienced in 6054. The surface condition of this cone was extremely poor, and the mandrel carried away portions of the initial deposit. The reason for the poor mandrel release is not known since ATJ graphite was used. Figures 258, 259 and 260 are the profile, radiograph and photograph of the deposit. The material lost at mandrel separation is evident in Figure 260. It was noted that the deposition rate of this initial deposit appeared to be higher than that in 6054.

All three of these deposits did modify the delamination pattern with respect to previous deposits. This change can be best seen by comparing the polished section photographs of these cones with those of the cones deposited in subtask 1.

Boron content was not determined for the deposits in this subtask. X-ray diffraction revealed an interesting observation. The unit cell height (C_o) at the first deposited surface for samples of this series was lower than that at the last deposited surface in contrast to the values obtained for cones in subtask 1. Since time at temperature was about identical for all these cones and since at least for run 6054 the boron concentration in the inlet gas streams was identical, these results would indicate that unit cell height in the solid is a function of nozzle position. Closer positions gave higher values of C_o and so, probably, less boron in the deposit.

Subtask 3.3.7-3. The four deposits made in subtask 3 are summarized in Table LV. In this task, the objective was to take advantage of profile and material modifications that might be associated with high deposition pressures and then combine these with subsequent lower deposition pressures in order to deposit an inner cone shell of conventional material. The original plan was to deposit serveral cones with different initial deposition pressures and, in each case, reduce the pressure during the run to a low of 1.5 mm for the last deposited material.

The first run (5061) was started at a set of conditions corresponding to "standard" conditions for this subtask, except that boron was reduced from the 0.083 cfh to 0.040 cfh. In this case, a reduced boron trichloride flow as selected because of concern for sooting which might be a problem at higher deposition pressures. The initial deposition pressure for 5061 was 5.0 mm with planned decreases in pressure every 5 hours during the 40 hour deposition.

This run was completed without any apparent difficulties and the results are shown as the profile (Figure 261), X-radiograph (Figure 262), and photograph (Figure 263). In this deposit, there was an increase in deposition rate in the first inch back along the wall from the nose tip. This increase in rate in close proximity to the nose caused a closure between the walls which formed a void in the nose region. The profile does not present an accurate appraisal of the cone since there is no way to show a void. The unit cell height (C_o) values indicated that the anticipated increase, which would be associated with a deposit of lower anisotropy and density, was not obtained. The cell height was, in fact, the lowest of any value in the task to this point.

In order to understand better the characteristics of higher pressure deposits, it was decided that subsequent runs would be made at constant pressures rather than grading to lower values during the runs. Any favorable results could then be combined with lower pressure deposition for the best composite process.

The second run (5062) was made at a constant pressure of 5.0 mm. The run was completed without difficulty and Figures 264, 265 and 266 are the profile, X-radiograph and photograph respectively. Again in this case as in the first run, the profile was not representative because of a void in the nose region. The X-radiograph and photograph, however, provided a very clear picture of the profile and delamination characteristics. These results indicate that an undesirable profile resulted from the 5 mm deposition pressure. The third run (5064) was made at deposition conditions similar to runs 1 and 2 except the deposition pressure was maintained at 8.0 mm. The profile, X-radiograph and photograph, Figures 267 through 269, indicated that there was no void in this cone, but not because of a more desirable profile. The increase in deposition pressure apparently caused the point of initial maximum in deposition (note that in this case there were two maxima) but also caused the position to recede from the nose. If this run had continued, closure at 2 or 2-1/2 inches from the nose would have occurred.

To verify this trend and determine if a change in nature of the profile might be experienced with considerably higher deposition pressure, the next run (5068) was made at 18.0 mm. This run was terminated early due to a large growth on the nozzle which interfered with gas flow. the results of this run are shown as the profile, X-radiograph and photograph in Figures 270 through 272. In this case, the point of initial maximum deposition rate is still further displaced from the nose, at about 4-1/2 inches.

A review of the runs in this subtask combined with the knowledge gained in Task 3.5.1 indicated that increasing deposition pressure above about 3.0 mm causes an increased tendency to create voids in the nose region. The runs in this subtask are summarized in Figure 273 where deposition rates for each deposit are plotted agains position along the cone axis. In the case of runs 1 and 2, the peak rate is not evident since it is masked by the closure and resulting void. Runs 3 and 4, however (8 and 18 mm respectively) identify the problem by showing the shift from the nose tip region of the maximum deposition rate as pressure is increased. To prevent voids, the maximum deposition rate must be at the nose tip.

It was also worth noting that the C_o values did not increase with increasing deposition pressure. In all cases, the material appeared to be normal in appearance and in measured characteristics. No indication of lower density and anistropy were obtained.

Although subtask 3 was originally planned as a 6-run evaluation, the final two runs were cancelled, since increasing difficulty with extraneous growths could be expected with further increases in pressure. Neither was it expected that any pressure between the 8 and 18 mm would produce a better deposit than those two.

Subtask 3.3.7-4. Work in this subtask consisted of three runs, as summarized in Table LVI. The objective was to evaluate the effects of gas preheating on the delamination pattern and profile. The gas preheat was accomplished by attaching graphite caps to the injector nozzles to provide a heated surface in contact with the gas prior to its contact with the mandrel. In each case, the cap was attached by using SermeTel Allen PBX ceramic cement.

Run 5056 was made using deposition conditions which were normal for nose cones of this radius and half-angle. Figure 274 is a sketch of the nozzle cap used for the run. Run 5056 was terminated shortly after gas was turned on due to an obstruction in the gas line unrelated to the processing conditions selected or the nozzle cap design. Run 5057 was made with the same cap and deposition conditions as 5056. The profile, X-radiograph and photograph of the deposit are shown as Figures 275 through 277, and indicate that the cap had no significant effect on the deposit. The hole in this cap was essentially free of deposit.

Run 4067 was made using a cap as shown in Figure 278. In this case, additional surface for heating was provided. The divergent nature of this design was to prevent the deposit from closing the gas path. The run was made with reduced boron trichloride flow to further insure minimum difficulty with cap closure.

The deposit was made without difficulty and post run examination indicated that cap closure was not a problem since the deposit on the inlet side was only a few mils thick. This cap was not effective in improving the profile or delamination pattern and appeared to have

undesirably reduced the deposition rate in the nose region, as shown in Figures 279 through 281. This reduction in deposition rate may be associated with a difference in flow patterns as a result of the cap design.

The unit cell height, boron analysis and delamination characterizations did not offer any additional information as to the influence of pre-heating caps.

Subtask 3.3.7-5. This work had not been included in the original planning but was added when studies outside this contract indicated the importance of mass flow rates in small-angle nose cone deposition.

Small-angle nose cones (with half-angles less than 10 degrees) are desirable for aerospace hardware use. Many of the problems encountered in 10 degree half-angle cones are worse in the smaller angle cones, particularly if they also have small nose radii. The tendency to form voids in the nose tip region when the maximum deposition rate is not precisely at the tip, is much greater in the smaller angle cones. The narrow channel available for gas flow restricts the nozzle size and may require that the nozzle be positioned farther from the tip than might be desired.

For this subtask cones with half angles of 10 degrees and 6 degrees were used, both with nose radii of 1/4 inch. All deposits were made at 3750°F and at a pressure of 2 mm Hg. Flows were selected from the values 7, 10, 15 and 20 cfh and nozzle positions were 7 or 9 inches from the cone tips. The 10 cfh flow was not used for 10 degree cones since that combination was already used in other sub-tasks.

The standard 13/16 inch diameter nozzle was used for 10 degree half-angle cones, with an orifice 0.069 inches in diameter. For the 6 degree half-angle cones, however, the nozzle diameter was reduced to 1/2 inch to decrease its cross-sectional area. In both cases, the cold nozzle surface was shielded from the gases by the use of thin, full-length graphite sleeves. Such shields reduce the tendency to form large, abnormal growths on the nozzle surfaces. The shields increased the effective diameters of the nozzles to 1-1/4 inches and 43/64 inches respectively.

The nozzle shields did not function perfectly since some runs were terminated early as a result of large, abnormal growths on the shields themselves. In the case of 5066 (10° cone, 20 cfh, 7" nozzle position) the run was terminated so early by such a growth that a second attempt was made. In the second try, the deposition period was much longer but operating records indicate that there was some difficulty in maintaining the 20 cfh gas flow just 8 hours after the beginning of the run. Post-deposition examination revealed a growth on the top of the nozzle which had choked the discharge orifice.

With two exceptions, these deposits were evaluated using the same sampling procedures and tests as in the other subtasks. Boron analyses

A review of the runs in this subtask combined with the knowledge gained in Task 3.5.1 indicated that increasing deposition pressure above about 3.0 mm causes an increased tendency to create voids in the nose region. The runs in this subtask are summarized in Figure 273 where deposition rates for each deposit are plotted agains position along the cone axis. In the case of runs 1 and 2, the peak rate is not evident since it is masked by the closure and resulting void. Runs 3 and 4, however (8 and 18 mm respectively) identify the problem by showing the shift from the nose tip region of the maximum deposition rate as pressure is increased. To prevent voids, the maximum deposition rate must be at the nose tip.

It was also worth noting that the C_o values did not increase with increasing deposition pressure. In all cases, the material appeared to be normal in appearance and in measured characteristics. No indication of lower density and anistropy were obtained.

Although subtask 3 was originally planned as a 6-run evaluation, the final two runs were cancelled, since increasing difficulty with extraneous growths could be expected with further increases in pressure. Neither was it expected that any pressure between the 8 and 18 mm would produce a better deposit than those two.

Subtask 3.3.7-4. Work in this subtask consisted of three runs, as summarized in Table LVI. The objective was to evaluate the effects of gas preheating on the delamination pattern and profile. The gas preheat was accomplished by attaching graphite caps to the injector nozzles to provide a heated surface in contact with the gas prior to its contact with the mandrel. In each case, the cap was attached by using SermeTel Allen PBX ceramic cement.

Run 5056 was made using deposition conditions which were normal for nose cones of this radius and half-angle. Figure 274 is a sketch of the nozzle cap used for the run. Run 5056 was terminated shortly after gas was turned on due to an obstruction in the gas line unrelated to the processing conditions selected or the nozzle cap design. Run 5057 was made with the same cap and deposition conditions as 5056. The profile, X-radiograph and photograph of the deposit are shown as Figures 275 through 277, and indicate that the cap had no significant effect on the deposit. The hole in this cap was essentially free of deposit.

Run 4067 was made using a cap as shown in Figure 278. In this case, additional surface for heating was provided. The divergent nature of this design was to prevent the deposit from closing the gas path. The run was made with reduced boron trichloride flow to further insure minimum difficulty with cap closure.

The deposit was made without difficulty and post run examination indicated that cap closure was not a problem since the deposit on the inlet side was only a few mils thick. This cap was not effective in improving the profile or delamination pattern and appeared to have

undesirably reduced the deposition rate in the nose region, as shown in Figures 279 through 281. This reduction in deposition rate may be associated with a difference in flow patterns as a result of the cap design.

The unit cell height, boron analysis and delamination characterizations did not offer any additional information as to the influence of pre-heating caps.

Subtask 3.3.7-5. This work had not been included in the original planning but was added when studies outside this contract indicated the importance of mass flow rates in small-angle nose cone deposition.

Small-angle nose cones (with half-angles less than 10 degrees) are desirable for aerospace hardware use. Many of the problems encountered in 10 degree half-angle cones are worse in the smaller angle cones, particularly if they also have small nose radii. The tendency to form voids in the nose tip region when the maximum deposition rate is not precisely at the tip, is much greater in the smaller angle cones. The narrow channel available for gas flow restricts the nozzle size and may require that the nozzle be positioned farther from the tip than might be desired.

For this subtask cones with half angles of 10 degrees and 6 degrees were used, both with nose radii of 1/4 inch. All deposits were made at 3750°F and at a pressure of 2 mm Hg. Flows were selected from the values 7, 10, 15 and 20 cfh and nozzle positions were 7 or 9 inches from the cone tips. The 10 cfh flow was not used for 10 degree cones since that combination was already used in other sub-tasks.

The standard 13/16 inch diameter nozzle was used for 10 degree half-angle cones, with an orifice 0.069 inches in diameter. For the 6 degree half-angle cones, however, the nozzle diameter was reduced to 1/2 inch to decrease its cross-sectional area. In both cases, the cold nozzle surface was shielded from the gases by the use of thin, full-length graphite sleeves. Such shields reduce the tendency to form large, abnormal growths on the nozzle surfaces. The shields increased the effective diameters of the nozzles to 1-1/4 inches and 43/64 inches respectively.

The nozzle shields did not function perfectly since some runs were terminated early as a result of large, abnormal growths on the shields themselves. In the case of 5066 (10° cone, 20 cfh, 7" nozzle position) the run was terminated so early by such a growth that a second attempt was made. In the second try, the deposition period was much longer but operating records indicate that there was some difficulty in maintaining the 20 cfh gas flow just 8 hours after the beginning of the run. Post-deposition examination revealed a growth on the top of the nozzle which had choked the discharge orifice.

With two exceptions, these deposits were evaluated using the same sampling procedures and tests as in the other subtasks. Boron analyses

of runs 5071 and 6068 could not be completed prior to this report.

Figures 282 through 286 are the X-radiographs and 287 through 291 the polished-section photographs of the five 10 degree deposits made. The processing conditions and results of these runs as well as the 6 degree runs are summarized in Table LVII. Figure 292 summarizes the deposition profile of these deposits and also includes run 7028 from Task 3.5.1, which was considered representative of the profile of a deposit at a 9-inch nozzle position and 10 cfh natural gas flow.

The polished sections indicated that the characteristics of the delaminations were not changed except as they were influenced by profile. Figures 288 and 289 show irregularities in the nose tip regions of the 9-inch 15 cfh, and 9-inch 20 cfh deposits. It is difficult to determine reason for these irregularities. They might have been caused by soot but very normal values for C_o were reported for these deposits. It is believed the trouble was associated with the nozzle position-flow combination, and not with any extraneous factors such as accidental introduction of debris through the gas lines. In both cases, the relative nozzle position decreased as the nose thickness increased, and then the irregularities diminished and finally disappeared. There was no such structure problem at the 9-inch position with lower flows, such as 10 cfh.

The photograph of run 5071, (Figure 291) indicated an anomaly in the nose which was most probably caused by a mandrel flaw or debris in the gas stream. This same run, as mentioned earlier, was terminated early by blockage of the gas flow. The profile of the deposit was not considered representative of the nozzle and flow conditions. The irregularities are, instead, indicative of the processing problems associated with the conditions and geometry.

The results of variations for the 10 degree half-angle cone are best summarized by Figures 292 and 293. These summaries of deposition rates, irrespective of material quality and degree of processing difficulty, indicate the trend set by the nozzle and flow variations. In the case of the 9 inch nozzle position, the deposition rate in the nose tip increased as the flow was increased with no significant changes in the region immediately behind the nose, or in the skirt region. In contrast, the 7-inch nozzle position at 15 cfh deposit had a higher nose deposition rate than at 20 cfh. From experience, the nose rate for 7-inch 10 cfh would be estimated at 20-25 mils per hour. Considering run-to-run variations, it is difficult to say whether the rate is maximized at the 7-inch 15 cfh condition, or if it is relatively insensitive over a flow range of 10 to 15 cfh. The decrease to 18 mils per hour at 20 cfh is interpreted as indicating that increases in flow above about 15 cfh cause decreases in nose deposition rates. These observations are probably a result of many factors, including: a) inability of the system to heat the gas at higher mass flows and thus inability to produce active species for deposition at the nose, b) the reduced residence time between nozzle and nose at the high flows, and c) the increased influence of the nozzle as a heat sink at the closer positions .

In the case of the 9-inch position, it appears from the irregular structures in the nose region at 15 cfh (Figure 288) and 20 cfh (Figure 289) that undesirable deposition species were present. This may have been a result of the longer residence time, allowing gas phase reactions to proceed for a longer time before the gas reached the mandrel.

Outside of the nose region, most of the deposits were nearly identical. The one exception was run 5065 (the 7-inch 15cfh deposit) which had a measurably higher wall deposition rate. This increase in rate did not improve the delamination pattern because the minimum to maximum thickness ratio along the wall was still about two to one. Most of the deposits had a thin spot rate of about 5 mils per hour, and a skirt rate of about 10. In run 5065, the rates were 7 and 14.

From the point of view of favorable delamination patterns, the 7-inch nozzle position, 20 cfh, deposit was best. The rate of change of deposition rate coming out of the nose region was minimized and the delaminations approached the exterior surface at the lowest angle. However, this set of processing conditions was difficult to use and full term deposits were not obtained. There might be assembly design variations which could correct this. If such changes were made, then these conditions would be the most favorable. On the other hand, with this deposition assembly the 7-inch 15 cfh, and 9-inch 10 cfh combinations were the best compromises.

Table LVII summarizes the operating conditions and results for the 6 degree half-angle cones. Figures 294 through 314 are deposition profiles, X-radiographs and photographs for the seven deposits. As indicated in the table and by reference to the above figures, all of the deposits had deposition profiles which caused voids, or would have caused voids if the runs had been continued. It is difficult to discuss deposition rates in a nose where a void was formed, since the time at which closure occurred and the conditions preceding it are not known accurately. No figure equivalent to Figure 292 could be prepared. In this case, the results were evaluated subjectively by comparing the size and location of the void. Figure 315 shows a sketch of the deposits arranged with respect to flow and nozzle position. The length and shape of the voids are determined by the position of the deposition peak that caused the void, the deposition rate at this point and deposition rate profile forward of the closure point. A closure such as for 4076 indicates a maximum rate quite a distance from the nose with a relatively high rate of change in deposition rate from this point forward. If this void were narrow, it would indicate a relatively small difference in rate between the peak and points forward. If the void were shorter, such as is the case for 4075, it would indicate that the peak rate causing closure was farther forward.

Both the 7-and 9-inch positions were less desirable as the flow was increased from 15 to 20 cfh. For the 9-inch position, the 15 cfh flow was most favorable. The 7-inch position was also most favorable at

15 cfh, although there was little difference between the 15, 10 and 7 cfh. Of the two nozzle positions, 7 inches is favored because it gave close to the desired results over a broader flow range.

The results all confirm that this narrow cone is more sensitive to the location of maximum deposition rate and, in addition, responds to flow and nozzle position changes differently than the 10 degree cone.

A deposit made using a 6-inch position with from 10-15 cfh gas flow might give the best results, considering the results of the previous runs. When considering a nozzle position as close as 6 inches, however, it must be recognized that the clearance between the nozzle and cone wall is very small (5/8 inches if a 1/2 inch unshielded nozzle is used; and only 1/2 for a nozzle with a 43/64 inch graphite shield). The heat sink effect of the nozzle would also be very pronounced and might lead to cooling of the mandrel near the nozzle.

Another useful variation might be a process using a 10-inch position with a flow of 15 cfh, if the profile improved as it did by changing from 7 inch to 9 inch at 15 cfh.

Subtask 3.3.7-6. At this point in time, three additional deposits were made. One run (6067) was made to improve the results of Task 3.3.7-2 and two (7082 and 5074) were made to extend the flow and nozzle position combinations of the 6 degree cone geometry from Task 3.3.7-5.

Run 6067 was made at deposition conditions similar to run 6055. The conditions for 6055 are shown in Table LIV, and for 6067 in Table LVIII. In the latter run, the flow used for the initial deposition period was reduced from 4 to 3 cfh to produce a more uniform initial deposit than in 6055. The conditions for the normal deposition period were similar to 6055, except that the deposition time was extended to produce a 1 inch thick nose and approximately 200 mil thick wall. The results of the run are shown as the profile (Figure 316), the X-radiograph (Figure 317), and the photograph (Figure 318).

This photograph is not representative of the complete deposit since a thin shell of pyrolytic graphite cracked and separated from the deposit prior to the mounting and polishing. The X-radiograph made before the shell separated shows that the desired uniform coat was achieved but was thin (approximately 10 to 15 mils thick). The photograph shows that the balance of the deposit had the conventional delamination pattern expected for the processing conditions used.

The other two runs of this subtask are also summarized in Table LVIII. The concluding remarks of Subtask 3.3.7-5 suggested several processing combinations improving the deposition profile of the 6 degree half-angle cone.

The 6-inch nozzle position was not selected for study because of the limitations of clearance and cooling effect discussed earlier. Run 7082 was made at the recommended 10-inch position and 15 cfh gas flow. All other processing variables and design factors were the same as for the 6 degree cones in 3.3.7-5. The results of this run are illustrated by Figures 319, 320 and 321. This nozzle position turned out to be very undesirable with a very low depositon rate in the nose region and a deposition peak 4 inches back from the nose, which would have caused a void if the run had been continued.

The last run of this series (5074) was a repeat of the 9 inch 15 cfh deposit (4072) made in 3.3.7-5. Run 4072 had the smallest void of any deposition in that series. The repeat of that run was made to determine if a void-free nose could be deposited with those conditions. The results of run 5074 (Figures 322 through 324) show that the first run was the better.

These runs have pointed up the extreme difficulty, particularly for narrow half-angles, in depositing nose cones with improved profiles and delamination patterns.

SUMMARY

The work in this task represented a large number of experimental variations whose purpose was to modify delamination patterns in nose cones. Two types of studies were carried out: a) the use of favorable combinations of known processes, and b) development of new processes or techniques.

For nose cones with 10 degree half angles and 1/4 inch radii, the results can be summarized as follows:

1) In-process nozzle movements between 6-and 10-inch positions at 10 cfh flow did not improve the delamination pattern.

2) The delamination pattern was favorably altered when nozzle positions were varied in combination with gas flows. Long initial nozzle to nose tip distances in combination with low flows provided a uniform coat, displacing the first delamination inward and forming it parallel to the outside of the deposit.

3) Higher pressures had a deleterious effect on the profile. Increasing pressure gave decreased nose tip deposition rates and increased wall rates.

4) Graphite caps, intended to preheat the gas and allow higher deposition rates at the nose tip, had little or no effect.

In addition to these results, others were obtained on the effects of flow rate variations in the same cone shape and in a 6 degree half angle, 1/4 inch radius type.

For the 10 degree cone, correlation between flows and thickness profile characteristics were obtained over a relatively wide flow range. For the 6 degree cone, no such correlations were possible because every cone had a void in the nose tip region. The size and shape of the void changed as deposition conditions were varied and indicated that an even closer nozzle position (6 inches from the nose tip) with flows of 7 to 20 cfh might lead to success. Smaller half-angle cones, whether they be of large or small nose radius, are more difficult to deposit and the allowable range of process conditions is much smaller than for 10 degree cones.

RECOMMENDATIONS

Recommendations can be made in three categories: Process conditions which are not recommended for use or further study, process conditions which are recommended for further study, and process conditions which are recommended for use.

Process conditions which are not recommended for use are:

1) Deposition pressures greater than 3 mm. (This upper limit might be altered by setup design and equipment design however.)

2) Gas preheating by use of graphite nozzle caps.

3) Nozzle positions of 7 through 10 inches with flows of 7 through 20 cfh for deposition of 6 degree half-angle, 1/4 - inch radius cones. These do not yield a satisfactory profile. However, this may be influenced by the design of the gas injector. This study used a 1/2 inch o.d. nozzle with a 0.069 inch diameter orifice.

Those process conditions which warrant further study or have application as an improvement in areas other than delamination patterns, are:

1) Use of nozzle positions of 6 inch (and closer if possible) for deposition of 6 degree half-angle cones. A satisfactory profile might be obtained at this nozzle position. Because of the narrow angle, the nose radius of this cone type is an important variable and should be included in any experiments. As the half angle increases, the influence of nose radius decreases so that for 9 degree and 10 degree cones, the radius is not so important a variable.

2) Nozzle position/gas flow combinations selected from the results in Figures 292 and 293. These provide a good reference for selecting combinations which best meet the profile requirements of a given nose cone to be deposited.

3) Gas preheating. Although not effective as done here with the graphite caps, this technique should not be ruled out as a method for controlling profile and material properties.

Those process conditions which are recommended for use are:

1) Nose cone deposition in a two-step technique, beginning deposition with a set of processing conditions which yield a relatively uniform deposit thickness and then switching to deposition conditions which give the desired preferential deposition rate in the nose region. Such a uniform initial deposit favorably alters the delamination pattern by displacing inward the first delamination a uniform and planned distance from the exterior surface. The processing conditions recommended for such an initial coating in 1/4 inch, 10 degree half-angle cones, are:

Temperature	3750°F
Pressure	2 mm Hg
Gas Flow	4 cfh Methane or Natural Gas
BCl_3 Flow	0.1-1% of Methane
H_2 Flow	10 cfh
Nozzle Position	12 inches
Deposition Rate	~3 mils/hour

2) The use of a flow of 10-15 cfh with a nozzle position of 7 inches for deposition of 10 degree half-angle cones which gives the best delamination pattern. It is suggested, however, that after sufficient material has been deposited to establish the delamination pattern that the nozzle might be withdrawn one inch to increase the deposition rate in the nose region.

B. PROCESS OPTIMIZATION FOR NOSE CONES (TASK 3.5.2)

According to the Work Statement, "The results of all prior tasks will be combined and deposition will be made to optimize the process. A process specification will be written incorporating the optimum deposition parameters."

BACKGROUND

The results from the previous task in this Advanced Studies Section and also from the Special Studies Section were expected to modify the process specifications for the production of nose cones and other aerospace hardware. It was anticipated that these modifications would be combined and/or optimized in Task 3.5.2. The results of the Advanced and Special Studies, however, did not indicate that drastic changes were required and so the selection of an optimum process for a 10 degree half-angle cone was not as difficult as it might have been. The process conditions used for the cones in Task 3.5.1 were actually close to those which would now be selected after the additional experience.

The case of the 6 degree cone is somewhat different. This was a new configuration, added to the program as a result of its desirability as aerospace hardware. A wide variety of flow and nozzle positions were investigated in Task 3.3.7 for this cone with negative results. The work did, however, indicate the direction that further study should take.

To best satisfy the objectives of this task and of the overall program, the work was divided into two phases. The first phase was to demonstrate the improved state-of-the-art by making and characterizing a limited number of the 1/4-inch radius, 10 degree half-angle cones, using the best design and process parameters. The second phase was to extend the 6 degree half-angle work from Task 3.3.7 to successfully deposit cones of this geometry and, if possible, to recommend an acceptable process for such a configuration.

EXPERIMENTAL CONDITIONS SELECTED

For the 1/4" radius, 10 degree half-angle cone, a process specification was written incorporating all desirable processing conditions developed in this contract, as well as applicable experience from earlier work. This process specification is included as Appendix II. The specification includes all of the pertinent process and design details required for producing these cones at another facility. Three runs were planned for Phase 1, using this process specification as a guide. It was necessary, because of equipment difficulties which could not be repaired in time to complete the runs on schedule, to eliminate that portion of the process which required a 12-inch nozzle position. This was done with some reluctance since this position, and the portion of the process eliminated by the lack of it, does affect the delamination pattern of the deposit. The results of each run, therefore, would ideally be modified by a 35 to 40 mil uniform coating at the outer surface.

Six runs were planned in Phase 2 to develop a process specification for 1/4-inch radius, 6 degree cones. The experimental conditions selected for the initial run of the planned six was consistent with the recommendations of 3.3.7. In the 3.3.7 experiments, a graphite nozzle shield was used. A full nozzle shield was not used in the experiments here for fear that the coating on a full-length shield and the wall deposit would interfere and cause premature termination of the run. The processing conditions for the five subsequent runs were each selected on the basis of results of the previous runs.

Time did not permit a detailed evaluation of each deposit as for earlier tasks. These deposits were, for the most part, judged on their appearance, thickness profile, and the delamination pattern shown in the X-radiograph.

RESULTS

Table LIX summarizes the processing conditions and results for both the 6 degree and 10 degree runs of this task. In the case of the 10 degree cones, the table indicates that 4 deposits were made instead of the three planned. Run 5077 is not a representative run of the process specification for this part. An undetected failure in a furnace support part prior to (or during) deposition caused the deposition assembly to tilt. The other three 10 degree runs were deposited according to the specification included as Appendix II, as modified by the exclusion of the initial 12-inch nozzle position. A photograph of these deposits is shown as Figure 325. The profiles and X-radiographs are shown as Figures 326 through 331. The X-radiographs of the three deposits indicate that the cones are similar and the delamination patterns are the best that can be expected without the initial uniform coating. The nose deposition rate-to- minimum wall deposition rate ratio is approximately 6 to 1 for all three deposits. The process specification indicates that the desired ratio is 5 to 1. Assuming that it would have been possible to carry out the 12-inch nozzle position portion of the process, the wall thickness of each cone would have been increased by 40 mils and the nose-to-wall ratio would have been approximately the desired 5 to 1. Perhaps more important, the first delamination would have been displaced at least 40 mils from the outside surface.

Appendix II thus is a usable process specification which will produce a nose cone with good exterior surface finish, the desired nose-to-wall thickness ratio (5 to 1) and will give a delamination pattern in which the first delamination will be approximately 40 mils from the exterior suface.

The nose-to-wall deposition rate ratio remained relatively constant from one deposit to the next,although the absolute values of the thicknessess did vary. The lowest nose rate was 19 mils per hour, and the highest was 25 mils per hour. Since none of these runs had any unusual growths or exhaust-port closures, the reason for this variability is not understood. The premature termination of run 4083 was due to an obsruction in a gas-feed line and not associated with any factors of the process specification.

The Phase 2 study was started with a deposit using the recommended 6-inch nozzle position and a flow of 10 cfh. Figure 332 is the X-radiograph of this deposit and indicates that there was a small void in the nose region. The next run was made with a flow of 13 cfh. This run terminated after 31 hours due to closure of the exhaust ports in the mandrel support. Figure 333 is the X-radiograph of this deposit and indicates that a void-free nose was produced. The X-radiograph showed that a large nozzle growth was present and could have been an important factor in modifying the deposition profile. It was considered most important to determine the controlling factor in obtaining this desired profile.

The next run was planned for a deposition period shorter than the first, hoping to deposit as long as possible but purposely terminating

the deposition cycle before exhaust port closure. Nevertheless, closure and large growths were again encountered. This was also the experience in the following run. The X-radiographs of these deposits are shown as Figures 334 and 335 and, as in the case of run 4084, the profile was as desired. Run 4085, the fifth run of this series (the fourth at 13 cfh) was planned for only a 25-hour deposition cycle and was completed as scheduled. The results of this run are significant. Figure 336 is the X-radiograph of this deposit and indicates that the desired void-free nose was obtained. This deposit was generally thin compared to the others, indicating that the variation in nose and wall thicknesses for runs 4084, 6071 and 5078 were due to: a) the difference in deposition times, b) the shape of the growths that were formed, and c) the time at which such growths became an influencing factor. The nose and wall thickness of this last experimental deposit (4085) and the other deposits without voids were not thick enough to meet anticipated user specifications. The required thicknesses would most likely be a 1.5 to 2-inch thick nose, with a wall thickness of about 200 mils. With only one planned run left in the program, the simplest technique for increasing the nose and wall thickness was tried. The exhaust holes of the standard setup for this shape were increased from three 5/8-inch diameter holes to three 7/8-inch diameter holes, an increase of 96 percent in exhaust area.

Although scheduled for 50 hours, this run terminated after 46 hours, due to exhaust-port closure. No large nozzle growth was formed in this run although the cone was filled with a low density soot due to the closure. The results here, as shown in Figure 337, indicate the deposition rate in the nose region was decreased by the larger exhaust-port size. The deposition rate on the side walls was somewhat lower but the longer deposition time more than made up for this, so that increased wall thickness was obtained. Although the deposition rates in the nose were reduced, the void-free characteristics of this cone make it similar to the previous runs.

This observation suggests that increased thickness might be obtained by using a larger exhaust port, such as in run 5079, but maintaining the nozzle position at 6 inches, just long enough to change the shape to one which can be deposited from a 7- or 8-inch nozzle position. At these positions, the nose and wall deposition rates might be improved and the increased carbon stripping efficiency would decrease the rate of exhaust closure, permitting a deposition period of sufficient length to develop the desired thicknesses.

RECOMMENDATIONS

The recommended process for a 1/4 inch, 10 degree half-angle cone is shown as Appendix II. Experience indicates that this basic specification, with only minor changes, is applicable to cones with half angles of 8-1/2 degrees to 11 degrees and radii of 0.20 to 0.40 inches.

A process for the narrower angle cones, typified in these studies by a 1/4-inch radius, 6 degree half-angle cone, was not developed well enough that a final process specification could be prepared. The last deposits of this task did, however, indicate conditions which might allow such a cone to be deposited with a nose thickness of 1.5 to 2 inches and a minimum wall of 200 mils. These conditions are:

Temperature	3750°F
Pressure	2 mm Hg.
Gas Flow	13 cfh methane or natural gas
BCl_3 Flow	Graded uniformly from 1% to 0.1% over length of deposition period.
Nozzle Size	1/2 inch o.d.-0.069 inch diameter orifice.
Nozzle Shield	None.
Nozzle Position	6 inches for first 2 hours 8 inches for balance of run
Exhaust path	Three 5/8-inch holes.
Deposition time	50 hours.

If successful, this process could be further enhanced by adding an initial deposition period with conditions set for a uniform coating. The initial period recommended for the 10 degree cone would probably be satisfactory for this configuration.

XI. AUXILIARY TASKS

A number of tasks were related to the primary tasks in a support role and these have not been discussed separately. Thus, Task 3.1 covered the preparation of a program plan and Task 3.1.1 its acceptance by USAF-MATC.

Task 3.4.1.4 covered the evaluation of materials produced in Tasks 3.4.1.1 through 3.4.1.3. Task 3.4.2.2 covered the evaluation of materials produced in Task 3.4.2.1.

Task 3.4.4 covered the development of analytical techniques for predicting residual stress patterns. Appendix IV of this report shows the work done by Dr. T. McDonough of General Electric Company, Re-Entry Systems Department, in this task for application to the separators developed in Tasks 3.3.1 and 3.3.2.

Task 3.4.5, on the development of nondestructive test techniques, was de-emphasized when the revised Work Statement eliminated the deposits intended in the scale-up work for the original version of Task 3.5.2. Such technique development will be carried out on a continuing basis by General Electric Re-Entry Systems Department, however, and any of the GE-RSD Subcontract Engineers listed in the Foreword of this report may be contacted for discussion in this area.

BIBLIOGRAPHY

Ref. 1 Basic Carbon Corp., Bulletin No. 115, June 1964 "Standard Solid Grades, Comparative Data".

Ref. 2 Union Carbide Corp., Carbon Products Division, "The Industrial Graphite Engineering Handbook". Sections 4 and 5A.

Ref. 3 Great Lakes Carbon Corp., Graphite Products Division, Tech. Data Sheet No. 5530D, "Typical Physical Properties of Development Stock".

Ref. 4 Currie, L. M., V. C. Hamister and H. G. MacPherson, Union Carbide Corp., National Carbon Company, "The Production and Properties of Graphite for Reactors", presented at the United Nations International Conference on the Peaceful Uses of Atomic Energy, Geneva, August 8-20, 1955. Chapter V.

Ref. 5 "Pyrographite Research and Development," Final Report, April 1, 1961. Raytheon Company Report No. S-347 to Lockheed Missiles and Space Company.

Ref. 6 Bortz, S. A. and H. H. Lund, Proc. Fourth Carbon Conference, Pergamon Press, New York, (1959) p. 531.

Ref. 7 "Pyrographalloy Research and Development," Confidential Final Report, July 16, 1962 - May 31, 1964. Raytheon Company Report No. S-682 to Re-Entry Section Special Projects Office, Department of the Navy.

Ref. 8 Franklin, R. E., Acta Cryst. 4, 253 (1951)

Ref. 9 Fischbach, D. B., "Kinetics of Graphitization," TR No. 32-532, Jet Propulsion Laboratory, February 1, 1966.

Ref. 10 Diefendarf, R. J., "Refractory Pyrolytic Materials" General Electric Company Report 63-RL-3527M, December, 1963.

Ref. 11 Lowell, C. E., "Solid Solution of Boron in Graphite", J. Am. Ceram. Soc., Vol. 50, No. 3, pp. 142-144,(Mar. 1967).

Ref. 12 Elliot, R. P., "The Boron-Carbon Systems", Final Technical Report ARF-2200-12 for U.S. Atomic Energy Commission, Contract No. AT(11-1)-578, May 1, 1960-April 30, 1961.

Ref. 13 Turnbull, J. A., M. S. Stagg and W. T. Eeles, "Annealing Studies of Boron Doped Graphite by Electron Microscopy and X-ray Diffraction", Carbon, Vol. 3, pp. 387-392 (1966).

Ref. 14 Hennig, G., "Diffusion of Boron in Graphite", J. Chem. Phys., Vol. 42, pp. 1167-1172 (1965).

Ref. 15 Mayer, R. M., "Large Interstitial Loops in Graphite Containing Boron", Brit. J. Appl. Phys., Vol. 17, pp. 431-432 (1966).

Ref. 16 Hennig, G., "Electron Microscopy of Graphite Containing Boron", J. Appl. Phys., Vol. 34, p. 237, (1963).

Ref. 17 Soule, D. E., "The Effect of Boron on the Electronic Properties of Graphite", Proc. of the Fifth Conf. on Carbon, Pergamon Press, (1963) Vol. 1, pp. 13-21.

Ref. 18 Klein, C. A. and Lepie, "Operational Performance Characteristics of Pyrolytic Graphite Thermocouples", Solid State Electronics, Vol. 7, pp. 241-252 (1964).

Ref. 19 Klein, C. A., "Electronic Transport in Pyrolytic Graphite", Marcel Dekker, Inc., New York (1966), Chapter 5 in Chemistry and Physics of Carbon, Vol. 2, edited by P. L. Walker, Jr.

Ref. 20 Gasparoux, H., A. Pacault and E. Poquet, "Thermal Variations of Diamagnetism and Crystallographic Structure of Pyrolytic Carbon Doped with Boron", Carbon, Vol. 3, pp. 65-72 (1965).

Ref. 21 Tombrel, F., "Effect of Boron on the Structure and Mechanical Properties of Pyrolytic Carbon at High Temperature", Rev. Intern. Hautes Temp. Refractaires, Vol. 3, pp. 79-84 (1966).

Ref. 22 Kotlensky, W. V., R. N. Donadio and L. M. Hagen, "Graphitization of Boron Pyrolytic Graphite", Paper MI63 presented at the Eighth Conference on Carbon, Buffalo, N.Y., June 1967, Raytheon Co. Research Div., Waltham, Mass.

Ref. 23 Kotlensky, W. V. and H. E. Martens, "Structural and High-Temperature Tensile Properties of Boron Pyrolytic Graphite", Tech. Rept. No. 32-299, Jet Propulsion Laboratory, Cal. Inst. of Tech., Pasadena, Cal., December 16, 1963.

Ref. 24 Bovarnick, B., "On the Establishment of Pyrolytic Graphite Alloys", paper presented at the Fifth Conference on Carbon, Penn. State Univ., June, 1961, Raytheon Co. Research Div., Waltham, Mass.

Ref. 25 Pappis, J., R. Donadio, L. Hagen and A. Capriulo, "Properties of Boron Doped Pyrolytic Graphite", paper presented at the Second ASTM Symposium on Pyrolytic Materials, Palm Springs, May, 1966, Raytheon Co. Research Div.

Ref. 26 Kotlensky, W. V., A. J. Capriulo, R. N. Donadio, L. M. Hagen and J. Pappis, "Effect of Boron Content on the Mechanical and Physical Properties of Boron Pyrolytic Graphite Cylinders", Paper MI64 presented at the Eighth Conference on Carbon, Buffalo, N. Y., June, 1967, Raytheon Co., Research Div., Waltham, Mass.

Ref. 27 Mehan, R. L., "Experimental Mechanical Property Data on HTM Boron Pyrolytic Graphite and HTM Pyrolytic Graphite Plate", General Electric Missile and Space Vehicle Dept. PIR No. 8155-242, October 31, 1963.

Ref. 28 Zlupko, J. and P. Bolinger, "Thermal Expansion Measurements of Boron Alloyed Pyrolytic Graphite Material from Nose Tips", General Electric Missile and Space Vehicle Div., PIR No. 8157-622, May 16, 1966.

Ref. 29 Stover, E. R., "Structure of Whiskers in Pyrolytic Graphite", Report No. 64-RL-3609M, March, 1963, General Electric Co. Research Laboratory, Schenectady, N.Y. Also Tombrel, F. and J. Rappeneau, "Preparation and Structure of Pyrolytic Carbons", Vol. II, Chap. XXV, in Les Carbones, by the French group for the study of carbons, Masson, Paris (1965).

Ref. 30 Blumenthal, H., "Determination of Boron in Metal Borides", Anal. Chem., Vol. 23, pp. 922-924, (1951), Kriege, O. H., "Analysis of Refractory Borides, Carbides, Nitrides and Silicides", Rept. No. LA-2306, Contract No. W-7405-ENG-36, March 1959.

Ref. 31 McKinley, G. J. and H. F. Wendt, "Determination of Boron in Refractory Borides by Pyrohydrolysis", Anal. Chem. Vol. 37, pp. 947-950 (1965).

Ref. 32 Wachi, F. M., D. E. Gilmartin and K. C. Jefferson, "Determination of Boron in Boron Pyrolytic Graphite", TDR-669 (6250-40) -6, Aerospace Corporation, (Jan. 1966).

Ref. 33 Fischbach, D. B., "Kinetics of Graphitization I. The High-Temperature Structural Transformation in Pyrolytic Carbons", Tech. Rept. No. 32-532, Jet Propulsion Laboratory, California Inst. of Tech. (Feb. 1, 1966).

Ref. 34 Malnick, A. M., Re-Entry Systems Dept., General Electric Co., personal communication, 1967.

Ref. 35 Feingold, E., Space Sciences Laboratory, General Electric Co., personal Communication, 1967.

Ref. 36 Thomas, J. M., C. Roscoe, G. G. Cookson, T. H. Owen, and R. Tushingham, "Determination of Boron in Boronated Graphite Crystals Using a Spark Source Mass Spectrograph", Carbon, Vol. 4, pp. 457-458, (1966)

Ref. 37 Barrington, A. E., R. F. K. Herzog, and W. P. Poschenrieder, "The Ion Microprobe Mass Spectrometer", Progress in Nuclear Energy, Series IX, Analytical Chemistry, Vol. 7, pp. 243-273, (1966)

Ref. 38 Wachi, F. M. and D. E. Gilmartin, "Boron-Content-Profile of a Boron-Pyrolytic Graphite Nose Cone Model", TR-669 (6250-40)-15, Aerospace Corporation, (July, 1966).

Ref. 39 Feldman, C. and J. Y. Ellenburg, "Spectrochemical Determination of Boron in Carbon and Graphite", Anal. Chem. 27, pp. 1714-1721 (1955).

Ref. 40 Bonini, G. M., Jarrell-Ash Corporation, personal communication.

Ref. 41 Pasztor, L. C., and J. D. Bode, "Photometric Determination of Boron by Solvent Extraction Using Monomethylthionine", Anal. Chem. Vol. 32, pp. 1530-1531 (1960).

Ref. 42 Pasztor, L. C., J. D. Bode and Q. Fernando, "Determination of Micro Quantities of Boron in Steel by a Solvent Extraction Method", Anal. Chem. Vol. 32, pp. 277-281 (1960).

Ref. 43 Umland, F., D. Thieng and G. Mueller, "Photometric Determination of Picogram Amounts of Boron", Z. Anal. Chem. Vol. 215, pp. 401-406 (1966).

Ref. 44 Goward, G. W., and V. R. Wiederkehr, "Sensitivities and Other Properties of Reagents for the Spectrophotometric Determination of Boron", Anal. Chem. Vol. 35, pp. 1542-1545 (1963).

Ref. 45 Grob, R. L., J. Cogan, J. J. Mathias, S. Mazza and A. P. Piechowski, "1.1' -Bis (6-Chloroanthraquinonyl) amine As a Reactent for Trace Amounts of Boron", Anal. Chem. Acta, Vol. 39, pp. 139-141 (1967).

Ref. 46 "Accelerated Stress Relief Program", Raytheon Company Report No. S-346, Final Report to Lockheed Missiles and Space Division, 15 September 1961. Also "Analysis Calculations", Raytheon Company, Structures Memo Report 61-65, Final Report to Aerojet General Corporation, 12 December 1961.

Ref. 47 Vapor Deposition, by Powell, Oxley and Blocher, Chapter 7, "Stresses in Deposits", John Wiley and Sons, Inc., New York (1966).

Ref. 48 Garber, A. M., "Residual Stress Considerations in the Manufacture of Pyrolytic Graphite Structures", Paper presented at ASTM Symposium on Pyrolytic Graphite in Palm Springs, California, (March 30-31, 1964).

Ref. 49 "Pyrographalloy Research and Development", confidential Final Report to Special Projects Office, Department of the Navy, Raytheon Report No. S-682, May 1964.

Ref. 50 Clark, T. J., and R. J. Larsen, Final Report on Work Statement No. 87, "Residual Stress Studies", General Electric Report P 1-WS-0232, Metallurgical Products Department, Detroit (1961).

Ref. 51 Coffin, L. F. Jr., Journal of the American Ceramic Society 47, p. 473 (1964). Also L. F. Coffin, Jr., "A Note on the Structure-Property Relationships for Pyrolytic Graphite", General Electric Research Laboratory Report 62-RL-2945M, February 1962.

Ref. 52 Bovarnick, B., "On the Establishment of Pyrolytic Graphite Alloys", presented at the 5th Carbon Conference, Pennsylvania State University, June 19-23, 1961.

Ref. 53 Pappis, J., R. Donadio, L. Hagen, A. Capriulo, "Properties of Boron Doped Pyrolytic Graphite", presented at the Second ASTM Symposium on Pyrolytic Materials, Palm Springs, May 10-11, 1966.

Ref. 54 Albert, P., and J. Parisot, Proceedings 3rd Carbon Conference, Pergamon Press, pp. 467-474, (1959).

Ref. 55 Delhaes, P., and A. Marchand, Carbon, 3, 125-140 (1965).

Ref. 56 [illegible], D. E., Proceedings 5th Carbon Conference, Vol. 1, pp. [illegible]-21, Pergamon Press (1962).

Ref. [illegible] Mayer, R. M., British Journal of Applied Physics, Vol. 15, [illegible] (1964).

Ref. 58 Turnbull, J. A., M. S. Stagg and W. T. Eeles, Carbon, 3, pp. 387-92 (1966).

Ref. 59 Gasparoux, H., A. Pacault, and E. Poquet, Carbon, 3, pp. 65-72 (1965).

Ref. 60 Tombrel, F., Revue Hautes Temperature et Refractoire, 3, pp. 79-84 (1966).

Ref. 61 Delhaes, P., and A. Marchand, Carbon, 3, pp. 115-124, (1965).

Ref. 62 Klein, C. A., "Electronic Transport in Pyrolytic Graphite", Chapter 5 in Chemistry and Physics of Carbon, Vol. 2, edited by P. W. Walker, Jr., Marcel Dekker, Inc., New York (1966).

Ref. 63 Fischbach, D. B., Technical Report No. 32-532, Jet Propulsion Laboratory, February 1, 1966.

Ref. 64 Tsuzuku, T., "Graphitization Stresses and Dislocations in Polycrystalline Carbon", Proceedings 4th Carbon Conference, p. 403, Pergamon Press, (1960).

Ref. 65 Mrozowski, S., "Mechanical Strength, Thermal Expansion and Structure of Cokes and Carbons", Proceedings 1st and 2nd Carbon Conferences, p. 31, Waverly Press, Inc. (1956).

Ref. 66 Vickers, J. M. F., "Heat Transfer Coefficients Between Fluid Jets and Normal Surfaces", Ind. and Eng. Chem., 51, pp. 967-972, (Aug. 1959).

Ref. 67 Kestin, J., and P. F. Maeder, "Influence of Turbulence on Transfer of Heat from Cylinders", NACA TN 4018, Oct. 1957.

Ref. 68 Roy, J., Aeronaut, Soc., 41, p. 1109, (1937).

Ref. 69 Kay, William, National Cylinder Gas, Detroit, Michigan, personal communication.

Ref. 70 "Advantages of MAPP Gas", Advertizing Letter, Parkin Associates, Inc., September 1966.

Ref. 71 Torkelson, T. R., and V. K. Rowe, American Industrial Hygiene Association Journal, Vol. 25, pp. 554-559, (November-December, 1964).

Ref. 72 Dieferdorf, R. J., High Temperature Technology, pp. 119-[illegible], Butterworths (1964).

Ref. 73 Diefendorf, R. J., J. Chim. Physique, pp. 815-821 (1960).

Ref. 74 Harvey, J., D. Clark and J. N. Eastabrook, Special Ceramics, Academic Press, p. 181, (1965).

Ref. 75 Brown, A. R. G., A. R. Hall and W. Watt, Nature, 172, p. 1145 (1953).

Ref. 76 Grisdale, R. O., A. C. Pfeister and W. von Roosbroeck, Bell Systems Tech. J., Vol. 30, p. 271, (1951).

Ref. 77 Johnson, G. L., R. C. Anderson, Proc. Fifth Carbon Conference, 1, p. 395, Pergamon Press. (1961).

Ref. 78 Frazee, J. D., and R. C. Anderson, Proc. Third Carbon Conference, p. 405, Pergamon Press, (1959).

Ref. 79 U. S. Patent No. 3, 213, 177 Resistance Furnace, Diefendorf, R. J., assigned to General Electric Co.

Ref. 80 Ziskind, R., General Electric Co., PIR 8157-715, August 18, 1966.

TABLE I

CROSS-REFERENCE CHART - REVISED WORK STATEMENT

AF 33(615)-3136

Old Task No.	New Task No.	Subject
3.2.1.1	3.2.1.1	Flow Control - Cones
3.2.1.2	3.2.1.2	Chemical Additives
3.2.1.3	3.2.1.3	Turbulent Nozzles
3.2.1.4	---	Temperature Gradients
---	3.2.1.4	Turbulent Nozzles - BPG
3.2.2.1	3.2.2.1	Flow Control - Frustums
3.2.2.2	3.2.2.2	Hydrocarbon Replenishment
3.2.2.3	3.2.2.3	Dilution
3.3.1	3.3.1	Terminations (C & D)
3.3.2	3.3.2	Terminations (Roundness)
3.3.3	3.3.3	Mandrel Design
3.3.4	3.3.4	Mandrel Treatment
3.3.5	3.3.5	Graphite Grades
3.3.6	3.3.6	Interrupted Deposition
---	3.3.7	Delamination Control - Cones
3.4.1.1	3.4.1.1	Deposition Rate Variations
3.4.1.2	3.4.1.2	Boron Levels
3.4.1.3	3.4.1.3	Graded Boron
3.4.1.4	3.4.1.4	Property Correlations
3.4.1.5	---	Thermal Conductivity
---	3.4.1.5	Graphitization
3.4.2.1a	3.4.2.1a	Temperature Variation
3.4.2.1b	3.4.2.1b	Other Variables - Cones
3.4.2.2	3.4.2.2	Property Evaluations
3.4.2.3	3.4.2.3a	Acetylene - PG
---	3.4.2.3b	Acetylene - BPG
3.4.2.4	3.4.2.4	Hafnium - PG Cones
3.4.3	---	Annealing
3.4.4	3.4.4	Stress Predictions
3.4.5	3.4.5	Non-Destructive Testing Techniques
---	3.4.6	Boron (Deposition)
---	3.4.7	Boron (Assay)
3.5.1	3.5.1	State-of-Art Cones
3.5.2	---	Predictability - Pt. 1
---	3.5.2	Optimization
3.5.3	---	Furnace Modification
3.5.4	---	Machining
3.5.5	---	Scale-Up
3.5.6	---	Reproducibility
3.5.7	---	Predictability - Pt. 2
3.5.8	---	Cost Reductions

TABLE II
Task 3.5.1 Summary of Runs

Run No.	Lot No.	Gas Flow SCFH	BCl_3 Flow CFH	Temp °F	Press mm Hg	Sched Time Hrs.	Actual Time Hrs.	Nozzle Pos. In.	Results: Nose Thickness	Results: Thinnest Spot on Wall	Results: Locacion of Thin Spot	Results: Machined	Remarks
1	5019	10	.109 to .015	3750	2	53	53	8-1/2	1.82 in.	.260 in.	5 in.	Yes	
2	7027	10	.109 to .015	3750	2	53	53	8-1/2	1.68	.220	4	Yes	Large nodule starting with first deposited layer. High density inclusion.
3	5021	10	.109 to .015	3750	2	53	40.5	8-1/4	1.18	.130	3	Yes	Nozzle shield came loose and choked gas flow.
4	7028	10	.109 to .015	3750	2	53	53	8-1/2	1.12	.260	3	Yes	
5	7029	10	.109 to .015	3750	2	53	53	8-1/4	.94	.170	2	Yes	
6	4022	10	.109 to .015	3750	2	53	53	8-1/2	1.22	.130	3	Yes	Nozzle shield left out inadvertently.
7	4023	10	.109 to .015	3750	2	53	53	8-1/2	1.43	.160	3	Yes	Nozzle shield installed off center.
8	7030	10	.109 to .015	3750	2	53	53	8-1/2	.93	.140	3	Yes	
9	5024	10	.109 to .015	3750	2	53	53	8-1/2	1.52	.110	3	Yes	Nozzle shield installed off center.
10	7031	10	.109 to .015	3750	2	53	53	8-1/2	1.07	.200	3	Yes	

TABLE II continued
Task 3.5.1 Summary of Runs

Run No.	Lot No.	Gas Flow SCFH	BCl_3 Flow CFH	Temp °F	Press mm Hg	Sched Time Hrs.	Actual Time Hrs.	Nozzle Pos. In.	Results: Nose Thickness	Results: Thinnest Spot on Wall	Results: Location of Thin Spot	Results: Machined	Remarks
11	7032	10	.109 to .015	3750	3.6	50	50	8-1/2	.96	.210	2	Yes	
12	5025	10	.109 to .015	3750	3.6	50	50	8-1/2	1.52	.360	2	Yes	Void in nose 1/4" from tip, 1/2" long, .040 maximum width.
13	7033	10	.109 to .015	3750	3.6	50	50	8-1/2	1.70	.260	3		Void in nose, fine opening from base of nose to 3/8" from tip.
14	5026	10	.109 to .015	3750	3.0	55	55	8-1/2	1.90	.300	2		Void in nose. Small hole 1/4" from tip. Growth within the void.
15	4026	10	.109 to .015	3750	3.0	55	55	8-1/2	.100	-	-		Growth on side wall at 2" position interfered with nose deposition.
16	5027	10	.109 to .015	3750	3.0	55	55	8-1/2	1.65	.370	3	Yes	
17	4027	10	.109 to .015	3750	3.0	55	55	8-1/2	1.150	.280	2	Yes	
18	7034	10	.109 to .015	3750	3.0	55	55	8-1/2	1.080	.230	2	Yes	
19	5029	10	.109 to .015	3750	3.0	55	4-1/2	8-1/2	.120	.020	3		Gas regulator diaphragm ruptured.
20	5030	10	.109 to .015	3750	3.0	55	27-3/4	8-1/2	1.000	.180	2		

TABLE II continued
Task 3.5.1 Summary of Runs

Run No.	Lot No.	Gas Flow SCFH	BCl_3 Flow CFH	Temp °F	Press mm Hg	Sched Time Hrs.	Actual Time Hrs.	Nozzle Pos. In.	Results: Nose Thickness	Results: Thinnest Spot on Wall	Results: Location of Thin Spot	Results: Machined	Remarks
21	7035	10	.109	3750	3.0	55	8-1/2	8-1/2	.180	.050	3		Gas regulator diaphrahm ruptured.
22	7036	10	.109	3750	3.0	55	25-1/4	8-1/2	.860	.150	3	Yes	BCl_3 Flowmeter leak.
23	7037	10	.109 to .015	3750	3.0	55	49	8-1/2	1.100	.230	2	Yes	
24	5031	10	.109 to .015	3750	3.0	55	40	8-1/2	1.430	.300	3	Yes	
25	7038	10	.109 to .015	3750	3.0	55	55	8-1/2	1.080	.250	2	Yes	
26	5032	10	.109 to .015	3750	3.0	55	55	8-1/2	1.250	.290	2	Yes	
27	7039	10	.109 to .015	3750	3.0	55	49-3/4	8-1/2	1.000	.230	2	Yes	

TABLE III

GRAPHITE GRADES
SUMMARY OF PROPERTIES

Identification	Density	Grain Size In.	Ash %	Ranges of Sizes Available	
"B"	1.68	.008	.06	3/8" to 2-3/4" dia. x 48"	
"B"	1.68	.033	.06	3" to 7" dia. x 48"	
"B"	1.68	.033	.08	8" to 30" dia. x 48"	
"B"	1.65	.008	.06	1-1/2" I.D. to 5-7/8" I.D. x 72" Tube	
"G"	1.89	All other properties and sizes same as "B"			
"D"	1.78	.016		3" dia. x 72"	Manufacturer only reports Ash for 16" thru 24" - .4%
"D"	1.78	.033		4" to 14" dia. x 72"	
"D"	1.74	.033		16" to 38" dia. x 72"	
"E"	Same as above except purified to reduce ash to .06% Typical				
"F"	1.83	All other properties same as "D" grades above - all sizes available			
"C"	1.75	.006	.25	10" to 16-1/2" dia. x 24"	
"H"	1.72	.03	.09	3" to 10" dia. x 72"	
"K"	1.72	.03	1.18	12" to 18" dia. x 72"	
"L"	1.70	.03	1.24	20" to 24" dia. x 72"	
"M"	.7[illegible]	.03	.981	30" to 50" dia. x 72"	
[illegible]	1.[illegible]	.016	.03	3" to 8" dia. x 44"	
[illegible]	[illegible]	.03	.03	9" to 18" dia. x 44"	
[illegible]	[illegible]	[illegible]	.128	9" x 20" x 24" and 16-1/2" dia. x 14"	

[illegible], Air Force Materials Laboratory, WPAFB.

TABLE IV

RATING FACTORS* FOR GRAPHITE GRADE EVALUATIONS

Graphite	K_a	K_{sf}	K_{ms}	Rating Factor
"A"	1	2	2	4
"C"	1	2	2	4
"B"	2	1.5	1	3
"E"	2	1	0	0

* See text for explanation of terms and values.

TABLE V

PROCESSING CHARACTERIZATION FOR CYLINDER DEPOSITS

GEDC[(a)] Run No.	Nominal Run Variable	Nominal Temp (°C)	Depo Time (hrs)	Nominal Furnace Pressure (torr)	Gas Flow Rates (lpm) CH_4	N_2 or A	BCl_3
1	3/8% B TMB	2000	7	20	7.5	---	---
2	15 mils/hr PG	1900	10	20	8.0	1	---
3A	10 mils/hr PG	1900	5	10	12.0	2	---
4B	3/4% TMB	2000	6	10	12.0	---	---
5A	5 mils/hr PG	1900	18	10	7.0	7	---
6A	1-1/2% B TMB	2000	6	10	11.0	---	---
7A	3% B TMB	2000	9	10	10.0	---	---
8A	3/4% B BCl_3	2000	11	10	12.0	2	0.015
9A	15-5 mils/hr PG	1900	9	10	18 to 8	2 to 12	---
10A	1-1/2% B BCl_3	2000	8	10	18.0	2	0.045
11A	3/8% B BCl_3	2000	6-1/2	10	18.0	2	0.02
12A	Repeat GEDC-2	2000	6	10	20.0	---	---
13A	Repeat GEDC-10A	2000	4-1/2	10	18.0	2	0.3
14B	Repeat GEDC-1	2000	5	10	13.5	---	---
15A	Repeat GEDC-2	2000	5-1/2	20	16.0	---	---
16A	Graded boron BCl_3 0.1 to 3/4%	2000	5	10	18	2	0.013 to 0.23
17A	Graded boron BCl_3 0.1 to 3/4%	2000	4	10	18	2	0.013 to 0.23
18A	Graded boron TMB 1-1/2 to 3/4%	2000	4-1/3	10	9 to 13	---	---
19A	Process Run No. 1 0.3% B TMB	2000	5	20	7	1.6	---
20A	Graded boron BCl_3 0.1 to 3/4%	2000	5	20	9	---	0.004 to 0.026
21A	Graded boron TMB 0.1 to 3/4%	2000	6	20	7	---	---
22A	Process Run No. 2 15-5 mils/hr PG	2000	10	20	9 to 4.5	0 to 4.5	---

(a) Tubes 1 and 2 deposited on oxidized mandrels using a through-flow system. Tubes 3 through 12 deposited using a 3-1/4 in. diameter baffle and 6 in. i.d. preheat chamber. Tubes 13 through 18 deposited using a 2 in. diameter baffle and 4 in. i.d. preheat chamber. Tubes 19 through 22 deposited using a through-flow system.

TABLE V (Cont'd)

GEDC[a] Run No.	N_2 Over TMB (lpm)	T B Used (g/min)	Cylinder Wall Thickness[b] (mils) Max	Min	Middle	Deposition Rate (mils/hr) Max	Min	Avg
1	1.5	2.4	132±9	118±3	127±7	18.9	17.0	18.0
2	---	---	111±17	102±17	111±17	11.1	10.2	10.9
3A	---	---	47±2	35.5±1.5	40.5±1.5	9.4	7.1	8.2
4B	2.0	1.1	99±1	87.5±1.5	92.5±1.5	16.5	14.6	15.5
5A	---	---	104±4	79±1	90±2	5.8	4.4	5.0
6A	3.0	1.85	95±1	81±1	84±2	15.4	13.5	14.5
7A	4.0	2.0	112±4	109±1	109±1	12.5	12.1	12.2
8A	---	---	113±3	98.5±0.5	101±1	10.3	9.0	9.5
9A	---	---	75±6	60.5±0.5	66±0.5	8.3	6.7	7.4
10A	---	---	133±4	110±4	123±4	16.7	13.7	15.1
11A	---	---	84.5±1.5	69±0	76±1	13.1	10.7	11.9
12A	---	---	70±3	53±1	60±2	11.7	8.9	10.2
13A	---	---	159±8	125±3	139±4	35.5	27.8	31.1
14B	0.5	0.126	99.5±1.5	78.5±1.5	87.5±1.5	19.9	15.7	17.5
15A	---	---	95.5±2.5	75.5±0.5	81.5±1.5	17.5	13.7	15.0
16A	---	---	139±13	103±1	115±6	27.9	20.8	24.0
17A	---	---	110±7	80±1	94±4	27.5	20.0	23.0
18A	5 to 1	1.55	81±3	71.5±1.5	80±2	18.7	16.5	18.1
19A	0.4	0.26	69±2	67±2	68.5±2.5	13.8	13.4	13.7
20A	---	---	85±1	79±1	84±2	17.0	15.8	16.6
21A	0.2 to 1.1	0.32	105±5	96±5	101±4	17.5	16.0	16.9
22A	---	---	109±5	95±6	101±4	10.5	9.5	10.1

(b) Maximum and minimum measured over center 7 in. section of tube.

TABLE VI

DENSITY AND BORON ANALYSIS FOR CYLINDERS

GEDC Run No.	Density (g/cc) Top	Base	Boron Analysis[a] (%) Top	Center	Base
1	2.22	2.20	1.2	0.9	1.6
2	2.17	2.17			
3A	1.98				
4B	2.22	2.23	1.3	1.0	1.0(1.0)
5A	1.94(1.94)	1.99			
6A	2.23	2.22	0.9	0.7	1.2(1.1)
7A	2.22	2.23	1.9	1.3	1.0
8A	2.20	---	0.14	0.13	0.14
9A	2.14	---			
10A	2.20	---	0.22	0.25	0.19
11A	2.20	---	0.12	0.11	0.10
12A	2.01(1.98)	---			
13A	2.23	---	0.9	---	1.0
14B	2.20	---	0.1	0.1	0.1
15A	2.19	---			
16A	2.21	---	$0.02_{/0.9}$	$0.01_{/--}$	$0.02_{/1.3(1.2)}$
17A	2.22	---	$0.5_{/1.3}$	---	$0.3_{/1.5}$
18A	2.23	---	$1.5_{/0.6}$	---	$1.7_{/0.7}$
19A	2.20	---	0.2	0.2	0.2
20A	2.21	---	$0.2_{/0.4}$	---	$0.1_{/0.3}$
21A	2.23	---	$0.2_{/1.2}$	$0.2_{/1.4}$	$0.2_{/1.2}$
22A	2.19	---			

(a) Boron results for graded deposits reported as outside/inside surfaces.

TABLE VII

MEASURED TANGENTIAL RESIDUAL STRESS (O.D.) FOR CYLINDERS

GEDC Run No.	Ring Gapping Technique			Strain Gauge Technique		
	Location	t/R	σ, psi	Location	t/R	σ, psi
3A				Center	0.026	+330
				Base	0.029	-920
4B				Center	0.06	-7200
				Base	0.06	-8200
6A				Top	0.05	-4200
				Center	0.054	-4500
				Base	0.06	-6800
8A	Center	0.065	-3850			
9A				Center	0.044	-1500
10A	Center	0.076	-5050			
11A				Center	0.049	-3900
12A				Center	0.039	-600
14B				Center	0.057	-4200
				Center	0.056	-3400
15A				Center	0.053	-3900
				Center	0.053	-3600
18A	Top	0.050	-2200	Top	0.048	-5700
	Center	0.053	-3500	Center	0.052	-6500
	Base	0.053	-4900	Base	0.054	-8600
19A	Top	0.041	-2500			
	Center	0.044	-2600	Center	0.046	-3100
	Base	0.041	-2500			
20A	Center	0.056	-5100	Center	0.056	-5700
				Center	0.056	-6000
22A	Base	0.064	-4100	Top	0.055	-2800

TABLE VIII

MECHANICAL PROPERTY DATA FOR CYLINDERS

	Location	Modulus psi ($X10^{-6}$) E	Poisson's Ratio (μ)	Ring Crushing Strength (psi)
3A	Top	4.3	-0.02	15,200
4B	Base	6.4	-0.15	21,200
6A	Center	5.8	-0.11	23,500
9A	Center	5.1	-0.06	28,300
11A	Center	5.2	-0.08	18,900
12A	Center	5.1	-0.04	27,000
14B	Center	4.7	-0.13	24,400
15A	Center	4.6	-0.10	15,000
18A	Top	7.8-8.2	---	24,400
	Center	7.6-8.3	-0.08	22,600
	Base	7.2-9.2	---	16,200
19A	Center	4.5	-0.12	25,700
20A	Center	6.0	-0.08	28,700
22A	Top	4.8	-0.10	13,300

TABLE IX

EFFECT OF ANNEALING ON MECHANICAL PROPERTY DATA FOR CYLINDERS

	As-Deposited			HT 2000°C 20 Hrs		
	1.7/0.6 GEDC-18A	0.1/0.4 GEDC-20A	0.2% B GEDC-19A	1.7/0.6 GEDC-18A	0.1/0.4 GEDC-20A	0.2% B GEDC-19A
t/R	0.051	0.056	0.046		0.055	0.046
σ (o.d. residual stress, psi)	-5700 to -8600	-6000	-3100	Ring Cracked	-12,600	-9700
σ (ring crush strength, psi)	16,200 to 24,400	28,700	25,700		16,700	19,100
$EX10^6$, psi	7.2 to 9.2	6.0	4.5		8.6	8.7
μ	-0.08	-0.08	-0.12	---	---	---
C_0 Out	6.76	6.85	6.86	6.74	6.81	6.80
C_0 In	6.84	6.83	6.86	6.75	6.76	6.78
	Percent Change After Annealing					
a-direction (width)	---	---	---	+2.8	+1.2	+1.1%
c-direction (thickness)	---	---	---	-5.2	-0.8	-1.4%
Wt	---	---	---	0	nil	0
O.D.	---	---	---	---	+0.7	+1.0%

TABLE X

EFFECT OF TIME ON THE GRAPHITIZATION OF BPG

GEDC Run No.	Boron (%)	As-Deposited C_0	As-Deposited Time (hrs)	20-Hr Anneal (2000°C) C_a
20A	0.1	6.85	5	6.81
19A	0.2	6.86	5	6.78
20A	0.4	6.83	1	6.76
18A	0.6	6.84	1	6.75
18A	1.7	6.76	4	6.74

TABLE XI

PROCESS CONDITIONS FOR FRUSTUMS DEPOSITED IN TASK 3.2.2.1

Run No.	Gas Flow cfh	H_2 flow cfh	BCl_3 flow cfh	Temp. °F*	Pressure mm	Velocity ips
9031	60	0	.32	3800	5.0	780 Inlet 4200 Exhaust
9032	60	0	.32	3800	5.0	2030 Inlet 5590 Exhaust
9033	60	0	.32	3800	5.0	2030 Inlet 4200 Exhaust

* NEARLY 2100°C

TABLE XII

PROCESS CONDITIONS FOR CYLINDERS DEPOSITED IN TASK 3.2.2.2

Run No.	Gas Flow cfh	H_2 Flow cfh	BCl_3 Flow cfh	Temp. ^{o}F	Pressure mm
8038	24 Lower 12 Upper	0	0	3800	5.0
8039	18 Lower 18 Upper	0	0	3800	5.0

TABLE XIII

PROCESS CONDITIONS FOR CYLINDERS DEPOSITED IN TASK 3.2.2.3

Run No.	Gas Flow cfh	H_2 Flow cfh	BCl_3 Flow cfh	Temp. ^oF	Pressure mm	Velocity ips	Mandrel I.D. in.
8035W	36	0	.19	3800	5.0	1610	5.0
8035E	36	14	.19	3800	5.0	2020	5.0
4040	36	7	.19	3800	5.0	1820	5.0
4041	32	6	.17	3800	5.0	1610	5.0
8043E	36*	12	.15	3800	5.0	2430	4.5
8043W	36*	0	.15	3800	5.0	1990	4.5
8036W	36	0	0	3800	5.0	1610	5.0
8036E	36	14	0	3800	5.0	2020	5.0

*Planned at 30 cfh, run in error at 36

TABLE XIV

DEPOSITION CONDITIONS FOR TASK 3.4.6

PRESSURE ↓	TEMPERATURE →		
	3800°F (~2100°C)	3640°F (~2000°C)	3450°F (~1900°C)
3 MM	(240:1 30:1)* (120:1 60:1)	(240:1 30:1) (120:1 60:1)	(120:1 60:1)
5 MM	(240:1 30:1) (120:1 60:1)	(240:1 30:1) (120:1 60:1)	(240:1 30:1) (120:1 60:1)
7 MM	(240:1 30:1) (120:1 60:1)		

*Figures in parentheses are volume ratios of hydrocarbon source gas-to-boron source gas flows. Detroit natural gas (predominantly methane) and boron trichloride were used for these studies.

TABLE XV

CALCULATED LINEAR VELOCITIES FOR TASK 3.4.6

Temperature (°F)	Pressure (MM)	Velocity (ips)
3800	3	3300
3800	5	2000
3800	7	1400
3640	3	3200
3640	5	1950
3640	7	1350
3450	3	3000
3450	5	1850
3450	7	1300

TABLE XVI

DEPOSITION CONDITIONS FOR TASK 3.4.6

Run	Temp	Press.	(CFH) CH_4	(CFH) BCl_3	CH_4/ BCl_3	Hrs. Time
8044-1	3800	5	36	0.60	60	7-2/3
8044-2	3800	5	36	1.20	30	7-2/3
8045-1	3800	5	36	0.15	240	10
8045-2	3800	5	36	0.30	120	10
8046-1	3800	3	36	0.15	240	10
8046-2	3800	3	36	0.30	120	10
8047-1	3800	3	36	0.60	60	10
8047-2	3800	3	36	1.20	30	10
8048-1	3800	7	36	0.60	60	10
8048-2	3800	7	36	0.30	120	10
8049-1	3800	7	36	0.15	240	7-5/6
8049-2	3800	7	36	1.20	30	7-5/6
8050-1	3640	5	36	0.30	120	8
8050-2	3640	5	36	0.60	60	8
8051-1	3640	5	36	0.15	240	14 Min.
8051-2	3640	5	36	1.20	30	14 Min.
8052-1	3640	5	36	0.15	240	8
8052-2	3640	5	36	1.20	30	8
8053-1	3640	3.4	36	0.30	120	8
8053-2	3640	3.4	36	0.60	60	8
8056-1	3640	3.5-4.5	36	0.15	240	8
8056-2	3640	3.5-4.5	36	1.20	30	8
*8060-1	3640	3	36	0.15	240	4-1/3
*8060-2	3640	3	36	1.20	30	4-1/3
8061-1	3640	5	36	0.15	240	7
8061-2	3640	5	36	0.08	450	7
8055-1	3450	5	36	0.30	120	8
8055-2	3450	5	36	0.60	60	8
8058-1	3450	3	36	0.30	120	8
8058-2	3450	3	36	0.60	60	8
8059-1	3450	5	36	0.15	240	8
8059-2	3450	5	36	1.20	30	8
8065-1	3450	7	36	0.15	240	7
8065-2	3450	7	36	0.30	120	7

* For analysis these two deposits will be reversed (See text)

TABLE XVII

TEST RESULTS FOR TASK 3.4.6

Run	Stress[1] psi Btm	Top	t/r^2 Btm	Top	Density g/cc Btm	Top	Boron Analysis[3] % Btm	Top
8044-1	4893	4464	.054	.050			.67	.66
8044-2	6152	5005	.064	.056	2.227	2.227	.94	.80
8045-1	5285	4746	.078	.068	2.232	2.224	.63	.52
8045-2	-	-	.079	.081	2.229	2.223	.65	.63
8046-1	-	-	.053	.047	2.212	2.208	.39	.28
8046-2	-	-	.052	.050	2.216	2.210	.47	.38-.43
8047-1	-	-	.055	.058	2.224	2.223	.55	.50
8047-2	4795	4416	.068	.059	2.231	2.228	.71	.63
8048-1	-	-	.083	.083	2.234	2.229	.915	.755
8048-2	6629	6124	.091	.080	2.237	2.232	.74	.69
8049-1	-	-	.081	.079	2.229	2.226	.40	.37
8049-2	5081	4995	.072	.068	2.225	2.224	.91	.84
8050-1	5126	4525	.059	.051	2.236	2.232	.90	.85
8050-2	4256	3937	.057	.049	2.226	2.228	1.05	.99
8051-1	-	-	-	-	-	-	-	-
8051-2	-	-	-	-	-	-	-	-
8052-1	3570	2660	.058	.049	2.223	2.219	.385	.30
8052-2	3070	1950	.058	.052	2.228	2.225	.87	.80
8053-1	3953	3267	.046	.039	2.232	2.228	.91	.87
8053-2	3961	2975	.046	.038	2.230	2.228	.96	.98
8056-1	-	-	-	-	-	-	-	-
8056-2	-	-	-	-	-	-	-	-
*8060-1	1647	1732	.022	.022	2.227	2.225	1.12	.92
*8060-2	1950	1577	.024	.021	2.220	2.213	.75	.60
8061-1	4653	4404	.049	.045	2.239	2.235	.85	.85
8061-2	3073	3341	.044	.043	2.232	2.234	.55	.62
8055-1	-	-	-	-	2.219	2.205	1.56	1.37
8055-2	-	-	-	-	2.204	2.209	1.63	1.35
8058-1	2956	2163	.040	.029	2.218	2.212	1.31	1.14
8058-2	2814	2268	.033	.026	2.207	2.207	1.29	1.14
8059-1	-	-	.049	.045	2.230	2.231	1.10	.97
8059-2	3100	986	.048	.042	2.221	2.221	1.46	1.28
8065-1	-	-	-	-	-	-	-	-
8065-2	-	-	-	-	-	-	-	-

*For analysis these two deposits will be reversed (See text)

TABLE XVII Continued

Footnotes:

(1) Stress determined by cut-ring displacement method assuming 4.5 x 10^6 psi as modulus of elasticity.

(2) t/r - thickness/radius of deposit.

(3) Boron analysis obtained from Task 3.4.7 by pyrohydrolysis technique.

TABLE XVIII

REPRODUCIBILITY OF STANDARDS IN SEMIQUANTITATIVE SPECTROGRAPHIC METHOD FOR BORON ASSAY

Mixture W/O B	Weight mg.	Sample No.	Percent Transmittance 2496.78 A	2497.73 A
0.50	2	1	95.5	90.9
		2	95.4	84.4
0.50	4	1	88.6	67.7
		2	85.5	65.5
2.00	2	1	74.4	51.5
		2	68.7	45.1
2.00	4	1	53.5	38.1
		2	42.5	28.3
8.00	2	1	32.7	23.0
		2	32.8	23.8
8.00	4	1	27.3	22.5

TABLE XIX

REPRODUCIBILITY OF BORON ASSAY BY COMPARISON WITH EXTERNAL STANDARDS IN LIGHT EMISSION SPECTROSCOPY

Deposit	Reading	Reported w/o B			Previous w/o B
		Shot 1	Shot 2	Average	
2-48	1	0.18	0.18	0.18	0.15
1-49	1	0.36	0.41	0.39	
	2	0.38	0.46	0.42	
	3	0.40	0.43	0.42	
	Av.	0.38	0.43	0.41	0.31
P-1-B	1	0.95	0.75	0.85	
	2	1.10	0.86	0.98	
	3	1.07	0.87	0.97	
	Av.	1.04	0.83	0.93	
P-1-D	1	0.80	0.94	0.87	
	2	0.95	1.20	1.08	
	3	0.92	1.07	1.00	
	Av.	0.89	1.07	0.98	
P-1-F	1	0.83	0.82	0.83	
	2	0.88	1.02	0.95	
	3	0.89	1.00	0.95	
	Av.	0.87	0.95	0.91	

TABLE XX

COMPARISON OF BORON ASSAY BY PYROHYDROLYSIS AND LIGHT EMISSION SPECTROSCOPY

Run(p.p.m.-CH_4/BCl_3) Loc.		Weight Per Cent Boron							Plate
		Pyrohydrolysis		Spectroscopy (SnO_2 standard)					
3600°F Deposits:		1.	2.	1.	2.	3.	4.	(Average)	
2-48 (3-1000)	1 in.	0.056		0.057	0.060	0.069	0.066	(0.065)	a
				0.057	0.054	0.053	0.057	(0.056)	b
				0.057	0.057	0.057	0.055	(0.057)	c
1-49 (3-250)	1 in.	0.34		0.37	0.36	0.38	0.39	(0.38)	a
				0.38	0.40	0.43	0.41	(0.40)	b
				0.40	0.39	0.39	0.37	(0.39)	c
8046-1(3-240)	B	0.39		0.42	0.40	0.41	0.41	(0.41)	b
	D	0.29	0.27	0.32	0.30	0.31	0.31	(0.31)	d
8046-2(3-120)	B	0.47		0.46	0.46	0.46	0.44	(0.46)	d
	D-f	0.38		0.35	0.34	0.35	0.35	(0.35)	d
	D-e	0.43		0.39	0.41	0.40	0.40	(0.40)	d
8047-1(3-60)	B	0.55		0.43	0.40	0.44	0.40	(0.42)	e
				0.49	0.52	0.51	0.48	(0.50)	j
	D	0.50		0.41	0.41	0.38	0.43	(0.43)	e
8047-2(3-30)	B	0.71		0.51	0.54	0.51	0.54	(0.53)	e
				0.83	0.84	0.81	0.81	(0.82)	j
	D	0.63		0.52	0.51	0.57	0.57	(0.54)	e
8043-2(5-240) +H_2	B	0.46	0.48	0.47	0.49	0.45	0.47	(0.47)	b
	D	0.43		0.45	0.45	0.47	0.44	(0.45)	b
8045-1(5-240)	B	0.63		0.86	0.89	0.90	0.91	(0.89)	i
	D	0.52		0.52	0.54	0.53	0.53	(0.53)	i
8045-2(5-120)	B	0.66	0.64	0.65	0.73	0.80	0.73	(0.73)	b
	D	0.63		0.60	0.63	0.63	0.62	(0.62)	d
8044-1(5-60) +H_2	B	0.67		0.76	0.79	0.77	0.79	(0.78)	f
	D	0.66		0.84	0.81	0.84	0.86	(0.84)	f

TABLE XX, Continued

Run(p,mm-CH_4/BCl_3)	Loc.	Weight Per Cent Boron: Pyrohydrolysis 1.	Pyrohydrolysis 2.	Spectroscopy (SnO_2 standard) 1.	2.	3.	4.	(Average)	Plate
3800°F Deposits, cont.:									
8044-2(5-30)	B	0.96	0.93	0.84	0.88	0.88	0.97	(0.89)	e
				0.86	0.89	0.88	0.92	(0.89)	f
				0.63	0.65	0.64	0.65	(0.64)	f
				0.99	0.92	0.92	1.00	(0.96)	j
	D	0.80		0.76	0.75	0.77	0.80	(0.77)	f
8049-1(7-240)	B	0.40	0.40	0.41	0.38	0.39	0.41	(0.40)	h
	D	0.37		0.36	0.39	0.35	0.38	(0.37)	h
8048-2(7-120)	B	0.74		0.55	0.56	0.57	0.57	(0.56)	g
				0.80	0.80	0.81	0.80	(0.80)	j
	D	0.69		0.75	0.79	0.79	0.77	(0.78)	g
8048-1(7-60)	B	0.90	0.91	0.68	0.72	0.71	0.71	(0.71)	g
				0.91	0.88	0.88	0.90	(0.89)	j
	D	0.76	0.75	0.81	0.81	0.84	0.84	(0.83)	g
8049-2(7-30)	B	0.91		0.90	1.02	0.87	1.05	(0.96)	h
	D	0.84		0.89	0.87	0.89	0.94	(0.90)	h
3640°F Deposits									
8052-1(5-240)	B	0.38	0.39	0.35	0.35	0.35	0.36	(0.35)	k
	D	0.30		0.34	0.32	0.32	0.32	(0.32)	k
8050-1(5-120)	B	0.91	0.89	0.87	0.85	0.93	0.90	(0.89)	i *
	D	0.85	0.84	0.80	0.86	0.85	0.84	(0.84)	i *
8050-2(5-60)	B	1.05		0.98	0.99	0.98	0.94	(0.97)	i *
	D	0.99		1.01	1.07	1.08	1.03	(1.05)	i *
8052-2(5-30)	B	0.87		1.02	1.03	1.01	1.01	(1.02)	k
	D	0.80		0.81	0.82	0.82	0.78	(0.81)	k
8060-2(3-30)	B	1.12		0.83	0.80	0.78	0.80	(0.80)	p *
				1.15	1.10	1.05	1.08	(1.09)	q
	D	0.92		0.68	0.69	0.70	0.69	(0.69)	p *
				0.90	0.91	0.90	0.89	(0.90)	q

TABLE XX, Continued

Run(p,m-CH_4/BCl_3)	Loc.	Weight Per Cent Boron: Pyrohydrolysis 1_a	Pyrohydrolysis 2_a	Spectroscopy (SnO_2 standard) 1_s	2_s	3_s	4_s	(Average)	Plate
3640°F Deposits, Cont.:									
8033-1(3.4-120)	B	0.91		0.97	0.97	0.99	1.05	(0.99)	1
	D	0.87		0.90	0.87	0.86	0.89	(0.88)	1
8033-2(3.4-60)	B	0.96		1.03	0.97	0.97	1.00	(0.99)	1
	D	0.98		0.94	0.91	0.93	0.90	(0.92)	1
8060-1(3-240)	B	0.75		0.50	0.46	0.49	0.47	(0.48)	p *
				0.73	0.70	0.74	0.71	(0.72)	q
	D.	0.60		0.43	0.43	0.44	0.44	(0.44)	p *
				0.61	0.60	0.63	0.63	(0.62)	q
3450°F Deposits									
8059-1(5-240)	B	1.15	1.05	1.00	0.95	0.95	1.00	(0.97)	o *
	D	0.97		0.90	0.95	0.90	0.90	(0.91)	o *
8055-1(5-120)	B	1.56	1.51						
	D	1.37		1.42	1.37	1.41	1.27	(1.37)	m *
8055-2(5-60)	B	1.63	1.63	1.36	1.36	1.42	1.40	(1.39)	g
				1.25	1.25	1.30	1.30	(1.28)	j
				1.50	1.46	1.46	1.46	(1.47)	n *
	D	1.35		1.41	1.41	1.37	1.46	(1.41)	n *
8059-2(5-30)	B	1.46		1.20	1.35	1.35	1.30	(1.30)	o *
	D	1.28		1.50	1.35	1.40	1.50	(1.44)	o *
8058-1(3-120)	B	1.31		1.40	1.35	1.40	1.38	(1.38)	m *
	D	1.14		1.22	1.25	1.27	1.25	(1.25)	m *
8058-2(3-60)	B	1.29		1.40	1.45	1.42	1.40	(1.42)	m *
	D	1.14		1.25	1.27	1.18	1.18	(1.22)	m *
3270°F Deposits (flat plate)									
P-1 (2-70)	3 in.	0.78	0.79	0.81	0.84	0.81	0.89	(0.84)	a
	5 in.	0.84	0.86	0.70	0.70	0.68	0.70	(0.70)	a
				1.03	0.97	0.95	1.01	(0.99)	b
				0.82	0.82	0.83	0.81	(0.82)	c
	6 in.	0.92	0.93	1.10	1.03	1.09	1.03	(1.03)	a

TABLE XX, Continued

NOTES: Spectroscopic analyses enclosed by brackets ({ }) were separate samples from the same bottle before mixing with SnO_2 as a standard. Letters in "Plate" column indicate spectroscopic data from the same photographic plate. Capital letters in "Loc." column indicate different positions along the gas flow stream (B=4 in., D=12 in.). small letters ("f" and "c") indicate different locations around the circumference at the same position. The * in the "Plate" column indicates that the powder was diluted with spectroscopic graphite a second time (1/4) before mixing with SnO_2; all others were diluted only once (1/9).

TABLE XXI

BORON ASSAY BY PYROHYDROLYSIS FOLLOWED BY TITRATION OR SPECTROPHOTOMETRY

Run(p,mm-CH_4/BCl_3)	Loc.	Weight Per Cent Boron	
		Titration (1 g sample)	Spectrophotometry (0.1 g. sample)
3450°F Deposit			
8065-1(7-240)	B	1.13, 1.12	
	D	1.40, 1.46	
8065-2(7-120)	B	1.23, 1.28	
	D	1.55	
3640°F Deposit			
8061-2(5-450)	B	0.55	(.064, 0.56)* 0.55, 0.56
	D	0.62	(0.56, 0.56)* 0.59, 0.60
8061-1(5-240)	B	0.85	(0.80, 0.80)* 0.77, 0.80
	D	0.85	
3270°F Deposit			
P1-F (2-70)	3 in.	0.78, 0.79	0.75, 0.74, 0.75, 0.72, 0.75, 0.75, 0.69 (0.73 average)

*Duplicate analyses of the same sample.

TABLE XXII

REPRODUCIBILITY OF RESULTS ON SMALL SAMPLES BY PYROHYDROLYSIS AND SPECTROPHOTOMETRY

Sample Description	Weight Per Cent Boron				
	1.	2.	3.	4.	(Average)
PG-6053, nose, last ½	0.17	0.20	0.20	0.21	(0.20)
PG-6065, skirt, last ½	0.51	1.03	0.88	0.83	(0.81)
PG-5065, skirt, last ½	1.11	0.85	0.91	0.84	(0.93)

TABLE XXIII

PROCESSING CHARACTERISTICS FOR CYLINDER DEPOSITS*

Cylinder	BCl_3 Flow (lpm)	Boron Assay** (%)	Wall Thickness*** (mils) Max.	Min.	Mid
GEDC-1R	0.03	---	38 ± 3	30 ± 3	36 ± 3
GEDC-2R	0.03	0.32 ± 0.08	100 ± 2	96 ± 3	99 ± 2
GEDC-3R	0.03	0.29 ± 0.03	75 ± 5	72 ± 4	74 ± 5
GEDC-4R	0.015	0.13 ± 0.02	77 ± 3	74 ± 2	76 ± 3
GEDC-5R	0.06	0.74 ± 0.1	79 ± 5	71 ± 3	78 ± 3
GEDC-6R	0.045	0.48 ± 0.05	81 ± 3	75 ± 3	80 ± 2
GEDC-7R	Graded 0.06 to 0.02	0.67/0.24	90 ± 5	83 ± 5	87 ± 5
GEDC-8R	Graded 0.045 to 0.02	0.40/0.22	75 ± 3	72 ± 2	74 ± 3

*Nominal 2000°C, 15 torr, CH_4 flow 9 lpm.

**Boron assay (weight percent) measured at center of cylinder. Reported as o.d./i.d. for graded deposits.

***Measured over central 7-inch section of cylinder. Min. at gas inlet side of cylinder.

TABLE XXIV

PROPERTY MEASUREMENTS ON AS-DEPOSITED MATERIAL

Ring Number	Failure Stress (psi)	Modulus psi, 10^6	Poisson's Ratio	Residual Stress (psi)	Ultimate Stress (psi)	t/r	Boron* (%)
GEDC-4R	24,000	4.4	-0.15	-4000	28,900	0.055	0.13
GEDC-3R	22,500	5.2	-0.09	-6700	29,200	0.052	0.29
GEDC-6R	18,400	5.8	-0.15	-6100	24,500	0.052	0.48
GEDC-5R	21,500	7.6	-0.15	-7100	28,600	0.054	0.74
GEDC-7R	22,200	7.1	-0.13	-7300	29,500	0.057	0.67/0.24
GEDC-8R	25,100	6.0	-0.12	-5800	30,900	0.052	0.40/0.22

*Given as o.d./i.d. for graded deposits

TABLE XXV

PROPERTY MEASUREMENTS ON RINGS ANNEALED AT 2000° C FOR 5 HOURS

Ring No.	Failure Stress (psi)	Modulus, (psi, 10^6)	Poisson's Ratio	Residual Stress (psi)	Ultimate Stress (psi)	t/r
GEDC-4R	19,300	6.0	-0.12	- 7,400	26,700	0.055
GEDC-3R	17,400	8.7	-0.07	-12,400	29,800	0.052
GEDC-6R	15,200	8.6	-0.11	-10,900	26,100	0.052
GEDC-5R	19,000	9.5	-0.14	-12,800	31,800	0.054
GEDC-7R	19,500	9.3	-0.15	-11,700	31,200	0.057
GEDC-8R	11,700*	8.1	-0.10	-10,500	22,200	0.052

*Ring delaminated during test.

TABLE XXVI

PROPERTY MEASUREMENTS ON RINGS ANNEALED AT 2000° C FOR 15 HOURS

Ring No.	Failure Stress (psi)	Modulus (psi, 10^6)	Poisson's Ratio	Residual Stress (psi)	Ultimate Stress (psi)	t/r
GEDC-4R	15,100	6.9	-0.11	- 9,200	24,300	0.055
GEDC-3R	17,500	8.9	-0.11	-12,400	29,900	0.052
GEDC-6R	16,300	9.3	-0.07	-12,200	28,500	0.052
GEDC-5R	13,800	10.2	-0.16	-13,700	27,500	0.054
GEDC-7R	18,900	10.0	-0.16	-11,700	30,600	0.057
GEDC-8R	11,300*	7.6	-0.11	- 9,200	20,500	0.052

*Ring delaminated during test.

TABLE XXVII

RELATIVE STRUCTURAL INTEGRITY*

Cylinder No.	As-Deposited	After Annealing at 2000° C 5-Hour Anneal	15-Hour Anneal
GEDC-4R	1.0	0.44	0.28
GEDC-3R	0.53	0.22	0.22
GEDC-6R	0.48	0.22	0.21
GEDC-5R	0.50	0.24	0.16
GEDC-7R	0.53	0.29	0.28
GEDC-8R	0.69	---	---

*Calculated as (t/r X failure stress) residual stress and normalized for as-deposited cylinder GEDC-4R equal one.

TABLE XXVIII

DIMENSIONAL CHANGES AFTER ANNEALING AT 2000° C

Cylinder Number	5-Hour Anneal Thickness (%)	5-Hour Anneal Width (%)	15-Hour Anneal Thickness (%)	15-Hour Anneal Width (%)
GEDC-4R	-1.0	+0.5	-1.6	+0.6
GEDC-3R	-2.4	+0.7	-3.5	+1.3
GEDC-6R	-2.5	+0.9	-3.4	+1.2
GEDC-5R	-2.0	+1.0	-2.2	+1.1
GEDC-7R	-1.4	+0.5	-2.1	+0.9
GEDC-8R	-1.6	+0.5	-2.9	+0.9

TABLE XXIX

UNIT CELL HEIGHT (C_o) FOR CYLINDER DEPOSITS

Cylinder	Boron* Assay, %	Unit Cell Height, C_o, Å	
		o.d. Surface	i.d. Surface
GEDC-4R	0.13 ± .02	6.85	6.85
GEDC-3R	0.29 ± .03	6.82	6.84
GEDC-6R	0.48 ± .05	6.78	6.81
GEDC-5R	0.74 ± .1	6.75	6.78
GEDC-7R	0.67/0.24	6.74	6.84
GEDC-8R	0.40/0.22	6.78	6.81

*Boron assay at center of cylinder, reported as o.d./i.d. for graded deposits.

TABLE XXVII

RELATIVE STRUCTURAL INTEGRITY*

Cylinder No.	As-Deposited	After Annealing at 2000° C 5-Hour Anneal	15-Hour Anneal
GEDC-4R	1.0	0.44	0.28
GEDC-3R	0.53	0.22	0.22
GEDC-6R	0.48	0.22	0.21
GEDC-5R	0.50	0.24	0.16
GEDC-7R	0.53	0.29	0.28
GEDC-8R	0.69	---	---

*Calculated as (t/r X failure stress) residual stress and normalized for as-deposited cylinder GEDC-4R equal one.

TABLE XXVIII

DIMENSIONAL CHANGES AFTER ANNEALING AT 2000° C

Cylinder Number	5-Hour Anneal Thickness (%)	5-Hour Anneal Width (%)	15-Hour Anneal Thickness (%)	15-Hour Anneal Width (%)
GEDC-4R	-1.0	+0.5	-1.6	+0.6
GEDC-3R	-2.4	+0.7	-3.5	+1.3
GEDC-6R	-2.5	+0.9	-3.4	+1.2
GEDC-5R	-2.0	+1.0	-2.2	+1.1
GEDC-7R	-1.4	+0.5	-2.1	+0.9
GEDC-8R	-1.6	+0.5	-2.9	+0.9

TABLE XXIX

UNIT CELL HEIGHT (C_o) FOR CYLINDER DEPOSITS

Cylinder	Boron* Assay, %	Unit Cell Height, C_o, Å	
		o.d. Surface	i.d. Surface
GEDC-4R	0.13 ± .02	6.85	6.85
GEDC-3R	0.29 ± .03	6.82	6.84
GEDC-6R	0.48 ± .05	6.78	6.81
GEDC-5R	0.74 ± .1	6.75	6.78
GEDC-7R	0.67/0.24	6.74	6.84
GEDC-8R	0.40/0.22	6.78	6.81

*Boron assay at center of cylinder, reported as o.d./i.d. for graded deposits.

TABLE XXX

EFFECT OF ANNEALING AT 2000° C ON UNIT CELL HEIGHT (C_o) Å

Cylinder No.	As-Deposited o.d.	As-Deposited i.d.	Annealed 5 Hours Whole Ring o.d.	Annealed 5 Hours Whole Ring i.d.	Annealed 5 Hours Cut Ring o.d.	Annealed 5 Hours Cut Ring i.d.	Annealed 15 Hours Whole Ring o.d.	Annealed 15 Hours Whole Ring i.d.	Annealed 15 Hours Cut Ring o.d.	Annealed 15 Hours Cut Ring i.d.
GEDC-4R	6.85	6.85	6.81	6.81	6.82	6.82	6.81	6.80	6.80	6.82
GEDC-5R	6.75	6.78	6.73	6.73	6.74	6.74	6.73	6.74	6.73	6.73
GEDC-7R	6.74	6.84	6.74	6.80	6.74	6.80	6.73	6.78	6.73	6.76

TABLE XXXI

COEFFICIENT OF THERMAL EXPANSION FROM 0 - 1000° C

Cylinder No.	Boron %	As-Deposited a-Direction	CTE X 10^6 c-Direction	After Heat Treating c-Direction X 10^6 HT 2000° C 15 hours
GEDC-4R	0.13	0.8 ± 0.2	24.3	25.0
GEDC-3R	0.29	"	25.5	27.0
GEDC-6R	0.48	"	26.1	23.0
GEDC-5R	0.74	"	28.1	25.8

TABLE XXXII

BORON ASSAY AND C_o CHARACTERIZATION FOR CYLINDER GEDC-9R

	Samples Taken At 3" above base (Wall thickness 145 mils)		Samples Taken At 5" above base (Wall thickness 158 mils)	
	Boron w/o	C_o Å	Boron w/o	C_o Å
o.d.	0.53	6.75	0.52	6.74
50 mils from o.d.	---	---	0.47	6.75
75 mils from o.d.	(0.6)	6.78	---	---
87 mils from o.d.	---	---	0.44	6.80
i.d.	0.21	6.85	0.21	6.84

Cylinder deposited at 2000° C, 15 mm furnace pressure, 9 lpm methane flow, graded BCl_3 flow from 0.053 lpm to 0.015 lpm in seven increments. Deposition time 8 hours.

TABLE XXXIII

PROCESSING CHARACTERISTICS FOR CYLINDERS GEDC-10R - 13R*

Cylinder No.	Nominal Boron o.d./i.d., %	Average t/r	Remarks
GEDC-10R	0.5/0.2	.076	Two delaminations, uncracked
GEDC-11R	0.5/0.3	.077	Single delamination, uncracked
GEDC-12R	0.4/0.2	.077	Cracked and delaminated
GEDC-13R	0.4/0.2	.073	Cracked and delaminated

*Nominal deposition conditions: T=2000° C, P=15 mm, CH_4 flow=9 lpm.

TABLE XXXIV

PROCESSING CHARACTERIZATION FOR CONE DEPOSITS

GEDP Run No.	Run Variable	Nominal Deposition Temp (°C)	Time (hrs)	Nozzle Orifice Size (mils)	Furnace Pressure (torr)	Gas Flow Rates (lpm) CH_4	Gas Flow Rates (lpm) BCl_3	Initial Exhaust Area (%)[a]	Initial Nozzle to Cone Tip Distance (in.)
1	Nozzle size	2000	45-3/4	75	3	4.7	0.04	50	8-1/2
2	Nozzle size	2000	6	150	3	4.7	0.04	50	8-1/2
3	Nozzle size	2000	35	100	3	4.7	0.04	50	8-1/2
4	Base-run	2000	40	89	3	4.7	0.04	50	8-1/2
5	Nozzle withdrawal	2000	35	89	3	4.7	0.04	23	8-1/2
6	Nozzle with increase T	1950-2100	25	100	3	4.7	0.04	50	8-1/2
7	Increase T	1950-2100	35	100	3	4.7	0.04	40	8-1/2
8	Graded B increase T	1950-2100	35	100	3	4.7	0.04-0.01	50	8-1/2
9	Increased boron	2000	30	100	3	4.7	0.08	34	8-1/2
10	Modified nozzle withdrawal	2000	30	100	3	4.7	0.04	23	7-1/2
11	Graded B	2000	30	100	3	4.7	0.08-0.04	23	8-1/2
12	Modified nozzle withdrawal	2000	30	100	3	4.7	0.04	23	7-1/2
13	Nozzle size	2000	14	89	3	4.7	0.04	46	8-1/2
14	Increased boron	2000	7-1/4	100	3.6	4.7	0.16	46	8-1/2
15	Nitrogen dilution	2000	24-3/4	100	3	4.7 (N_2=1)	0.04	46	8-1/2
R-1[b]	---	2000	20	100	3	4.7	0.04	46	7-1/2

(a) Initial exhaust area calculated as the percent area of the three 15/16 in. diameter holes at the base of the mandrel sleeve and area between nozzle sleeve mandrel base plate to the area at the base of the mandrel sleeve.

(b) Raytheon Company run.

TABLE XXXIV Continued

GEDP Run No.	Cold Finger[c]	Nominal Boron Level[d]	Nozzle Withdrawal[e]	Rotating Cone	Tip Closure[f]	Avg Wall Thickness[g] (mils) Tip	Max	Min
1	no	medium	no	yes	good	782	480±40	185±5
2	no	medium	no	yes	NE	75	145	70
3	no	medium	no	yes	good	1500	400±40	200±15
4	no	medium	no	yes	good	1700	530±100	360±110
5	no	medium	yes-fast	no	void	1200	320±55	190±40
6	yes	medium	yes-std.	yes	very good	800	250±5	150±30
7	no	medium	no	yes	good	1190	390±20	200±15
8	no	medium to low	no	yes	very good	625	255±35	135±20
9	no	high	no	yes	good	1250	370±50	170±20
10	yes	medium	yes-std.	yes	good	260	190±20	100±15
11	yes	high to medium	yes-std.	yes	very good	570	250±25	125±15
12	no	medium	yes-std.	yes	very good	400	280±60	120±30
13	no	medium	yes-std.	yes	good	370	150±5	80±10
14	no	very high	yes-std.	yes	NE	120	70±10	40±10
15	yes	medium	yes-modified	yes	NE	185	210±10	80±10
R-1	yes	medium	yes-std.	no	good	300	180±10	90±10

(c) Defined as unshielded 1-1/2 in. section of water-cooled nozzle.

(d) Boron level based on BCl_3 flow - low, 0.01 lpm; medium, 0.04 lpm; high, 0.08 lpm; very high, 0.16 lpm.

(e) Nozzle withdrawal rate defined as: fast, 1/4 in. per 5 hrs of deposition; STD, (standard), 1/8 in. after 5 and 10 hrs, 1/4 in. after 15 and 20 hrs, 1/2 in. after 25 hrs; modified, 1/8 in. per 5 hrs. of deposition.

(f) Tip closure rating based on curvature of delamination pattern from min. wall thickness region to the cone tip. NE = not examined (thin tip closure).

(g) Max measured at about 7 in. from tip; min measured over range 1 to 3 in. from tip.

TABLE XXXV

BORON ANALYSIS FOR CONES
(wt %)

GEDP Run No.	Tip of Cone			Base of Cone	
	Outer Surface	Center	Inner Surface	Outer Surface	Inner Surface
1	0.6	---	0.5	0.6	2.4
3	1.3	1.1	1.5	1.5	2.0
4	0.3	0.7	0.8	1.5	---
5	0.6	0.8	0.8	0.7	---
6	1.2	1.5	1.2	1.5	1.4
7	1.1	1.0	1.4	1.6	1.9
8	1.4	---	0.5	1.3	0.3
9	0.6	1.0	1.4	1.1	1.9
10	0.7	---	---	1.2	1.8
11	0.6	---	---	1.3	1.5
13	---	---	---	1.8	2.2

TABLE XXXVI

SUMMARY OF PROCESS PARAMETERS

TASK 3.2.1.3

Experiment	Reference Re∼10,000	Reference Re∿750	Diffuser Cap	Diffuser Cap	Orifice Insert	Diffuser Cap
Nose Cone No.	3213-1	3213-2	3213-3	3213-4[1]	3215-5	3213-6
RSD No.	1-13	2-20	1-19	2-27	1-21	1-22
Pressure (mm)	4.0	4.0	4.0	4.0	4.0	4.0
Temperature (°C)	2150	2150	2150	2150	2150	2150
Time (hours)	40	40	40	55	40	40
CH_4 flow (SCFH)	10	10	10	10	10	10
H_2 flow (SCFH)	5	5	5	5	5	5
Nozzle Position[2]	8 1/2	8 1/2	8 1/2	8 1/2	8 1/2	7 3/4
Nozzle Orifice (in)	.069	.25	.25	.25	.25	.25

1 Nose Cone Run 3213-4 was Cone 3213-3 with an additional 15 hours deposit.

2 Inches, nozzle tip to tip of nose cone mandrel.

TABLE XXXVII

SUMMARY OF RESULTS

Task 3.2.1.3

Experiment	Reynolds Number Effects		Diffuser Cap Studies			"Swirler" Insert
	Re 10,000	Re 750	40 Hrs.	55 Hrs.	7 3/4" Noz. Pos.	
Cone No.	3213-1	3213-2	3213-3	3213-4	3213-6	3213-5
Stag. Thick. (in)	.280	.220	.175	.400	.220	.105
Min. Wall Thickness (in)	.060	.060	.130	.150	.070	.060
Outer Surface	Spalled	Badly Spalled	Fair	Fair	Fair	Good
Inner Surface	Good	Good[1]	Good	Good[2]	Heavy Nodules	Nodules
Residual Stress Psi	6000	3800	--	1400	5000	1300

[1] 3 axial cracks developed when mandrel was removed.

[2] 1 axial crack was generated when trim ring was removed.

TABLE XXXVIII

OPERATING CONDITIONS--TASK 3.2.1.4

Run No.	Cap Position Inches	Pressure KM	Temp. °F	Gas Flows (CFH) Nat. Gas	Gas Flows (CFH) BCl_3	Time Hours Sched.	Time Hours Act.	Cap Number
6048	8-1/4	3.0	3800	10	--	40	40	304012
6049	8-1/4	3.0	3800	10	.050	30	1-1/4	304012
6051	8-1/2	3.0	3800	10	.050	30	1-1/4	304013
6052	8-1/2	3.0	3800	10	.050	30	30	304013
4064	7-1/2	3.0	3800	10	.050	30	30	304013
4065	9-1/2	3.0	3800	10	.050	30	30	304013
4066	8-1/2	3.0	3800	10	.050	30	10 Min.	304015

TABLE XXXIX

PROCESS CONDITIONS - TASK 3.4.2.3a - PHASE 1

Run No.	Temp. (°C)	Pressure (mmHg)	Gas Flow (SCFH)			Time (hrs)
			CH_4	C_2H_2	H_2	
1-42	2100	2	15	5	3	6
2-43	2100	4	15	5	3	5
1-39	2100	8	15	5	3	6
1-38	2100	2	10	10	3	6
1-36	2100	4	10	10	3	6
1-35	2100	8	10	10	3	6
2-42	2100	2	5	15	3	6
1-40	2100	4	5	15	3	6
1-41	2100	8	5	15	3	6
2-41	1925	4	10	10	3	6
2-40	1750	4	10	10	3	6

Gas velocity for all experiments - 3,000 in/sec.
Gas residence for all experiments - 3×10^{-3} sec.

TABLE XL

EXPERIMENTAL RESULTS PHASE I - 3" DIAMETER TUBES

GE-RSD Run No.	Experiment		Average Deposition Rate (mils/hr)	Density (gm/cm^3)		Average Residual Strain (in/in)
	CH_4/C_2H_2 Ratio	Pressure mmHg		Bottom	Top	
1-42	3	2	6.0	2.16	2.17	-0.420
2-43	3	4	8.2	2.13	2.09	0.006
1-39	3	8	12.2	2.17	2.18	0.020
1-38	1	2	8.3	2.16	2.17	-0.001
1-36	1	4	12.3	2.17	2.18	0.020
1-35	1	8	18.7	2.18	2.18	0.017
2-42	1/3	2	12.5	2.16	2.17	0.017
1-40	1/3	4	20.0	2.17	2.18	0.017
1-41	1/3	8	30.0	2.17	2.05	0.019
2-40*	1	4	10.0	-	1.10	0.015
2-41*	1	4	11.0	1.93	2.03	0.012

*No. 2-40 - Deposition Temperature 1750
*No. 2-41 - Deposition Temperature 1925
All other experiments - Deposition Temperature 2100°

TABLE XLI

PROCESS CONDITIONS - TASK 3.4.2.3a - PHASE 2

GE-RSD Run No.	Deposition Period (hrs)	Nozzle Position*	Deposition Pressure (mmHg)	Gas Flow (SCFH)			Temp. (°C)	Nozzle OD (inches)
				CH_4	C_2H_2	H_2		
1-43	0-10 10-20 20-30	5 7 8	4	2.5	7.5	3.0	2100	1
2-46	0-10 10-20 20-30	5 7 8	4	2.5	7.5	0	2100	13/16"
1-48	0-10 10-20 20-30	5 6 8	3	2.5	7.5	3.0	2100	13/16"

*Distance from tip of cone to injector nozzle

Notes: (1) Orifice for all nozzles - 0.069"

(2) The nozzle was rotated in each Run - 135°/2 hours.

(3) Run No. 2-46 had some pressure fluctuation after 12 hours deposition time.

TABLE XLII

DEPOSITION THICKNESS PROFILES - TASK 3.4.2.3a - PHASE 2

Axial Position	Run 1-46 Deposit Thickness (inches)	Run 2-46 Deposit Thickness (inches)	Run 1-48 Deposit Thickness (inches)
Stagnation Region	.96	.95	.35
Station 1	.39	.31	.21
Station 2	.28	.24	.13
Station 3	.20	.22	.13
Station 4	.19	.24	.13
Station 5	.18	.25	.13
Station 6	.18	.24	.12
Station 7	.17	.21	.12
Station 8	.17	.21	.11

TABLE XLIII

PROCESS CONDITIONS - TASK 3.4.2.3b

Run No.	Position Inches	Pressure MM	Temp °F	Gas Flows (CFH)					Time - Hours	
				Nat.	MAPP	Hyd.	Acet.	BCl_3	Sched.	Act.
5051	7-1/2	4.0	3800	2.5	--	--	7.5	--	30	30
5052	7-1/2	4.0	3800	2.5	--	--	7.5	.109	30	10 Min.
5053	8-1/2	2.0	3800	2.5	3.0	4.0	--	--	30	25-1/2
5054	8-1/2	2.0	3800	2.5	3.0	4.0	--	.109	26	4
5055	8-1/2	2.0	3800	2.5	3.0	4.0	--	.109	26	1-1/4
5058	7-1/2	4.0	3640	2.5	--	--	7.5	--	30	30
5060	7-1/2	4.0	3450	2.5	--	--	7.5	--	30	30

TABLE XLIV

SUMMARY OF RESULTS - TASK 3.4.2.3b

Run No.	Thickness - Inches			Density - g/cc		C_o	
		Wall					
	Nose	Min.	Max.	1st Deposit	Last Deposit	1st Deposit	Last Deposit
5051	1.320	.190	.360	2.084	1.917	6.854	6.854
5052	--	--	--	--	--	--	--
5053	.260	.190	.290	2.176	2.146	6.854	6.854
5054	--	--	--	--	--	--	--
5055	.200	.170	.250	--	--	--	--
5058	1.020	.300	.520	--	--	6.846	6.854
5060	0.700	.240	.410	--	--	6.846	6.823

TABLE XLV

PROCESSING MATRIX

Furnace Run No.	No.	Thickness of Ring (mils)					Max t/r of Each Ring					Part t/r
		Outer	2nd	3rd	4th	5th	Outer	2nd	3rd	4th	5th	
1-77	1-A	30	30	30	30	30	.02	.02	.02	.02	.02	.10
2-88	.1	30	30	30	30	30	.02	.02	.02	.02	.02	.10
2-90	2	50	50	50	--	--	.03	.04	.04	--	--	.10
1-82	3	75	75	--	--	--	.05	.05	--	--	--	.10
2-105	4	70	50	30	--	--	.05	.04	.02	--	--	.10
2-108	5	75	70	65	--	--	.05	.05	.05	--	--	.14

TABLE XLVI

PROCESSING PARAMETERS

Furnace Run No.	No.	Deposition Time (hrs)	Deposition Pressure (mm Hg)	Gas Flow SCFH			Temp. (°C)
				CH_4	H_2	BCl_3	
1-77	1-A	15	4	21	7	.1	2100
2-88	1	10.4	4	21	7	.1	2100
2-90	2	11.5	4	21	7	.1	2100*
1-82	3	12.0	4	21	7	.1	2100
2-105	4	12.5	4	21	7	.1	2100
2-108	5	17.25	4	21	7	.1	2100

*Due to an equipment malfunction the temperature could not be directly controlled. The power settings employed in Runs 1-77 and 2-88 were duplicated.

TABLE XLVII

RESULTS

Part No.	Thickness of Rings (mils)		Part Thickness (mils)		Avg. Thickness of Ring (mils)	Max. t/r For Ring From Sm. End (Top)	Axial Cracks	Part t/r		Density gm/cc		Avg. Res. Str. in/inx10^{-2}	
	Top	Bottom	Top	Bottom				Top	Bottom	Top	Bottom	Top	Bottom
Frustum No. 1-A													
Run No. 1-77			183	225				.150	.114				
(Rings) Outer	27	40	-	-	34	.020		-	-	2.22	2.23	-	-
2	35	43	-	-	39	.027	1	-	-	2.23	2.21	-	-
3	38	47	-	-	43	.029		-	-	2.24	2.24	-	-
4	40	50	-	-	45	.031		-	-	2.24	-	-	-
5	43	45	-	-	44	.033		-	-	2.2.	-	-	-
Frustum No. 1													
Run No. 2-88			120	142				.095	.071				
(Rings) Outer	15 (1)	21	-	-	18	.011		-	-	2.21	-	8.1	1.4
2	25	28	-	-	27	.019		-	-	2.22	2.23	-	-
3	25	29	-	-	27	.020	0	-	-	2.21	2.23	3.3	2.3
4	25	31	-	-	28	.020		-	-	2.22	2.23	5.7	6.2
5	30	33	-	-	32	.024		-	-	2.22	2.23	5.2	4.8
Frustum No. 2													
Run No. 2-90			131	167				.105	.084				
(Ring) Outer	48	60	-	-	54	.037		-	-	2.21	2.24	7.9	1.8
2	43	54	-	-	49	.035	0	-	-	2.23	2.24	3.4	-
3	40	53	-	-	47	.033		-	-	2.22	2.23	2.9	2.5
Frustum No. 3													
Run No. 1-82			150	151				.120	.076				
(Ring) Outer	75	76	-	-	75.0	.059	0	-	-	2.21	2.23	4.3	4.0
2	75	75	-	-	75.0	.059		-	-	2.22	2.24	4.4	2.3
Frustum No. 4													
Run No. 2-105			154	178				.109	.083				
(Ring Outer	66	76	-	-	70	.045		-	-	2.22	2.22	2.8	4.0
2	54	60	-	-	59	.039	0	-	-	2.24	2.24	4.6	4.0
3	37	37	-	-	35	.024		-	-	2.22	2.23	2.7	-5.0
Frustum No. 5													
Run No. 2-108			241	275				.174	.130				
(Ring) Outer	77	90	-	-	85.0	.053		-	-	2.22	2.23	-	-
2	80	90	-	-	86.0	.058	2	-	-	2.24	2.24	-	-
3	78	91	-	-	85.0	.060		-	-	2.24	2.24	-	-

(1) Delamination Not Continuous

TABLE XLVIII

DEPOSIT THICKNESS

(1)	Average Deposit Thickness in mils for Different Frustums					
	1-77	2-88	2-90	1-82	2-105	2-108
Top	198	133	145	150	154	241
1" from top	204	134	144	151	157	245
2" " "	209	136	146	153	161	250
3" " "	216	139	151	154	165	259
4" " "	217	143	157	155	170	266
5" " "	227	147	162	155	173	269
6" " "	233	149	169	155	176	273
7" " "	232	152	172	155	178	275

(1) Small End of Frustum

TABLE XLIX

COMPOSITION OF NATURAL GAS*

CH_4	94.60%
C_2H_6	3.27
C_3H_8	.63
Iso Butane	.10
N. Butane	.10
Iso Pentane	.05
Hexanes +	.05
CO_2	.80
N_2	.40
Total	100.00%

* Niagra Mohawk Power Corporation

TABLE L

LEVELS OF IMPURITIES

	Volume Percent	
	-	+
a = C_2H_6	.0%	5.78%
b = C_3H_8	.0%	2.10%
c = CO_2	.0%	2.10%
d = H_2	.0%	21.05%
e = BCl_3	.0%	1.05%

CH_4 added to bring total flow to 1.9 cfh.

TABLE LI

EFFECTS OF IMPURITIES ON THE DEPOSITION RATE

Treatment Combinations	Levels of Impurity					Slope	
	C_2H_6	C_3H_8	CO_2	H_2	BCl_3	Experimental	Calculated
1						1.6	1.6
a	+	-	-	-	-	2.9	2.5
b	-	+	-	-	-	2.4	2.1
ab	+	+	-	-	-	2.2	2.5
c	-	-	+	-	-	1.9	1.6
ac	+	-	+	-	-	2.5	2.5
bc	-	+	+	-	-	2.0	2.1
abc	+	+	+	-	-	2.6	2.5
d	-	-	-	+	-	1.0	1.1
ad	+	-	-	+	-	2.3	2.1
bd	-	+	-	+	-	1.6	1.7
abd	+	+	-	+	-	2.1	2.3
cd	-	-	+	+	-	1.2	1.1
acd	+	-	+	+	-	1.8	2.1
bcd	-	+	+	+	-	1.5	1.7
abcd	+	+	+	+	-	2.3	2.1
e	-	-	-	-	+	3.1	3.5
ae	+	-	-	-	+	6.7	6.3
be	-	+	-	-	+	5.1	4.5
abe	+	+	-	-	+	5.5	6.2
ce	-	-	+	-	+	3.7	3.5
ace	+	-	+	-	+	5.5	6.3
bce	-	+	+	-	+	3.9	4.5
abce	+	+	+	-	+	6.2	6.1
de	-	-	-	+	+	2.5	2.4
ade	+	-	-	+	+	5.3	5.3
bde	-	+	-	+	+	3.2	3.3
abde	+	+	-	+	+	5.9	5.7
cde	-	-	+	+	+	2.2	2.4
acde	+	-	+	+	+	5.8	5.1
bcde	-	+	+	+	+	3.6	3.5
abcde	+	+	+	+	+	5.8	4.9

1 - pure methane
a - ethane
b - propane
c - carbon dioxide
d - hydrogen
e - boron trichloride
"ab" would mean that unit concentrations ethane and propane were added to pure methane

TABLE LII

COMPOSITION OF SYNTHESIZED GAS

FOR FILAMENT RUNS

Run 1.	CH_4	99.95%
Run 2.	CH_4	94.22
	C_2H_6	5.78
Run 3.	CH_4	98.95
	BCl_3	1.05
Run 4.	CH_4	93.27
	C_2H_6	5.78
	BCl_3	1.05

TABLE LIII

TASK 3.3.7-1

SUMMARY OF OPERATING CONDITIONS AND RESULTS

Operating Conditions

Run No.	Nozzle Position Inches From Nose	Run Time Sched.	Run Time Act.	Flows (cfh) Nat. Gas	Flows (cfh) BCl_3	Pressure MM	Temp. °F
6050	7"- 9"	45	45	10	.083	2.0	3750
4063	6"-10"	45	28	10	.083	2.0	3750
6053	6"-10"	45	45	10	.083	2.0	3750
6056	6"-10"	45	45	10	.083	2.0	3750

Results

Run No.	Profile Nose Thickness	Profile Wall Min.	Profile Wall Max.	Boron % in Solid Nose First Half	Boron % in Solid Nose Last Half	Boron % in Solid Skirt First Half	Boron % in Solid Skirt Last Half	C_Ω Nose First Deposit	C_Ω Nose Last Deposit
6050	1.02	.11	.24	-	-	-	-	6.854	6.818
4063	0.42	.03	.22	.02	.04	.08	.07	6.862	6.843
6053	0.50	.08	.28	.17	.52	.61	.81	6.854	6.823
6056	0.78	.17	.29	.30	.75	.40	.74	6.849	6.815

TABLE LIV

TASK 3.3.7-2

SUMMARY OF OPERATING CONDITIONS AND RESULTS

Operating Conditions

Run No.	Nozzle Position Inches From Nose	Run Time Sched.	Run Time Act.	Flows (cfh) Nat. Gas	Flows (cfh) BCl_3	Pressure MM	Temp. °F
6054	12"-7"	45	44.5	10	.083	2.0	3750
6055	12"-8"	43	43	*4-10	*.028-.083	2.0	3750
6057	12"-7"	45	45	10	.040	2.0	3750

* See Text

Results

Run No.	Profile Nose Thickness	Profile Wall Min.	Profile Wall Max.	Boron % in Solid Nose First Half	Boron % in Solid Nose Last Half	Boron % in Solid Skirt First Half	Boron % in Solid Skirt Last Half	C_Q Nose First Deposit	C_Q Nose Last Deposit
6054	0.47	.11	.17	-	-	-	-	6.772	6.854
6055	0.48	.09	.25	-	-	-	-	6.825	6.843
6057	0.70	.12	.21	-	-	-	-	6.800	6.846

TABLE LV

TASK 3.3.7-3

SUMMARY OF OPERATING CONDITIONS AND RESULTS

Operating Conditions

Run No.	Nozzle Position Inches From Nose	Run Time Sched.	Run Time Act.	Flows (cfh) Nat. Gas	Flows (cfh) BCl_3	Pressure MM	Temp. °F
5061	8.5"	40	40	10	.040	5.0/1.5	3750
5062	8.5"	30	30	10	.040	5.0	3750
5064	8.5"	30	30	10	.040	8.0	3750
5068	8.5"	30	9.25	10	.040	18.0	3750

Results

Run No.	Profile Nose Thickness	Profile Wall Min.	Profile Wall Max.	Boron % in Solid Nose First Half	Boron % in Solid Nose Last Half	Boron % in Solid Skirt First Half	Boron % in Solid Skirt Last Half	C_Q Nose First Deposit	C_Q Nose Last Deposit
5061	*0.28	.28	.50	.34	.25	.30	.46	6.772	6.754
5062	*1.55	.28	.34	.17	.21	.26	.67	6.749	6.836
5064	0.12	.39	.60	.41	.76	.91	2.07	6.769	6.836
5068	0.06	.11	.28	.57	.43	.32	.46	6.724	6.846

* Deposit has void in nose region or, if run longer, would have had void.

TABLE LVI

TASK 3.3.7-4

SUMMARY OF OPERATING CONDITIONS AND RESULTS

Operating Conditions

Run No.	Nozzle Position Inches From Nose	Run Time Sched.	Act.	Flows (cfh) Nat. Gas	BCl_3	Pressure Mi	Temp. °F
5056	8.5"	45	1.5	10	.083	2.0	3750
5057	8.5"	45	45	10	.083	2.0	3750
4067	8.5"	45	45	10	.040	2.0	3750

Results

Run No.	Profile Nose Thickness	Wall Min.	Max.	Boron % in Solid Nose First Half	Nose Last Half	Skirt First Half	Skirt Last Half	Cu Nose First Deposit	Nose Last Deposit
5056	0.04	<.01	<.01	-	-	-	-	-	-
5057	0.88	.15	.33	.41	.56	.37	1.10	6.836	6.843
4067	0.50	.13	.27	.27	.45	.32	.62	6.854	6.782

TABLE LVIIa

TASK 3.3.7-5

SUMMARY OF OPERATING CONDITIONS AND RESULTS

Operating Conditions

Run No.	Cone Angle	Nozzle Position Inches From Nose	Run Time Sched.	Run Time Act.	Flows (cfh) Nat. Gas	Flows (cfh) BCl_3	Pressure MM	Temp. °F
5065	10°	7"	40	37.8	15	.126	2.0	3750
4071	10°	9"	40	40	15	.126	2.0	3750
6060	10°	9"	40	40	20	.165	2.0	3750
5066	10°	7"	40	21	20	.165	2.0	3750
5071	10°	7"	40	36	20	.165	2.0	3750
4072	6°	9"	40	39	15	.126	2.0	3750
6061	6°	9"	40	40	20	.165	2.0	3750
4074	6°	9"	40	40	10	.083	2.0	3750
4075	6°	7"	40	40	15	.126	2.0	3750
4076	6	7"	40	40	20	.165	2.0	3750
6065	6°	7"	40	40	10	.083	2.0	3750
6068	6°	7"	40	40	7	.0[illegible]	2.0	3750

TABLE IVIIb

TASK 3.3.7-5

SUMMARY OF OPERATING CONDITIONS AND RESULTS

Results

Run No.	Profile			Boron % in Solid				Co	
				Nose		Skirt		Nose	
	Nose Thickness	Wall Min.	Wall Max.	First Half	Last Half	First Half	Last Half	First Deposit	Last Deposit
5065	1.02	.26	.52	.42	.95	.67	1.11	6.832	6.813
4071	1.00	.17	.40	.28	.40	.37	.74	6.849	6.823
6060	1.48	.21	.34	.50	.70	.66	2.13	6.849	6.820
5066	0.40	.10	.24	.38	.66	.17	.34	6.849	6.813
5071	0.42	.04	.46	-	-	-	-	6.851	6.854
4072	1.70*	.12	.35	.58	.74	.24	.51	6.815	6.739
6061	2.00*	.13	.24	.36	.53	.55	.83	6.836	6.802
4074	2.20*	.15	.30	.58	.54	.44	1.07	6.779	6.754
4075	2.00*	.07	.25	.64	.73	.60	1.12	6.838	6.737
4076	2.70*	.08	.20	.47	.34	.50	1.08	6.823	6.836
6065	1.74*	.15	.28	.37	.55	.66	.51	6.831	6.785
6068	1.75*	.14	.30	-	-	-	-	6.747	6.818

* Deposit has void in nose region or, if run longer, would have had void.

TABLE LVIII

TASK 3.3.7-6

SUMMARY OF OPERATING CONDITIONS AND RESULTS

Operating Conditions

Run No.	Nozzle Position Inches From Nose	Run Time Sched.	Run Time Act.	Flows (cfh) Nat. Gas	Flows (cfh) BCl_3	Pressure MM	Temp. °F
6067	12"-9"	57	57	3-10**	.028-.083**	2.0	3750
7082	10"	40	40	15	.126	2.0	3750
5074	9"	40	40	15	.126	2.0	3750

** See Text

Results

Run No.	Profile Nose Thickness	Profile Wall Min.	Profile Wall Max.	Boron % in Solid Nose First Half	Boron % in Solid Nose Last Half	Boron % in Solid Skirt First Half	Boron % in Solid Skirt Last Half	C_Q Nose First Deposit	C_Q Nose Last Deposit
6067	1.00	.19	.40	-	-	-	-	6.742	6.841
7082	.05*	.08	.48	-	-	-	-	6.813	6.349
5074	2.40*	.20	.30	-	-	-	-	6.772	6.752

* Deposit has void in nose region or, if run longer, would have had void.

TABLE LIX

TASK 3.5.2

SUMMARY OF OPERATING CONDITIONS AND RESULTS

Run No.	Cone Angle	Nozzle Position Inches From Nose	Run Time Sched.	Run Time Act.	Flows (cfh) Nat. Gas	Flows (cfh) BCl_3	Pressure MM	Temp. °F	Profile Nose Thickness	Profile Wall Min.	Profile Wall Max.
6069	10°	7.5"-8.5"	50	50	10	.109-.015	2.0	3750	1.25	.20	.34
4083	10°	7.5"-8.5"	50	42.5	10	.109-.015	2.0	3750	1.00	.16	.33
5077	10°	7.5"-8.5"	50	50	10	.109-.015	2.0	3750	-	-	-
6072	10°	7.5"-8.5"	50	50	10	.109-.015	2.0	3750	.95	.17	.35
6070	6°	6"	50	50	10	.109-.015	2.0	3750	1.65	.12	.20
4084	6°	6"	50	31	13	.109-.028	2.0	3750	1.20	.16	.28
6071	6°	6"	30	28.5	13	.109-.034	2.0	3750	1.10	.19	.23
5078	6°	6"	30	26	13	.109-.034	2.0	3750	0.65	.13	.28
4085	6°	6"	25	25	13	.109-.034	2.0	3750	0.85	.08	.23
5079	6°	6"	50	46	13	.109-.015	2.0	3750	0.75	.13	.28

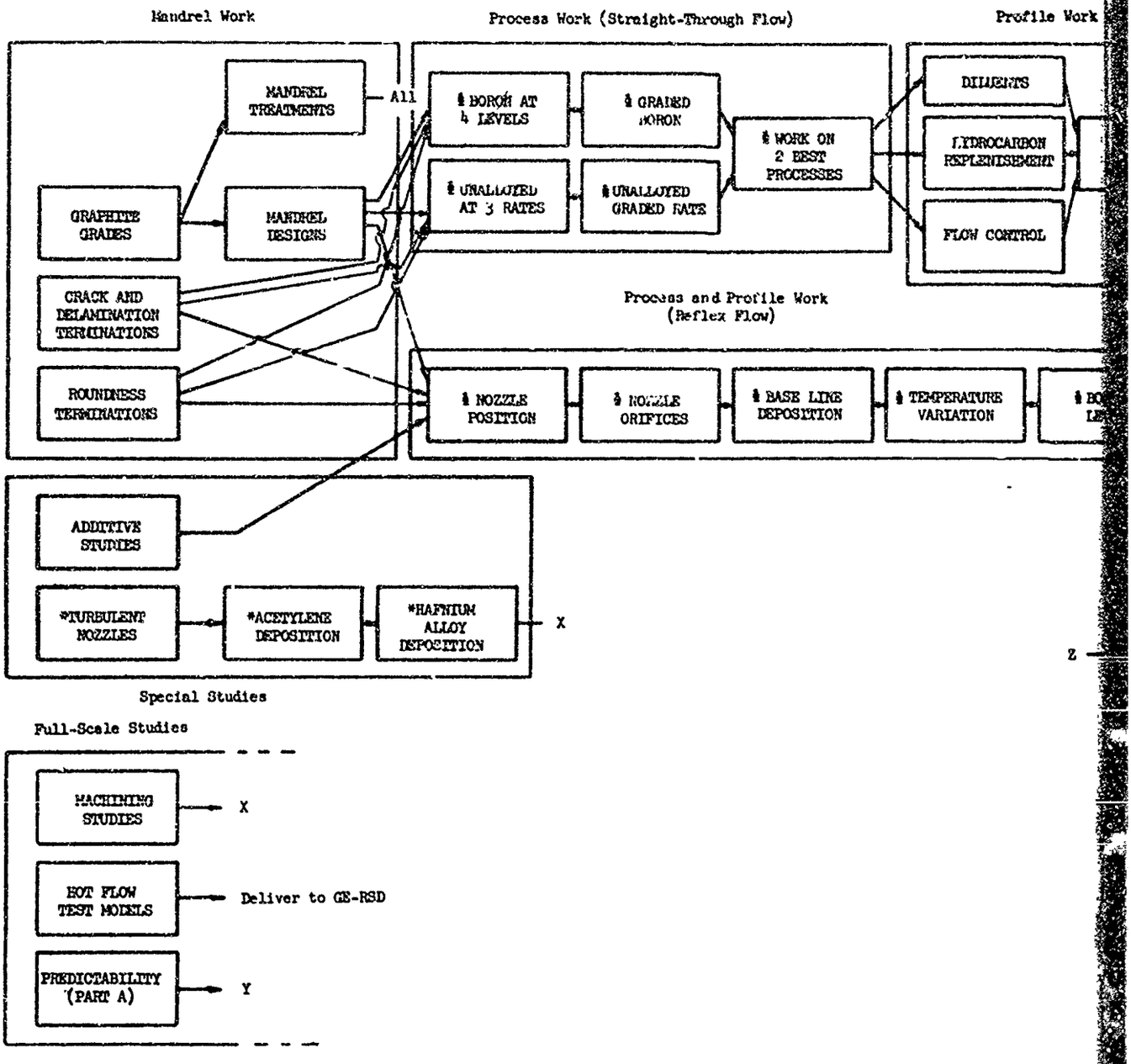
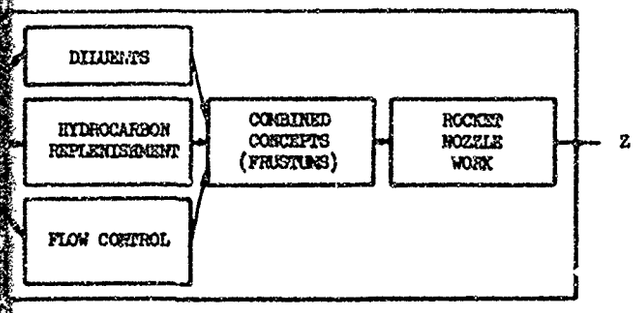
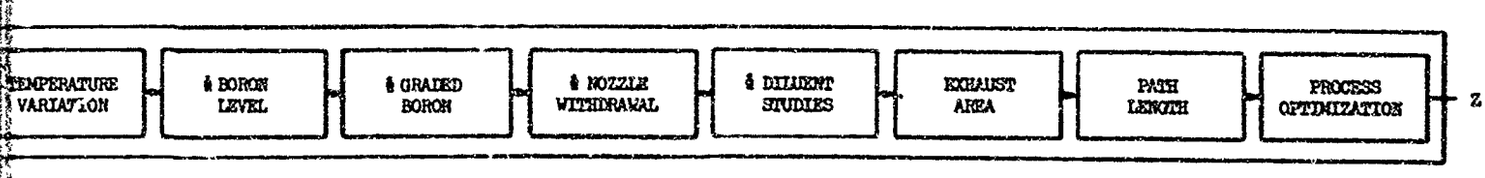


FIGURE 1.

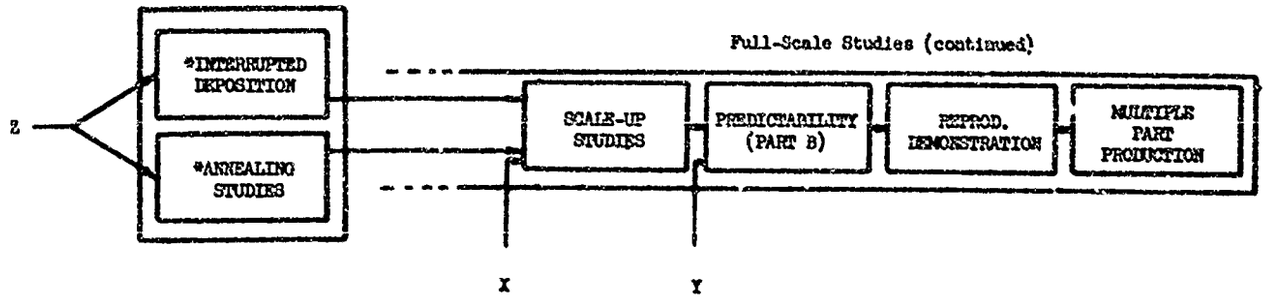
FLOW CHART AF 33(615)-3136

Profile Work (Straight-Through Flow)



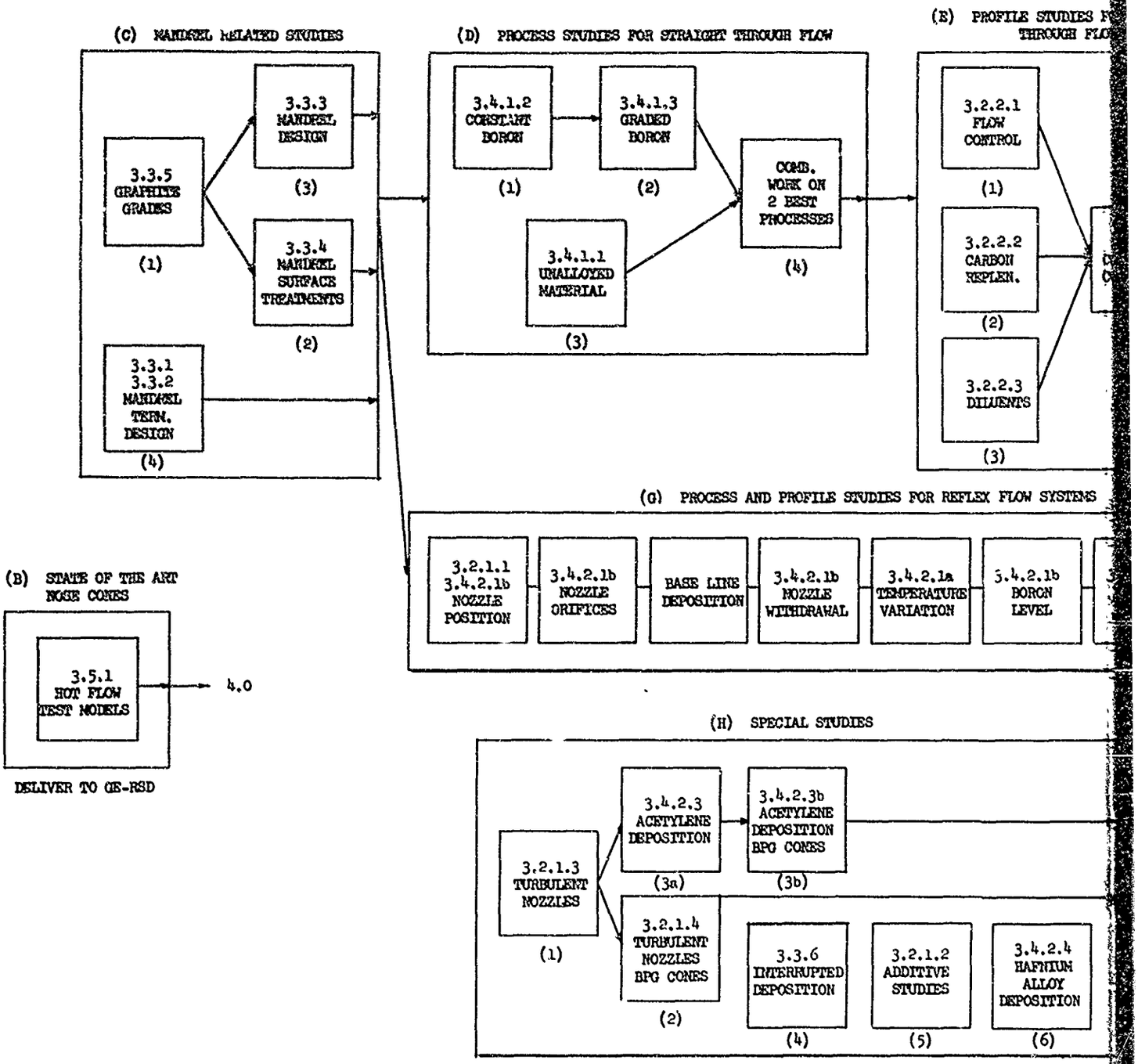


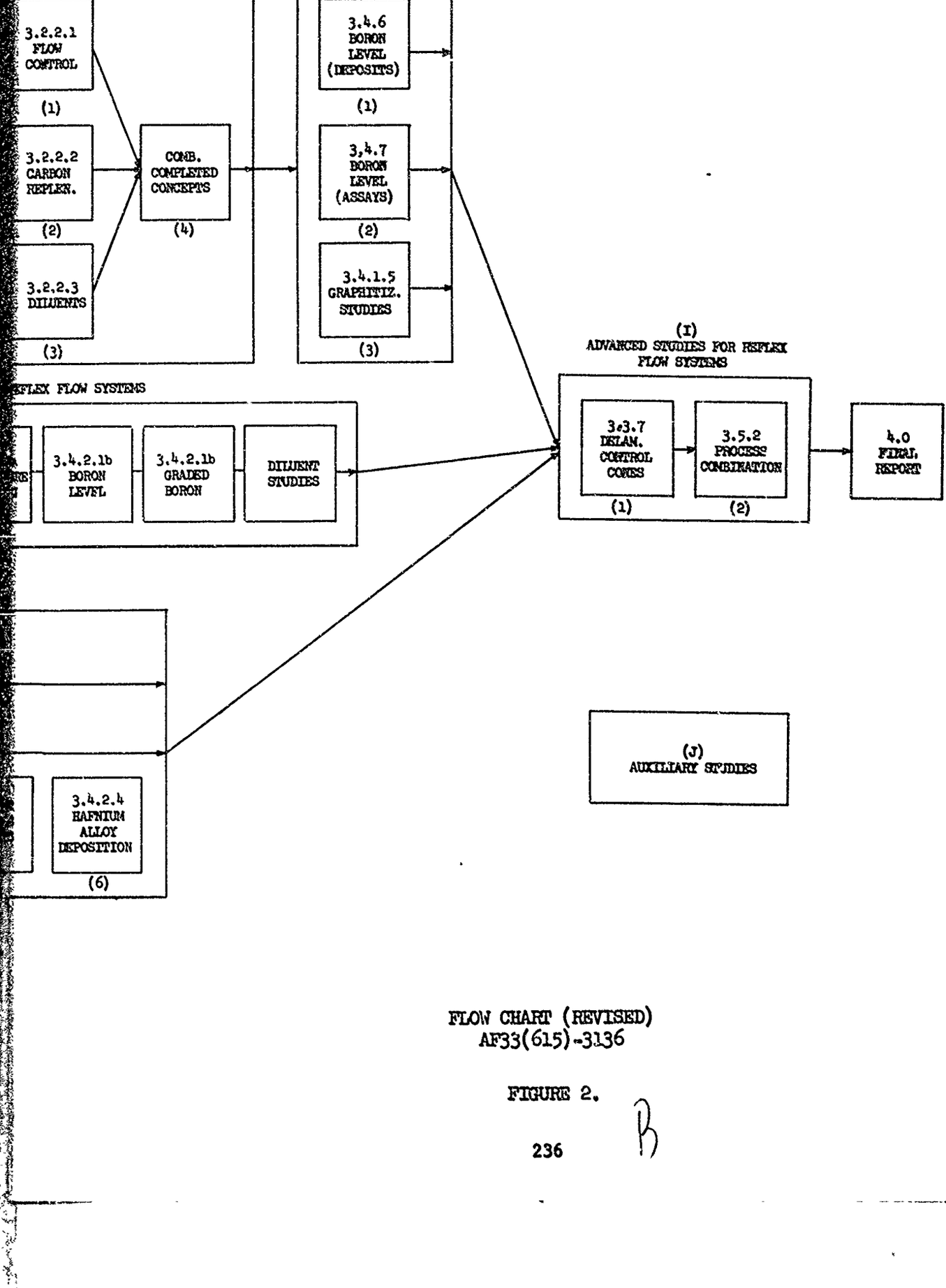
Residual Stress



Note:

* = GE (R&D) Subcontract Effort
â = Raytheon Subcontract Effort


(C) MANDREL RELATED STUDIES
3.3.5 GRAPHITE GRADES
(1)
3.3.3 MANDREL DESIGN
(3)
3.3.4 MANDREL SURFACE TREATMENTS
(2)
3.3.1 3.3.2 MANDREL TERM. DESIGN
(4)
(D) PROCESS STUDIES FOR STRAIGHT THROUGH FLOW
3.4.1.2 CONSTANT BORON
(1)
3.4.1.3 GRADED BORON
(2)
3.4.1.1 UNALLOYED MATERIAL
(3)
COMB. WORK ON 2 BEST PROCESSES
(4)
(E) PROFILE STUDIES F
THROUGH FLO
3.2.2.1 FLOW CONTROL
(1)
3.2.2.2 CARBON REPLEN.
(2)
3.2.2.3 DILUENTS
(3)
(G) PROCESS AND PROFILE STUDIES FOR REFLEX FLOW SYSTEMS
3.2.1.1 3.4.2.1b NOZZLE POSITION
3.4.2.1b NOZZLE ORIFICES
BASE LINE DEPOSITION
3.4.2.1b NOZZLE WITHDRAWAL
3.4.2.1a TEMPERATURE VARIATION
3.4.2.1b BORON LEVEL
(B) STATE OF THE ART NOSE CONES
3.5.1 HOT FLOW TEST MODELS
4.0
DELIVER TO GE-RSD
(H) SPECIAL STUDIES
3.2.1.3 TURBULENT NOZZLES
(1)
3.4.2.3 ACETYLENE DEPOSITION
(3a)
3.4.2.3b ACETYLENE DEPOSITION BPG CONES
(3b)
3.2.1.4 TURBULENT NOZZLES BPG CONES
(2)
3.3.6 INTERRUPTED DEPOSITION
(4)
3.2.1.2 ADDITIVE STUDIES
(5)
3.4.2.4 HAFNIUM ALLOY DEPOSITION
(6)



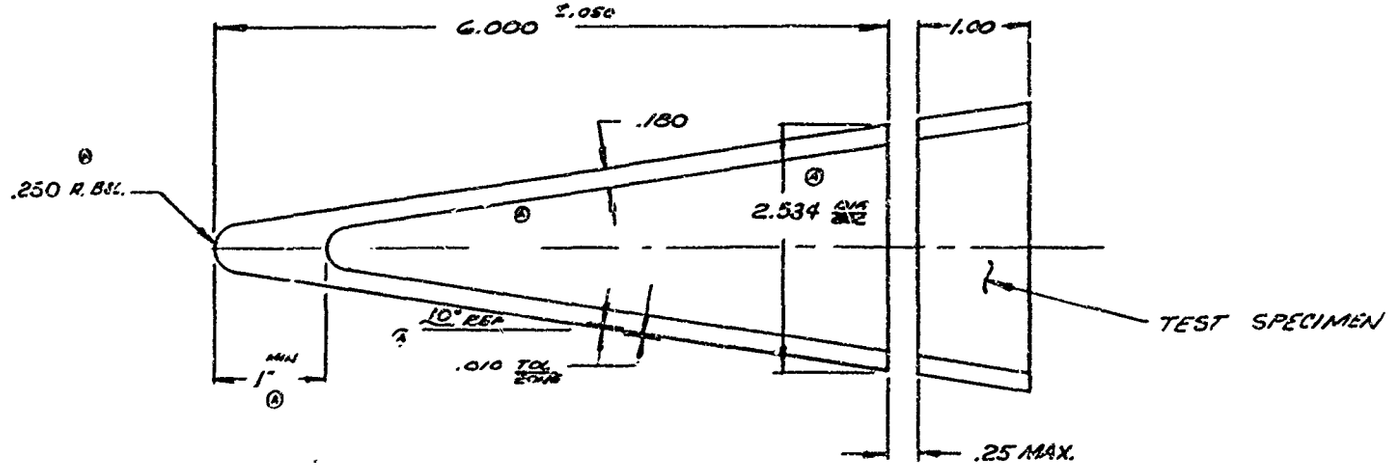
FLOW CHART (REVISED)
AF33(615)-3136

FIGURE 2.

WORK TO DIMENSIONS DO NOT SCALE DW'G.

DWG. NO. SA 317-1
2 SHEETS SHEET 1

A) CHANGED AS 3° CHAM WAS .827, CHD R WAS .10, I WAS 100, .010 TOL ZONE ON ID REMOVED.



NOTES
1. NO MACHINING REQUIRED IN STAGNATION AREA.
2. T.O. TO BE MACHINED WITHIN 2.5" MAX. FROM NOSE OF PART.

TOLERANCES
3 PLACE ±.010
2 PLACE ±.030

SCALE FULL
TOLERANCE
FRACTIONAL ONE ± ONE — UNLESS OTHERWISE SPECIFIED

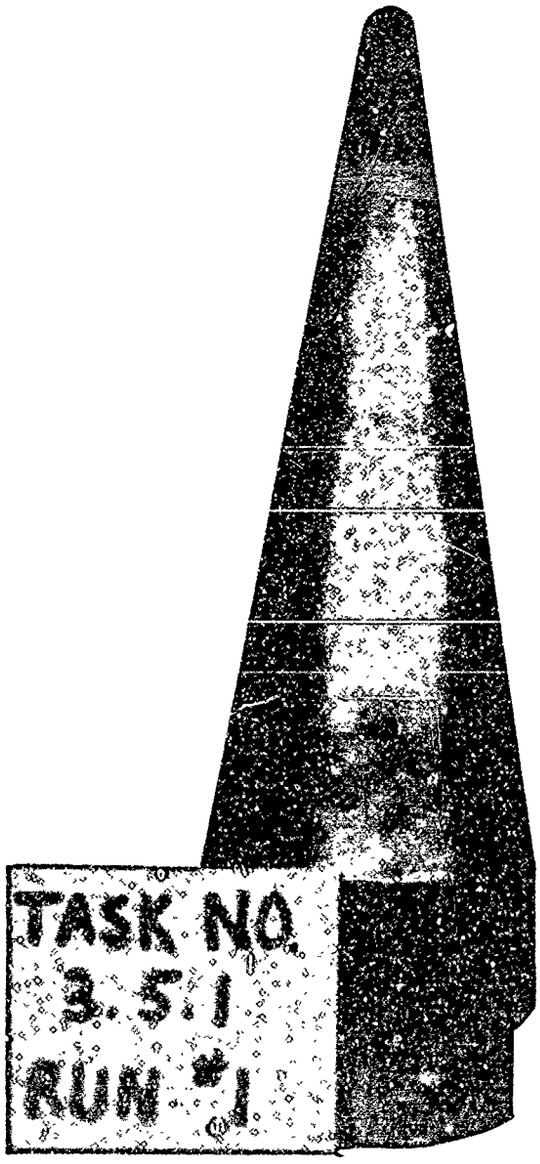
Figure 3

MARK:

GENERAL ELECTRIC
METALLURGICAL PRODUCTS DEPARTMENT

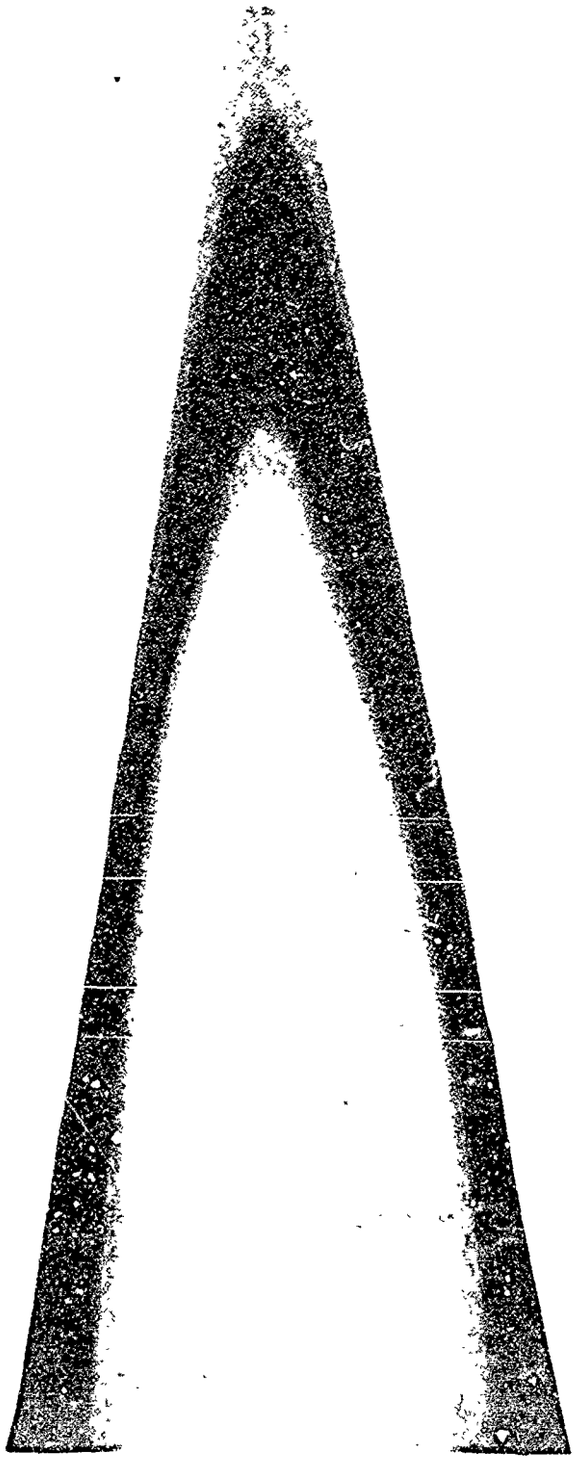
CUSTOMER			
NAME	PTM SHIELD CONE		
MATERIAL	BORON PYROLITIC GRAPHITE		
DRAWN MAS	DATE 7-27-65	DWG. NO. SA-317-A	
CHK'D FLS	DATE 7-27-65	SHEETS	SHEET

237



As deposited Nose Cone

Figure 4



Task 3.5.1 Radiograph of Nose Cone No. 1.

Figure 5.

SUMMARY OF NOSE CONE THICKNESS DATA. TASK 3.5.1.

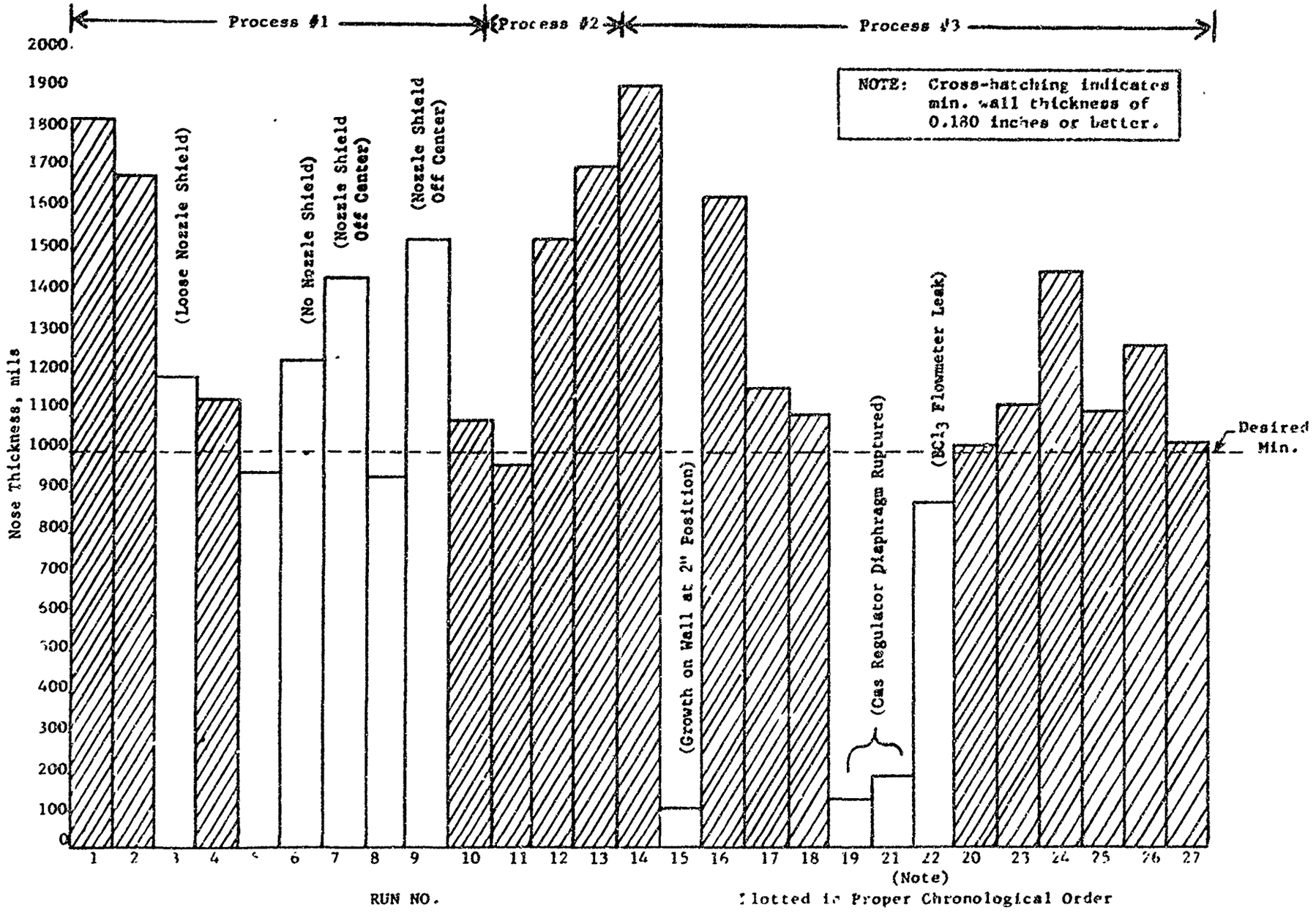


Figure 6

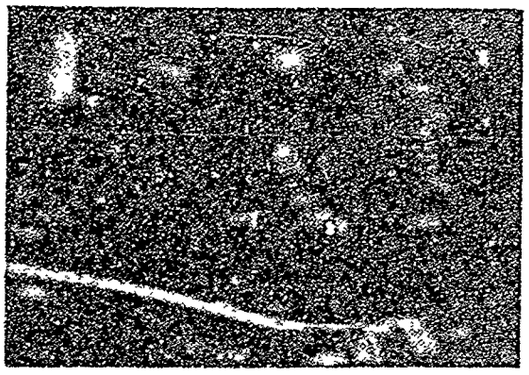


Figure 7.
Polished Surface, Grade B Graphite
(2 X)

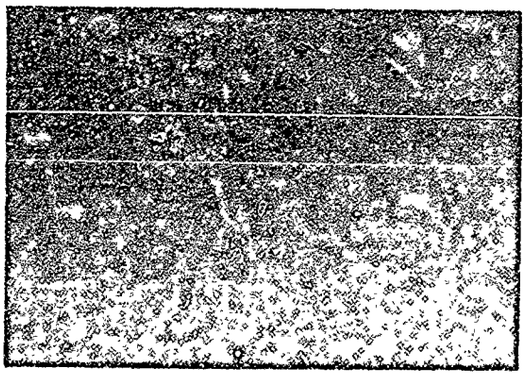


Figure 8.
Polished Surface, Grade C Graphite
(2 X)

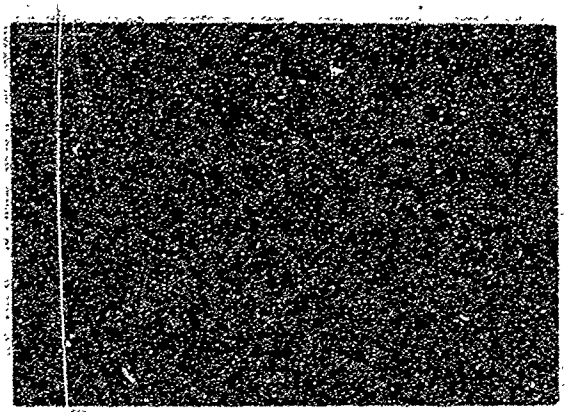


Figure 9.
Polished Surface, Grade A Graphite
(2 X)

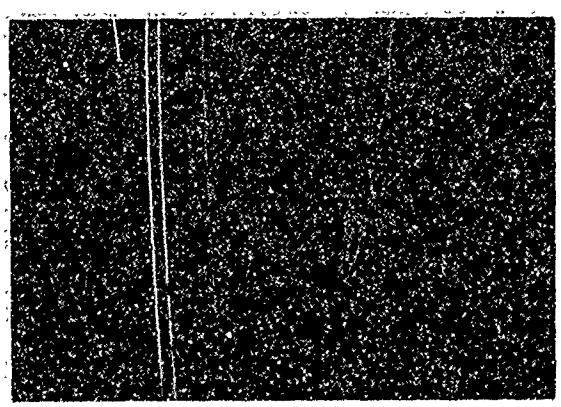


Figure 10.
Polished Surface, Grade D Graphite
(2 X)

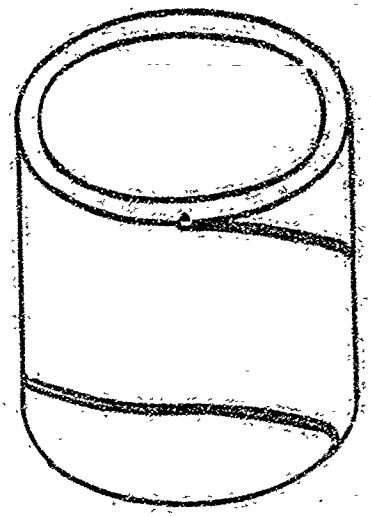


Figure 11

Single Spiral Undercut Mandrel

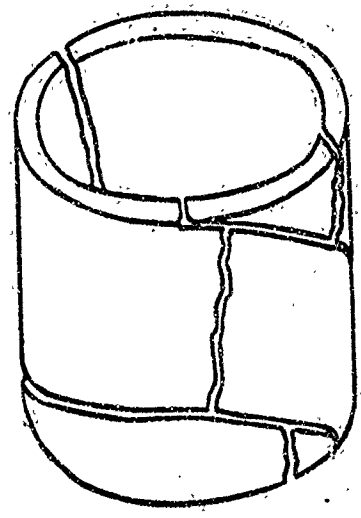
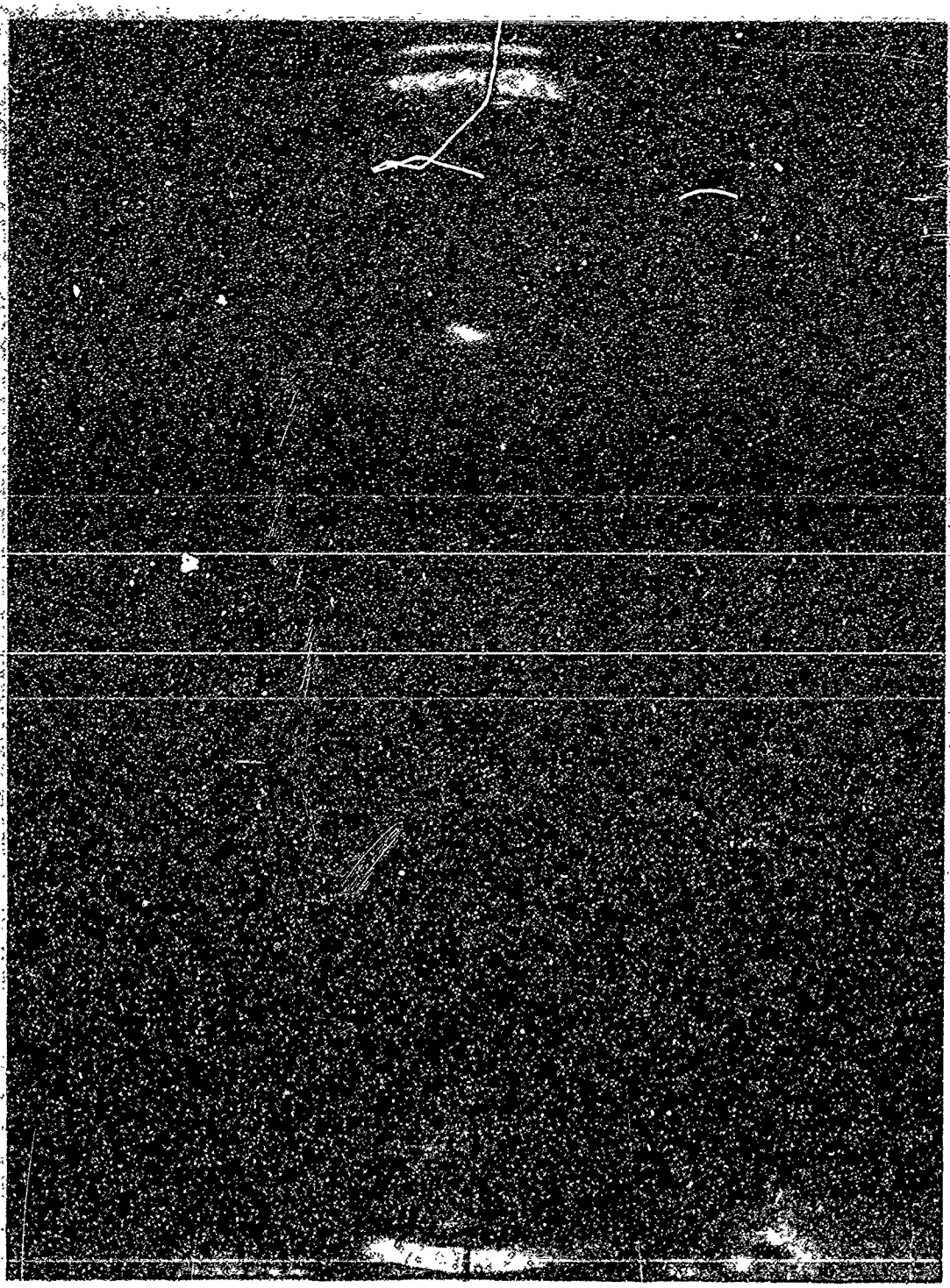


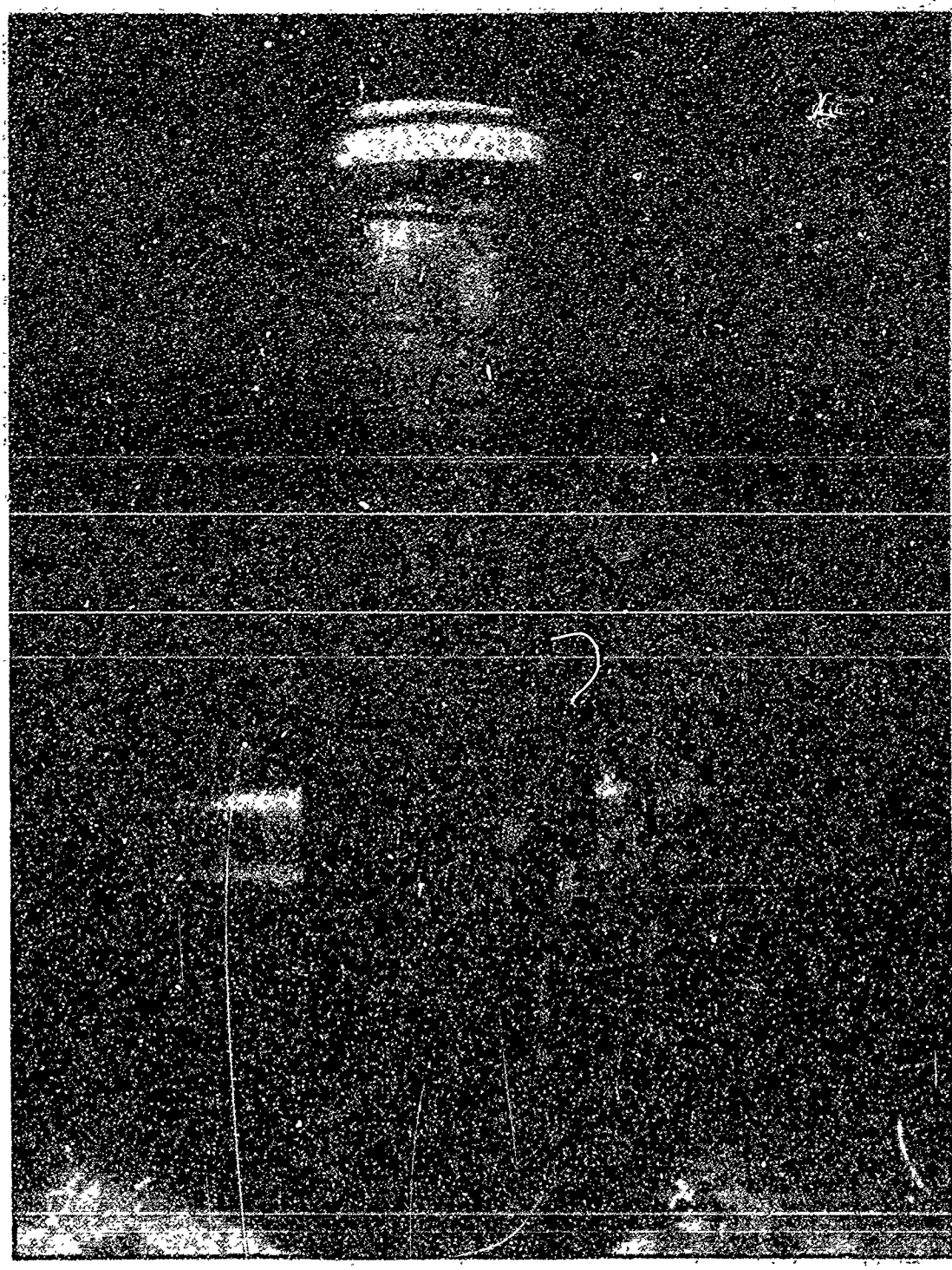
Figure 12

Spiral Undercut Mandrel After Failure



Typical Mandrel Failure Patterns

Figure 13.



Typical Failure of Spirally Undercut Mandrel

Figure 14.

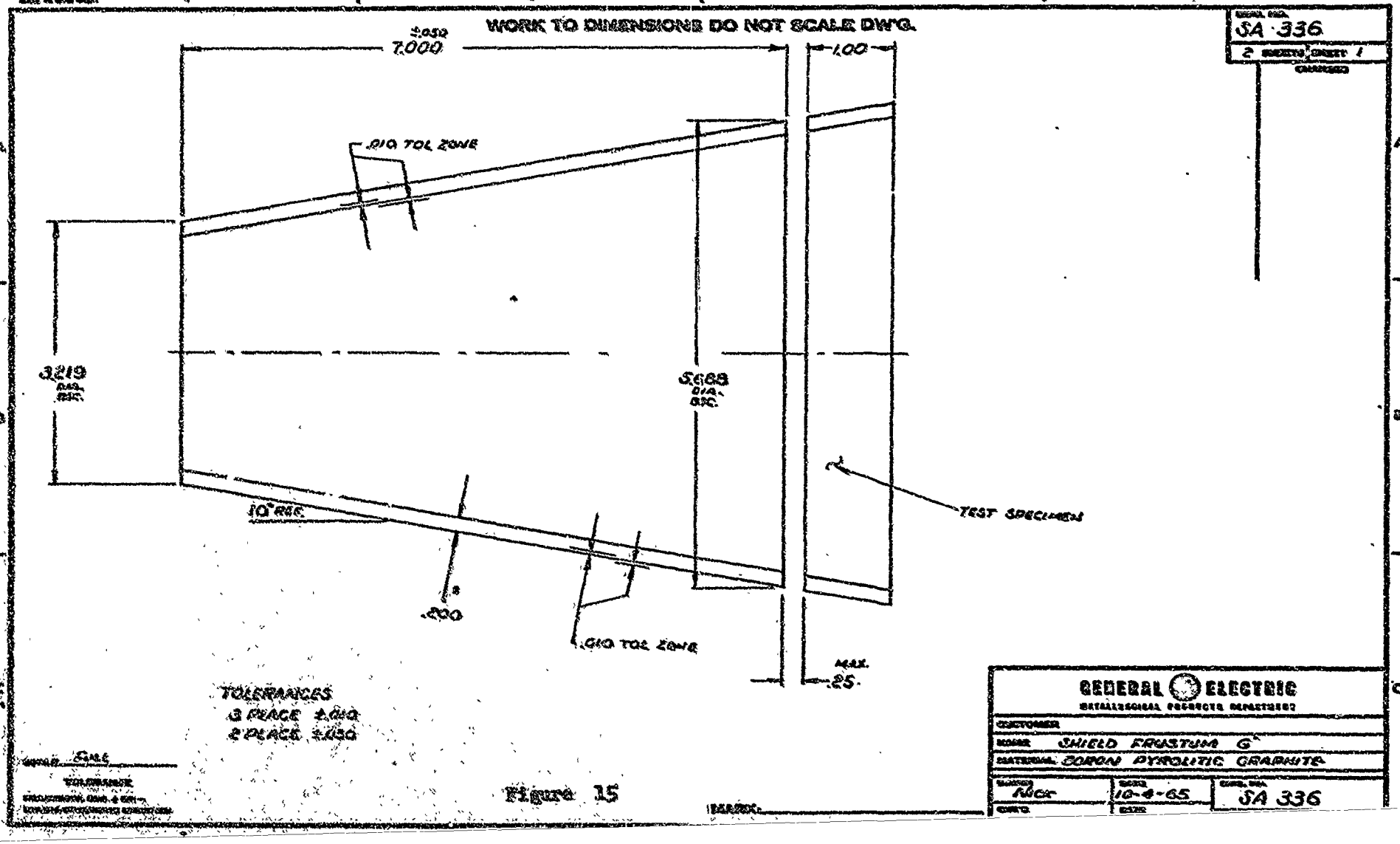
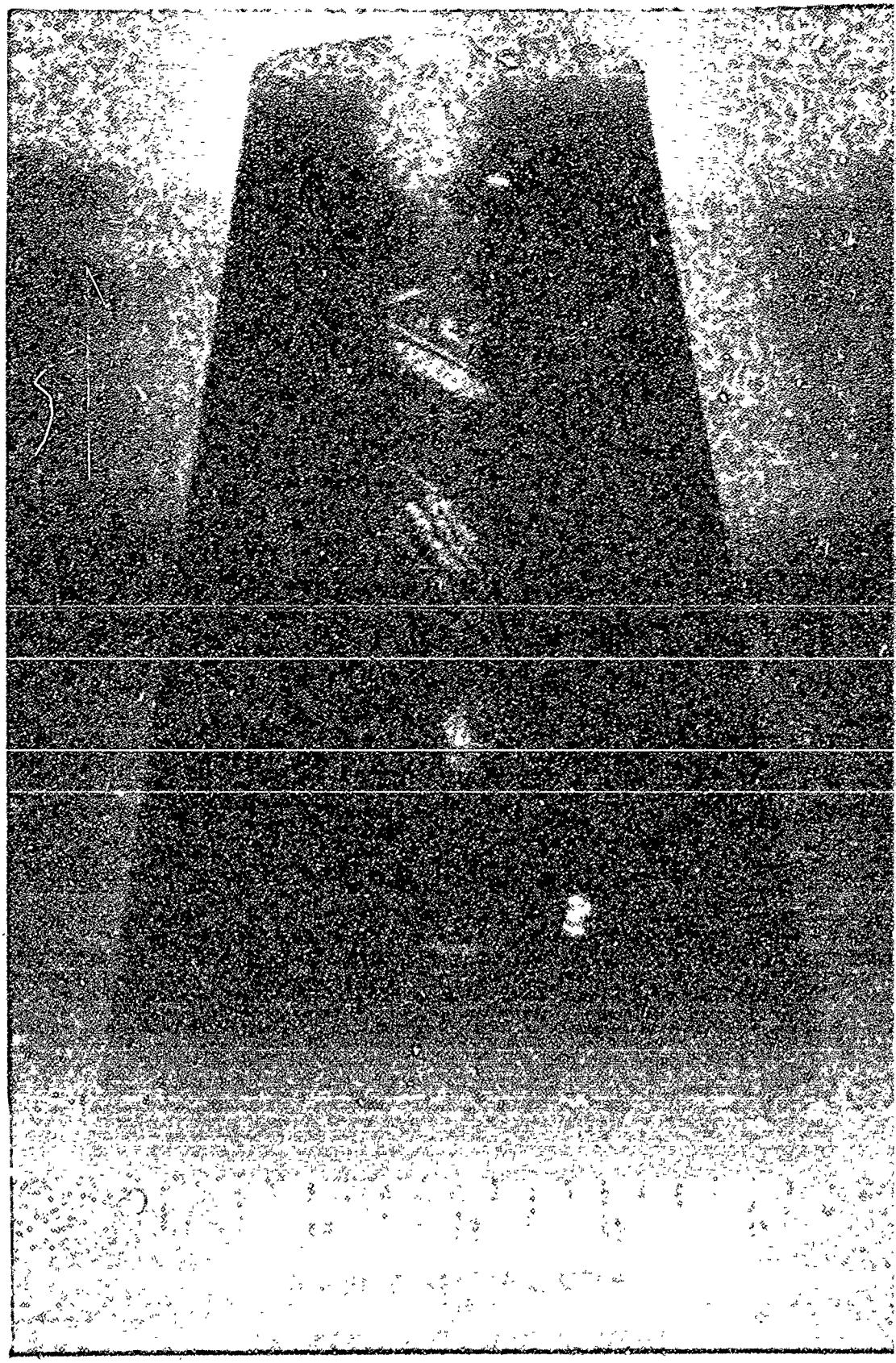

WORK TO DIMENSIONS DO NOT SCALE DWG.
SA 336
7.000
±.050
1.00
.010 TOL ZONE
3219
DIA.
BSC.
5668
DIA.
BSC.
10° REF.
TEST SPECIMENS
.010 TOL ZONE
.25
MAX.
TOLERANCES
3 PLACE ±.010
2 PLACE ±.050
GENERAL ELECTRIC
METALLURGICAL PRODUCTS DEPARTMENT
SHIELD FRUSTUM G
BORON PYROLITIC GRAPHITE
Rice
10-4-65
SA 336

Figure 15



Task 3.3.3 Spalled Surface of Frustum Deposited in tapered thickness mandrel.

Figure 16

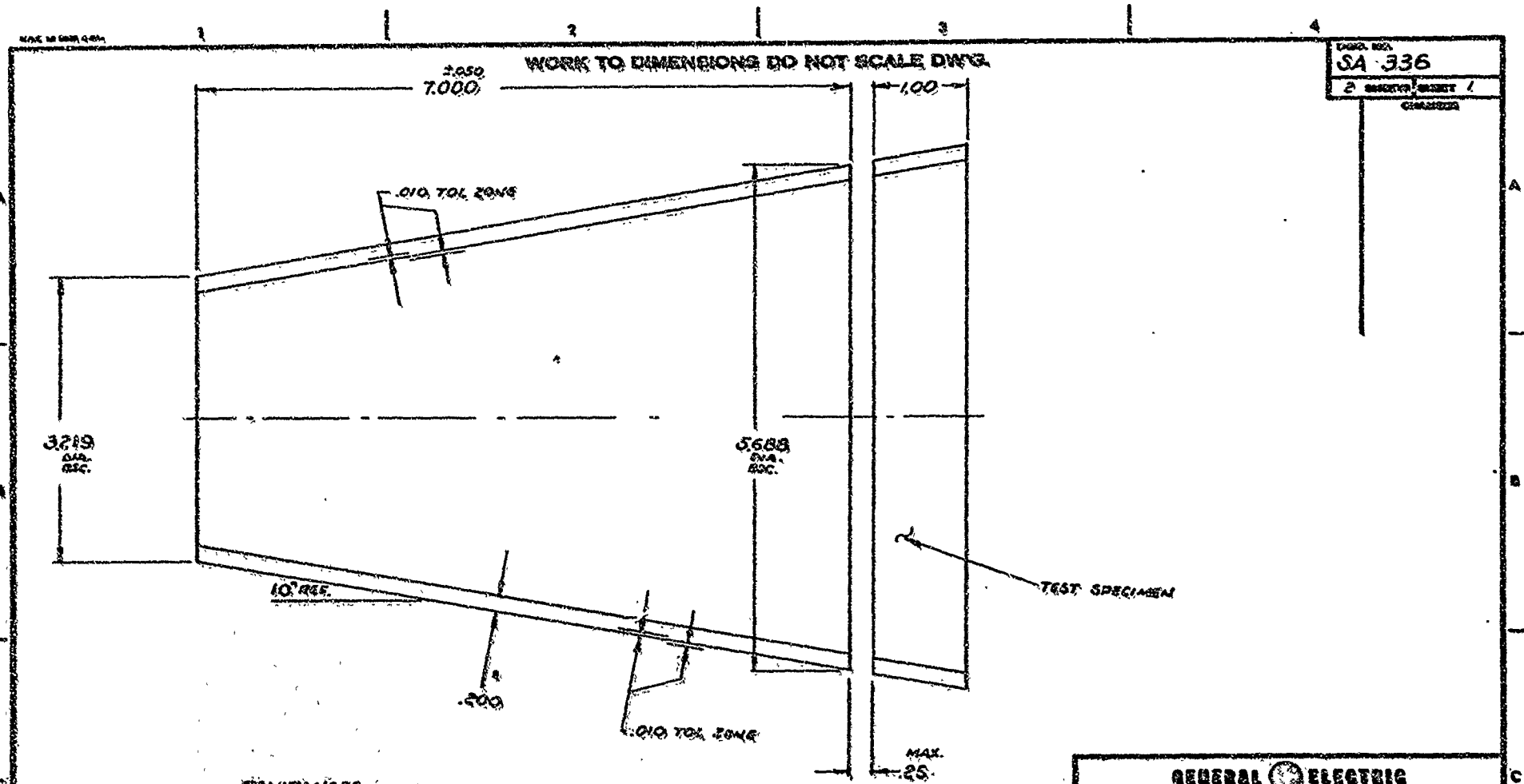
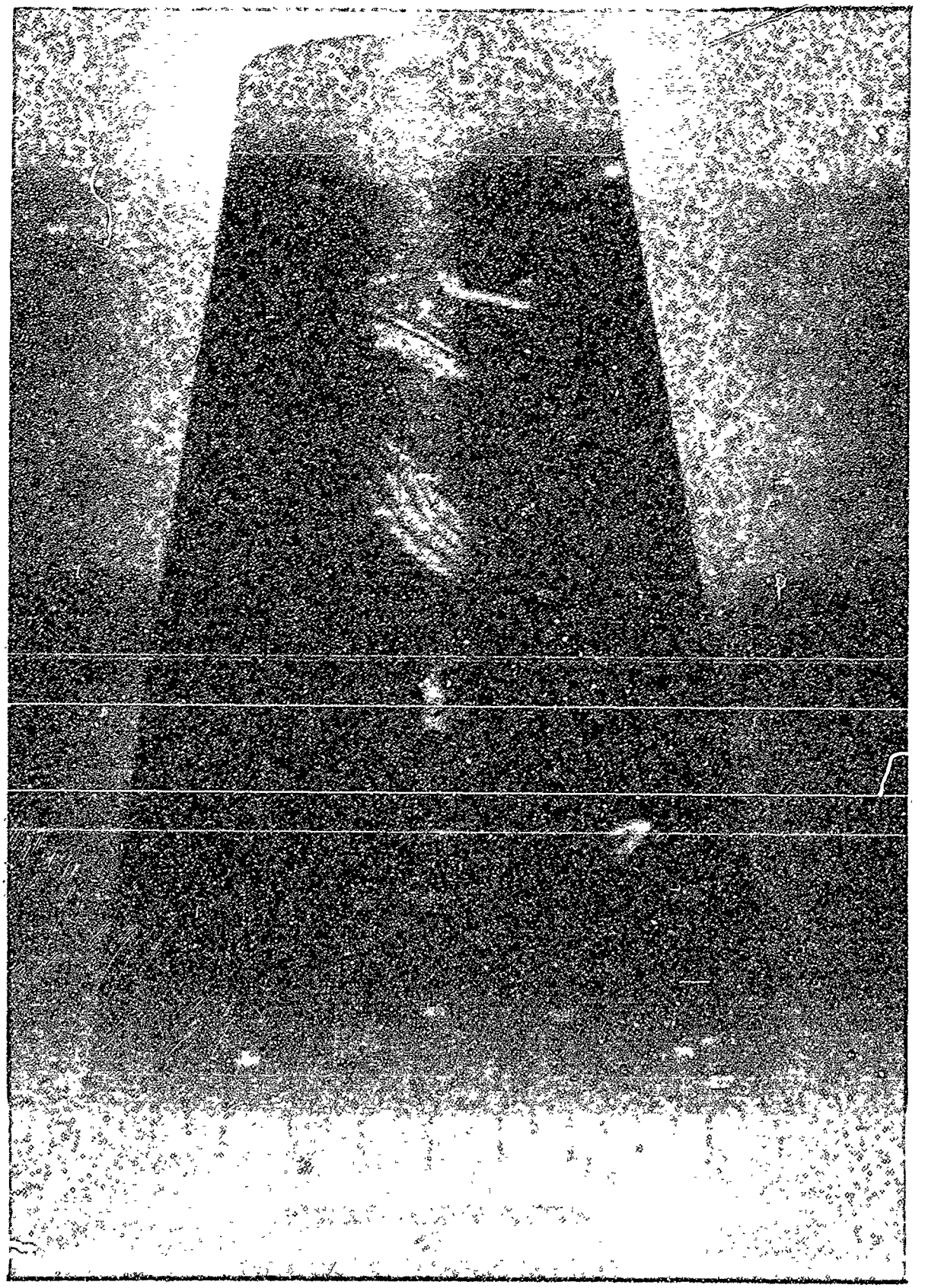
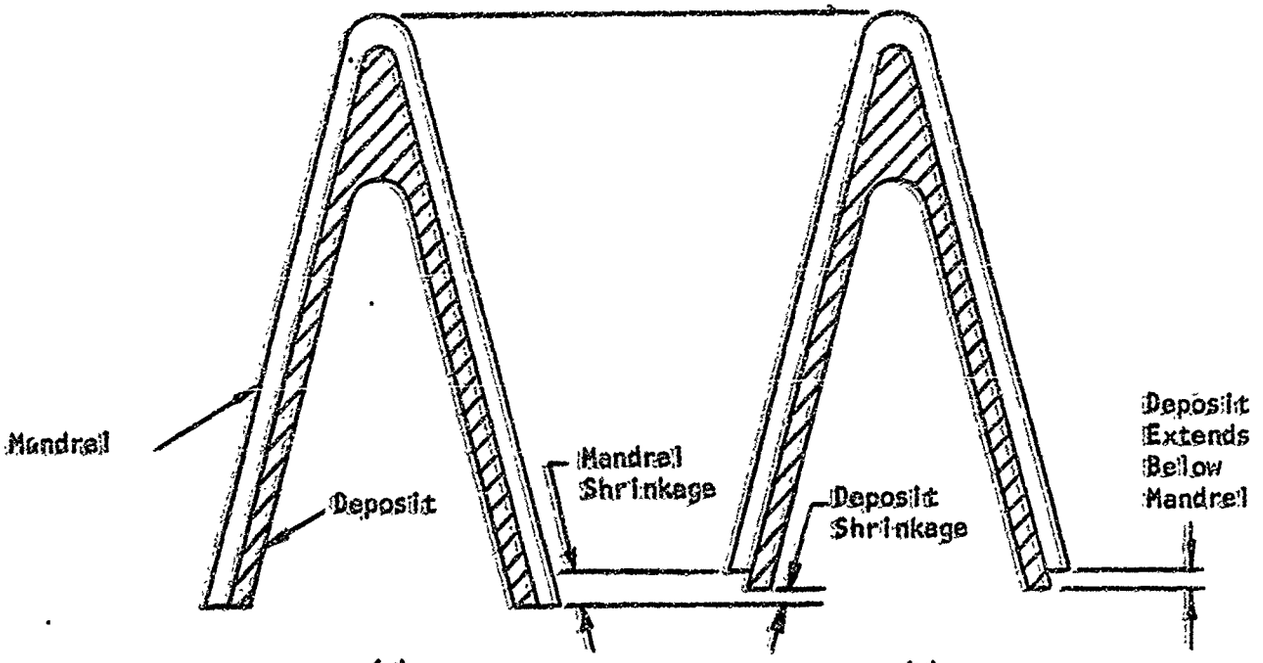

WORK TO DIMENSIONS DO NOT SCALE DWG.
SA 336
7.000 ±.050
1.00
.010 TOL ZONE
3.219 DIA. REF.
5.688 DIA. REF.
10° REF.
.200
.010 TOL ZONE
TEST SPECIMEN
MAX. .25
TOLERANCES
3 PLACE ±.010
2 PLACE ±.030
GENERAL ELECTRIC
METALLURGICAL PRODUCTS DEPARTMENT
CUSTOMER
NAME SHIELD FRUSTUM 6"
MATERIAL BORON PYROLETIC GRAPHITE
246

Figure 15



Task 3.3.3 Spalled Surface of Frustum Deposited in tapered thickness mandrel.

Figure 16



Nose Cone Cool-Down Without Mandrel Failure

Figure 17

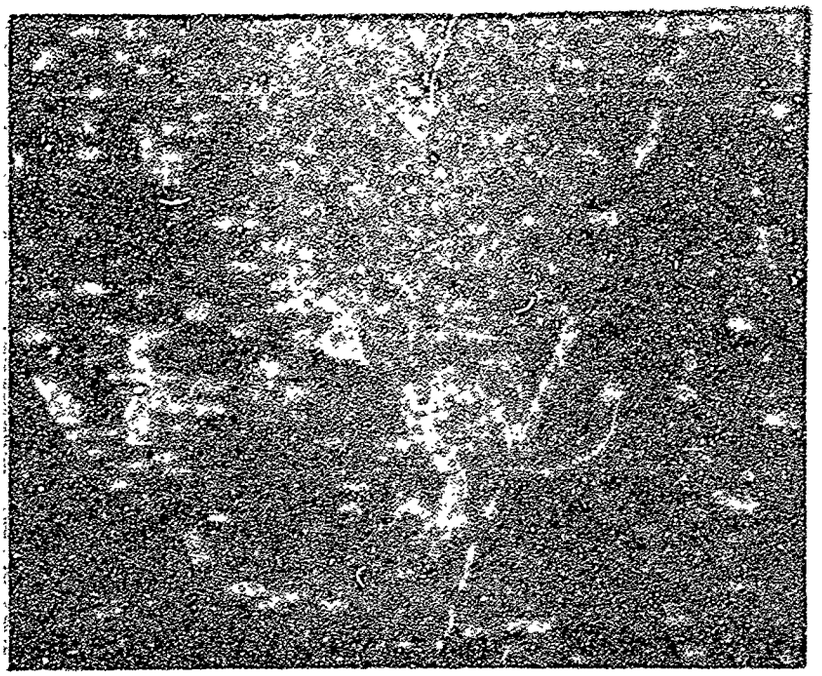


Figure 18a

Deposition surface resulting from mandrel polished with 600 grit paper followed by .0003" precoat. Original Magnification 2X

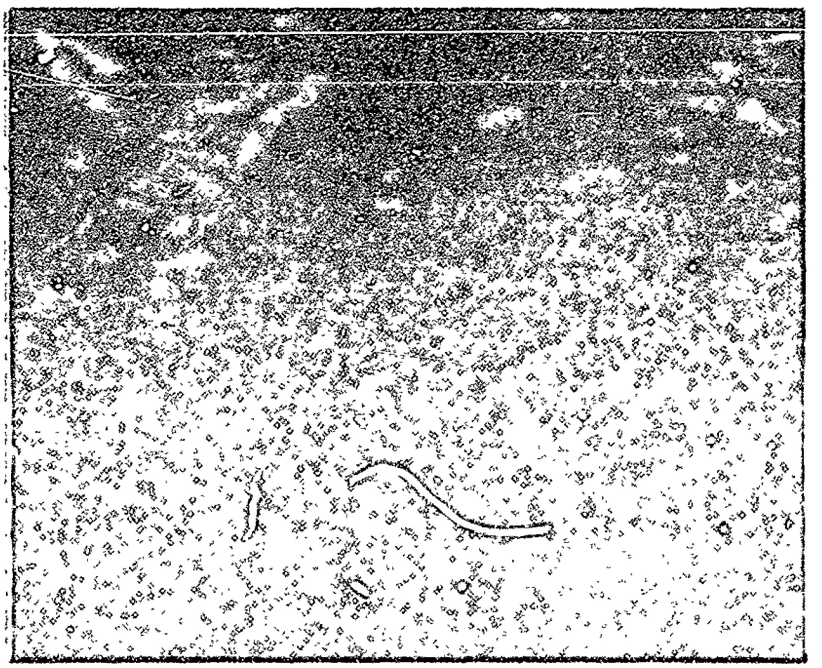


Figure 18b

Deposition surface resulting from mandrel oxidized 1 hour at 1050°F with no subsequent precoat. Original Magnification 2X

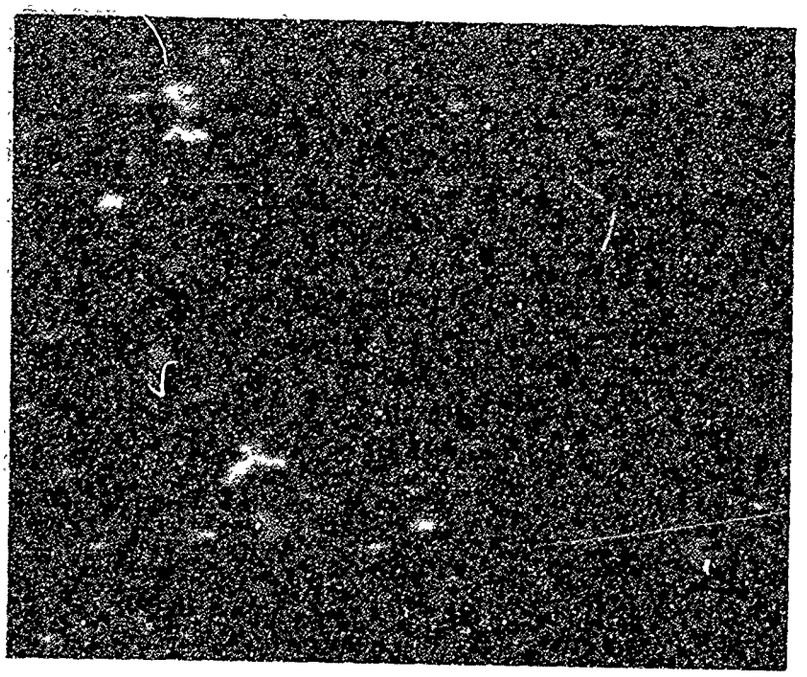


Figure 19a

Deposition surface resulting from mandrel oxidized 1 hour at 1050°F followed by .0003" precoat. Original Magnification 2X

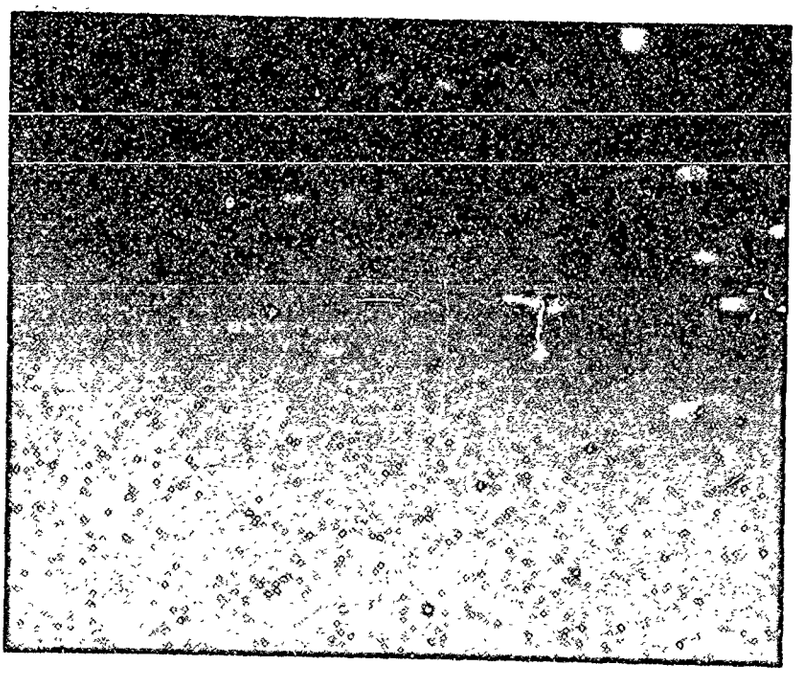
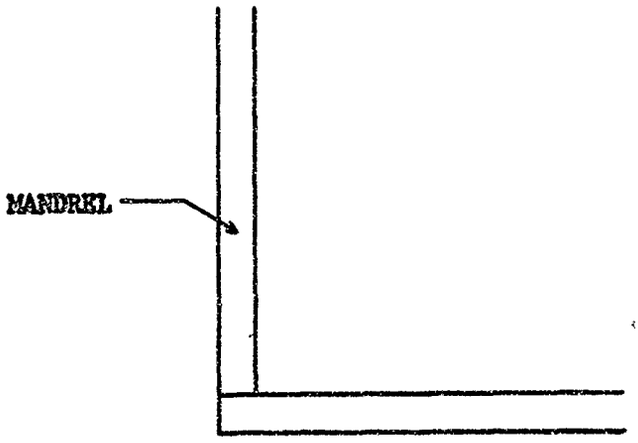
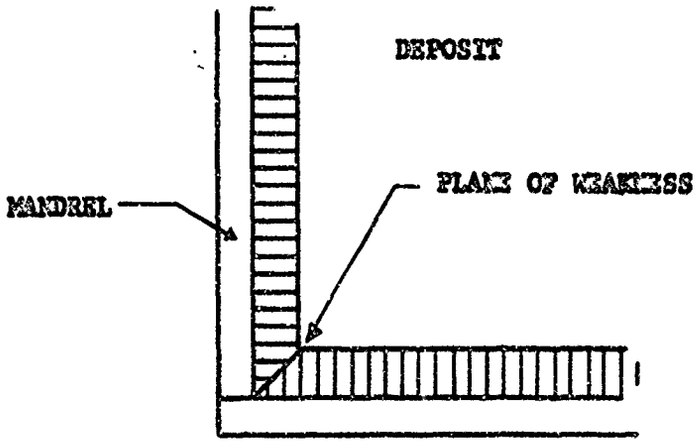


Figure 19b

Deposition surface resulting from mandrel oxidized 1 hour at 1150°F followed by .0003" precoat. Original Magnification 2X



(a) BEFORE DEPOSIT

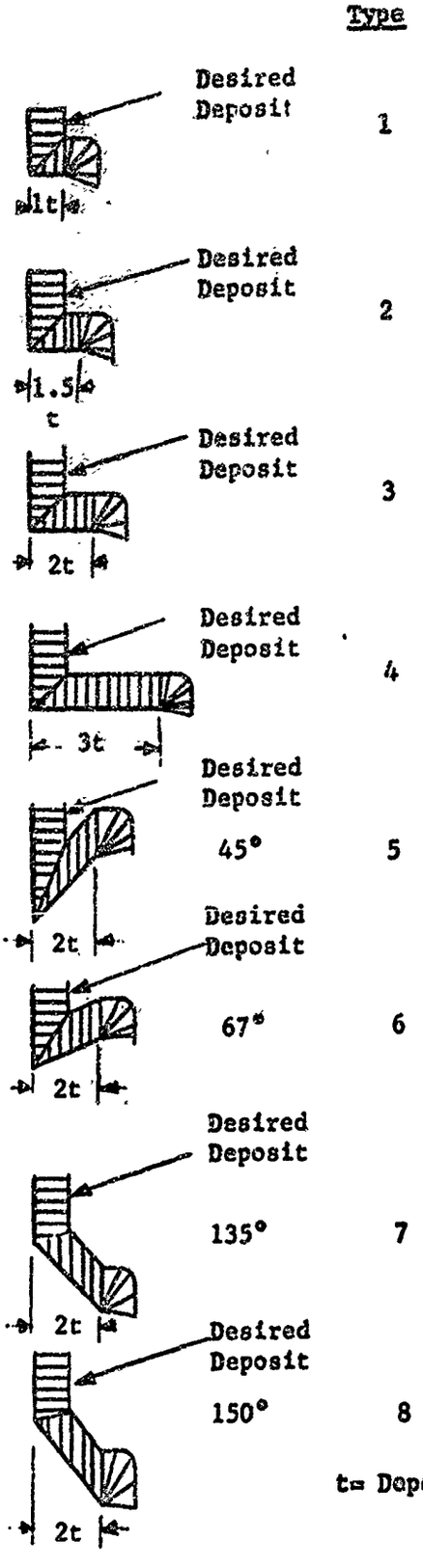


(b) AFTER DEPOSIT

Figure 20

DEPOSITION OF PYROLYTIC GRAPHITE
AT MANDREL JUNCTURE

CATEGORY A TERMINATIONS



t= Deposit Thickness

Figure 21

CATEGORY B TERMINATIONS

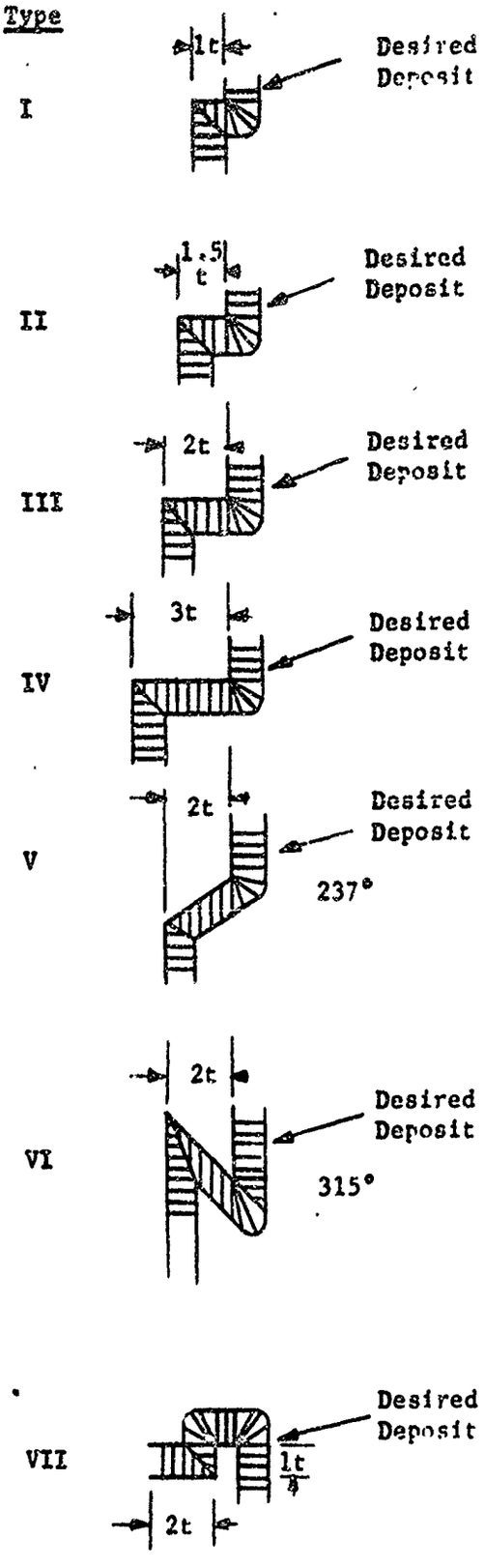


Figure 22

CATEGORY C TERMINATIONS

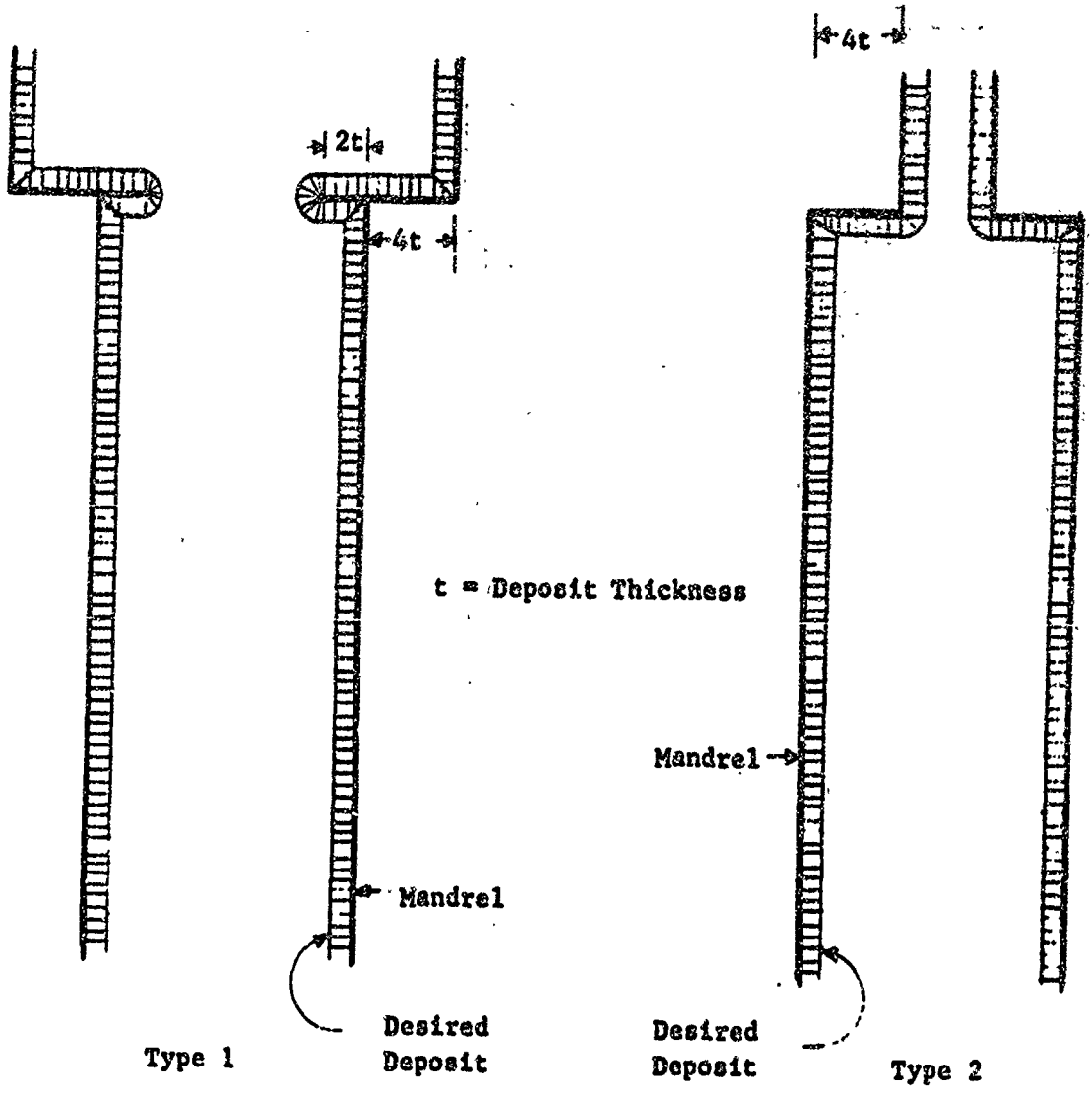


Figure 23

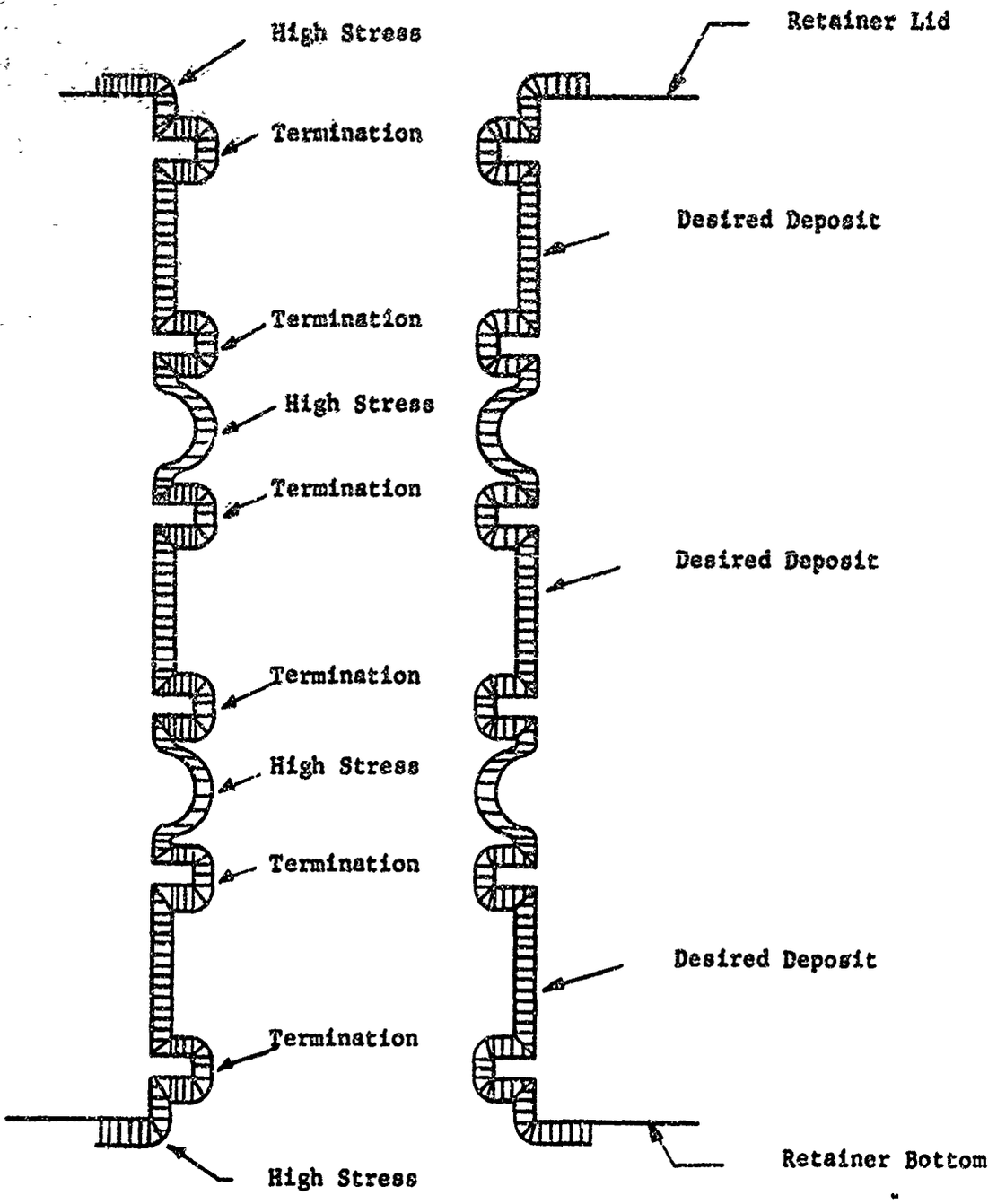


Figure 24

Schematic Arrangement of Parts in Multiple Tube Deposition Assembly for Evaluation of Termination Design

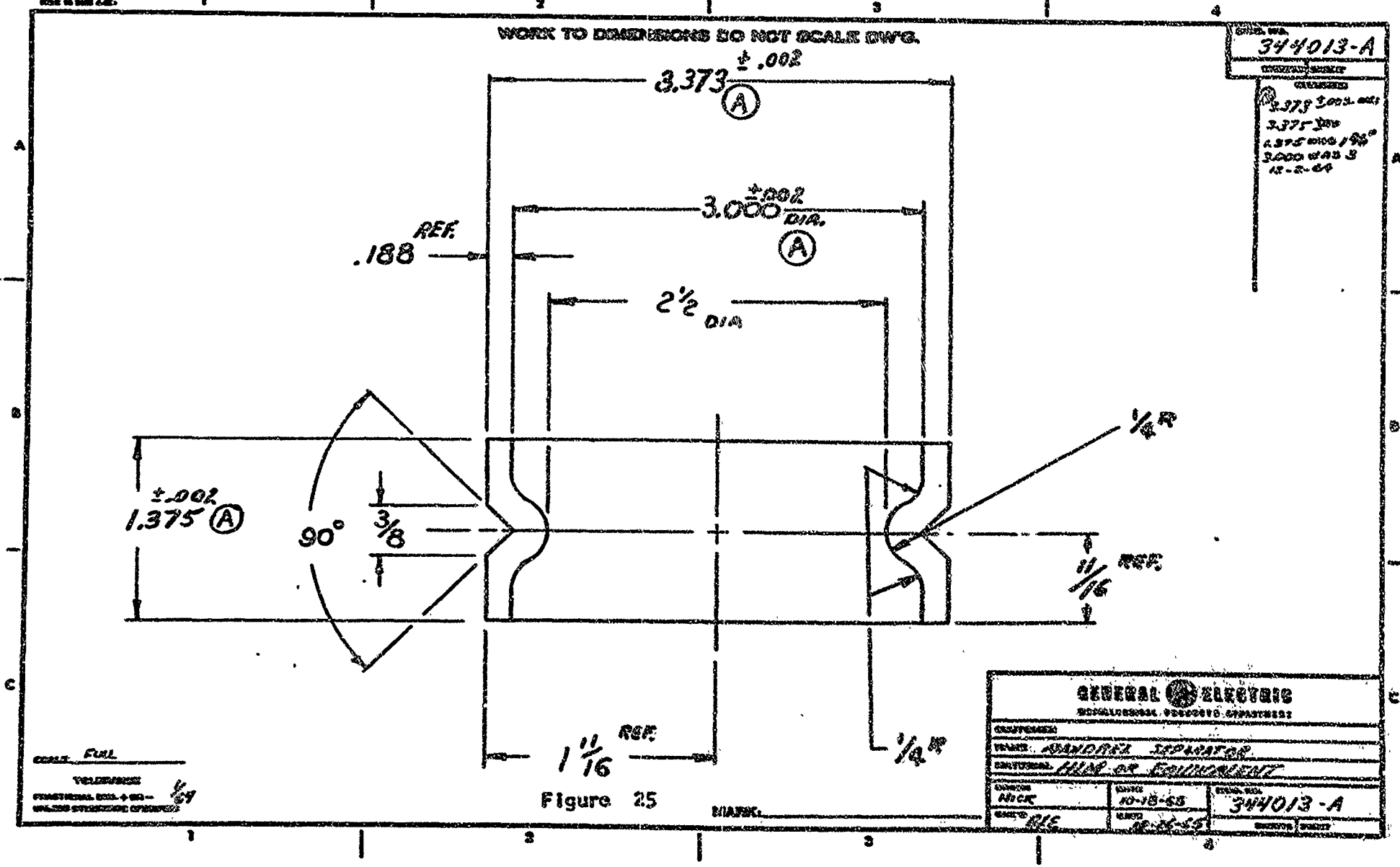
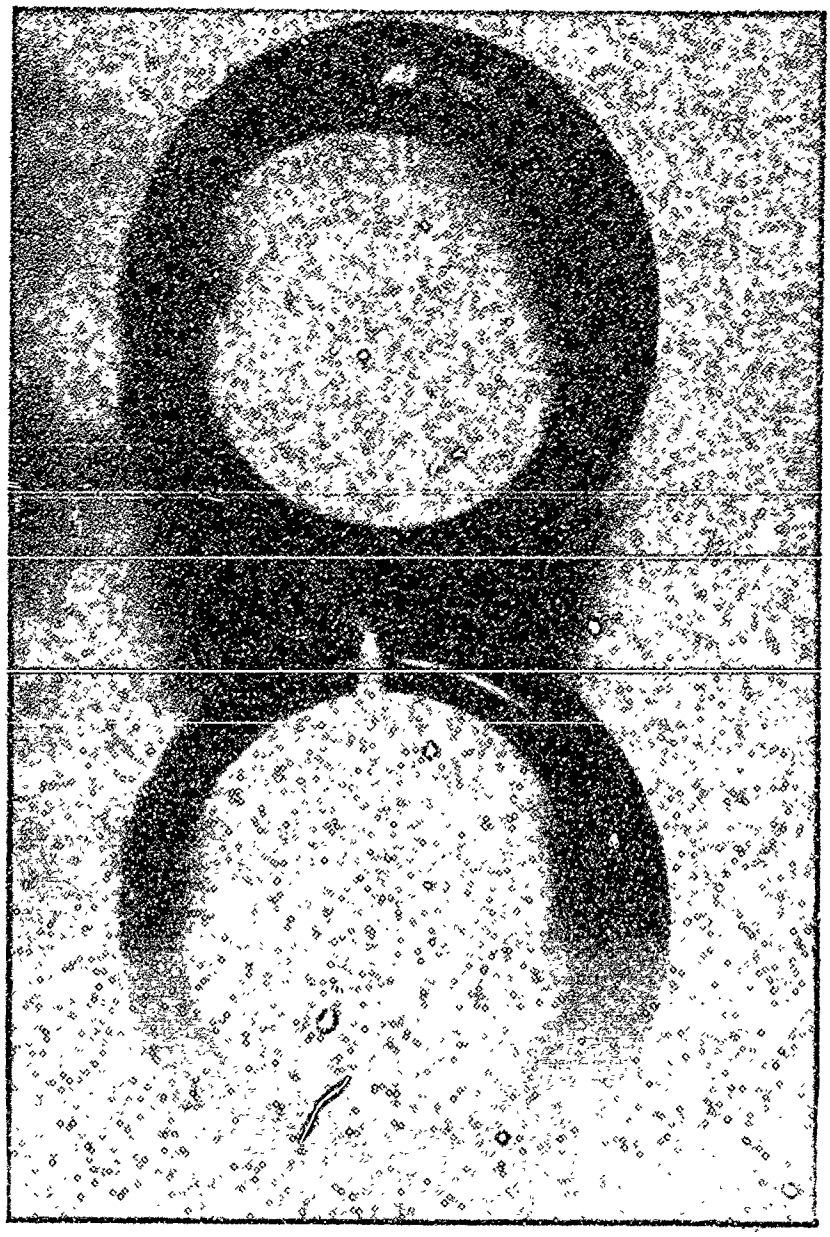

WORK TO DIMENSIONS DO NOT SCALE DWG.
3.373 ±.002 (A)
3.000 ±.002 DIA. (A)
.188 REF.
2½ DIA
±.002 1.375 (A)
90°
3/8
1/4 R
11/16 REF.
1 11/16 REF.
1/4 R
344013-A
3.373 ±.002
3.375
3.000 REAM 3
12-2-64
GENERAL ELECTRIC
ADAPTER SEPARATOR
HEAT SHIELD
HICK
10-18-65
344013-A
RLE
12-15-65
FULL
4/64

Figure 25



Characteristic Deposit With
Separator 344013 Attached

Figure 26.



Separator 344013 Before and After Axial Cut. Opening Demonstrates Inner Fiber Compressive Residual Stress.

Figure 27.

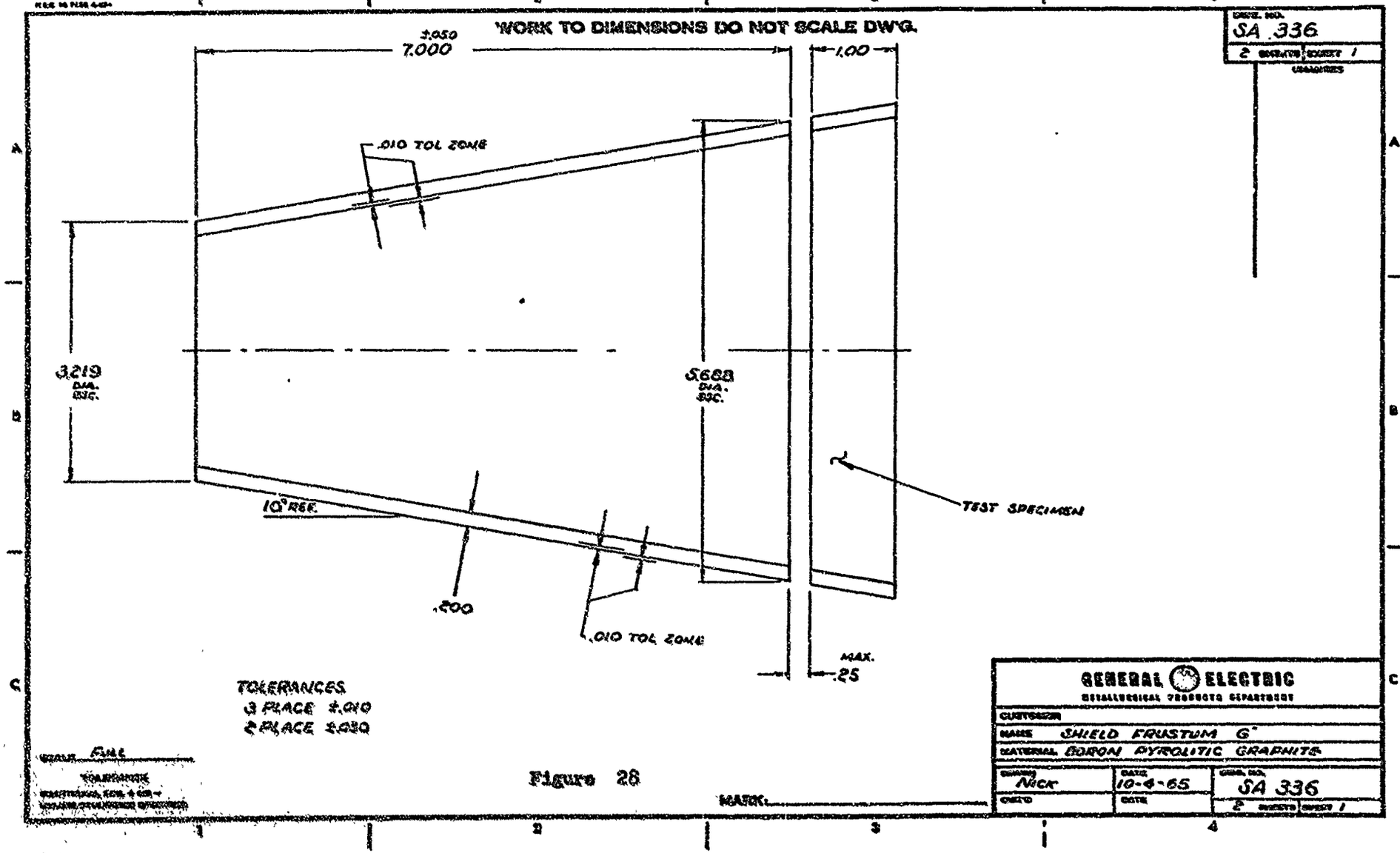
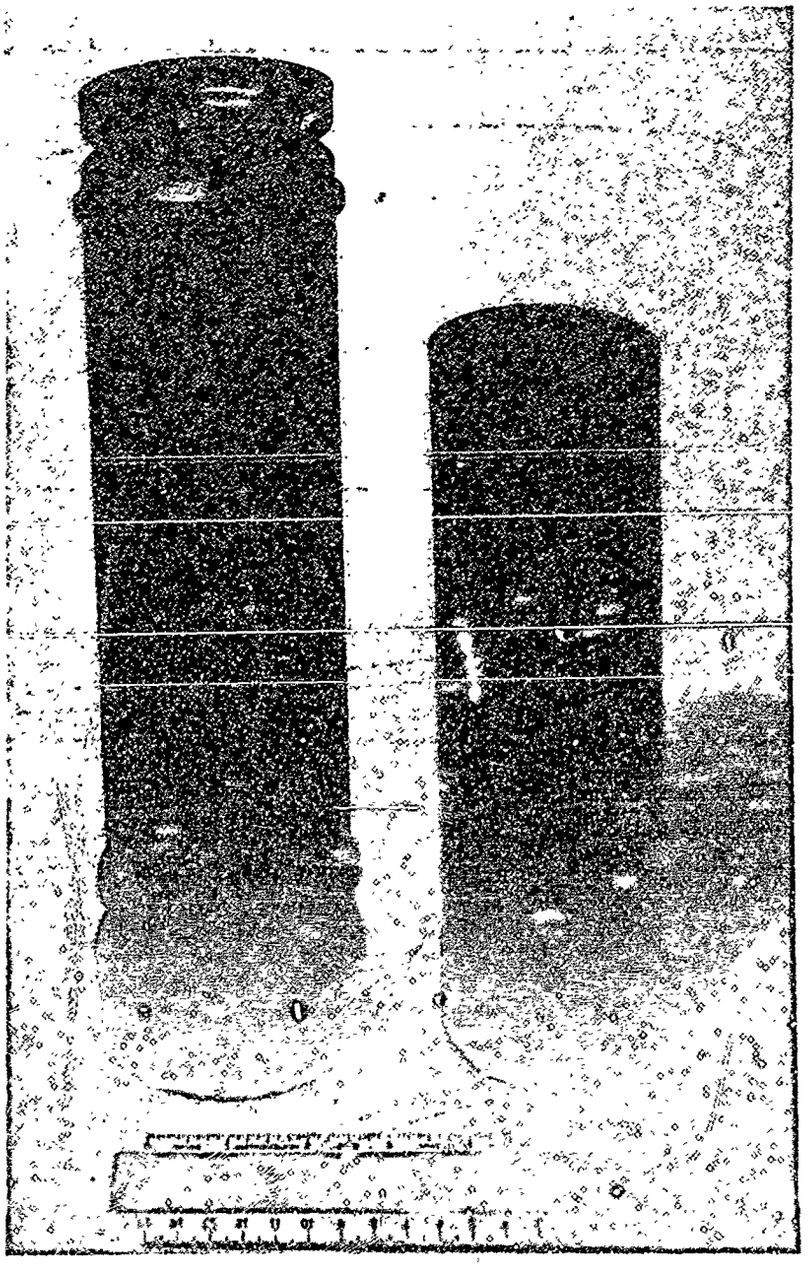
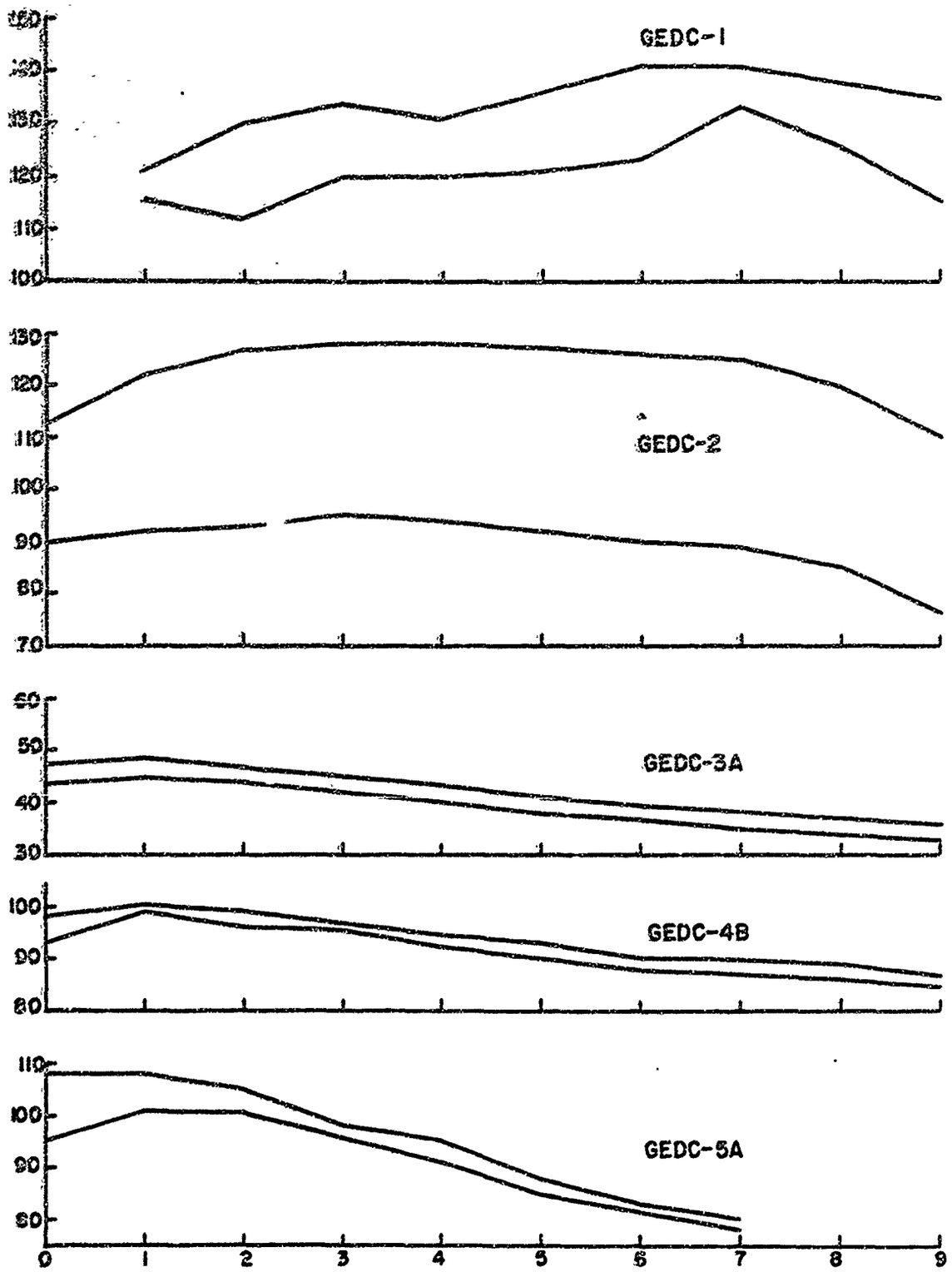

WORK TO DIMENSIONS DO NOT SCALE DWG.
7.000 ±.050
1.00
.010 TOL ZONE
3.219 DIA. BSC.
5.688 DIA. BSC.
10° REF.
TEST SPECIMEN
.200
.010 TOL ZONE
MAX. .25
TOLERANCES
3 PLACE ±.010
2 PLACE ±.030
DRWG. NO. SA 336
GENERAL ELECTRIC
METALLURGICAL PRODUCTS DEPARTMENT
NAME SHIELD FRUSTUM 6°
MATERIAL BORON PYROLITIC GRAPHITE
DRAWN Nick
DATE 10-4-65
SA 336

Figure 28



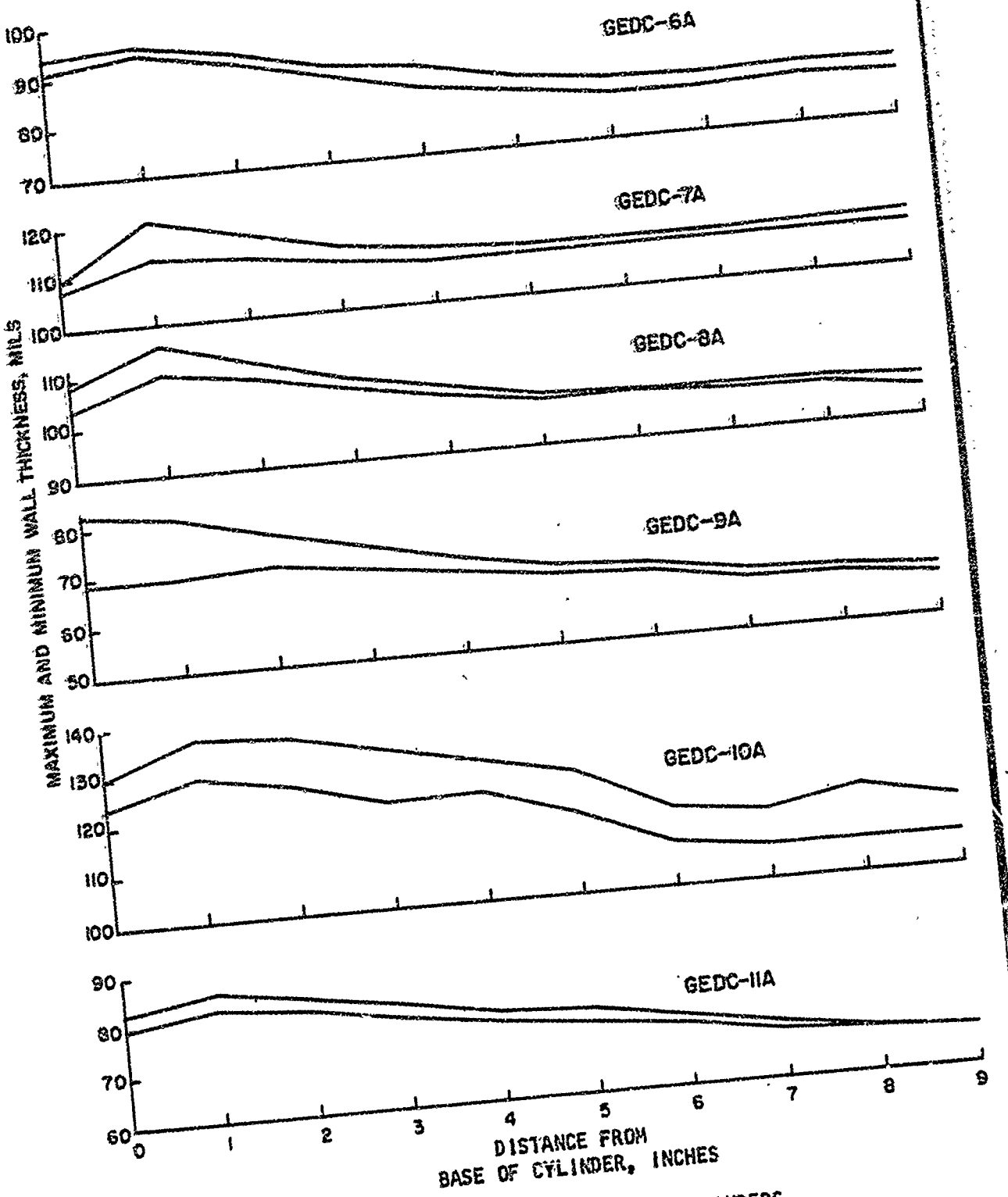
Photograph of Mandrel Assembly and Typical Tube Deposited.

Figure 29



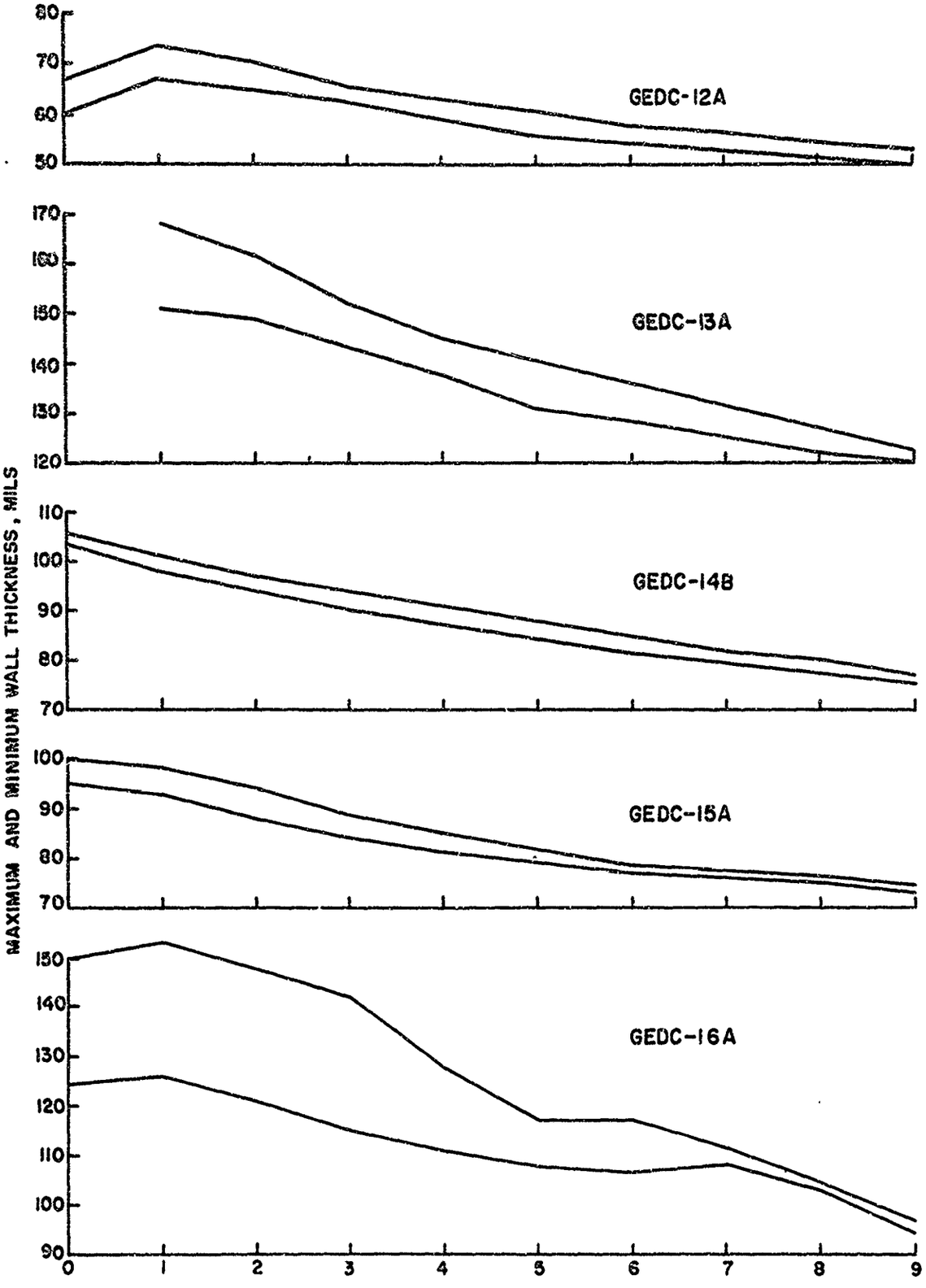
DEPOSITION PROFILE FOR CYLINDERS

Figure 30



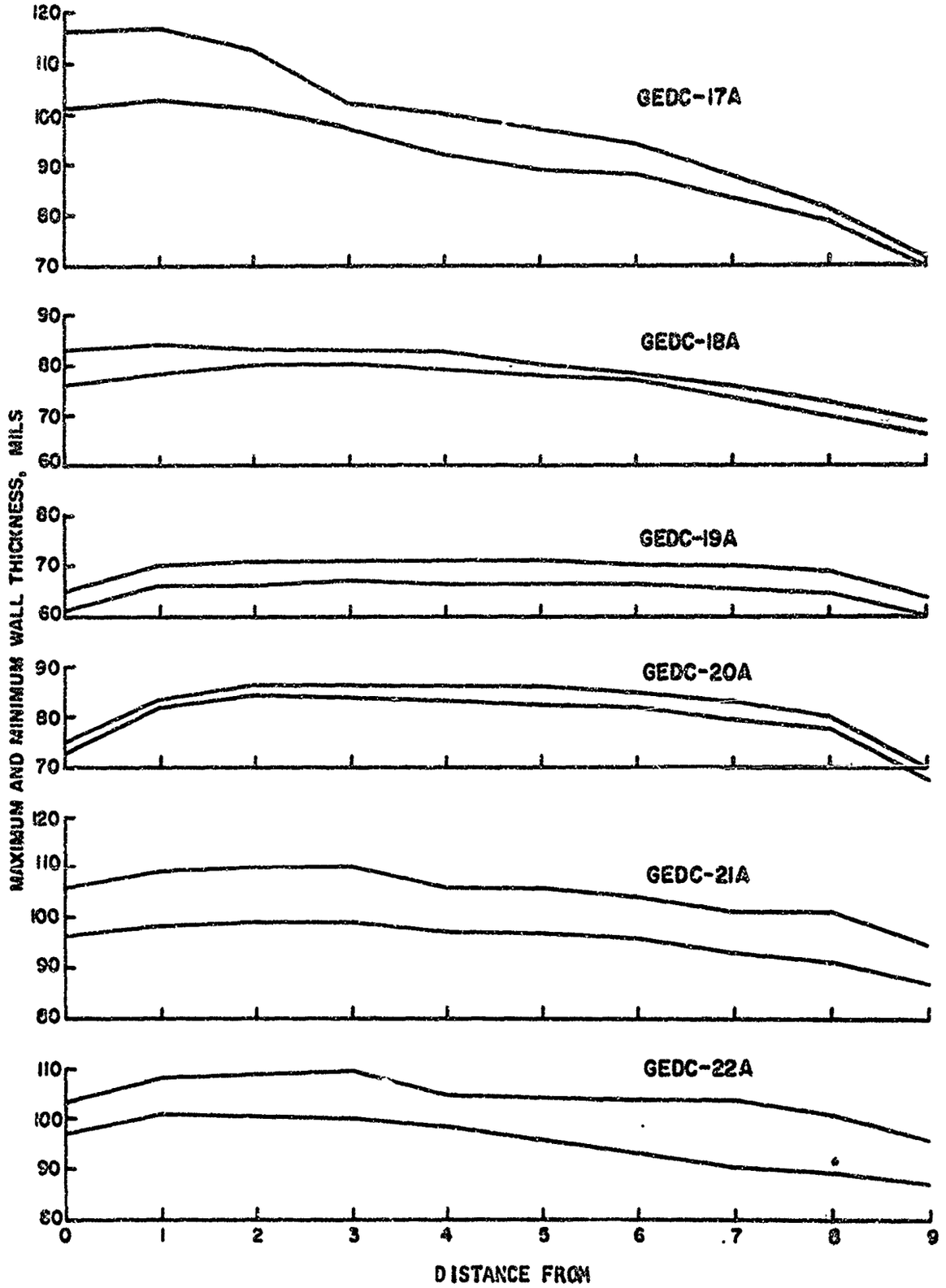
DEPOSITION PROFILE FOR CYLINDERS

Figure 31



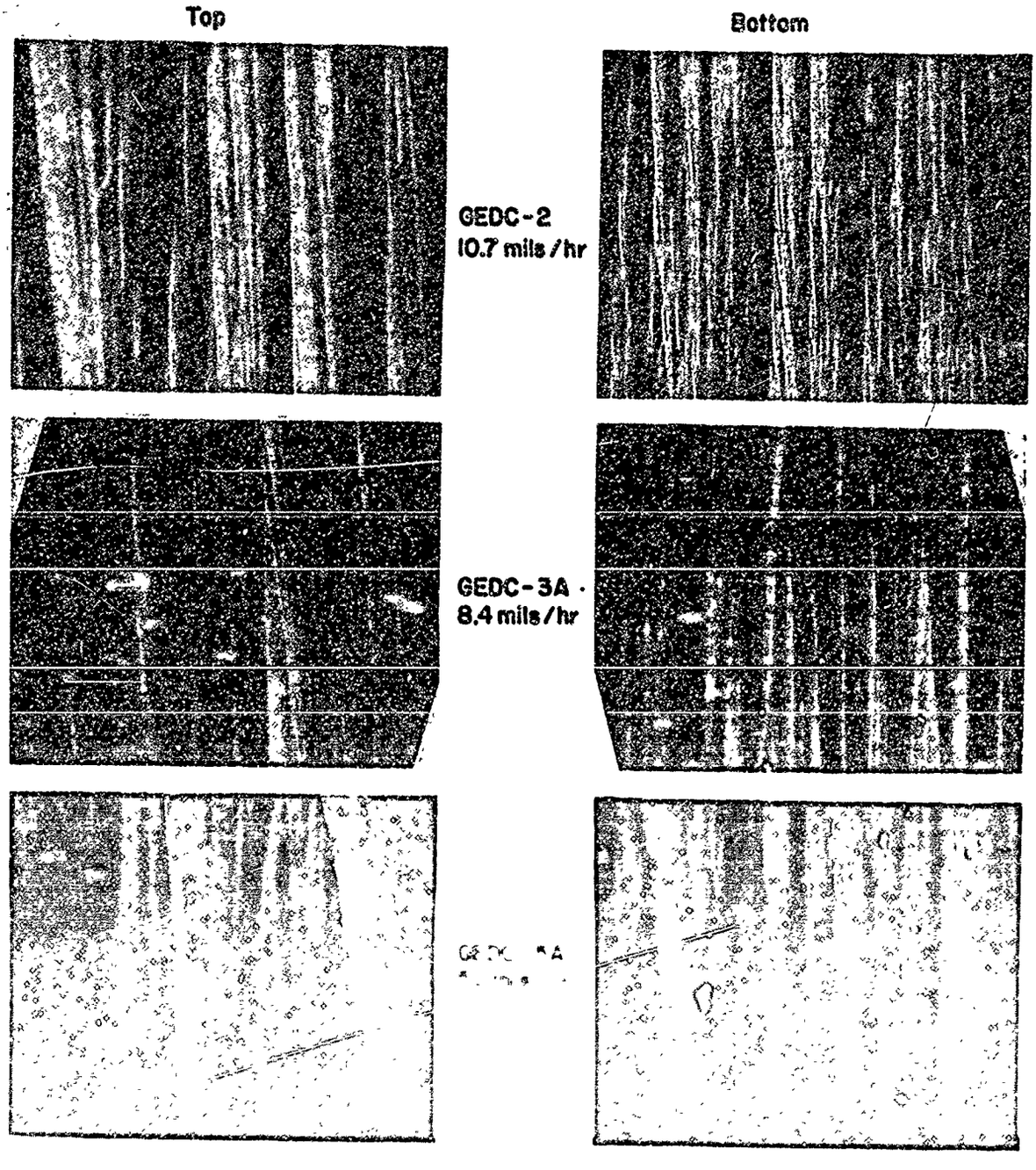
DEPOSITION PROFILE FOR CYLINDERS

Figure 32



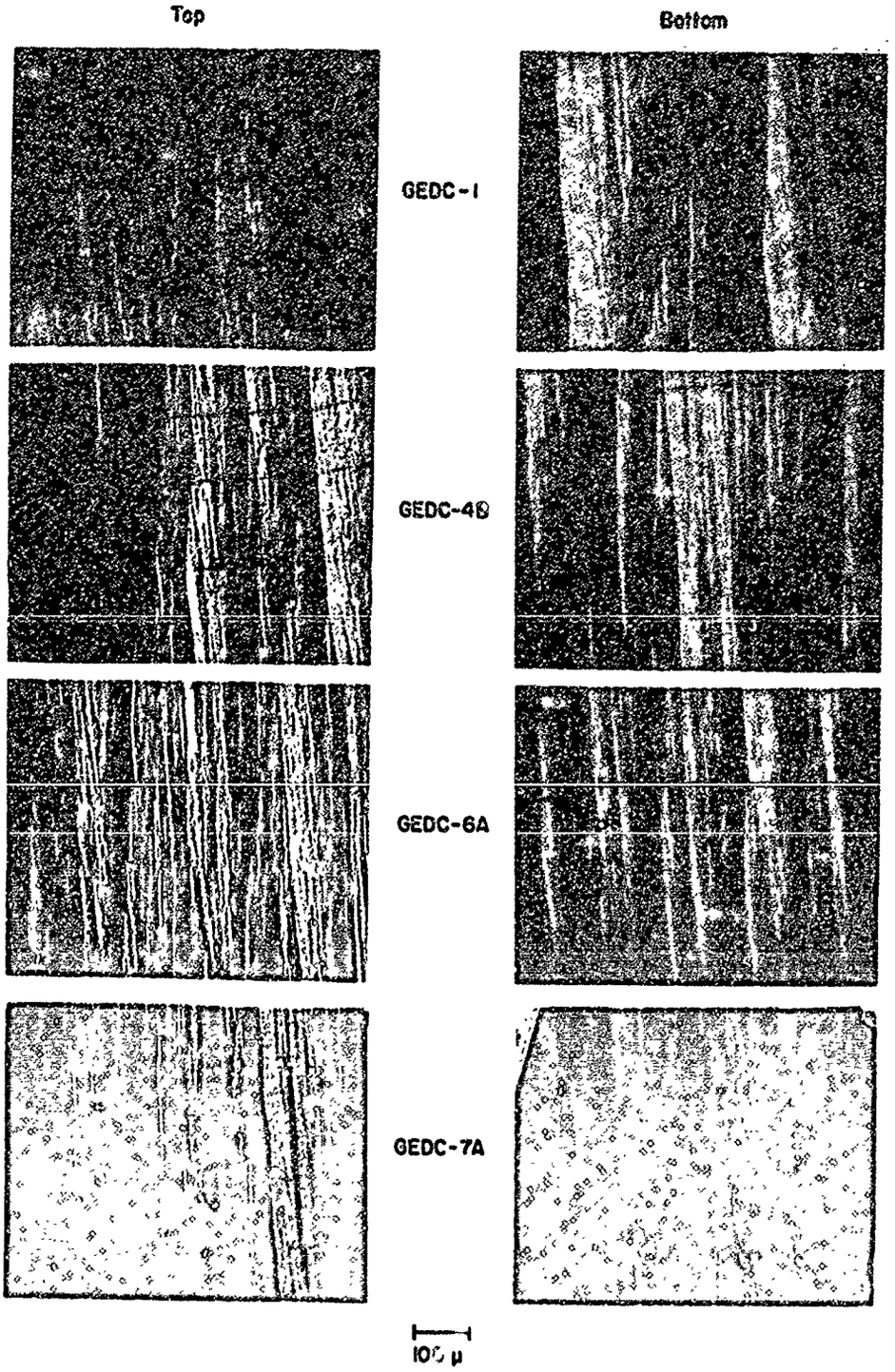
DEPOSITION PROFILE FOR CYLINDERS

Figure 33



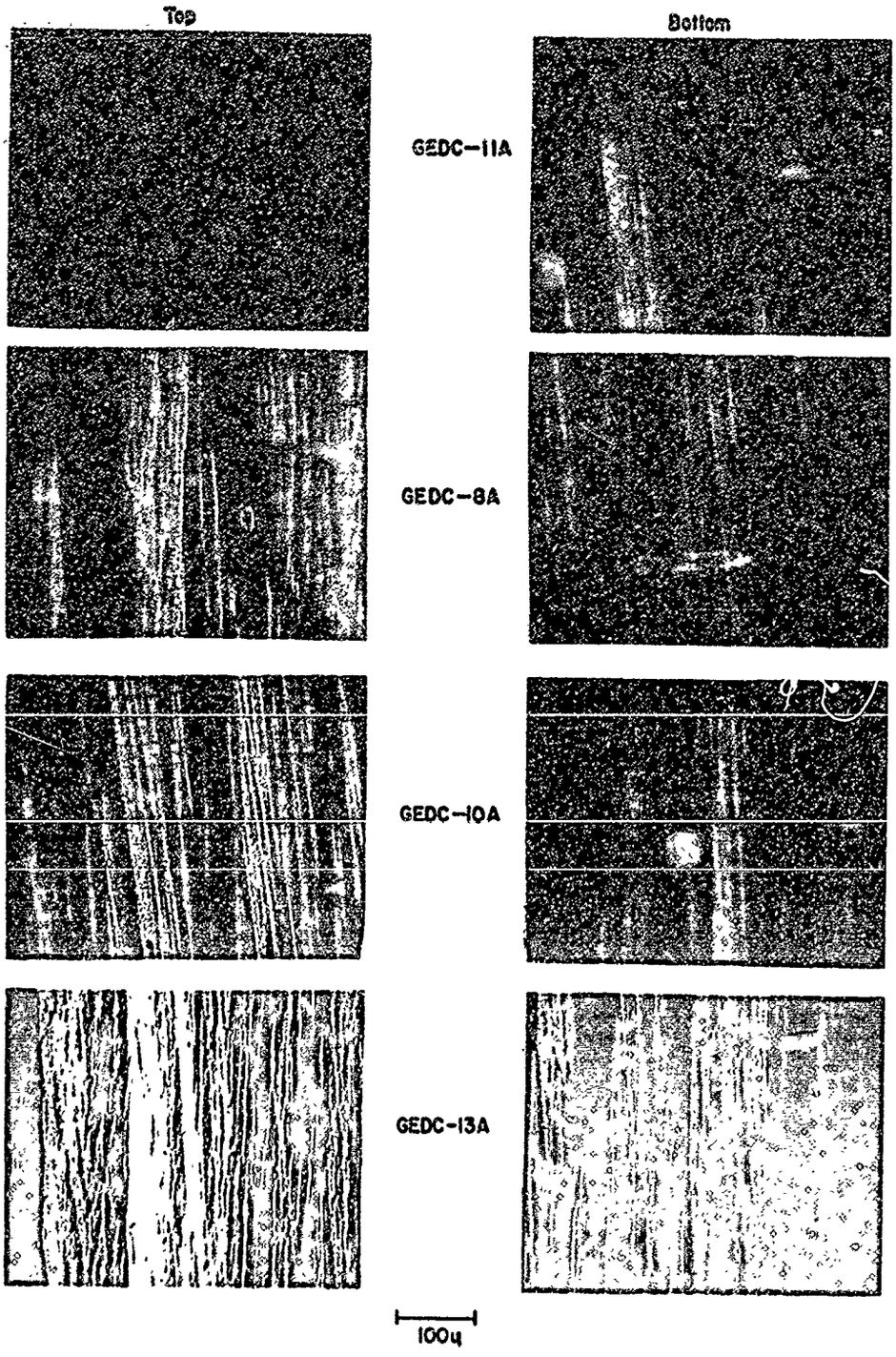
Micrographs for PG Cylinder Deposits. Deposition Rate Variable.

Figure 34



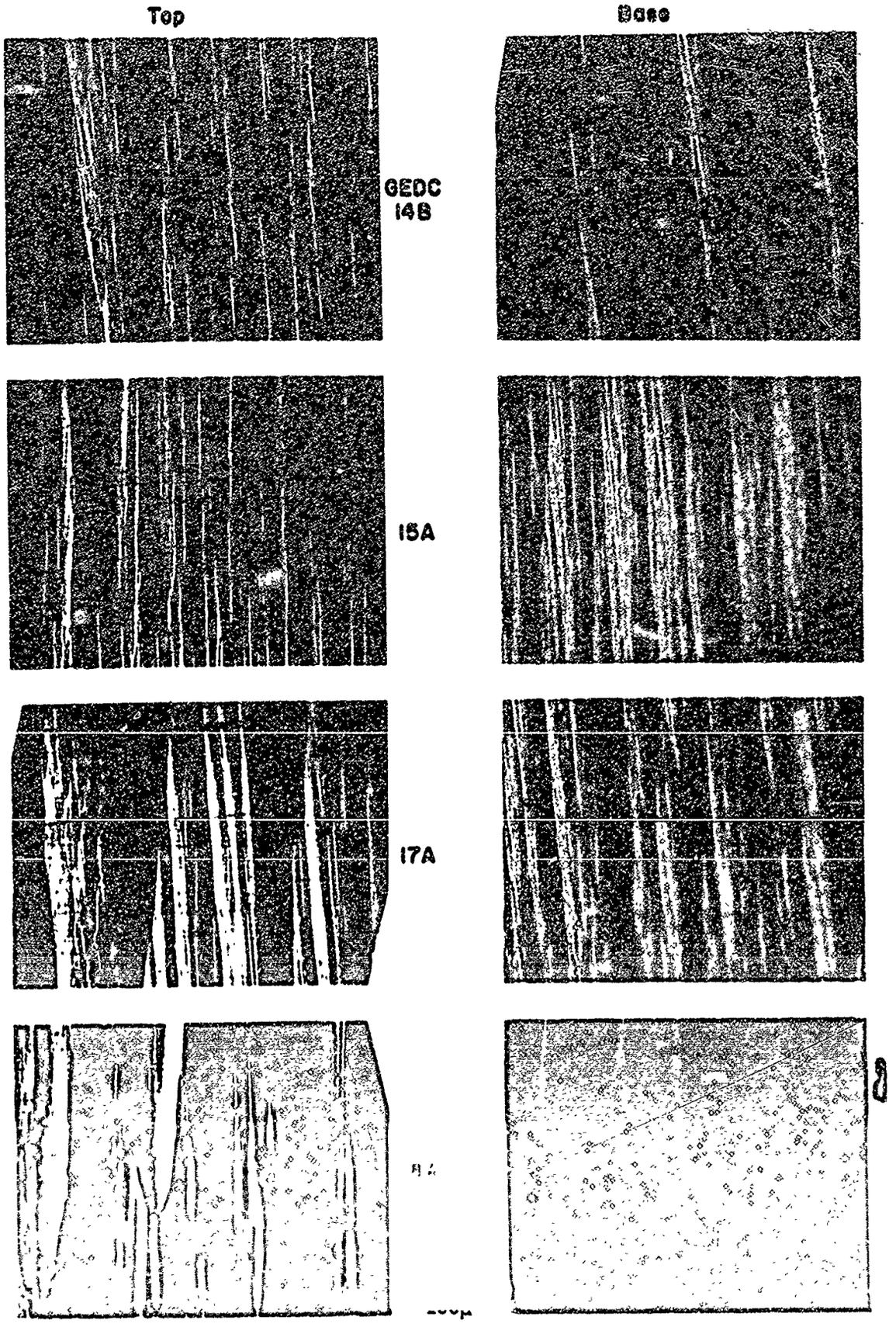
Micrographs for Boron PG cylinder deposits. Boron Content Variable from Trimethyl Borate and Methane.

Figure 35



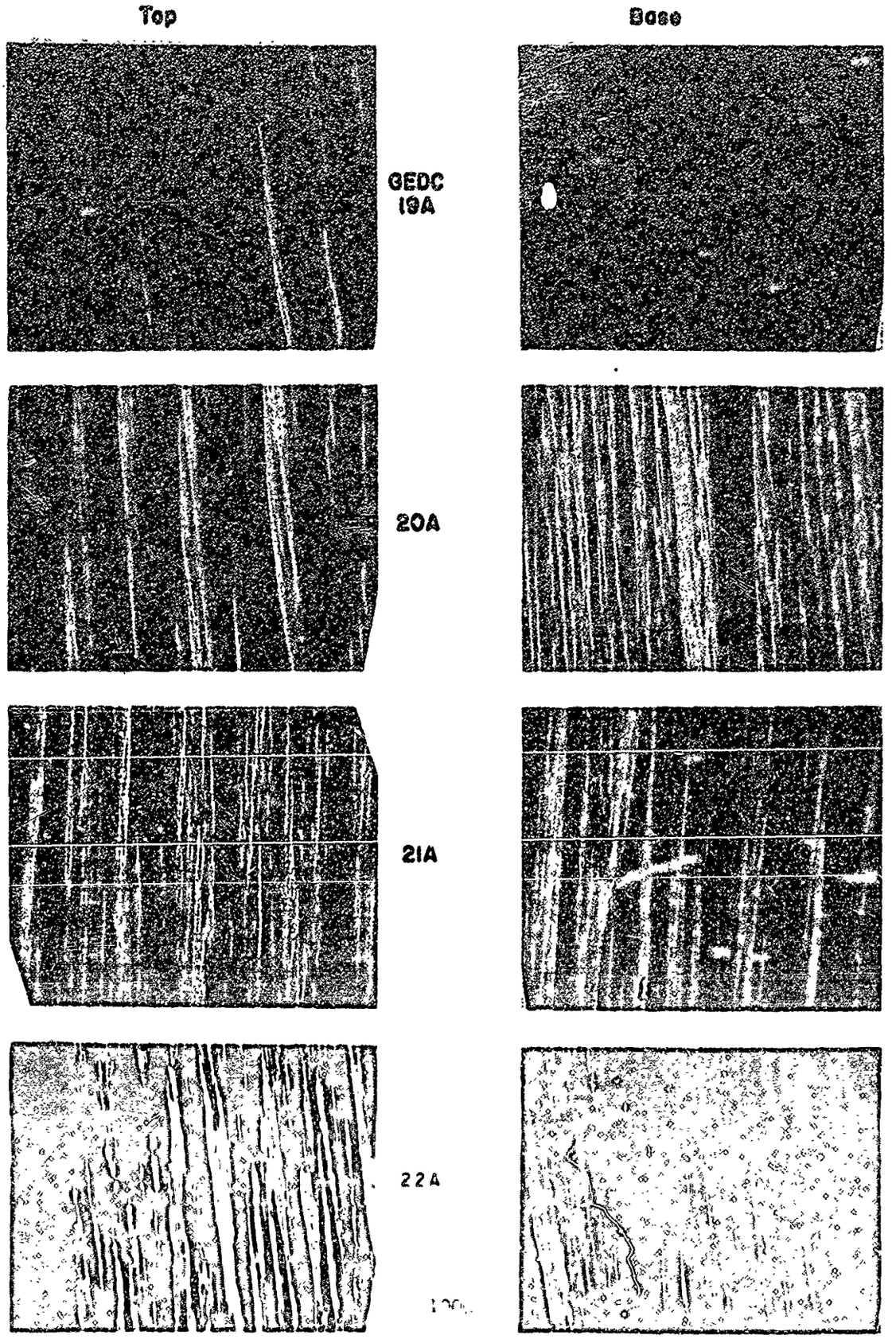
Micrographs for Boron PG cylinder deposits. Boron content Variable from Trimethyl Borate and Methane.

Figure 36



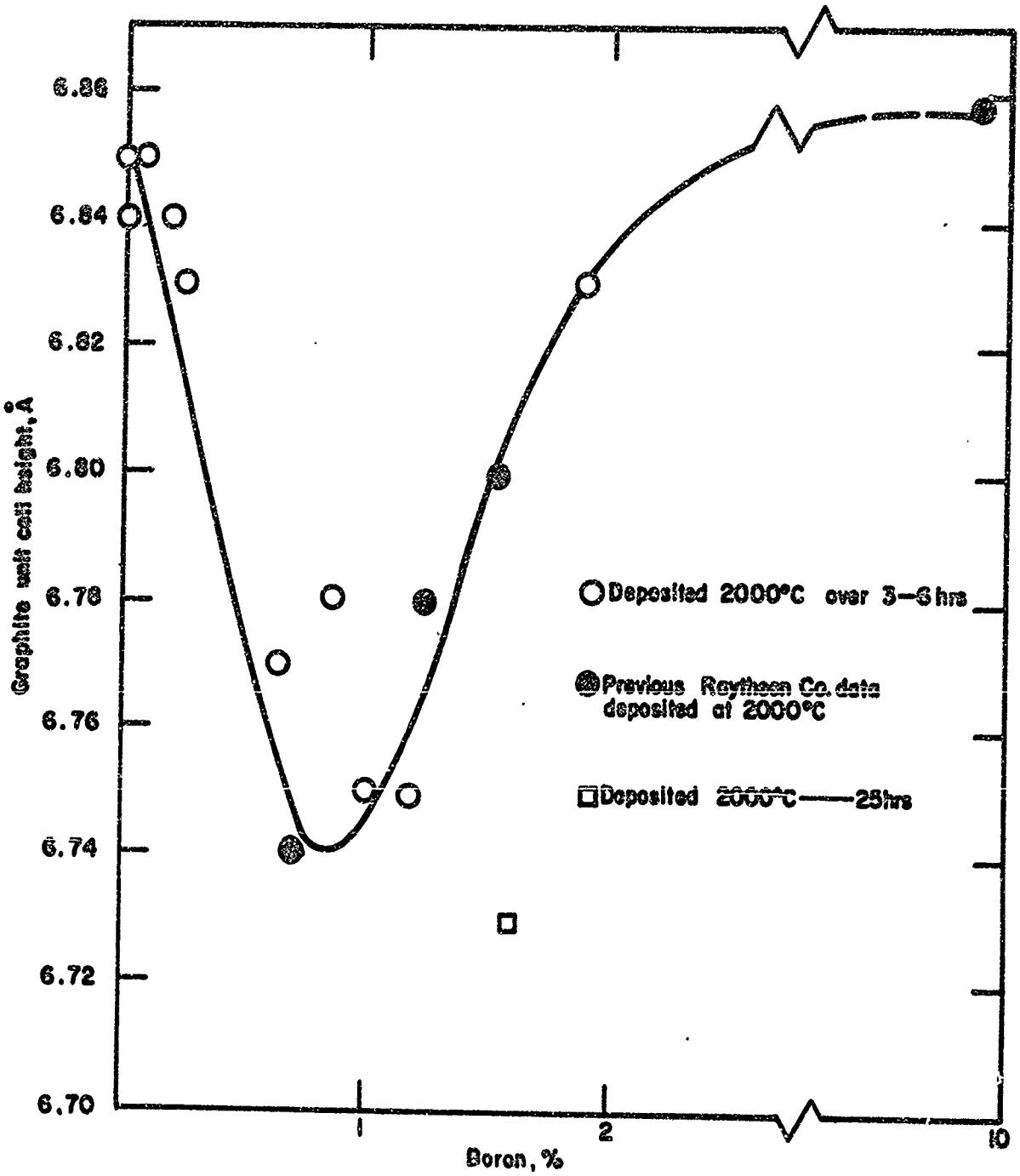
Micrographs for Cylinder Deposits

Figure 37



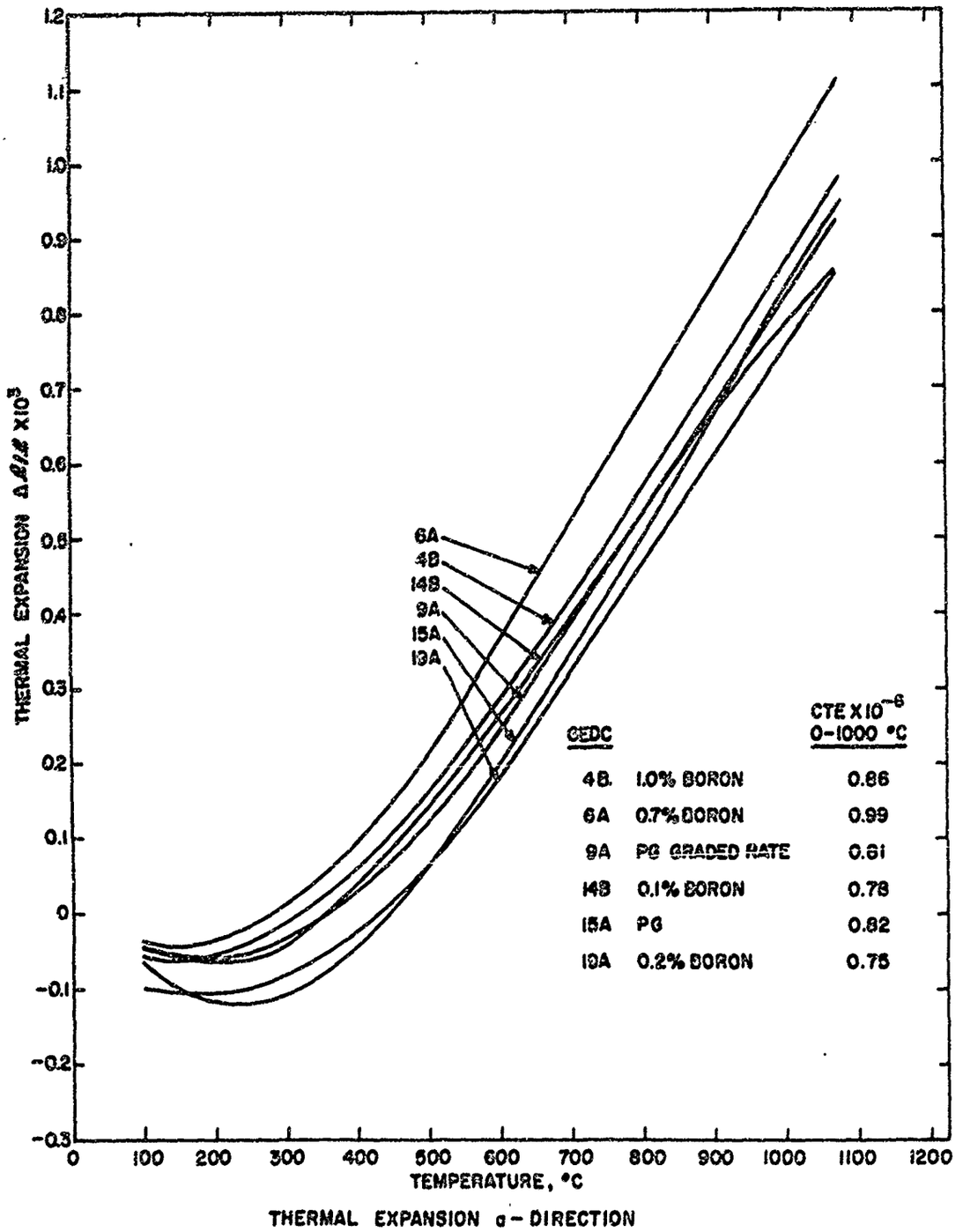
Micrographs for Cylinder Deposits

Figure 38



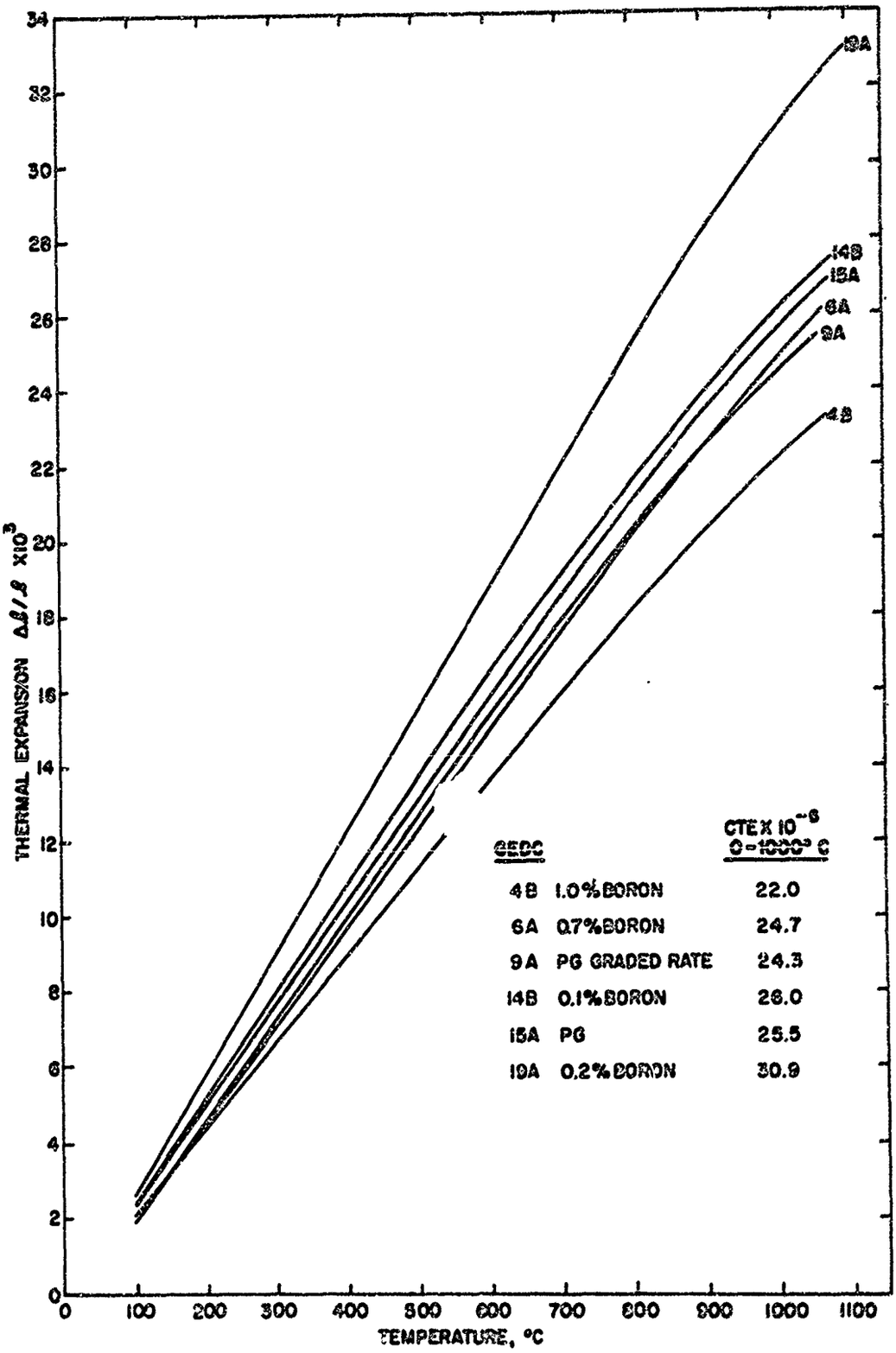
CORRELATION BETWEEN UNIT CELL HEIGHT AND PERCENT BORON

Figure 39



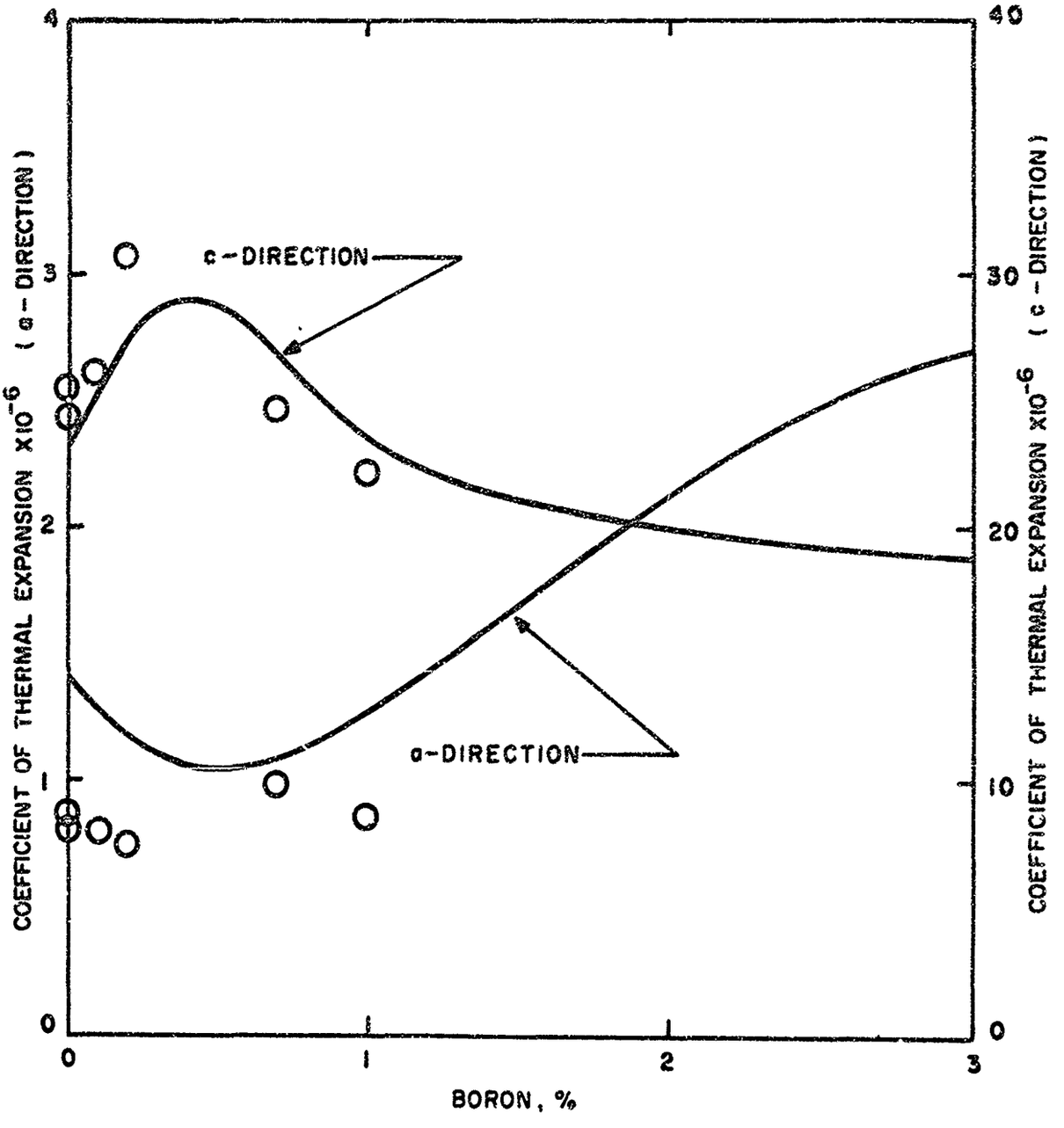
THERMAL EXPANSION a - DIRECTION

Figure 40



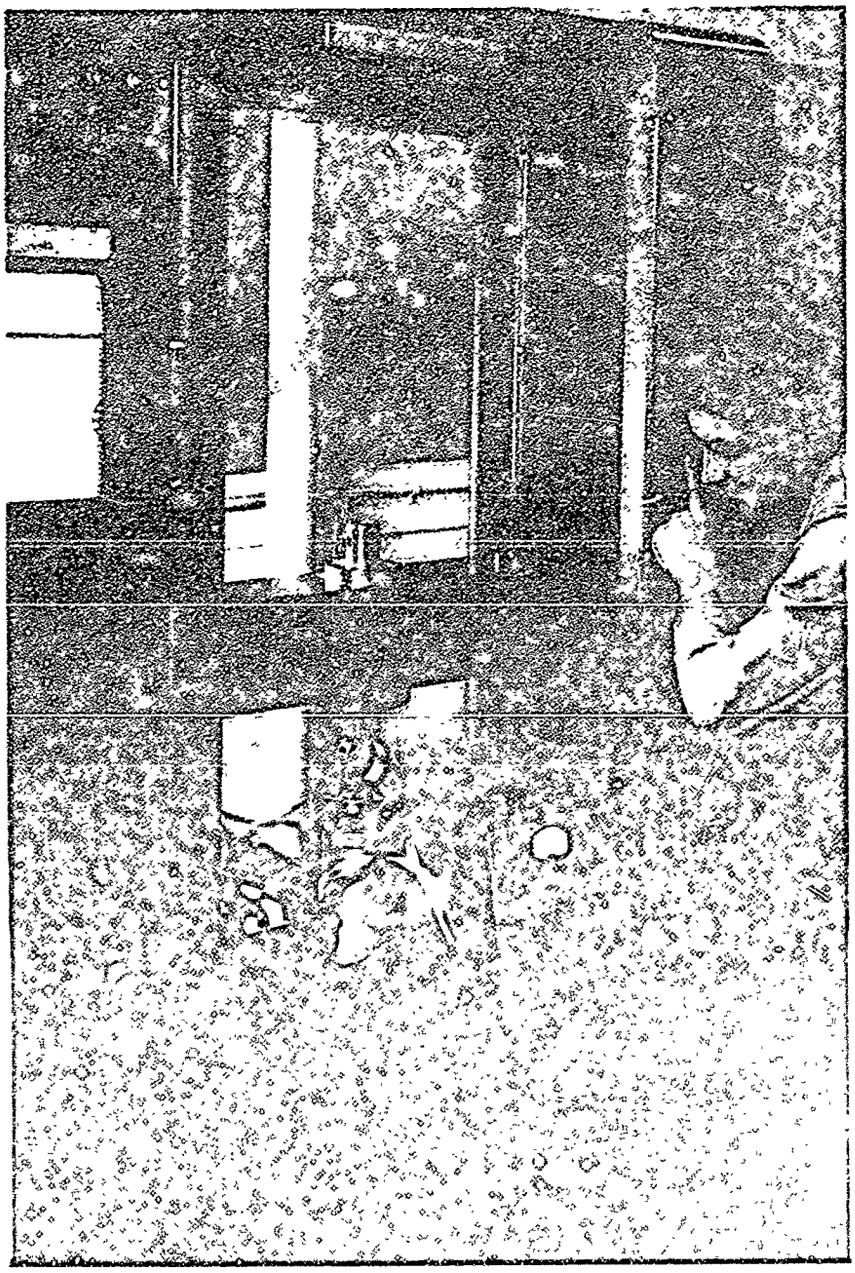
THERMAL EXPANSION c – DIRECTION

Figure 41



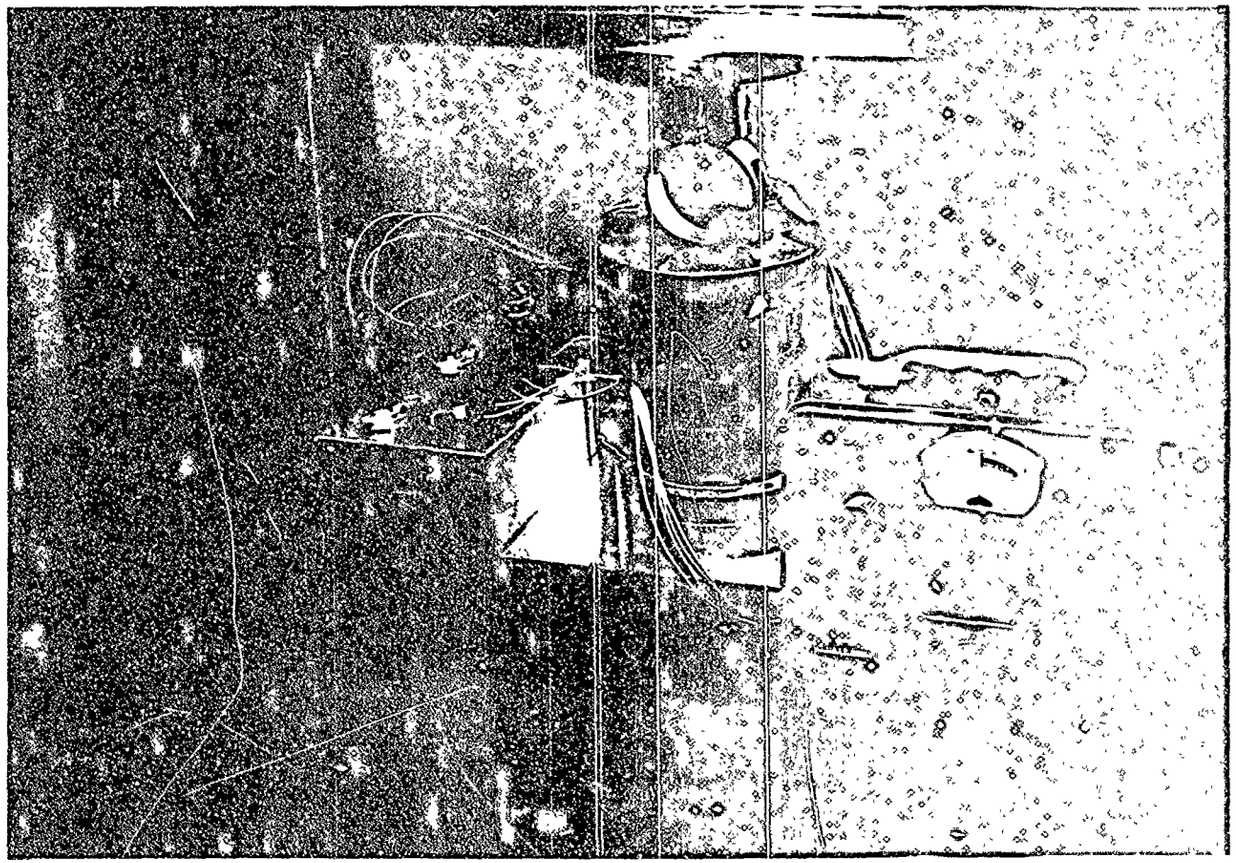
COEFFICIENT OF THERMAL EXPANSION FOR BPG FROM 0° TO 1000° C AS A FUNCTION OF BORON CONTENT, NOMINAL 2000° C DEPOSITS. CURVES BASED UPON PREVIOUS RAYTHEON CO. FLAT PLATE DEPOSITS CIRCLES FROM TUBE DEPOSITS

Figure 42



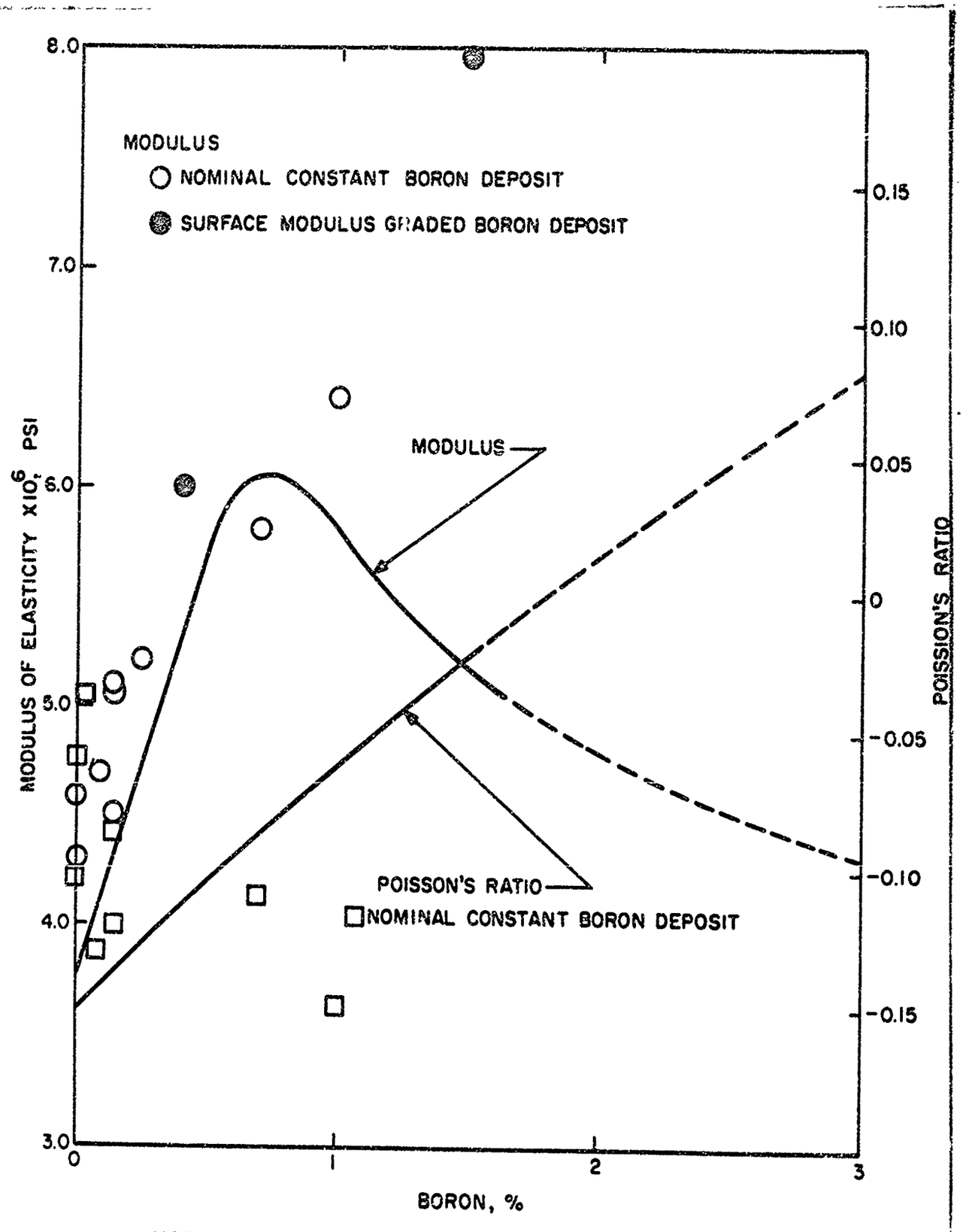
Photograph of Diametral Ring Compression Apparatus

Figure 43



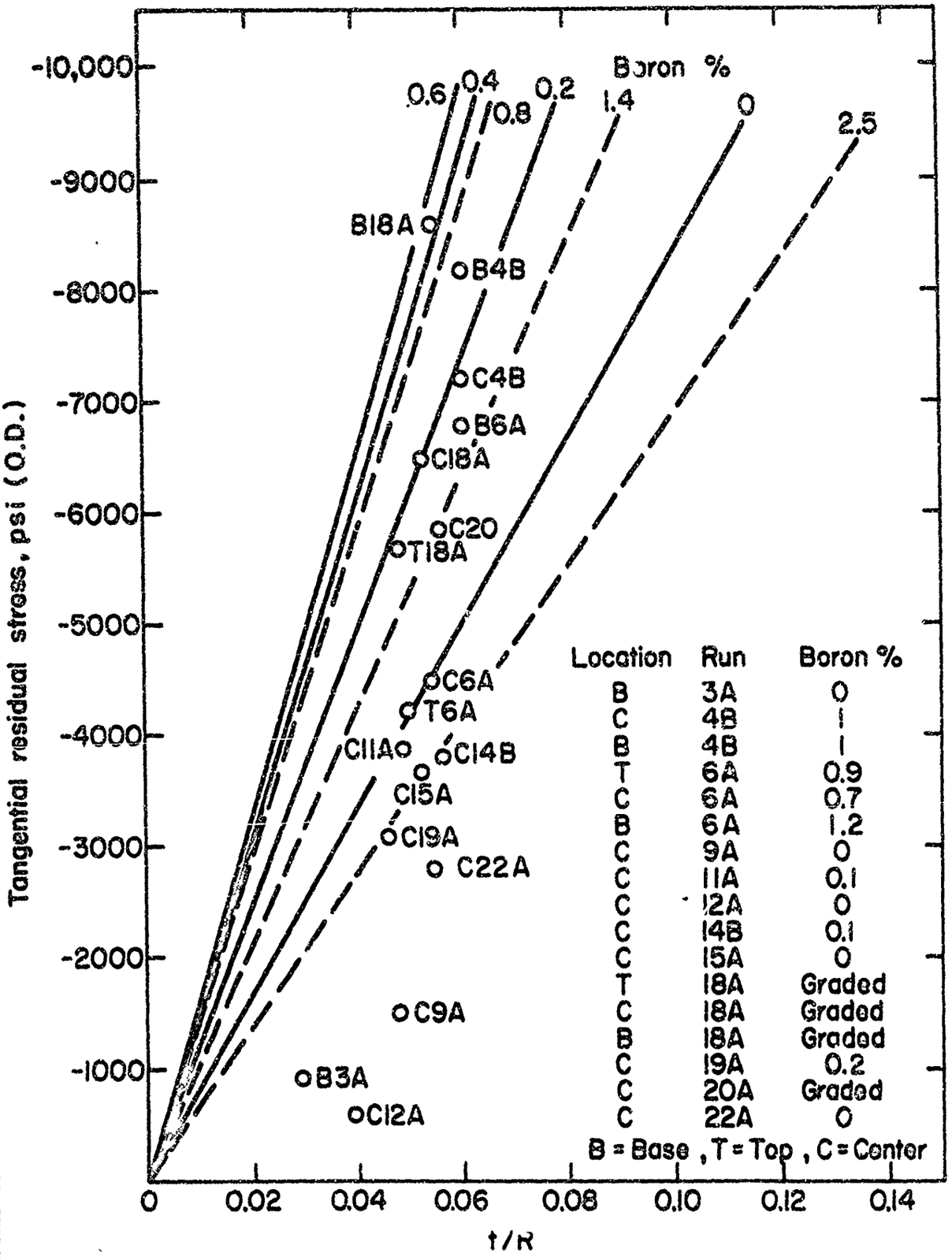
Photograph of Close Up of Diametral Ring Compress! Assem

Figure 44



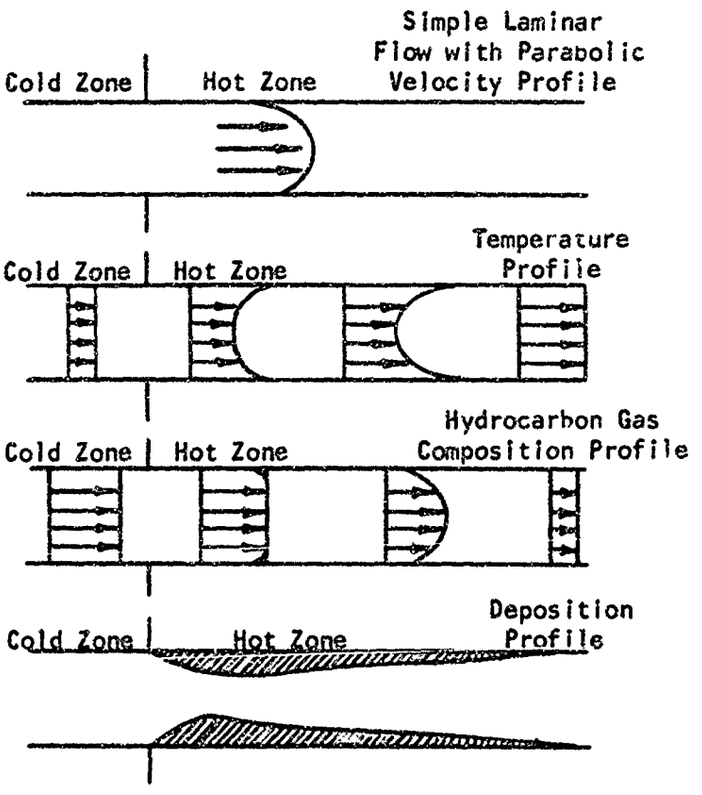
MODULUS OF ELASTICITY AND POISSON'S RATIO FOR BPG AS A FUNCTION OF BORON CONTENT. NOMINAL 2000° C DEPOSITS CURVES BASED UPON PREVIOUS RAYTHEON CO. FLAT PLATE DEPOSITS. CIRCLES AND SQUARES FROM TUBE DEPOSITS

Figure 45



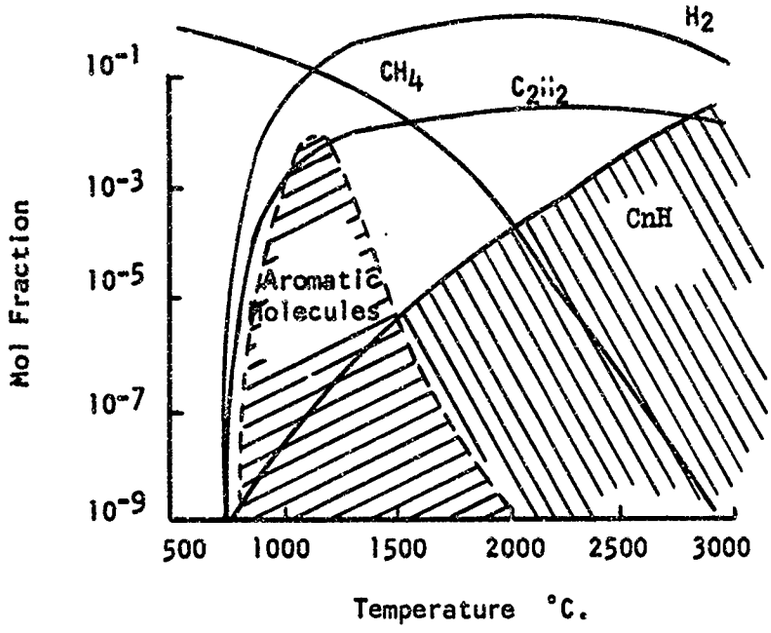
COMPARISON OF CALCULATED (Lines) AND MEASURED (Circles) RESIDUAL STRESS.

Figure 46



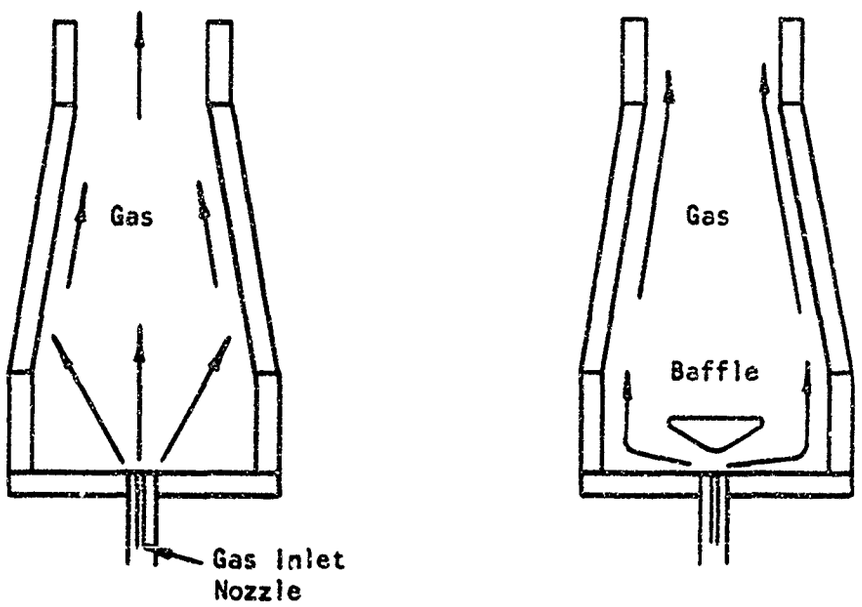
Characteristics of hydrocarbon gas flowing inside heated tube and deposition profile which results.

Figure 47.



Equilibrium Mol Fractions
of Various Gas Species in C-H System
at 0.1 Atmosphere Pressure and C/H Ratio of 1/4.

Figure 48.

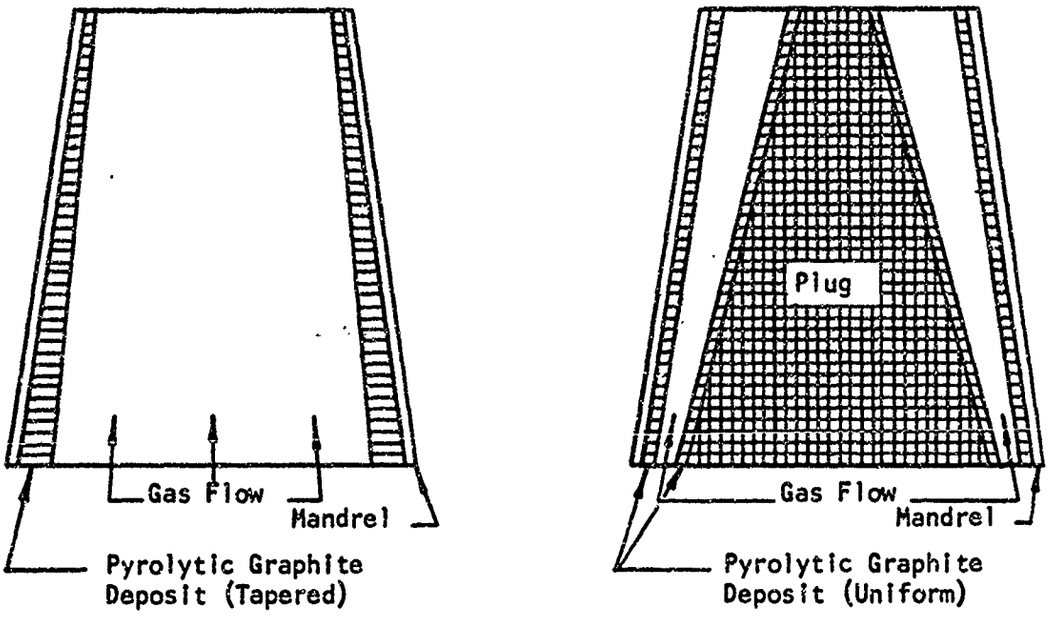


(A) Without Baffle

(B) With Baffle

Baffling Technique for Frustum Deposition

Figure 49.

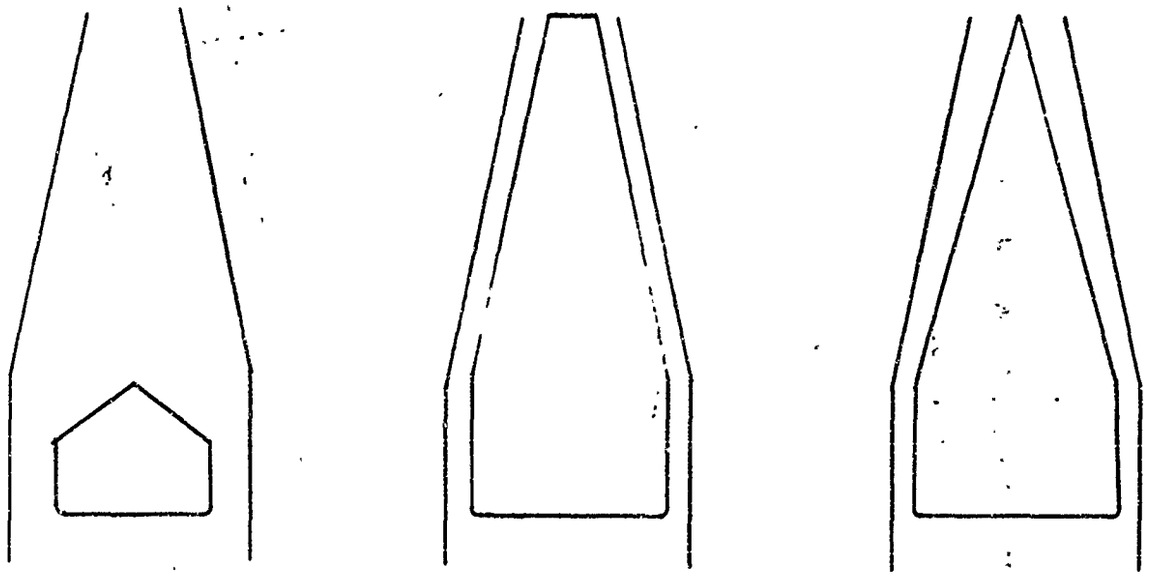


(A) Deposit in Frustum

(B) Deposit in Plugged Frustum

Plug Technique for Frustum Deposition

Figure 50.



(a)

Simple Baffle

PG-9031

(b)

Constant Gap
Baffle/Plug
PG-9032

(c)

Constant Area
Baffle/Plug
PG-9033

Figure 51
FRUSTUM PLUG AND BAFFLE DESIGNS

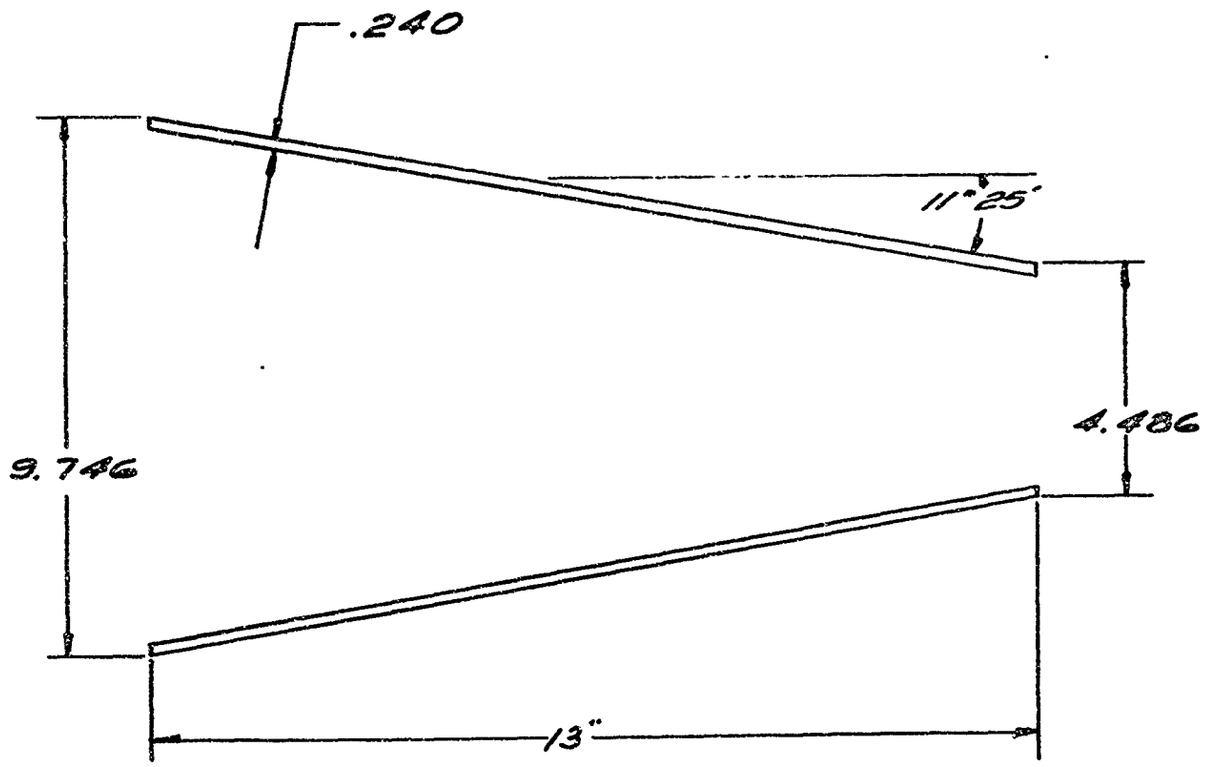


Figure 52

FRUSTUM MANDREL FOR TASK 3.2.2.1

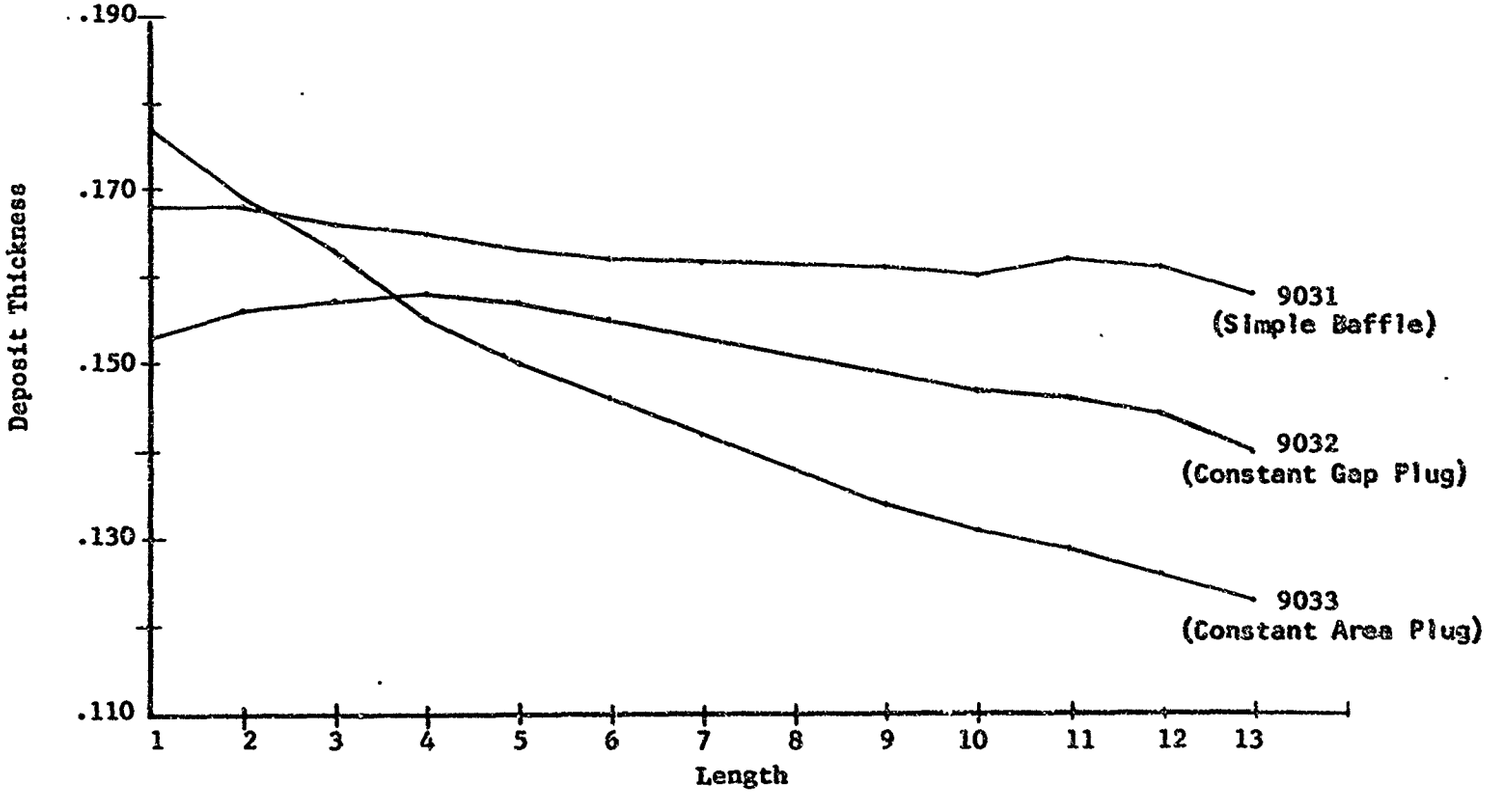
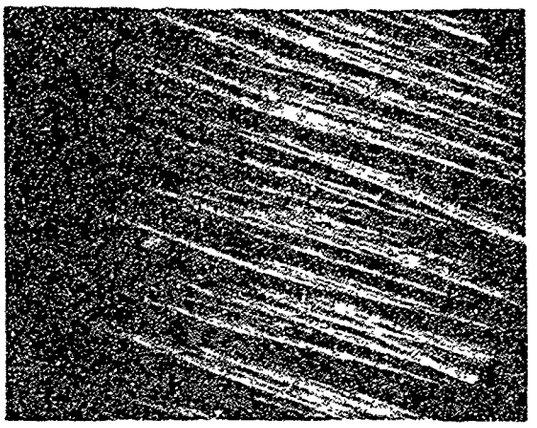


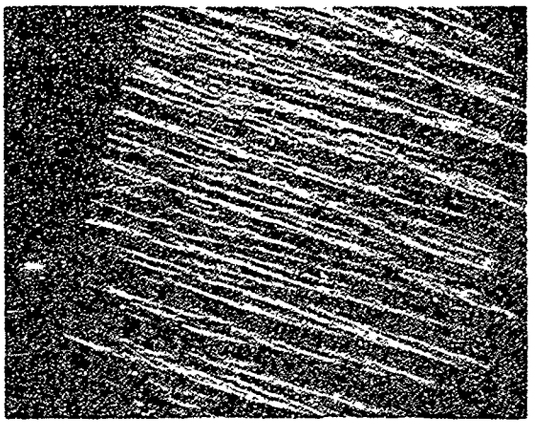
Figure 53

THICKNESS PROFILES

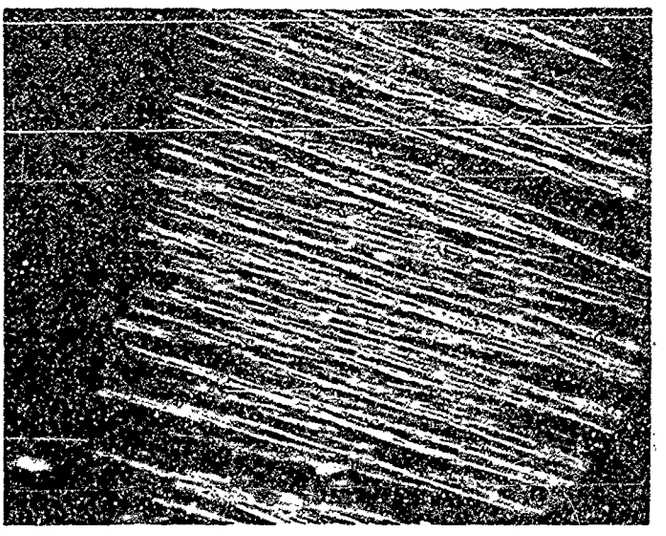
FOR TASK 3.2.2.1



Run 9031



Run 9032



Run 9033

Figure 54

MICROSTRUCTURE FROM EXHAUST END OF FRUSTUMS
DEPOSITED IN TASK 3.2.2.1 30X

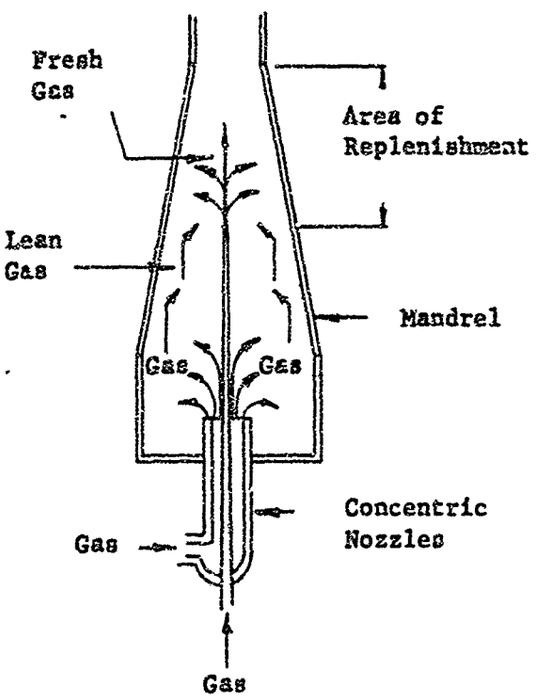


Figure 55

SCHEMATIC REPRESENTATION OF A POSSIBLE GAS-REPLENISHMENT TECHNIQUE FOR ACHIEVING UNIFORM WALL THICKNESSES IN LONG FRUSTUMS

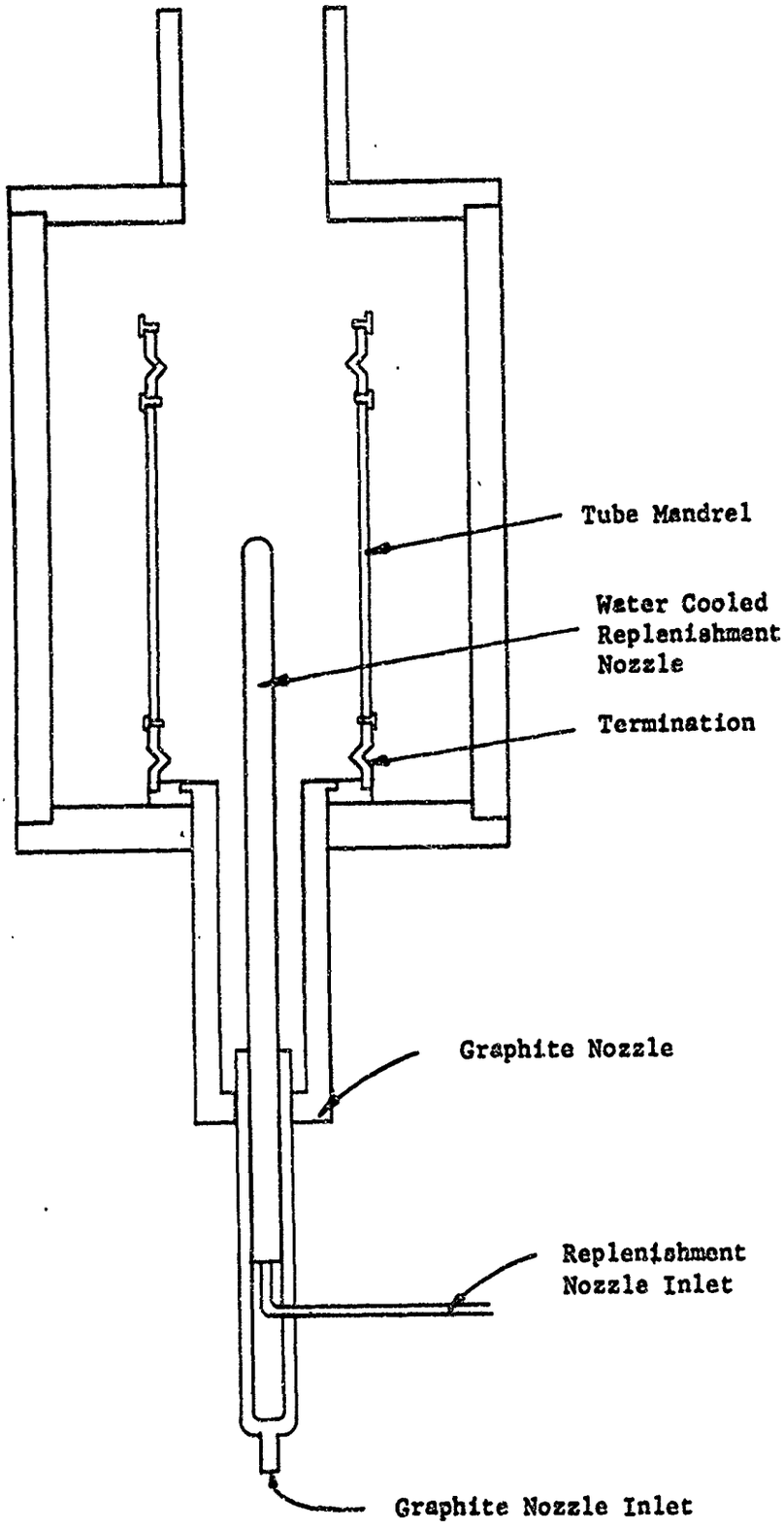


Figure 56

DEPOSITION ASSEMBLY FOR REPLENISHMENT EXPERIMENT

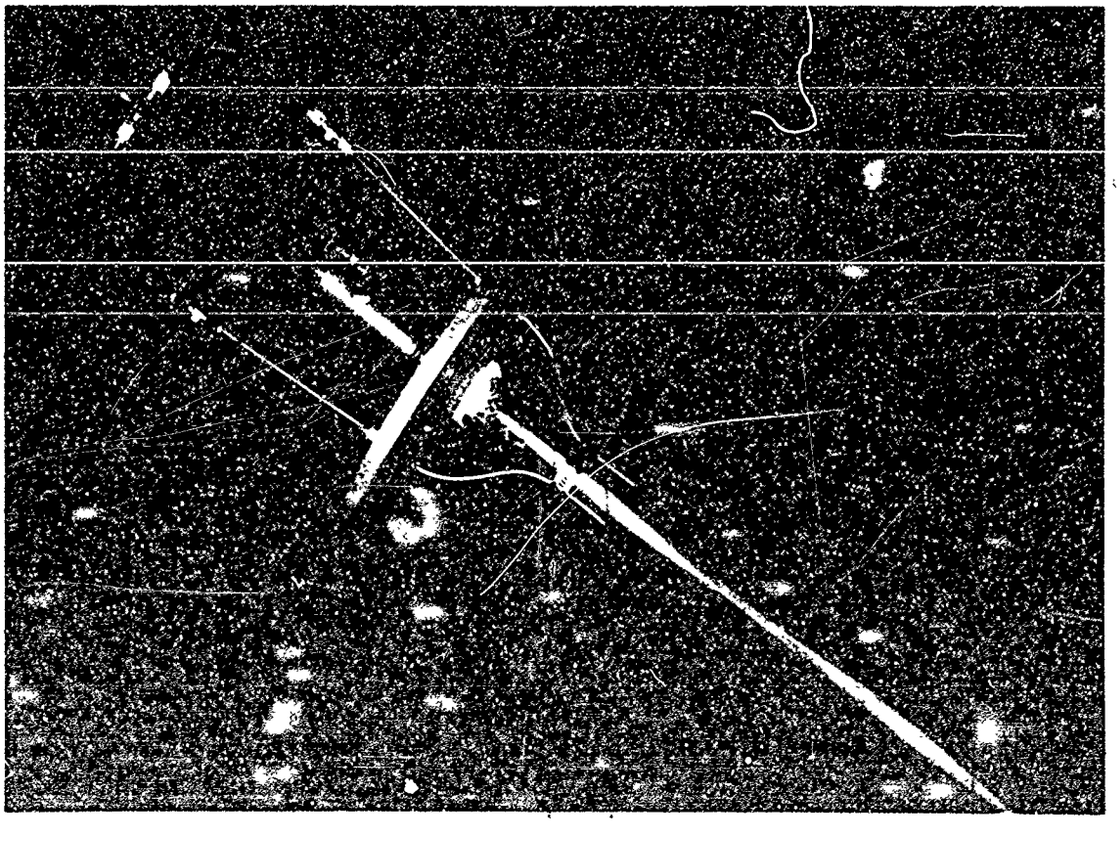
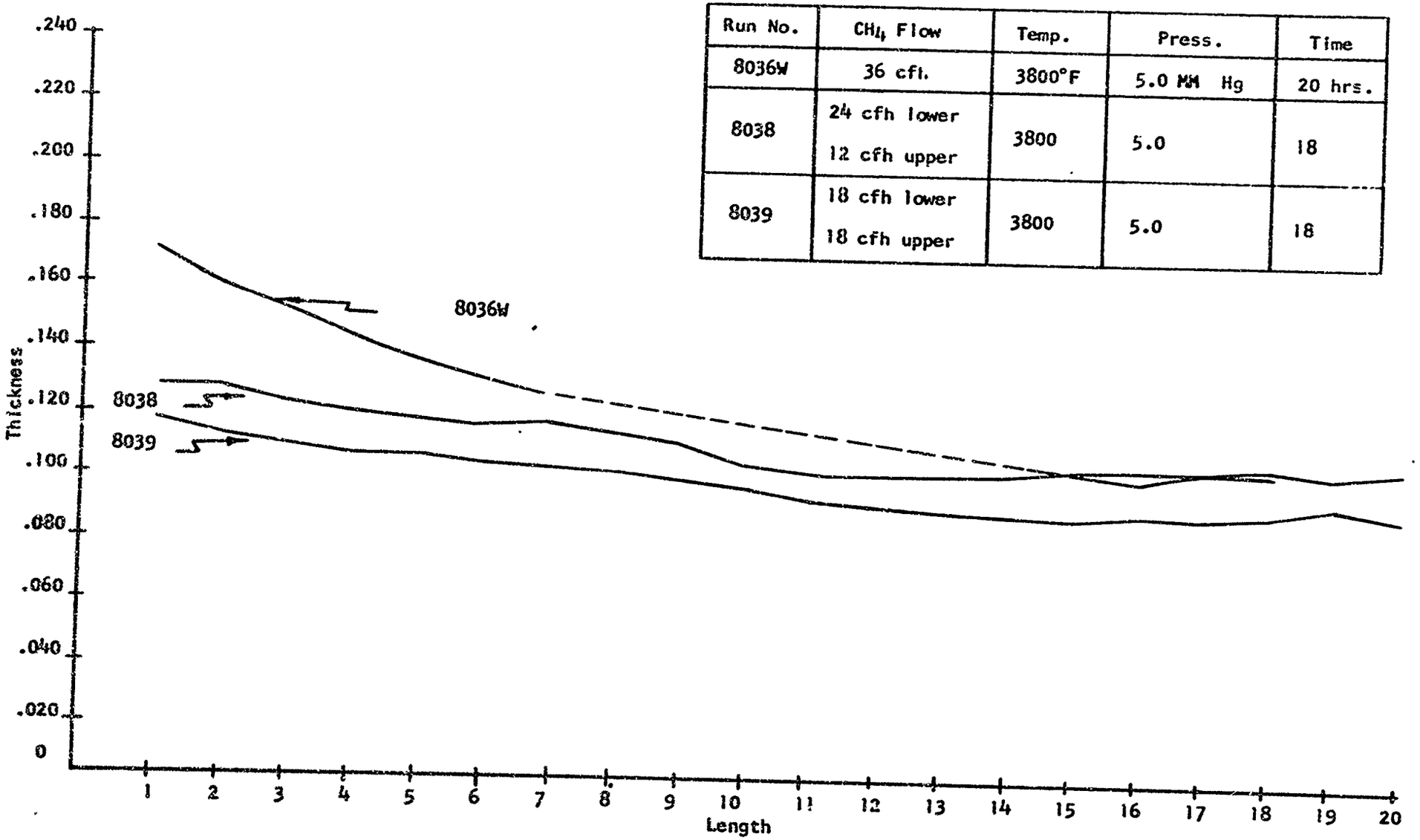


Figure 57

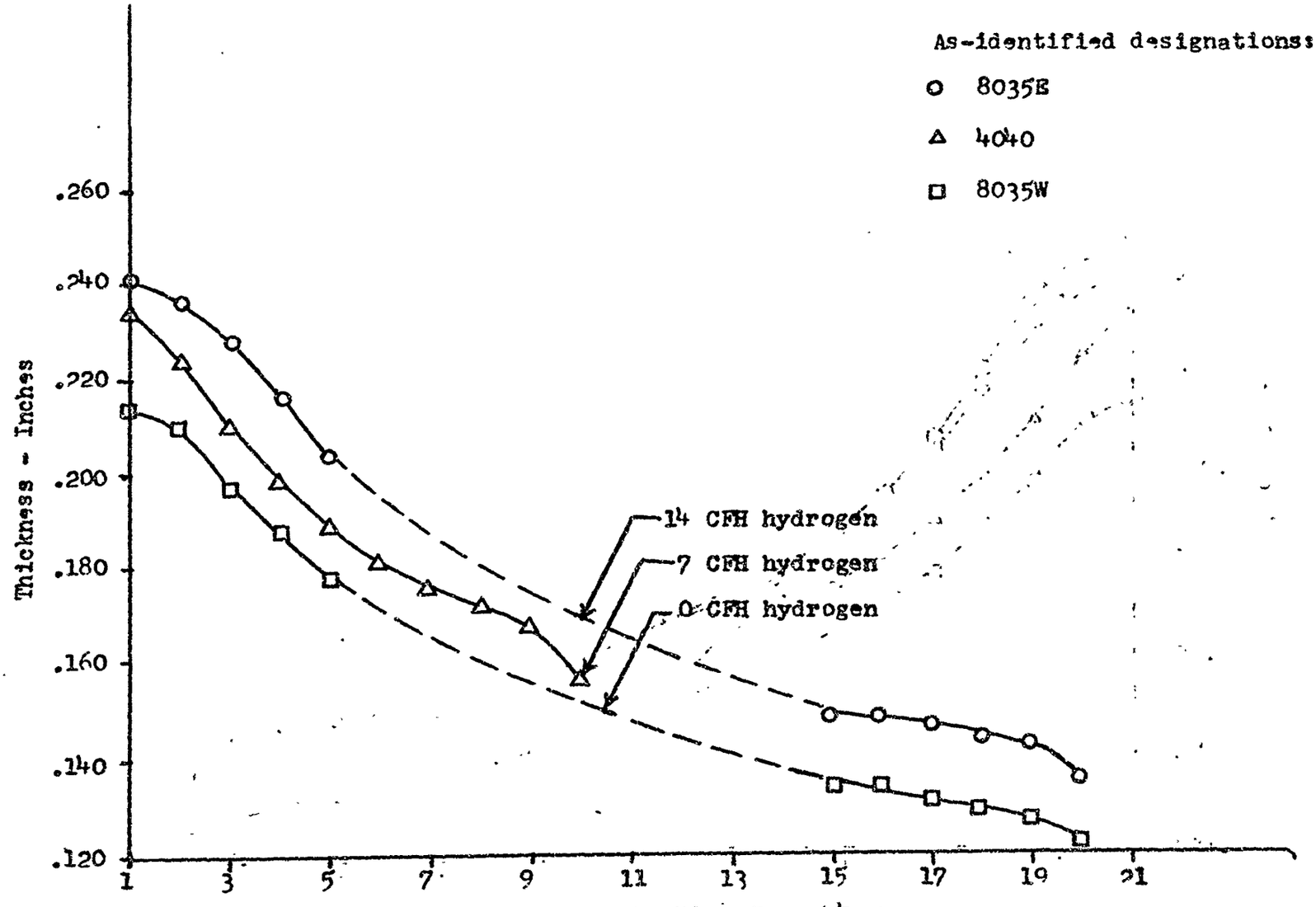
REPLENISHMENT NOZZLE ASSEMBLY
INCLUDING GRAPHITE NOZZLE GAS FEED

Run No.	CH_4 Flow	Temp.	Press.	Time
8036W	36 cfh.	3800°F	5.0 MM Hg	20 hrs.
8038	24 cfh lower 12 cfh upper	3800	5.0	18
8039	18 cfh lower 18 cfh upper	3800	5.0	18



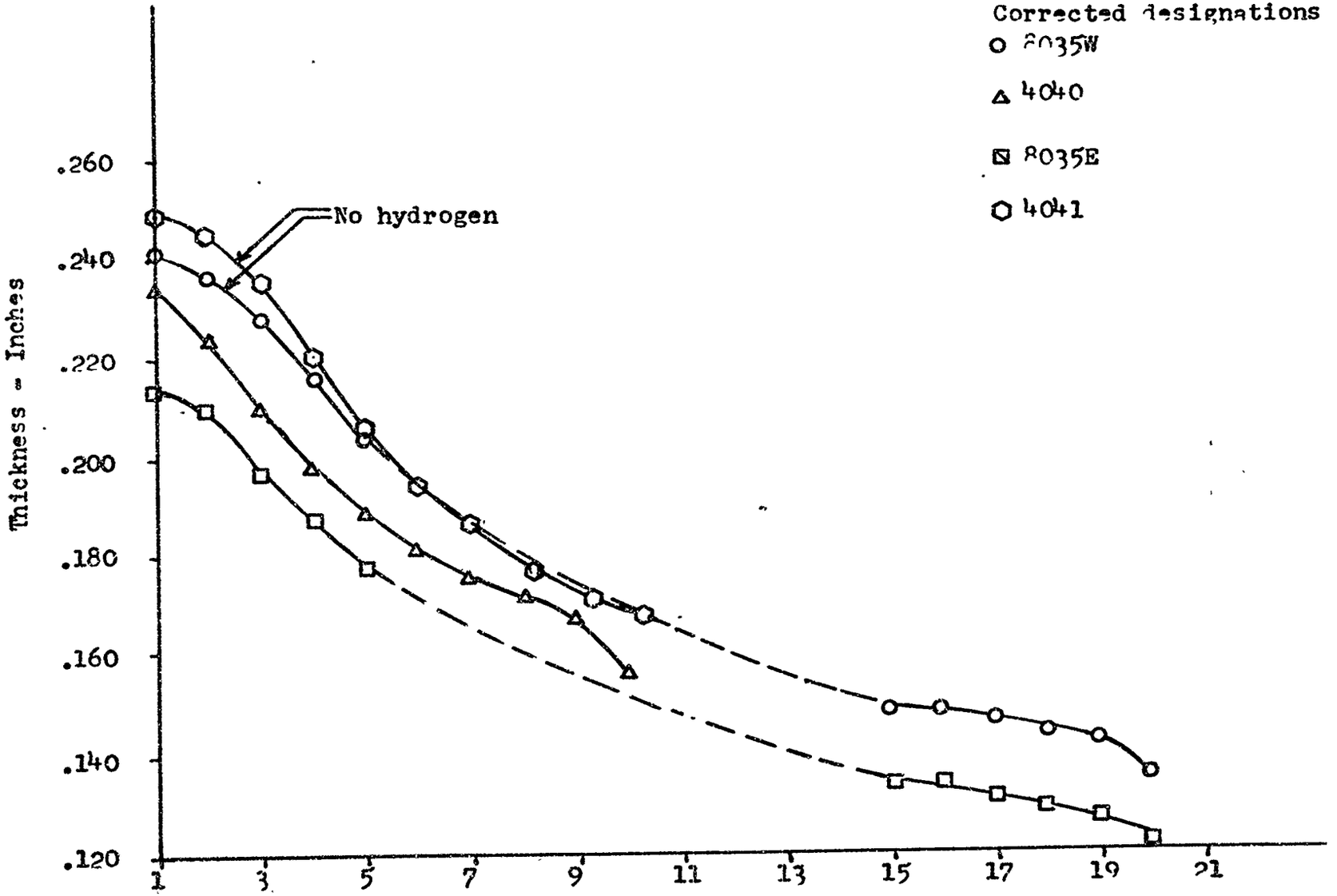
Task 3.2.2.2 Deposition Thickness Profiles

Figure 58



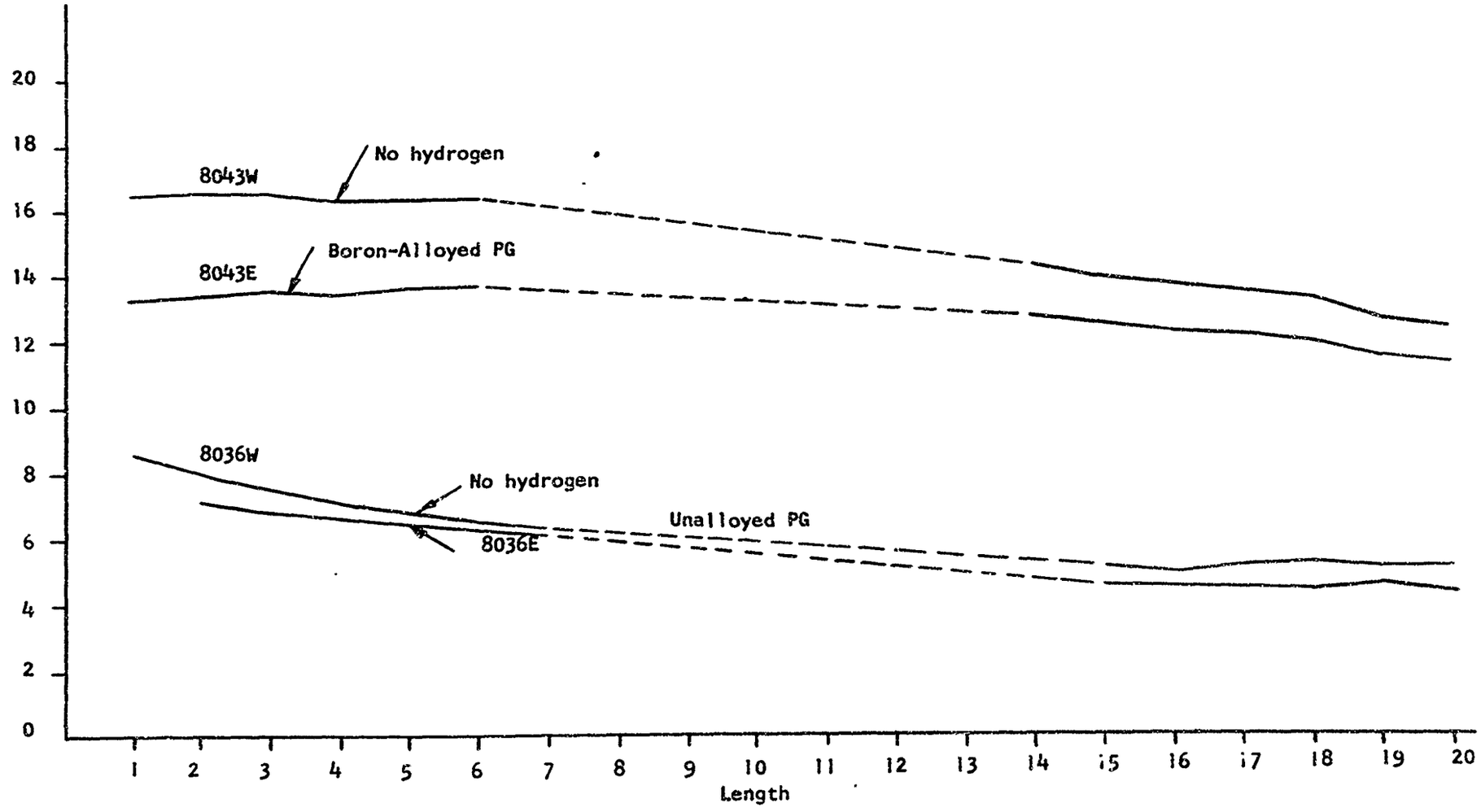
Task 3.2.2.3 Initial Deposition Thickness Profiles

Figure 59



Task 3.2.2.3 Deposition Thickness Profiles

Figure 60



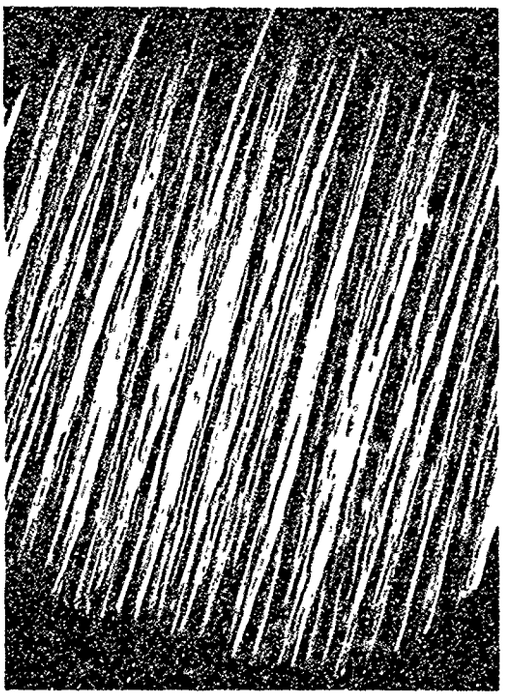
Effects of Hydrogen Dilution In Boron-alloyed and Unalloyed PG Deposition

Figure 61



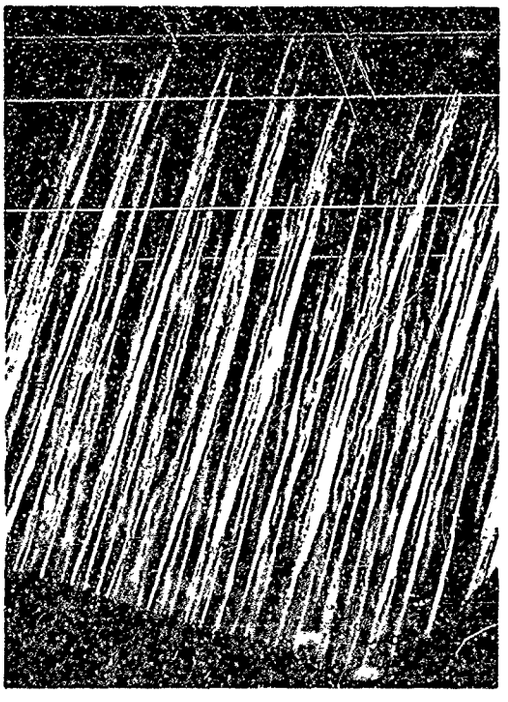
8043W Near Center

DENSITY--2.213



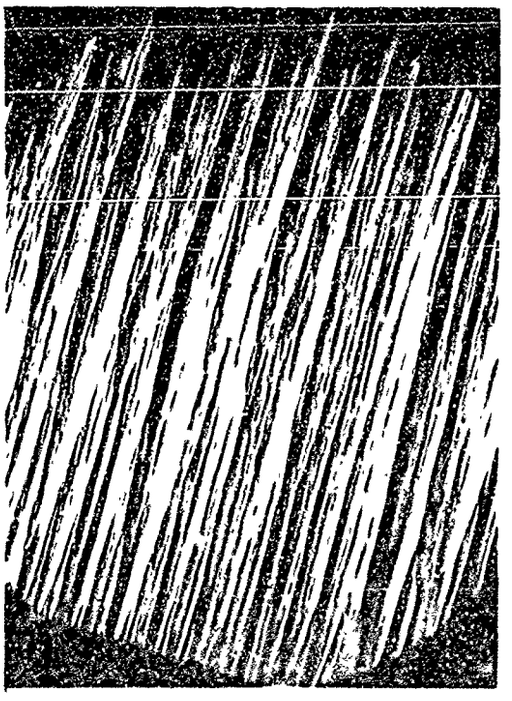
8043W Near Inlet 30X

DENSITY--2.218



8043E Near Center 30X

DENSITY--2.224

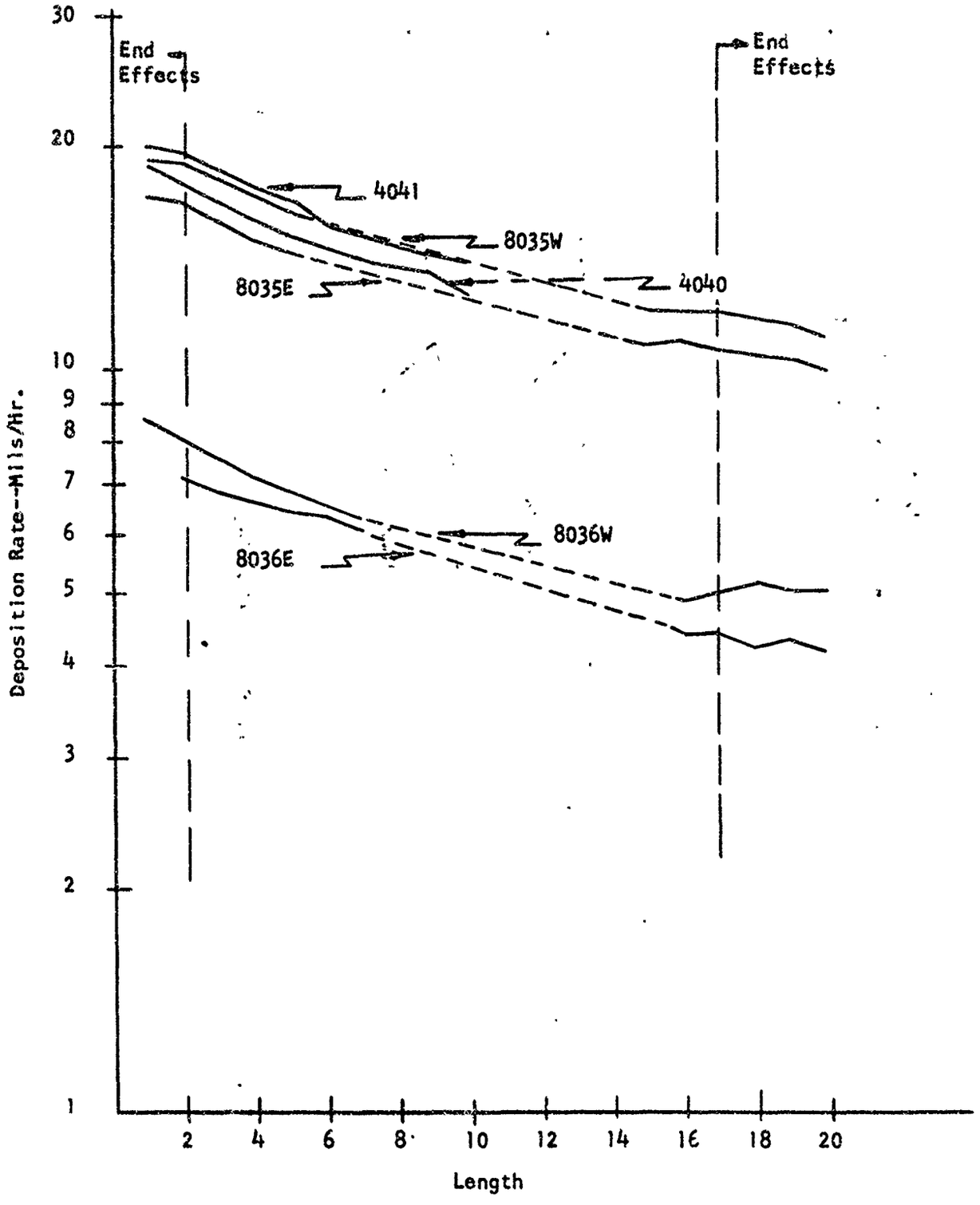


8043E Near Inlet 30X

DENSITY--2.229

Figure 62

MICROSTRUCTURE AND DENSITY--Run 8043



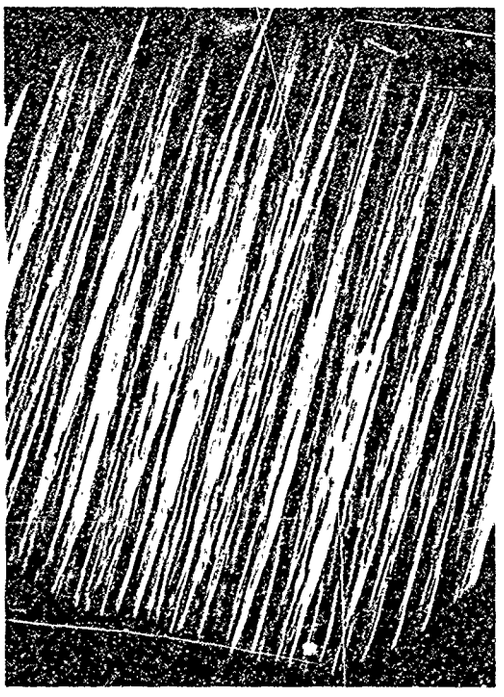
Task 3.2.2.3 Comparison of Characteristic Slopes

Figure 63



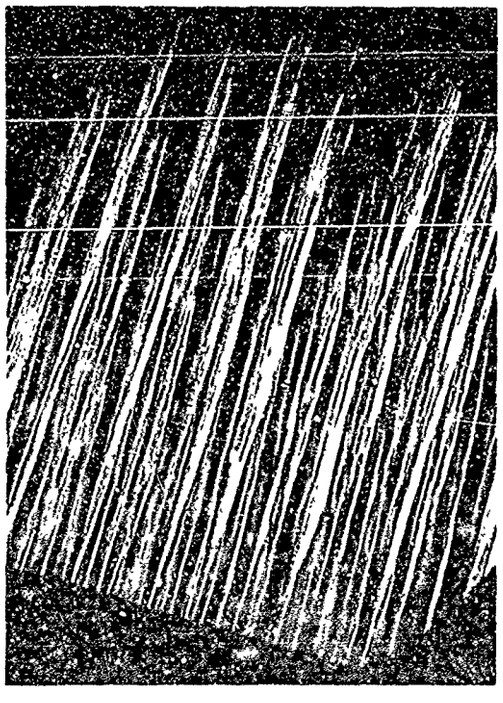
8043W Near Center

DENSITY--2.213



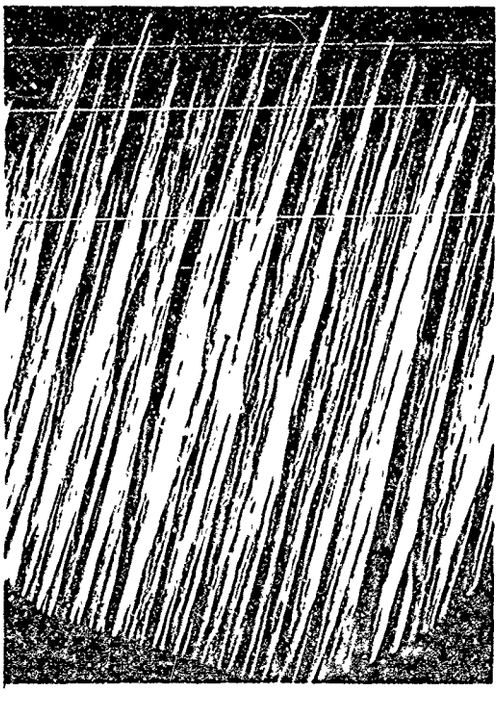
8043W Near Inlet 30X

DENSITY--2.218



8043E Near Center 30X

DENSITY--2.224

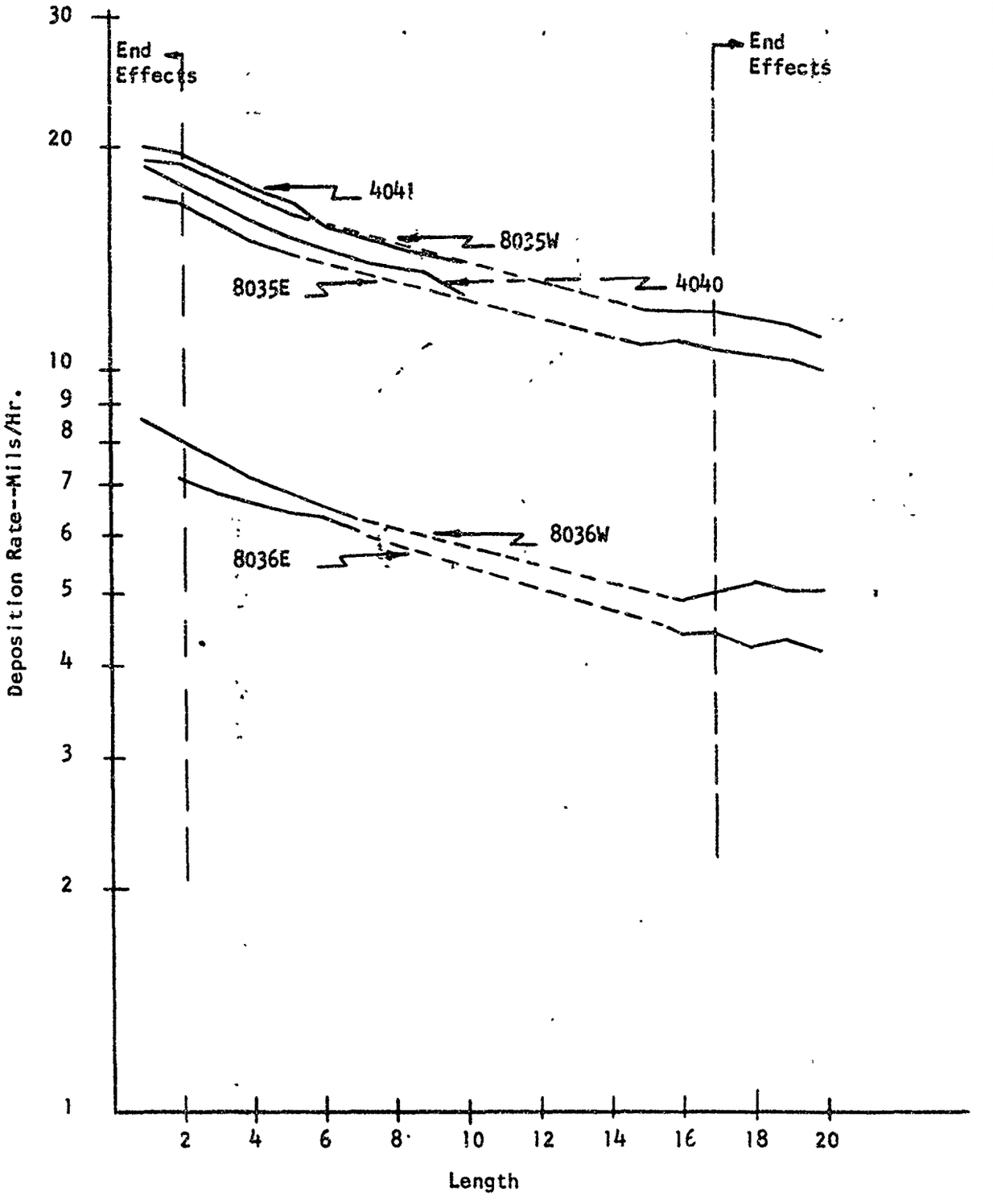


8043E Near Inlet 30X

DENSITY--2.229

Figure 62

MICROSTRUCTURE AND DENSITY--Run 8043



Task 3.2.2.3 Comparison of Characteristic Slopes

Figure 63

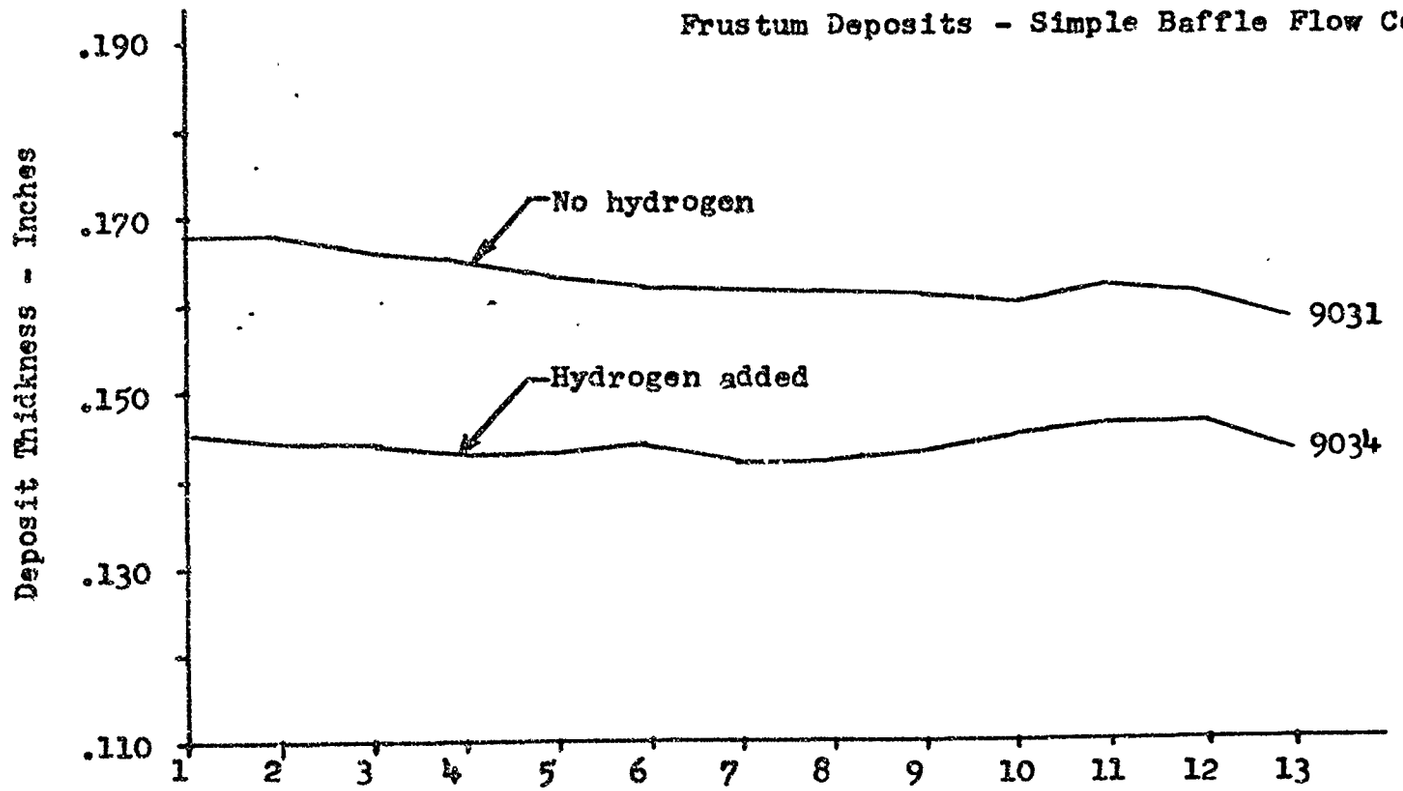
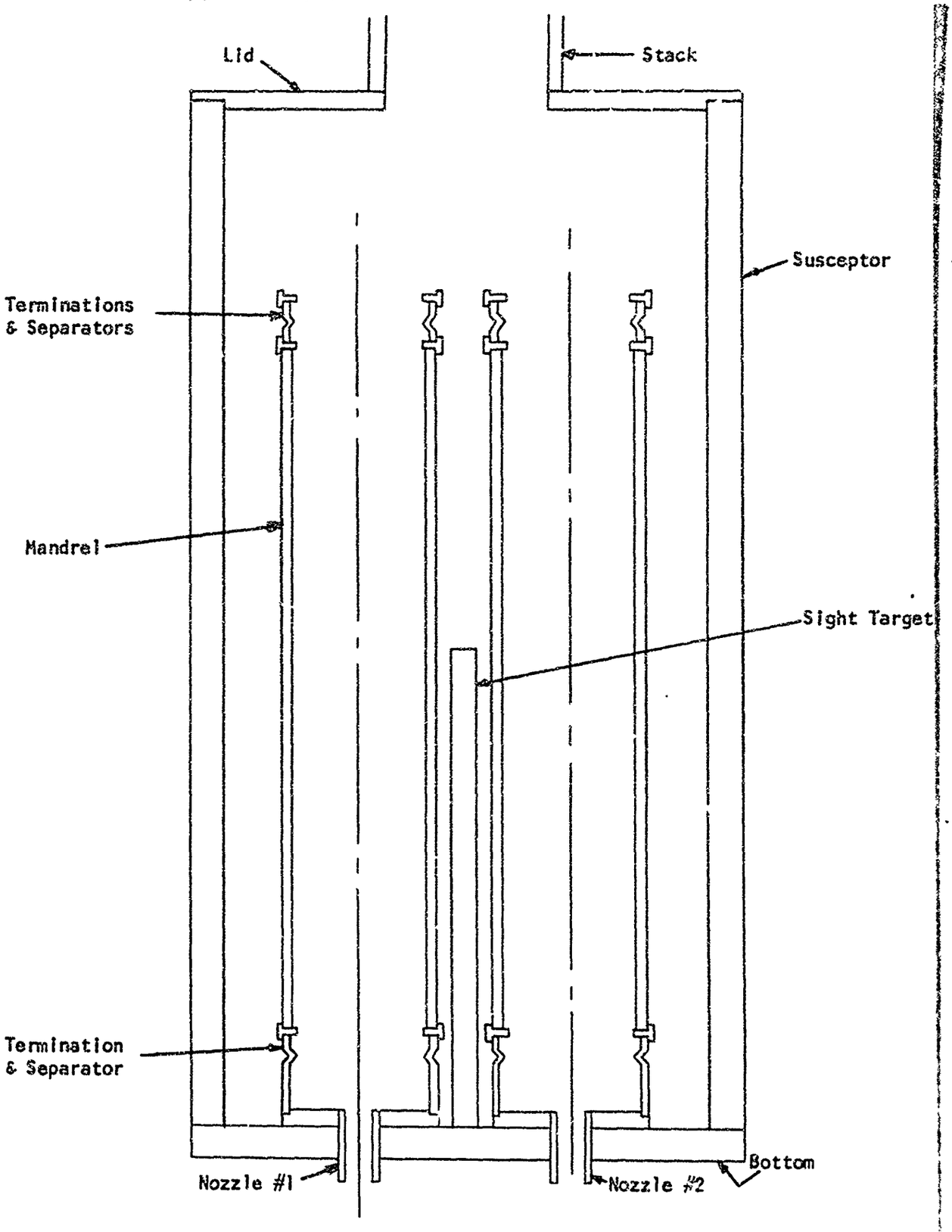
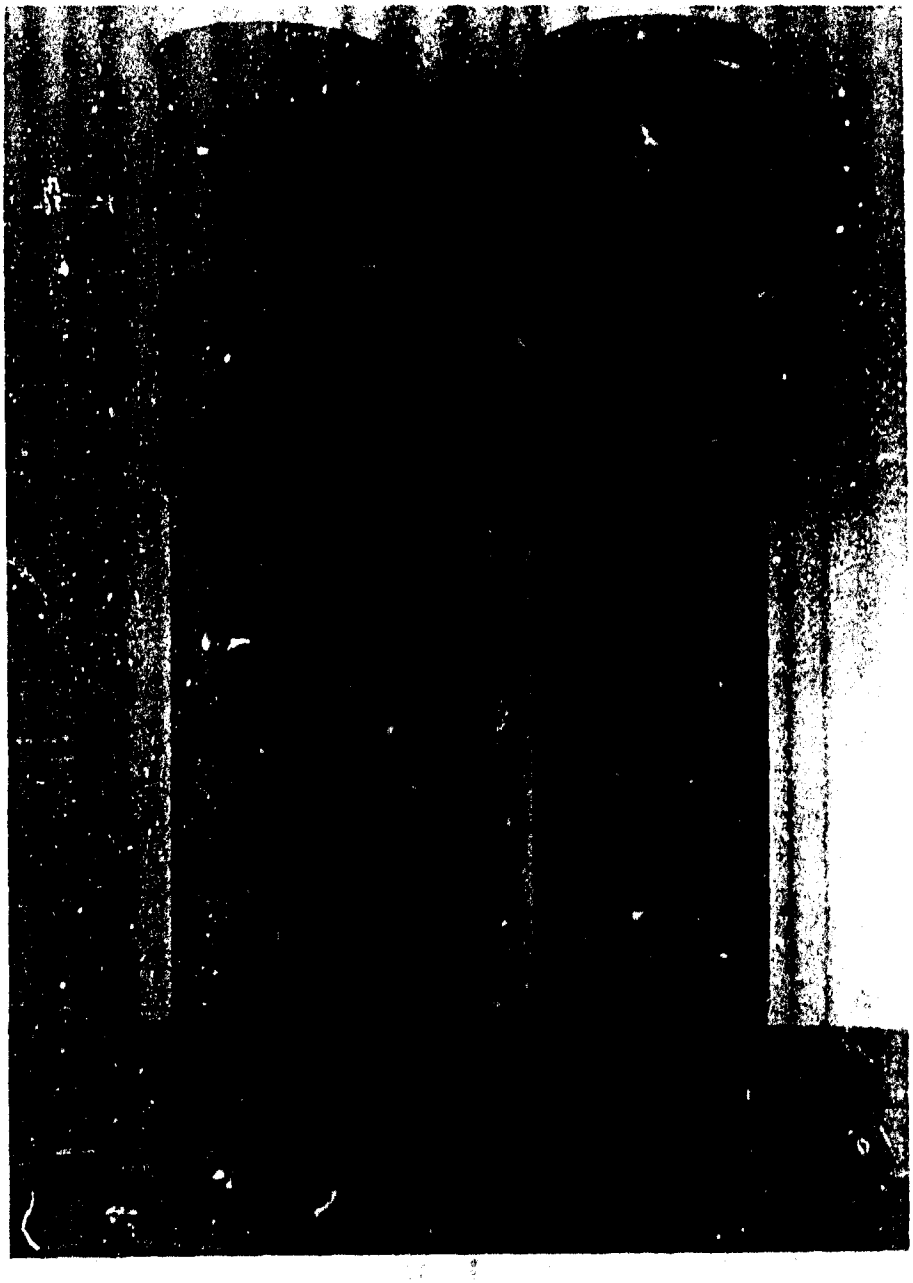

Frustum Deposits - Simple Baffle Flow Control
.190
.170
.150
.130
.110
Deposit Thickness - Inches
No hydrogen
9031
Hydrogen added
9034
1
2
3
4
5
6
7
8
9
10
11
12
13
Distance from Inlet - Inches

Figure 64



Deposition Assembly for Task 3.4.6

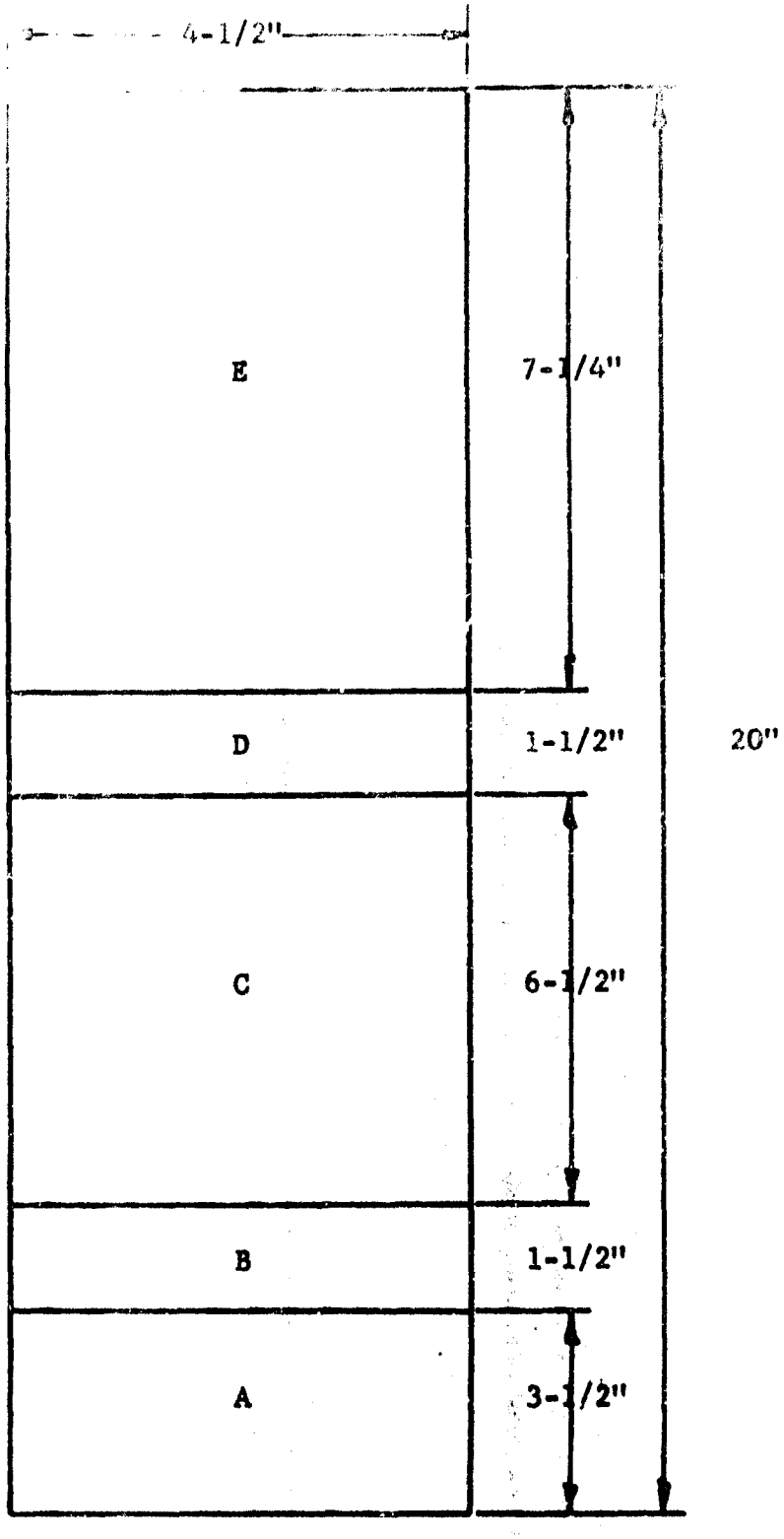
Figure 65.



TASK 3.4.6

Typical Cylinders Prior to Mandrel Removal

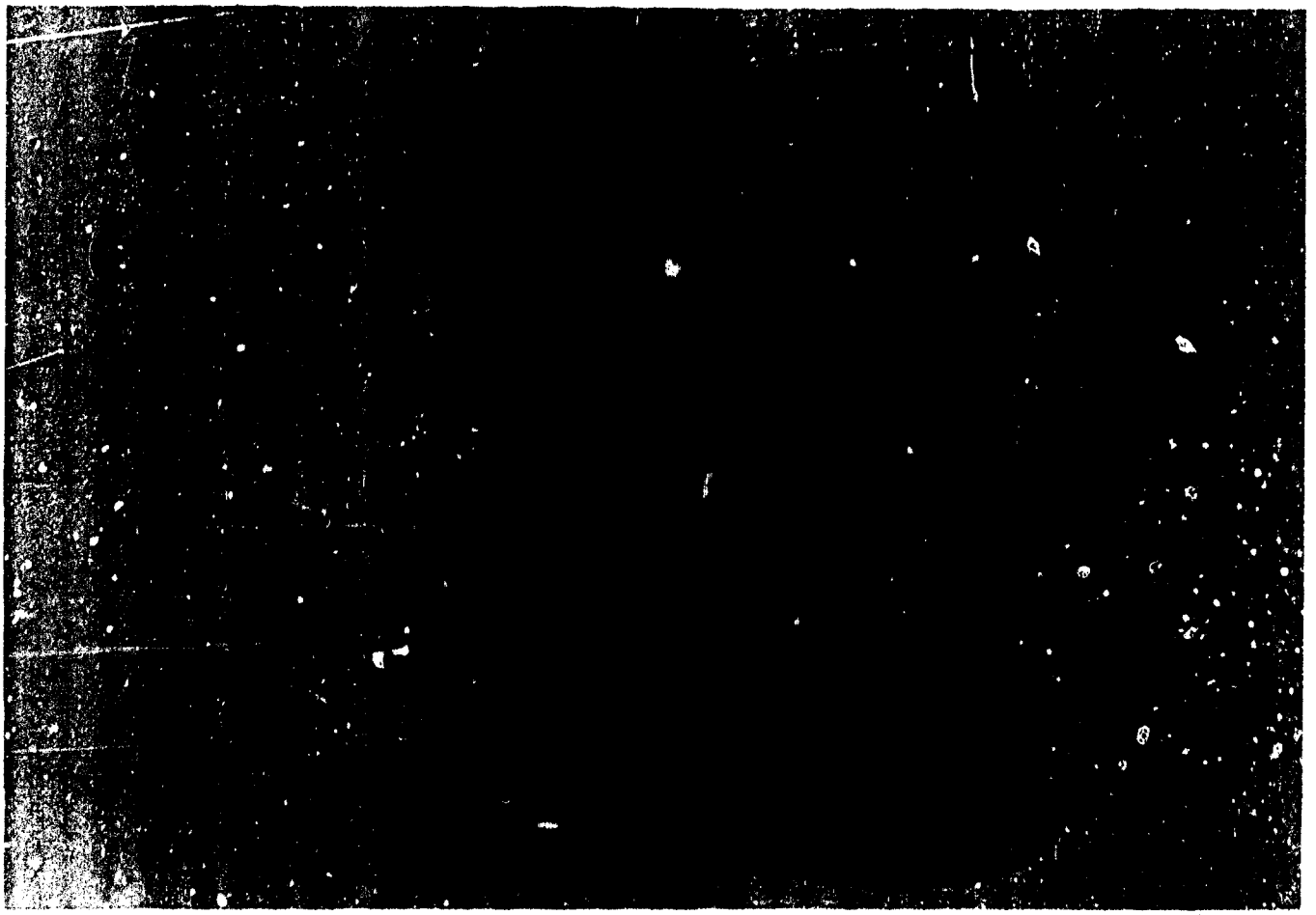
Figure 66.



TASK 3.4.6

Sampling Plan

Figure 67.



TASK 3.4.6

Typical Deposit, Cut for Sampling

Figure 68.

Deposition Profiles for Cylinders

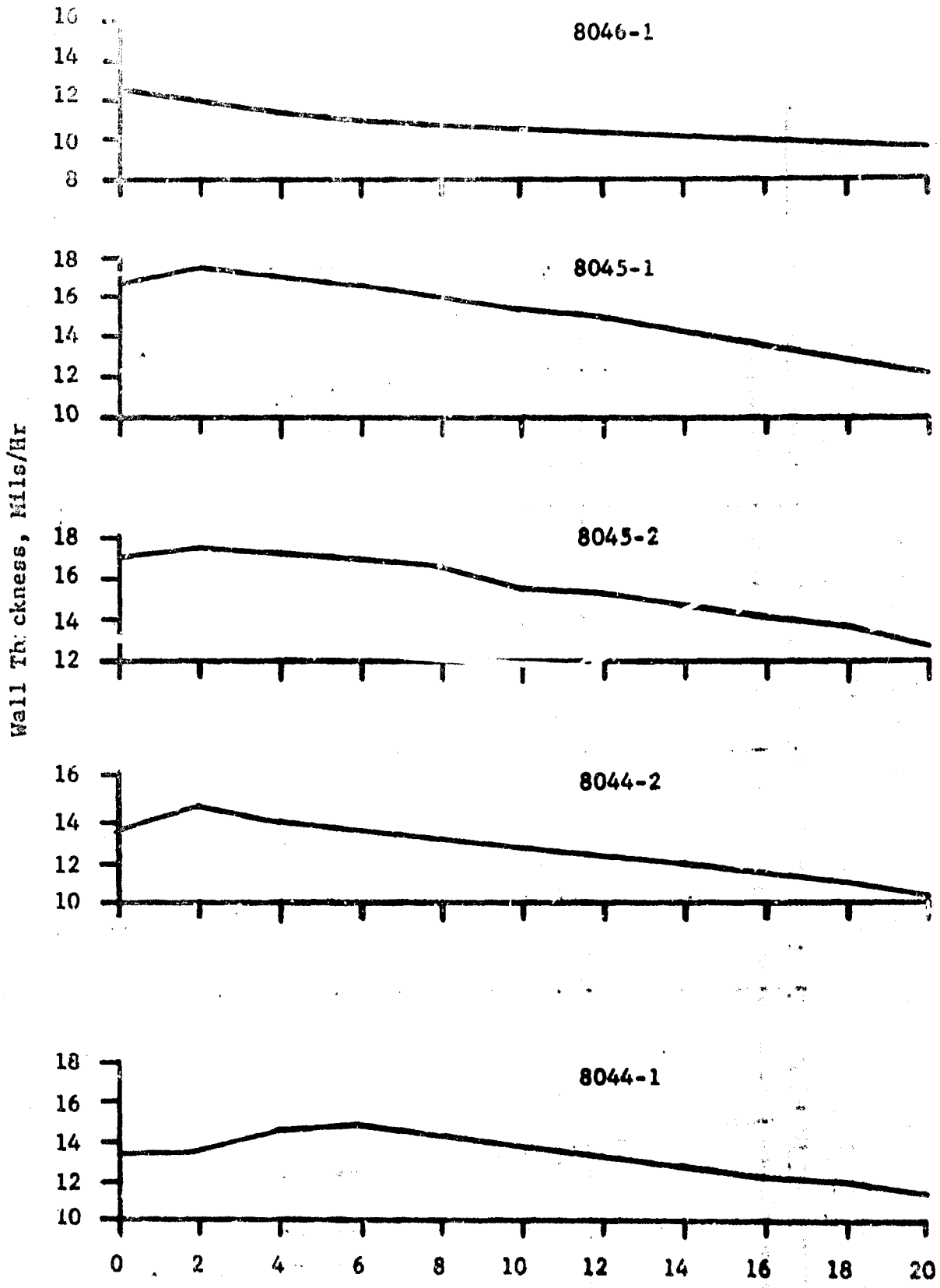


Figure 69.

TASK 3.4.6

Deposition Profile for Cylinders

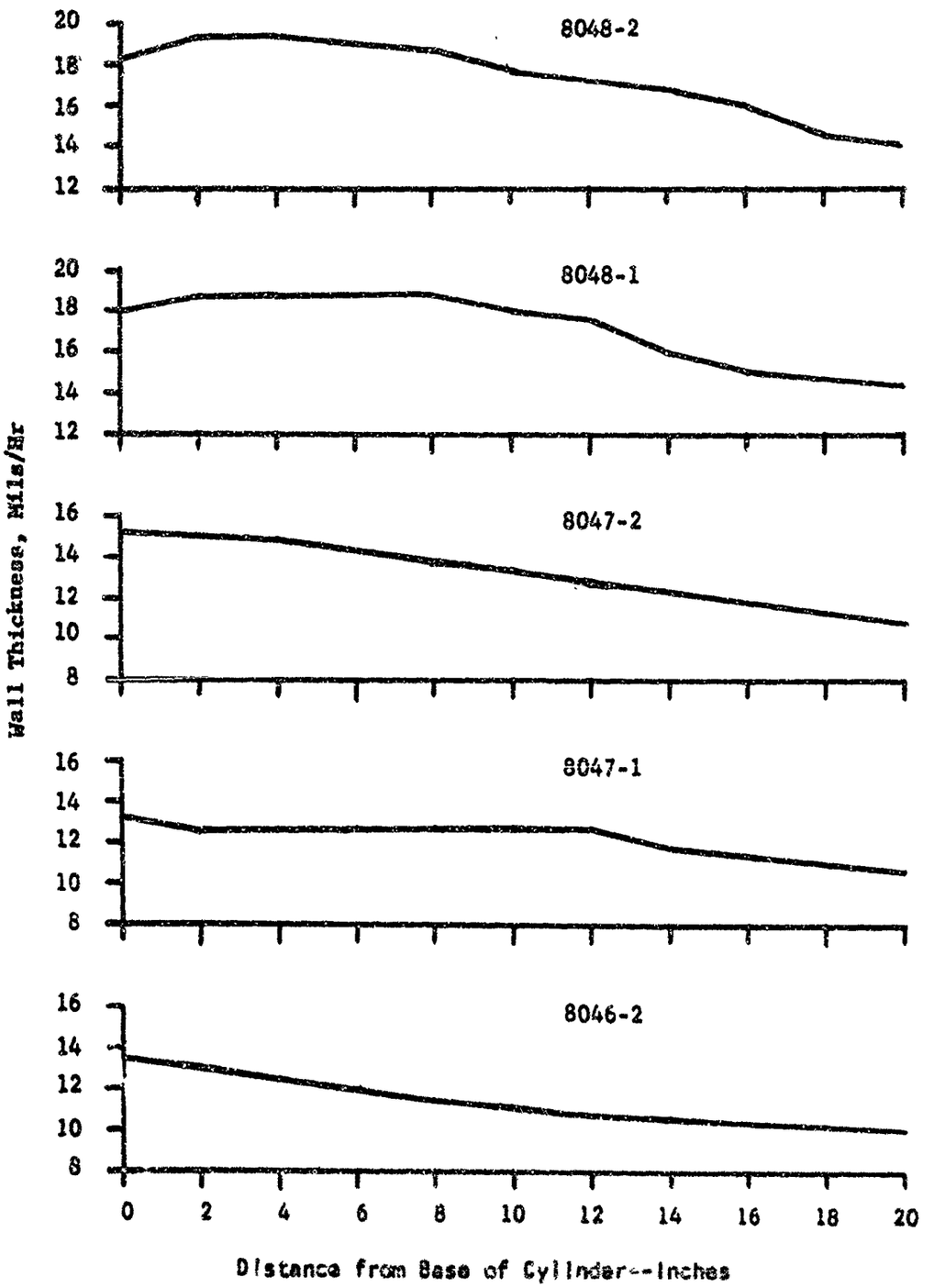


Figure 70.

TASK 3.4.6

Deposition Profile for Cylinders

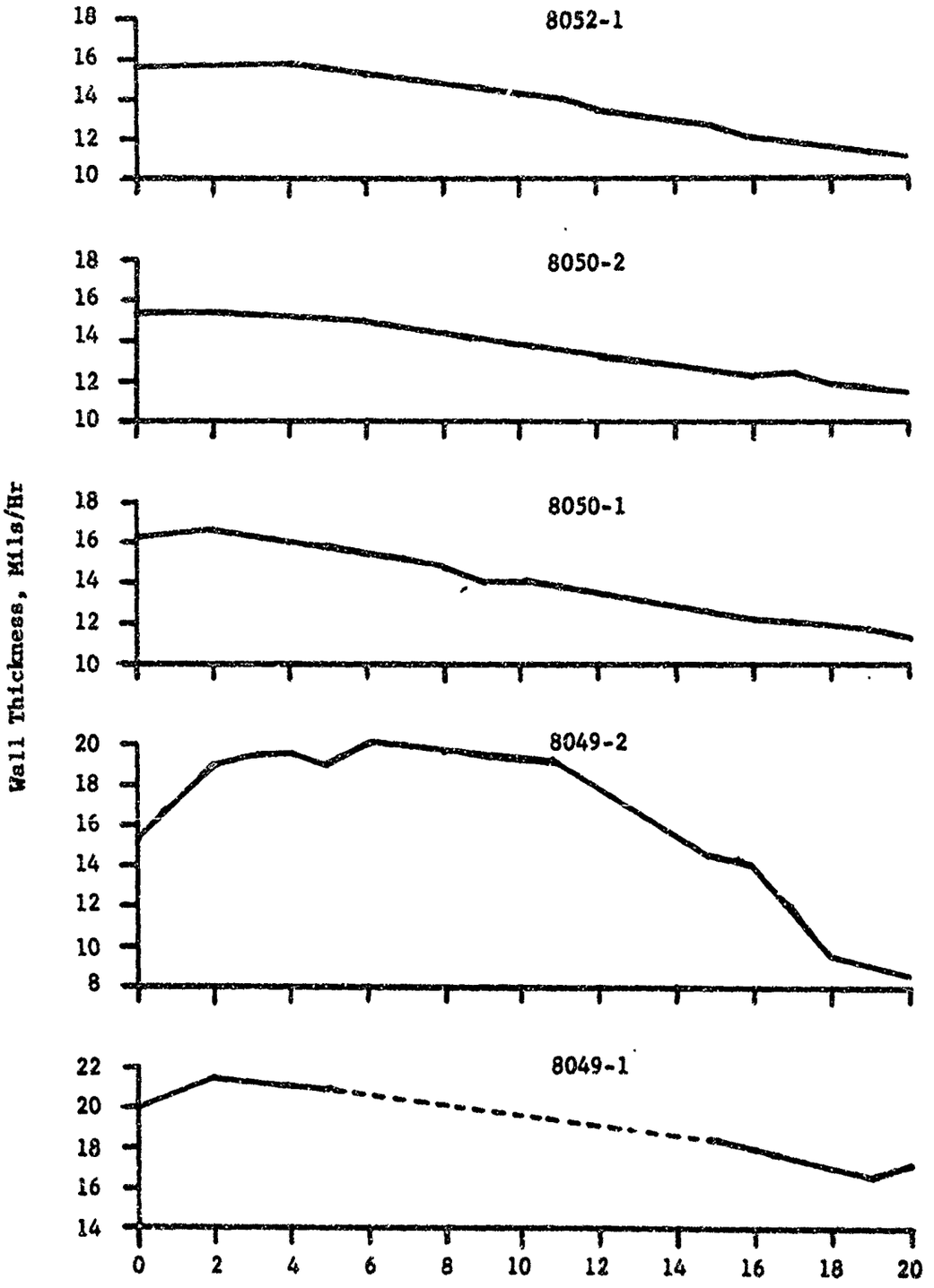


Figure 71.

TASK 3.4.6

Deposition Profile for Cylinders

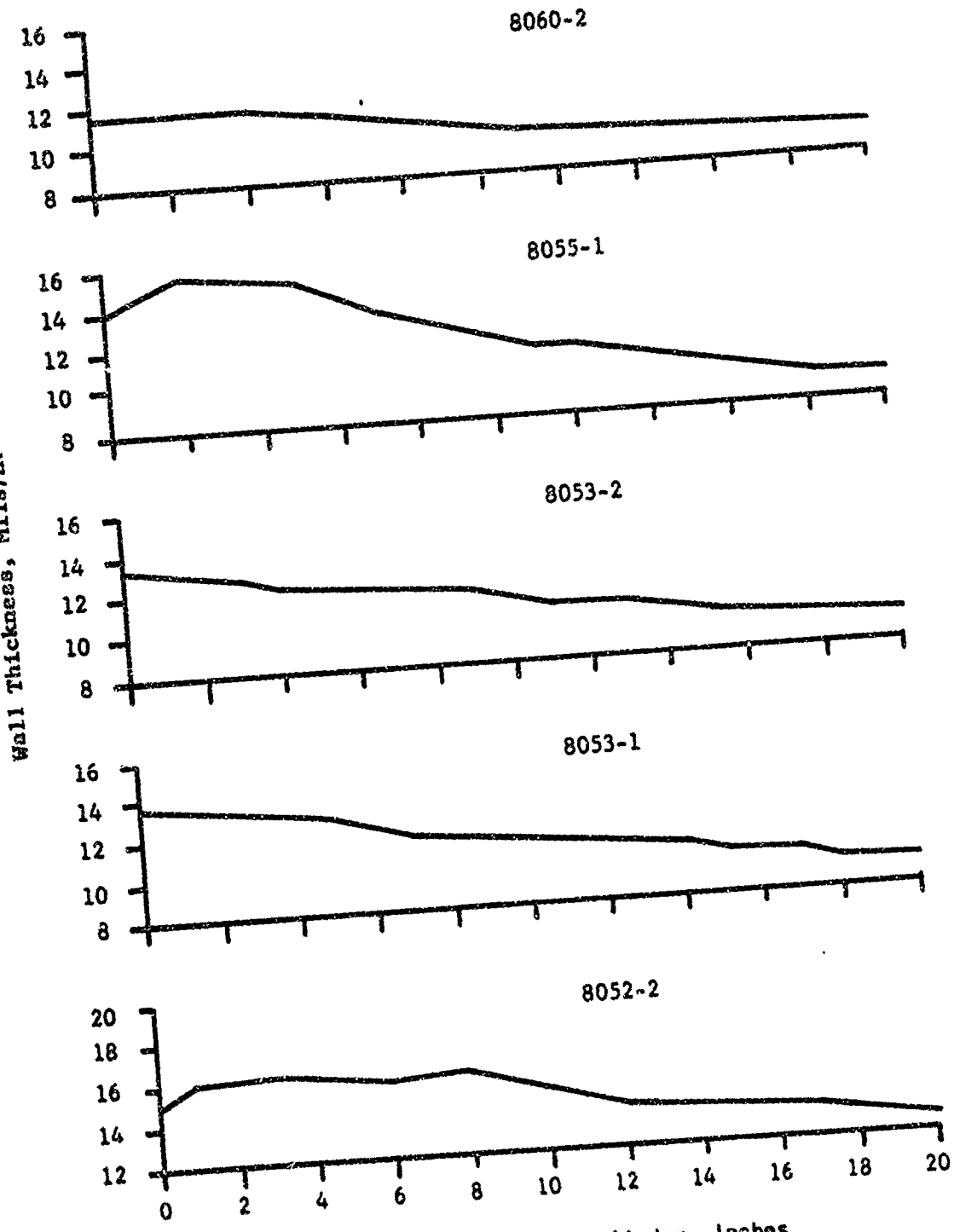


Figure 72.

TASK 3.4.6

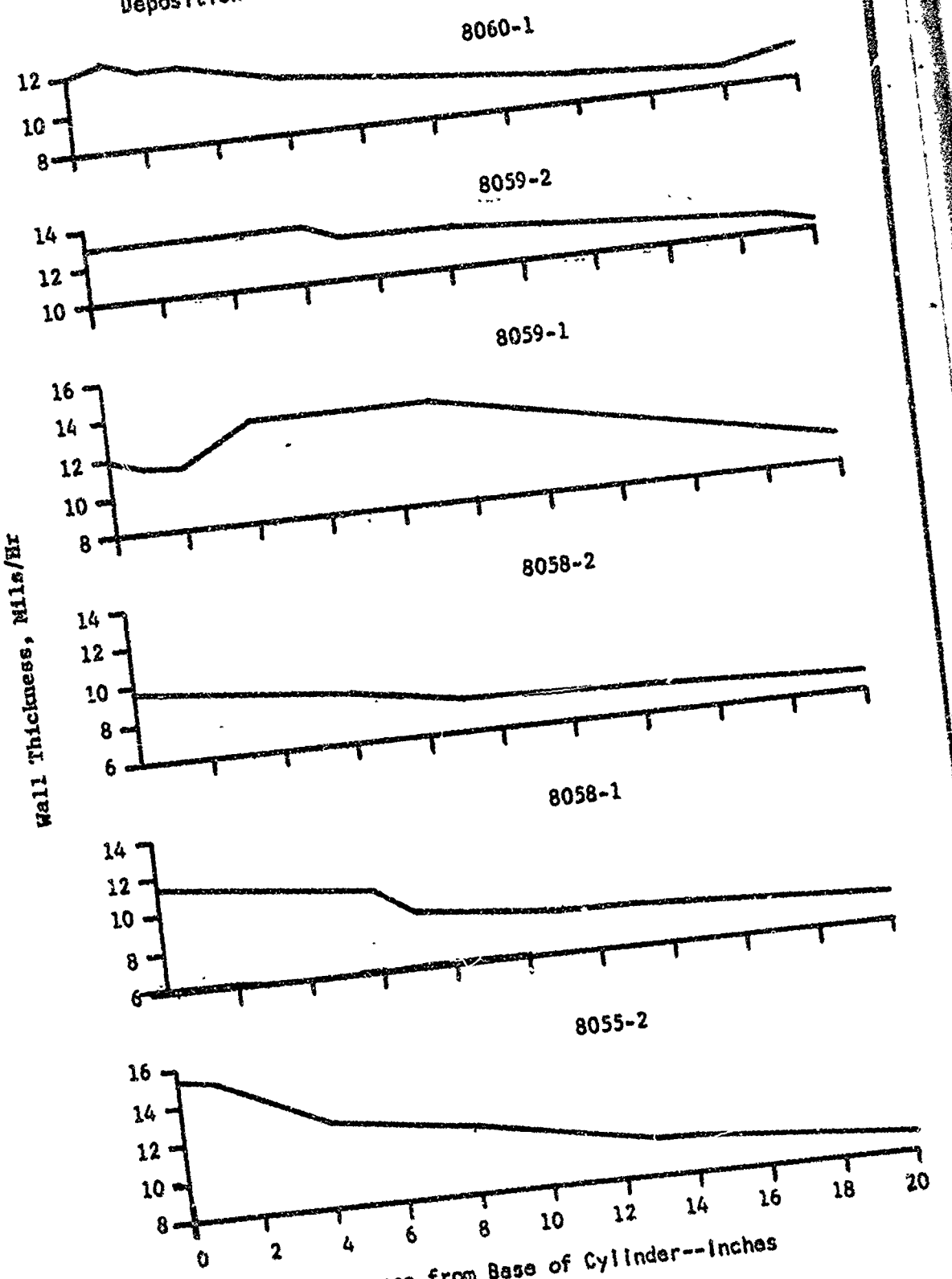


Figure 73.

TASK 3.4.6

Deposition Profile for Cylinders

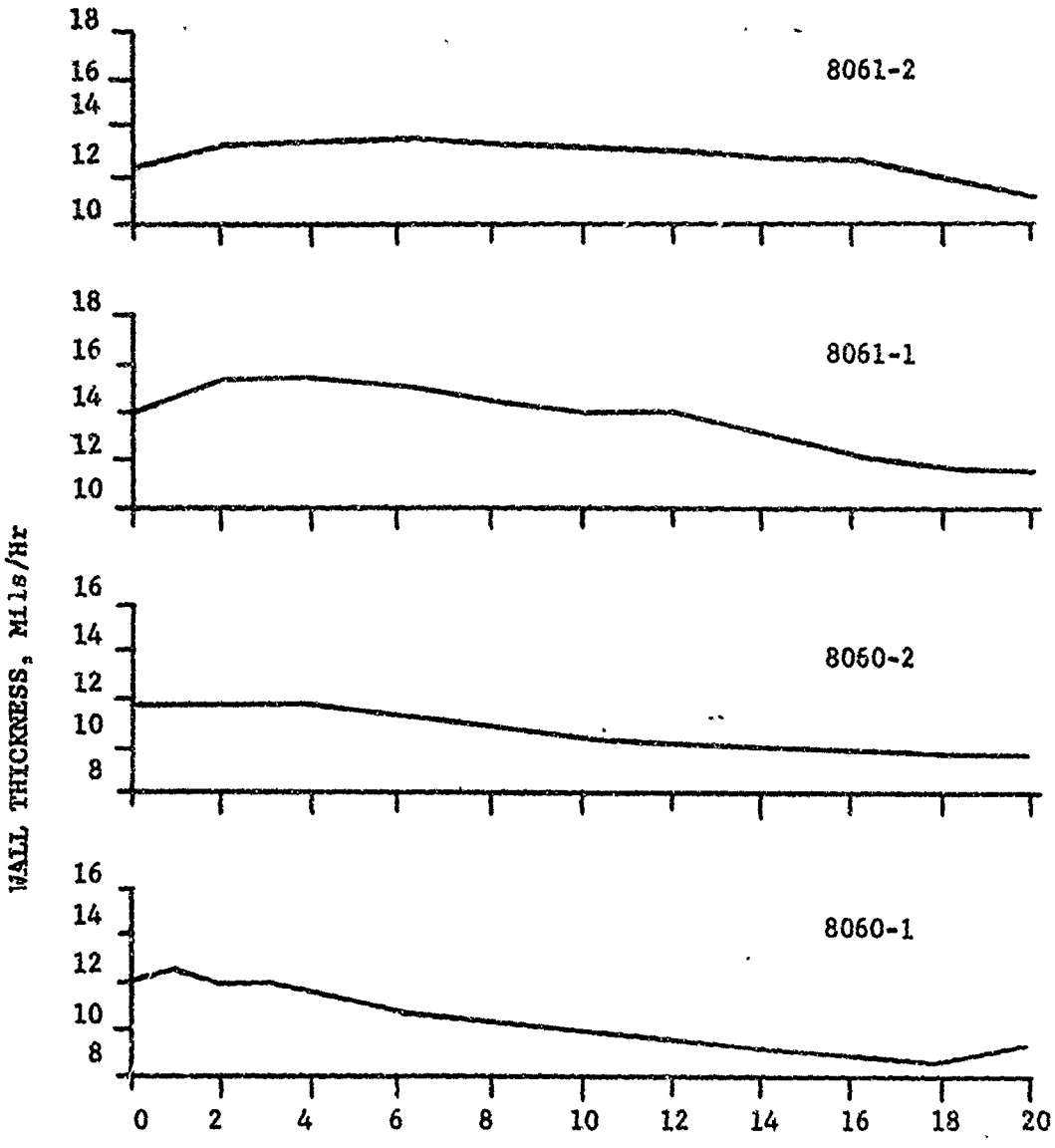


Figure 74

TASK 3.4.6

Deposition Profile for Cylinders

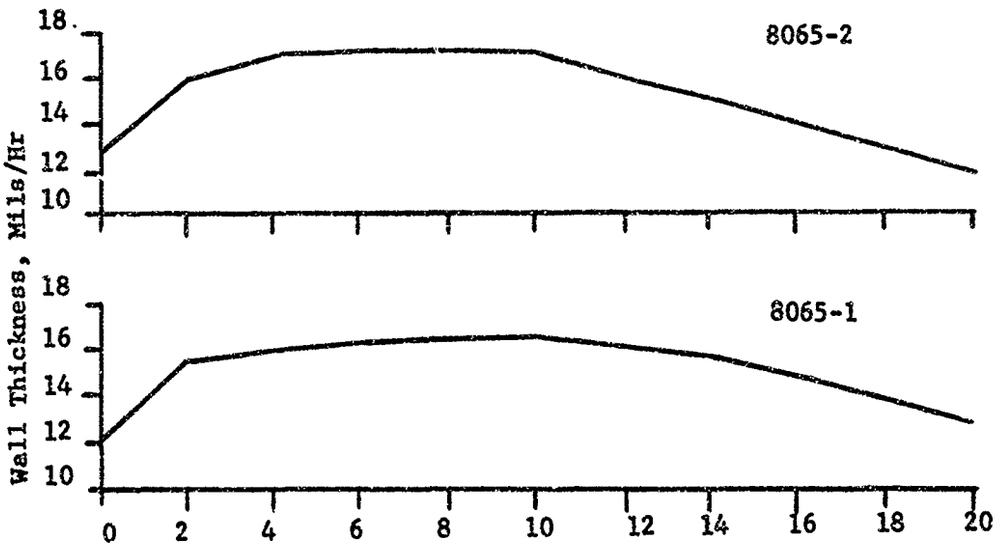
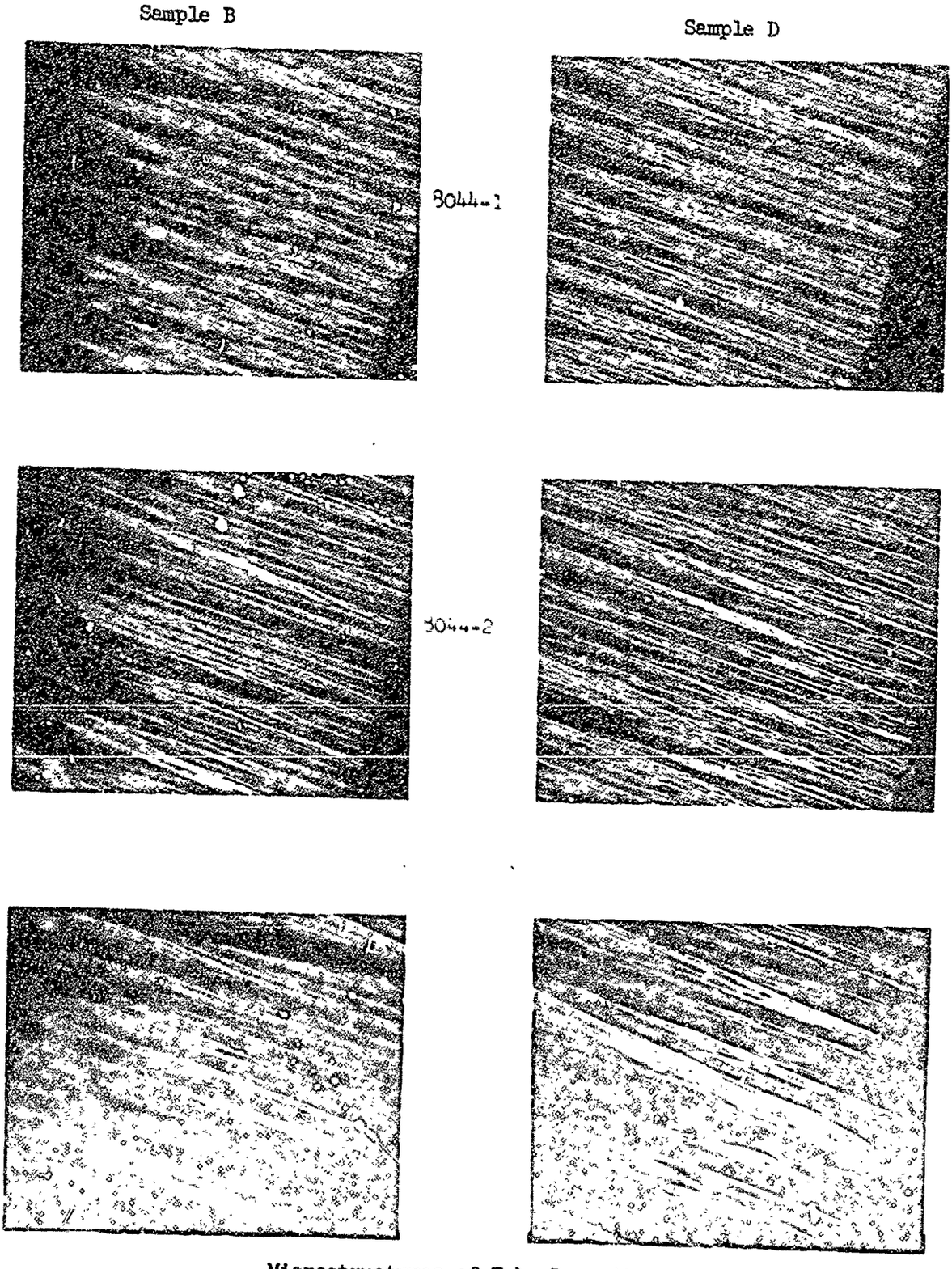


Figure 75

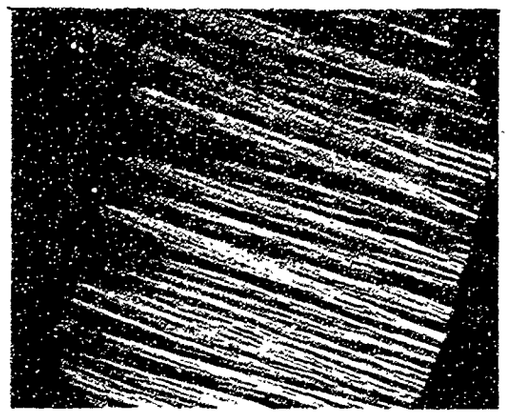


Microstructures of Tube Deposits
Task 3.4.6 Orig. Mag: 50X

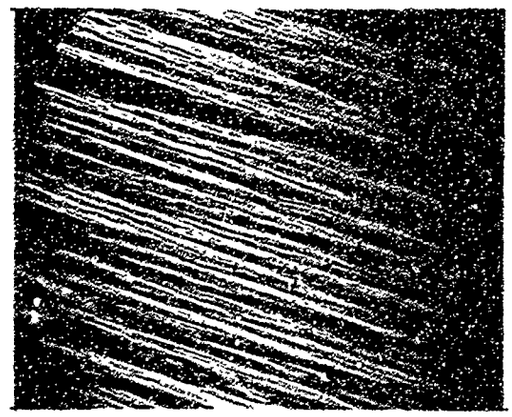
Figure 76

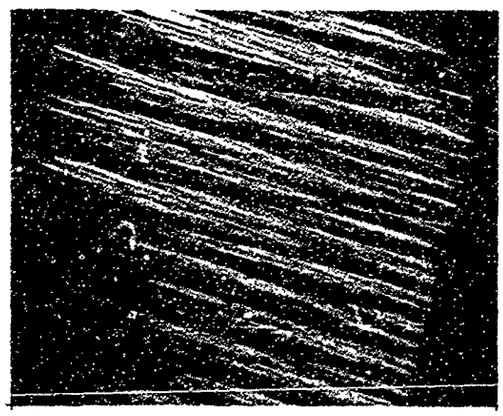
Sample B

Sample D

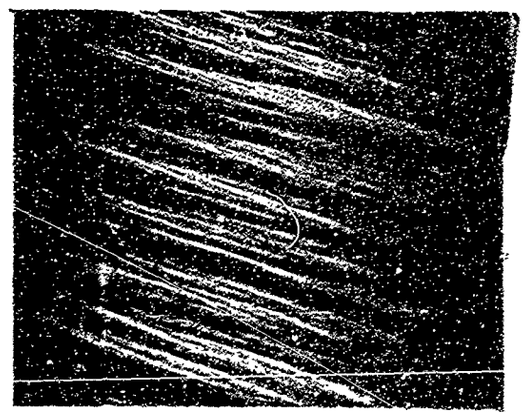


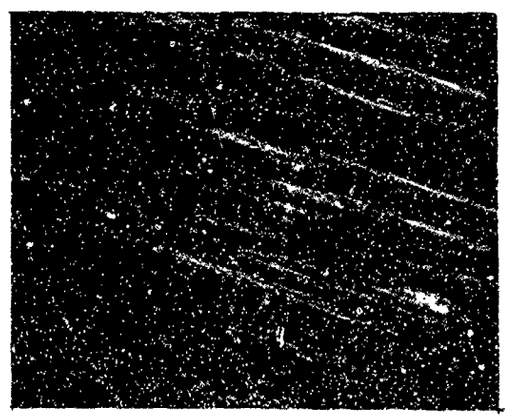
8045-2



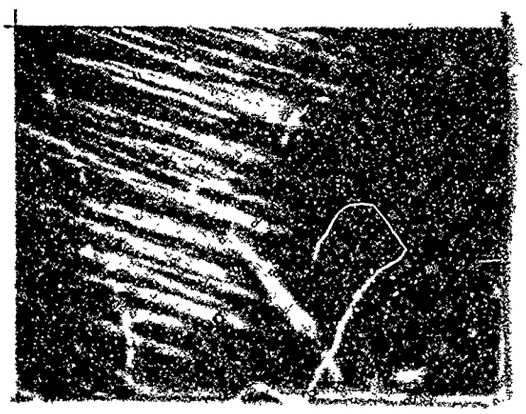


8046-1

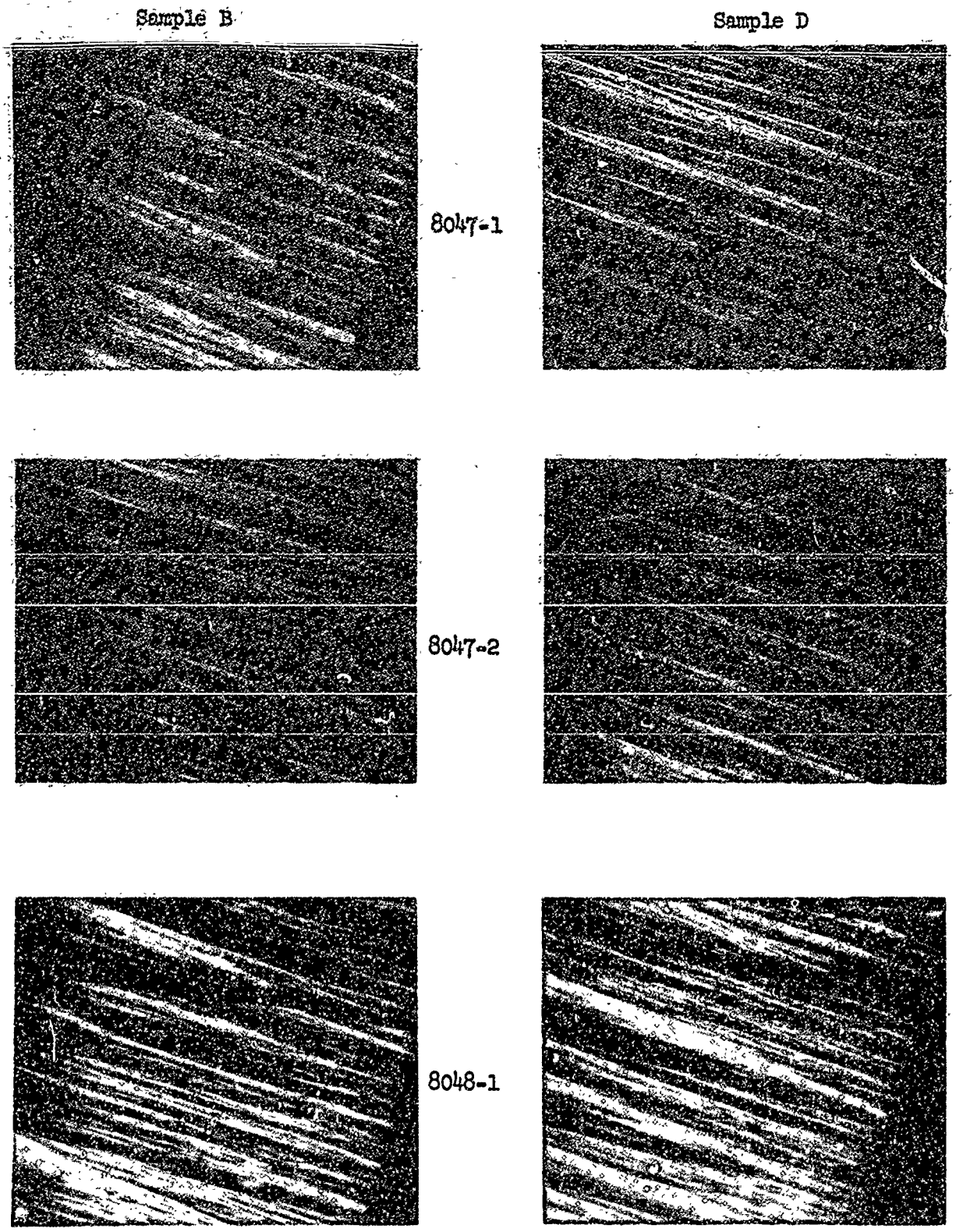




8046-2

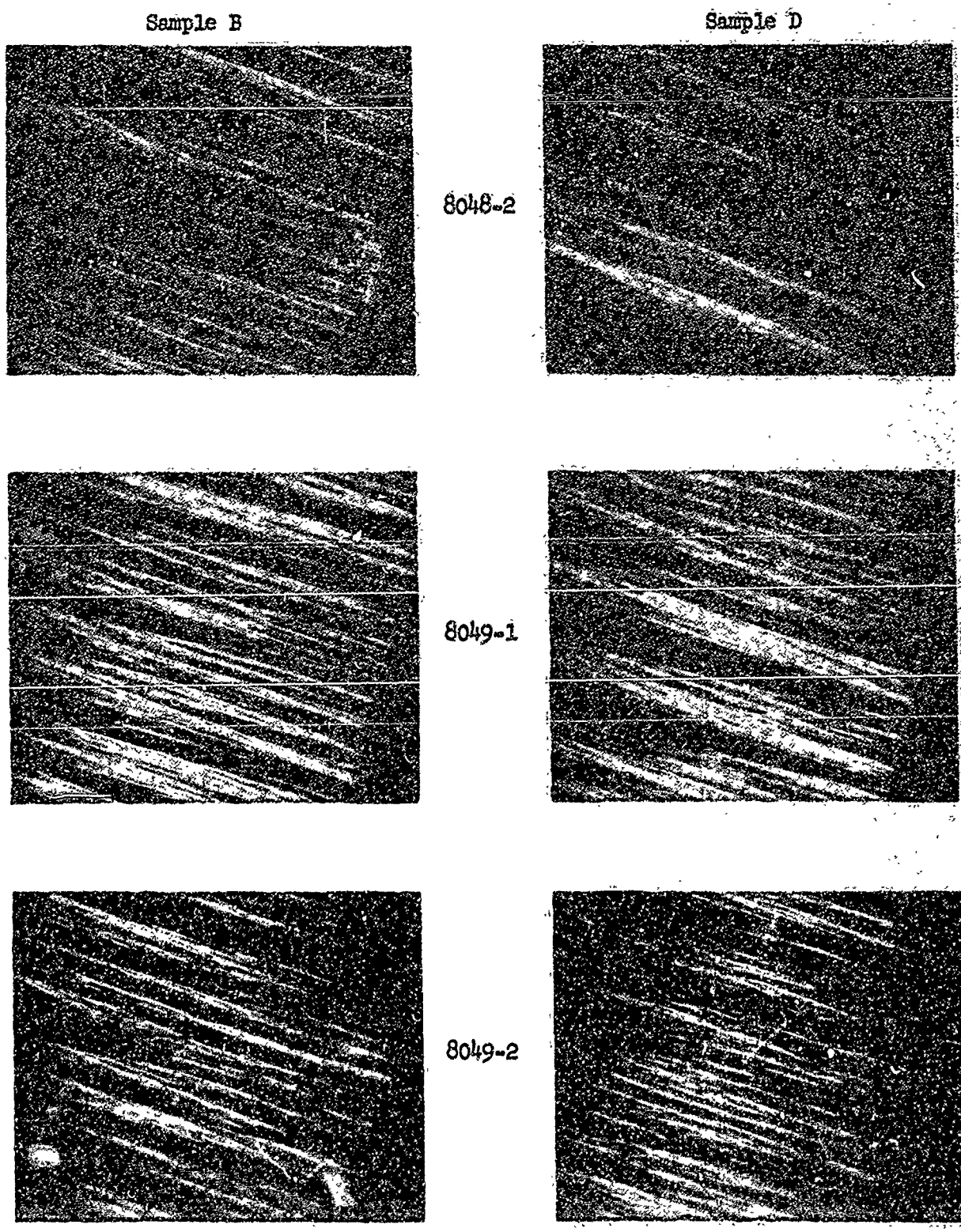


Microstructures of [illegible]
Task 3.4.[illegible] [illegible]



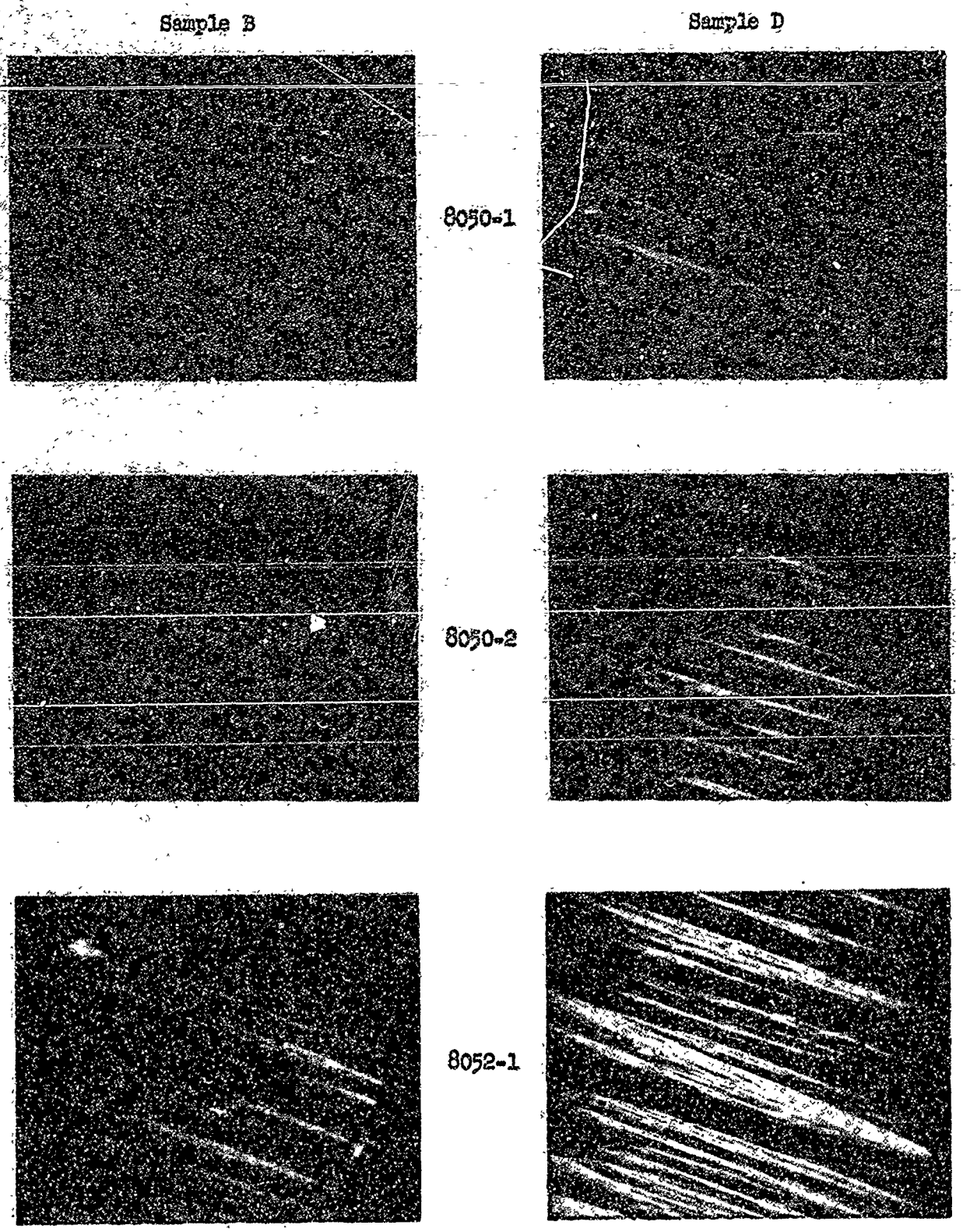
Microstructures of Tube Deposits
Task 3.4.6 Orig. Mag: 50X

Figure 78



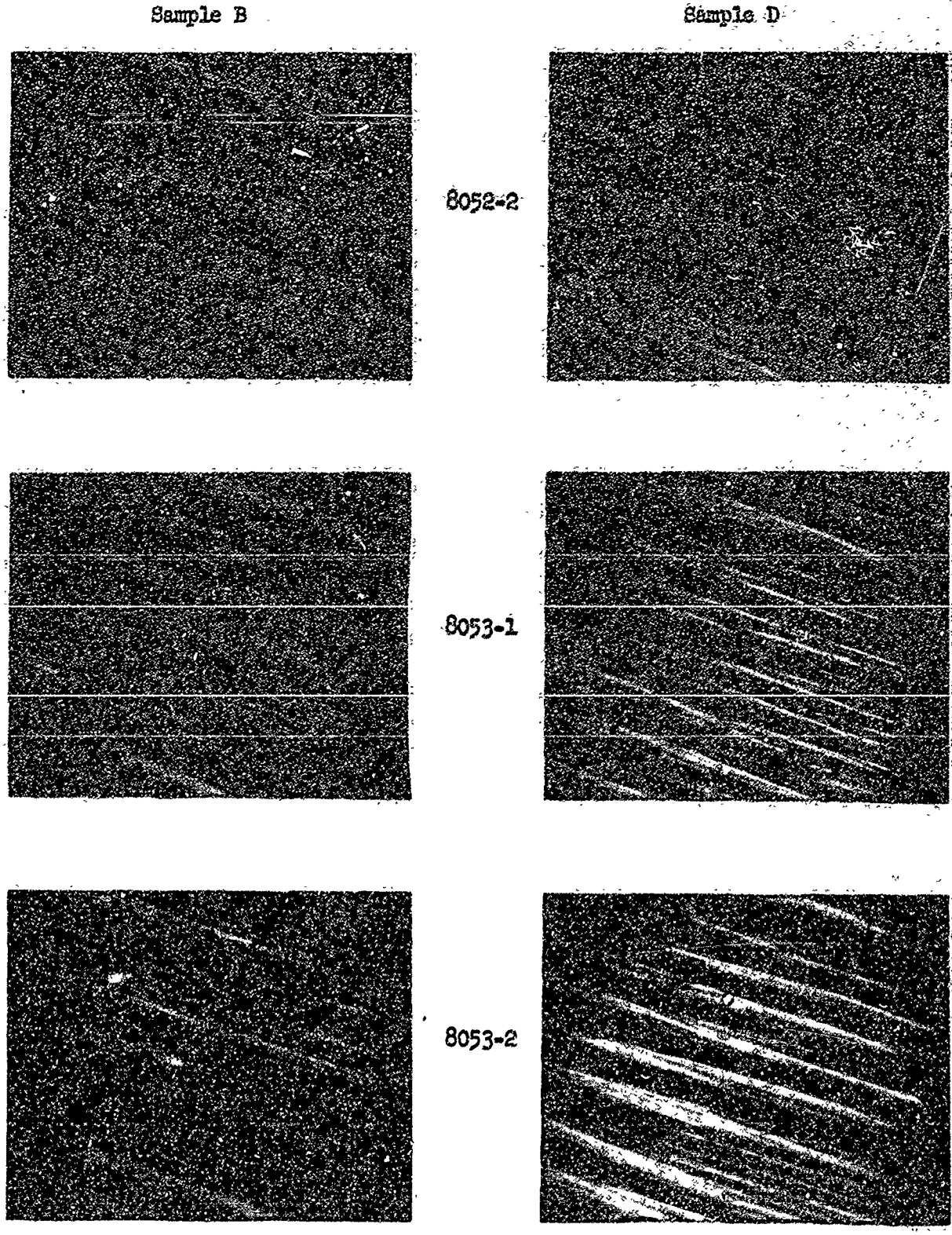
Microstructures of Tube Deposits
Task 3.4.6 Orig. Mag: 50X

Figure 79



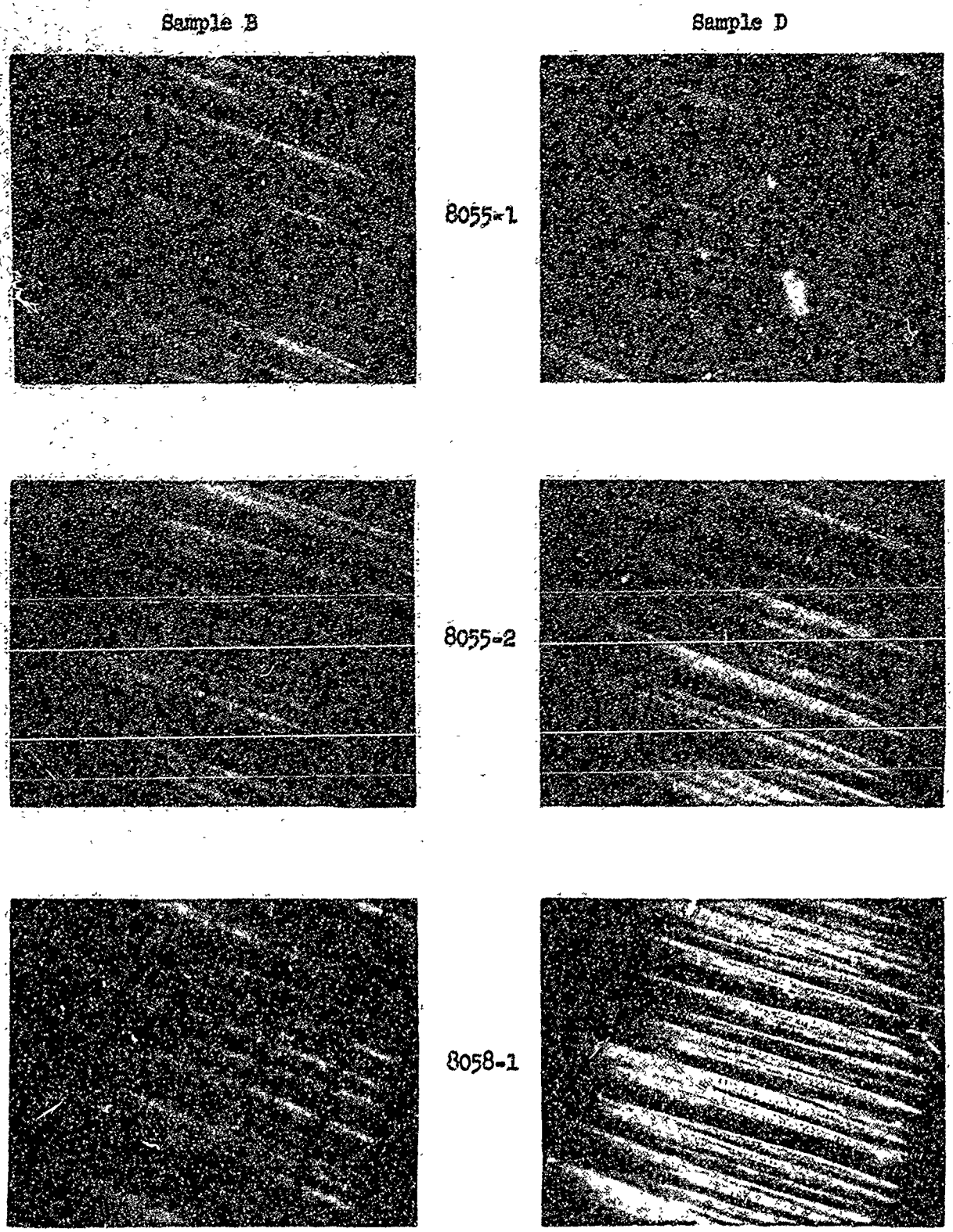
Microstructures of Tube Deposits
Task 3.4.6 Orig. Mag: 50X

Figure 80



Microstructures of Tube Deposits
Task 3.4.6 Orig. Mag: 50X

Figure 81

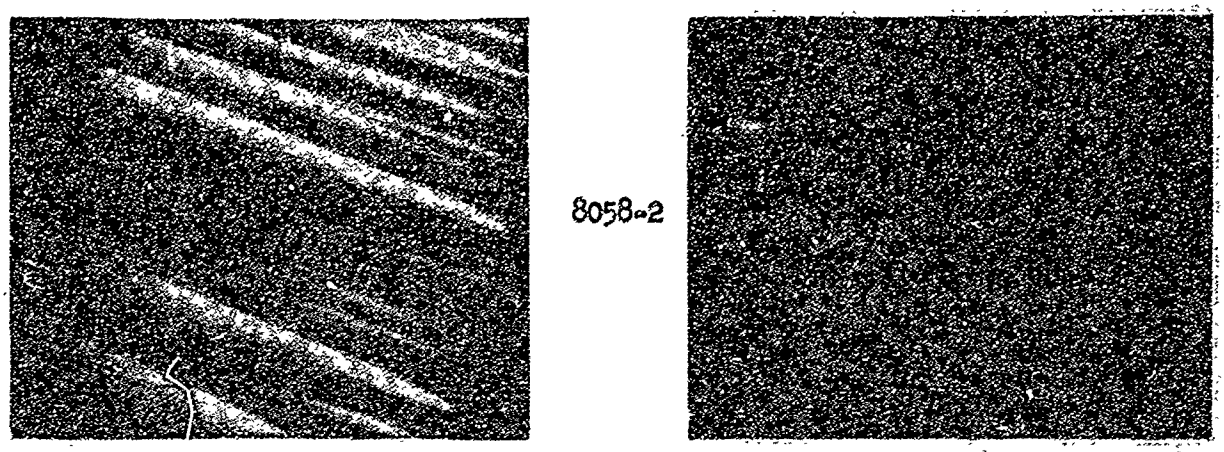


Microstructures of Tube Deposits
Task 3.4.6 Orig. Mag: 50X

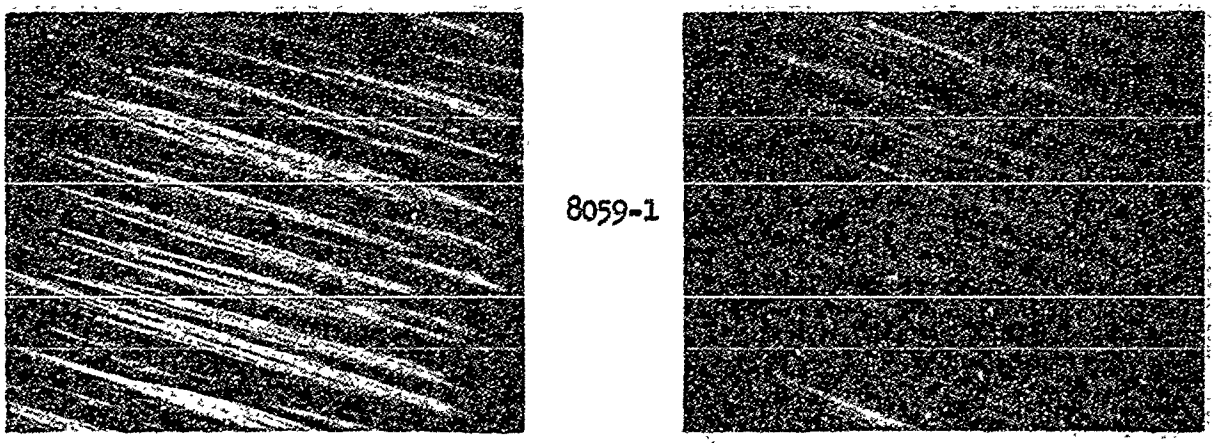
Figure 82

Sample B

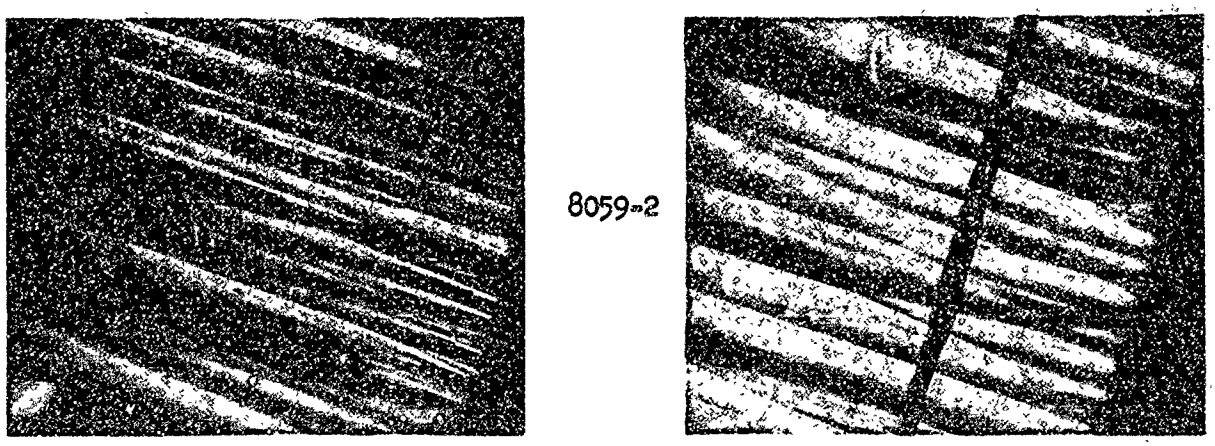
Sample D



8058-2



8059-1



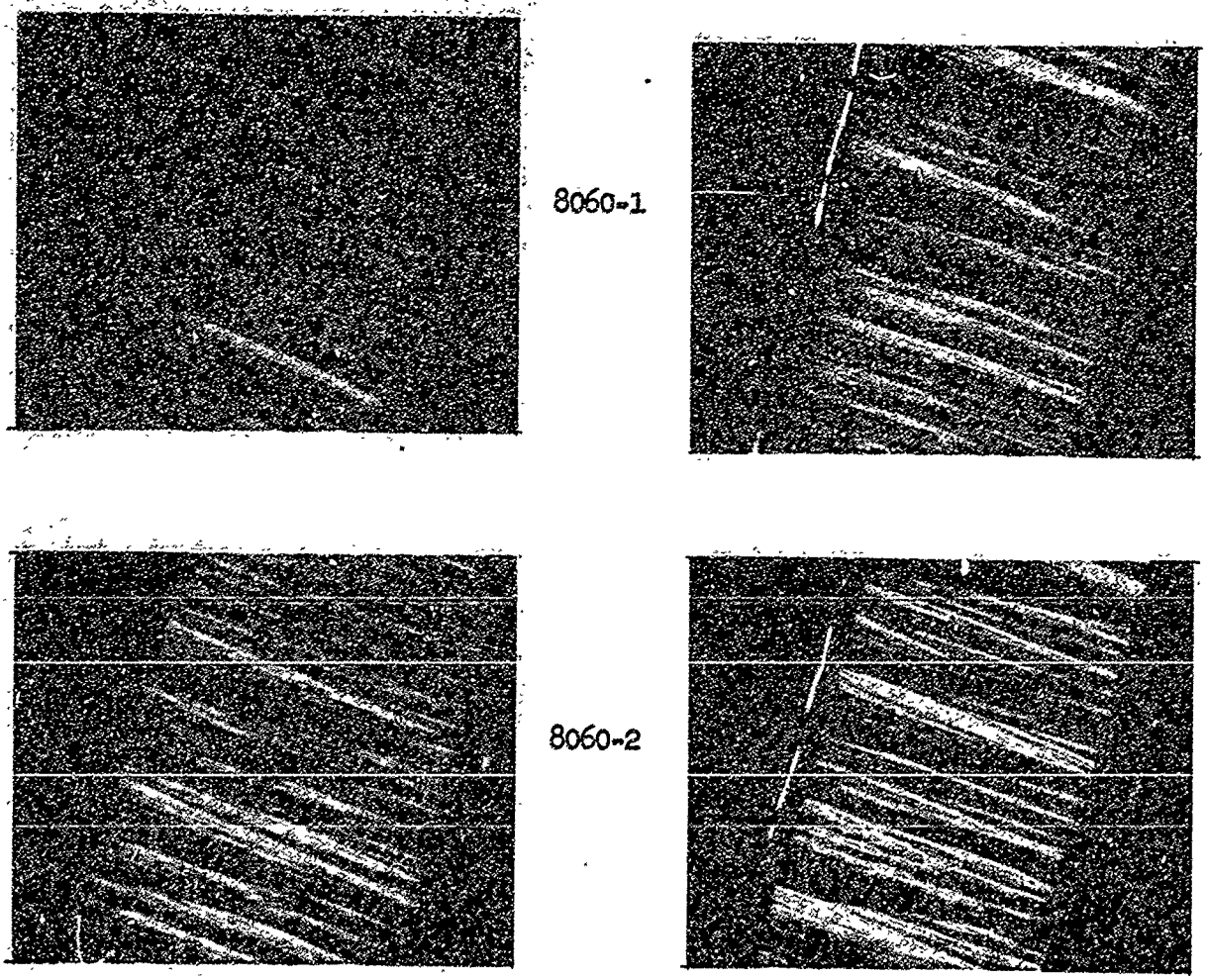
8059-2

Microstructures of Tube Deposits
Task 3.4.6 Orig. Mag: 50X

Figure 83

Sample B

Sample D

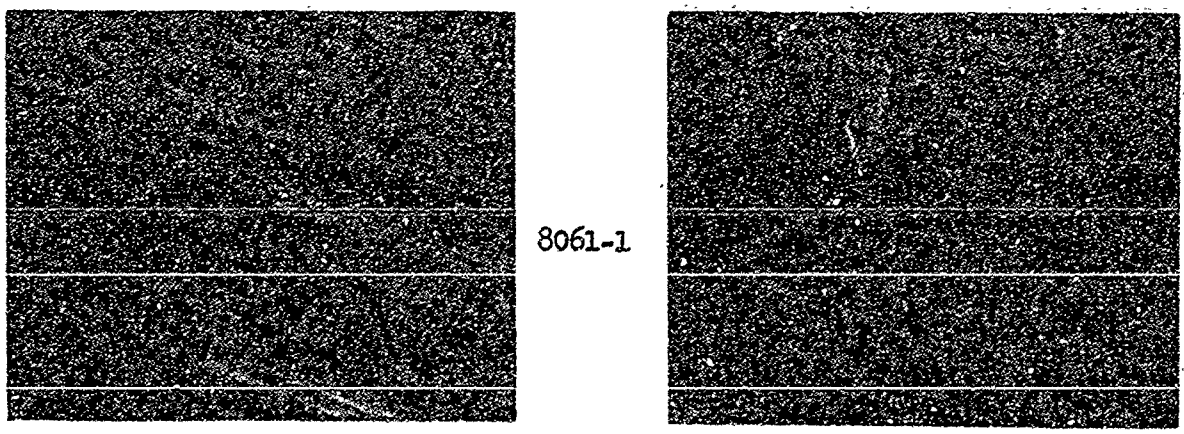


Microstructures of Tube Deposits
Task 3.4.6 Orig. Mag: 50X

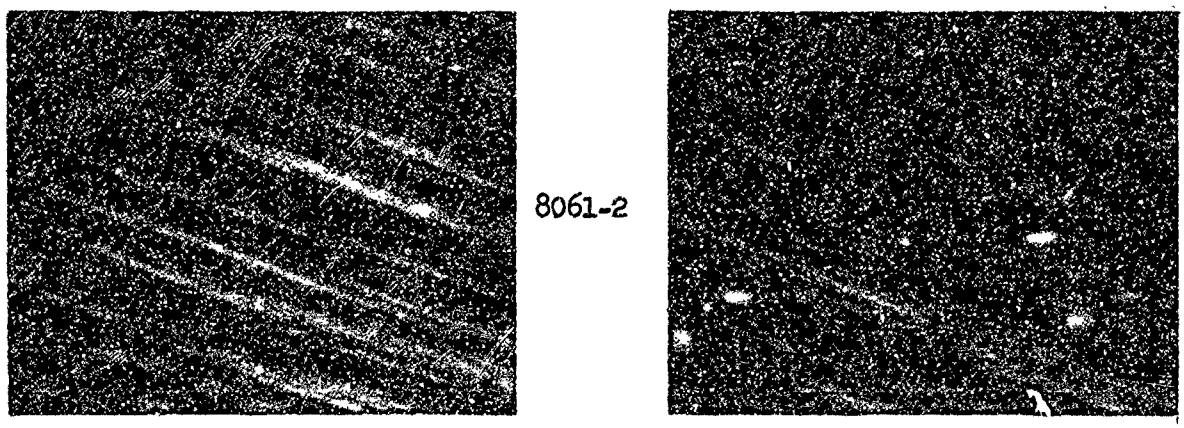
Figure 84

Sample B

Sample D



8061-1



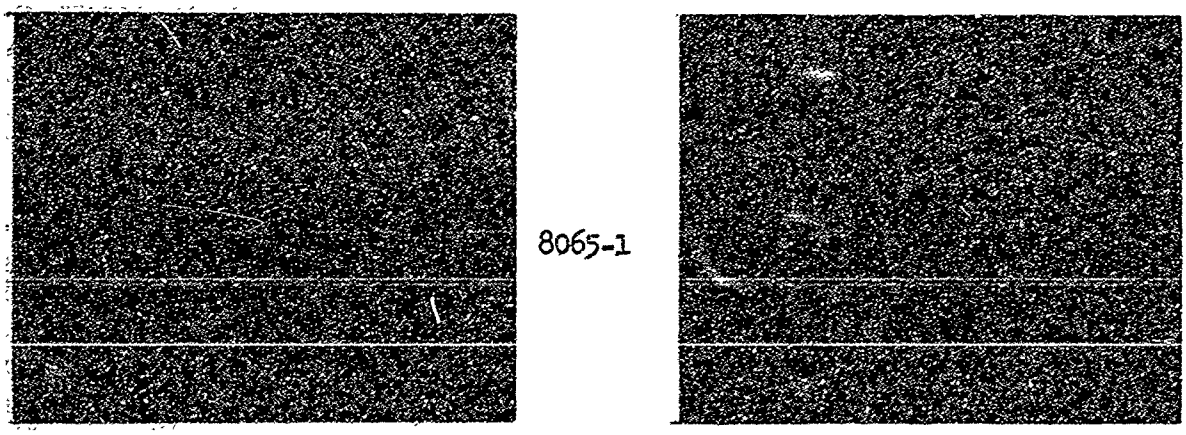
8061-2

Microstructures of Tube Deposits
Task 3.4.6 Orig. Mag: 50X

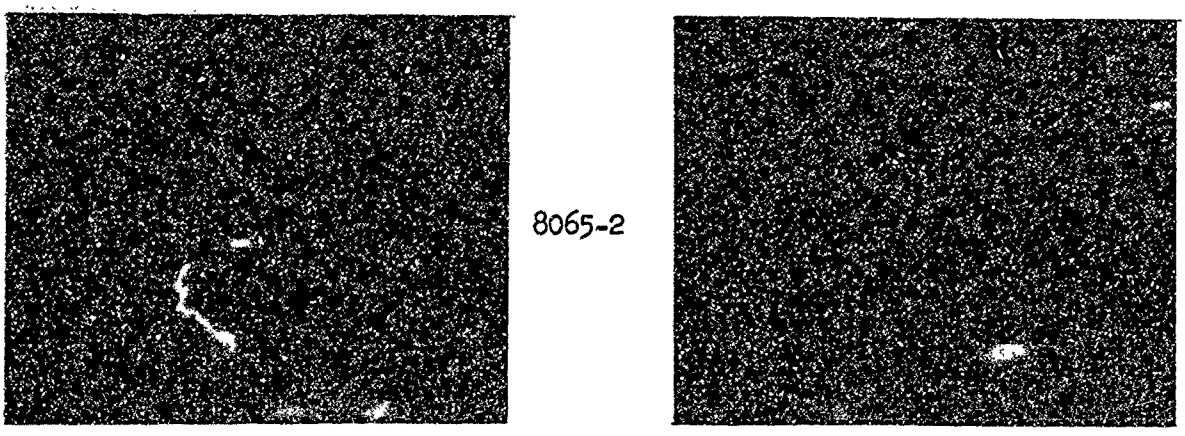
Figure 85.

Sample B

Sample D



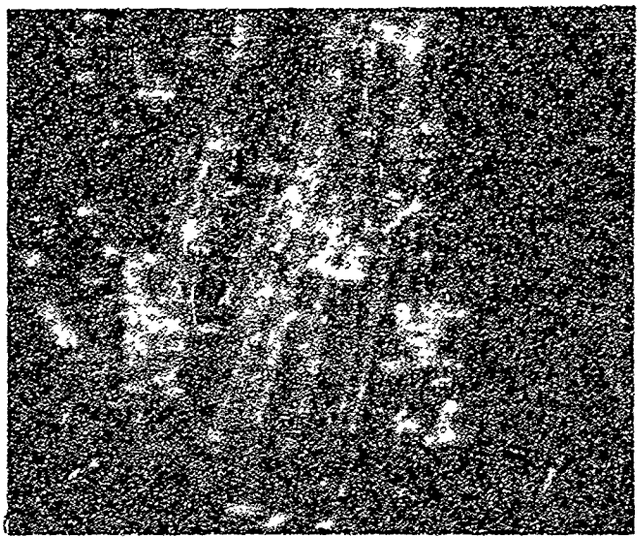
8065-1



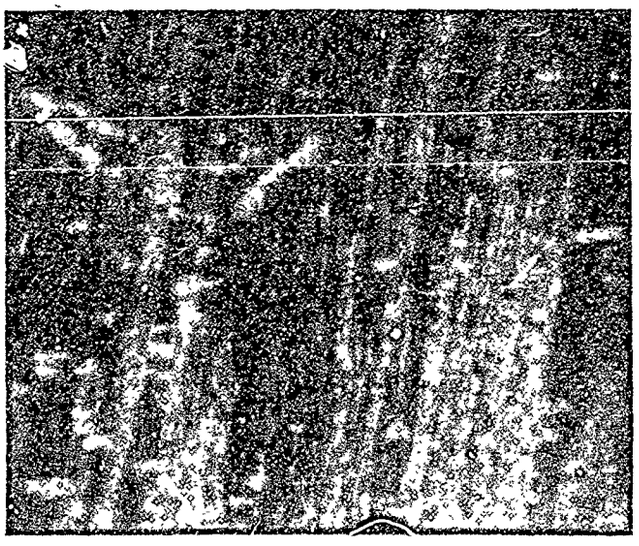
8065-2

Microstructures of Tube Deposits
Task 3.4.6 Orig. Mag: 50X

Figure 86.



Mag: 500X



Mag: 800X

TASK 3.4.6

Deposit 8059-1B

Figure 87

TASK 3.4.6

% Boron in Solid vs. Temperature

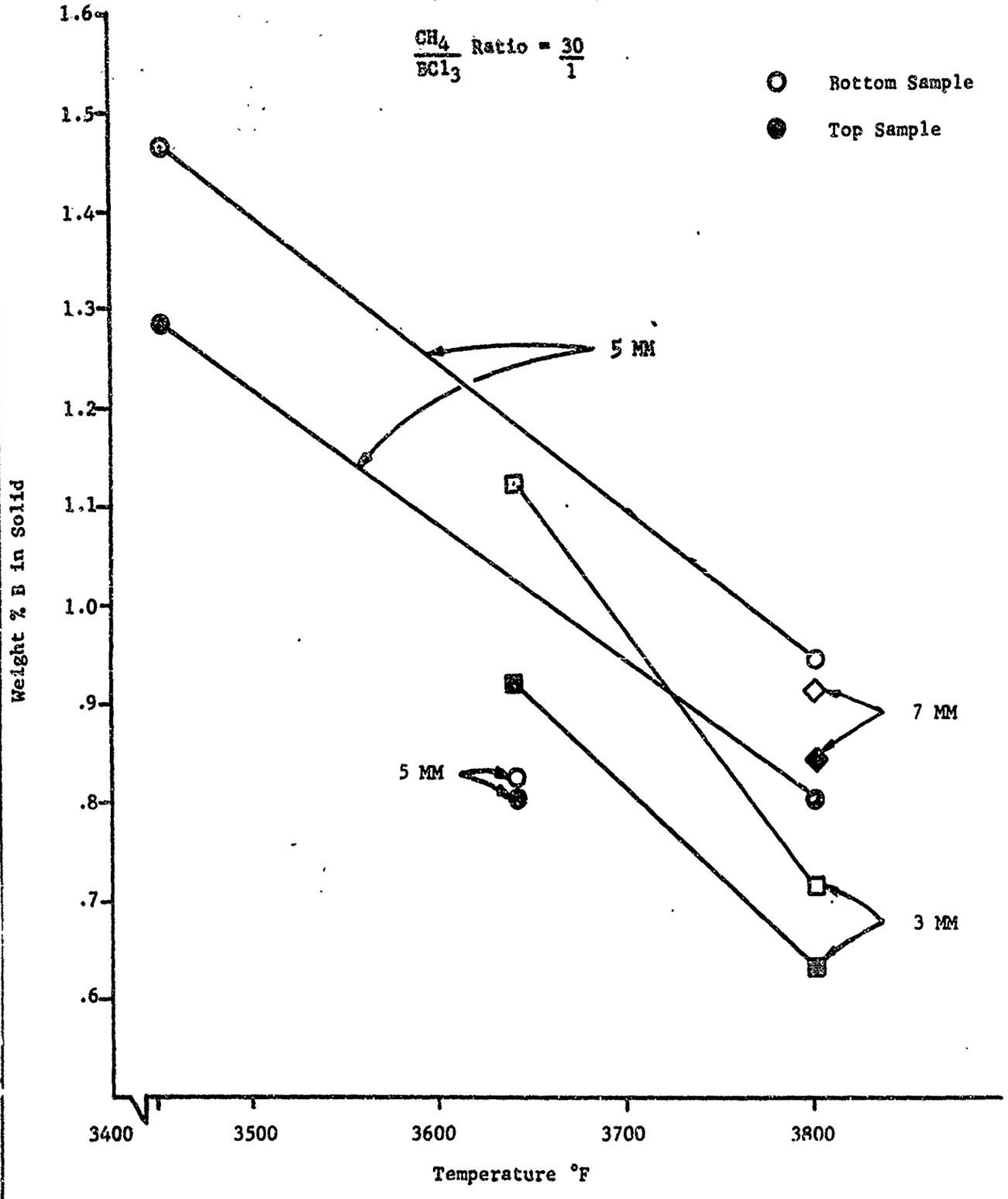


Figure 88

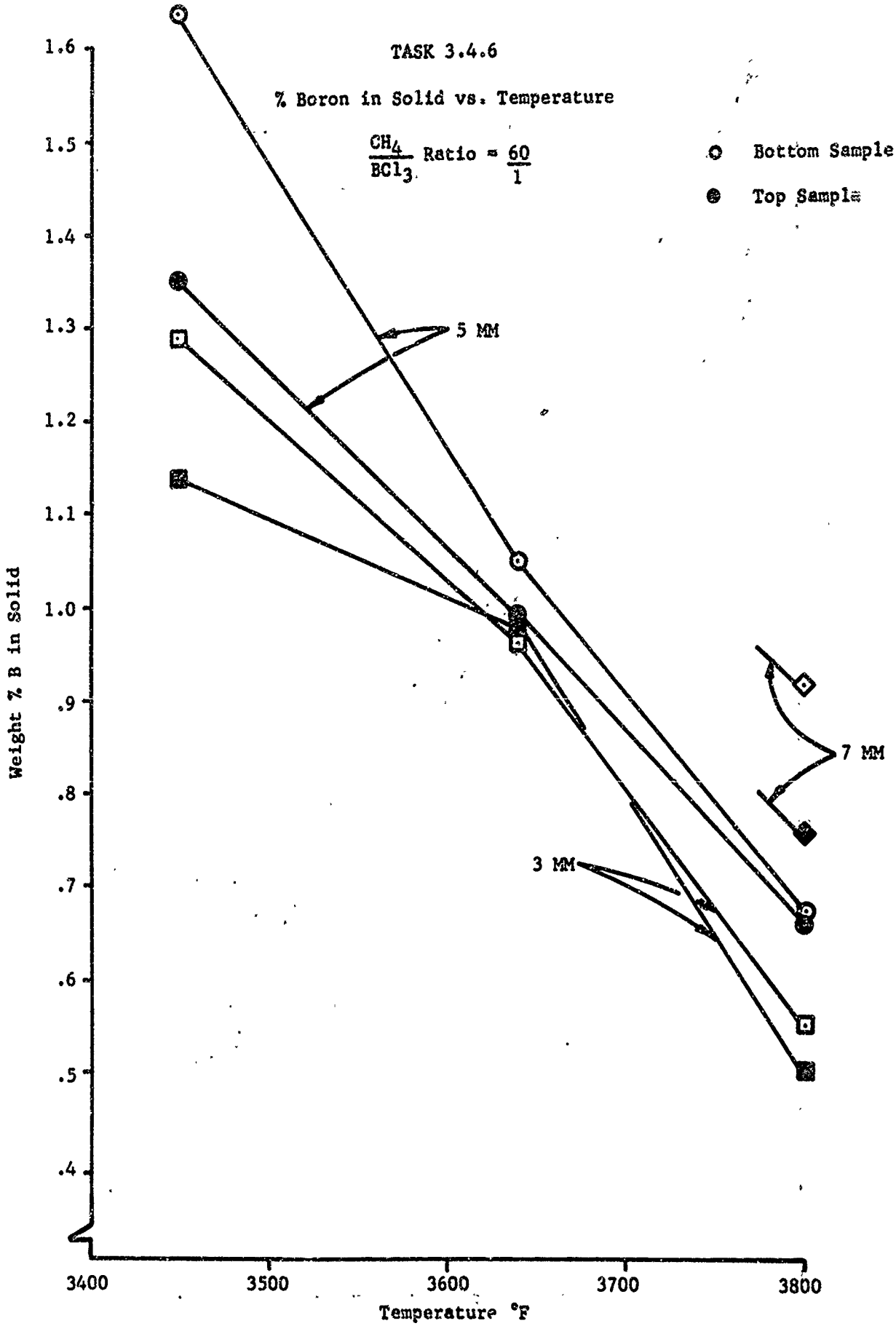

TASK 3.4.6
% Boron in Solid vs. Temperature
$\frac{CH_4}{BCl_3}$ Ratio = $\frac{60}{1}$
Bottom Sample
Top Sample
5 MM
7 MM
3 MM
Weight % B in Solid
1.6
1.5
1.4
1.3
1.2
1.1
1.0
.9
.8
.7
.6
.5
.4
3400
3500
3600
3700
3800
Temperature °F

Figure 89

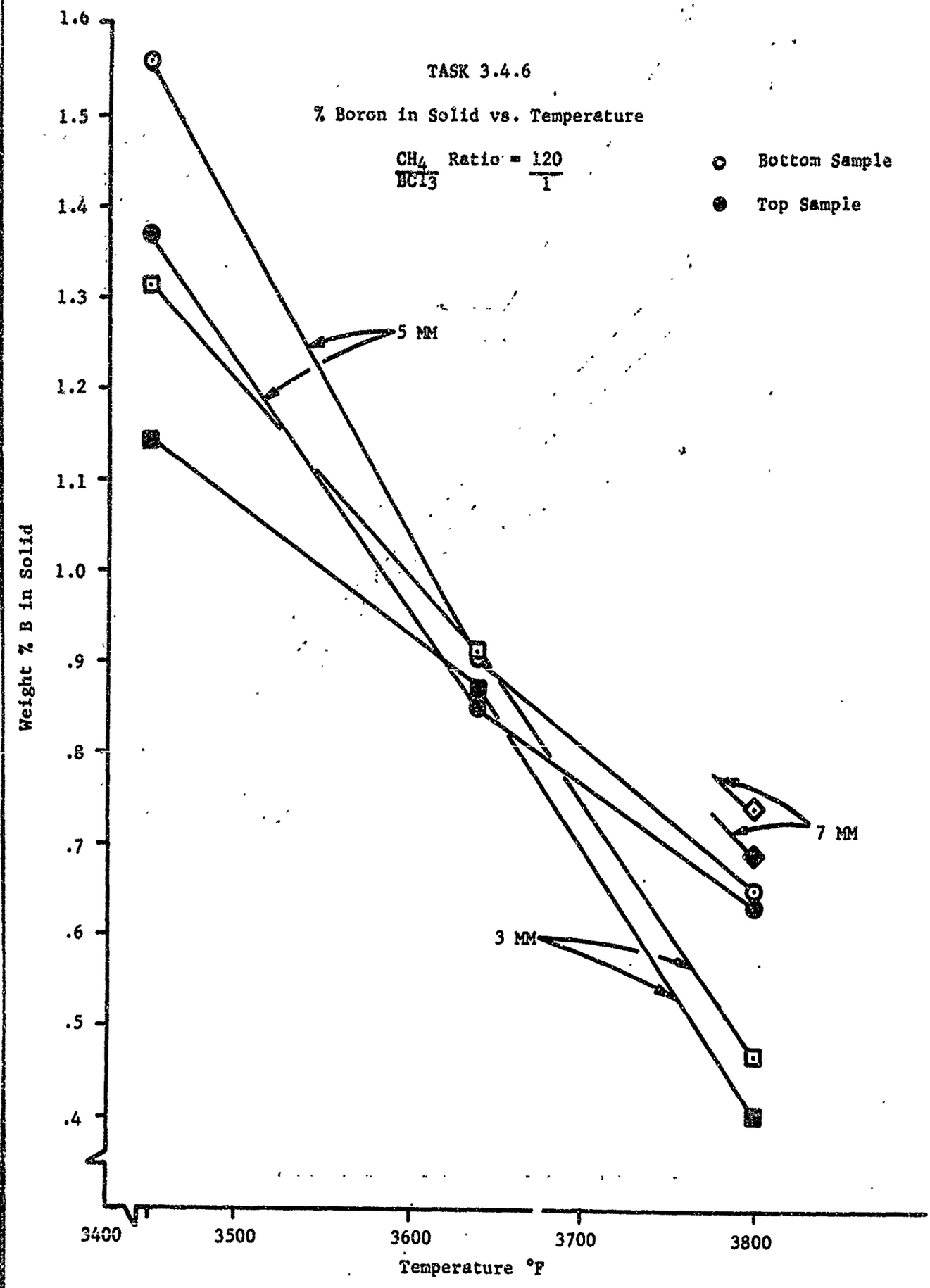

TASK 3.4.6
% Boron in Solid vs. Temperature
$\frac{CH_4}{BCl_3}$ Ratio = $\frac{120}{1}$
Bottom Sample
Top Sample
5 MM
7 MM
3 MM
Weight % B in Solid
1.6
1.5
1.4
1.3
1.2
1.1
1.0
.9
.8
.7
.6
.5
.4
3400
3500
3600
3700
3800
Temperature °F

Figure 90

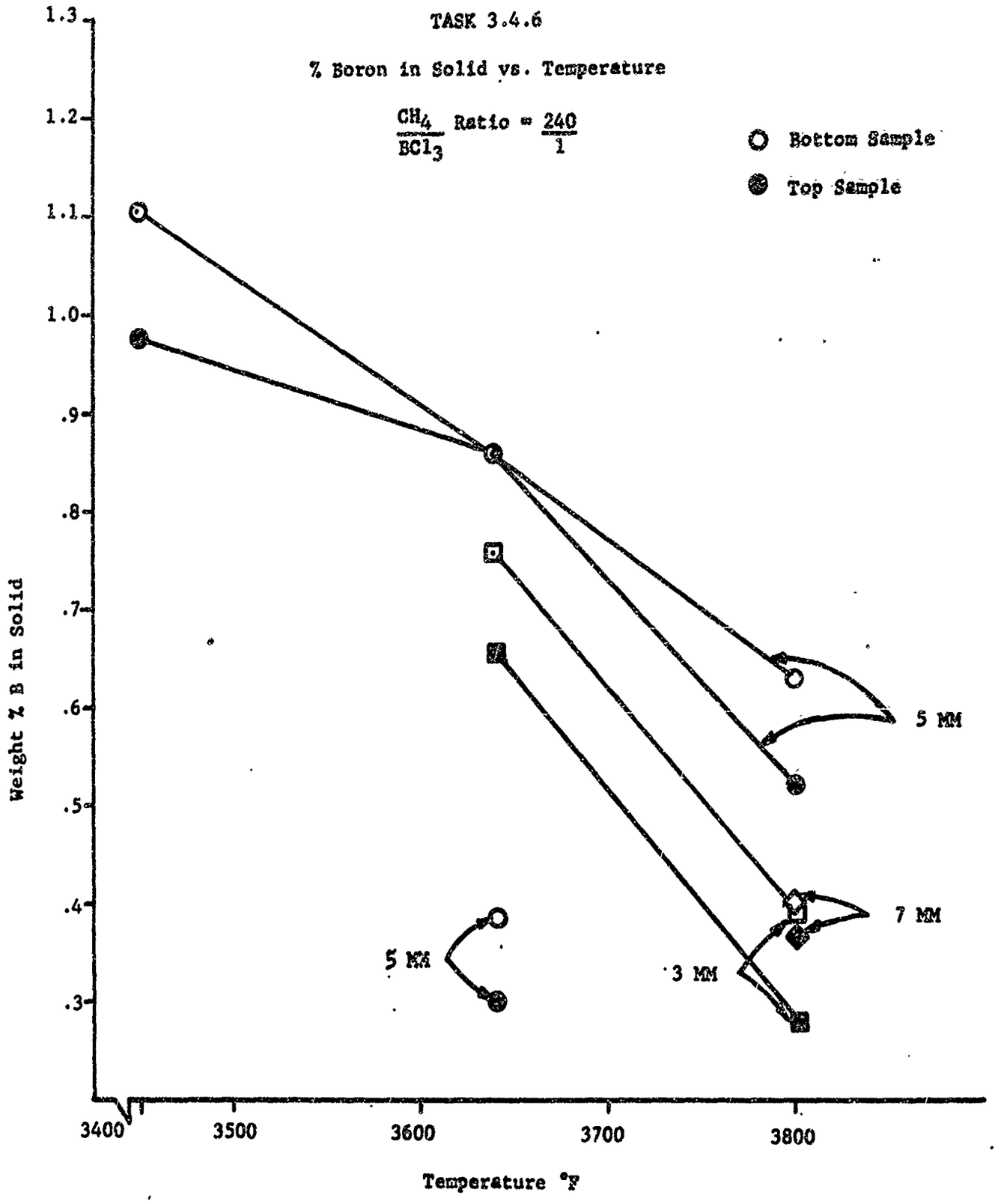

TASK 3.4.6
% Boron in Solid vs. Temperature
$\frac{CH_4}{BCl_3}$ Ratio = $\frac{240}{1}$
Bottom Sample
Top Sample
Weight % B in Solid
1.3
1.2
1.1
1.0
.9
.8
.7
.6
.5
.4
.3
5 MM
7 MM
5 MM
3 MM
3400
3500
3600
3700
3800
Temperature °F

Figure 91



TASK 3.4.6

Soot Deposit as Exposed at Inlet End Cylinder 8059-2

Figure 92.

TASK 3.4.6

Boron in Solid vs. Pressure for 3800°F

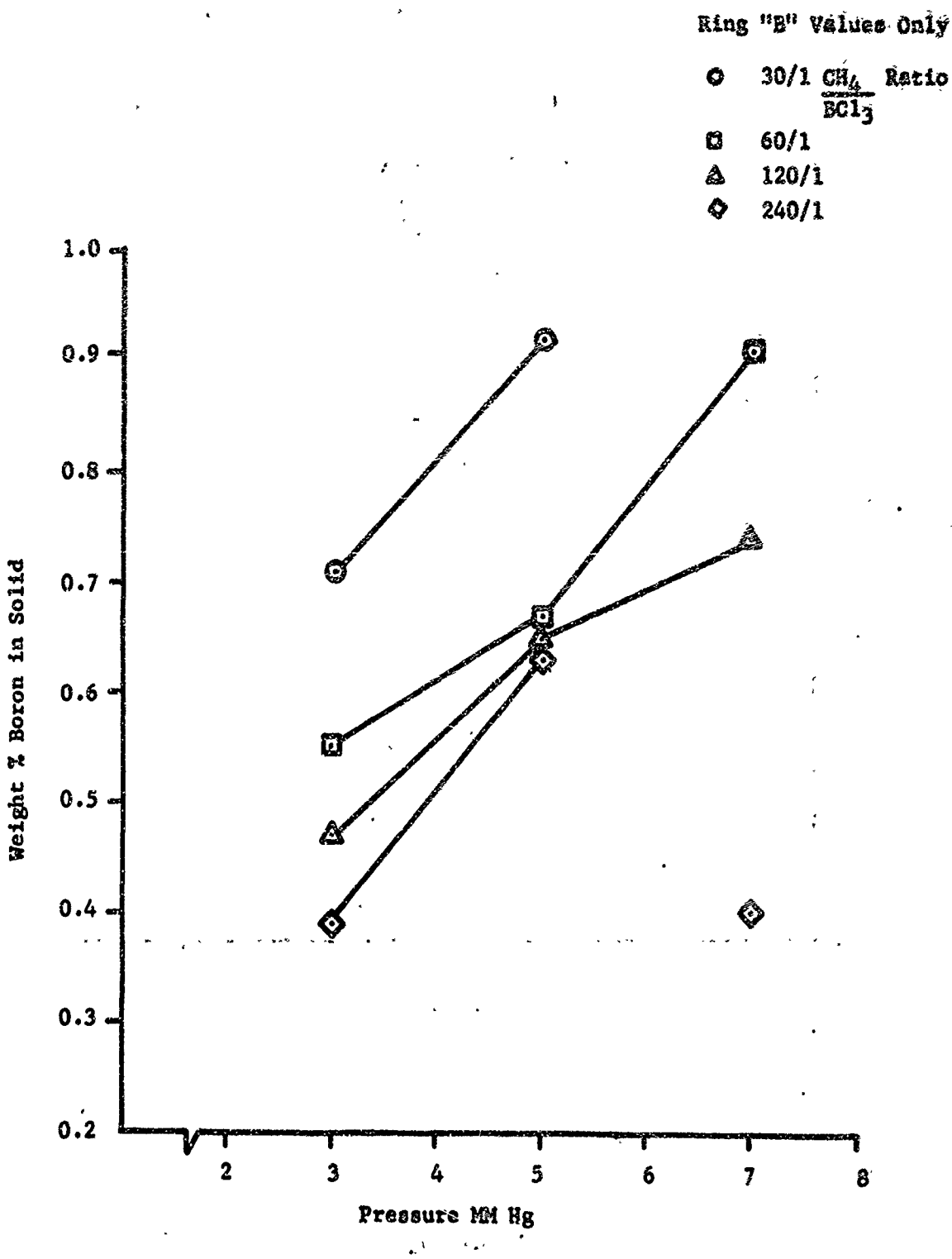


Figure 93

TASK 3.4.6

Boron in Solid vs. Pressure for 3640°F

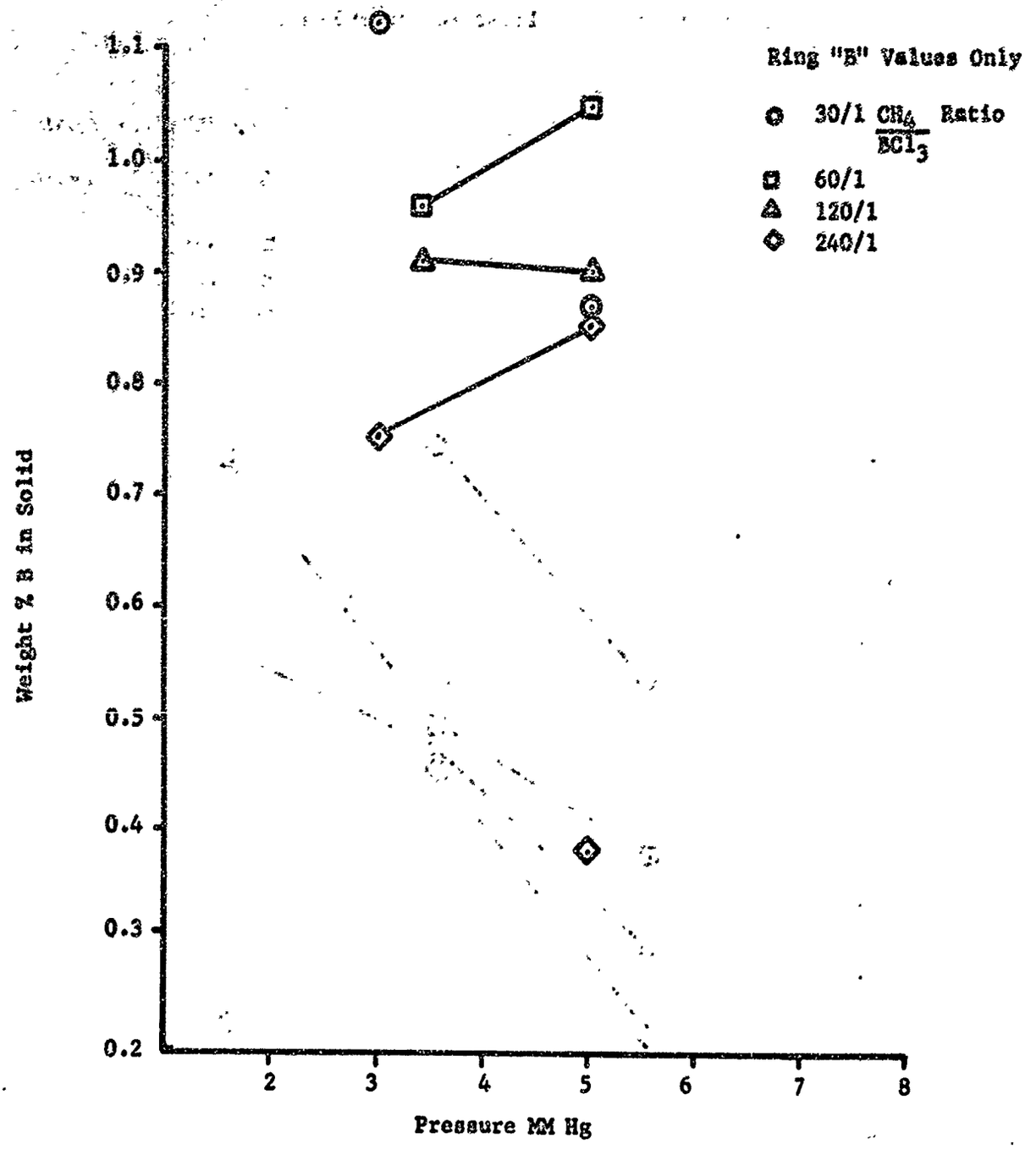


Figure 94

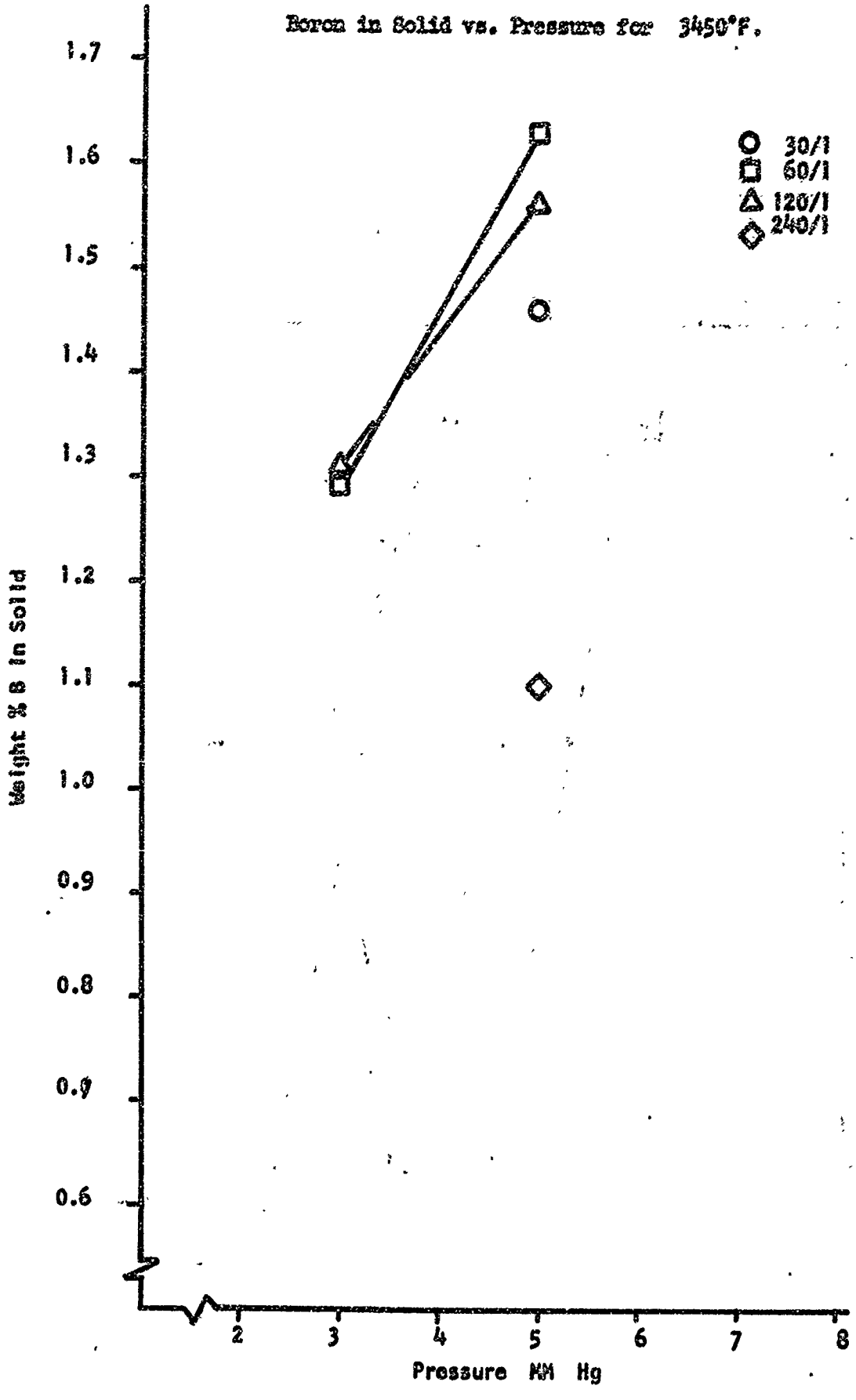

Boron in Solid vs. Pressure for 3450°F.
30/1
60/1
120/1
240/1
Weight % B in Solid
1.7
1.6
1.5
1.4
1.3
1.2
1.1
1.0
0.9
0.8
0.7
0.6
2
3
4
5
6
7
8
Pressure MM Hg

Figure 95

TASK 3.4.6

Boron in Solid vs. Boron Trichloride Concentration in Reactant

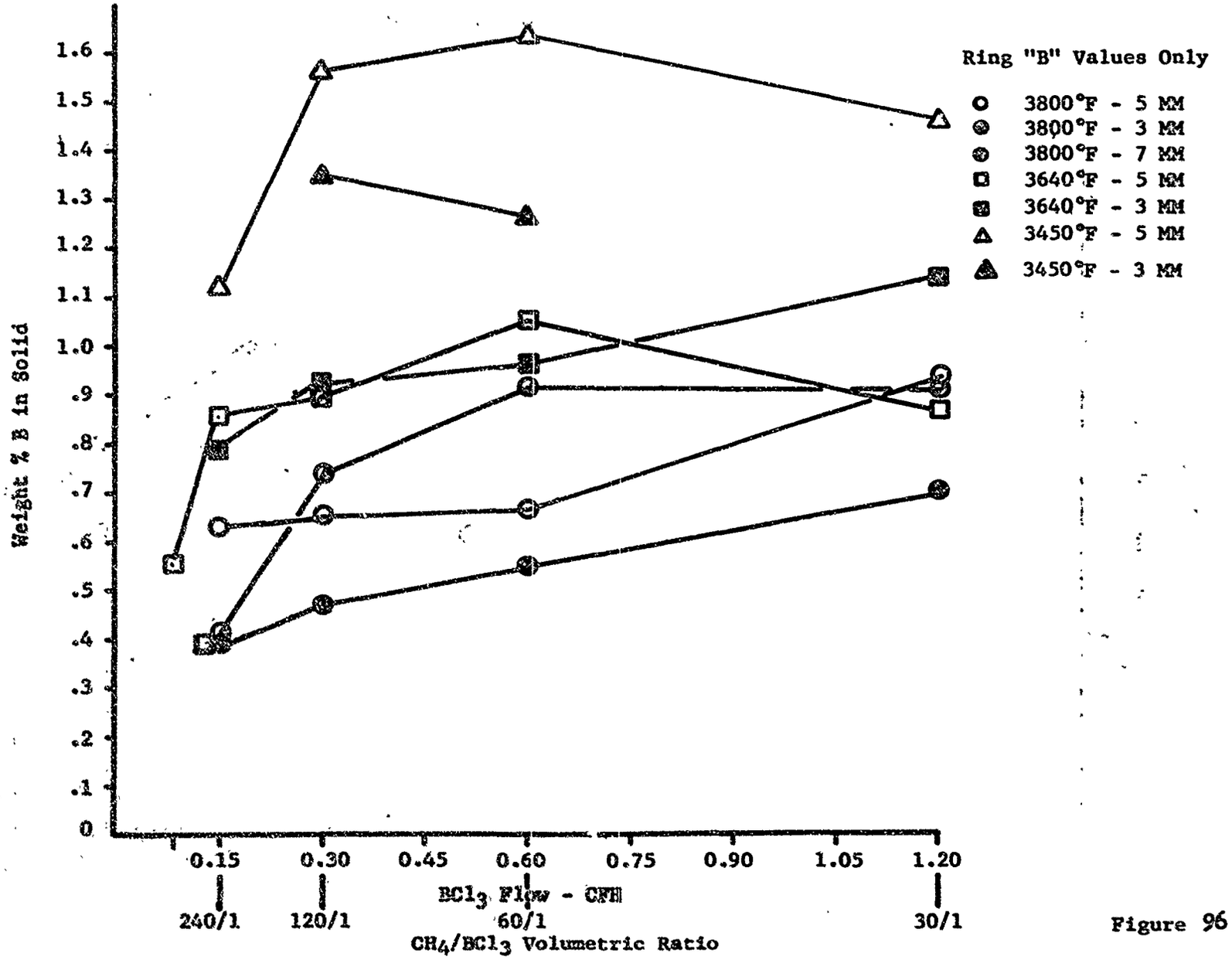
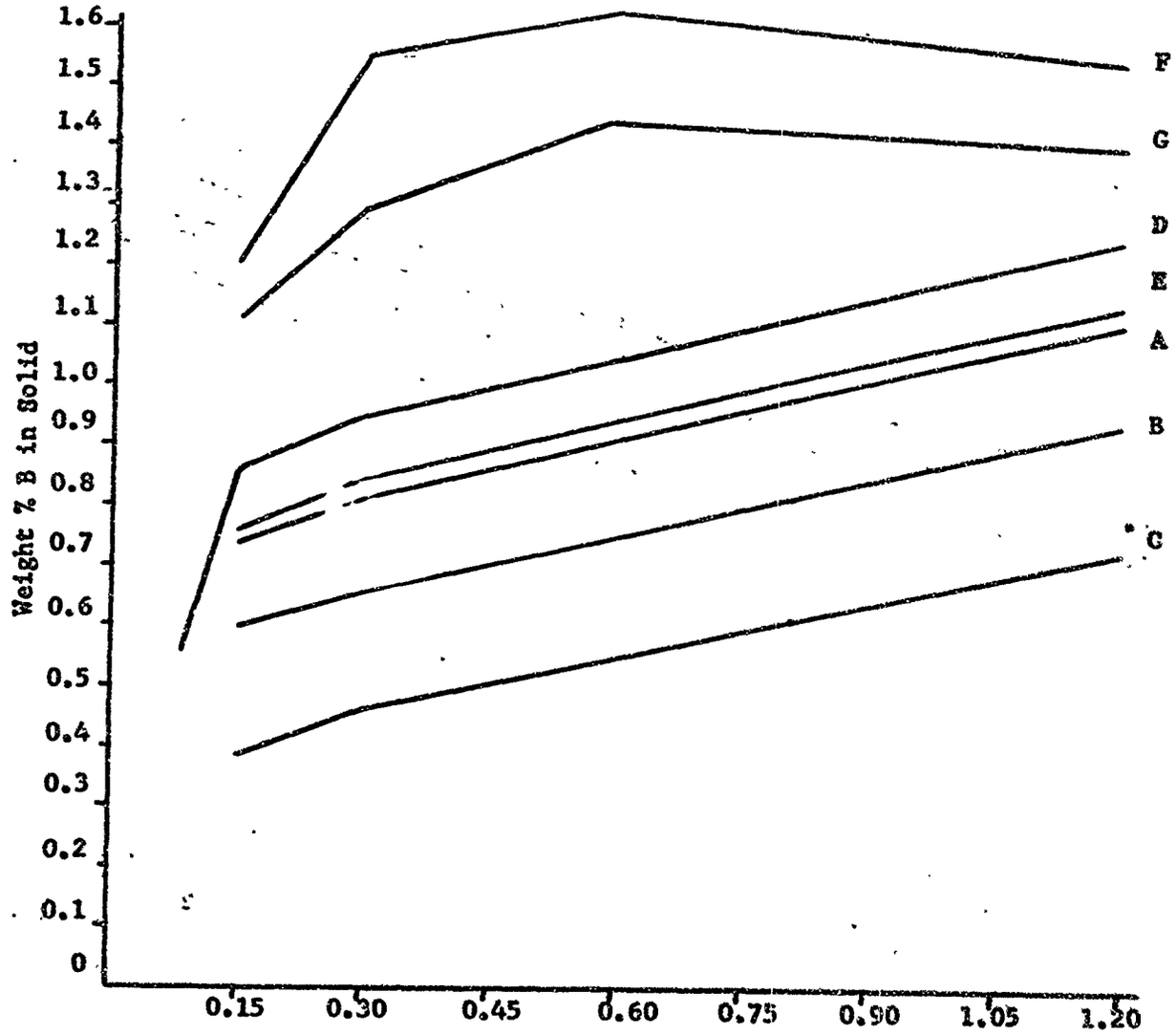


Figure 96

Task 3.4.6

Smoothed Calibration Curve - Ring "B" Values

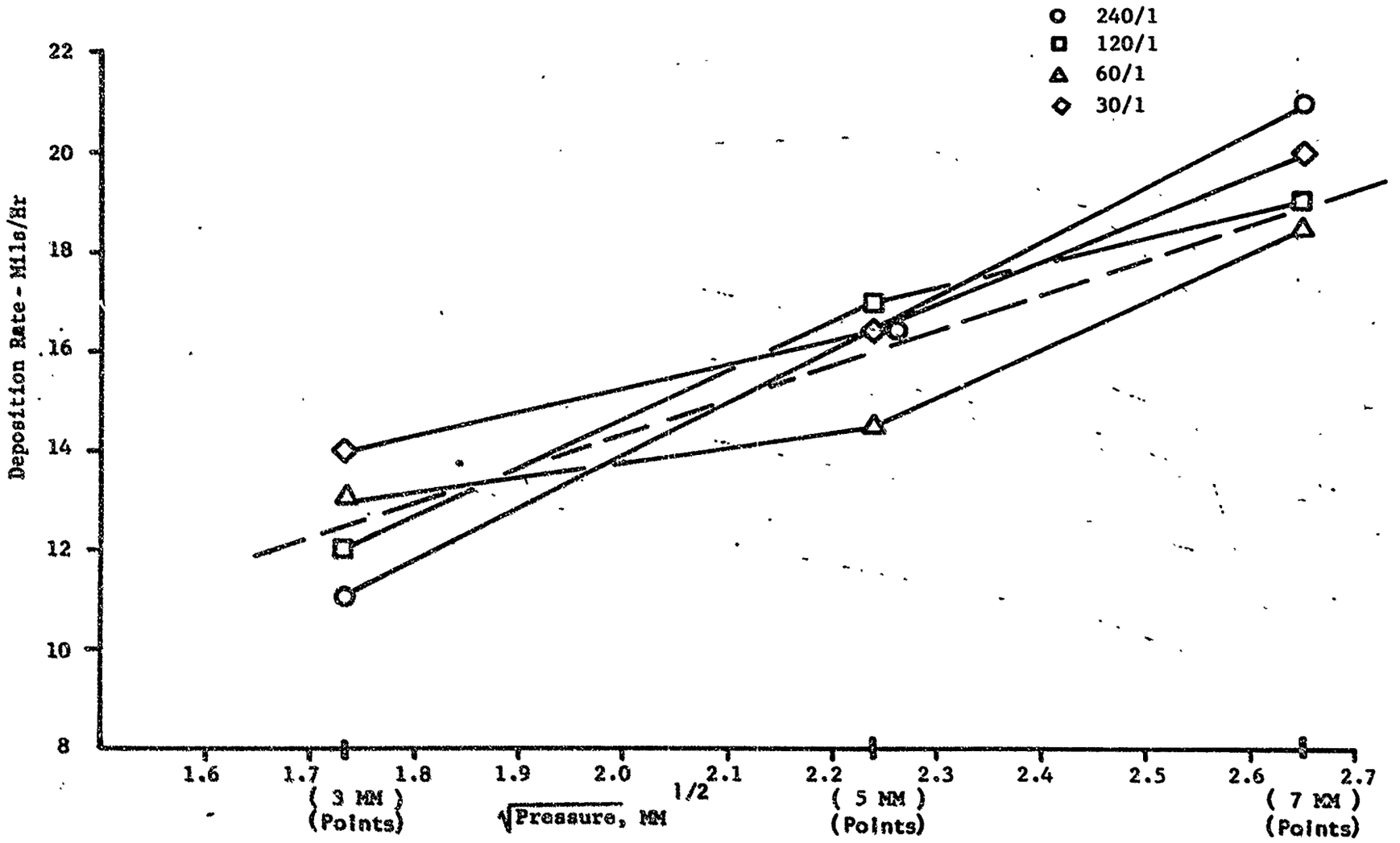


	Temp.	Pressure
A	3800°F	7MM
B	3800°F	5MM
C	3800°F	3MM
D	3640°F	3MM
E	3640°F	3MM
F	3450°F	5MM
G	3450°F	3MM

Figure 97

TASK 3.4.6

Deposition Rate vs. $(P)^{1/2}$ - Temp. 3800°F



328

Figure 98

TASK 3.4.6

Deposition Rate vs. $(P)^{1/2}$ - Temp. 3640°F

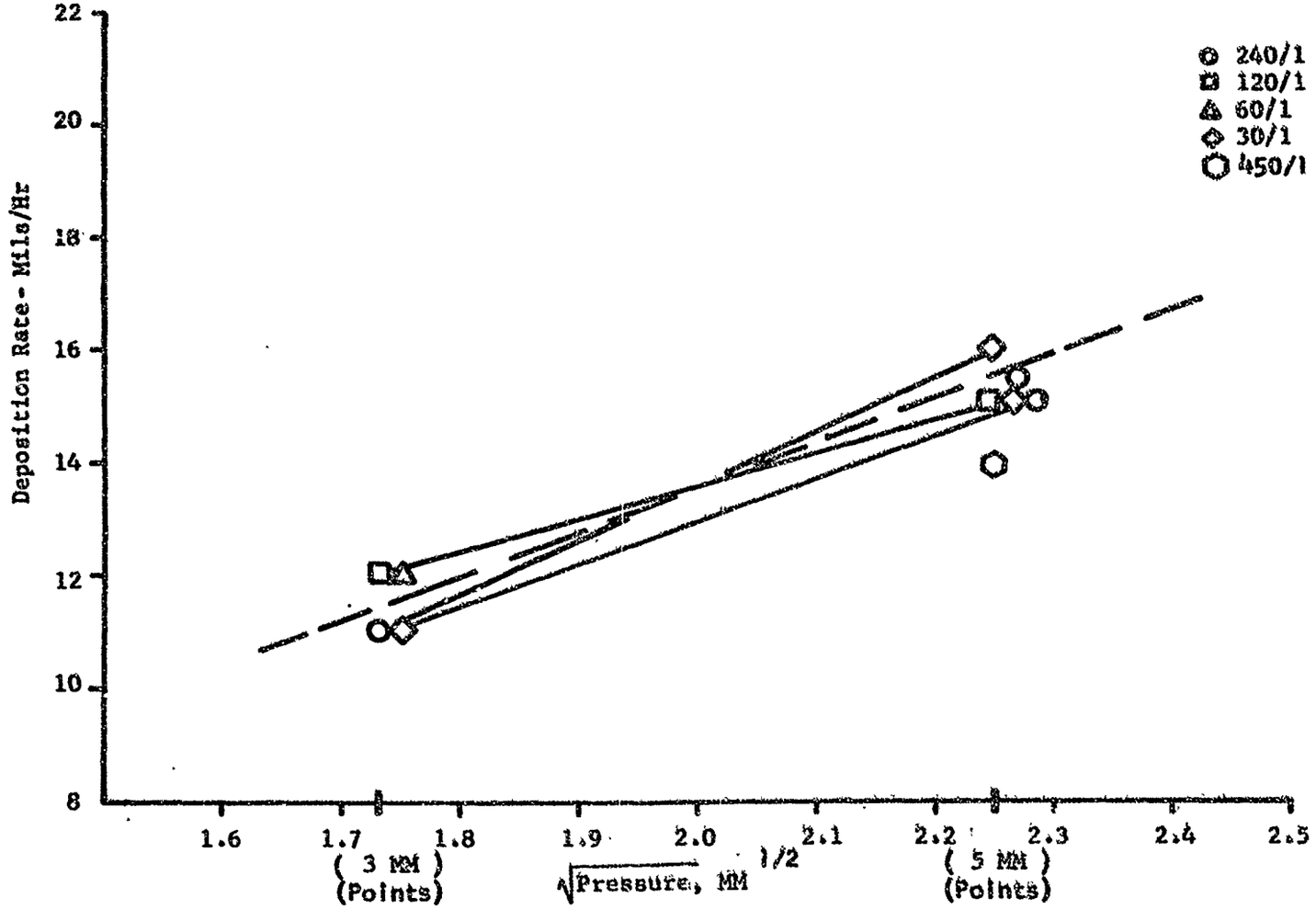


Figure 99

TASK 3.4.6

Deposition Rate vs. $(P)^{1/2}$ - Temp. 3450°F

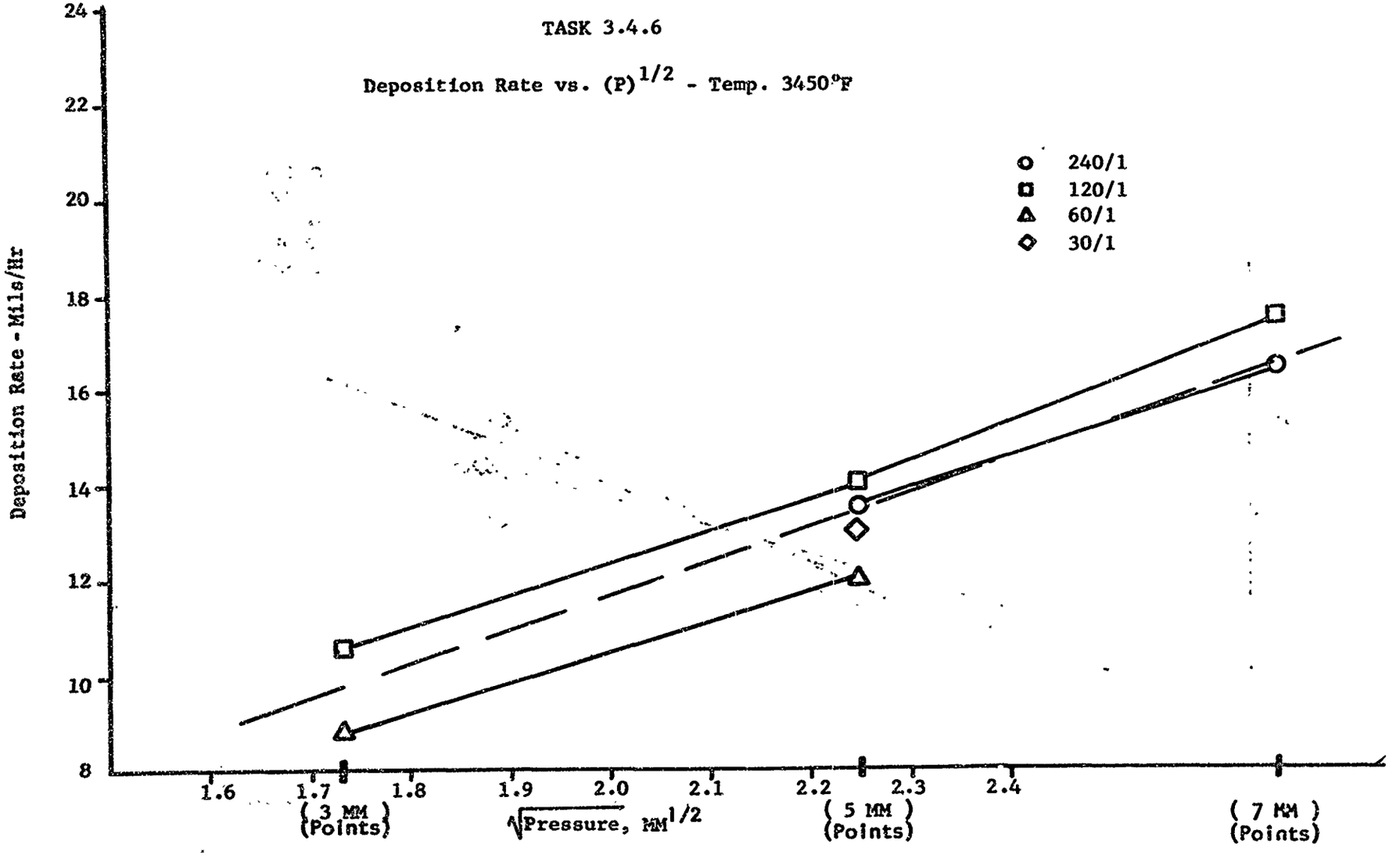


Figure 100

TASK 3.4.6

Deposition Rate vs. Temperature

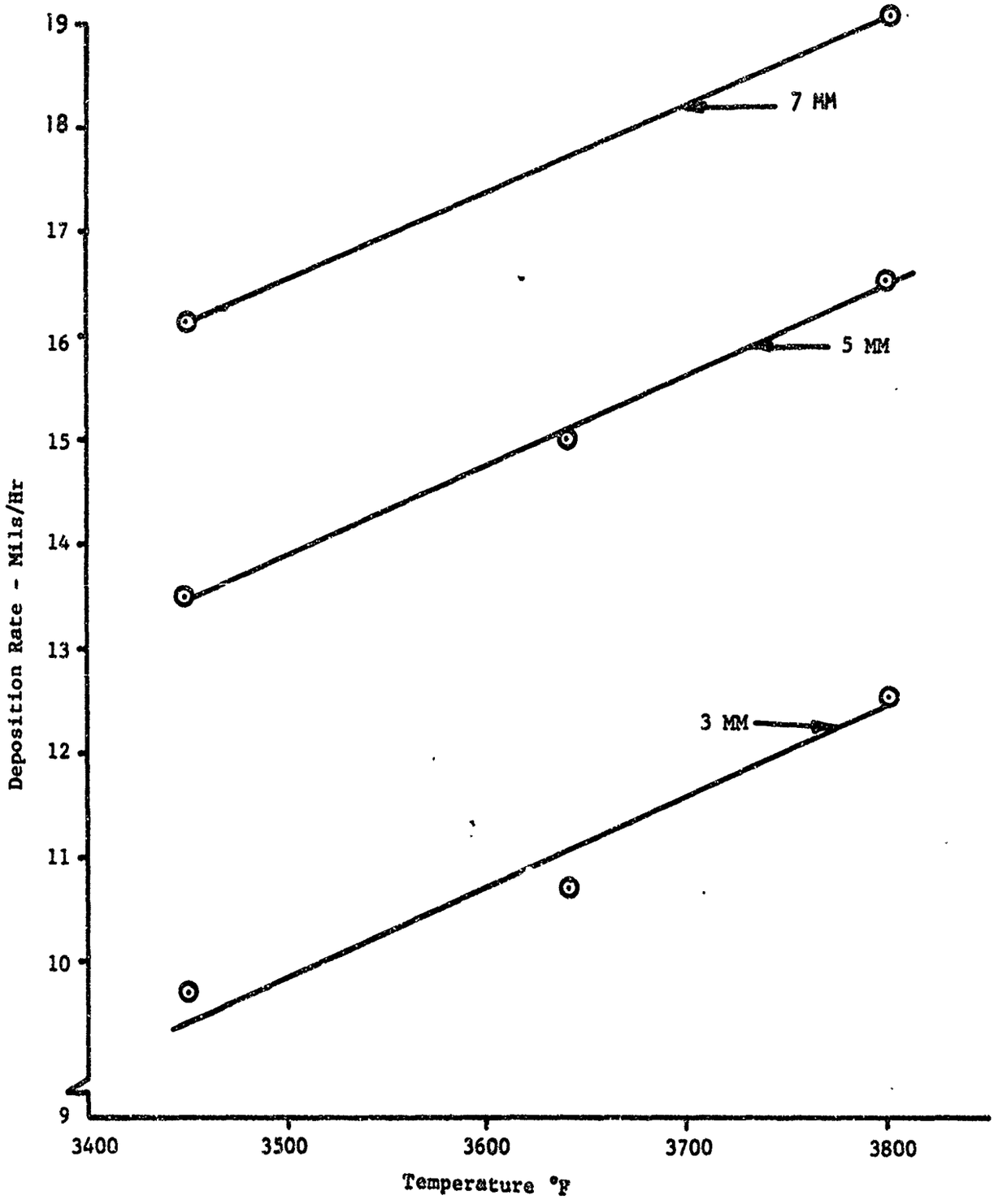
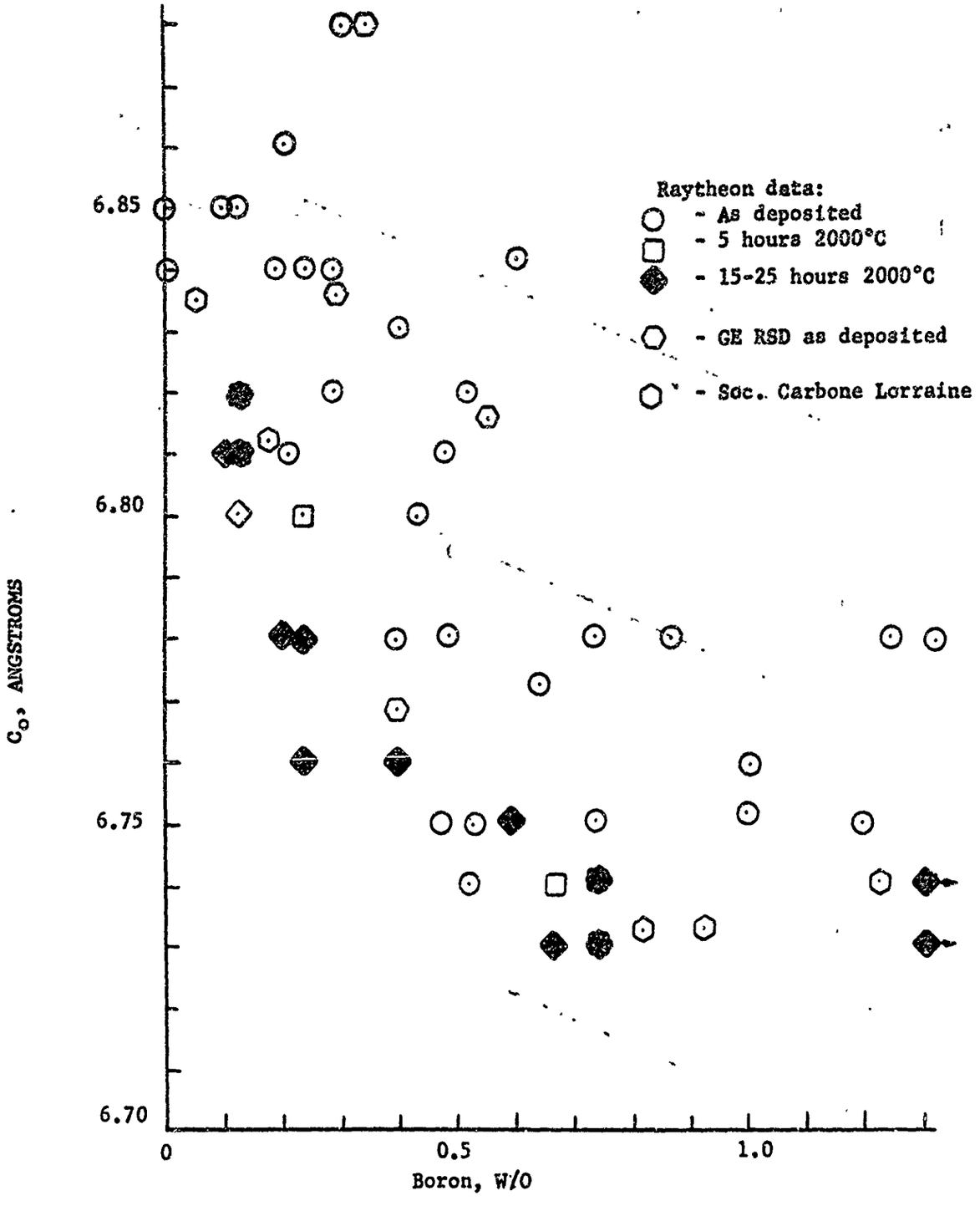
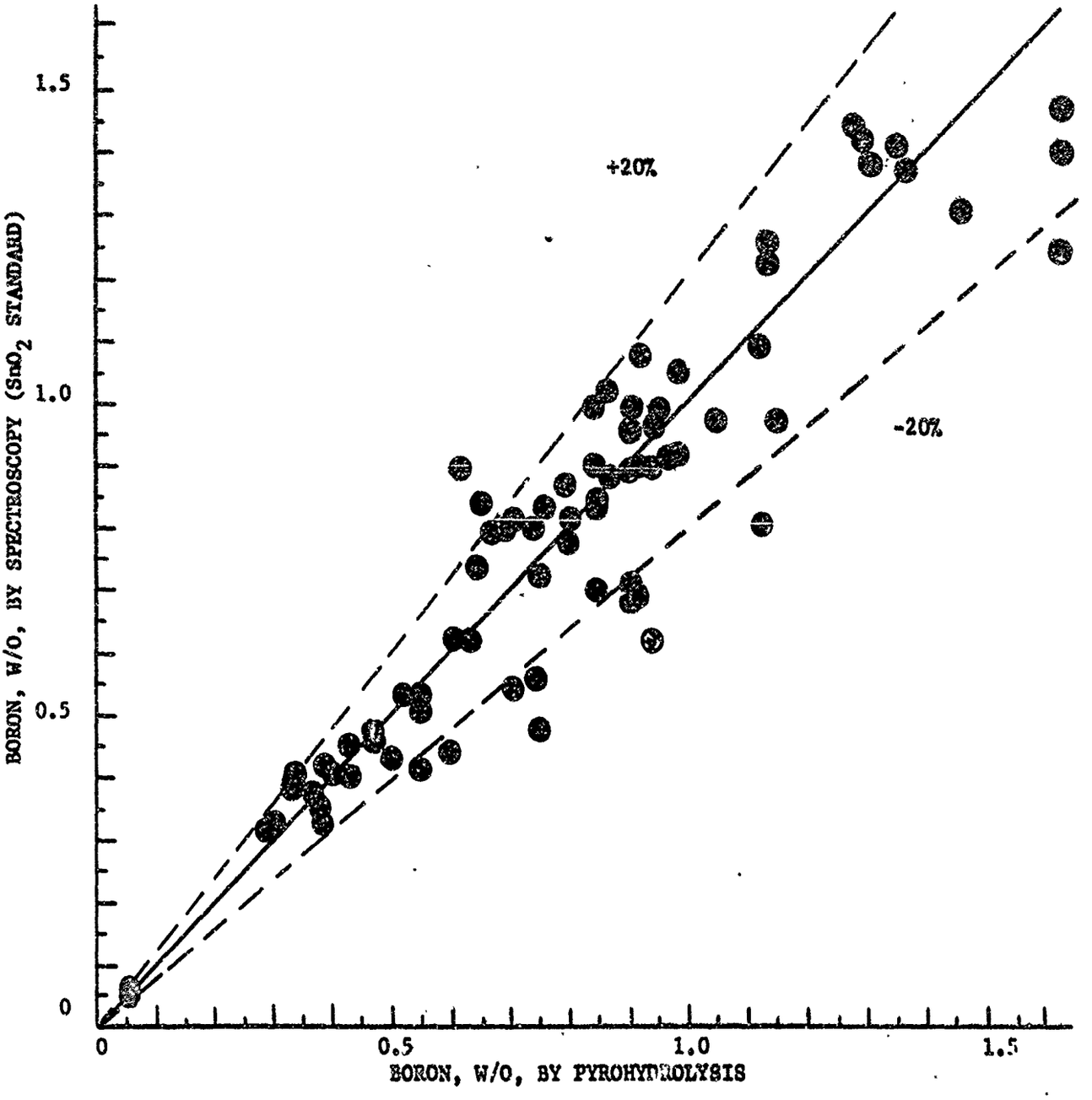


Figure 101



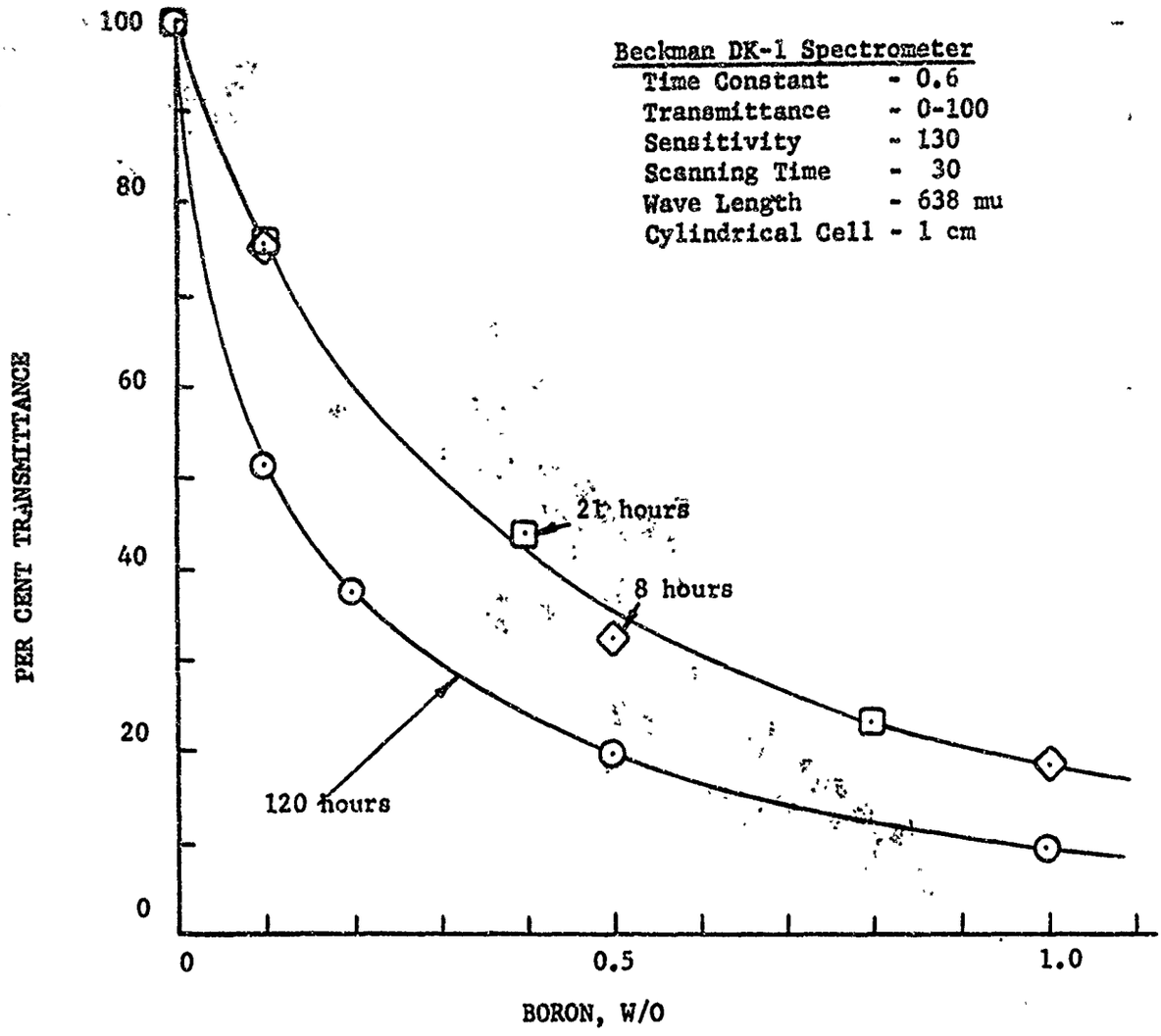
Unit cell height as a function of boron content in pyrolytic graphite as-deposited and after annealing; scatter in data is due in part to inaccuracies in boron assay by spectroscopy.

Figure 102



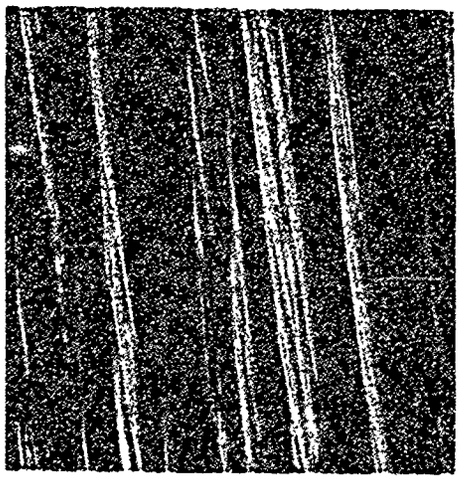
Comparison of data on the same samples by pyrohydrolysis and titration (1.4 gram samples) with data by emission spectroscopy with an internal standard (0.01 gram samples)

Figure 103

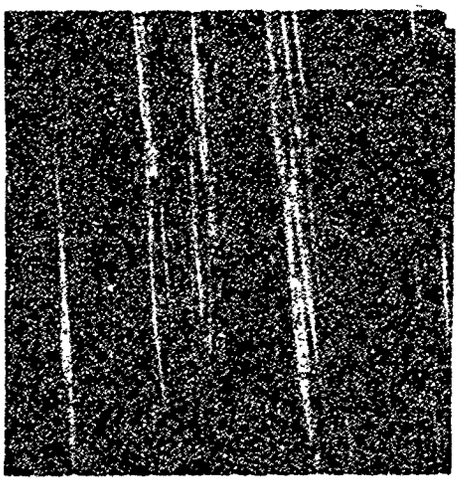


Standard curves for boron determination by the spectrophotometric method as a function of time of reaction between H_3BO_3 and HF. Azure C - tetrafluoborate complex is extracted with 25% CCl_4 in dichloroethane.

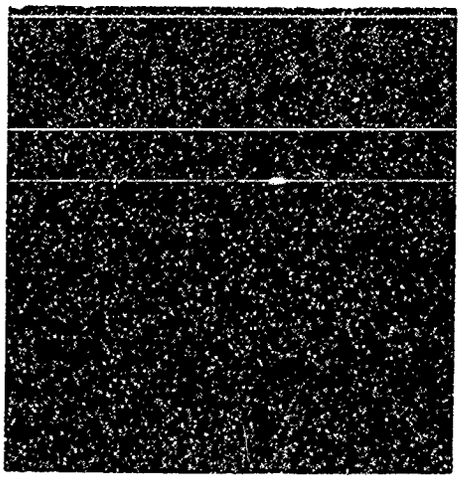
Figure 104



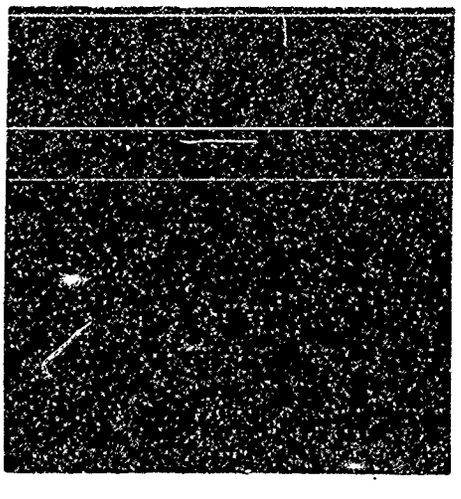
GEDC-3R



GEDC-6R



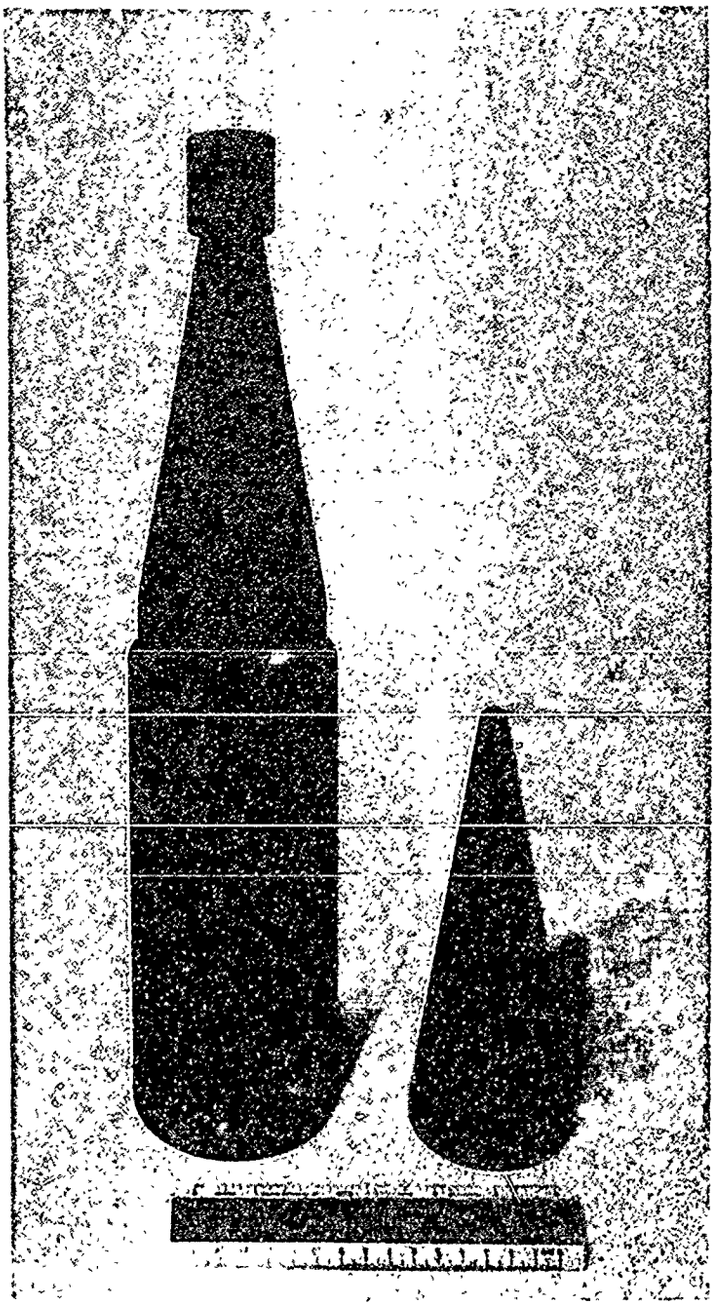
GEDC-7R



GEDC-8R

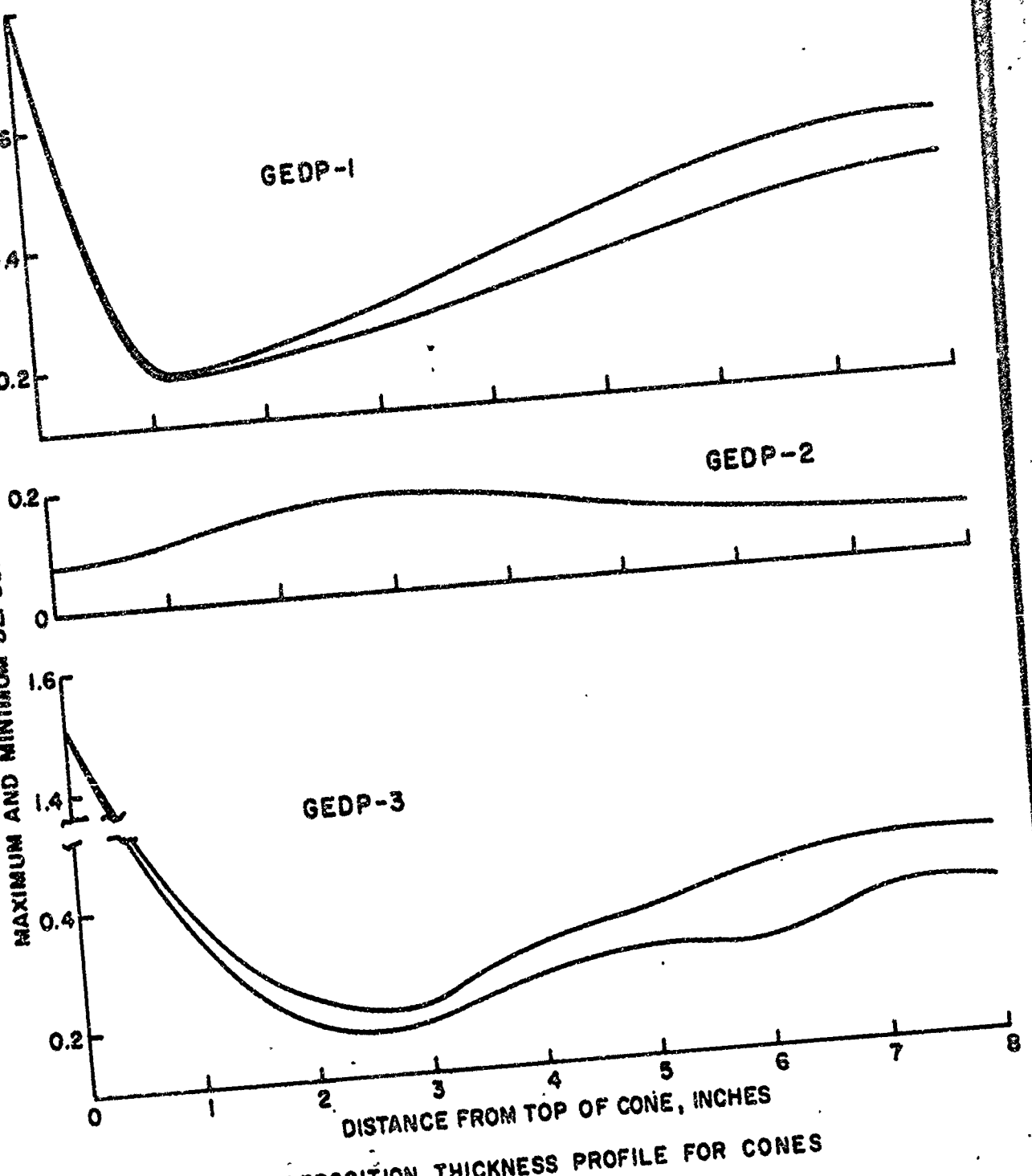
Typical Microstructures of Cylinders
Polarized Light, 100X Magnification.

Figure 105



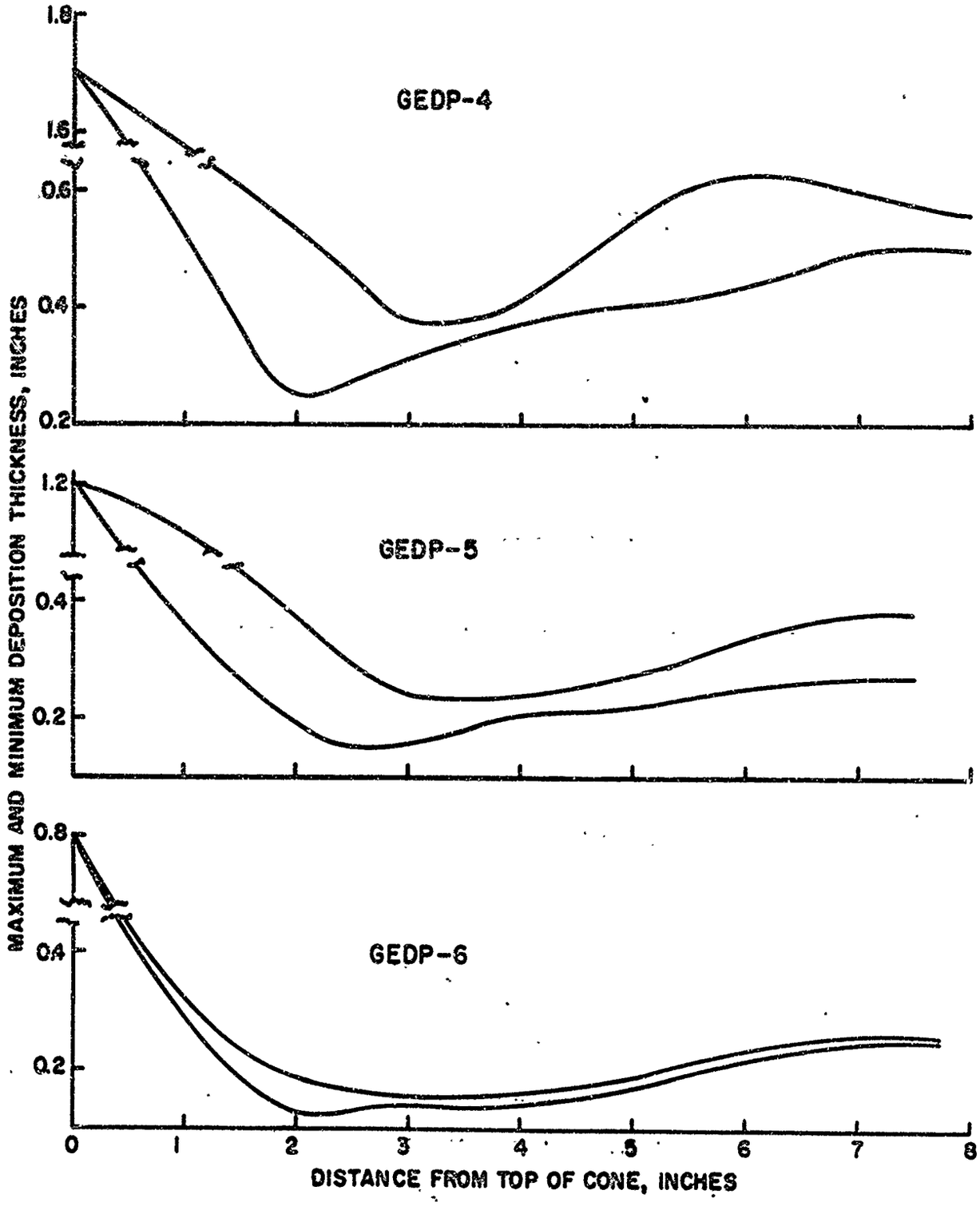
Photograph of Mandrel Assembly and
Typical Cone Deposited.

Figure 106

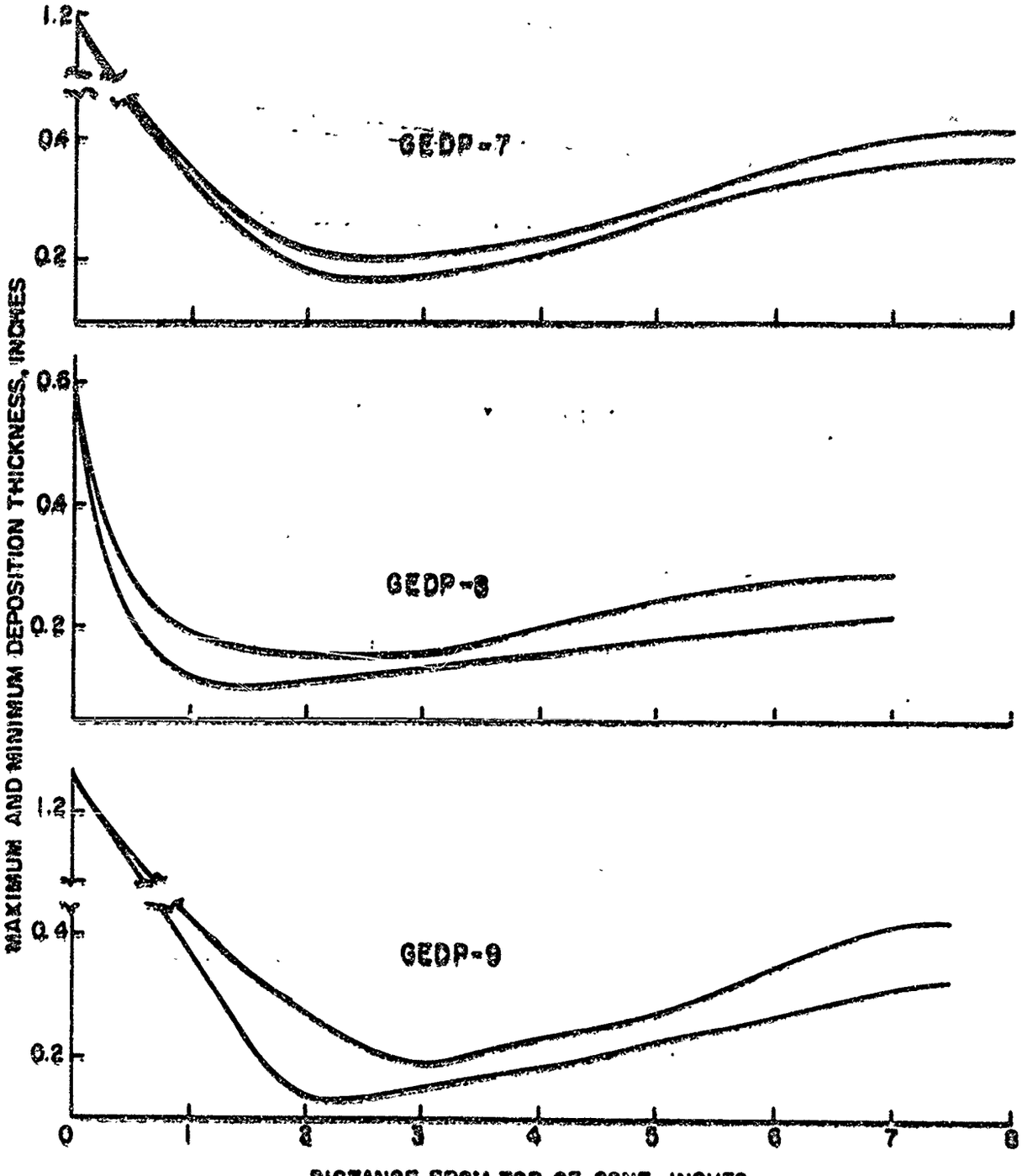


DEPOSITION THICKNESS PROFILE FOR CONES

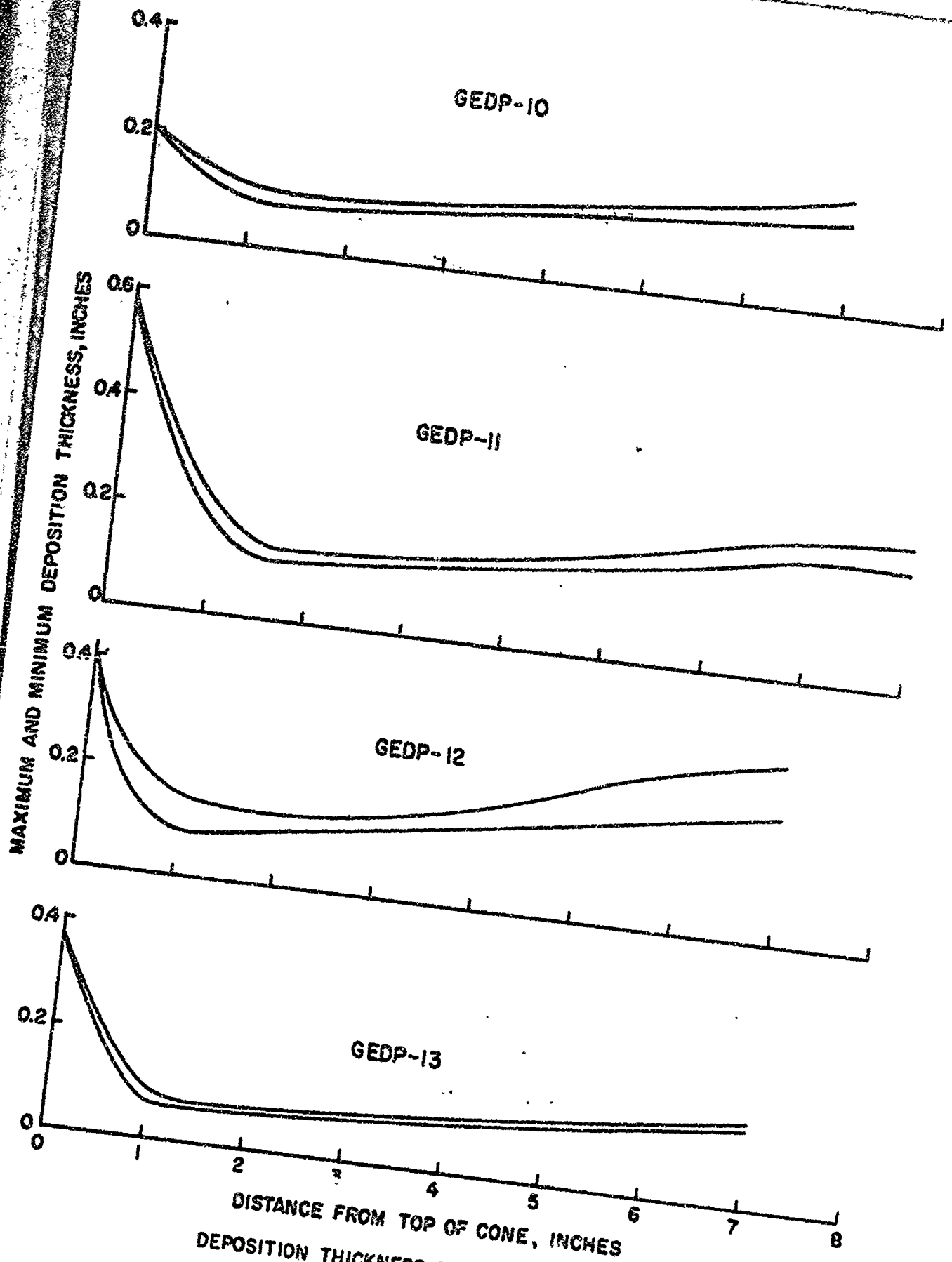
FIGURE 107



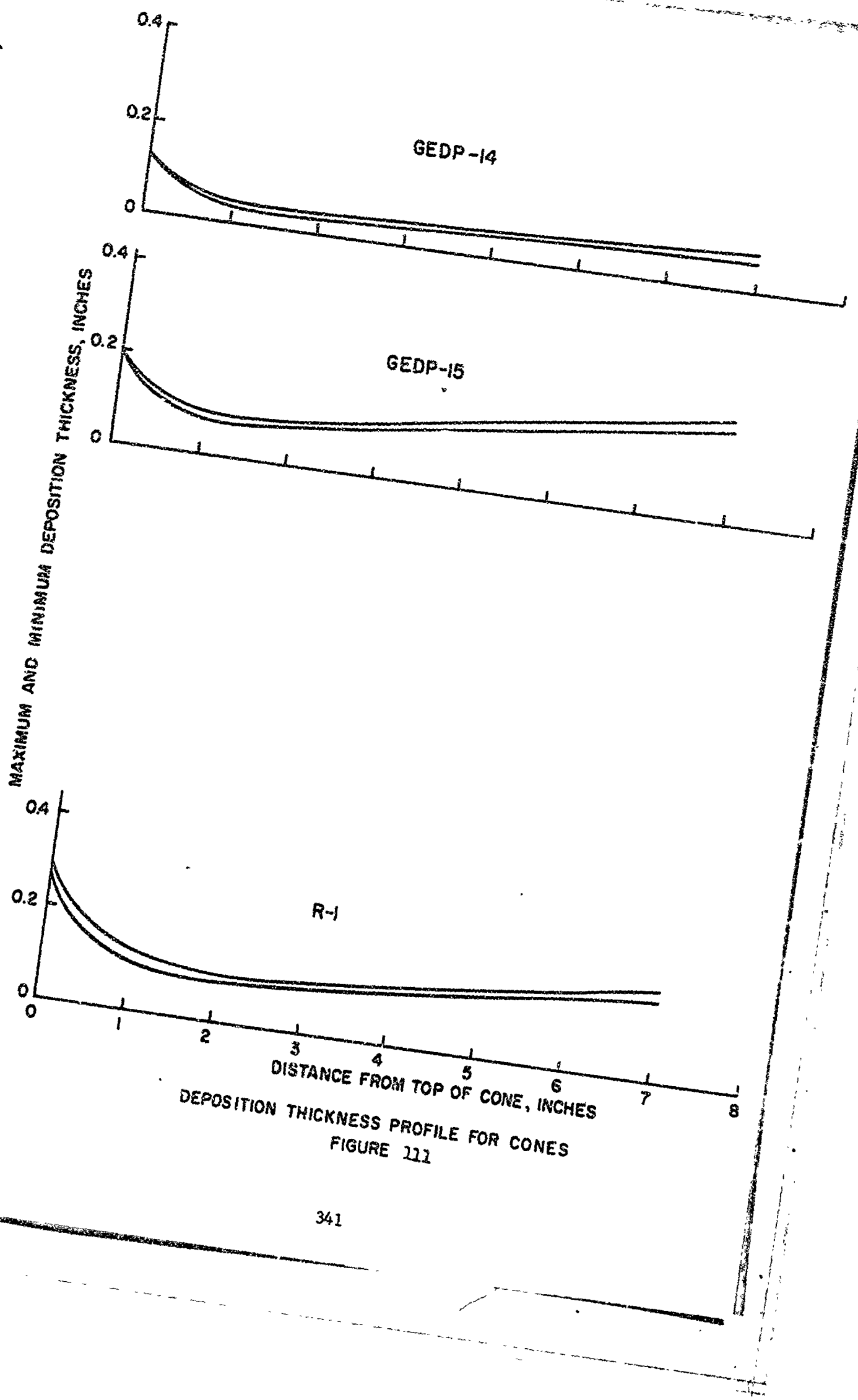
DEPOSITION THICKNESS PROFILE FOR CONES
FIGURE 108



DEPOSITION THICKNESS PROFILE FOR CONES
FIGURE 109



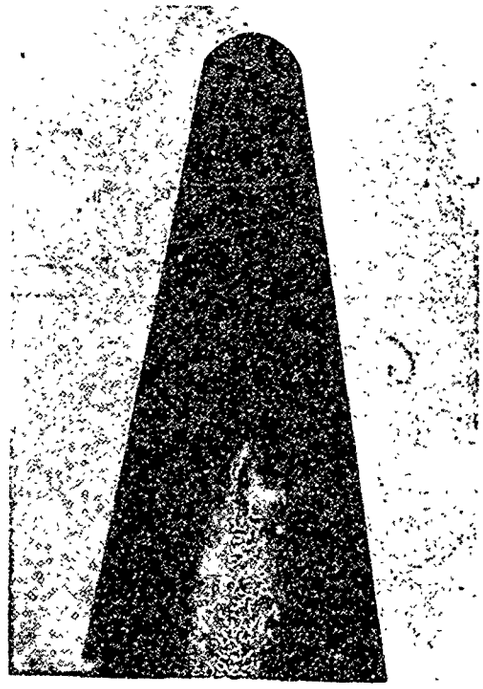
DEPOSITION THICKNESS PROFILE FOR CONES
FIGURE 110



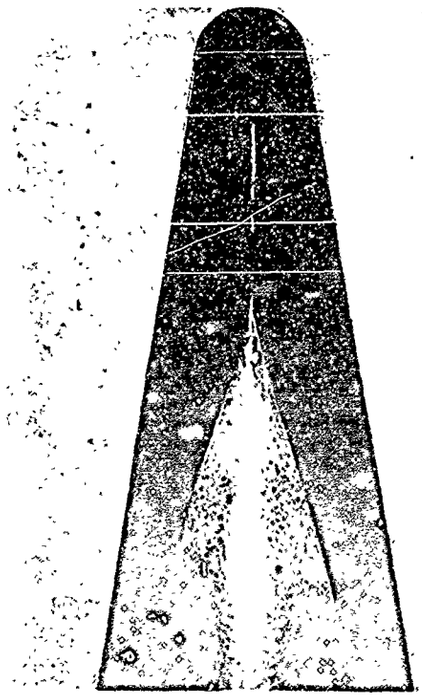
DEPOSITION THICKNESS PROFILE FOR CONES
FIGURE 111



GEDP-3



GEDP-4



GEDP-5



GEDP-6

Photographs of Polished Tip Sections.
Magnifications from 1 1/4 to 2X.

Figure 112



GEDP-1



GEDP-7



GEDP-8



GEDP-9

Photographs of Polished Tip Sections. Magnification ~1 1/4X

Figure 113



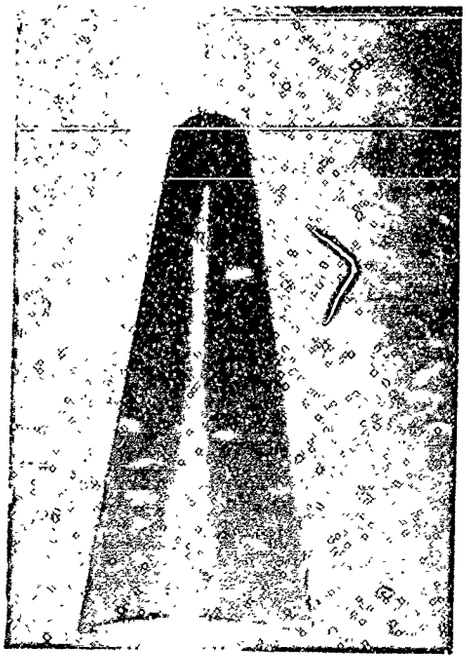
GEDP-10



GEDP-11



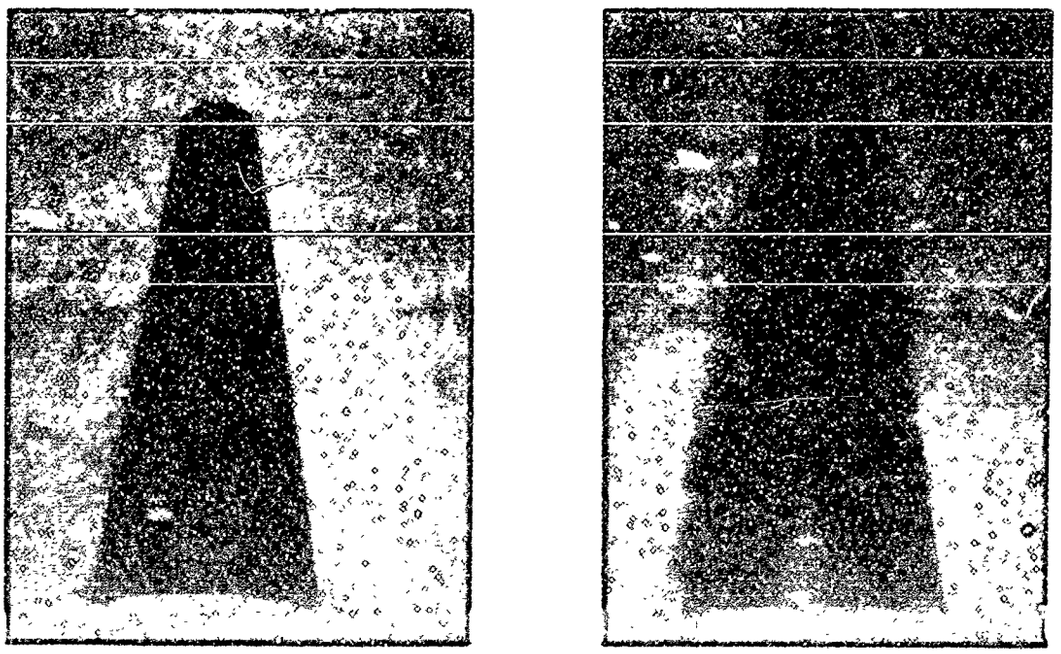
GEDP-12



GEDP-13

Photographs of Polished Tip Sections. Magnifications ~ 1 to 1 1/4X.

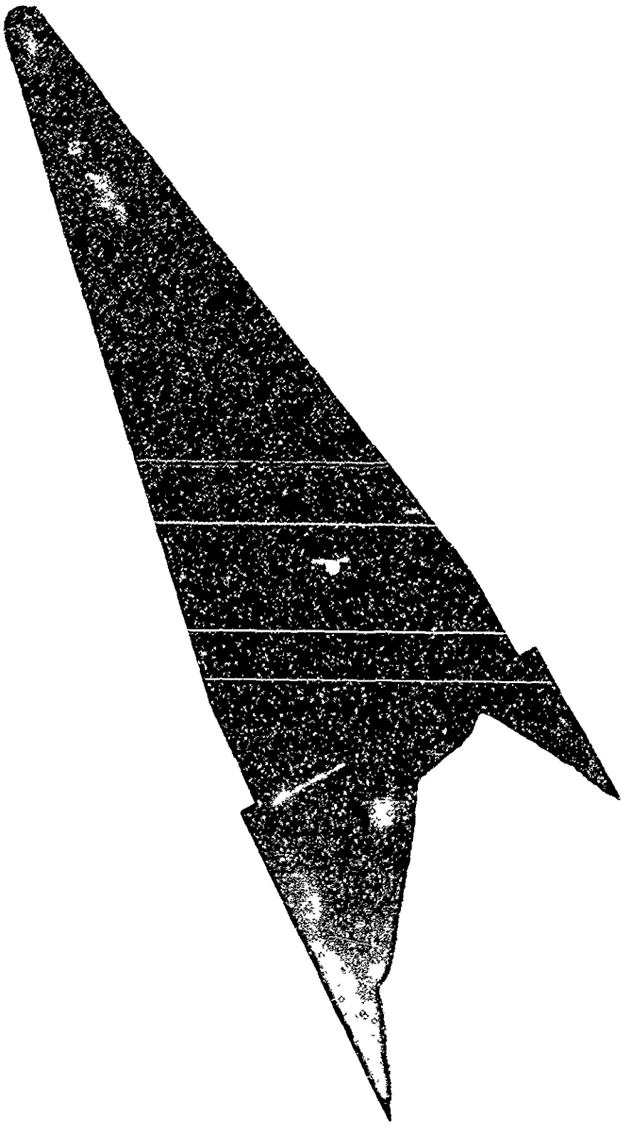
Figure 114



GEDP-15 R-1

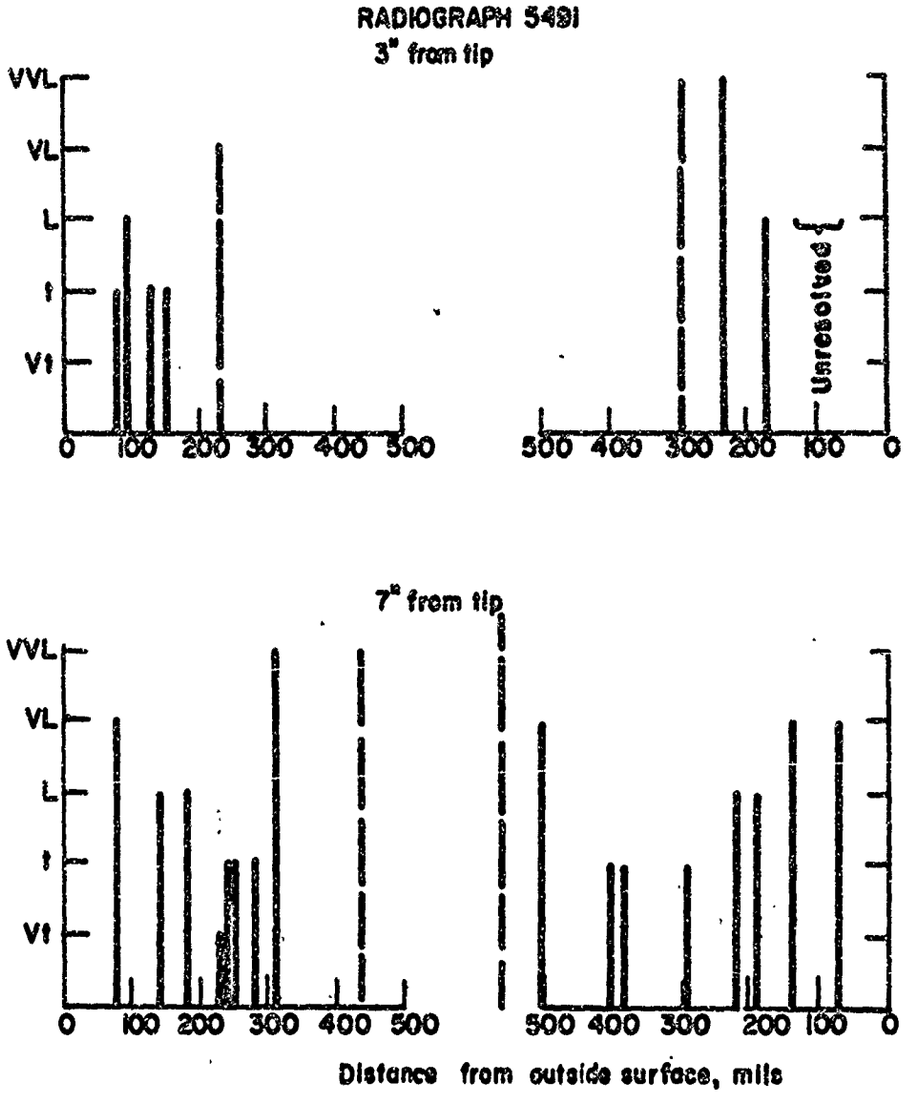
Photographs of Polished Tip Sections. Magnification ~ 1X.

Figure 115



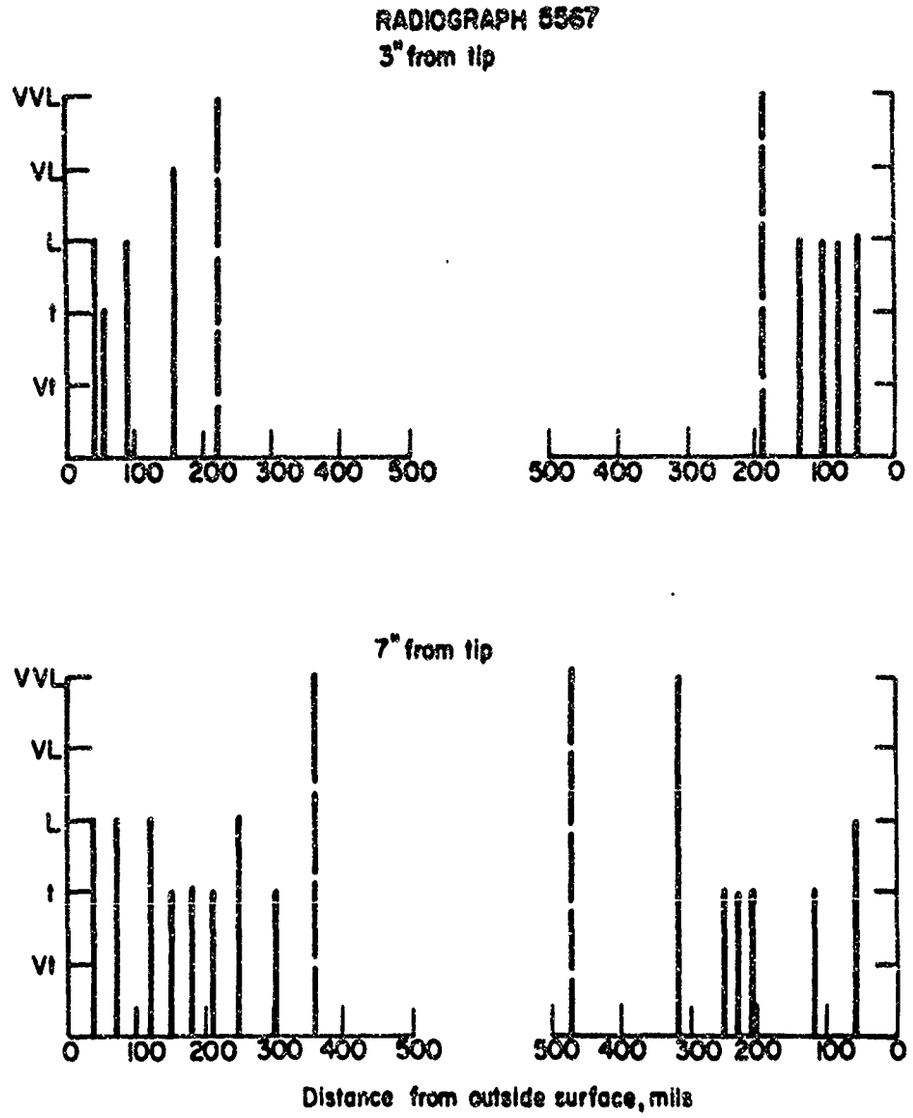
Photograph of GEDP-2

Figure 116



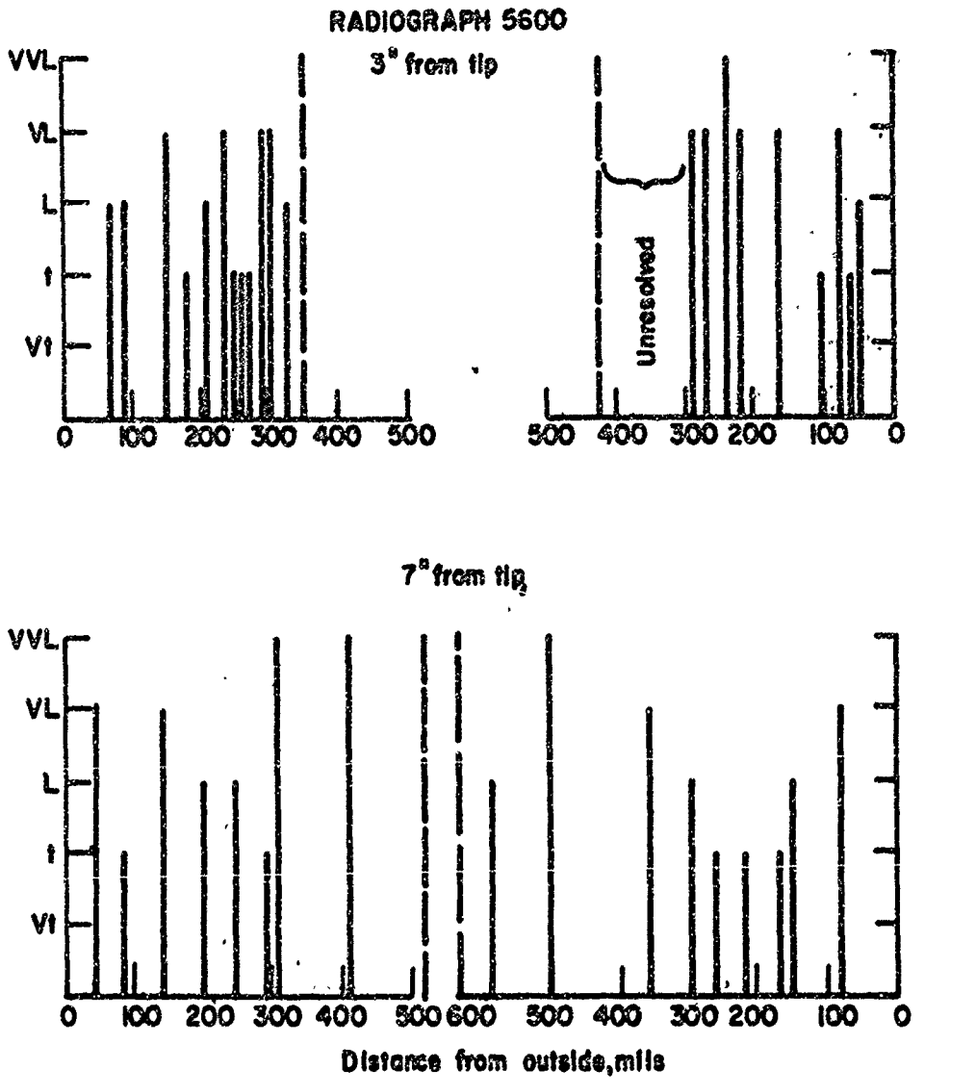
WALL DELAMINATION PROFILE FOR CONE GEDP-I

FIGURE 117



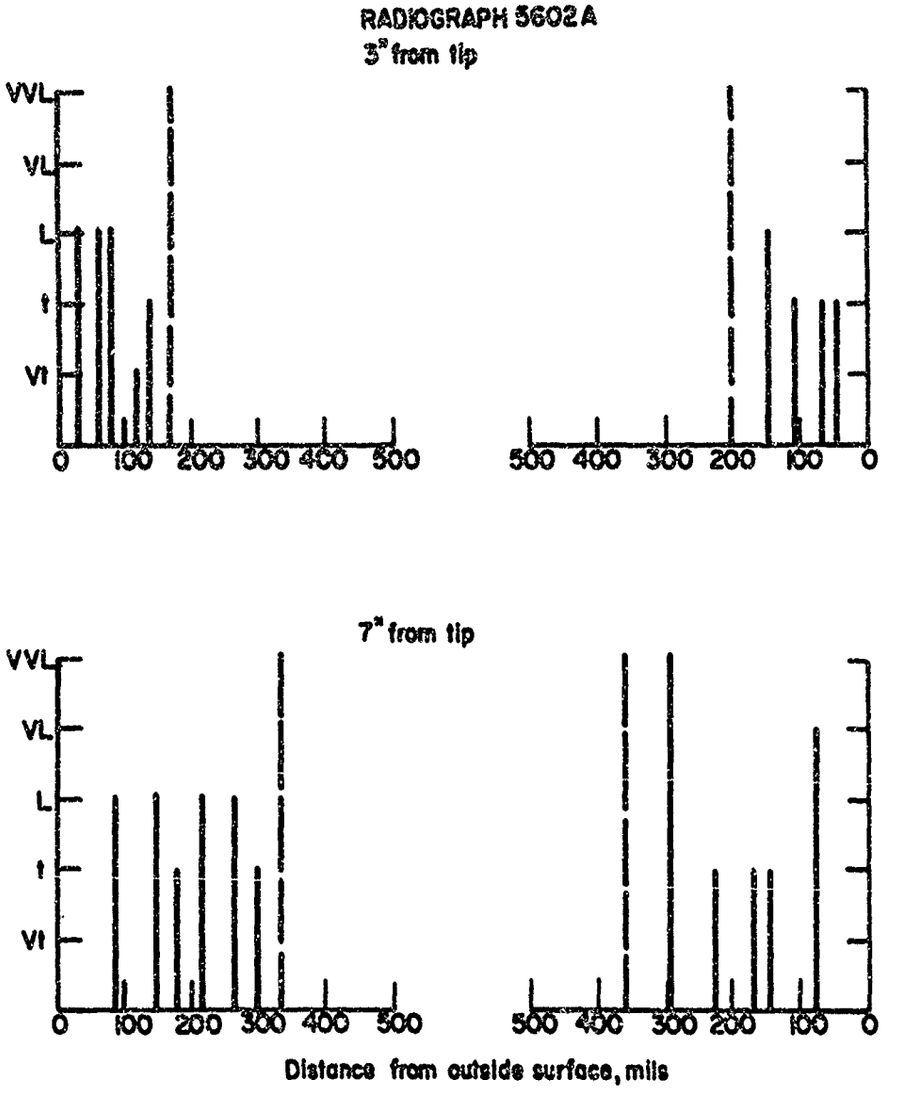
WALL DELAMINATION PROFILE FOR CONE GEDP-3

FIGURE 118



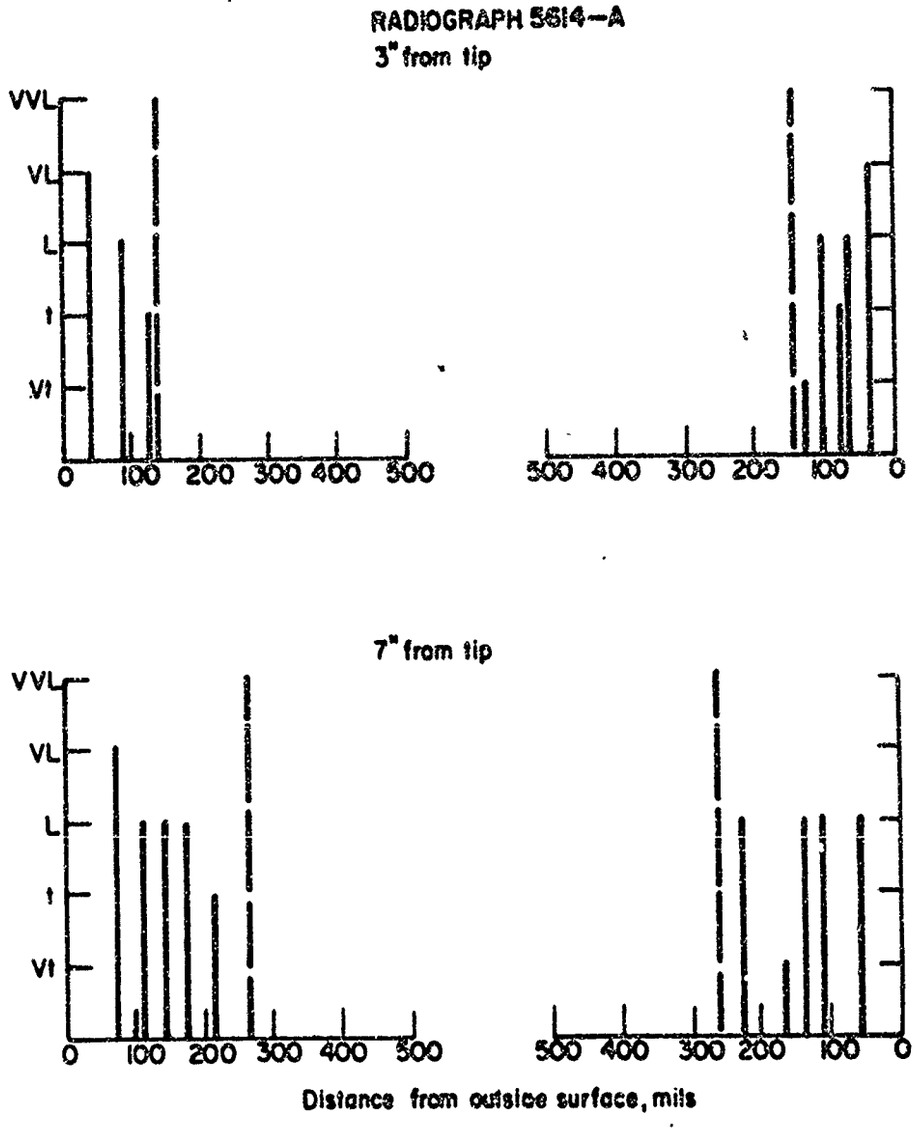
WALL DELAMINATION PROFILE FOR CONE GEDP—4

FIGURE 119



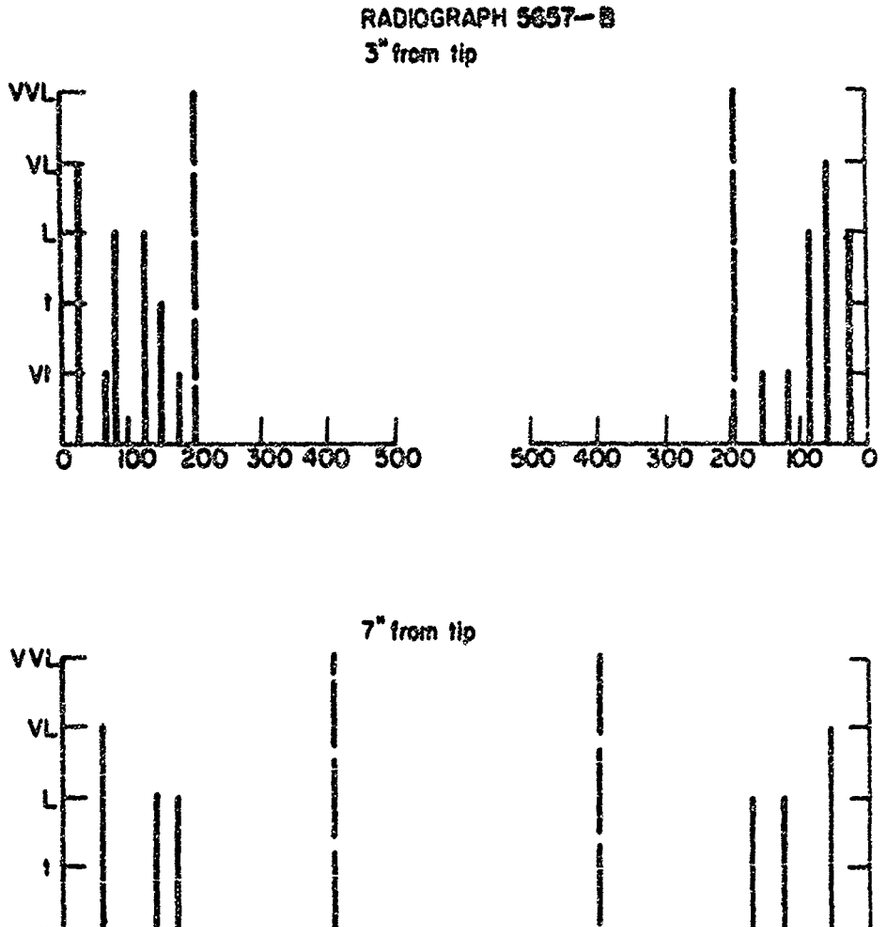
WALL DELAMINATION PROFILE FOR CONE GEDP-5

FIGURE 120



WALL DELAMINATION PROFILE FOR CONE GEDP—6

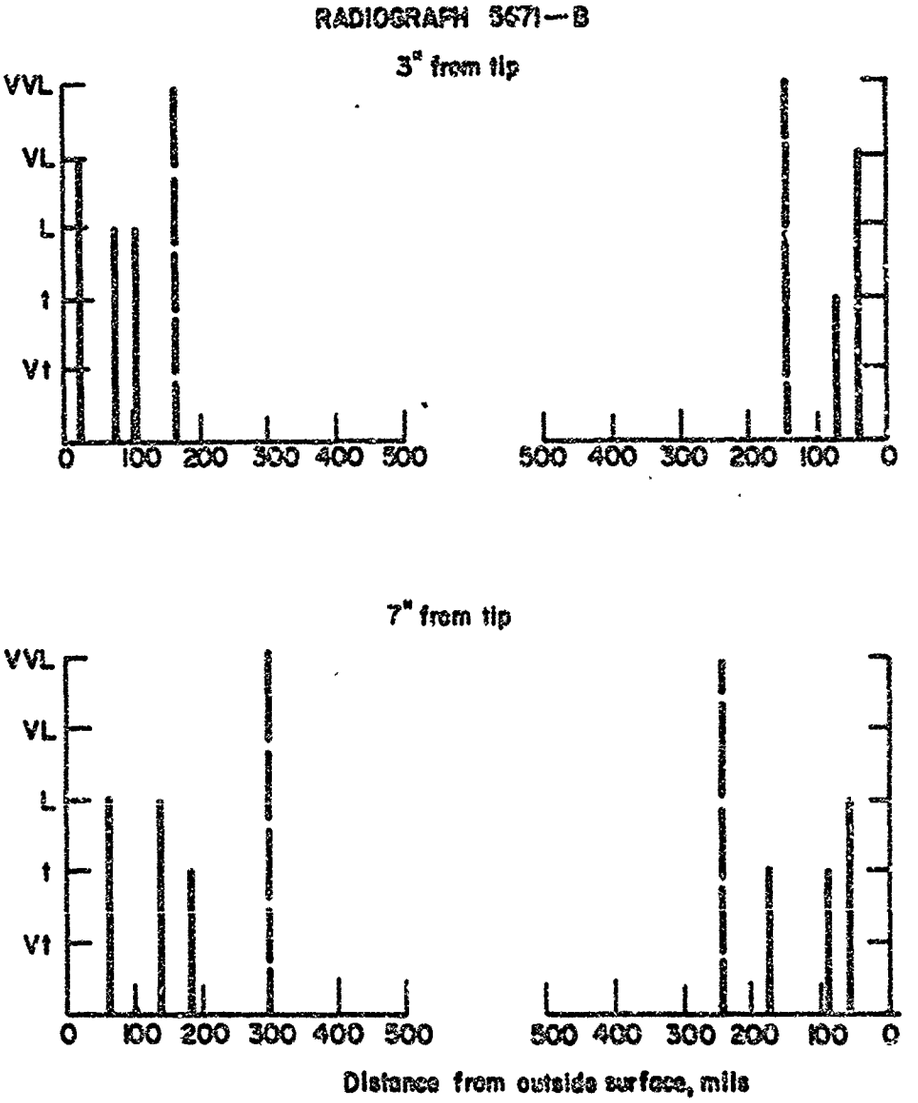
FIGURE 121



WALL DELAMINATION PROFILE FOR CONE GEDP–7

FIGURE 122

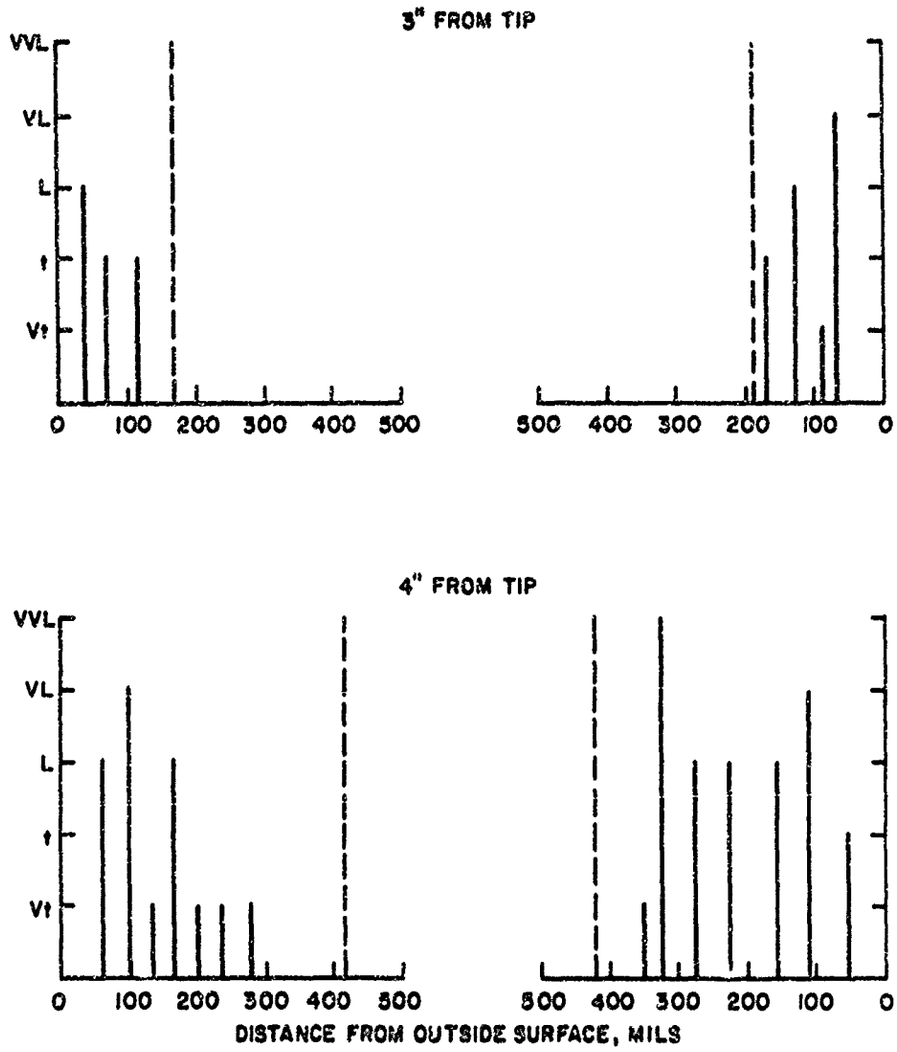
RADIOGRAPH 5671—B



WALL DELAMINATION PROFILE FOR CONE GEDP—8

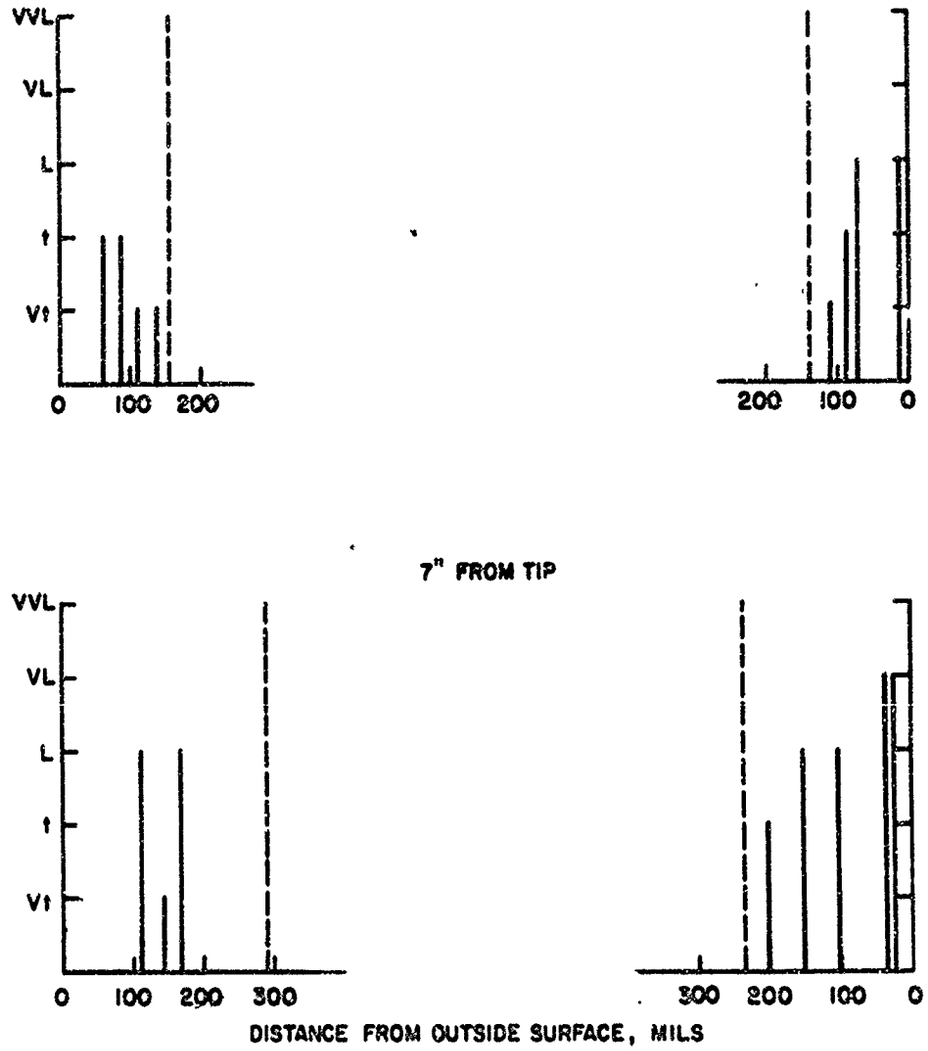
FIGURE 123

RADIOGRAPH 5709



WALL DELAMINATION PROFILE FOR CONE GEDP-9
FIGURE 124

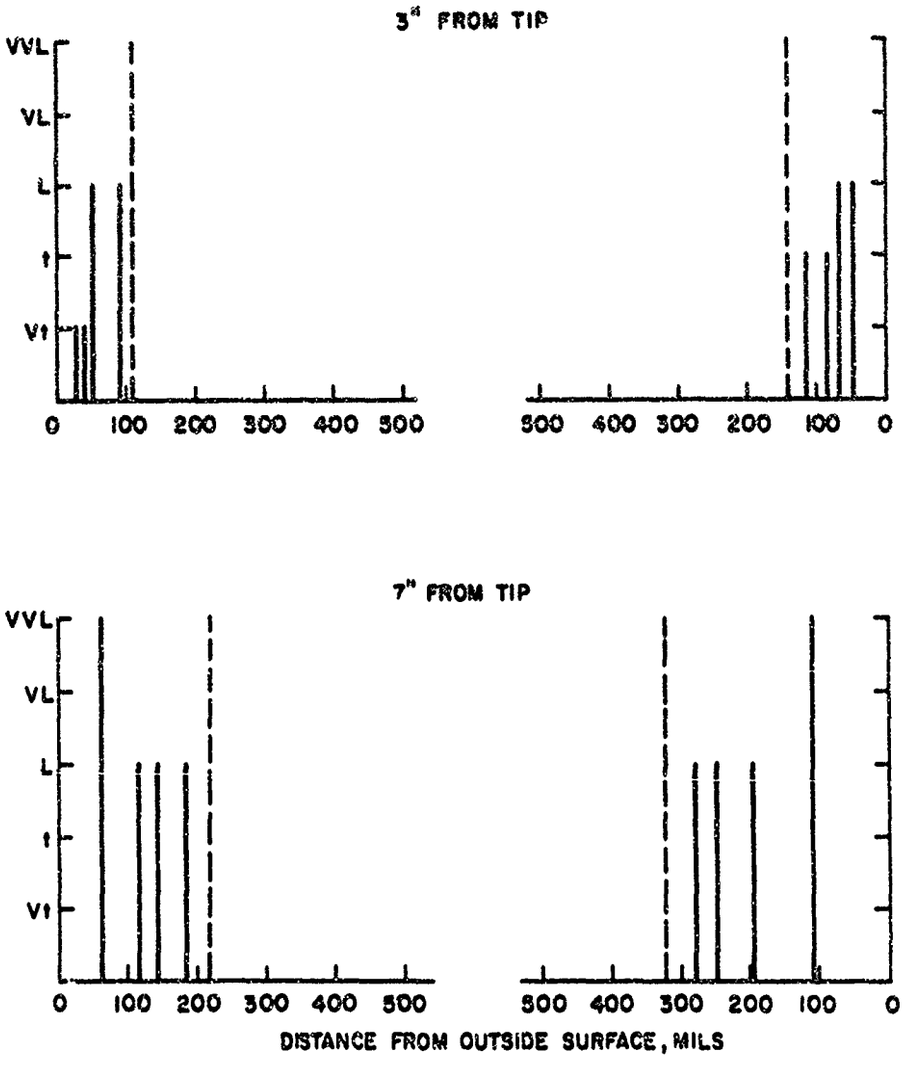
RADIOGRAPH 5739-A



WALL DELAMINATION PROFILE FOR CONE GEDP-11

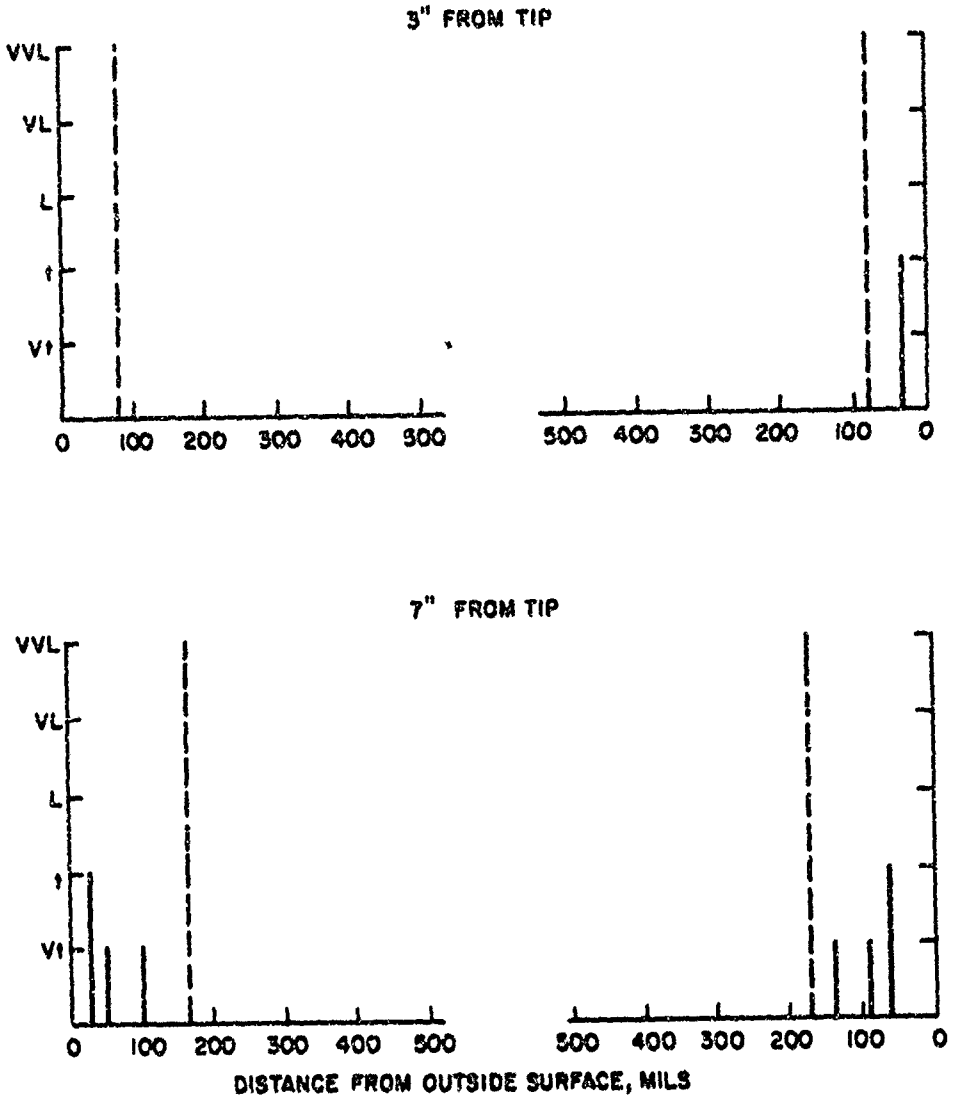
FIGURE 125

RADIOGRAPH 5776A



WALL DELAMINATION PROFILE FOR CONE GEDP-12
FIGURE 126

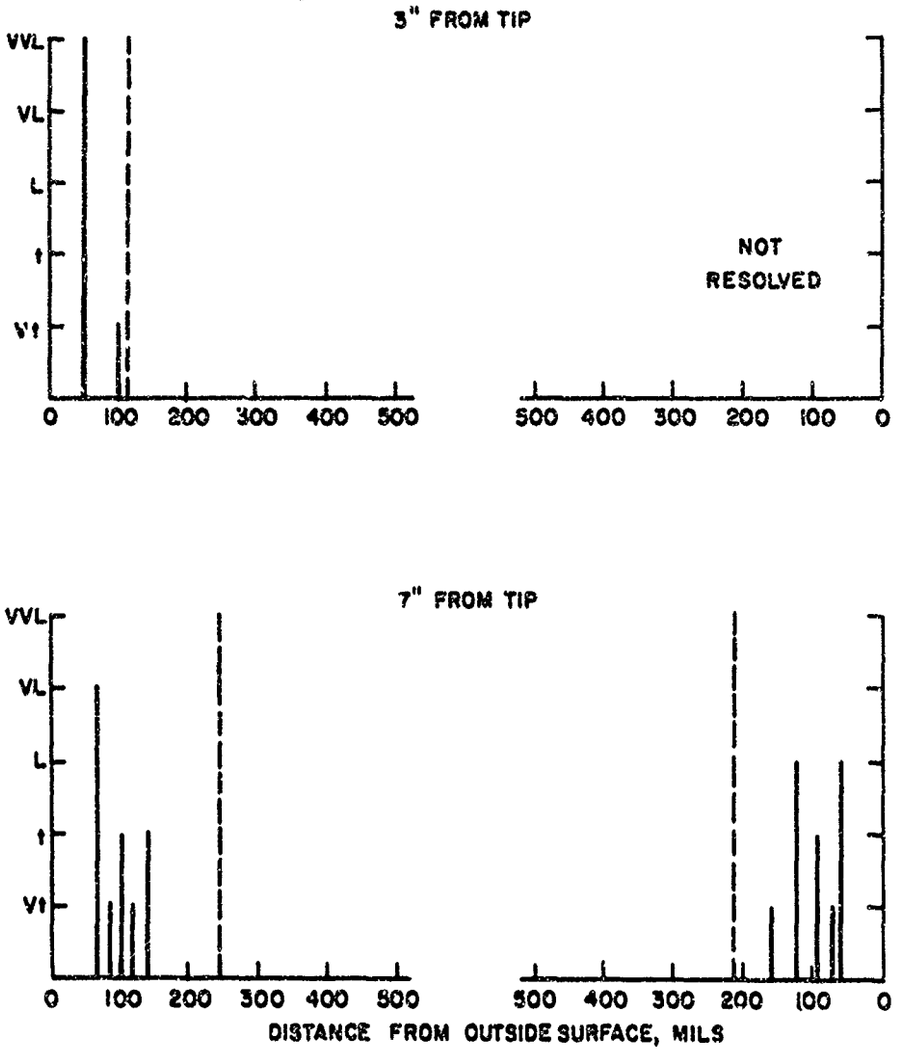
RADIOGRAPH 5787



WALL DELAMINATION PROFILE FOR CONE GEDP – 13

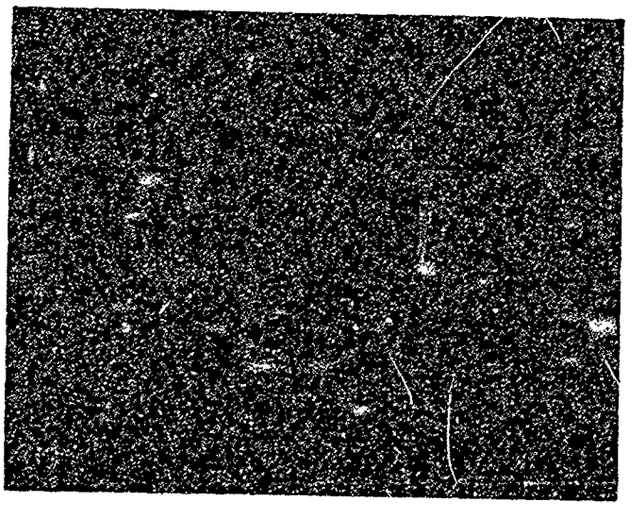
FIGURE 127

RADIOGRAPH 5799

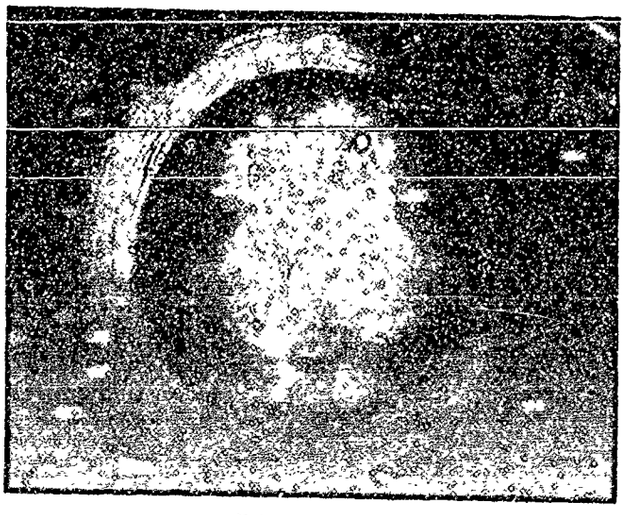


WALL DELAMINATION PROFILE FOR CONE GEDP– 15

FIGURE 128



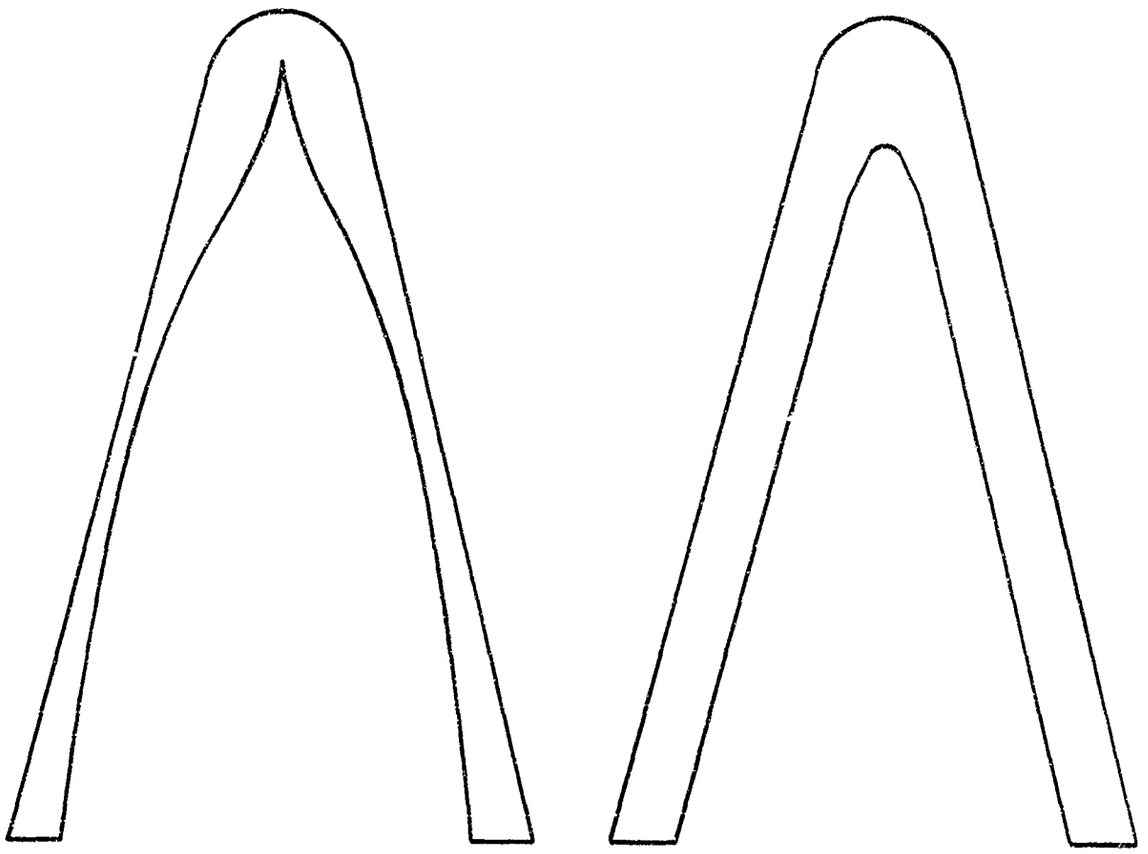
(a)



(b)

Photograph of Polished Sections of Cone GEDP-7 at a - 3 in. and b - 7 in. from tip showing Circumferential Delaminations.

Figure 129



a

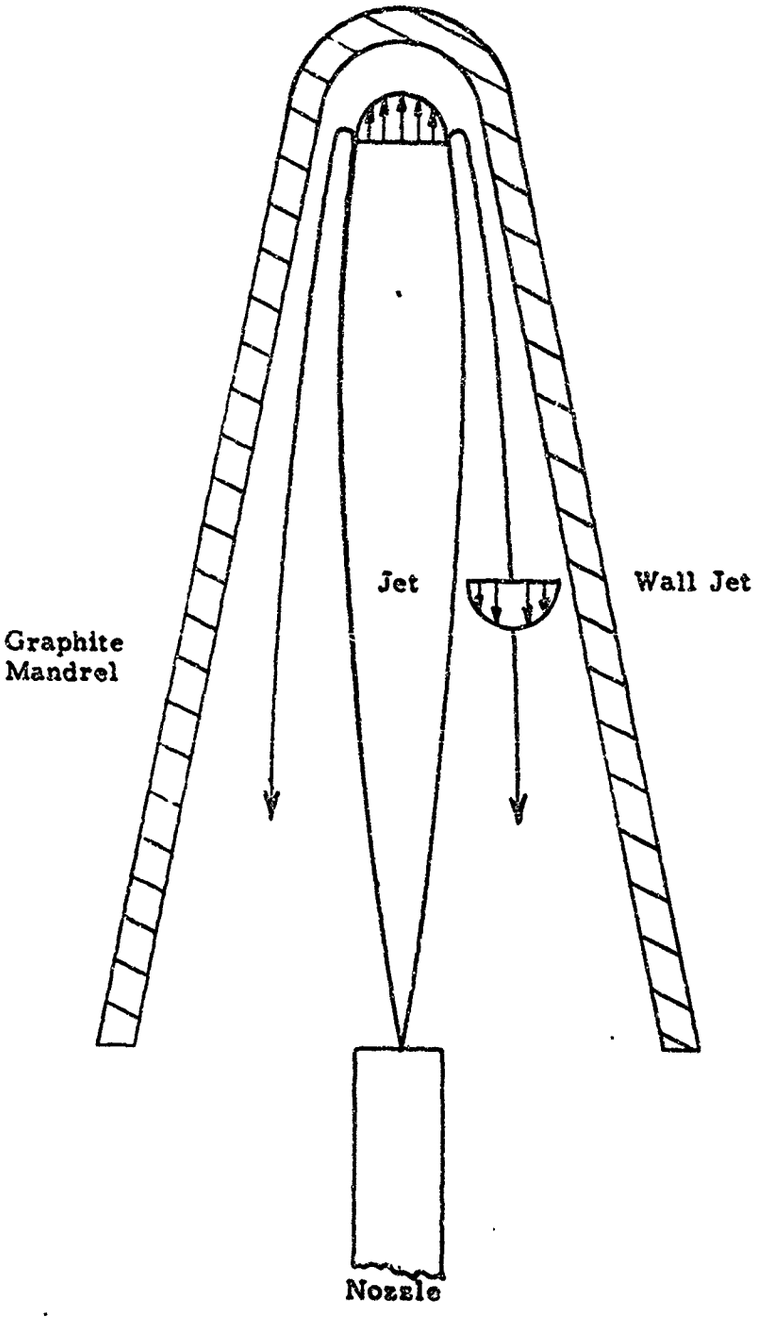
STATE-OF-ART GROWTH PROFILE

b

DESIRED GROWTH PROFILE

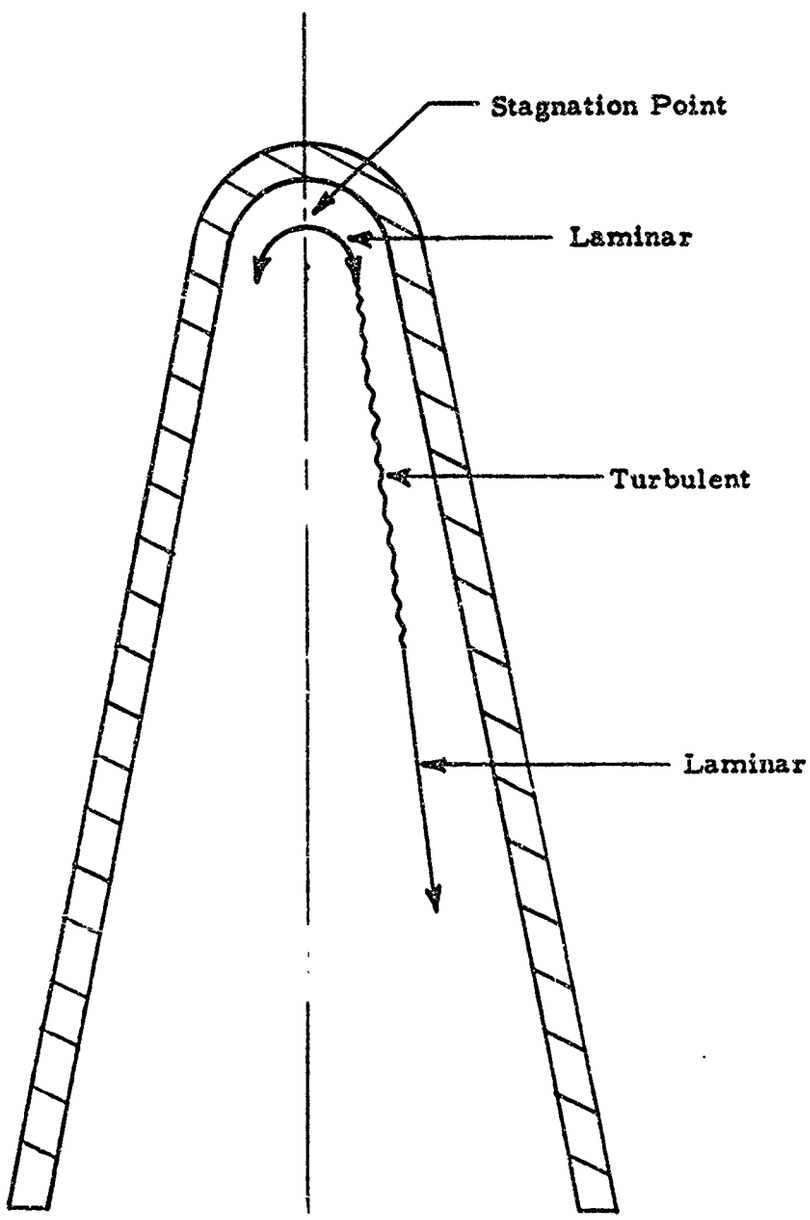
Schematic Diagrams of State of the Art and Desired Growth Profiles.

Figure 130



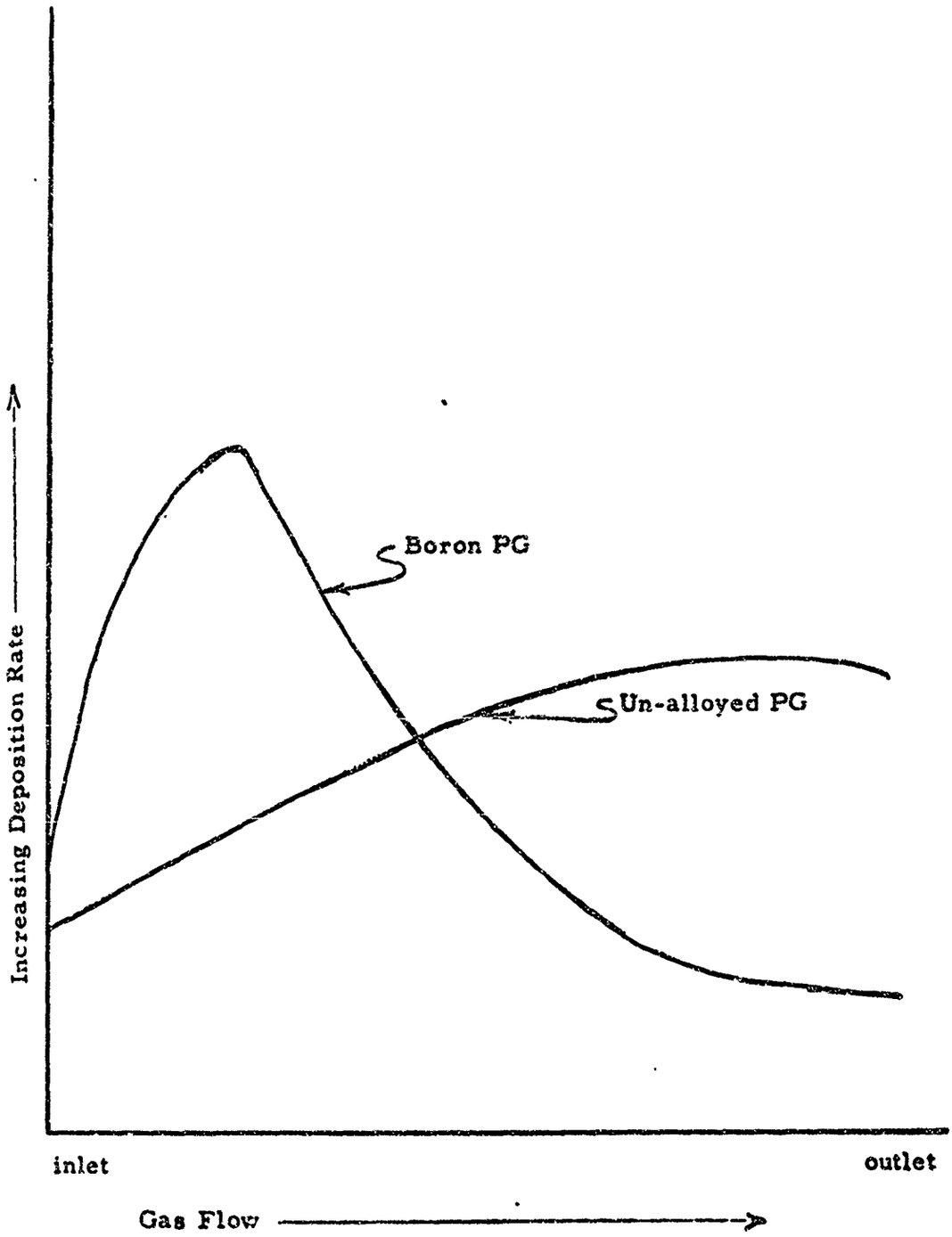
Schematic Diagram of Fluid Mechanics
Model of Pyrolytic Graphite Deposition

Figure 131



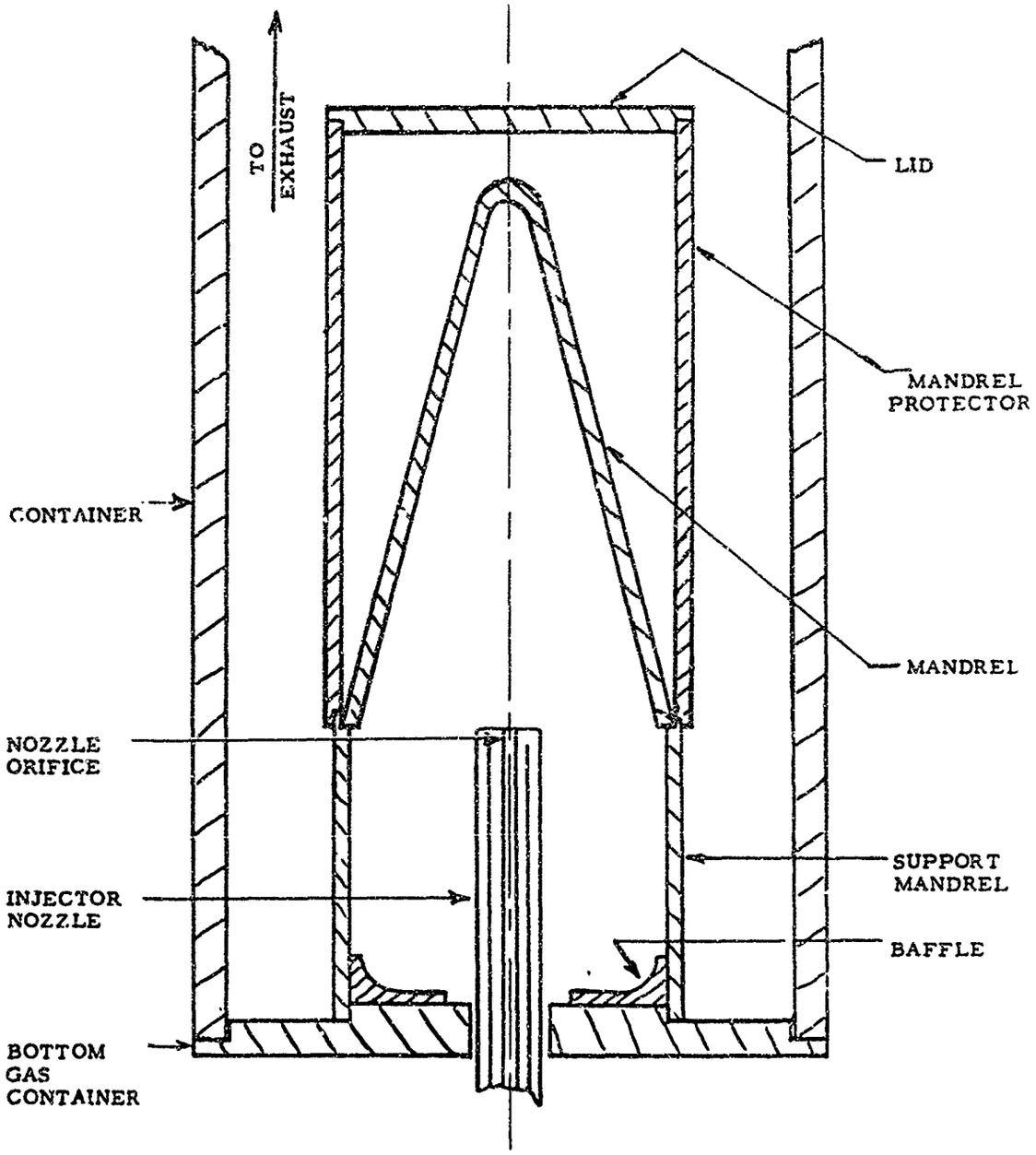
Local Wall Jet
Flow Regimes

Figure 132



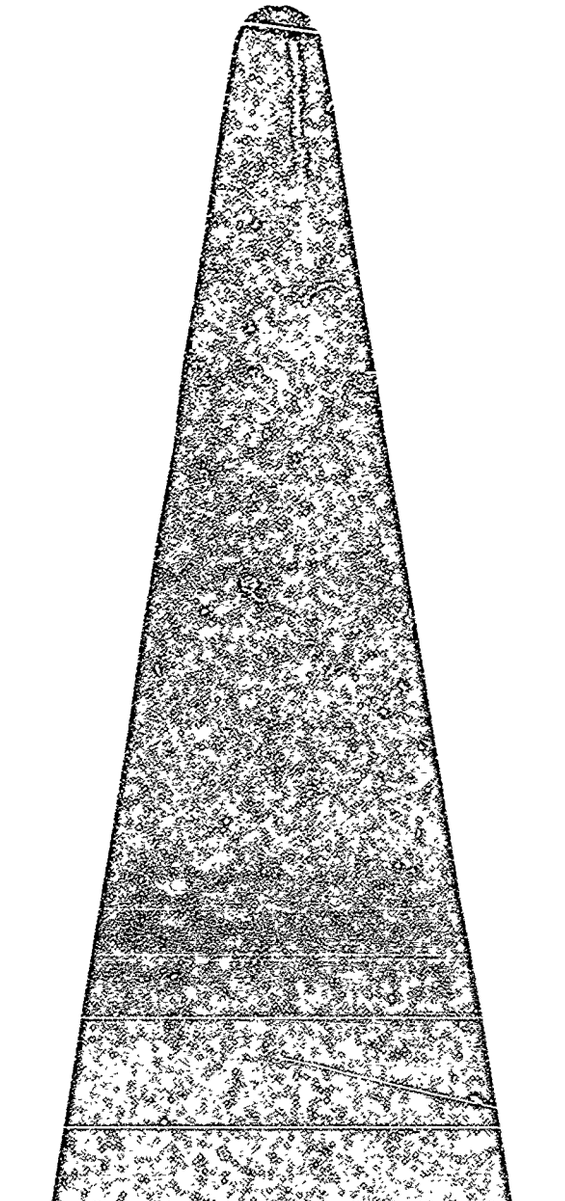
Schematic Diagram of Boron Catalytic
Effects on Pyrolytic Graphite Deposition

Figure 133



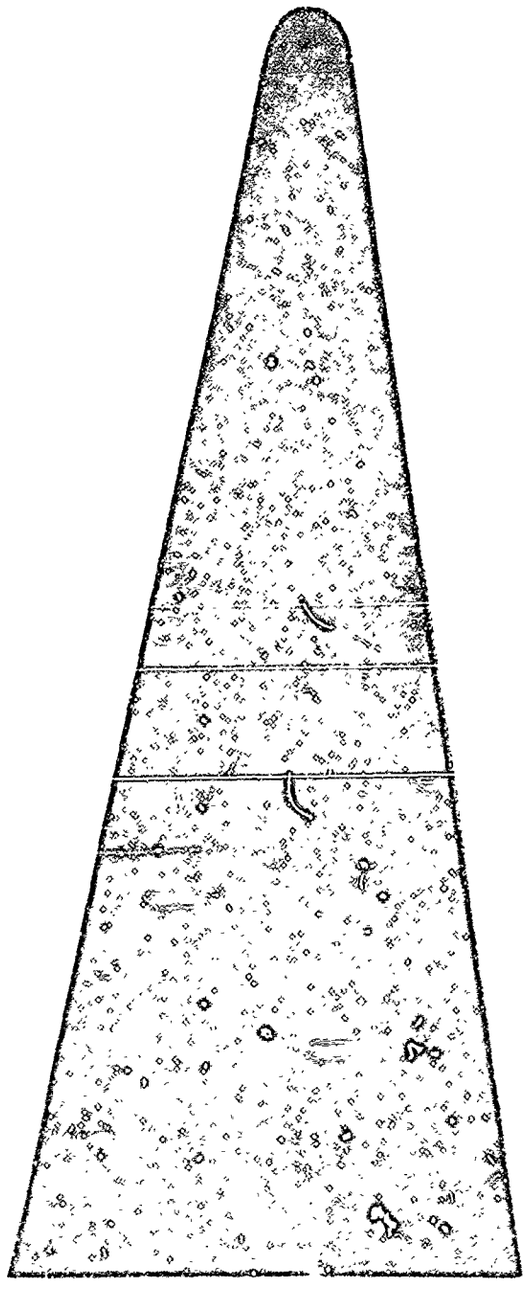
Furnace Set-up for all Nose Cone Tip Deposition Experiments

Figure 134

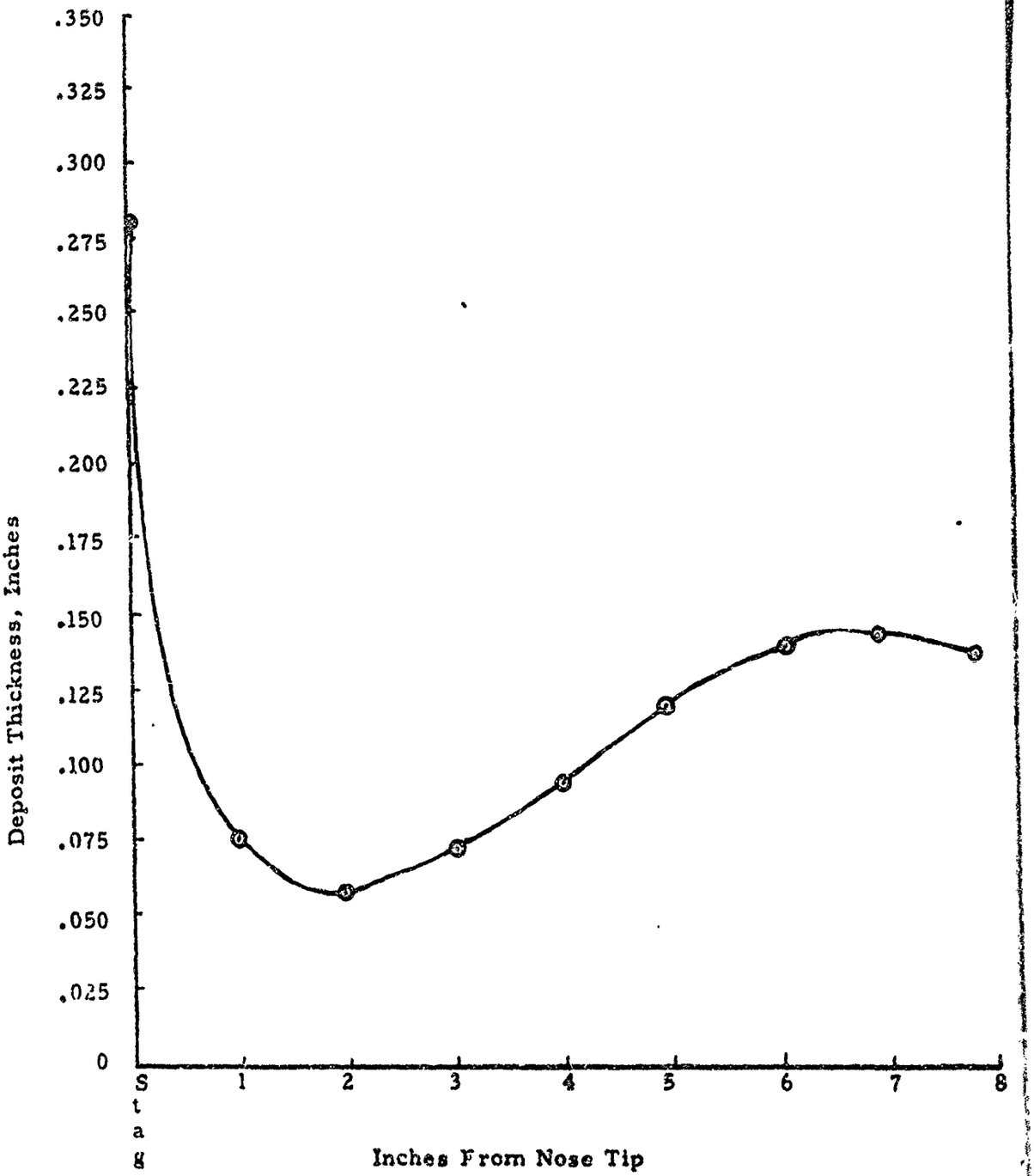


Photograph of Nose Cone Tip 3213-1

Figure 135

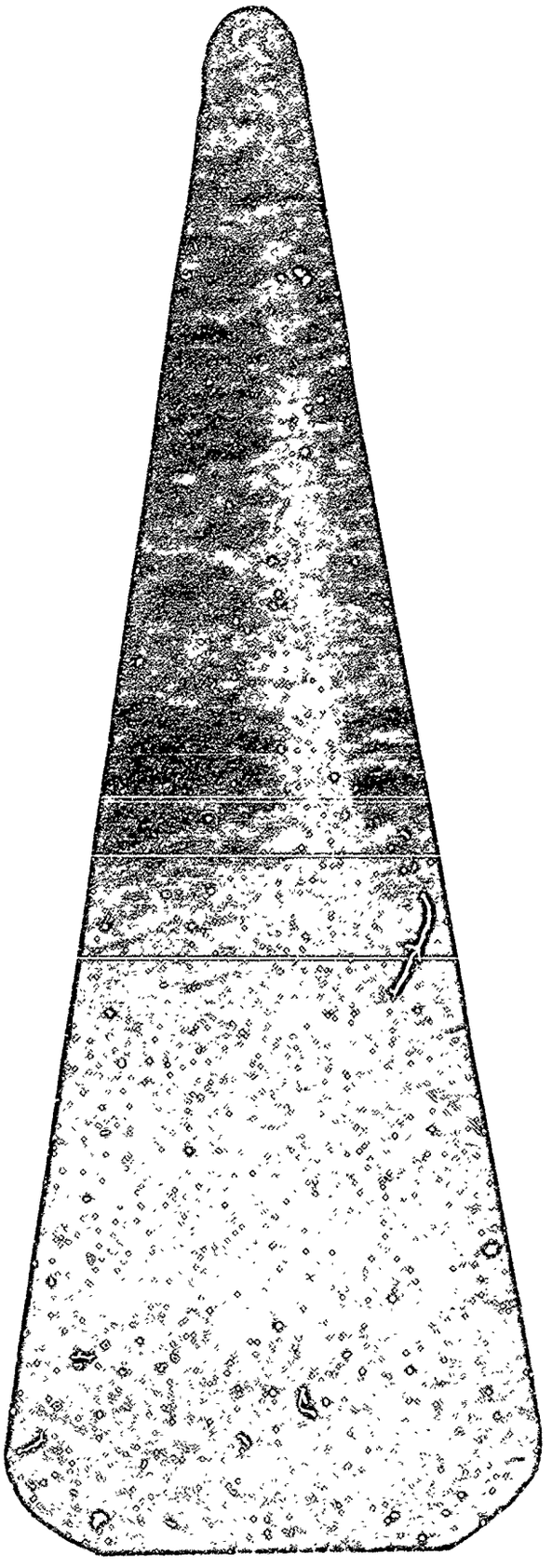


...tive Nose Cone Tip 3213-1
... Orifice 0.069"



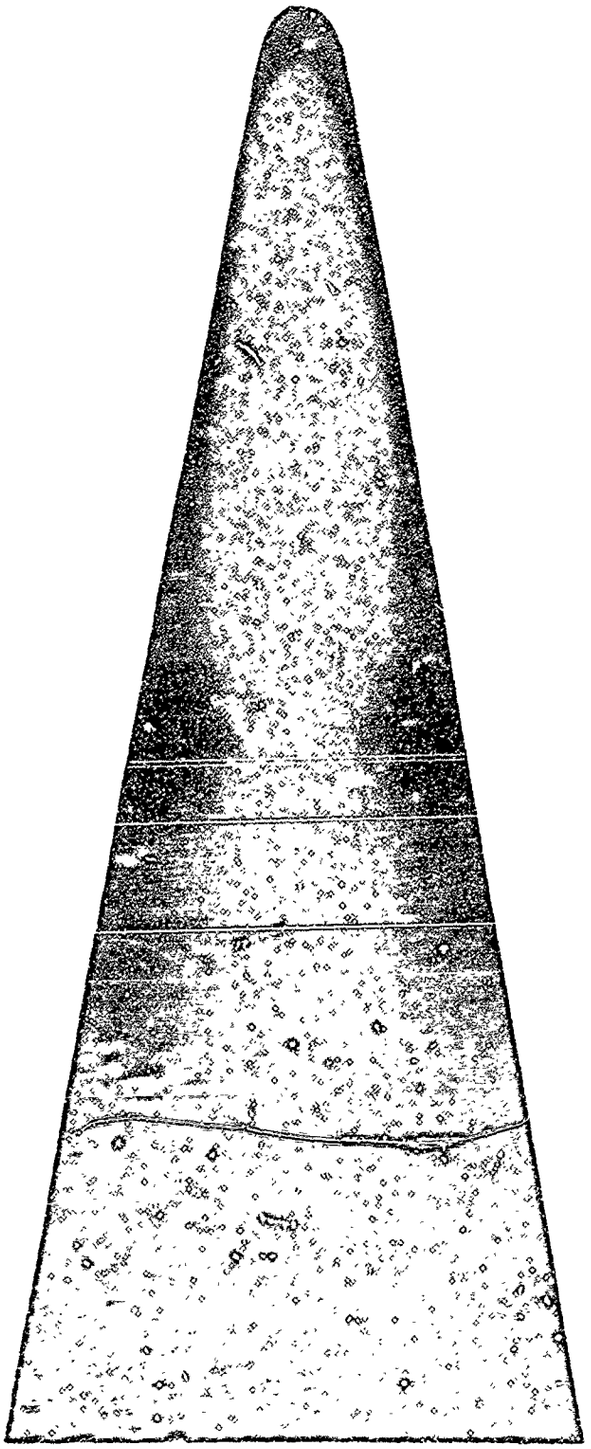
Deposit Profile Nose Cone Tip 3213-1
Base Line Run No. 1 Orifice 0.069"

Figure 137

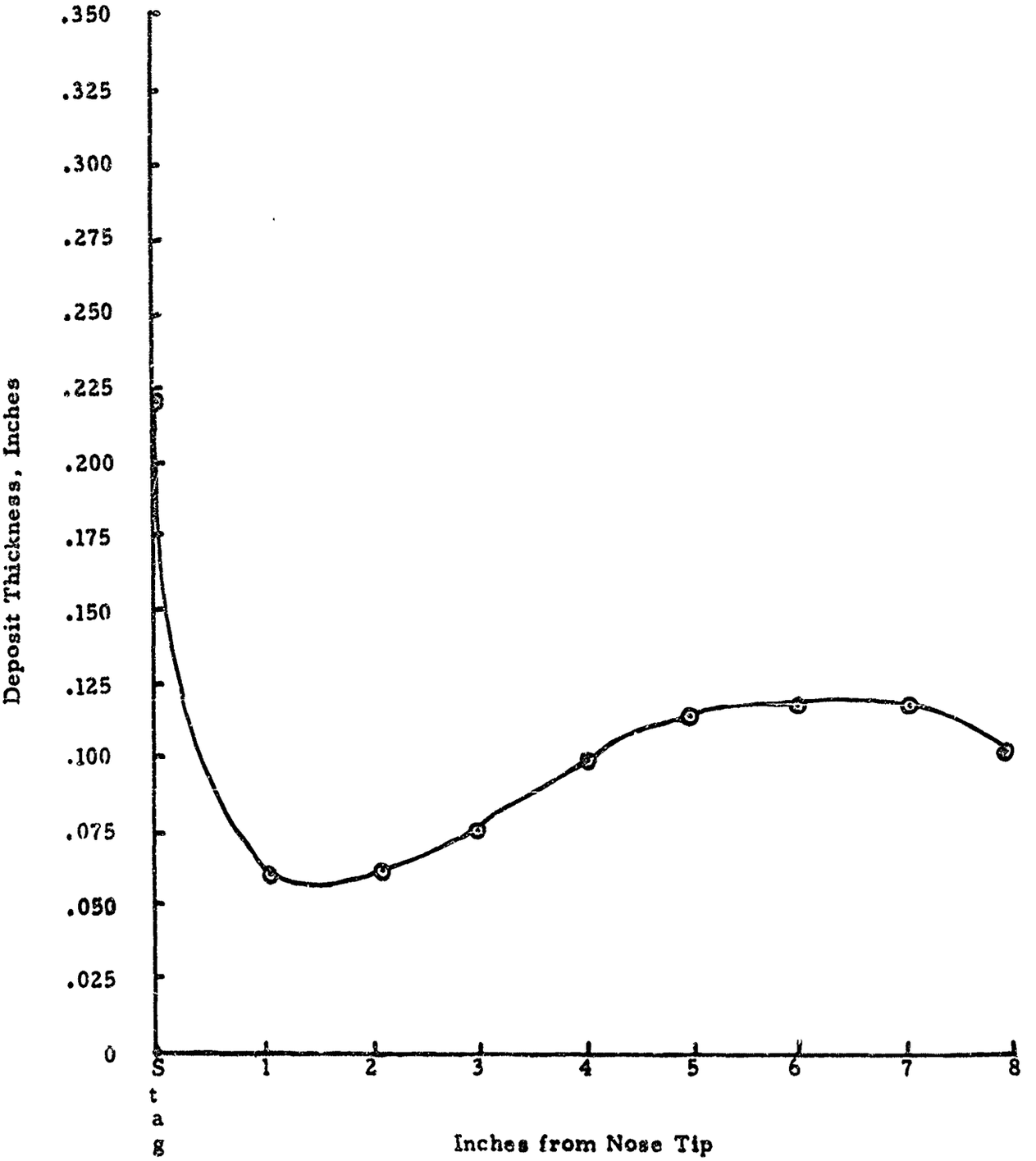


Photograph of Nose Cone Fin 3218-2

Figure [illegible]

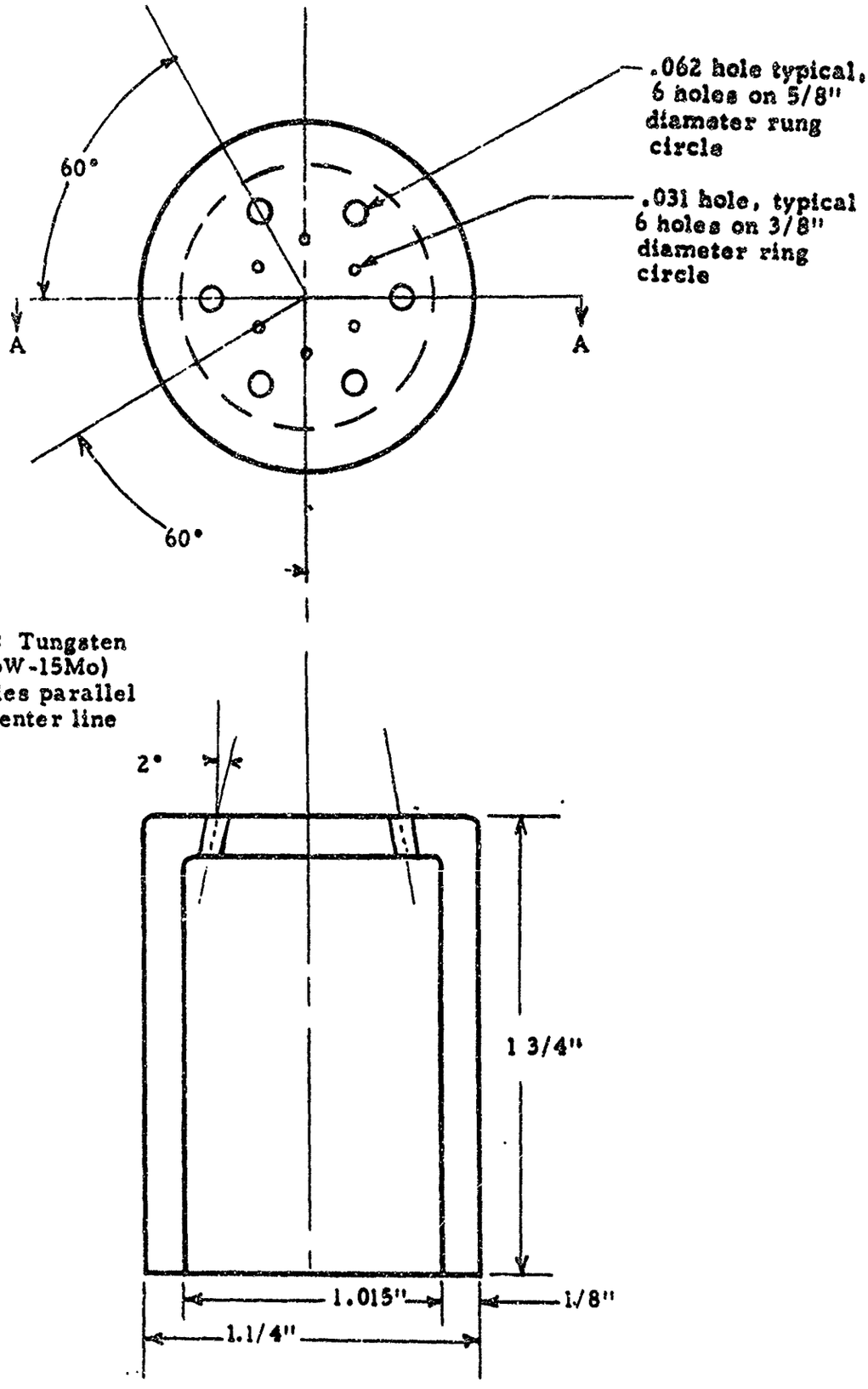


Radiographic Positive Nose Cone Tip 3213-2
Base Line Run 2 Nozzle Orifice 0.250"



Deposit Profile Nose Cone Tip 3213-2
Base Line Run No. 2 Orifice 0.250"

Figure 140



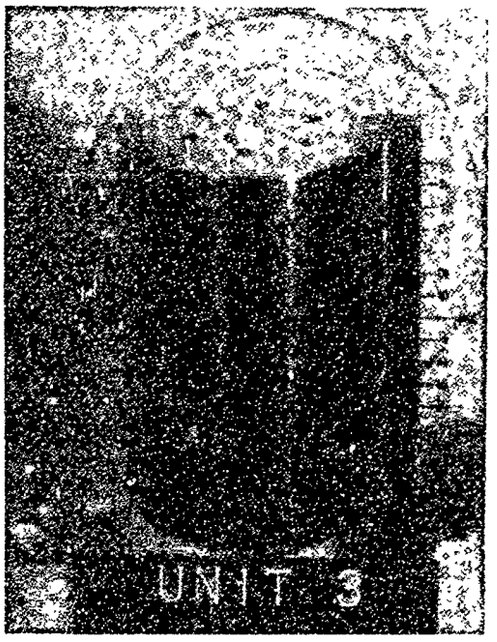
Notes:

(1) Material: Tungsten Alloy (85W-15Mo)
(2) .031" holes parallel to part center line

Section AA

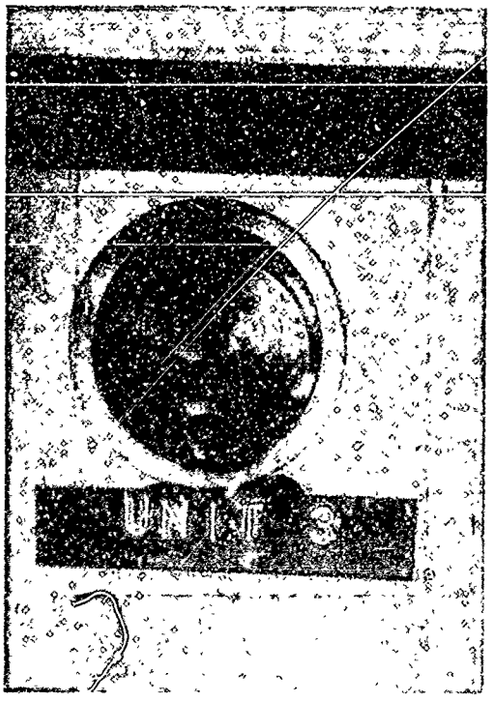
Nozzle Diffuser Cap No. 3

Figure 141



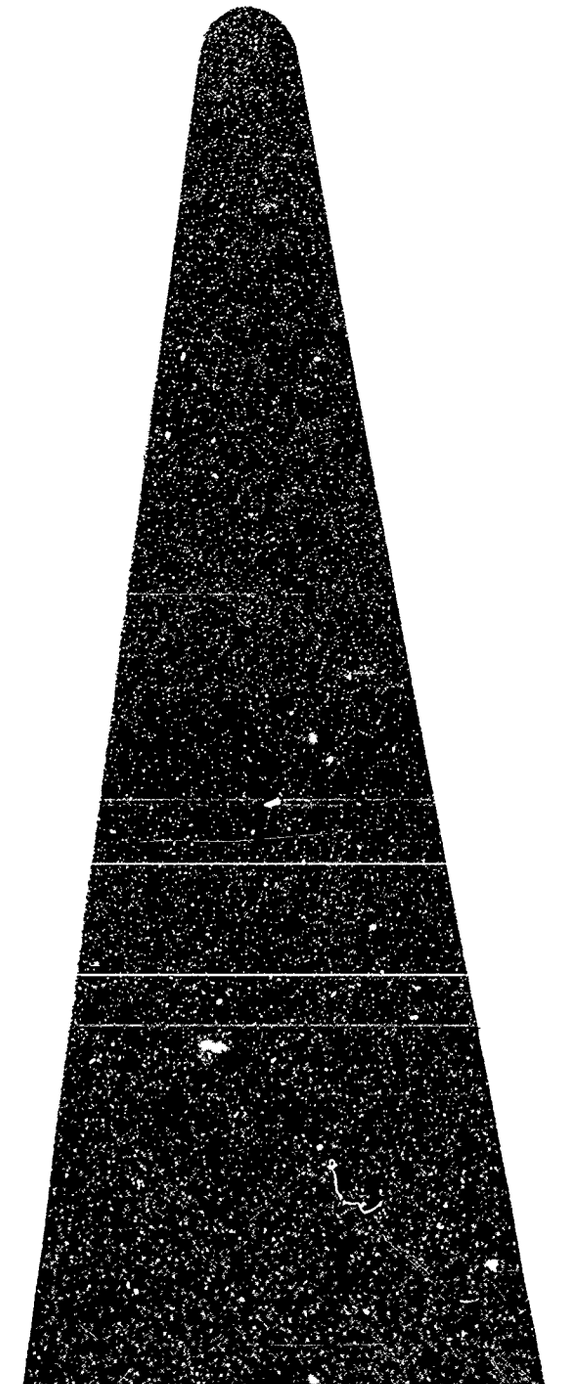
Photograph of Diffuser Cap - Side View

Figure 142



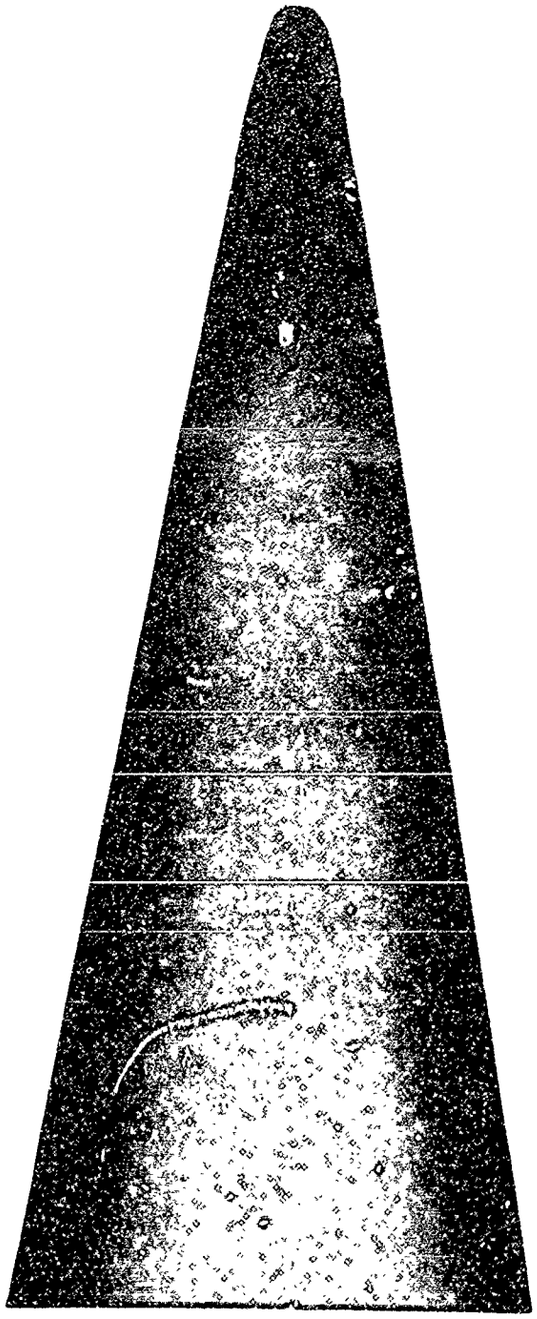
Photograph of Diffuser Cap - Bottom View

Figure 143



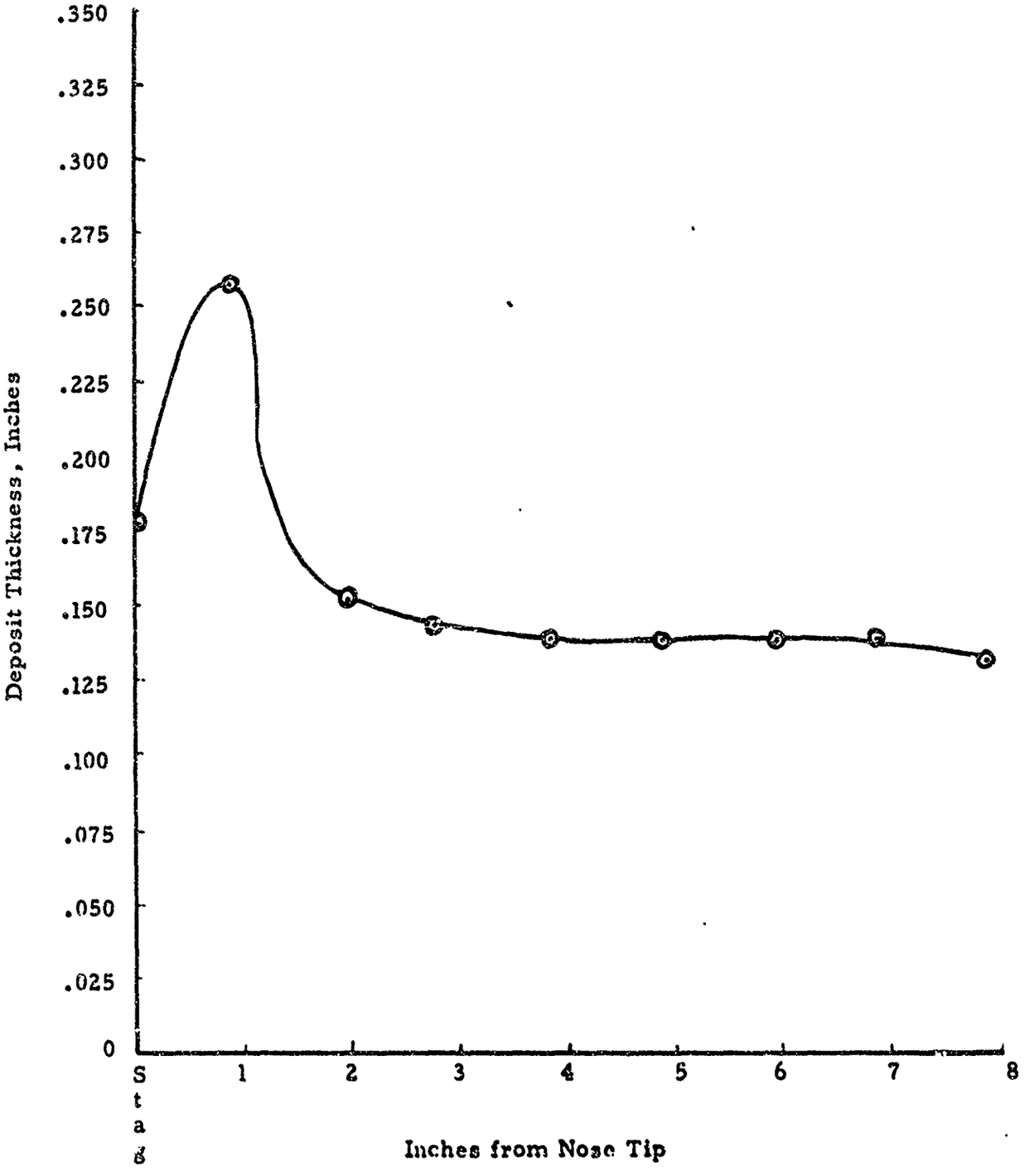
Photograph Nose Cone Tip 3213-3

Figure 144



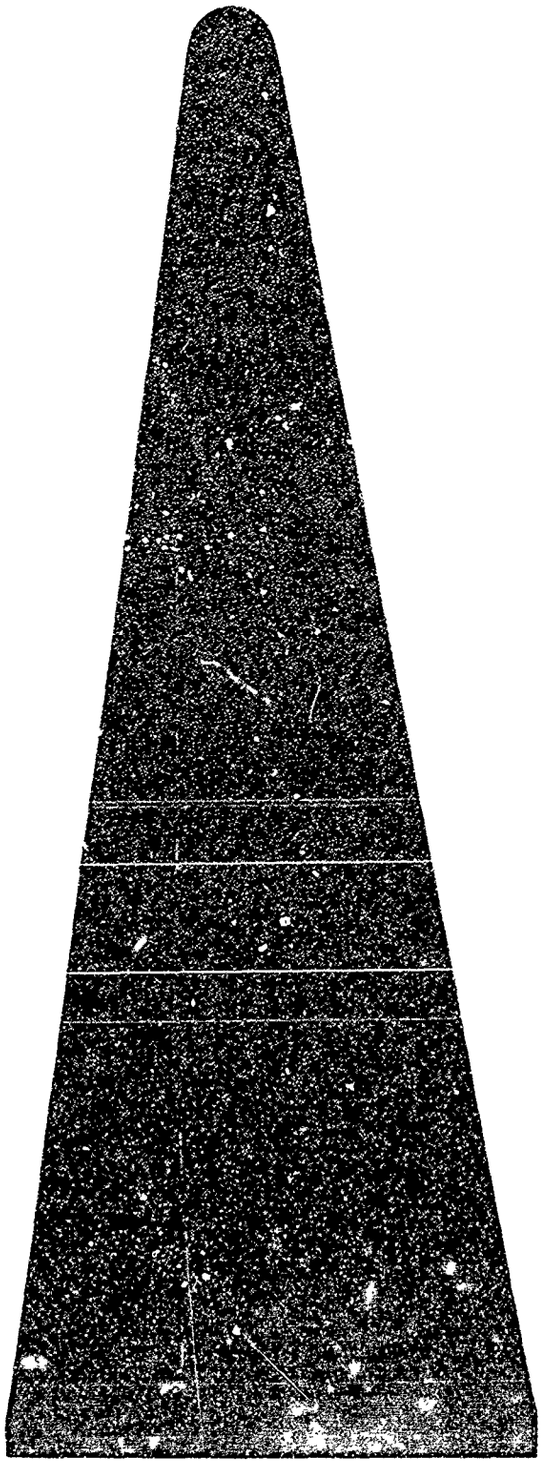
Radiographic Positive Nose Cone Tip 3213-3
Turbulent Diffuser Cap No. 3

Figure 145



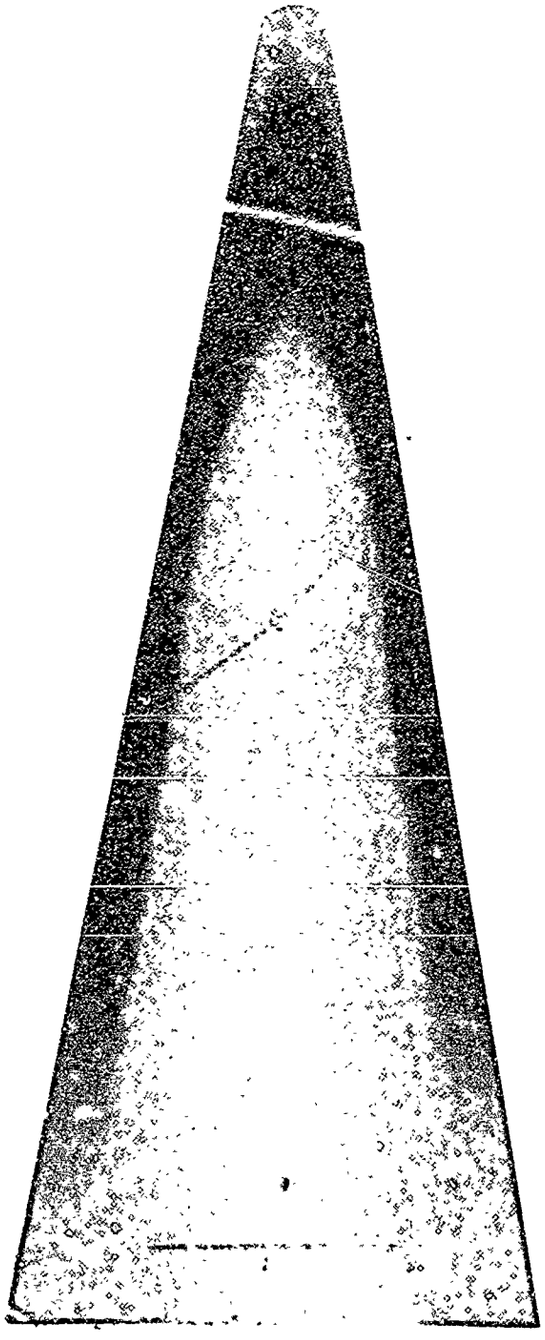
Deposit Profile Nose Cone Tip 3213-3 (Diffuser Cap)

Figure 146



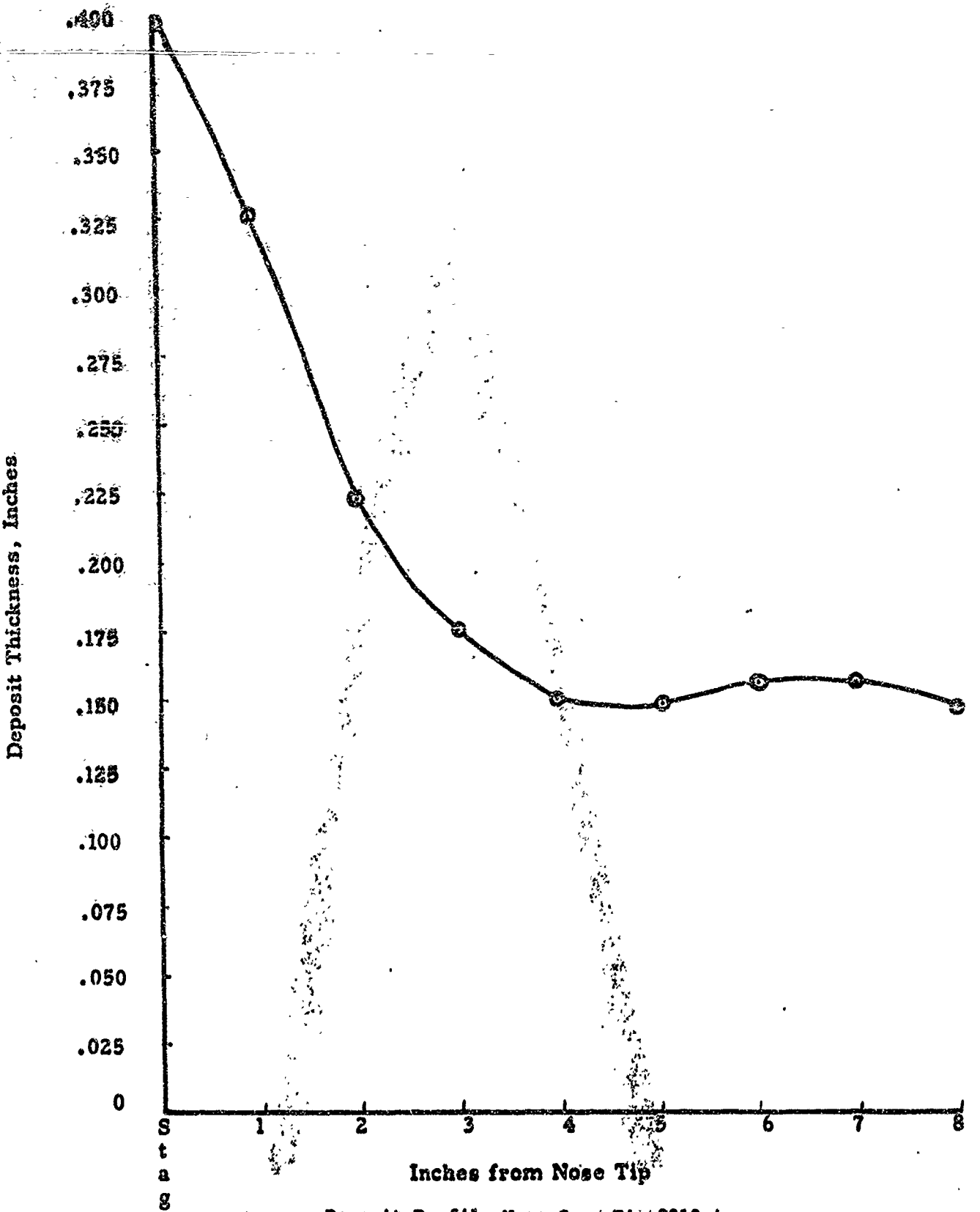
Photograph of Nose Cone Tip 3213-4

Figure 147



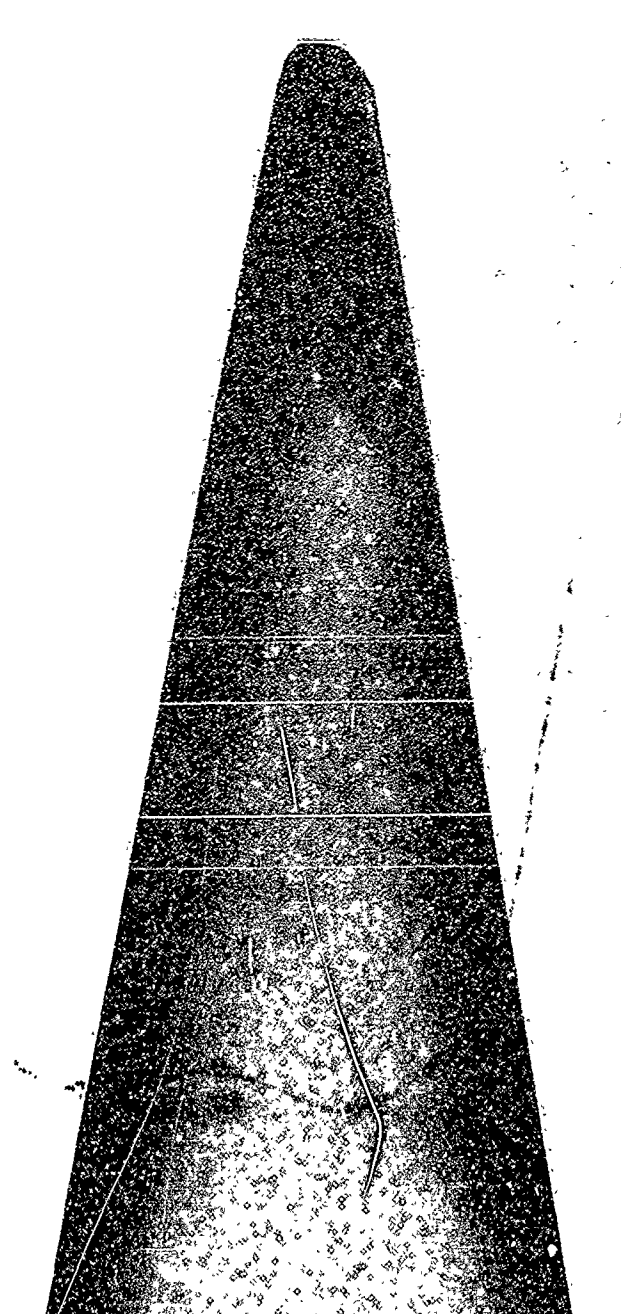
Radiographic Positive Nose Cone Tip 3213-4
(Nose Cone Tip 3213-3 with an additional
15 hours of deposition time).

Figure 148



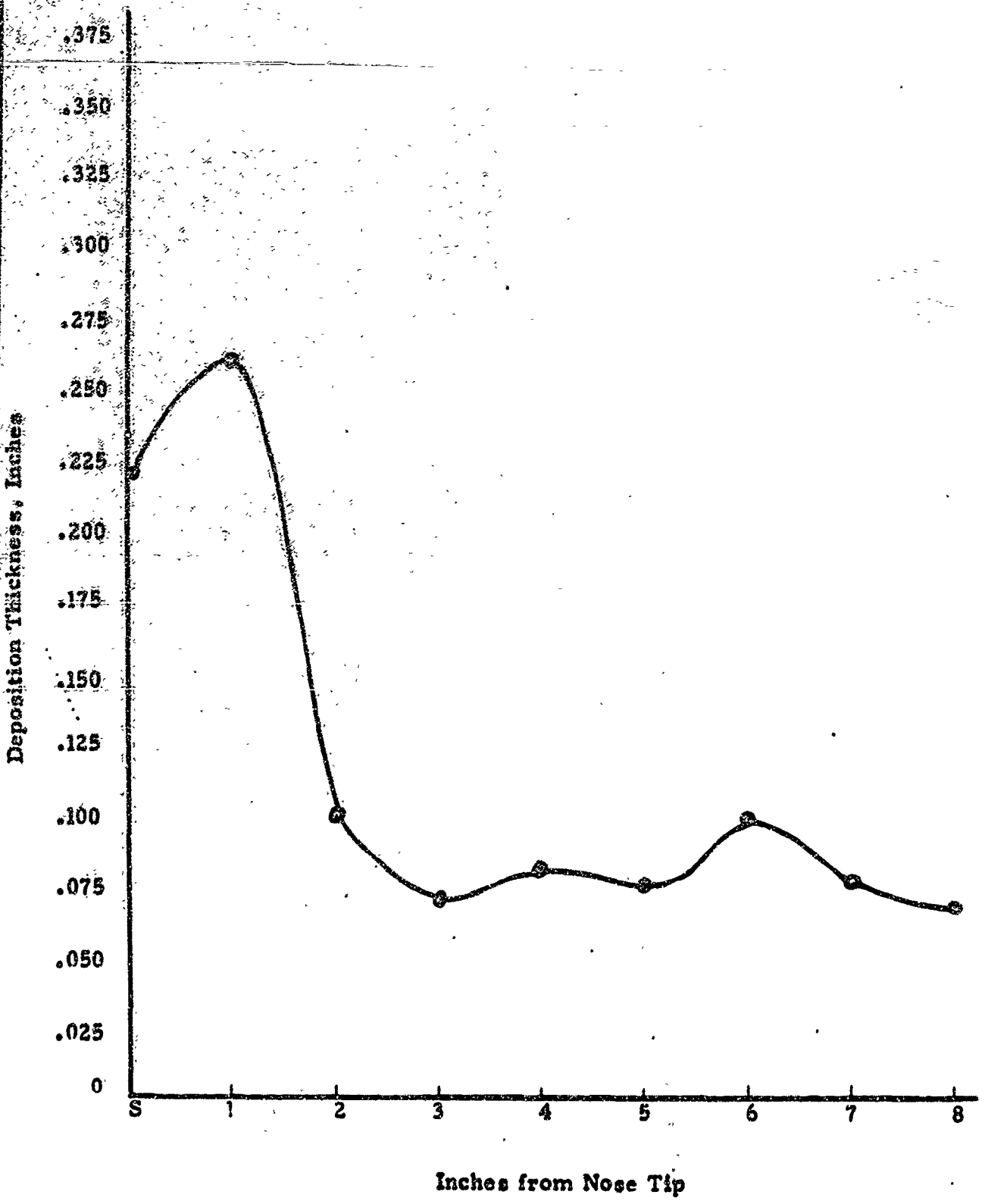
Deposit Profile Nose Cone Tip 3213-4
(Nose Cone Tip 3213-4 with additional
15 hours deposit).

Figure 149



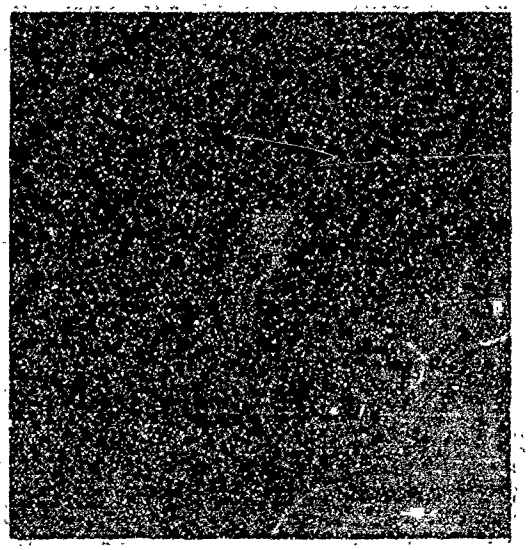
Radiographic Positive Nose Tip 3213-6

Figure 150



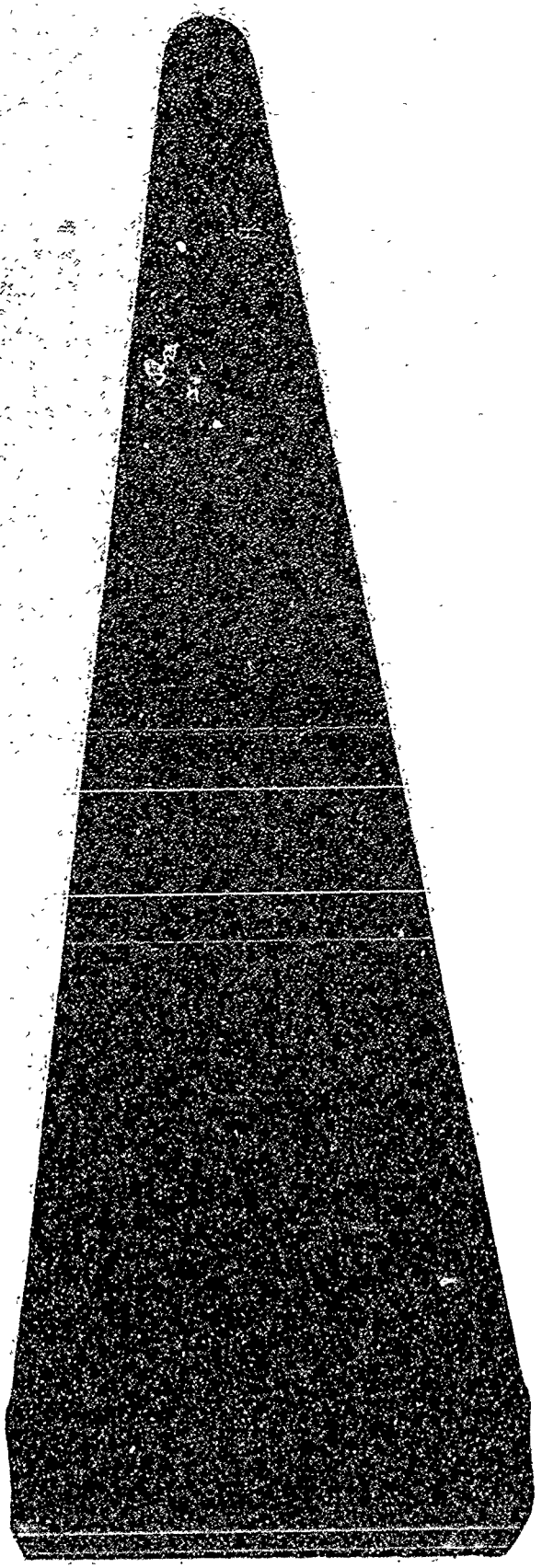
Deposit Profile Nose Cone Tip 3213-6
(Diffuser Cap No. 3 with 7-3/4" Nozzle Position).

Figure 151



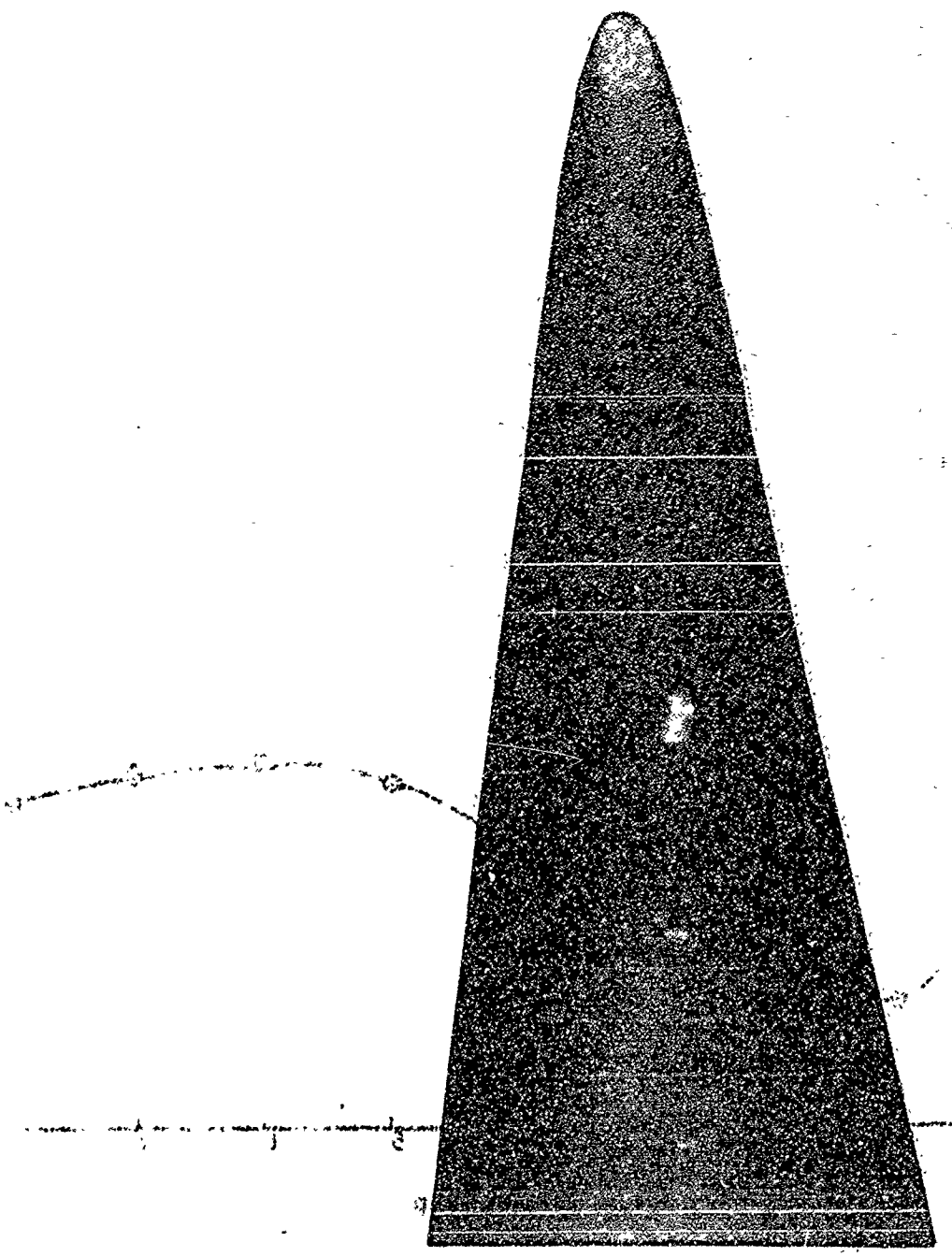
Photograph of Orifice Insert (Swirler)

Figure 152



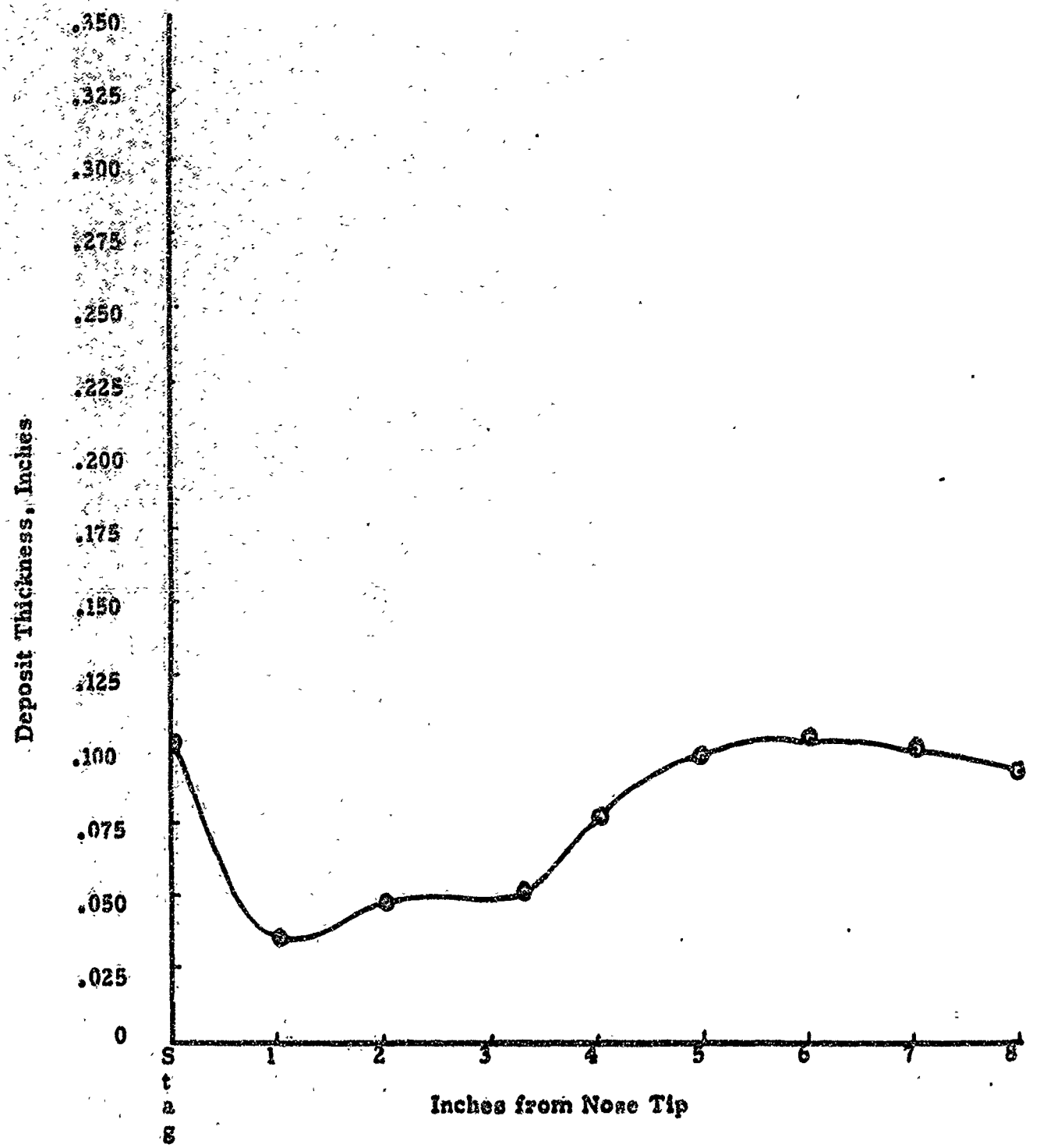
Photograph of Nose Cone Tip 3213-5

Figure 153



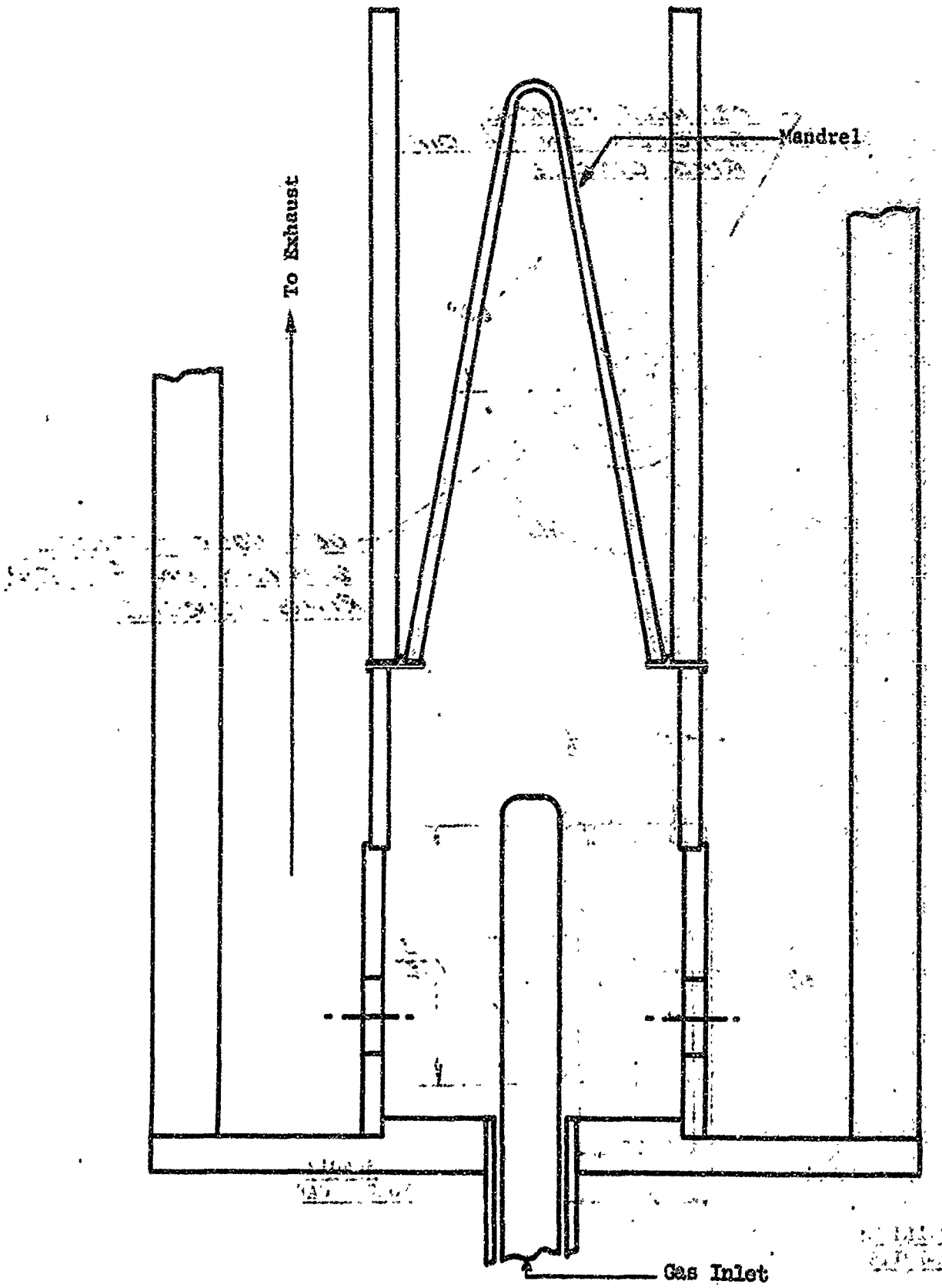
X-ray Positive Nose Cone Tip 3213-5 (Swirler Insert)

Figure 154



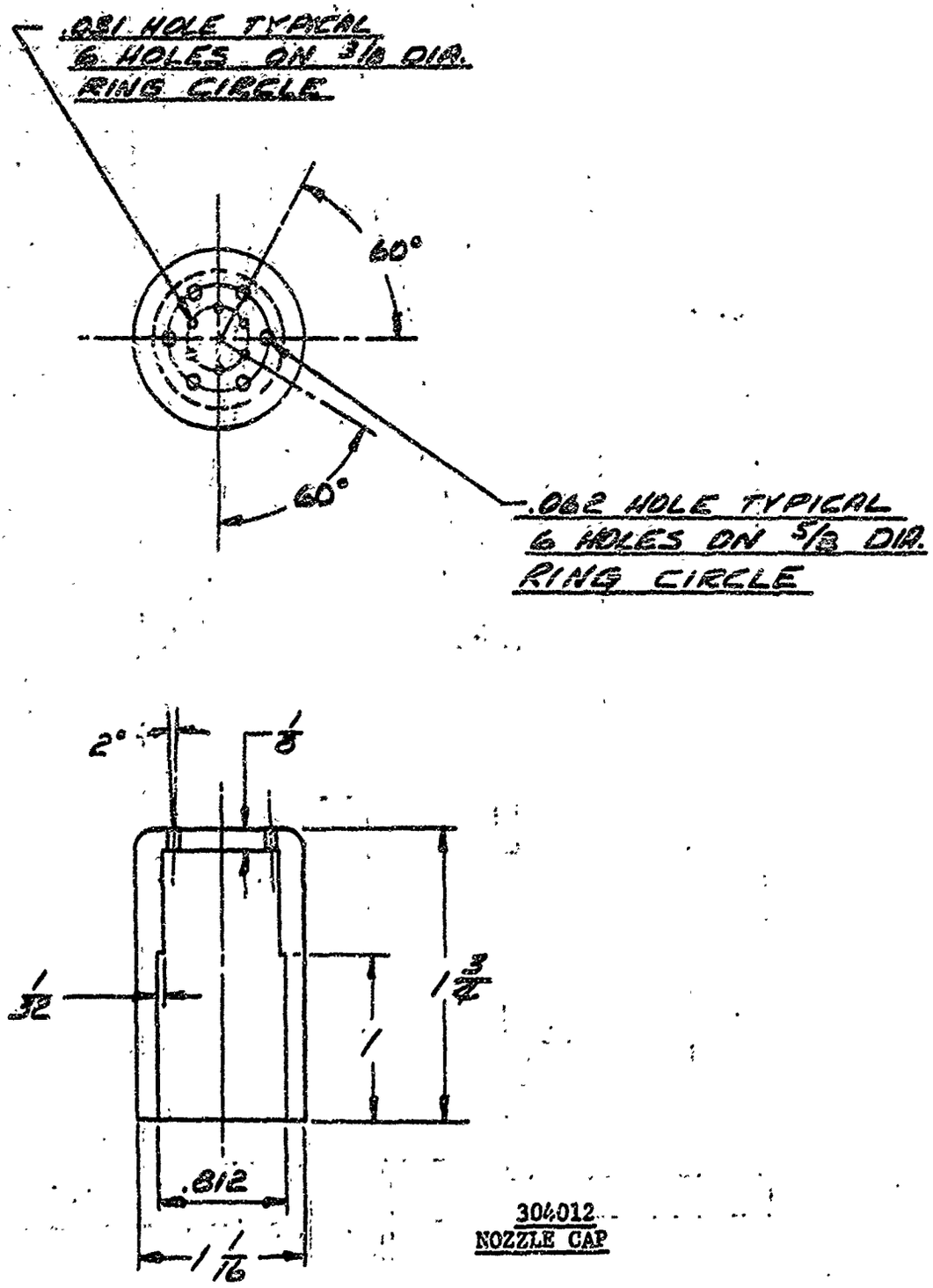
Deposit Profile Nose Cone Tip 3213-5
(Swirler Insert in Nozzle Orifice)

Figure 155



Deposition Assembly for Nose Cones

Figure 156



304012
NOZZLE CAP

MATERIAL:
GRAPHITE

Figure 157



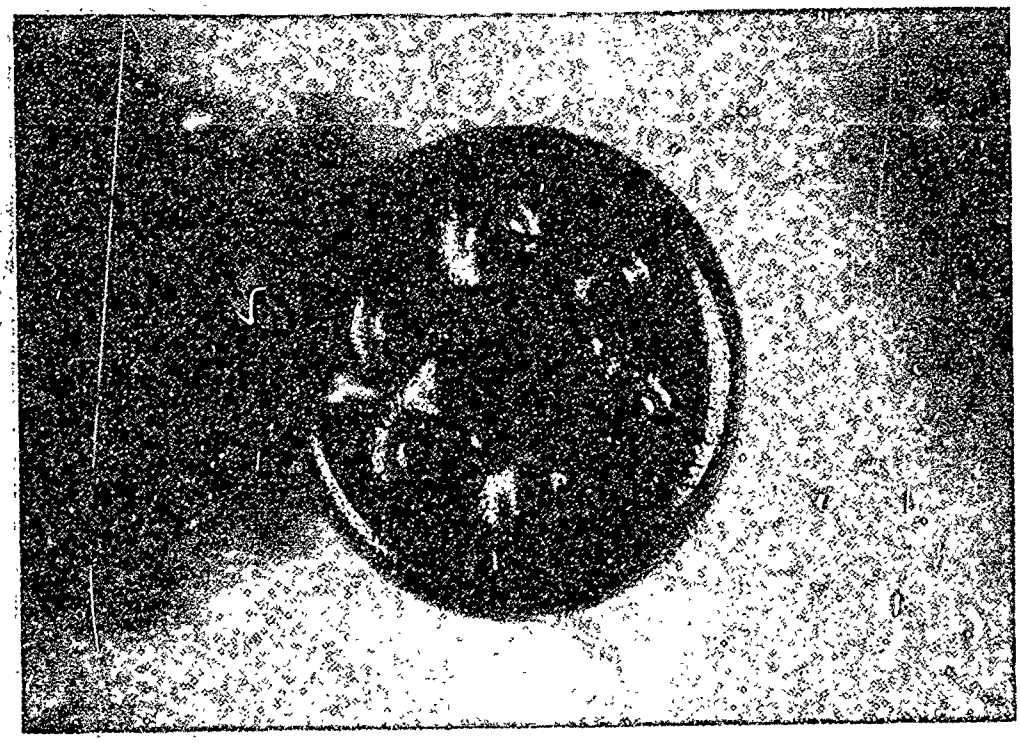
Nozzle Cap Before Deposition

Figure 158



Nozzle Cap After Deposition

Figure 159



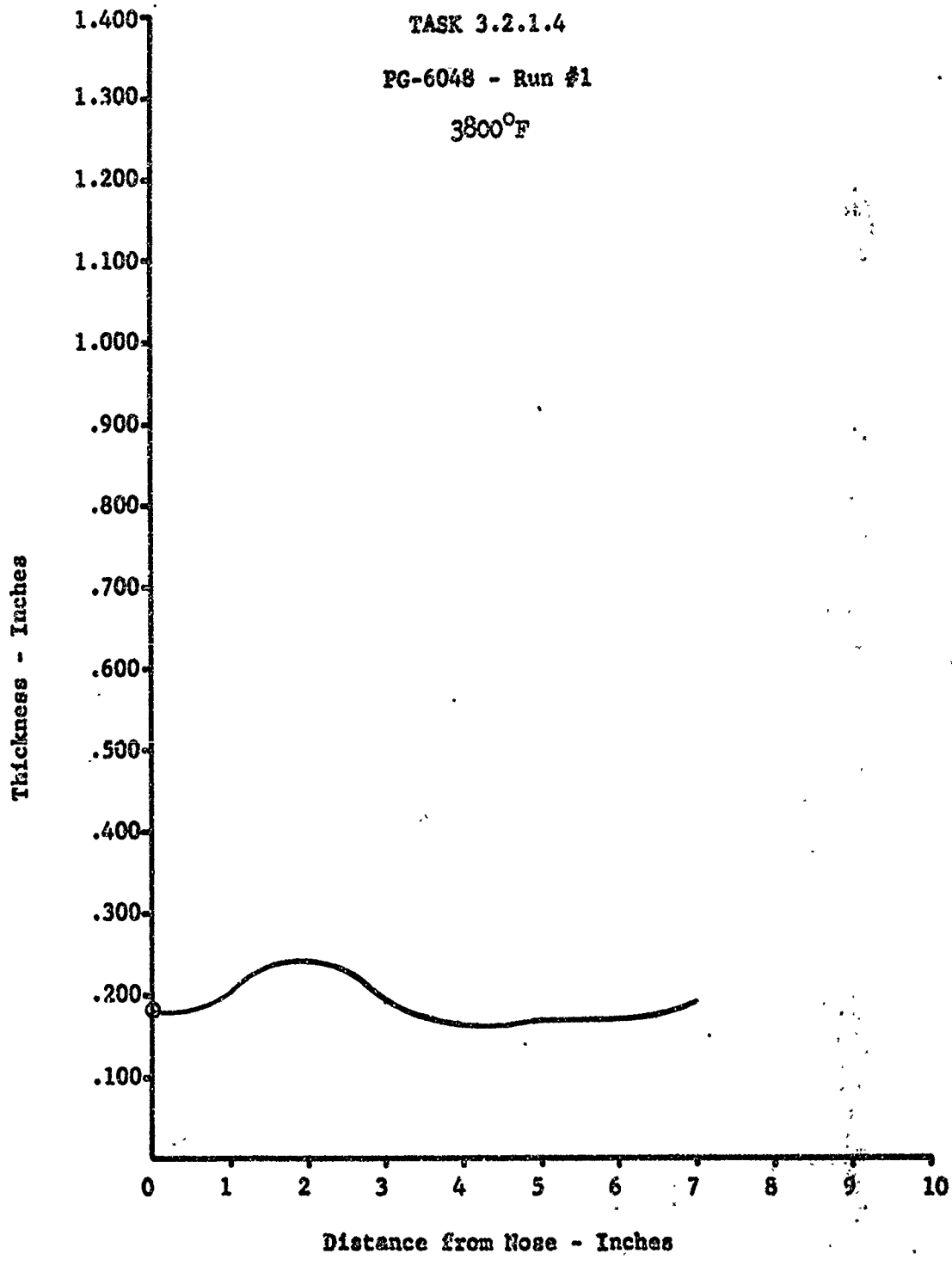
Run 6048 - Nozzle Cap Closeup of Discharge Holes After Deposition

Figure 160



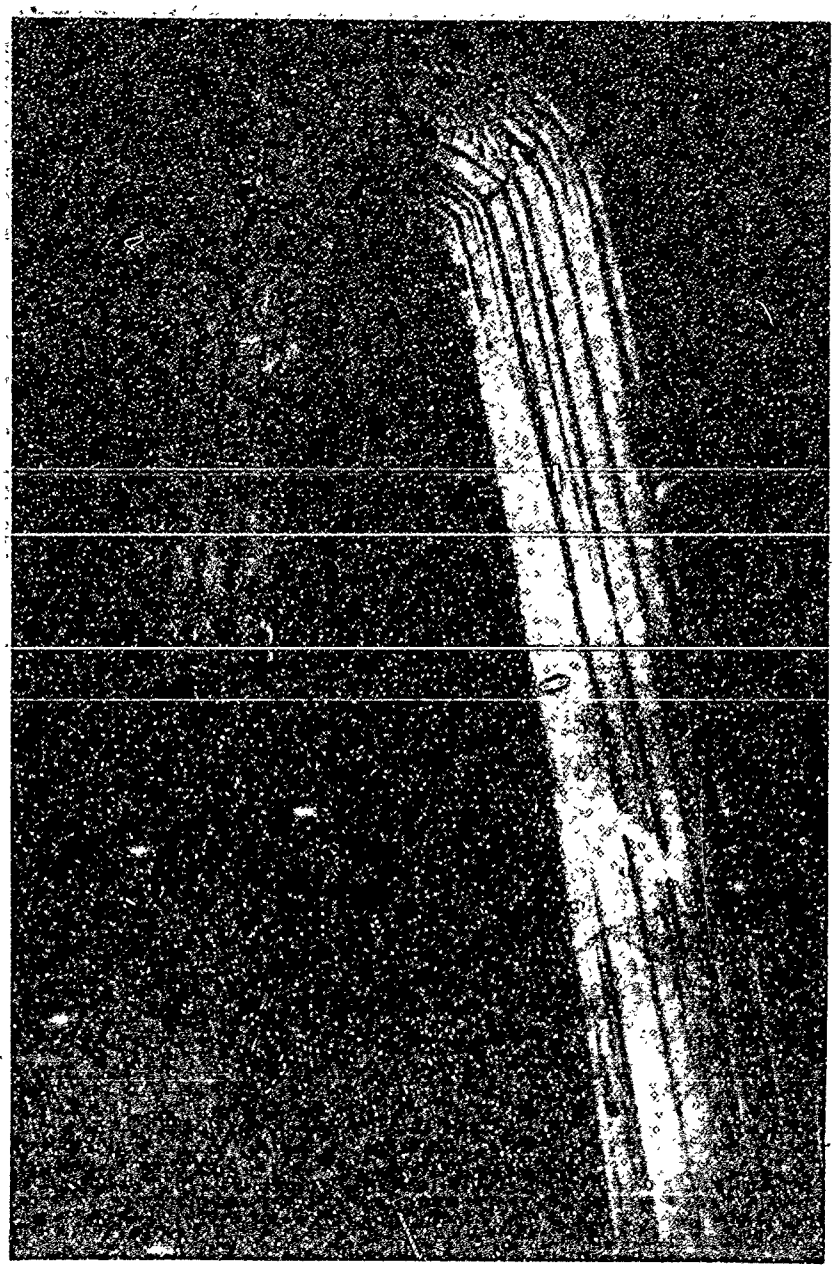
Run 6048 - Nozzle Cap Cross Section After Deposition

Figure 161



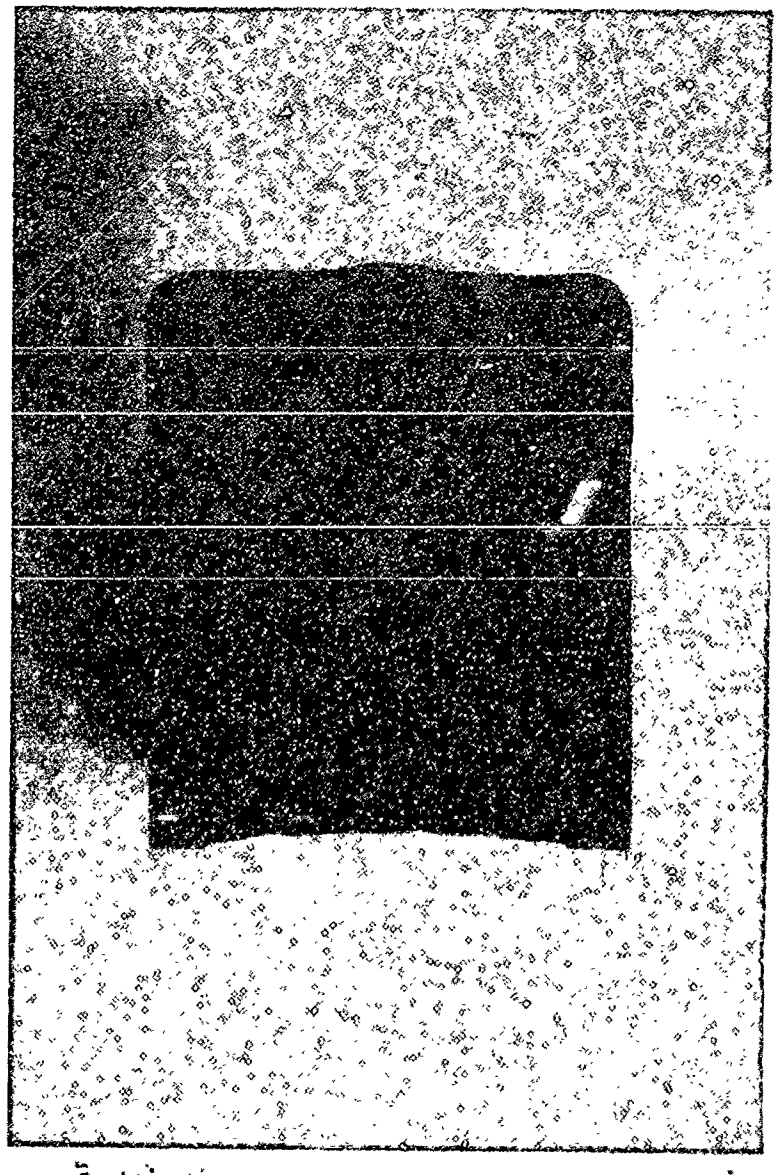
Deposition Thickness Profile

Figure 162



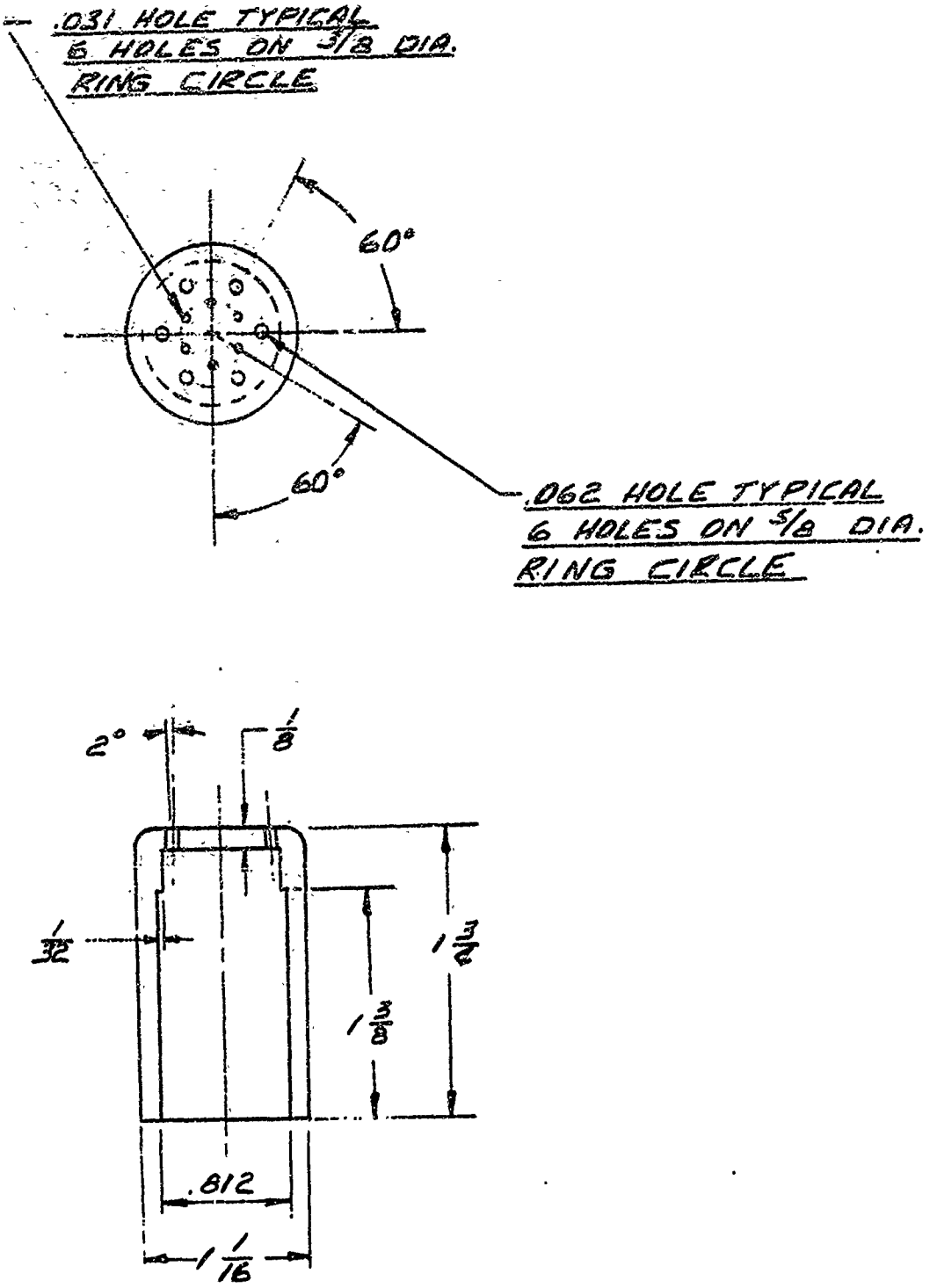
Run 6048 - Nose Region Cross Section -- 5X

Figure 163



Run 6049 - Nozzle Cap Cross Section After Deposition

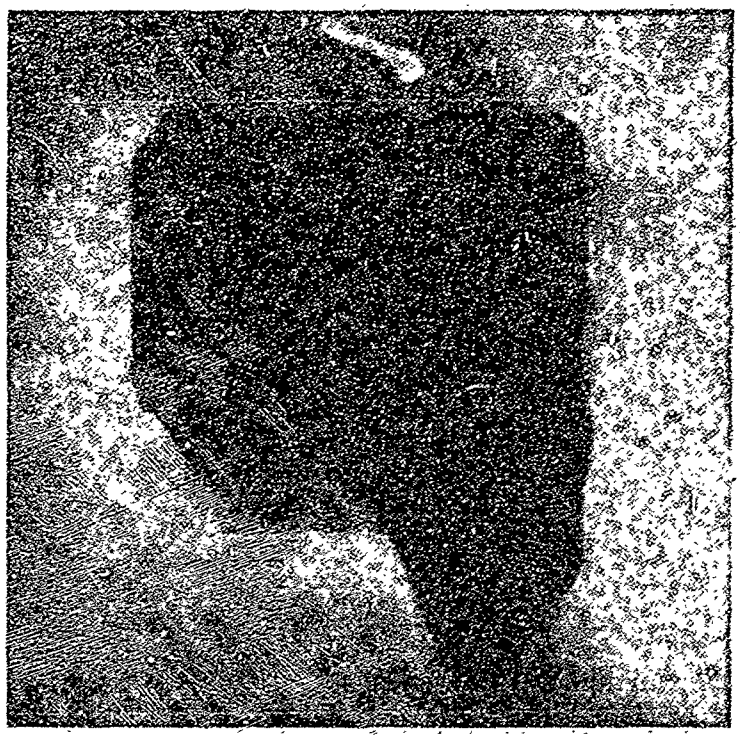
Figure 164



MATERIAL:
GRAPHITE

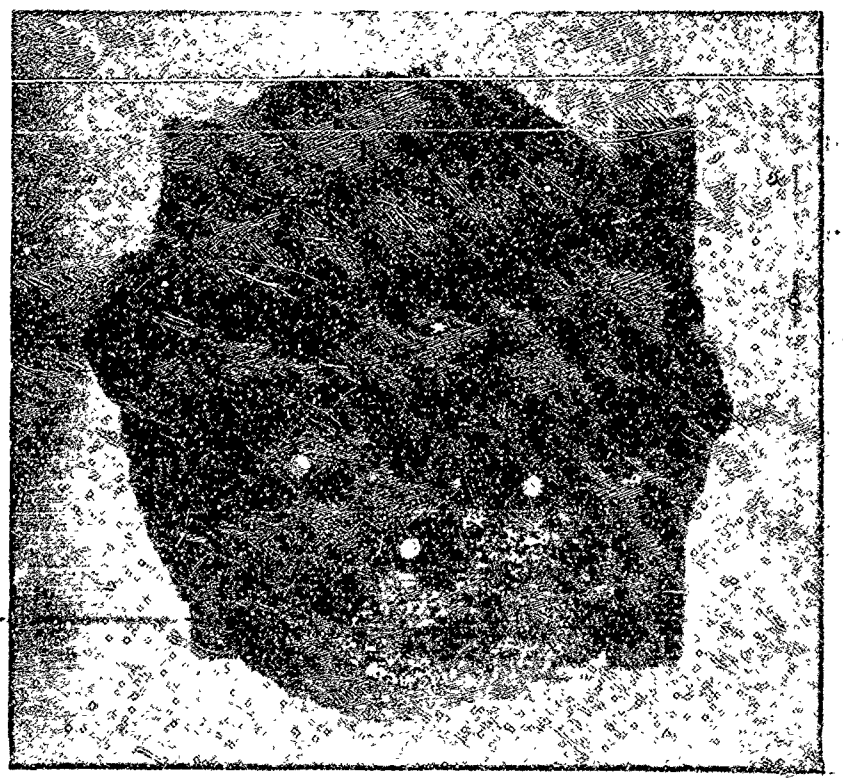
304013
NOZZLE CAP

Figure 165



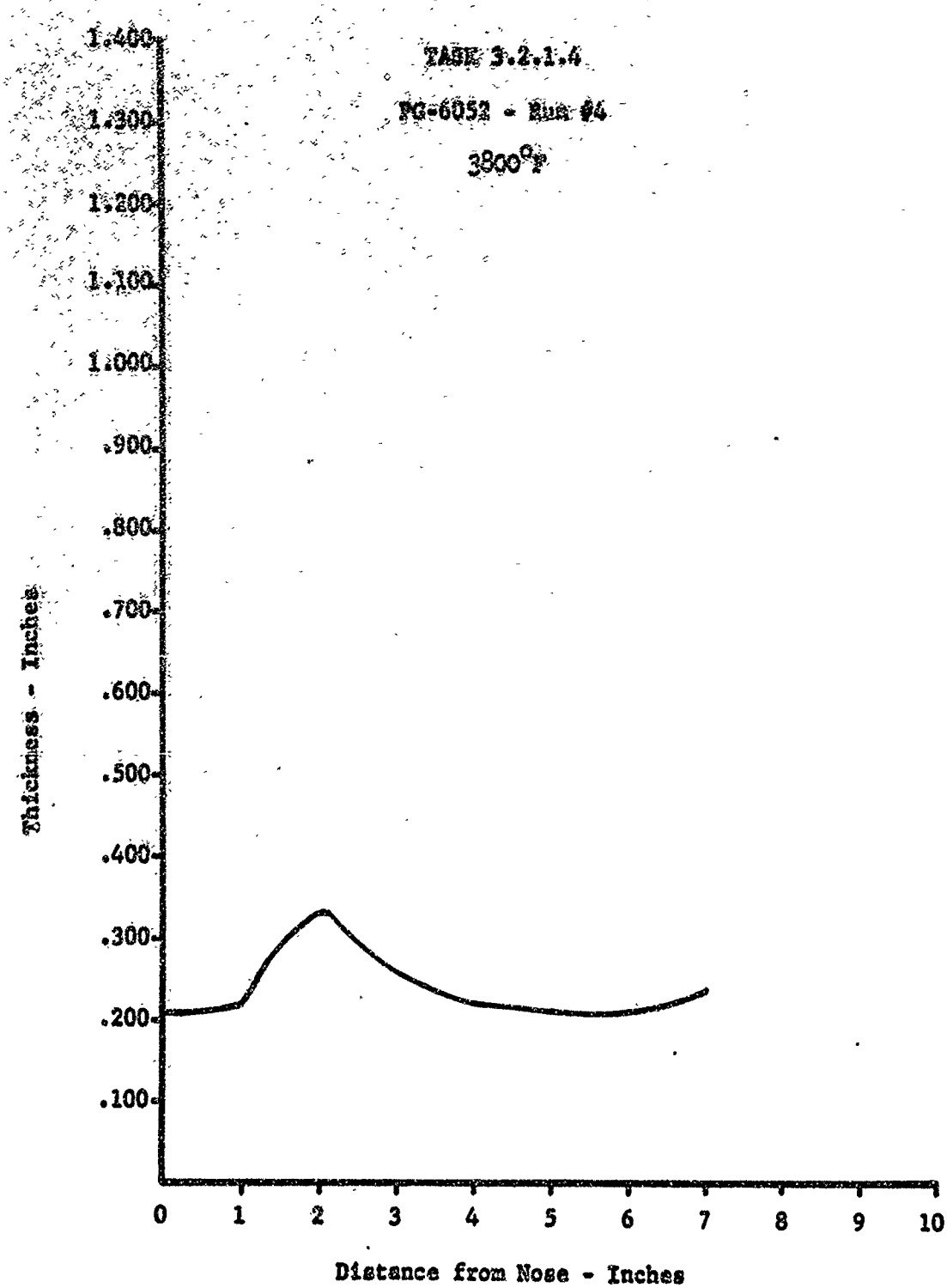
Run 6052 - Nozzle Cap Cross Section After Deposition

Figure 166



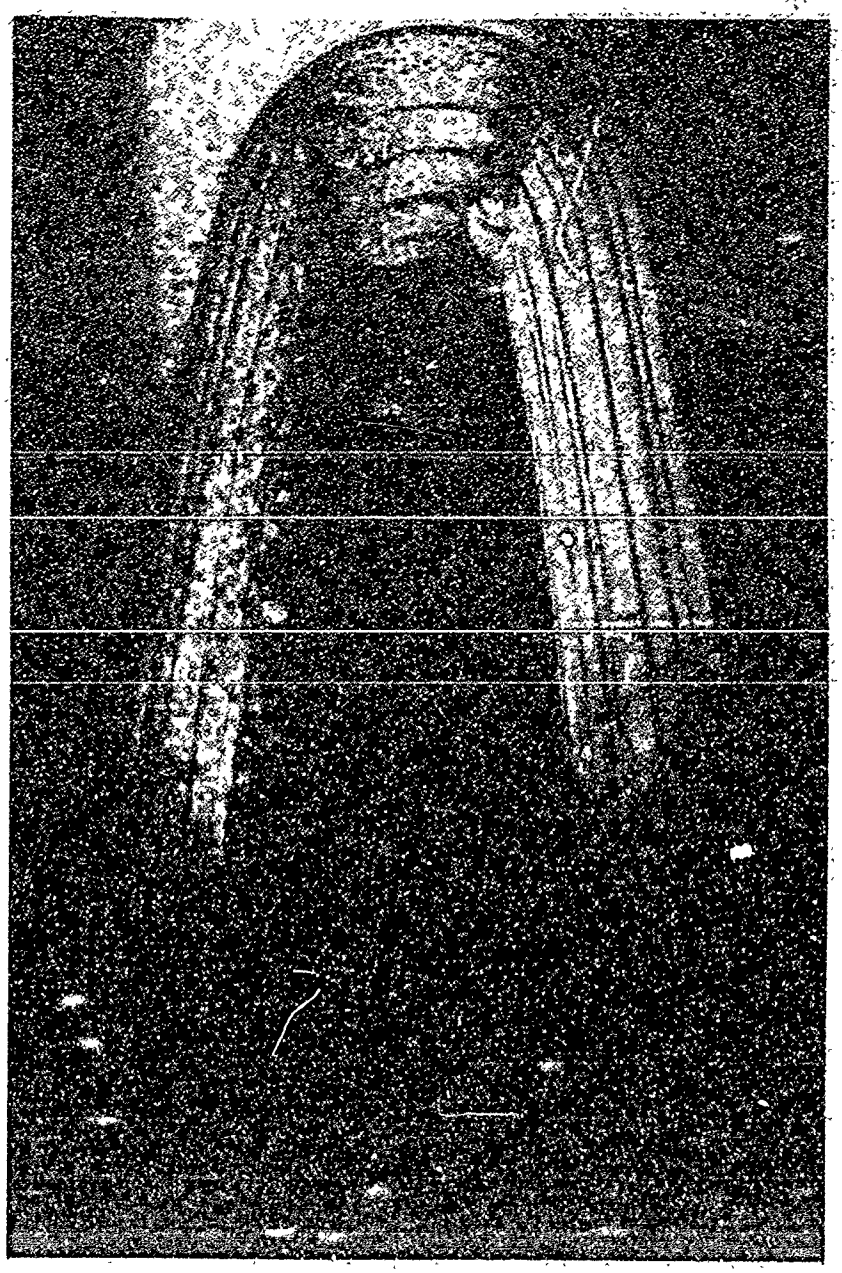
Run 6052 - Nozzle Cap Closeup of Discharge Holes After Deposition

Figure 167



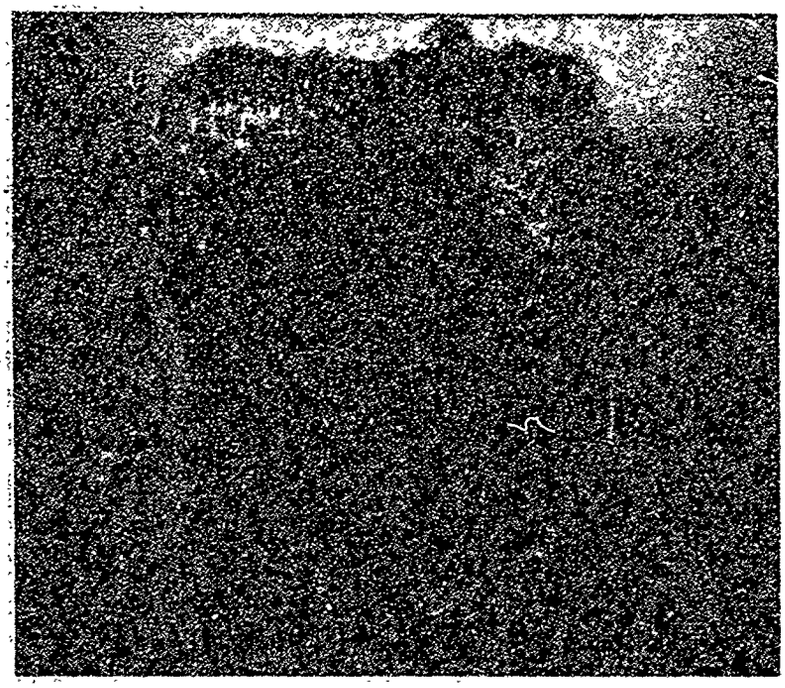
Deposition Thickness Profile

Figure 168



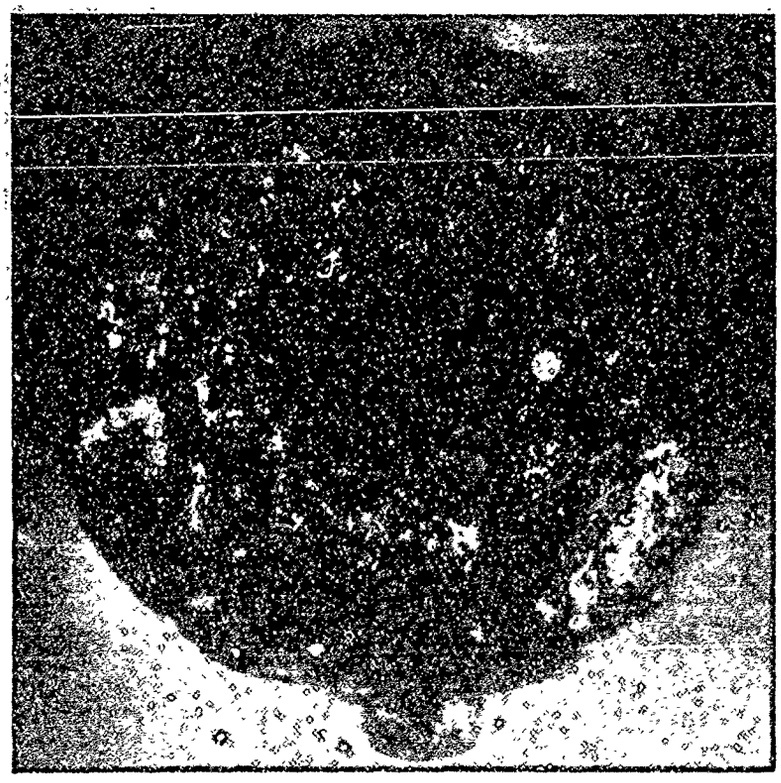
Run 6052 - Nose Region Cross Section -- 5X

Figure 169



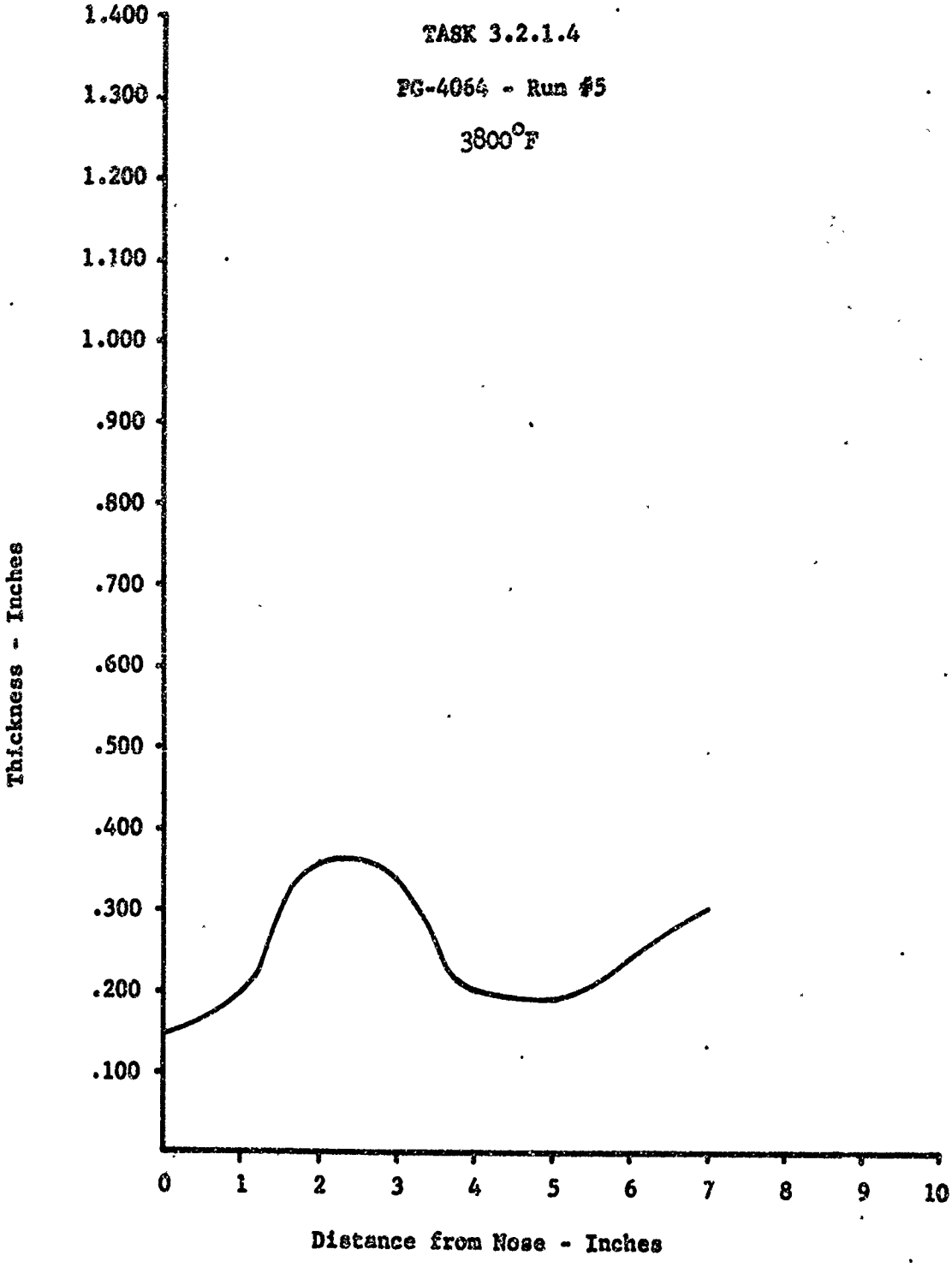
Run 4064 - Nozzle Cap Side View After Deposition

Figure 170



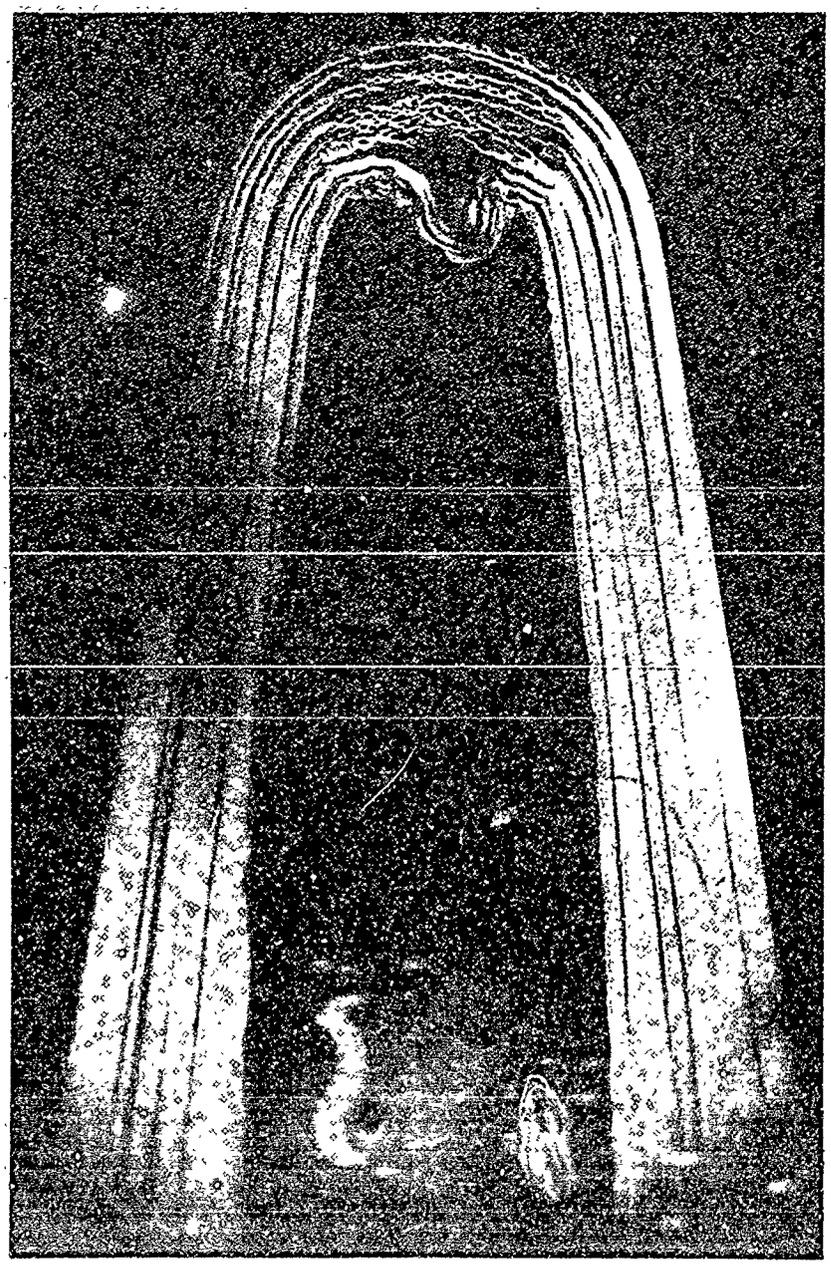
Run 4064 - Nozzle Cap Discharge Holes After Deposition

Figure 171



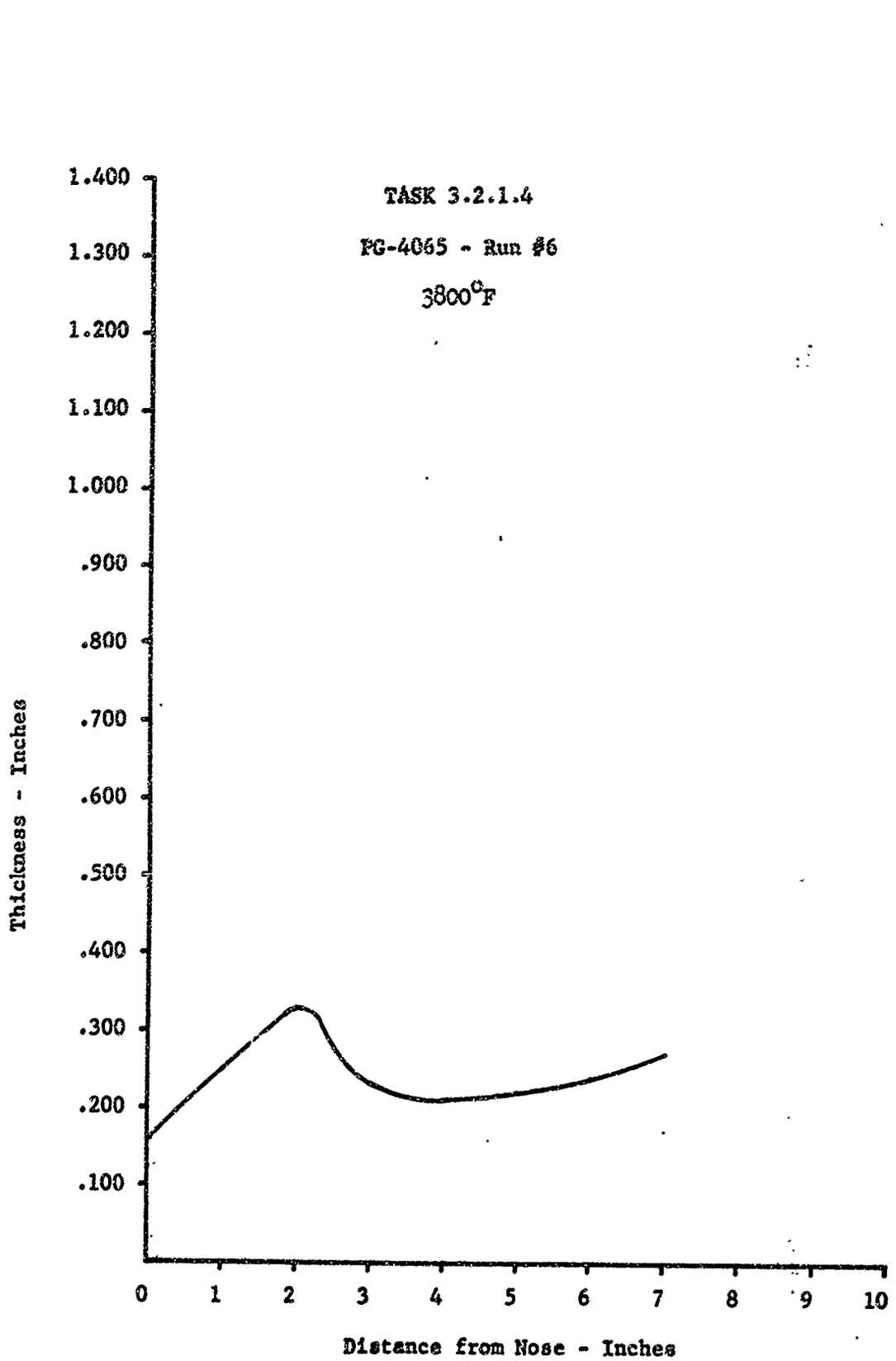
Deposition Thickness Profile

Figure 172



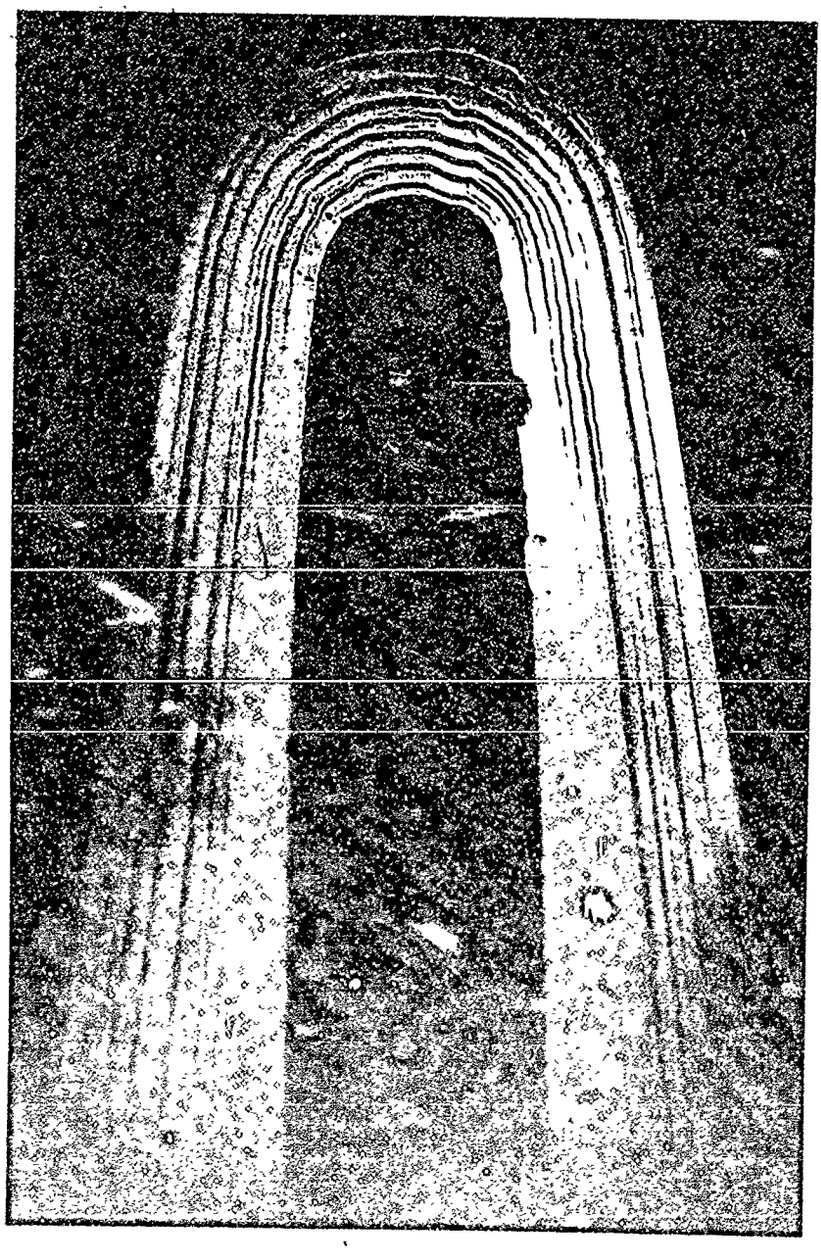
Run 4064 - Nose Region Cross Section -- 5X

Figure 173



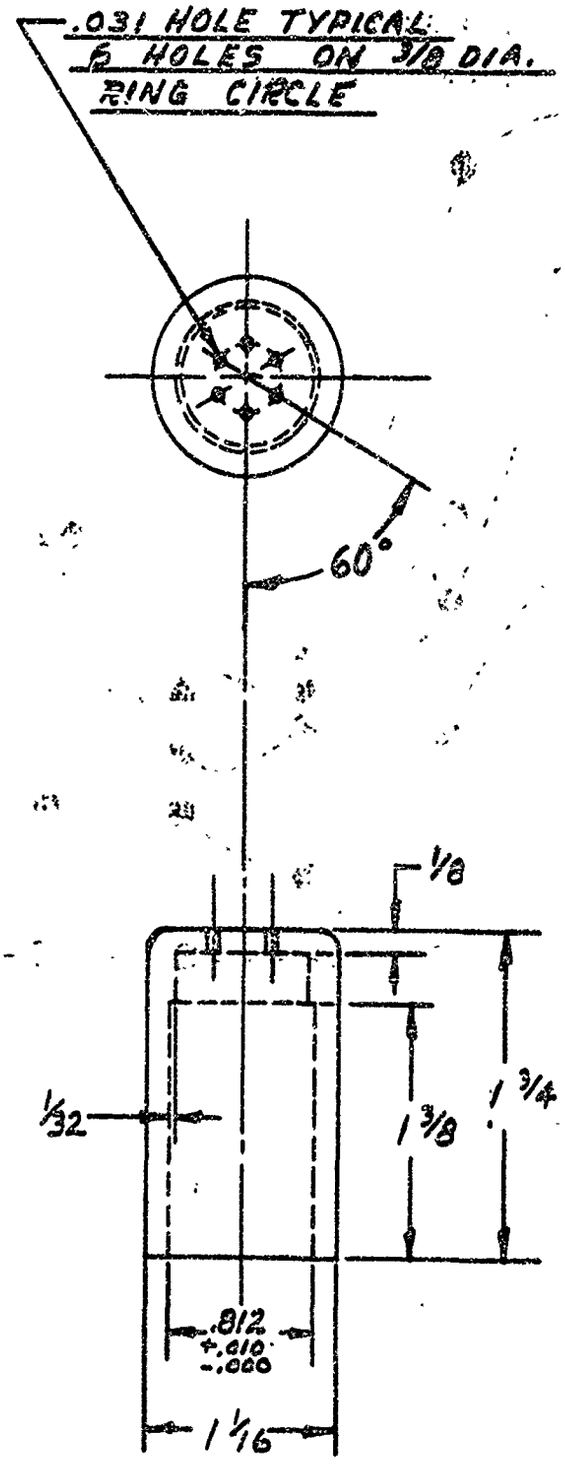
Deposition Thickness Profile

Figure 174



Run 4065 - Nose Region Cross Section -- 5X

Figure 175



MATERIAL :
GRAPHITE

304015
NOZZLE CAP

Figure 176

Task 3.2.1.4

Deposition Profile Summary

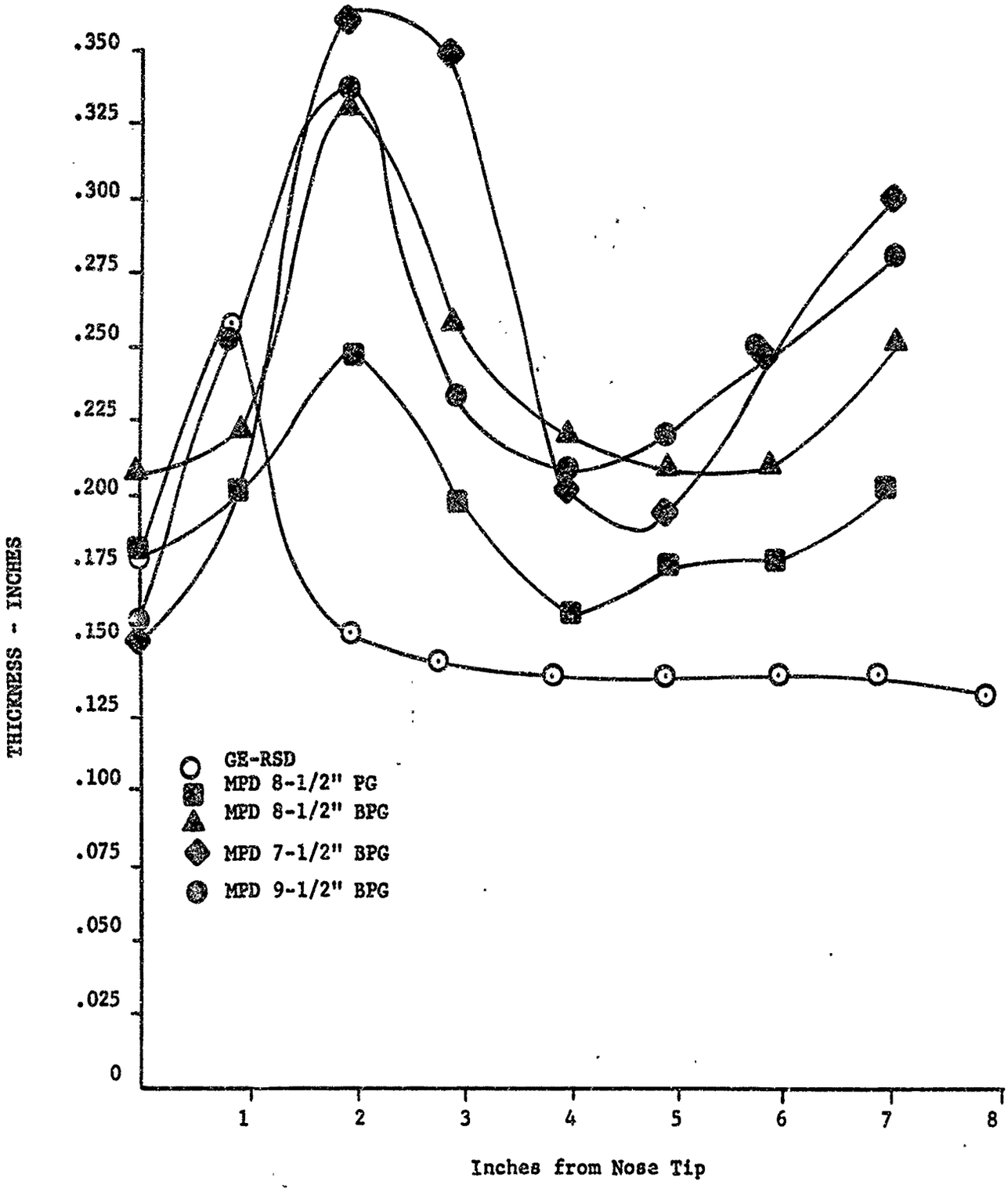


Figure 177

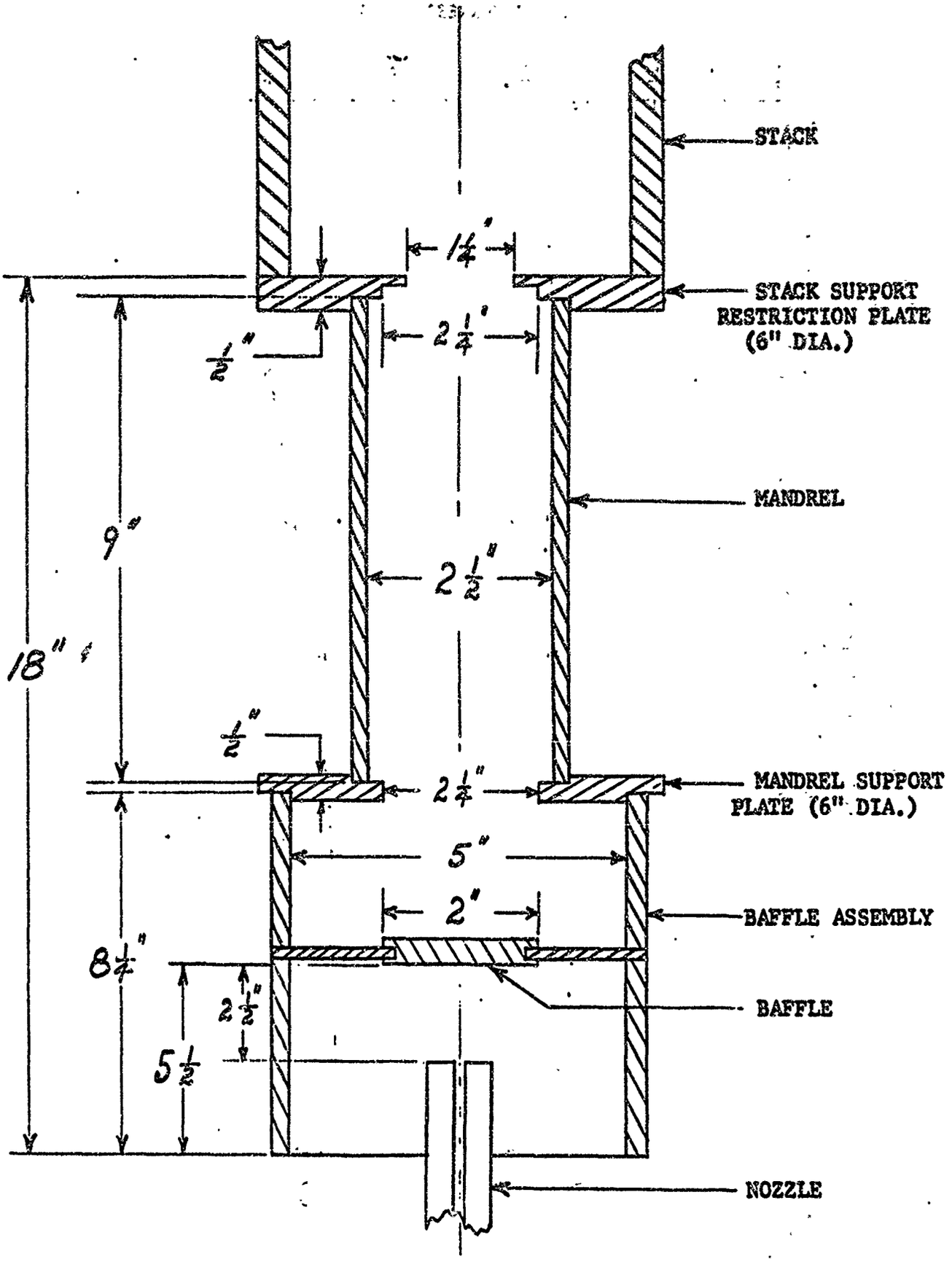


Figure 178

SCHEMATIC DIAGRAM ILLUSTRATING PHASE I FURNACE ASSEMBLY

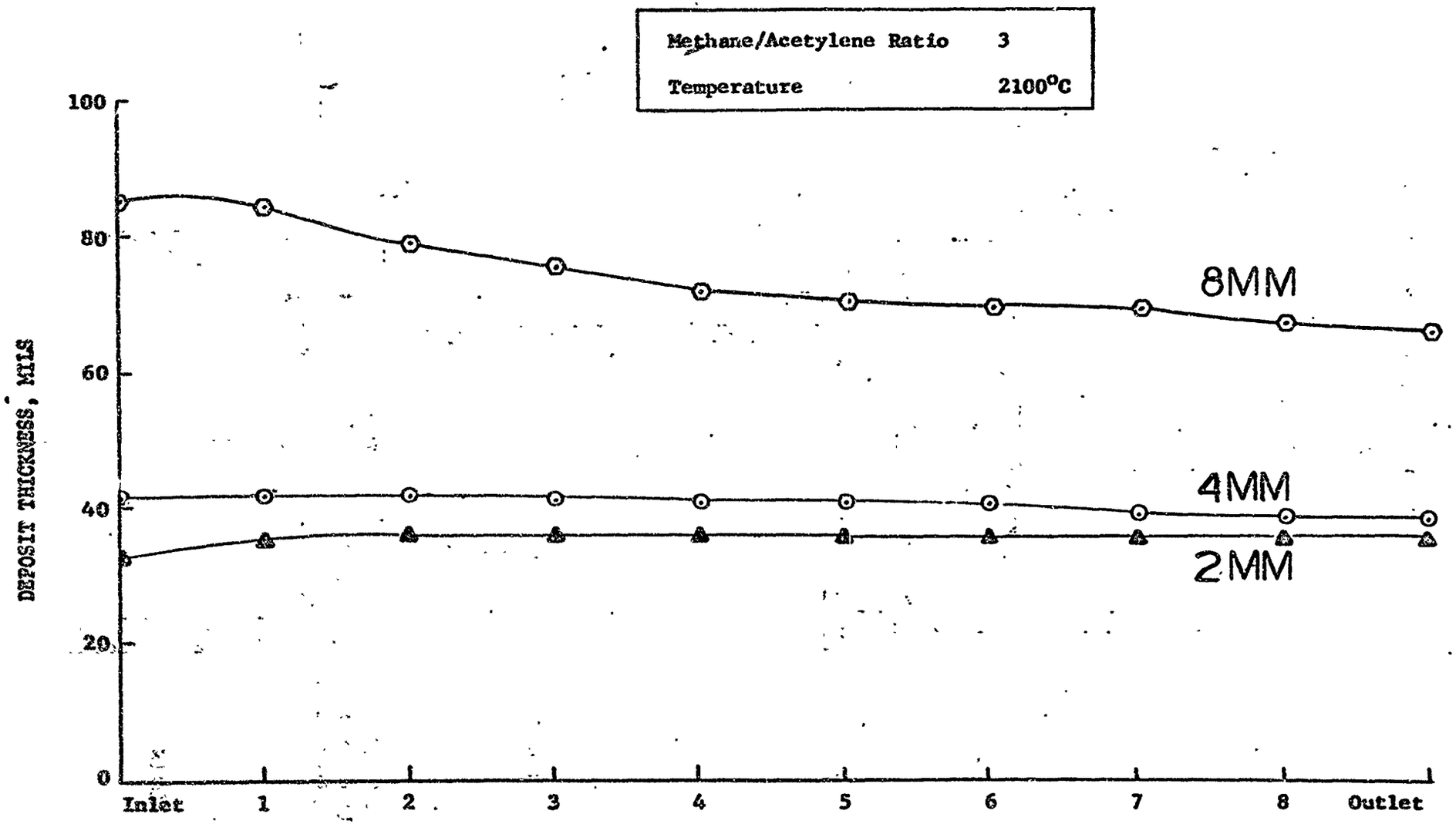


Figure 179

EFFECT OF DEPOSITION PRESSURE ON DEPOSIT THICKNESS PROFILE

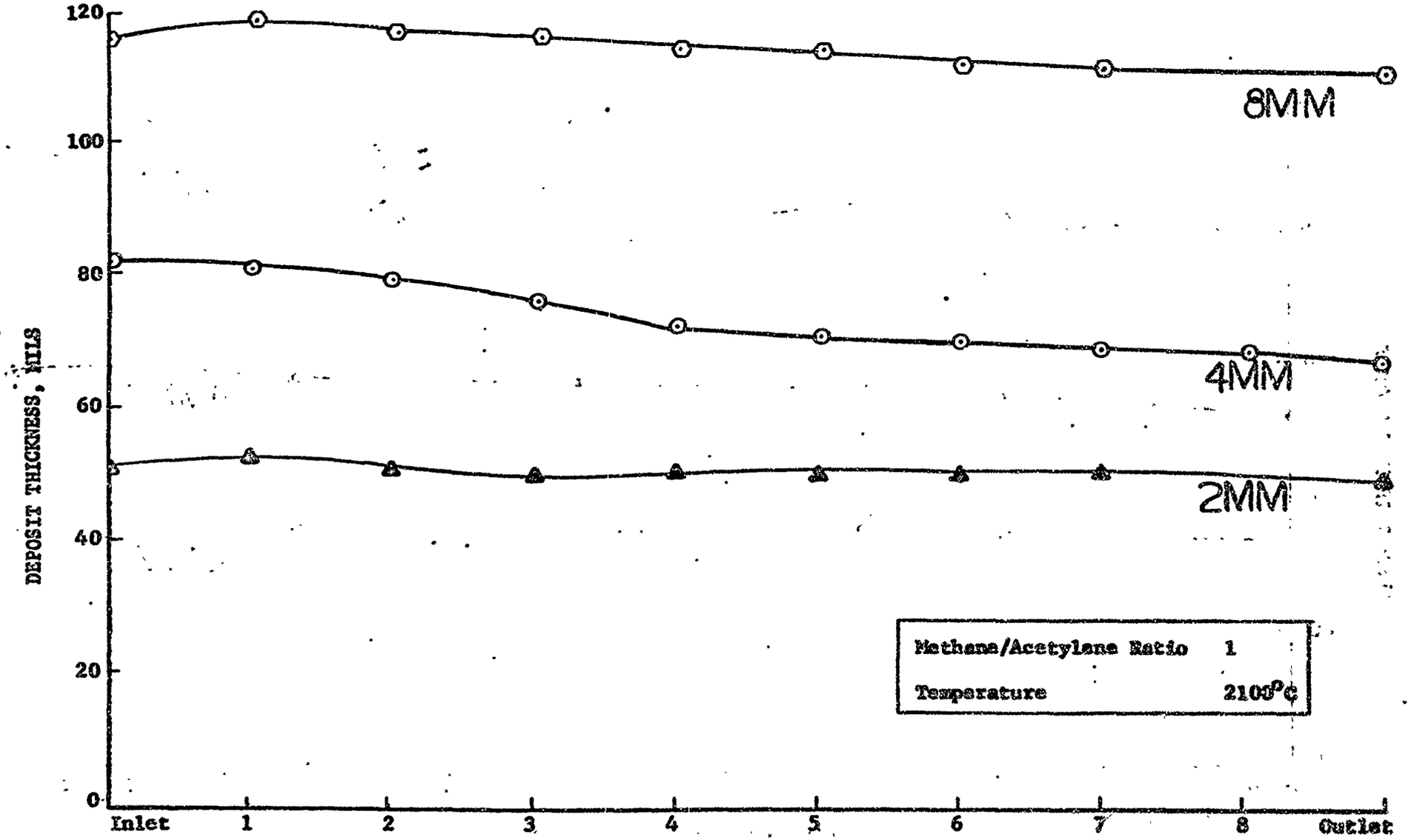
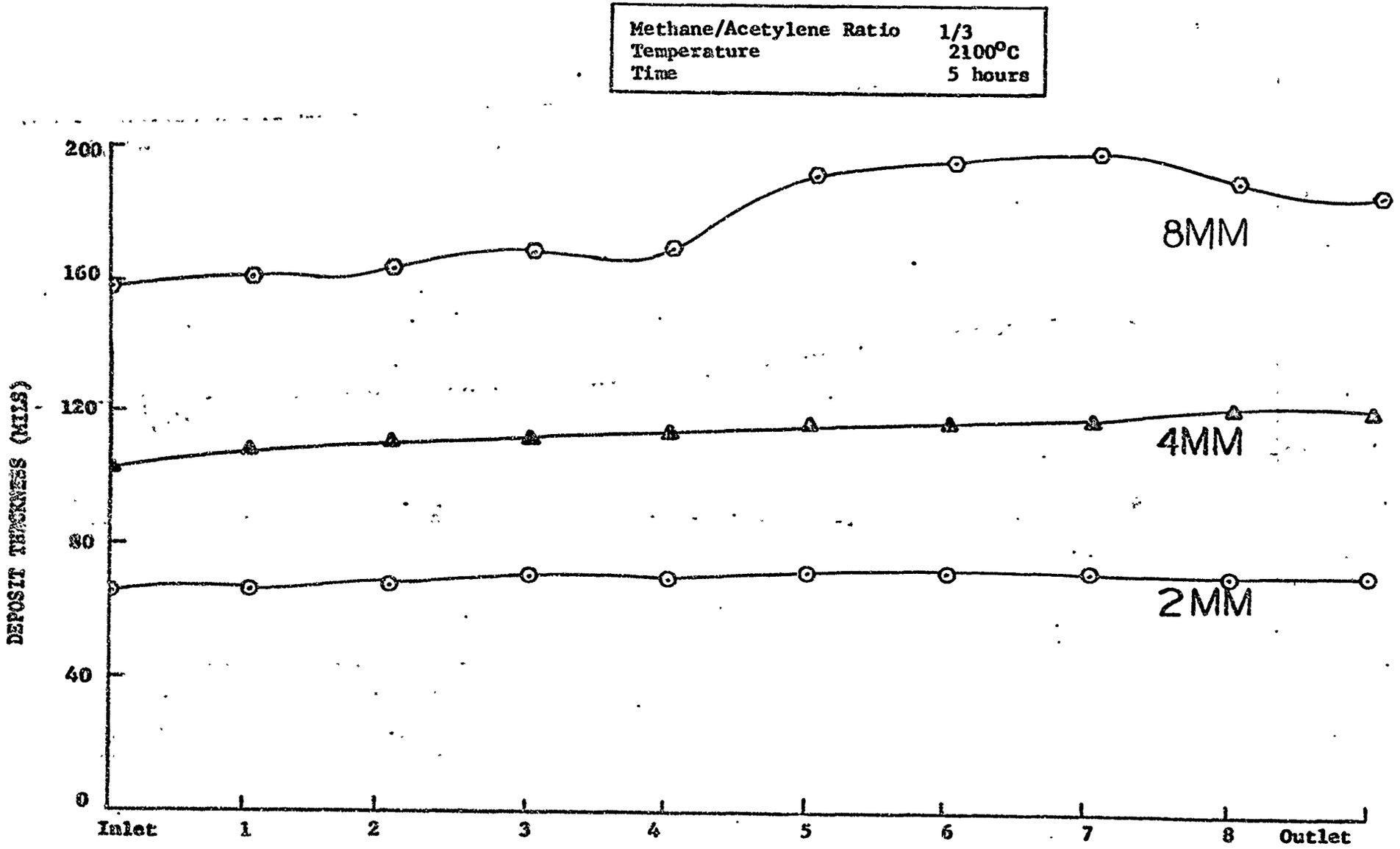


Figure 180

EFFECT OF DEPOSITION PRESSURE ON DEPOSIT THICKNESS PROFILE



406

Figure 181

EFFECT OF DEPOSITION PRESSURE ON DEPOSIT THICKNESS PROFILE

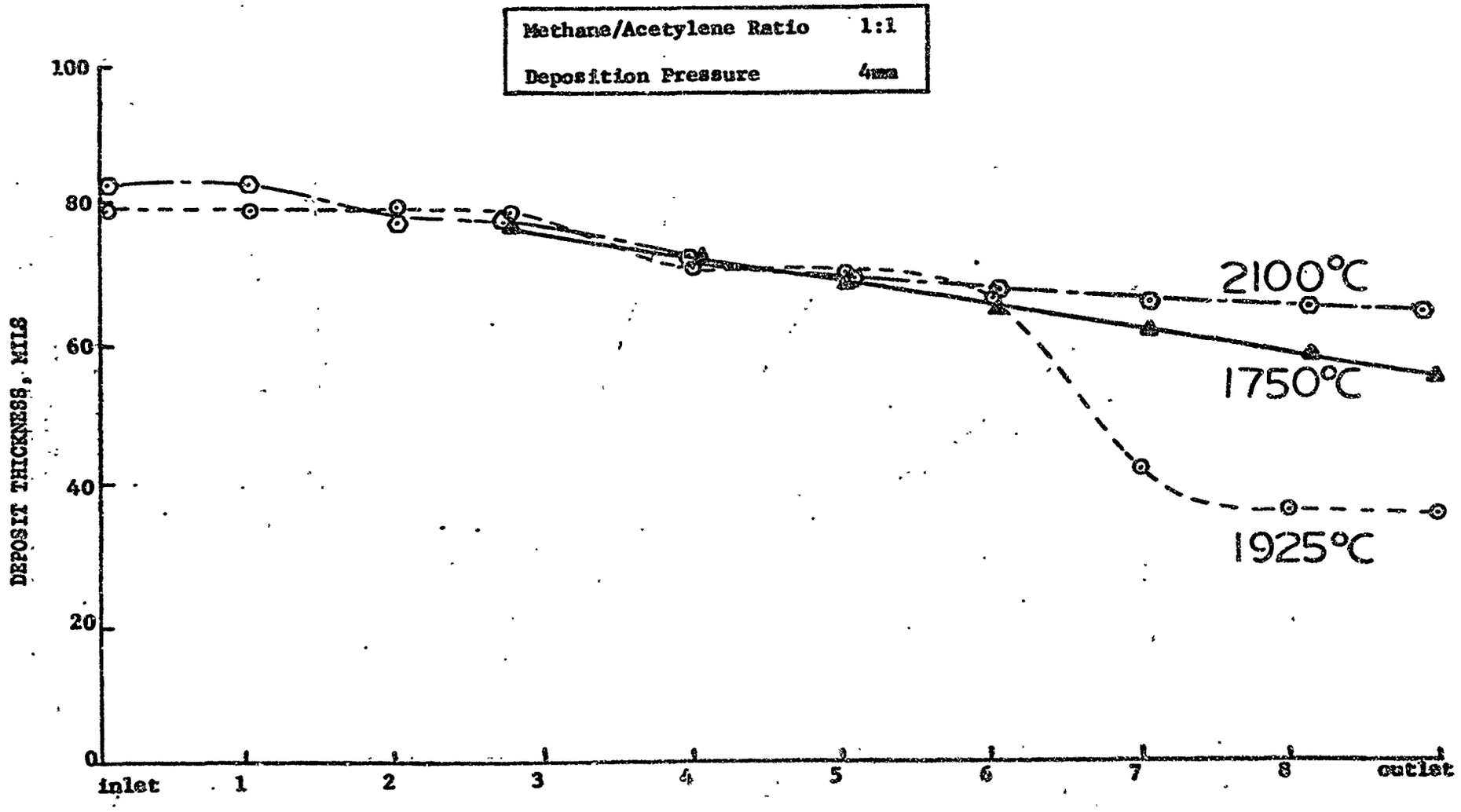


Figure 182

EFFECT OF DEPOSITION TEMPERATURE ON DEPOSIT THICKNESS PROFILE

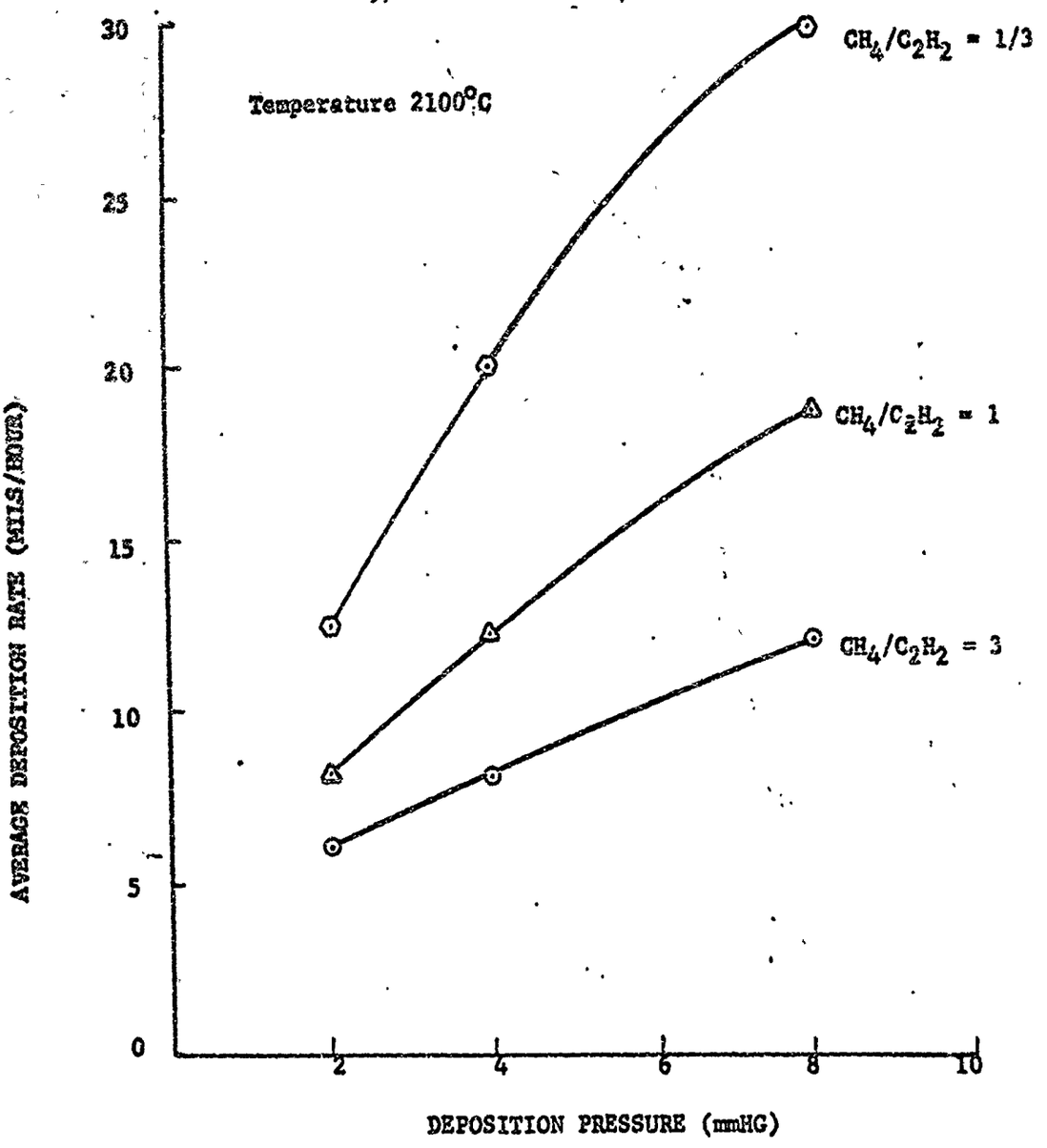


Figure 183

EFFECT OF METHANE/ACETYLENE RATIO ON DEPOSITION RATE AT VARIOUS DEPOSITION PRESSURES (3" DIAMETER TUBES)

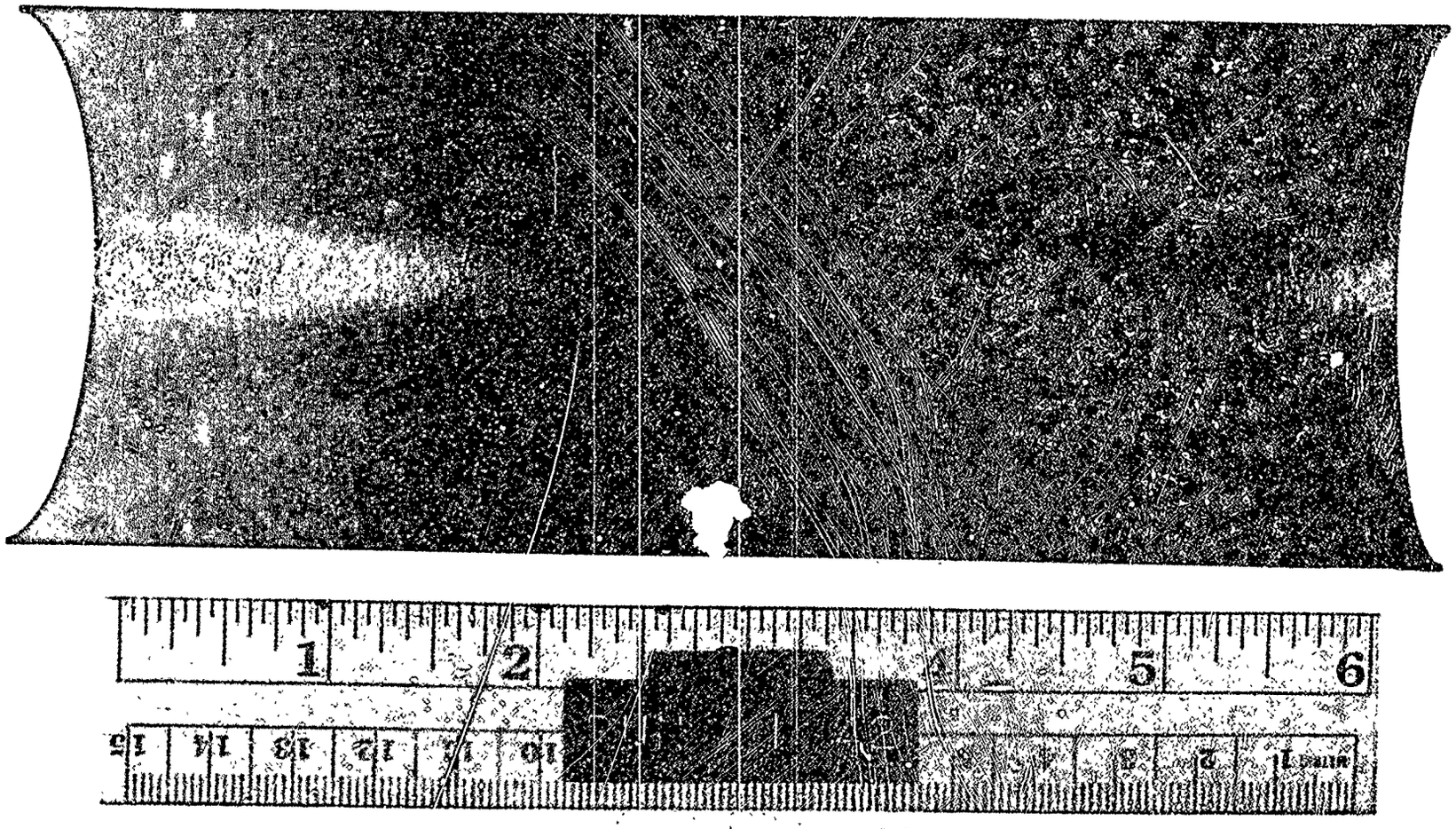


Figure 184

PHOTOGRAPH OF CYLINDER 1-42 ILLUSTRATING THE INNER SURFACE CONDITION AND OVERALL APPEARANCE (CH_4/C_2H_2 = 3, PRESSURE 2 mm Hg, TEMP., 2100°C

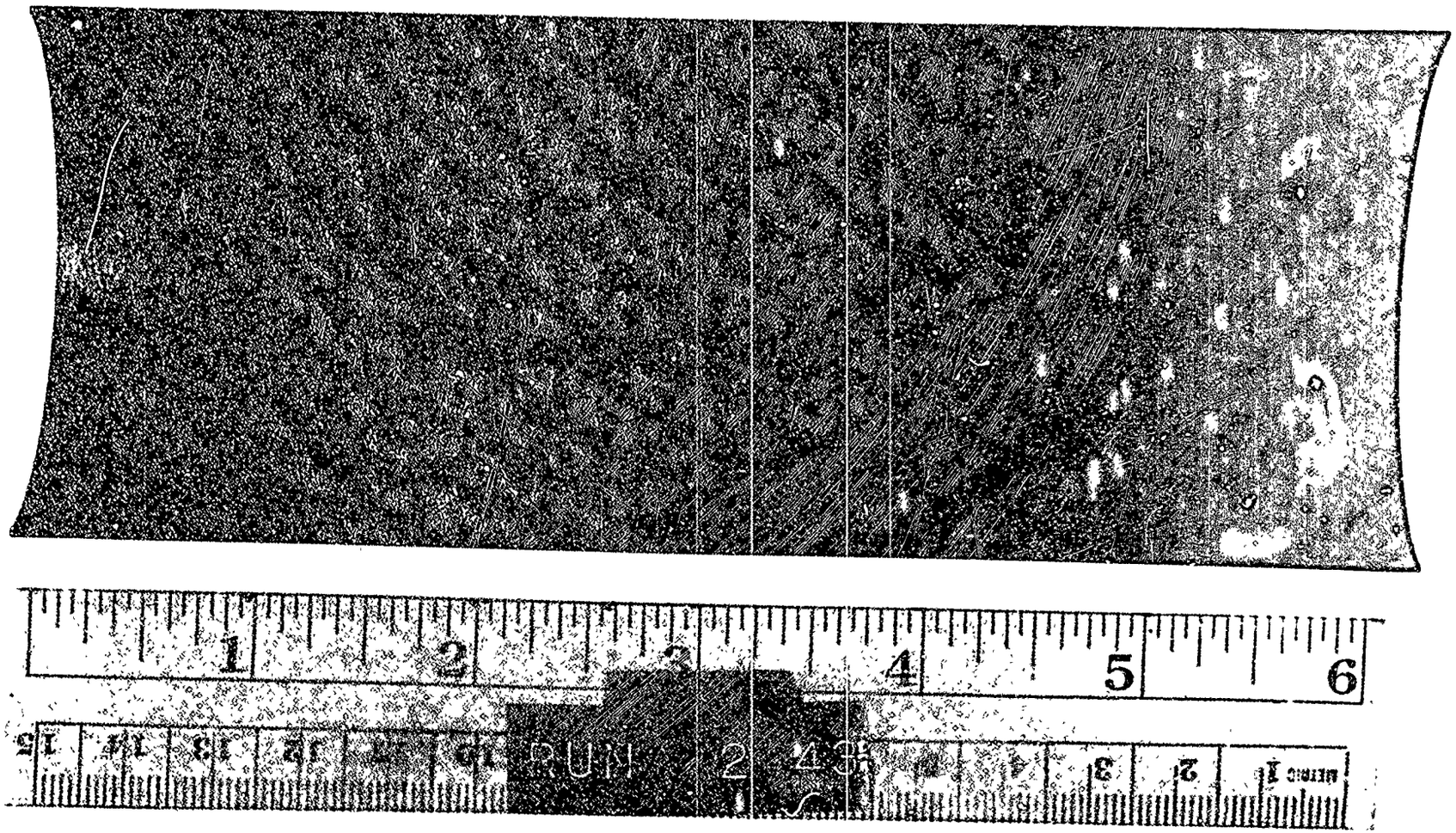


Figure 185

PHOTOGRAPH OF CYLINDER NO. 2-43 ILLUSTRATING THE INNER SURFACE CONDITION AND OVERALL APPEARANCE (CH_4/C_2H_2 = 3, PRESSURE 4 mm Hg, TEMP. 2100°C)

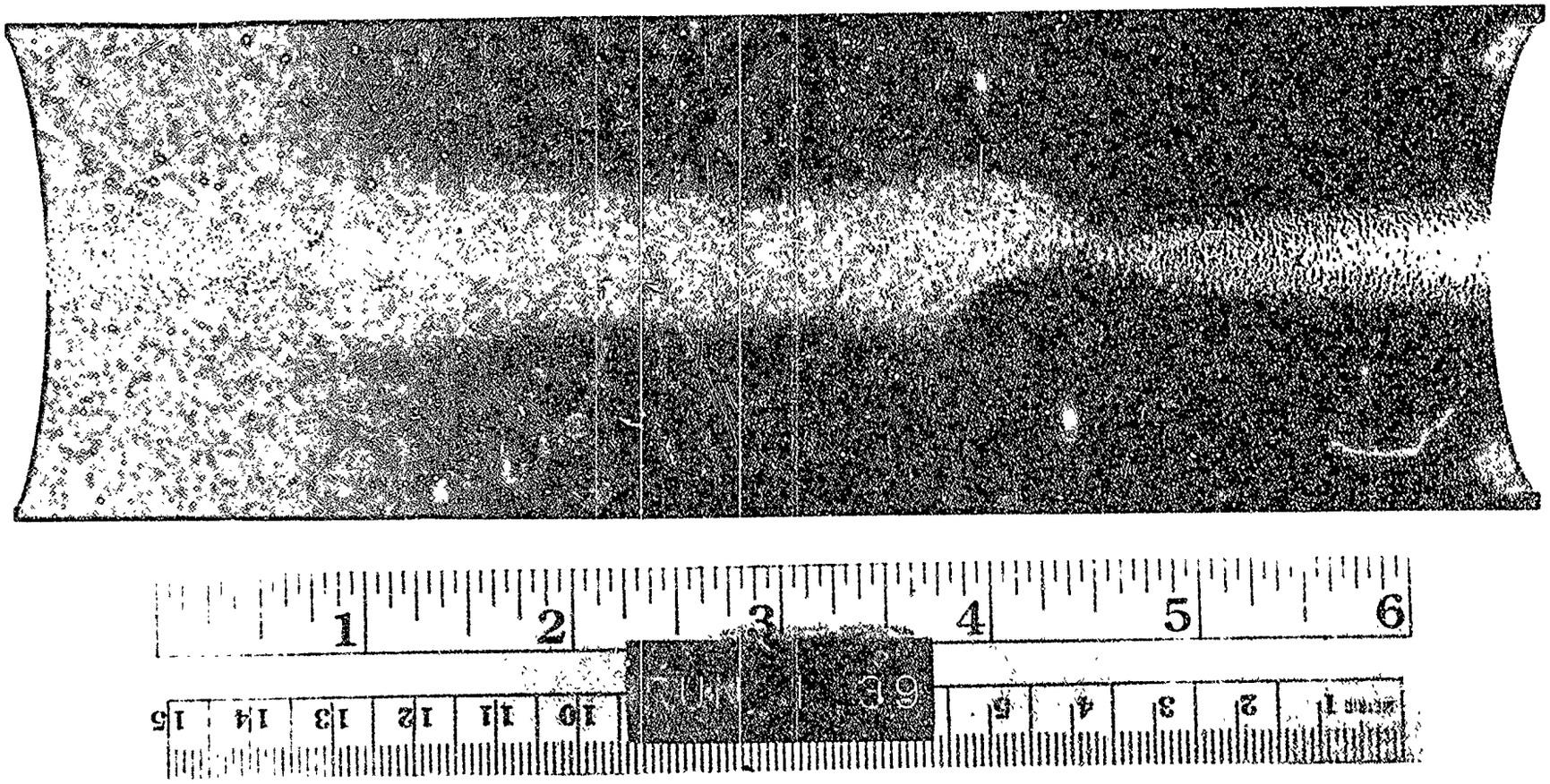


Figure 186

PHOTOGRAPH OF CYLINDER 1-39 ILLUSTRATING THE INNER SURFACE CONDITION AND OVERALL APPEARANCE (CH_4/C_2H_2 = 3, PRESSURE 8 mm Hg, TEMP. 2100°C)

PHOTOGRAPH OF CYLINDER 1-38 ILLUSTRATING THE INNER SURFACE CONDITION AND OVERALL APPEARANCE (CH_4/C_2H_2 = 1, PRESSURE 2 mm Hg, TEMP. 2100°C)

Figure 187

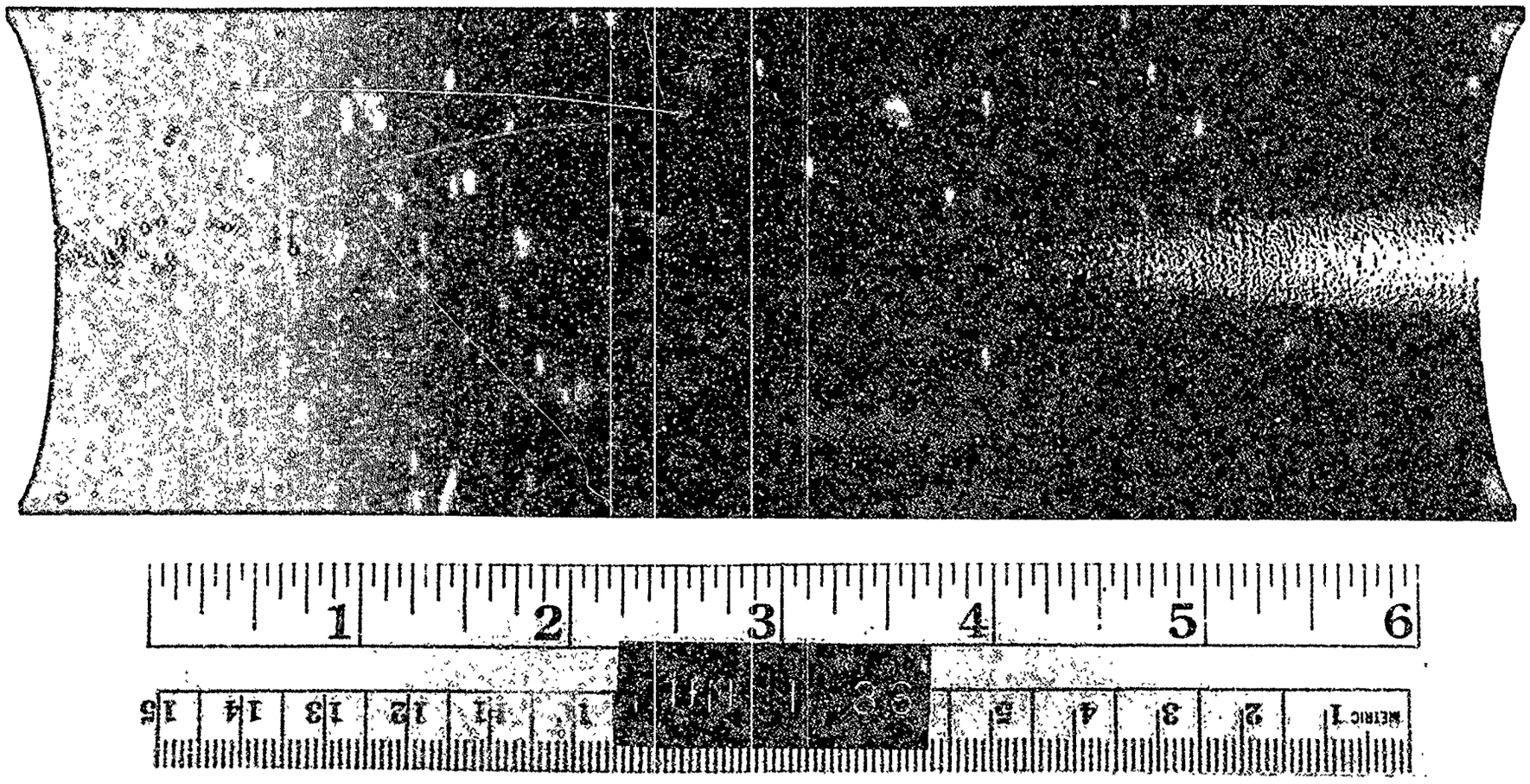


Figure 188

PHOTOGRAPH OF CYLINDER 1-36 ILLUSTRATING THE INNER SURFACE CONDITION AND OVERALL APPEARANCE (CH_4/C_2H_2 = 1, PRESSURE 4 mm Hg, TEMP. 2100°C)
NOTE: HEAVIER CONCENTRATION OF MEDIUM SIZED NODULES

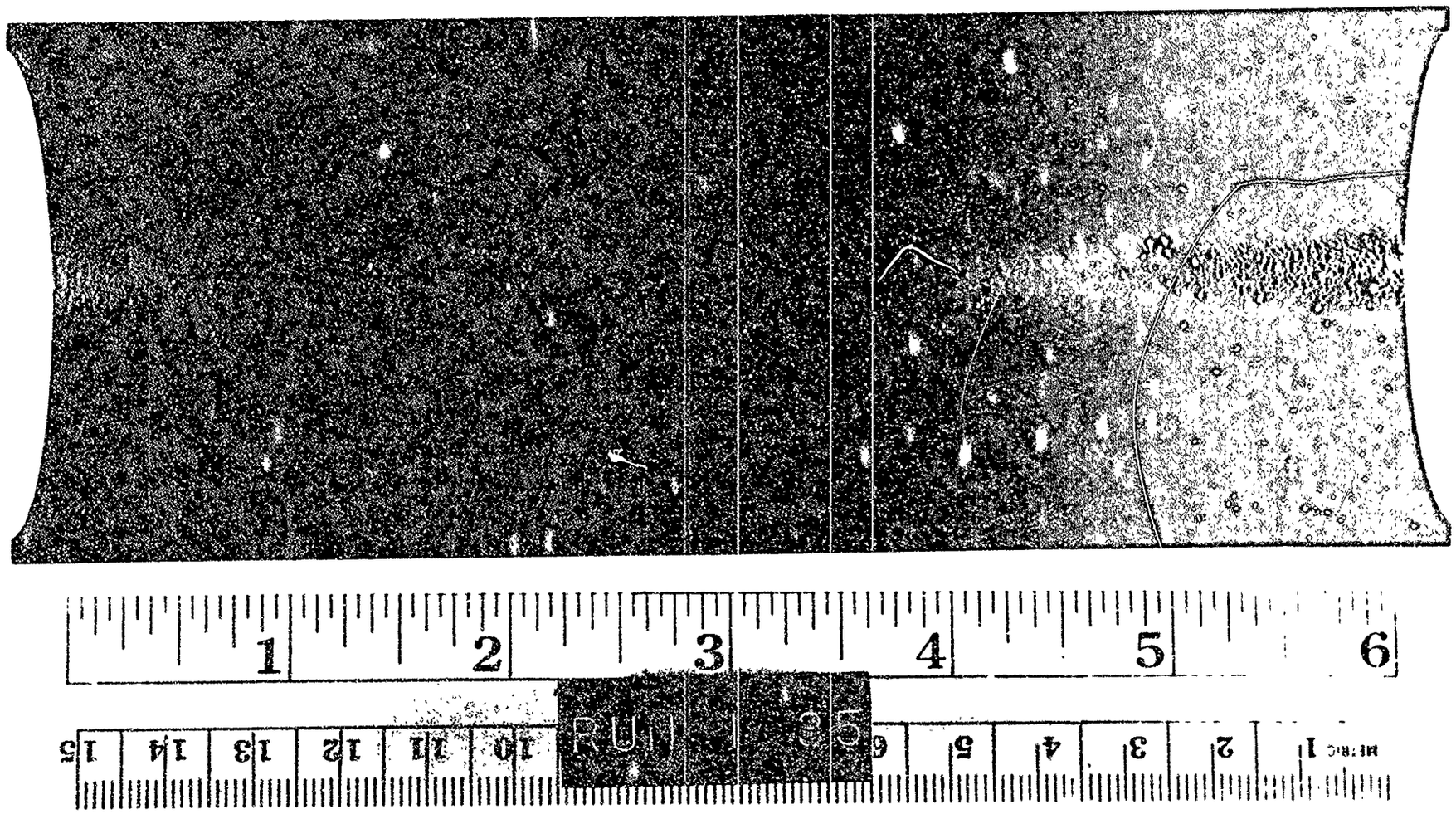


Figure 189

PHOTOGRAPH OF CYLINDER 1-35 ILLUSTRATING THE INNER SURFACE CONDITION AND OVERALL APPEARANCE (CH_4/C_2H_2 = 1, PRESSURE 8 mm Hg, TEMP. 2100°C)
NOTE: SCATTERING OF SOME LARGE NODULES

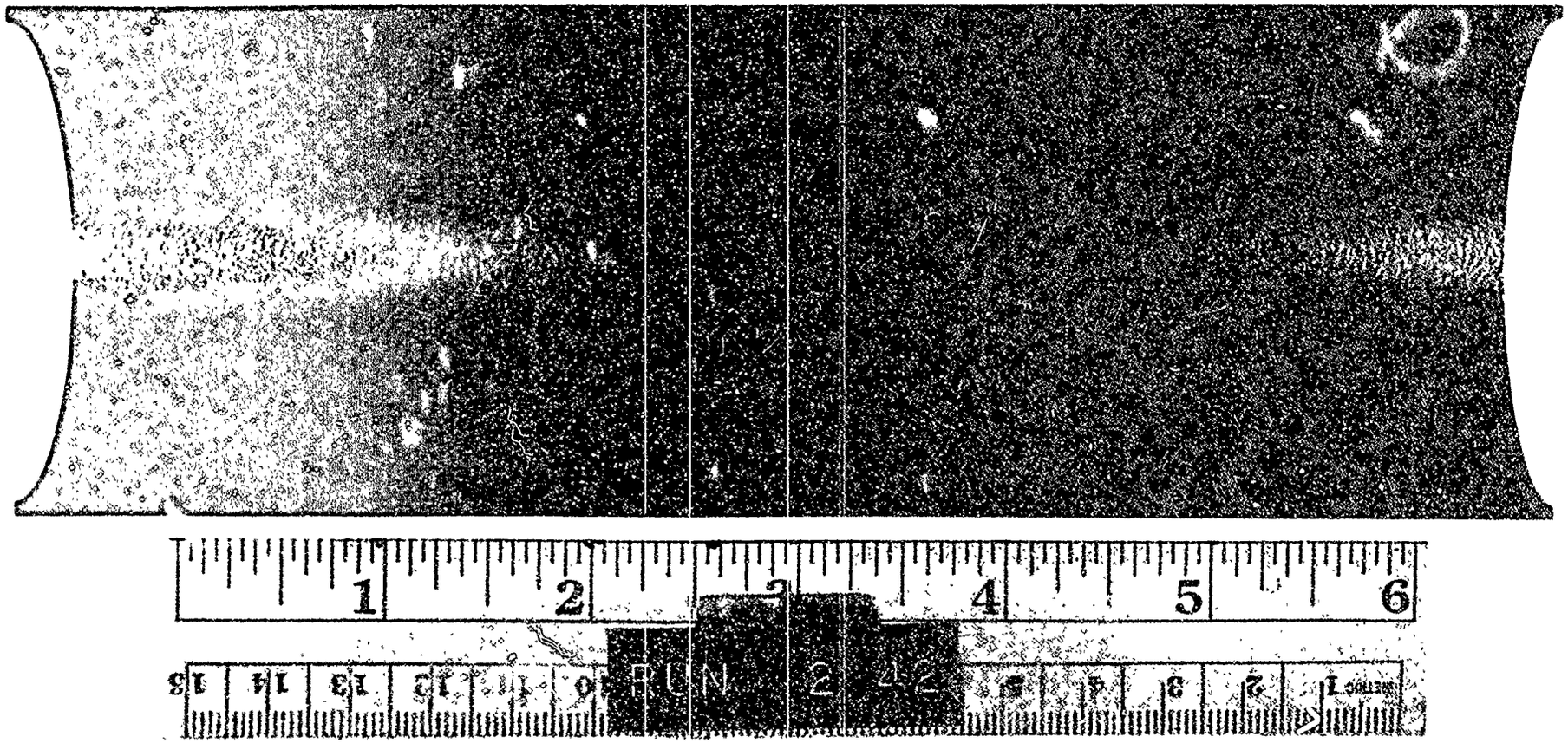


Figure 190

PHOTOGRAPH OF CYLINDER 2-42 ILLUSTRATING THE INNER SURFACE CONDITION AND OVERALL APPEARANCE (CH_4/C_2H_2 = 1/3, PRESSURE 2 mm Hg, TEMP. 2100°C)

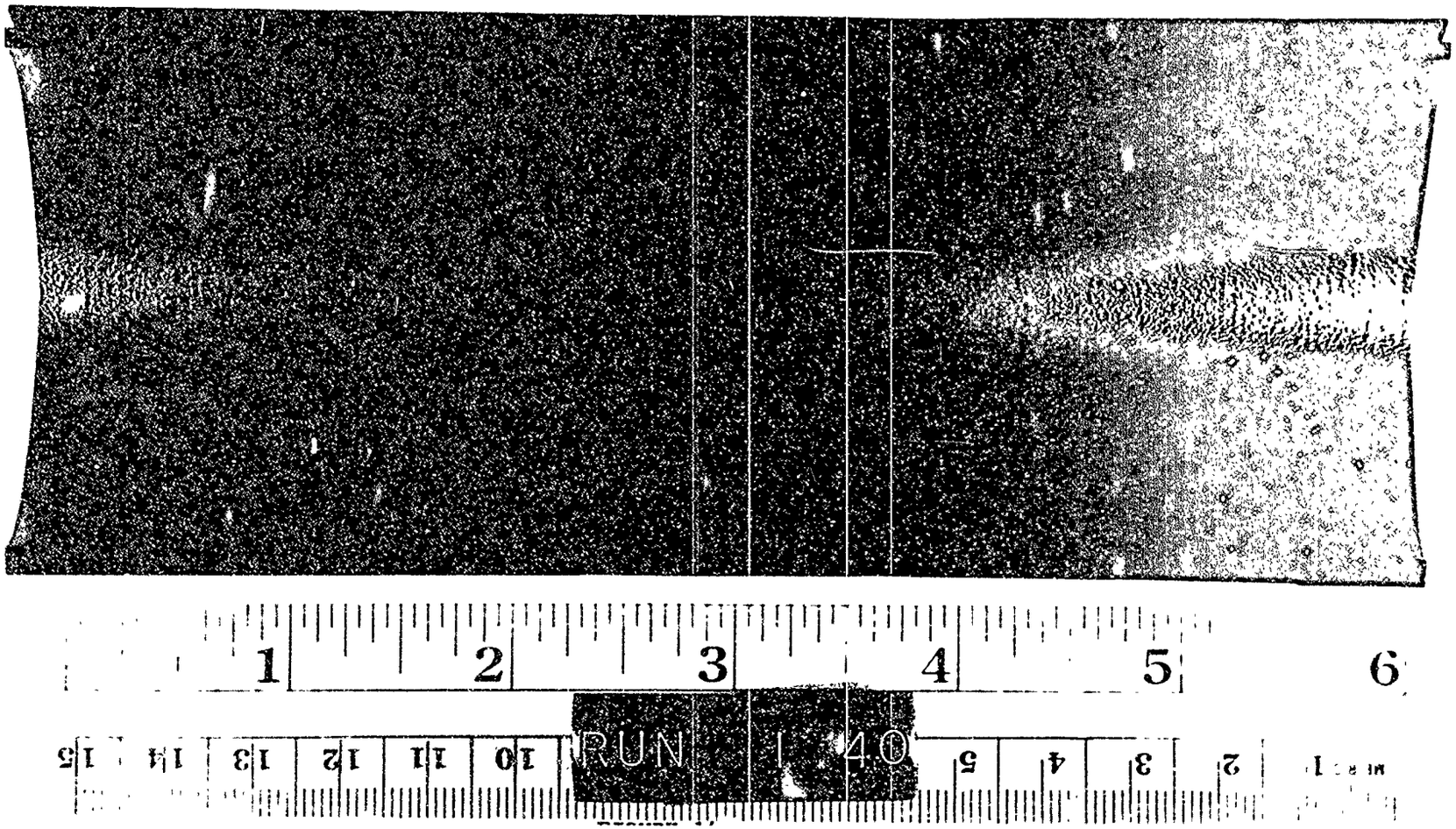


Figure 191

PHOTOGRAPH OF CYLINDER 1-40 ILLUSTRATING THE INNER SURFACE CONDITION AND OVERALL APPEARANCE (CH_4/C_2H_2 = 1/3, PRESSURE 4 mm Hg, TEMP. 2100°C) NOTE: COMPLETE SEPARATION OF OUTER SHELL AFTER CYLINDER WAS CUT. THIS TUBE HAD ONE LARGE DELAMINATION AND A HIGH T/R FOR UNALLOYED PYROLYTIC GRAPHITE.

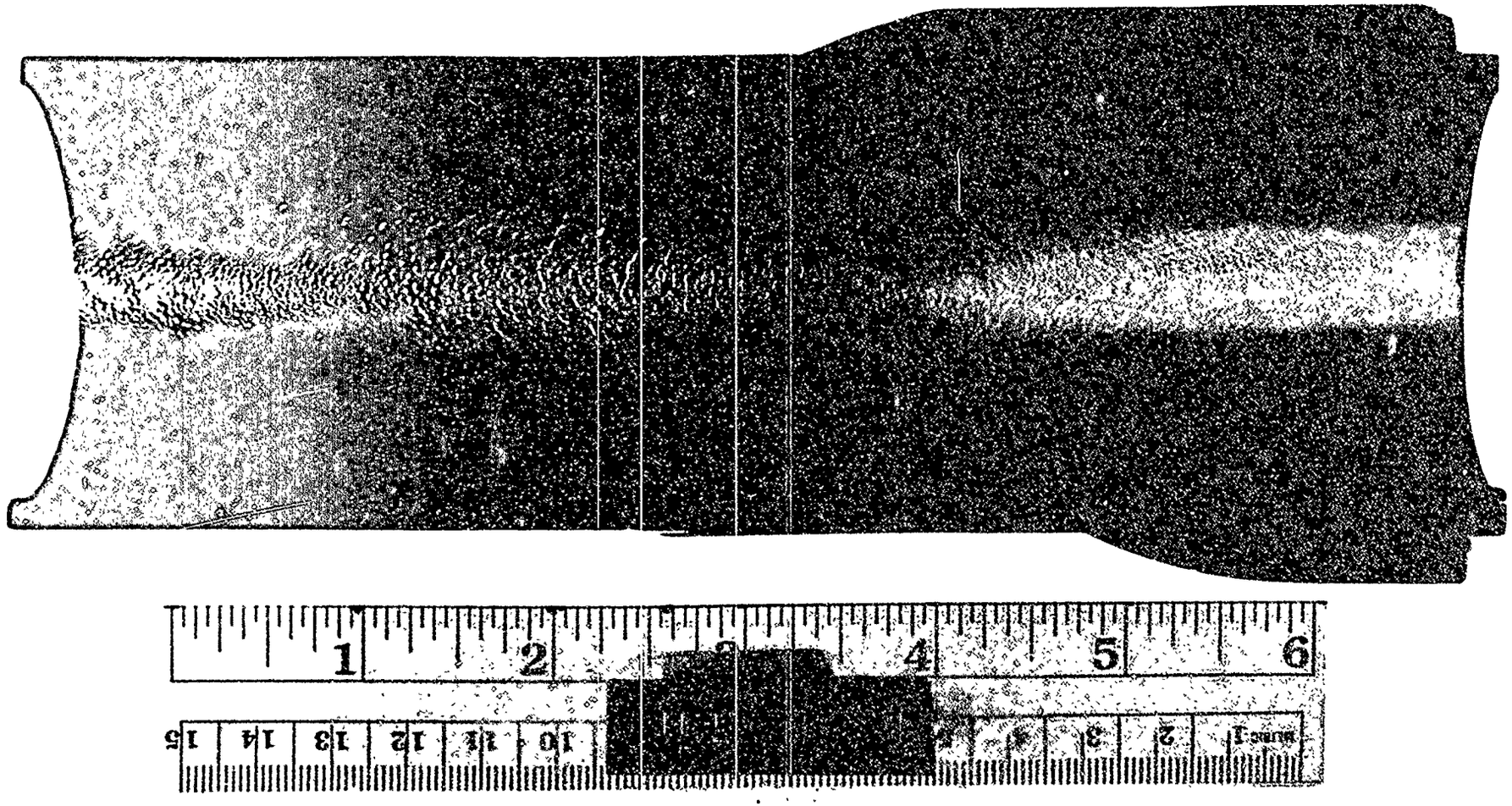


Figure 192

PHOTOGRAPH OF CYLINDER 1-41 ILLUSTRATING THE INNER SURFACE CONDITION AND OVERALL APPEARANCE (CH_4/C_2H_2 = 1/3, PRESSURE 8 mm Hg, TEMP. 2100°C) NOTE: THE NON-UNIFORM SURFACE CONDITION. THE GASES ENTERED FROM HEAVILY NODULATED END OF THE TUBE. THE T/R OF THIS CYLINDER WAS EXTREMELY HIGH FOR UNALLOYED PYROLYTIC GRAPHITE. ALSO NOTE SECTION OF MANDREL STILL ATTACHED TO THE P.G. TUBE DUE TO VERY POOR MANDREL SEPARATION.

Figure 193

PHOTOGRAPH OF CYLINDER 2-41 ILLUSTRATING THE INNER SURFACE CONDITION AND OVERALL APPEARANCE (CH_4/C_2H_2 = 1, PRESSURE 4 mm Hg, TEMP. 1925°C)
NOTE: THE SURFACE CONDITION OF THE GAS OUTLET END OF THE TUBE WAS POOR DUE TO SPALLATION.

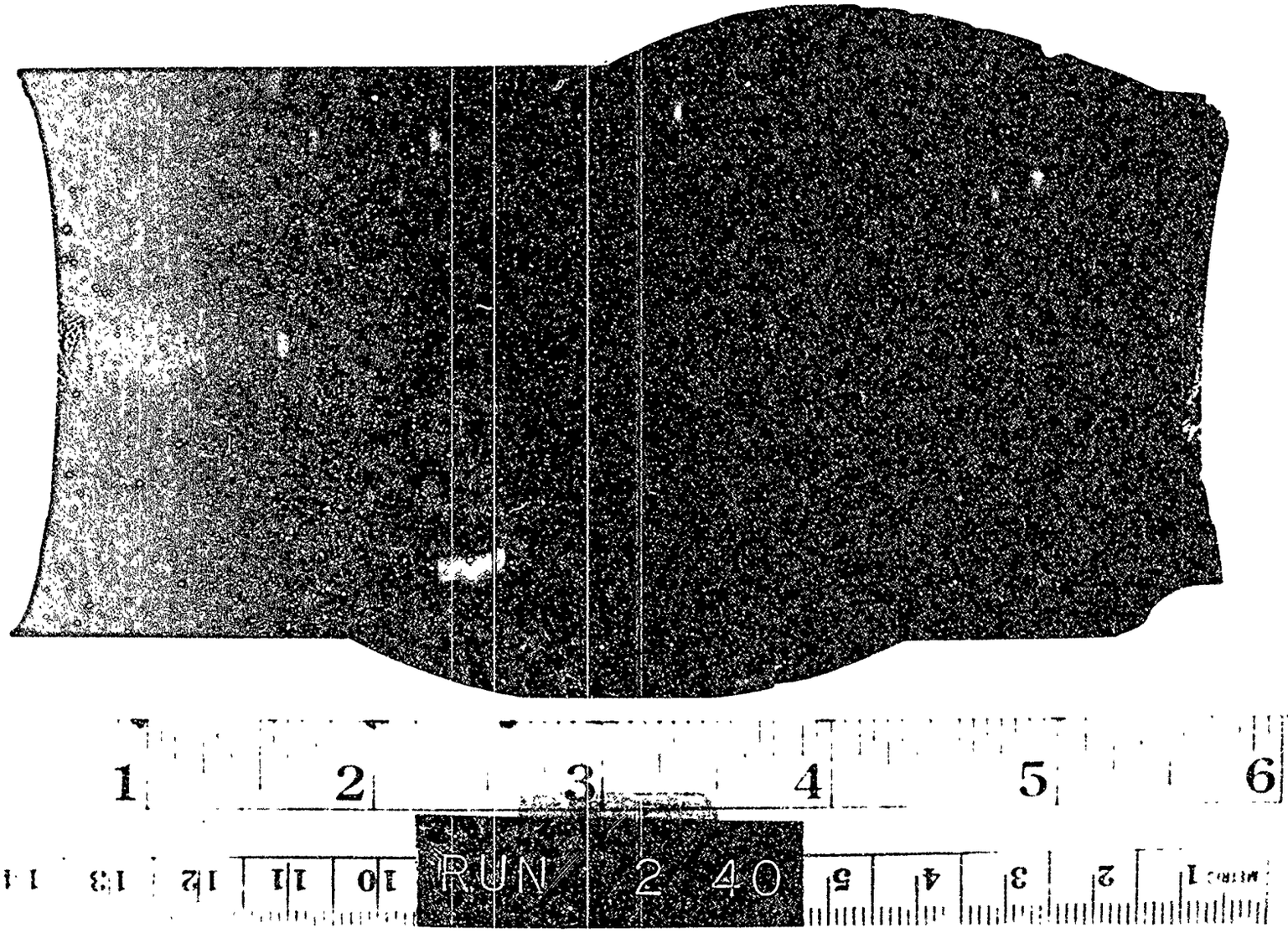
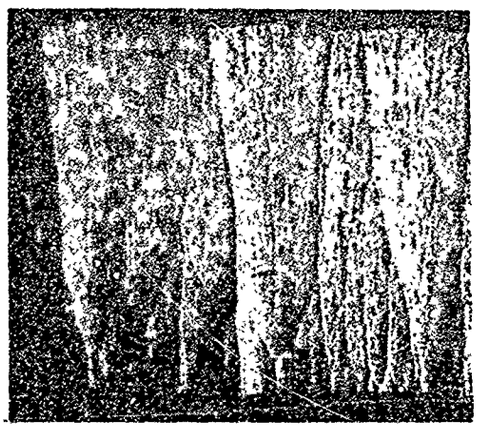
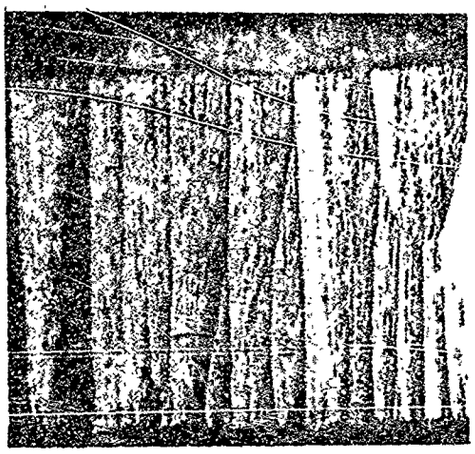


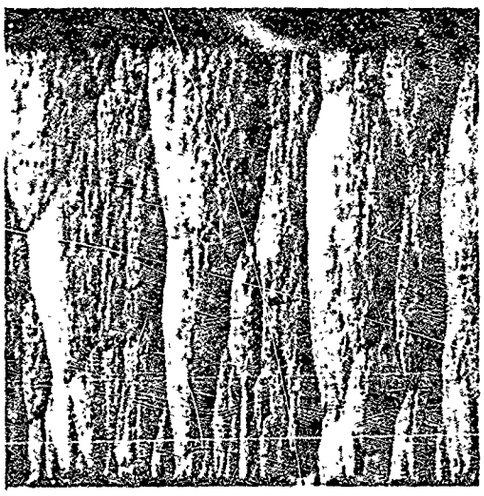
Figure 194

PHOTOGRAPH OF CYLINDER 2-40 ILLUSTRATING THE INNER SURFACE CONDITION AND OVERALL APPEARANCE (CH_4/C_2H_2 = 1, PRESSURE 4 mm Hg, TEMP. 1750°C)
NOTE: SECTION OF MANDREL STILL ATTACHED TO TUBE DUE TO POOR MANDREL SEPARATION.



RUN NO. 1-42 (TOP)
CH_4/C_2H_2 = 3
Pressure = 2 mmHg
Density = 2.17 gm/cc





(TOP) Density = 2.09 gm/cc (BOTTOM) Density 2.13 gm/cc
RUN NO. 2-43 CH_4/C_2H_2 = 3, PRESSURE = 4 mmHg



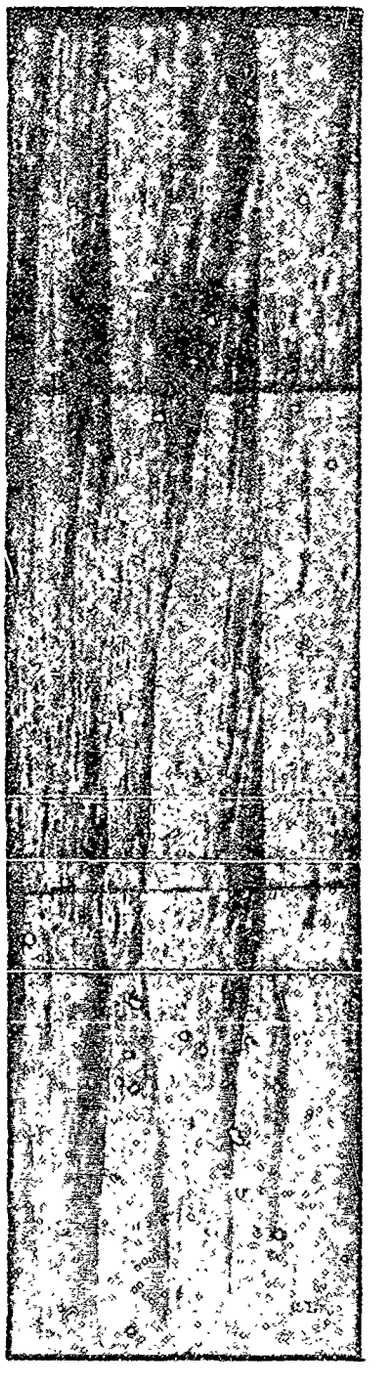
RUN NO. 1-39 (TOP)
CH_4/C_2H_2 = 3
Pressure = 8 mmHg
Density = 2.18 gm/cc

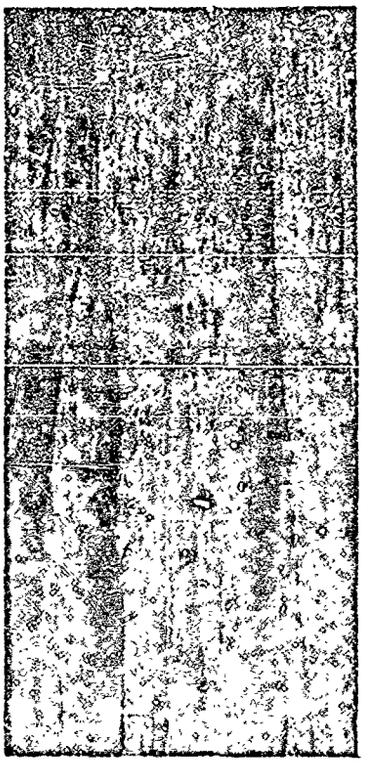
PHOTOMICROGRAPHS THROUGH DEPOSIT THICKNESS SHOWING MICROSTRUCTURE OF THESE TUBES 60X

Figure 195



Run No. 1-38 (TOP)
CH_4/C_2 = 1
Pressure = 2 mmHg
Density = 2.17 gm/cc



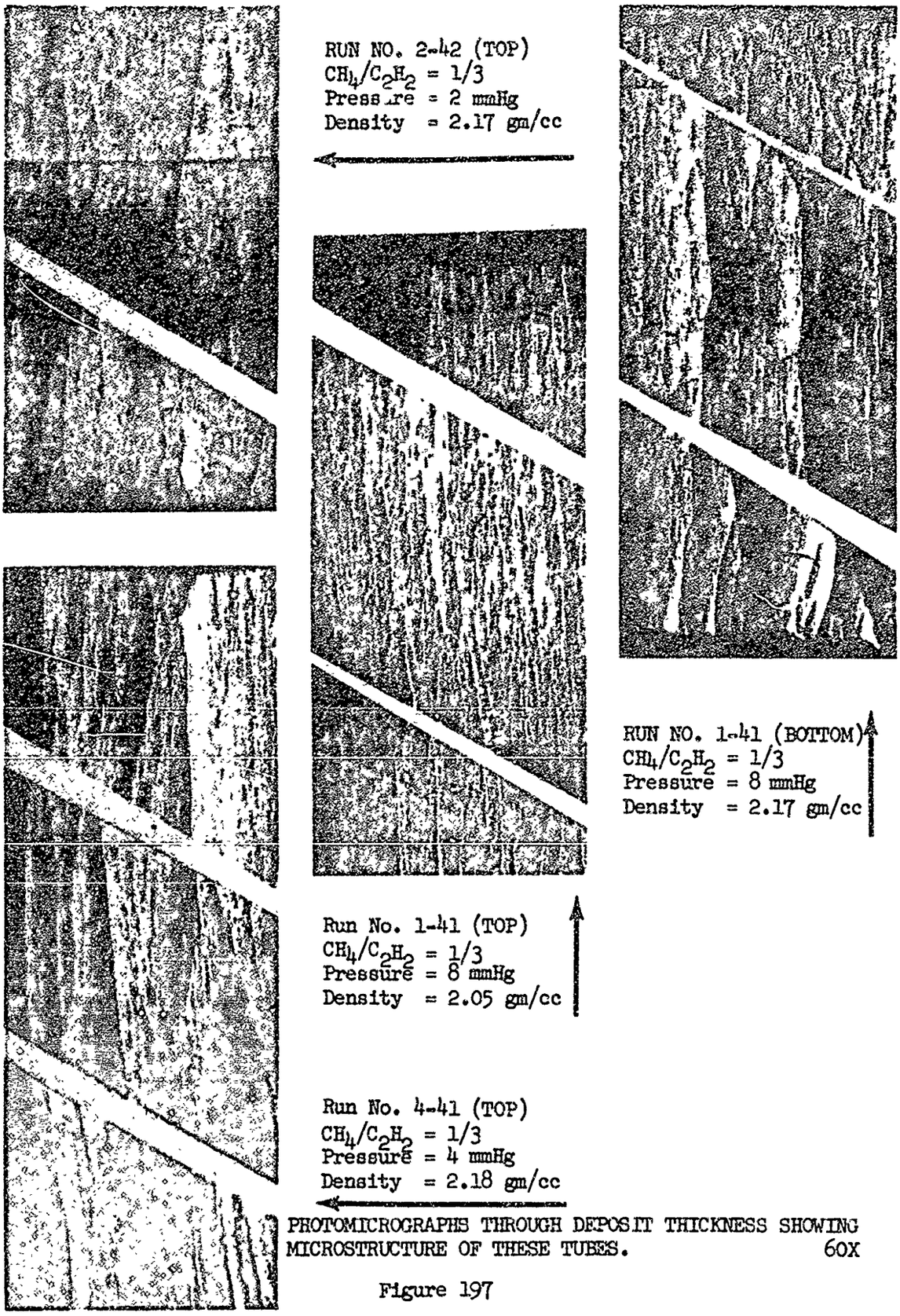


Run No. 1-36 (TOP)
CH_4/C_2H_2 = 1,
Pressure = 4 mmHg
Density = 2.18 gm/cc

Run No. 1-35 (TOP)
CH_4/C_2H_2 = 1,
Pressure = 8 mmHg
Density = 2.18 gm/cc

PHOTOMICROGRAPH THROUGH DEPOSIT THICKNESS SHOWING MICROSTRUCTURE OF THESE TUBES. 60X

Figure 196



RUN NO. 2-42 (TOP)
CH_4/C_2H_2 = 1/3
Pressure = 2 mmHg
Density = 2.17 gm/cc

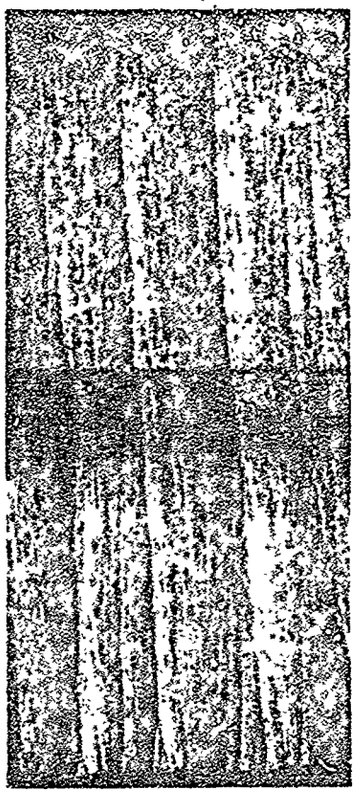
RUN NO. 1-41 (BOTTOM)
CH_4/C_2H_2 = 1/3
Pressure = 8 mmHg
Density = 2.17 gm/cc

Run No. 1-41 (TOP)
CH_4/C_2H_2 = 1/3
Pressure = 8 mmHg
Density = 2.05 gm/cc

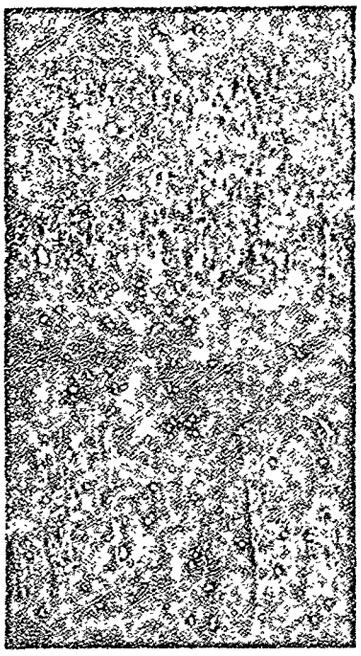
Run No. 4-41 (TOP)
CH_4/C_2H_2 = 1/3
Pressure = 4 mmHg
Density = 2.18 gm/cc

PHOTOMICROGRAPHS THROUGH DEPOSIT THICKNESS SHOWING MICROSTRUCTURE OF THESE TUBES. 60X

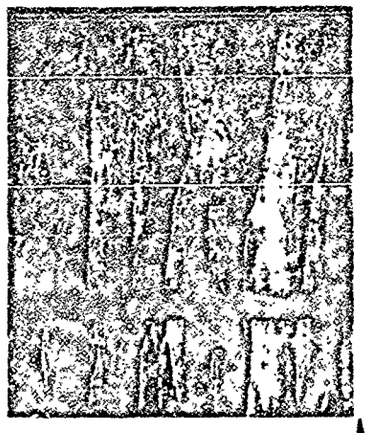
Figure 197



RUN NO. 1-36 (TOP)
CH_4/C_2H_2 = 1
Pressure = 4 mmHg
Density = 2.18 gm/cc
Temp. = 2100°C



RUN NO. 2-40 (TOP)
CH_4/C_2H_2 = 1
Pressure = 4 mmHg
Density = 1.10 gm/cc
Temp. = 1750°C



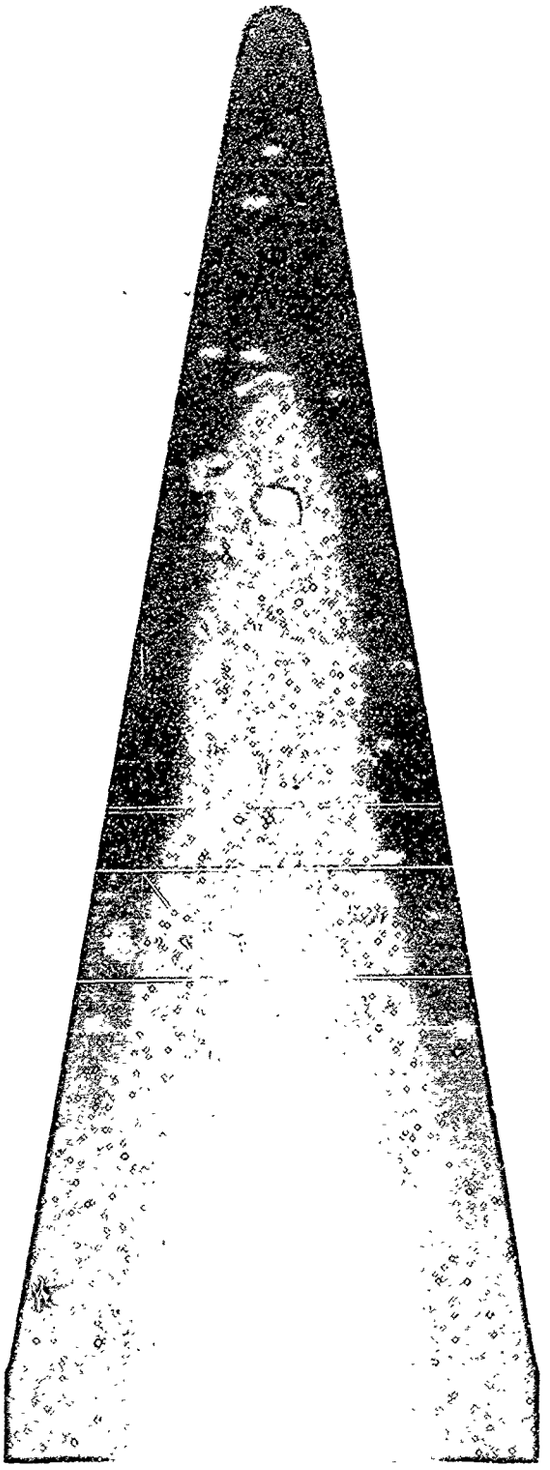


RUN NO. 2-41 (BOTTOM)
CH_4/C_2H_2 = 1
Pressure = 4 mmHg
Density = 1.93 gm/cc
Temp. = 1925°C

RUN NO. 2-41 (TOP)
CH_4/C_2H_2 = 1
Pressure = 4 mmHg
Density = 2.03 gm/cc
Temp. = 1925°C

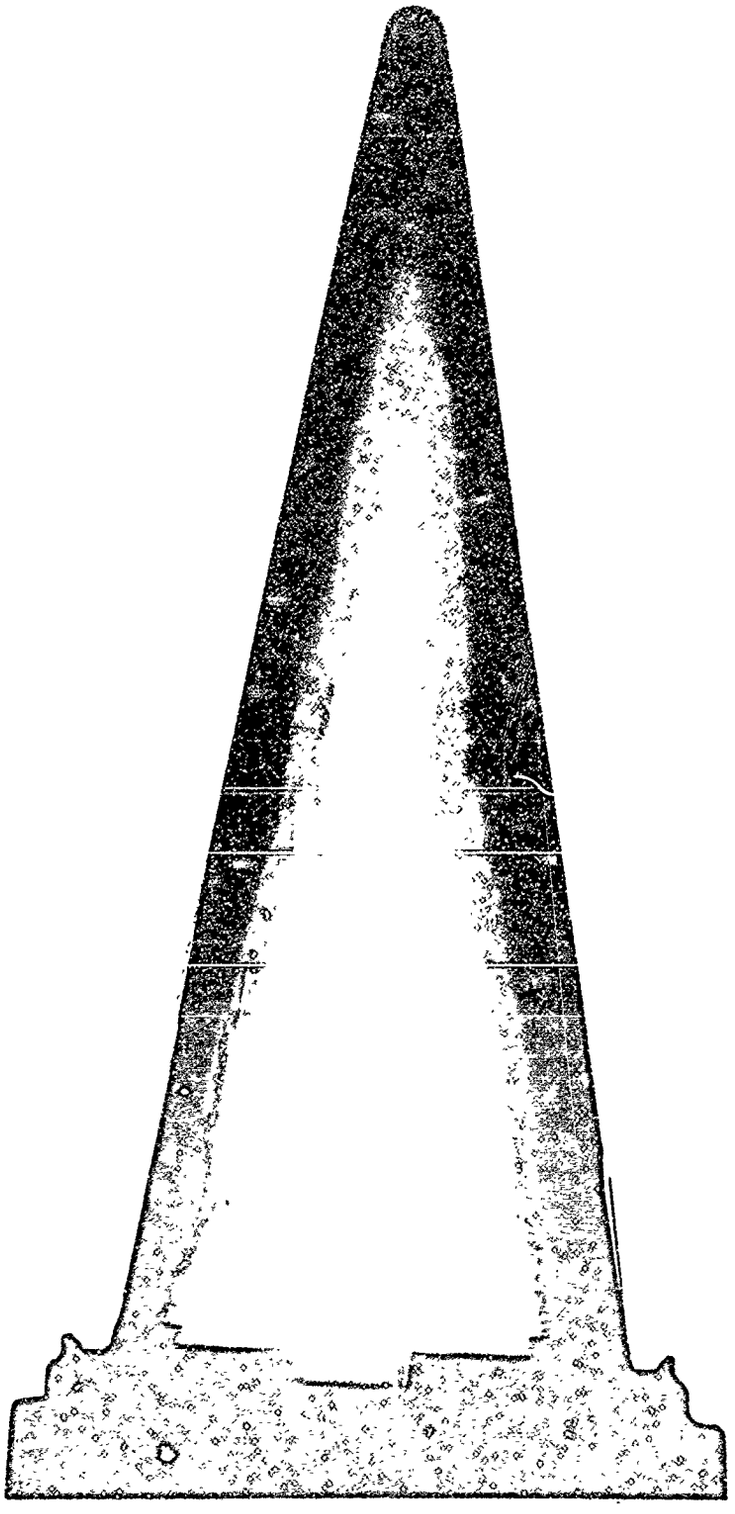
PHOTOMICROGRAPHS THROUGH DEPOSIT THICKNESS SHOWING MICROSTRUCTURE OF THESE TUBES. 60X
NOTE: DENSITY VARIATION WITH CHANGE IN DEPOSITION TEMPERATURE.

Figure 198



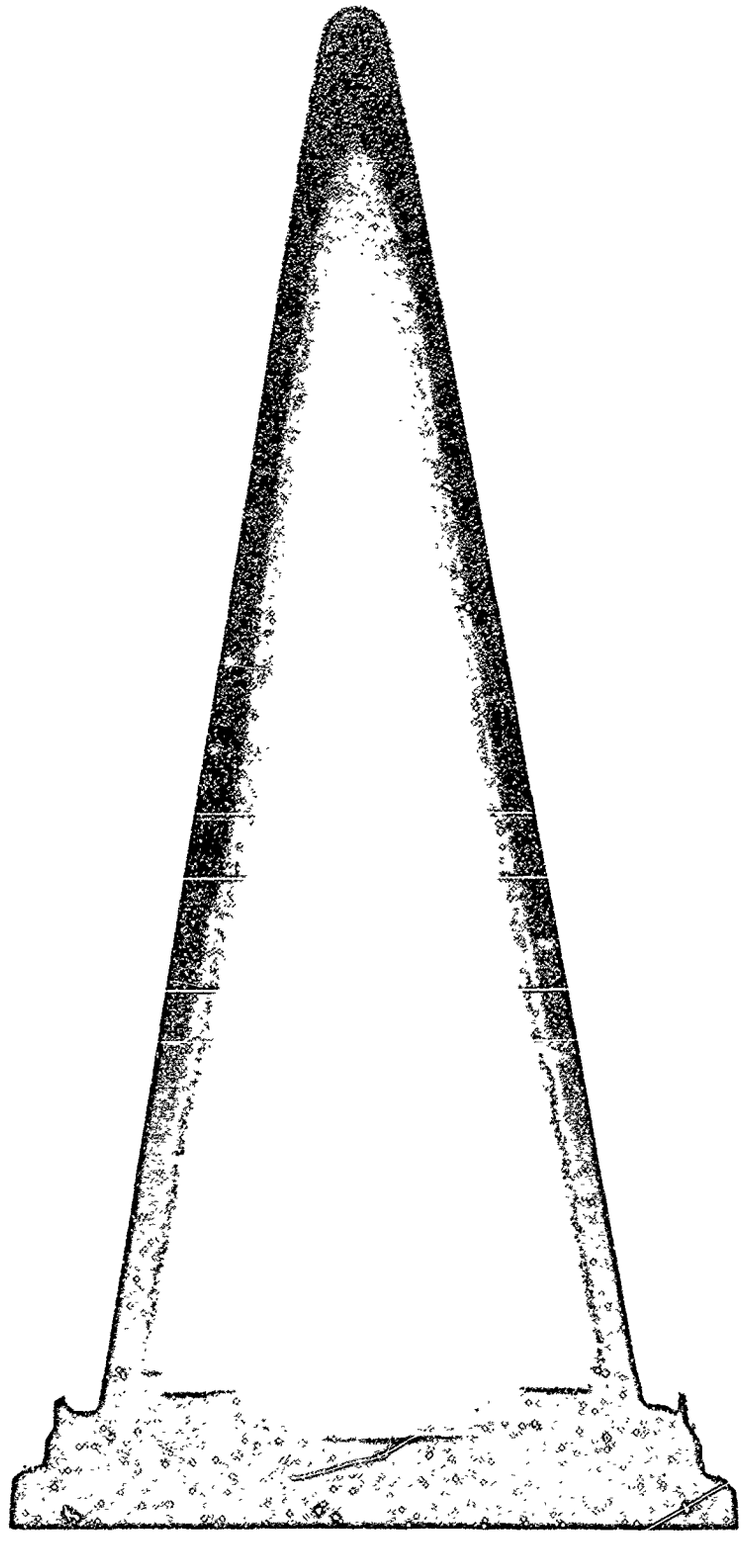
Radiographic Positive Nose Cone 1-43
Illustrating the General Growth Pattern

Figure 199



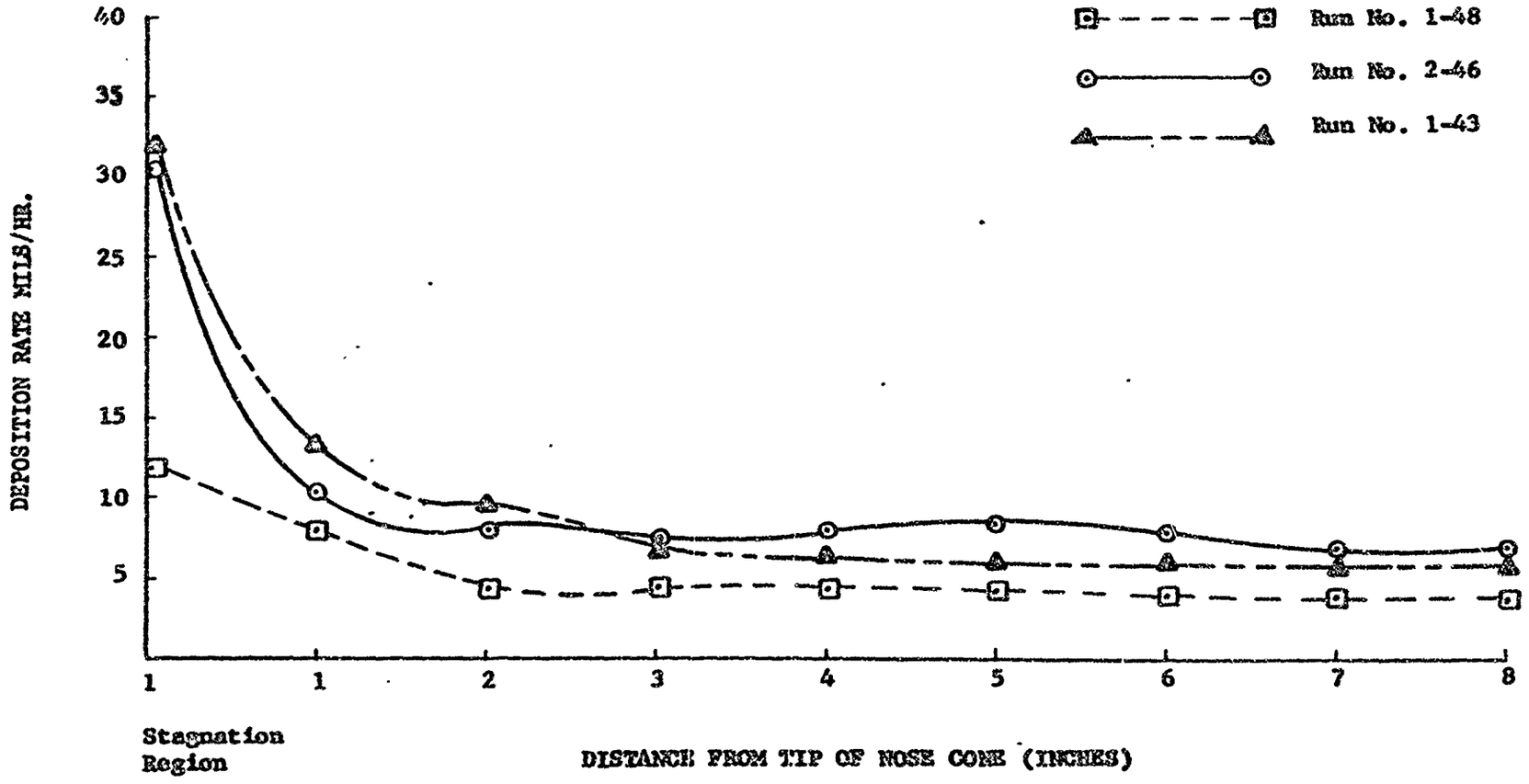
Radiographic Positive Nose Cone 2-46
Illustrating the General Growth Pattern

Figure 200



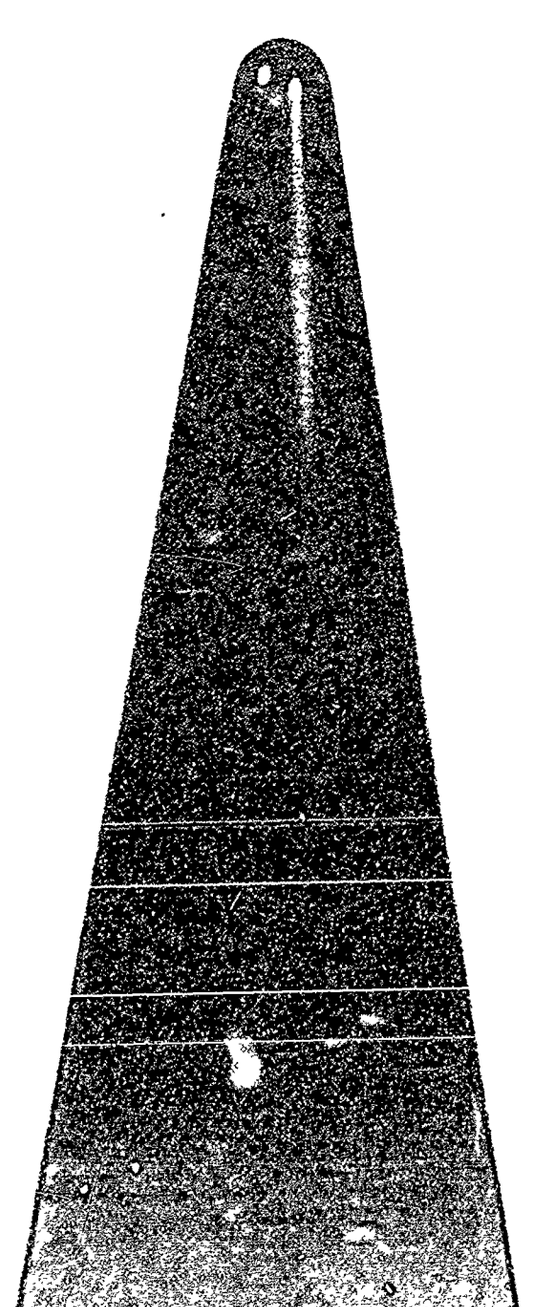
Radiographic Positive Nose Cone 1-48
Illustrating the General Growth Pattern

Figure 201



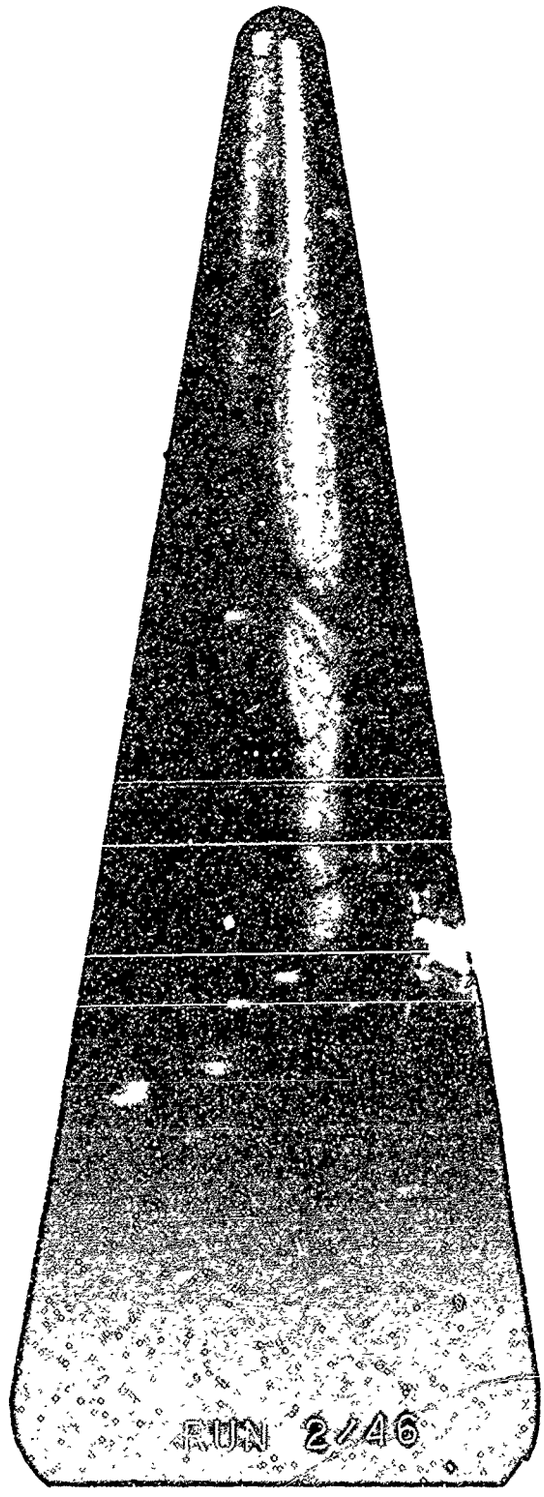
Deposition Thickness Profile - Nose Cones 1-43, 2-46 and 1-48
(Data Taken from Radiograph Film)

Figure 202



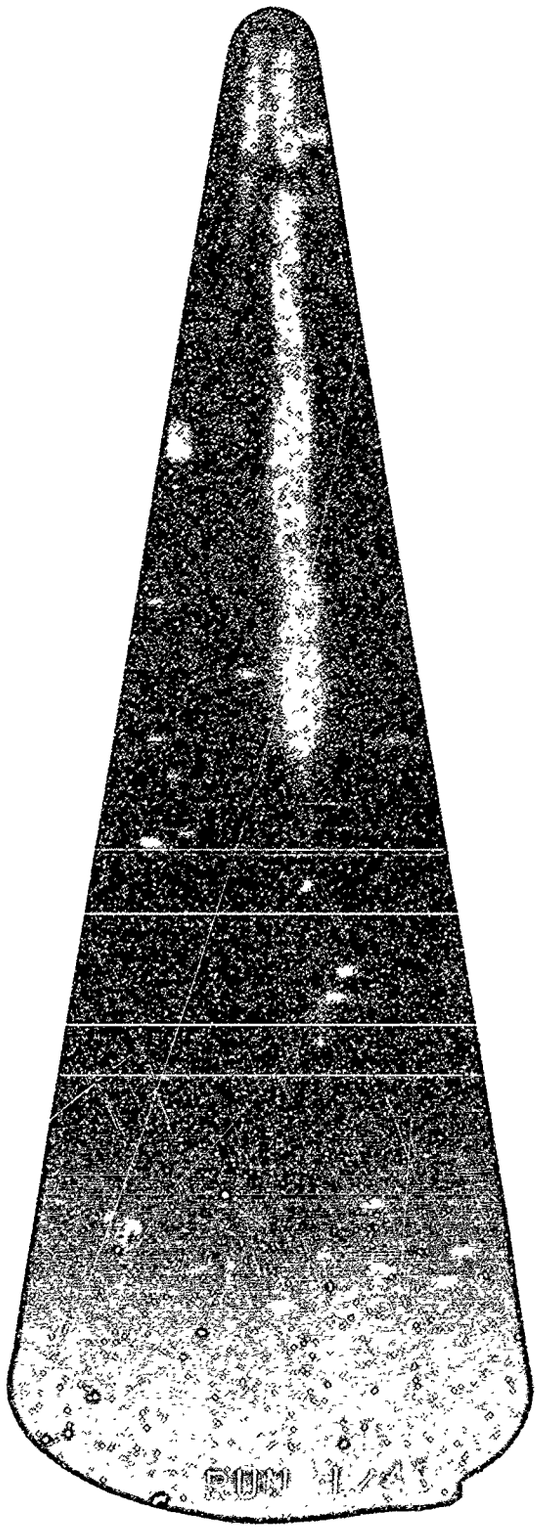
Photograph of Nose Cone 1-43 Illustrating
Surface Condition and Overall Appearance
Note the Slight Spallation of Very Thin Precoat

Figure 203



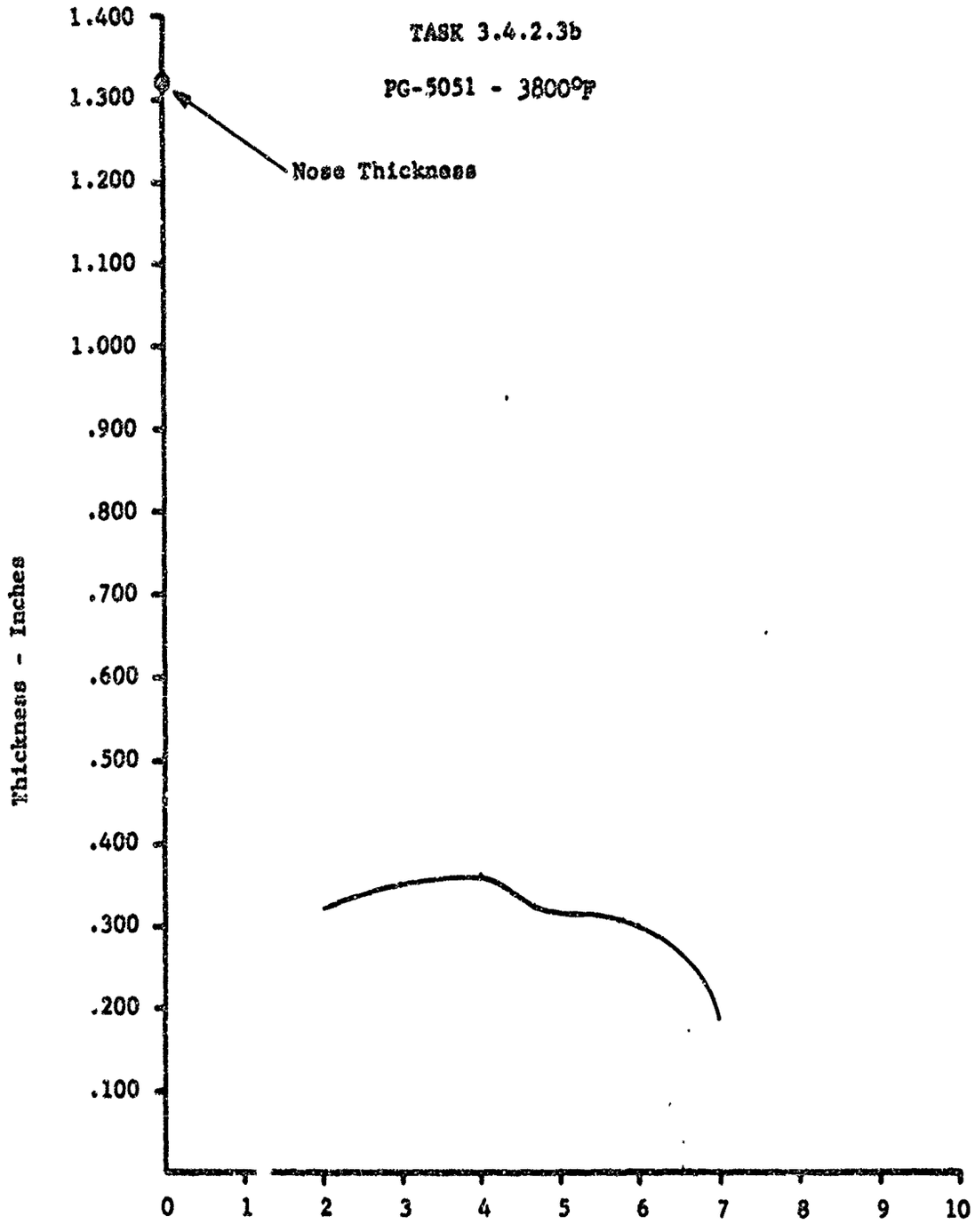
Photograph of Nose Cone 2-46 Illustrating Surface Condition and Overall Appearance Note Extremely Heavy Spallation Due to Residual Stresses Introduced by Process Fluctuations.

Figure 204



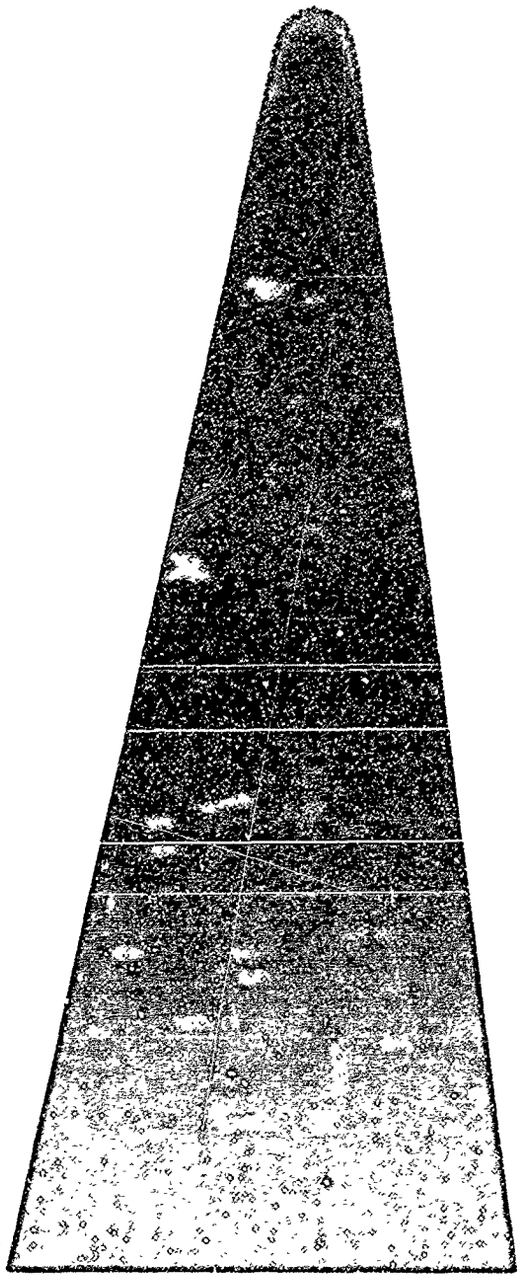
Photograph of Nose Cone 1-48 Illustrating
Surface Condition and Overall Appearance

Figure 205



Deposition Thickness Profile

Figure 206



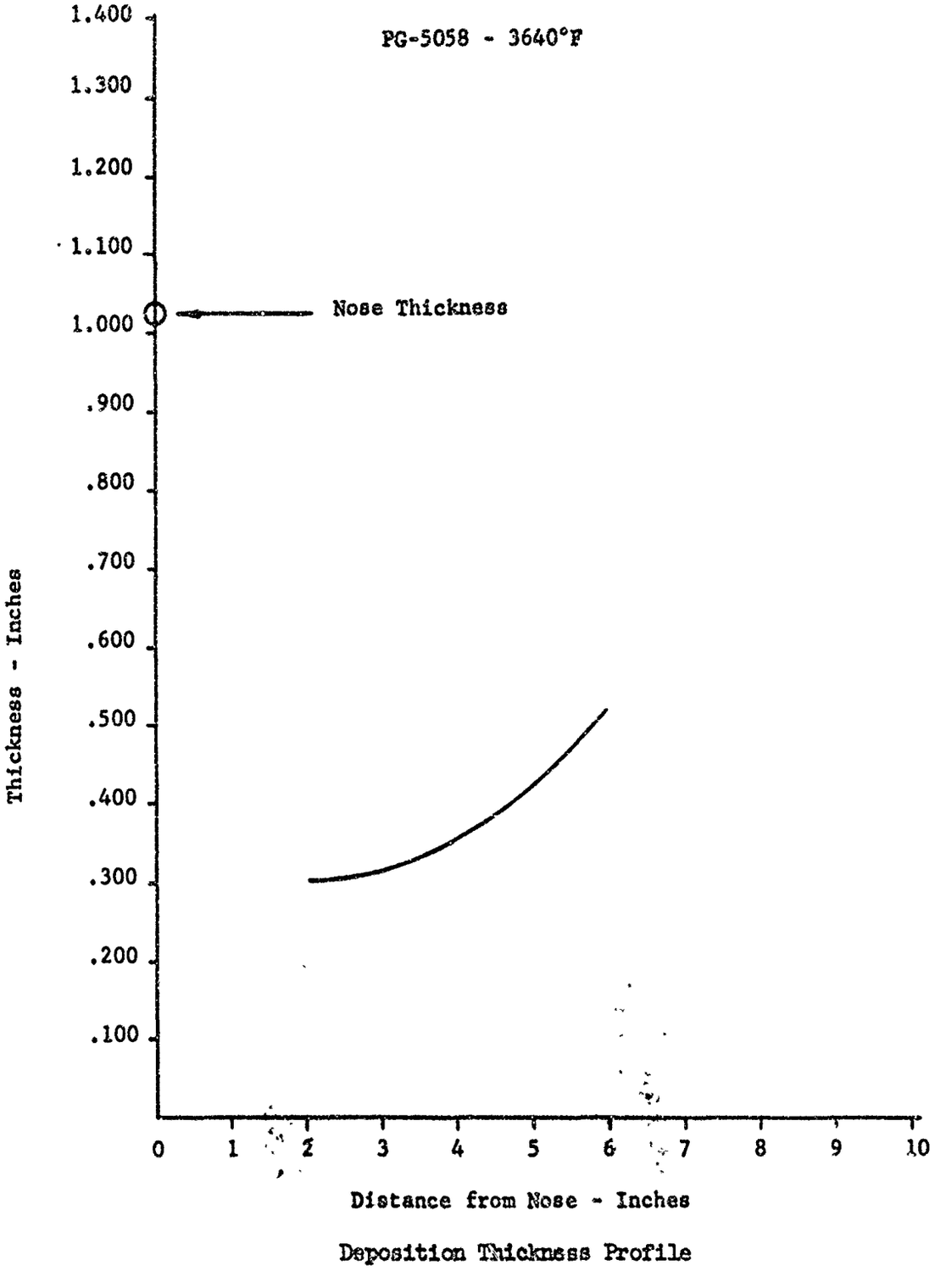
Task 3.4.2.3b

Radiograph of 5051

Figure 207

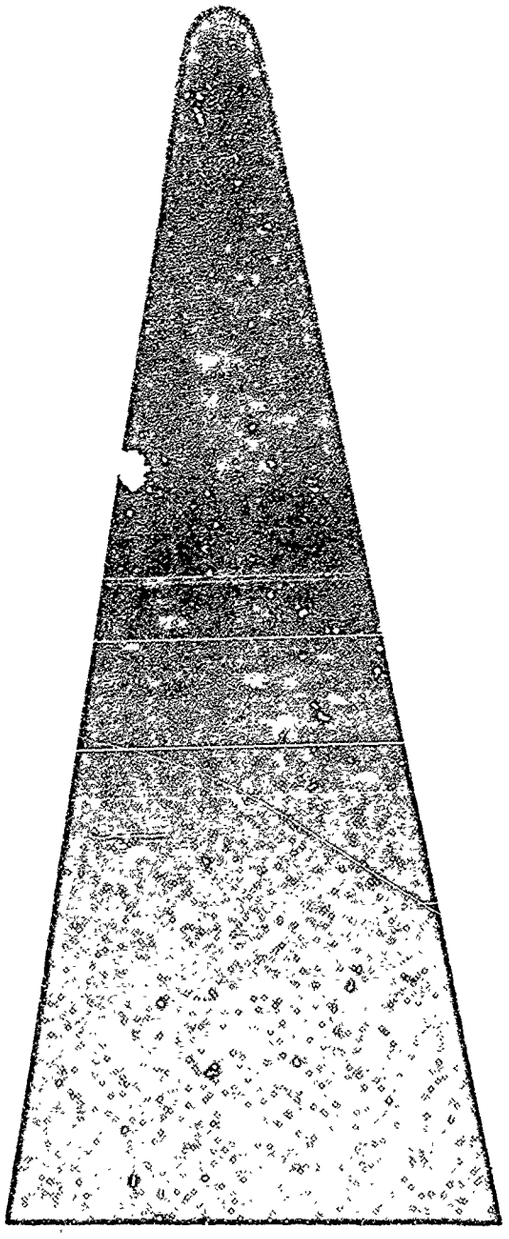
Task 3.4.2.3b

PG-5058 - 3640°F



Deposition Thickness Profile

Figure 208



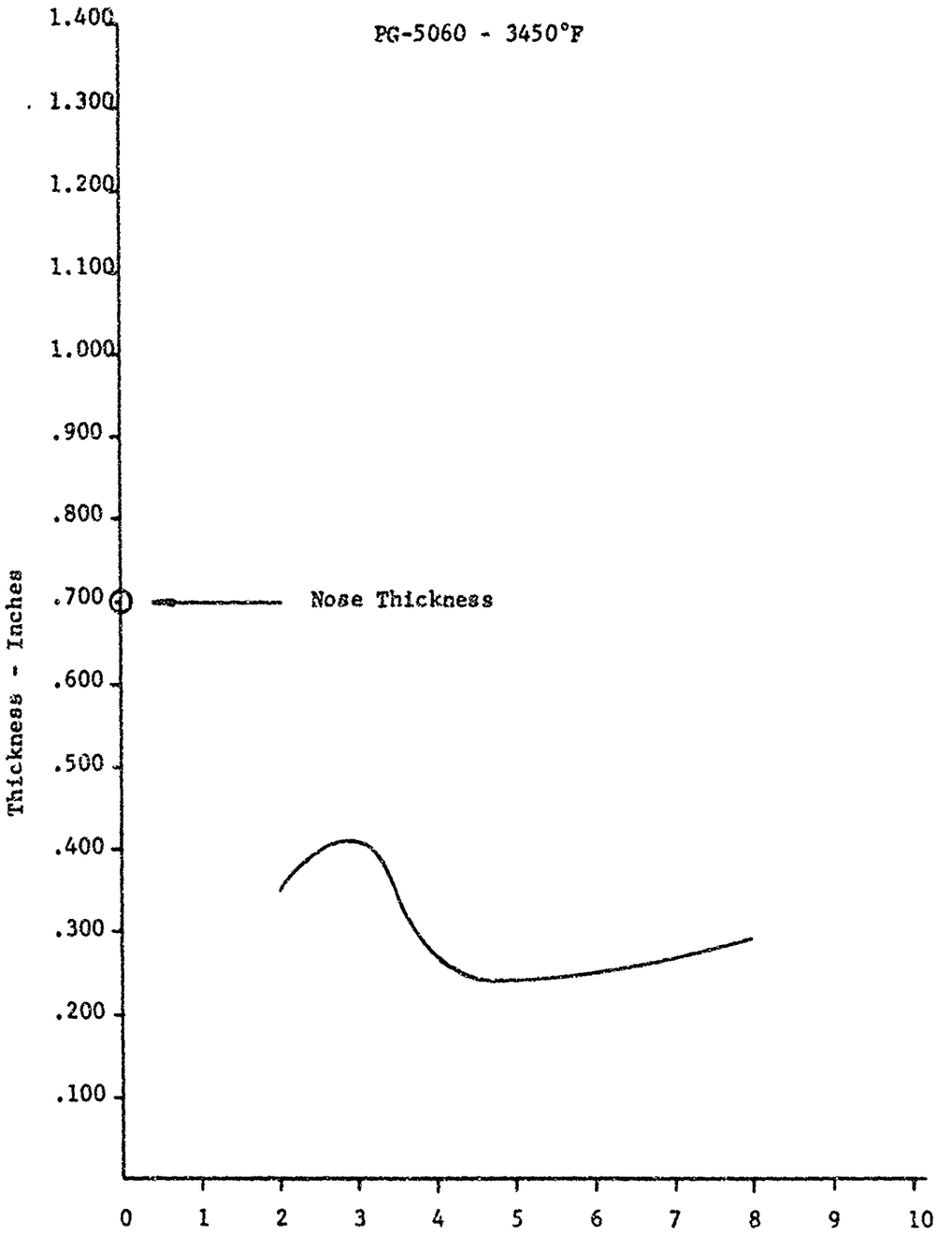
Task 3.4.2.3b

Radiograph of 5058

Figure 209

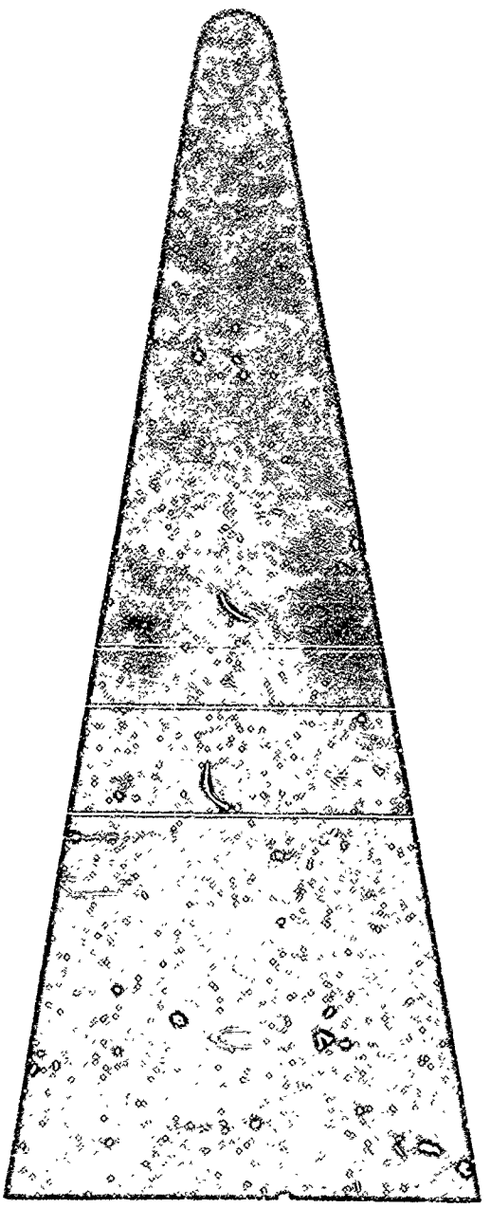
Task 3.4.2.3b

PG-5060 - 3450°F



Deposition Thickness Profile

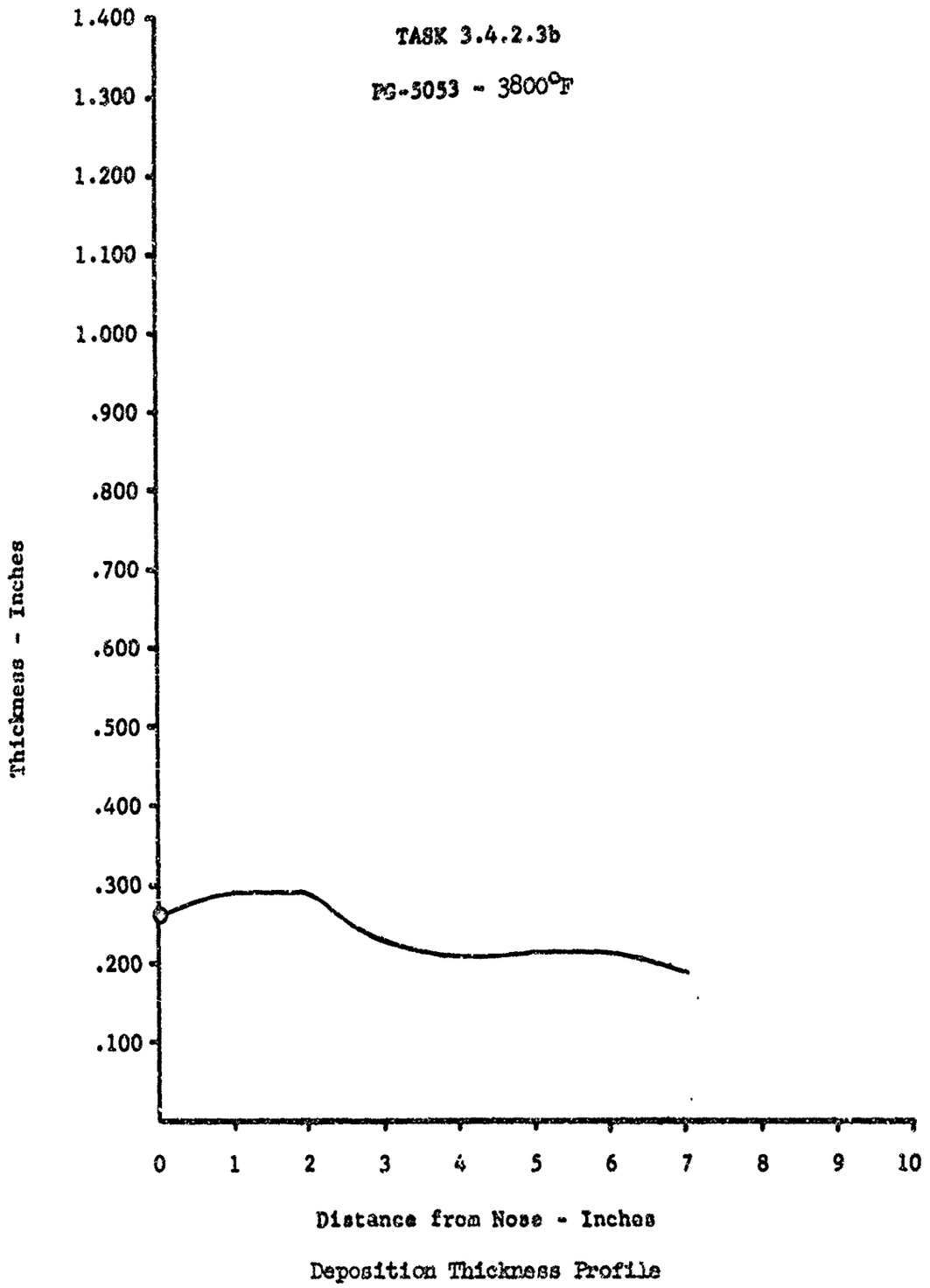
Figure 210



Task 3.4.2.3b

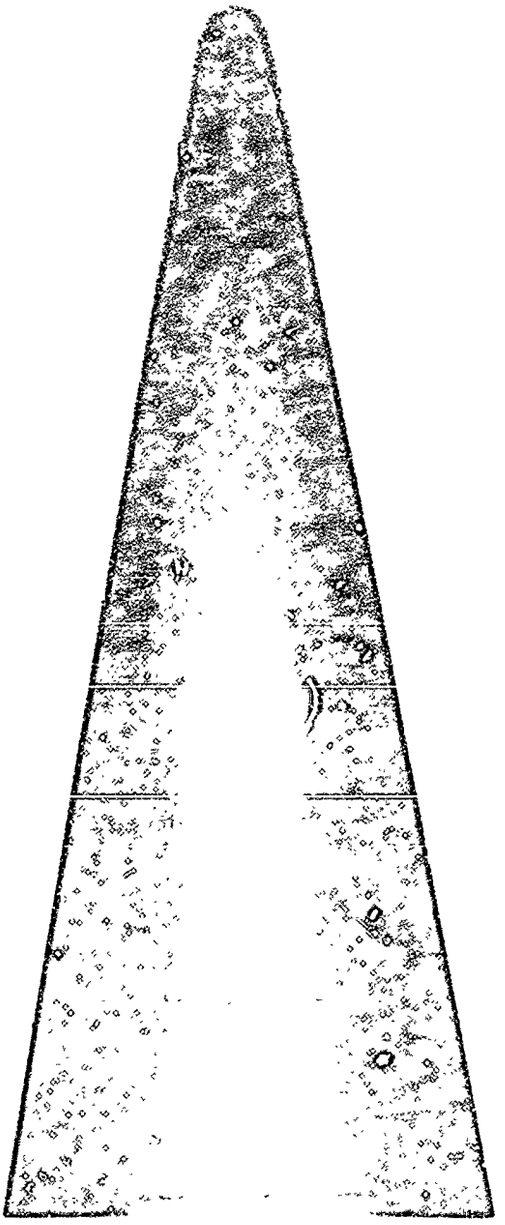
Radiograph of 5060

Figure 211



Deposition Thickness Profile

Figure 212



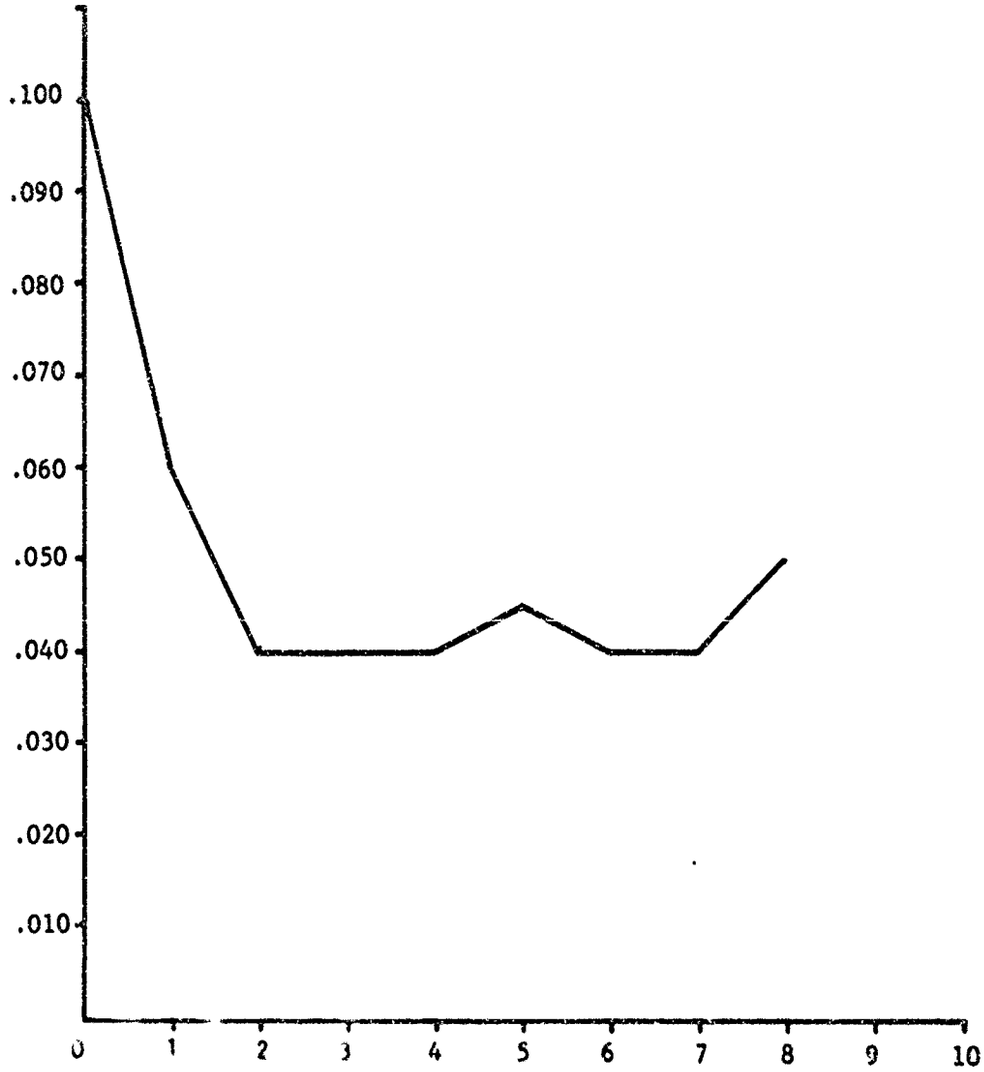
Task 3.4.2.3b

Radiograph of 5053

Figure 213

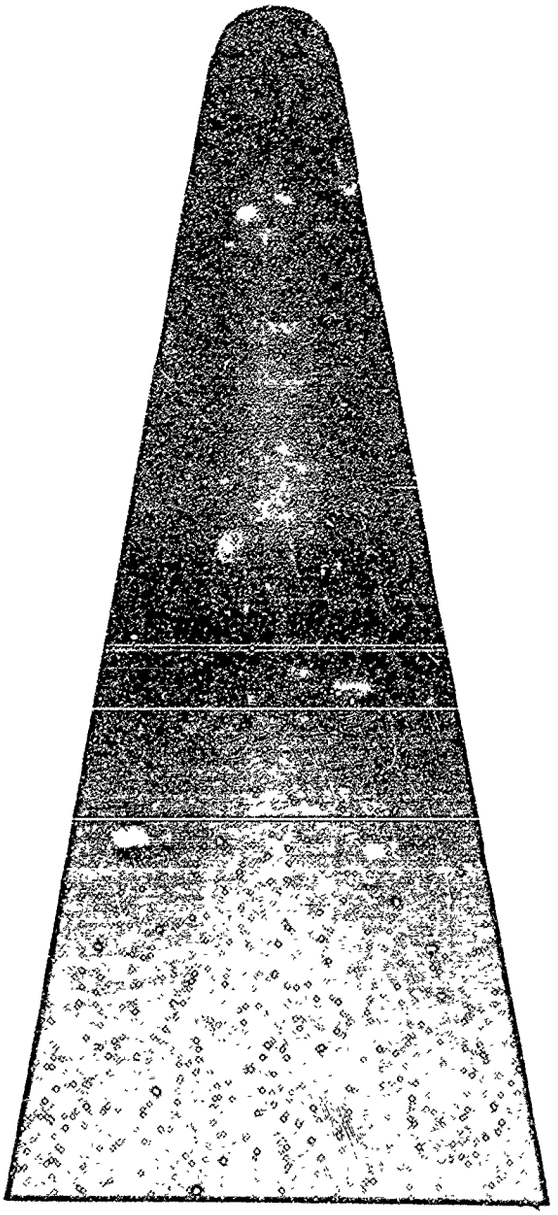
TASK 3.4.2.3b

PG-5054 - 3800°F



Deposition Thickness Profile

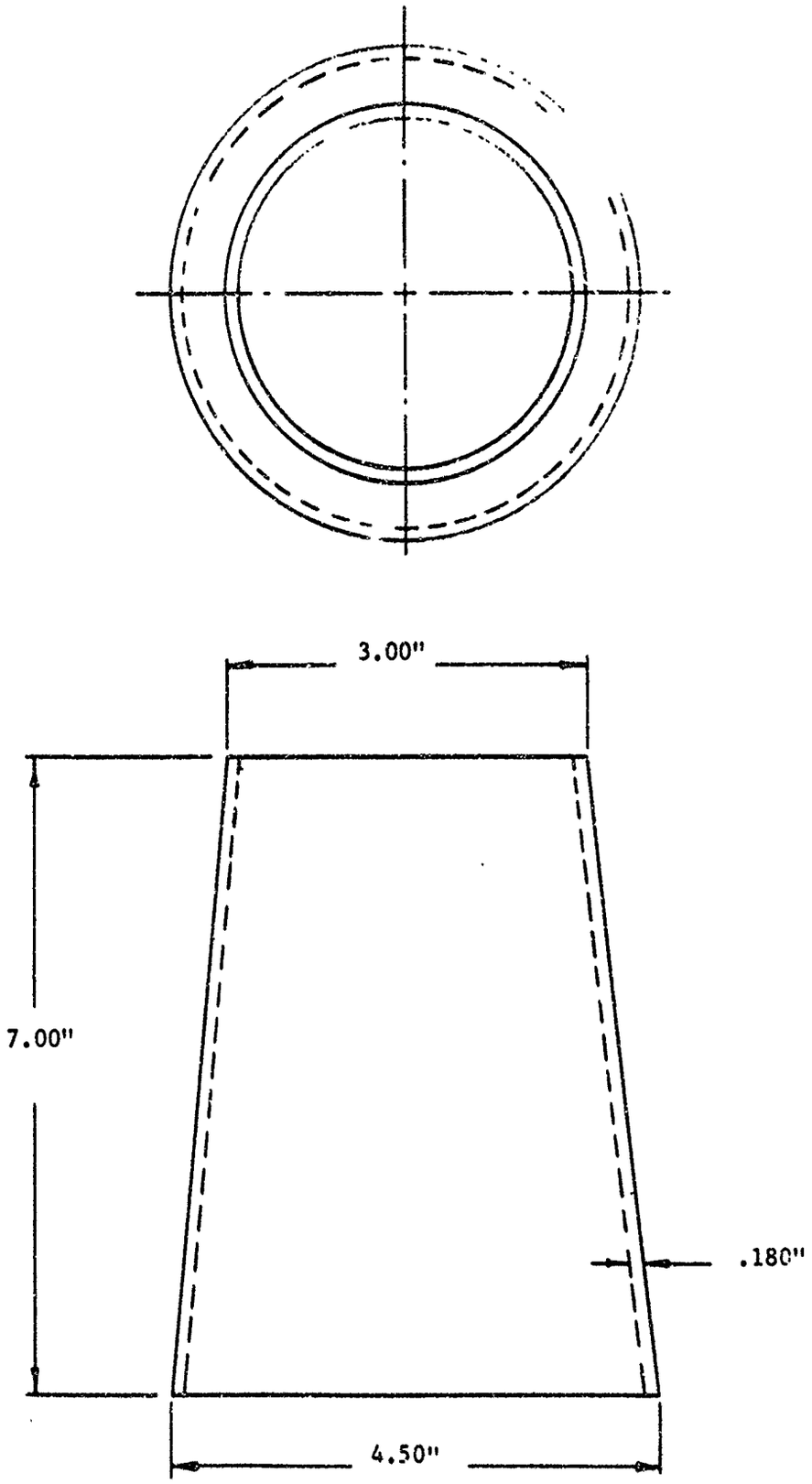
Figure 21b



Task 3.4.2.3b

Radiograph of 5054

Figure 215



FRUSTUM

Figure 216

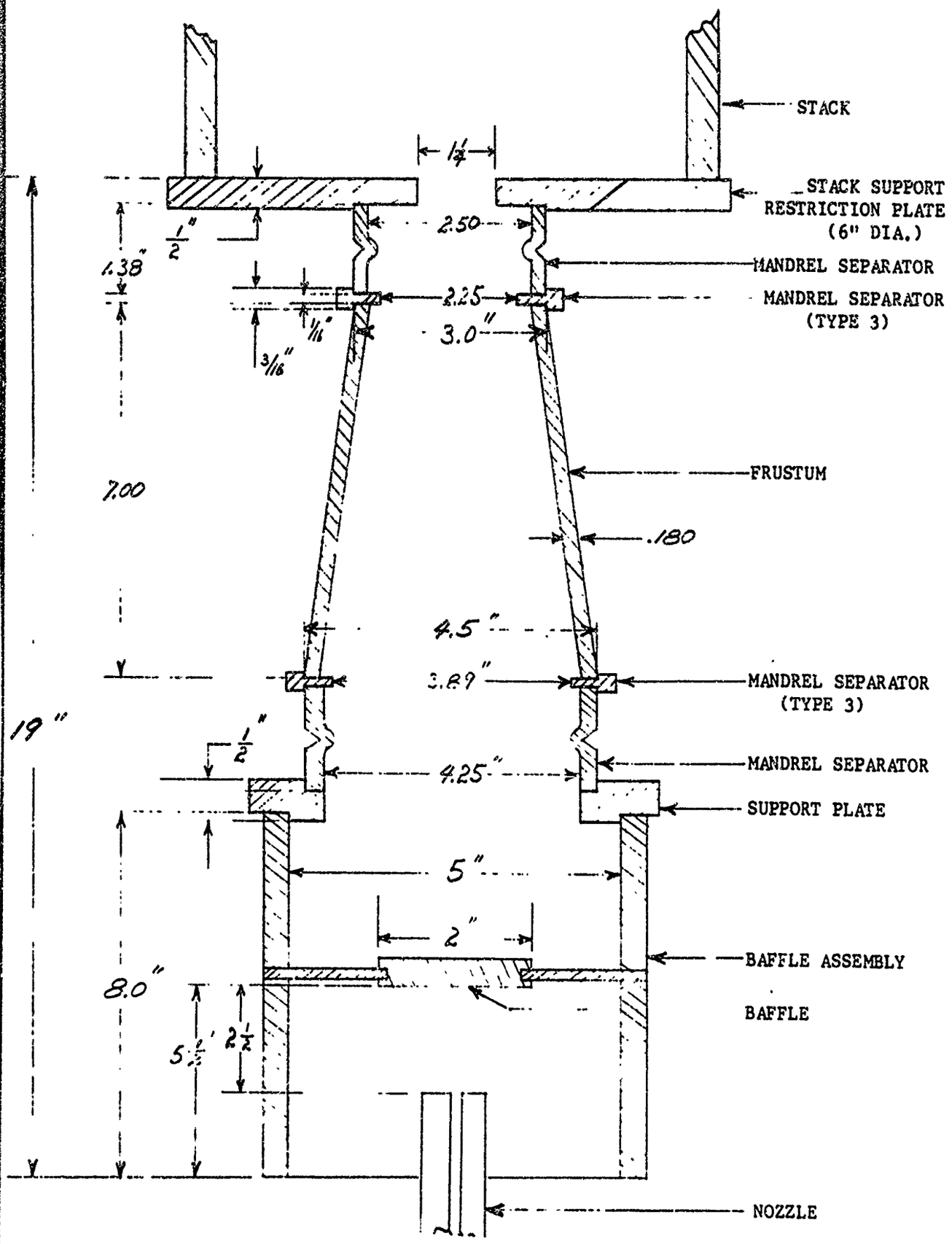


FIGURE 217

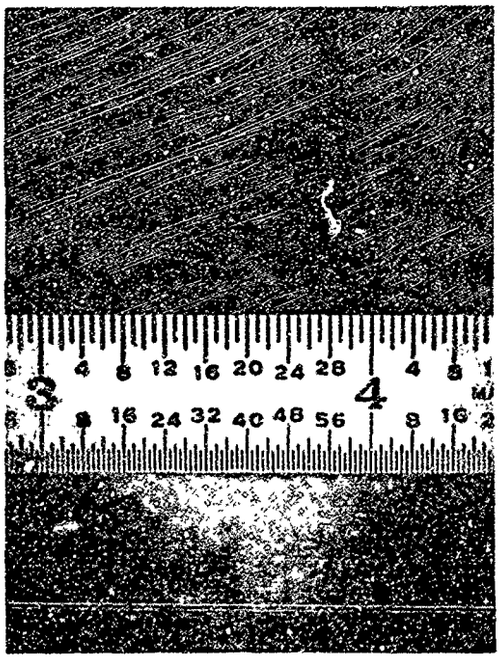
SCHEMATIC DIAGRAM ILLUSTRATING FURNACE ASSEMBLY
USED FOR THE FABRICATION OF THE FRUSTUMS

FIGURE 218

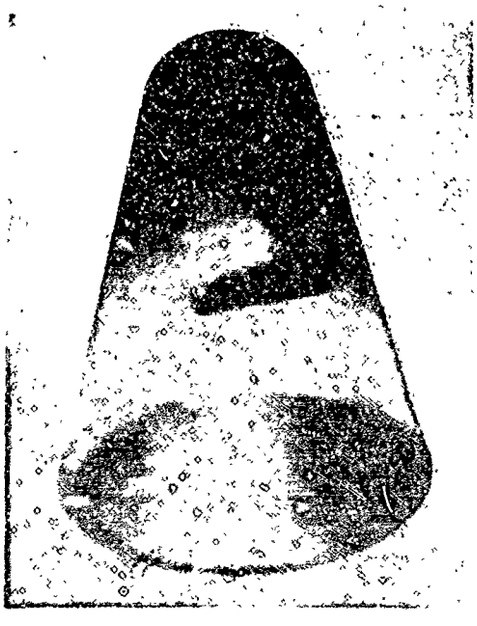
PHOTOGRAPHS OF FABRICATED PART NO. 1-77



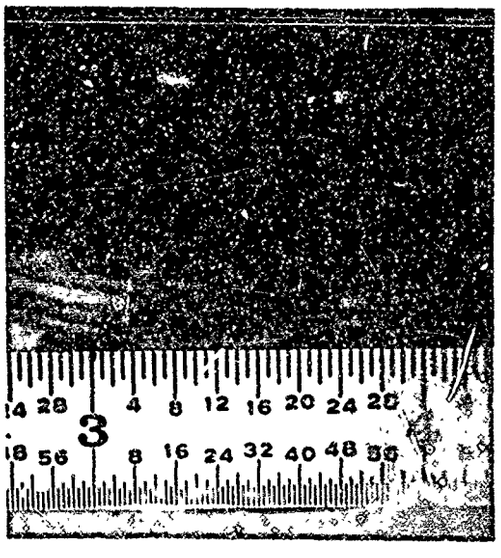
Note Spallation on Outer Surface.



Concentric Rings Separated by Distinct Delaminations.



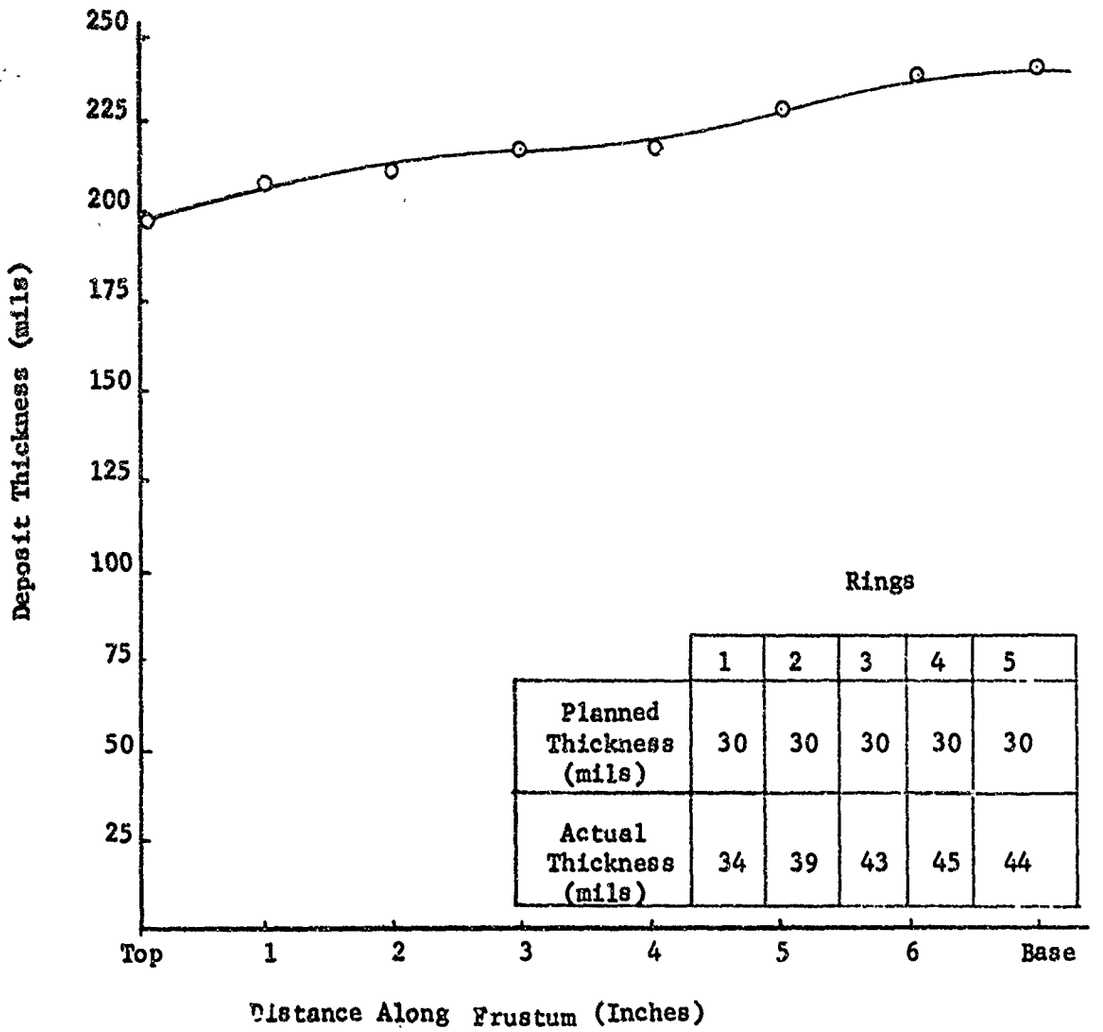
Note Crack on Inner Surface.



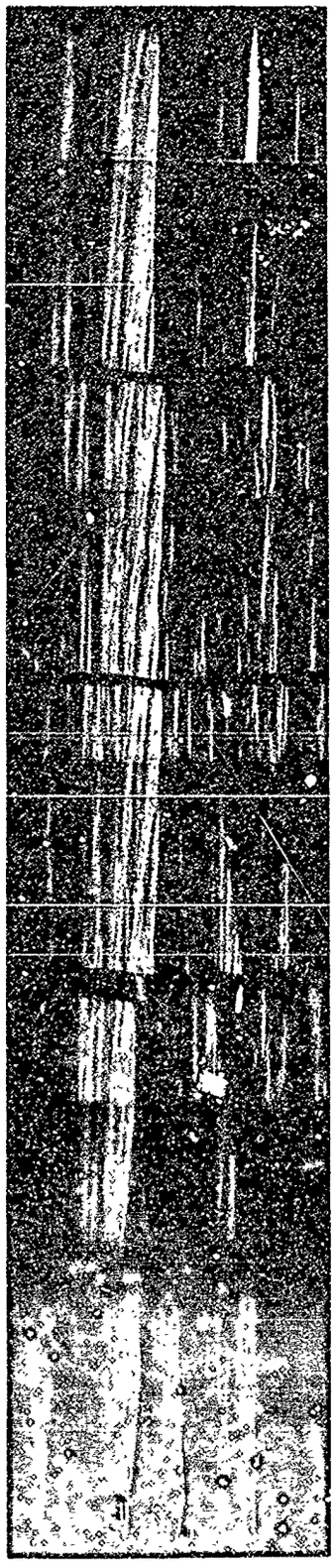
Interdelamination Crack at Large End of Frustum.

FIGURE 219

DEPOSITION THICKNESS PROFILE FOR FRUSTUM NO. 1-77



	Rings				
	1	2	3	4	5
Planned Thickness (mils)	30	30	30	30	30
Actual Thickness (mils)	34	39	43	45	44



Microstructure of Five Concentric Rings from Small End of Frustum. Structure is Basically substrate nucleated with some additional nucleation at the delaminations.

Microstructure of Concentric Rings from Large End of Frustum. Note the Missing Delamination near top of Photograph. Yet nucleation sites are still present.



Photomicrographs Through the Deposit Thickness Showing Microstructure of Material from Top and Bottom of Fructum 1-77.

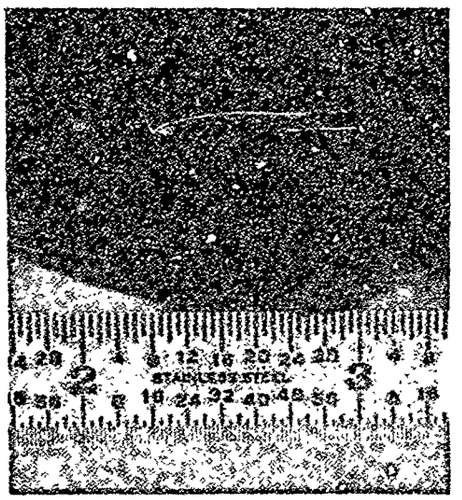
Figure 220

FIGURE 221

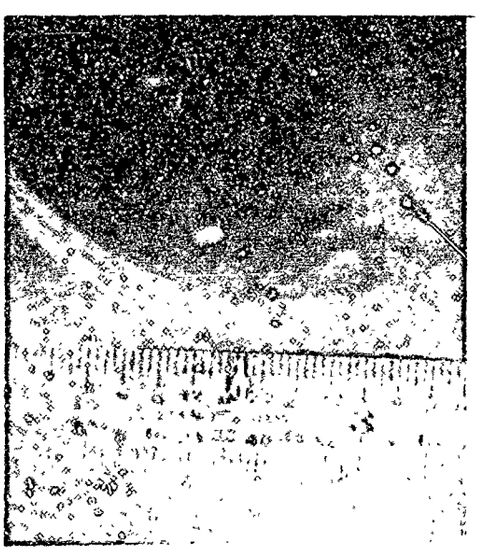
PHOTOGRAPHS OF FABRICATED PART RUN NO.2-88



Illustrating Excellent Outer Surface Condition



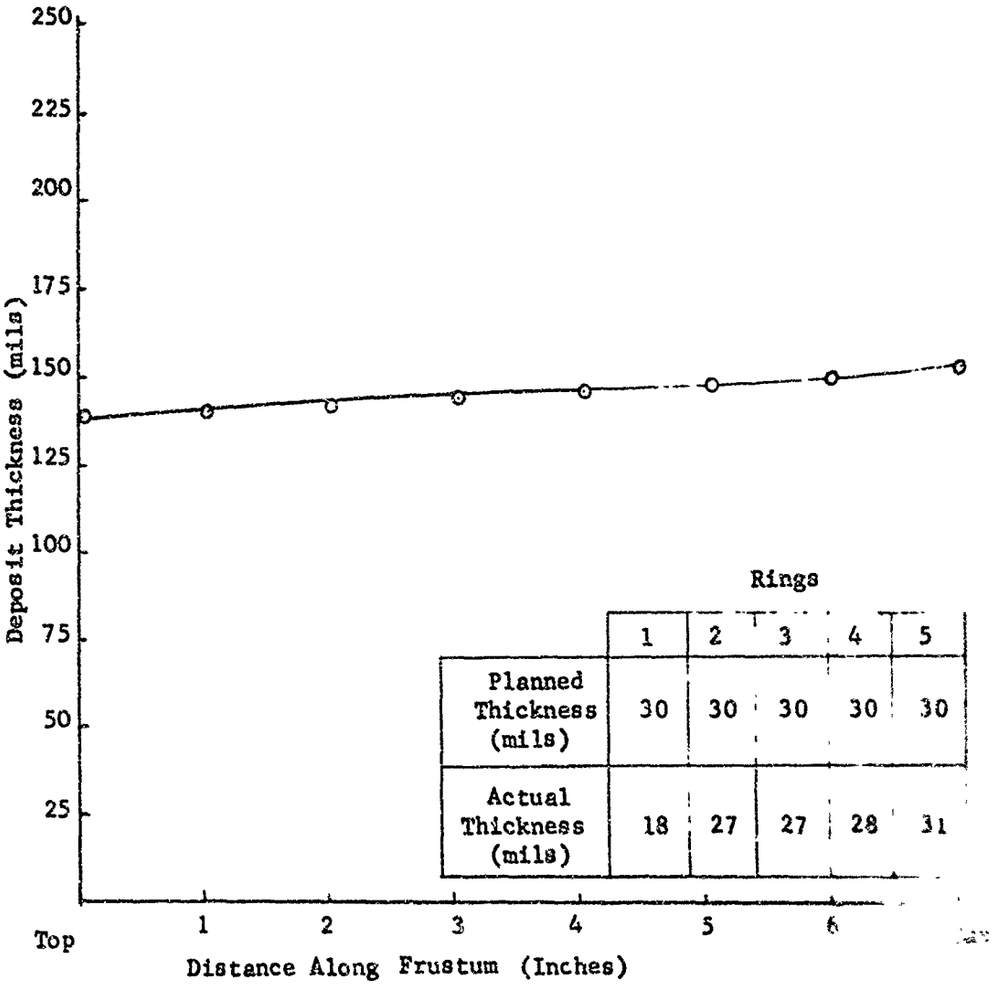
Note Crack in Center Ring.



Concentric Rings Separated by Delaminations. (Note: Outer Ring Did not Separate Distinctly)

FIGURE 222

DEPOSITION THICKNESS PROFILE FOR FRUSTUM NO. 2-8S



	Rings				
	1	2	3	4	5
Planned Thickness (mils)	30	30	30	30	30
Actual Thickness (mils)	18	27	27	28	31



Microstructure of five concentric rings from small end of frustum. Material is basically substrate nucleated.

Microstructure of concentric rings from large end of frustum. Note distinct delaminations separating all rings, except the second and third rings from the inner surface.



Top

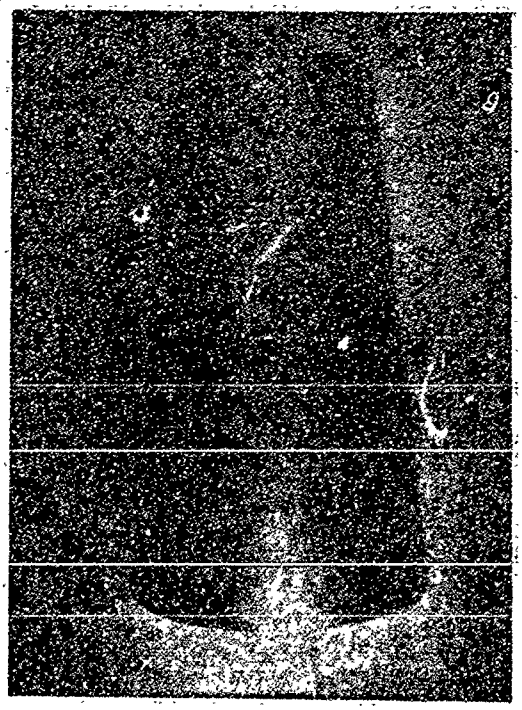
Bottom

Photomicrographs through deposit thickness showing microstructure of material from the top and bottom of frustum 2-88.

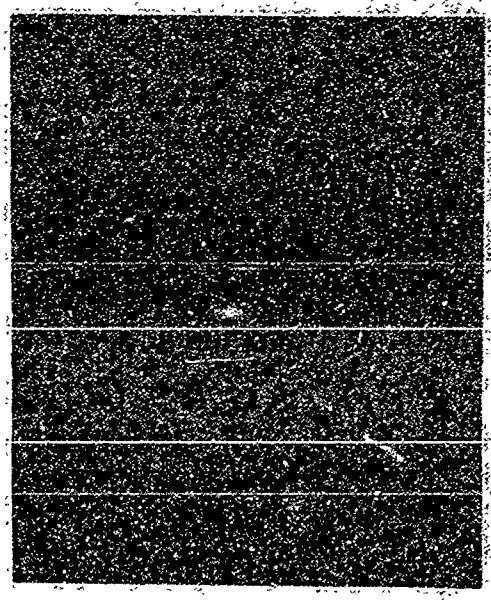
Figure 223

FIGURE 224

PHOTOGRAPHS OF FABRICATED PART (RUN NO. 2-90)



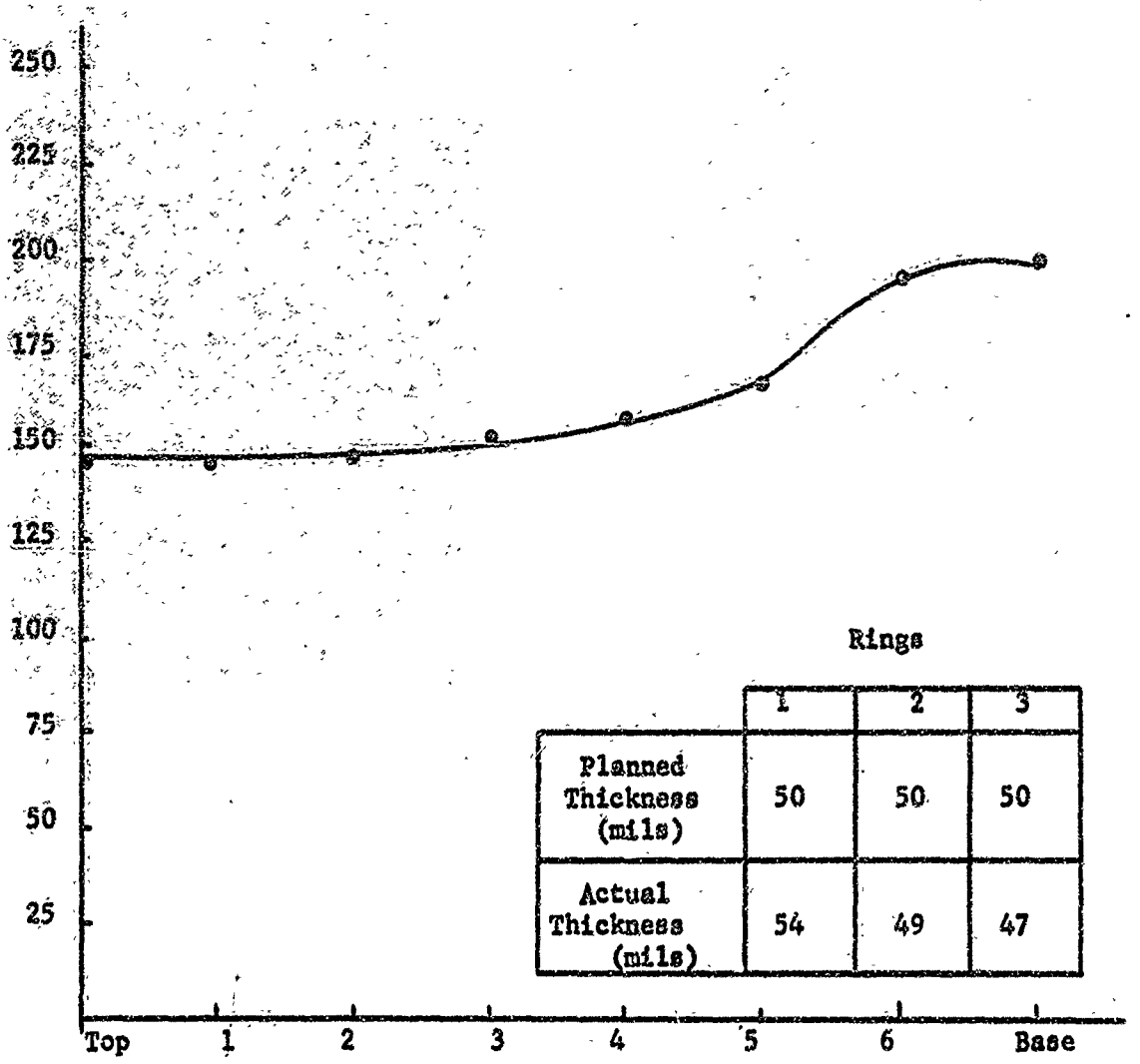
Outer Surface of Frustum Was Clean and Uncracked.



3 Concentric Rings Through Deposit Thickness. Separated by Distinct Delaminations.



Stress Relieving in One Ring. (Note Crack in Outer Ring)

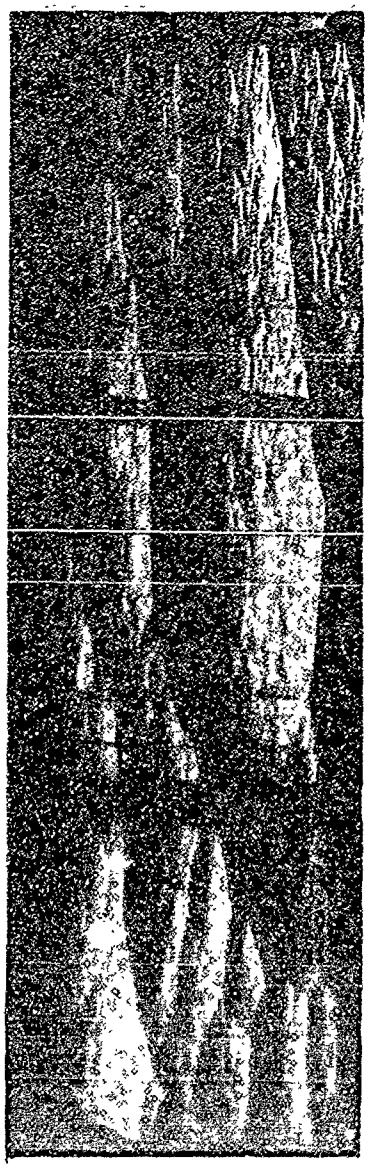


Rings

	1	2	3
Planned Thickness (mils)	50	50	50
Actual Thickness (mils)	54	49	47

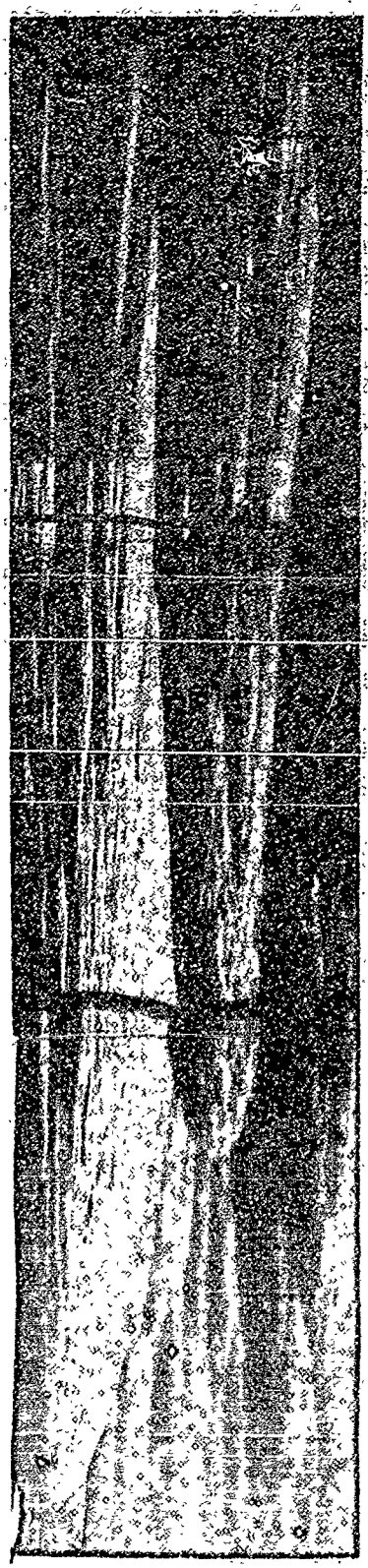
Deposition Thickness Profile for Frustum No. 2-90

Figure 225



Microstructure of three concentric rings from small end of frustum

Microstructure of concentric rings from large end of frustum Structure is mainly substrate nucleated

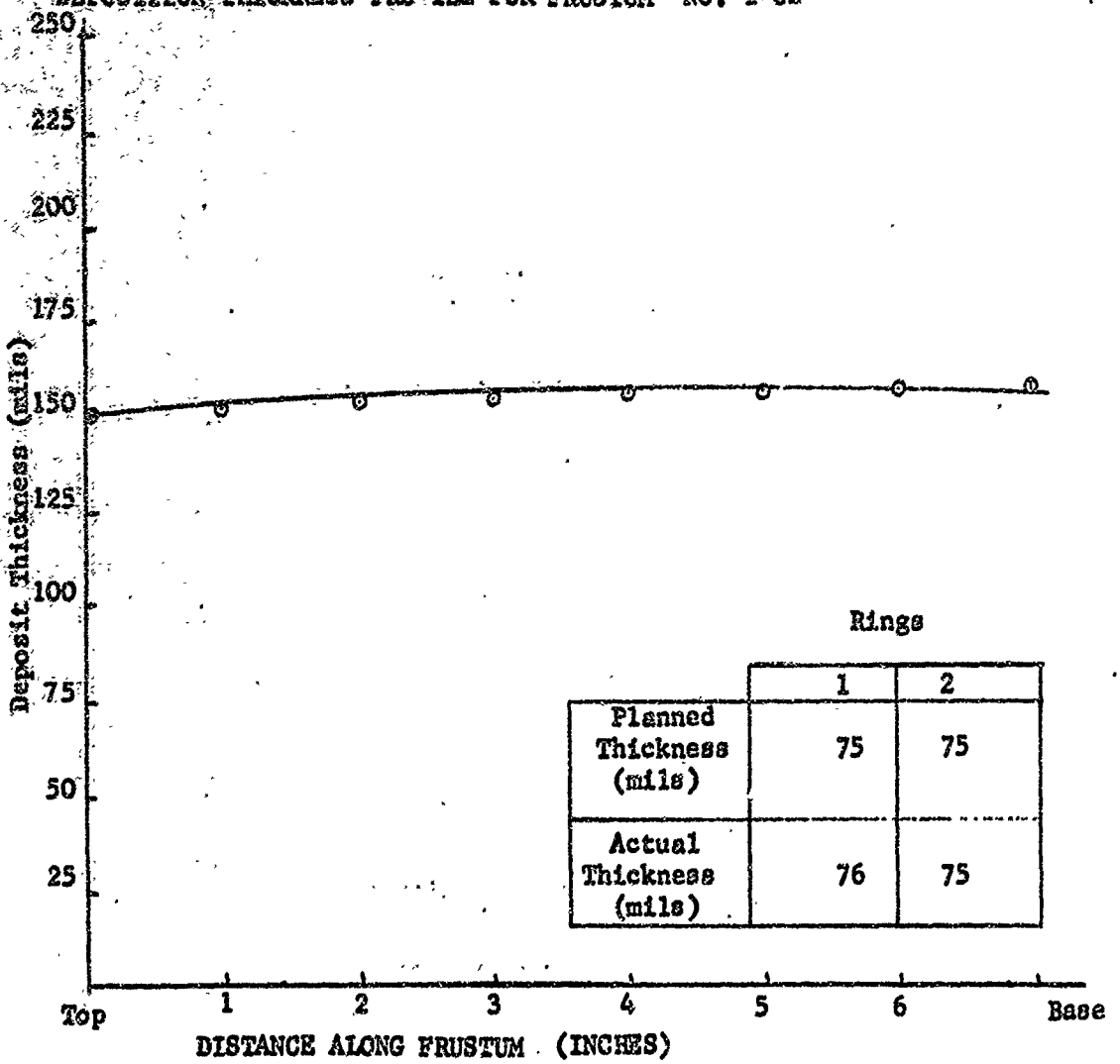


Photomicrographs through deposit thickness showing microstructure of material from the top and bottom of frustum 2-90

Figure 226

FIGURE 227

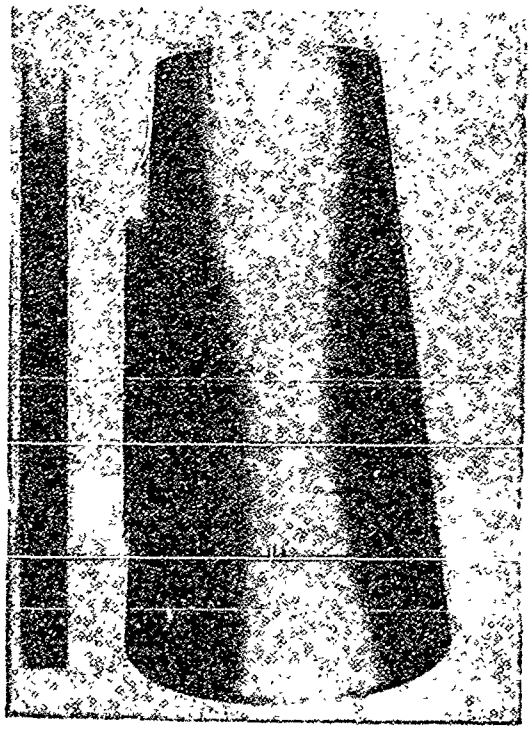
DEPOSITION THICKNESS PROFILE FOR FRUSTUM NO. 1-82



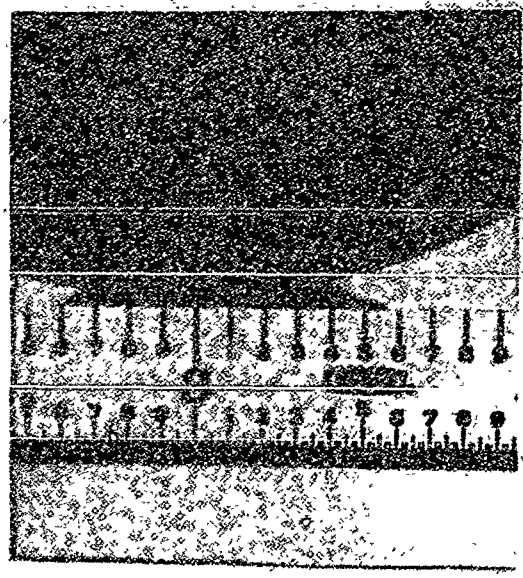
	Rings 1	2
Planned Thickness (mils)	75	75
Actual Thickness (mils)	76	75

FIGURE 228

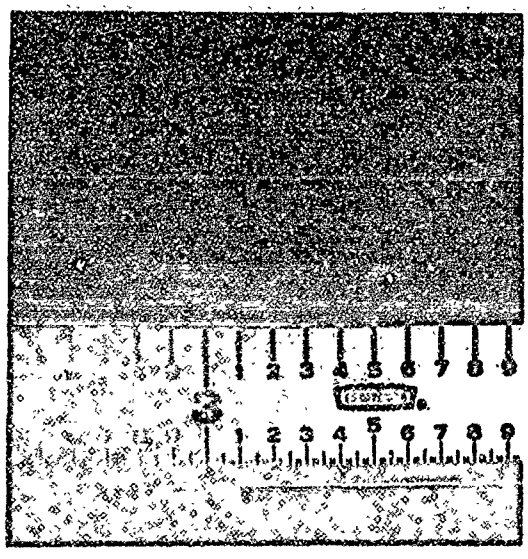
PHOTOGRAPH OF FABRICATED PART (RUN NO. 1-82)



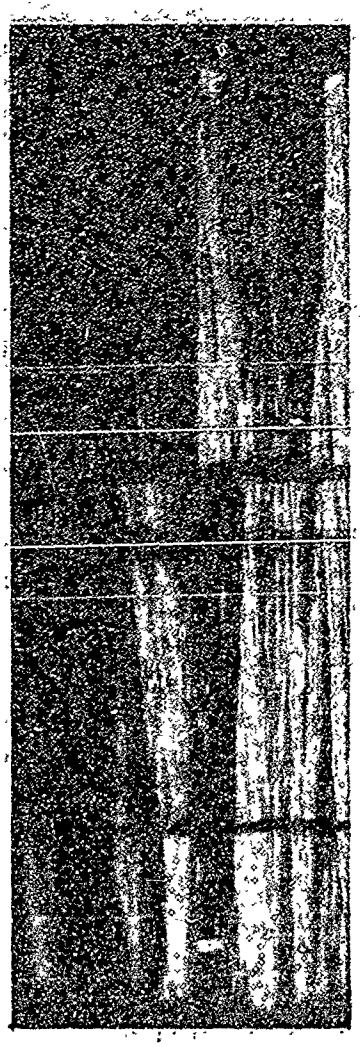
Illustrating Outer Surface and General Condition of Frustum.



2 Concentric Rings Through Deposit Thickness. Separated by One Delamination

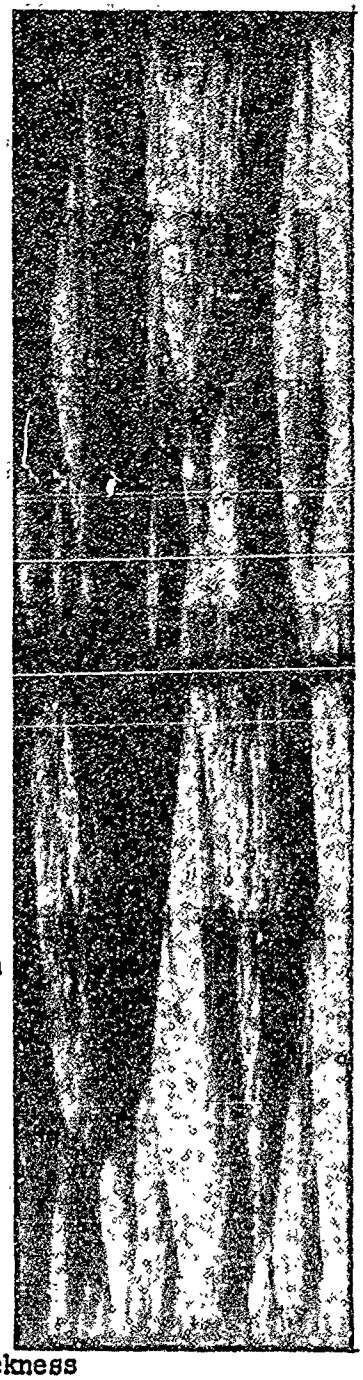


Note Stress Relieving by Formation of Additional Delaminations. Due to High t/r of Small End of Frustum.



Microstructure of two planned concentric rings. Note second delamination in first ring which developed during sample preparation.

Microstructure of concentric rings from large end of frustum. Note new nucleation sites at delamination..

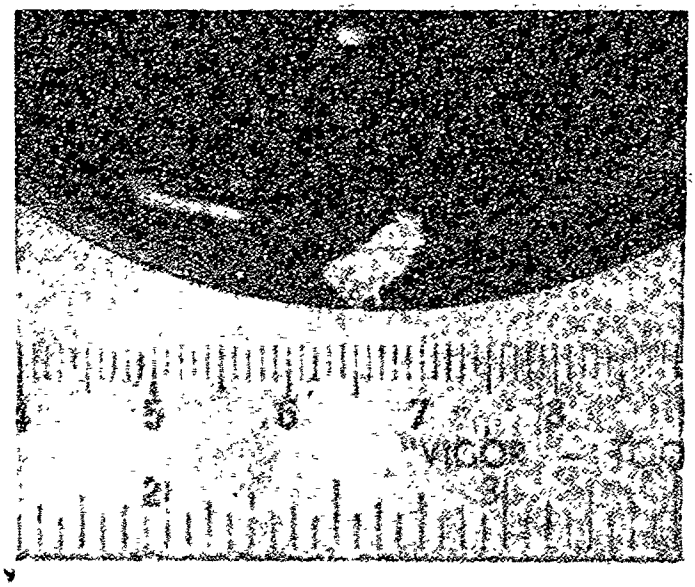


Photomicrographs through deposit thickness showing microstructure of material from top and bottom of frustum 1-82.

Figure 229



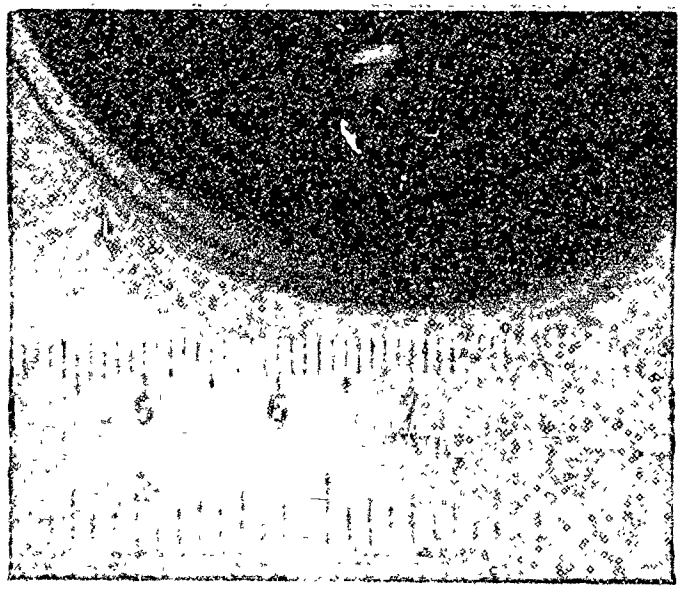
Illustrating excellent outer surface condition.



Material through deposit thickness at small end of frustum - No random delaminations or interdelamination cracks.



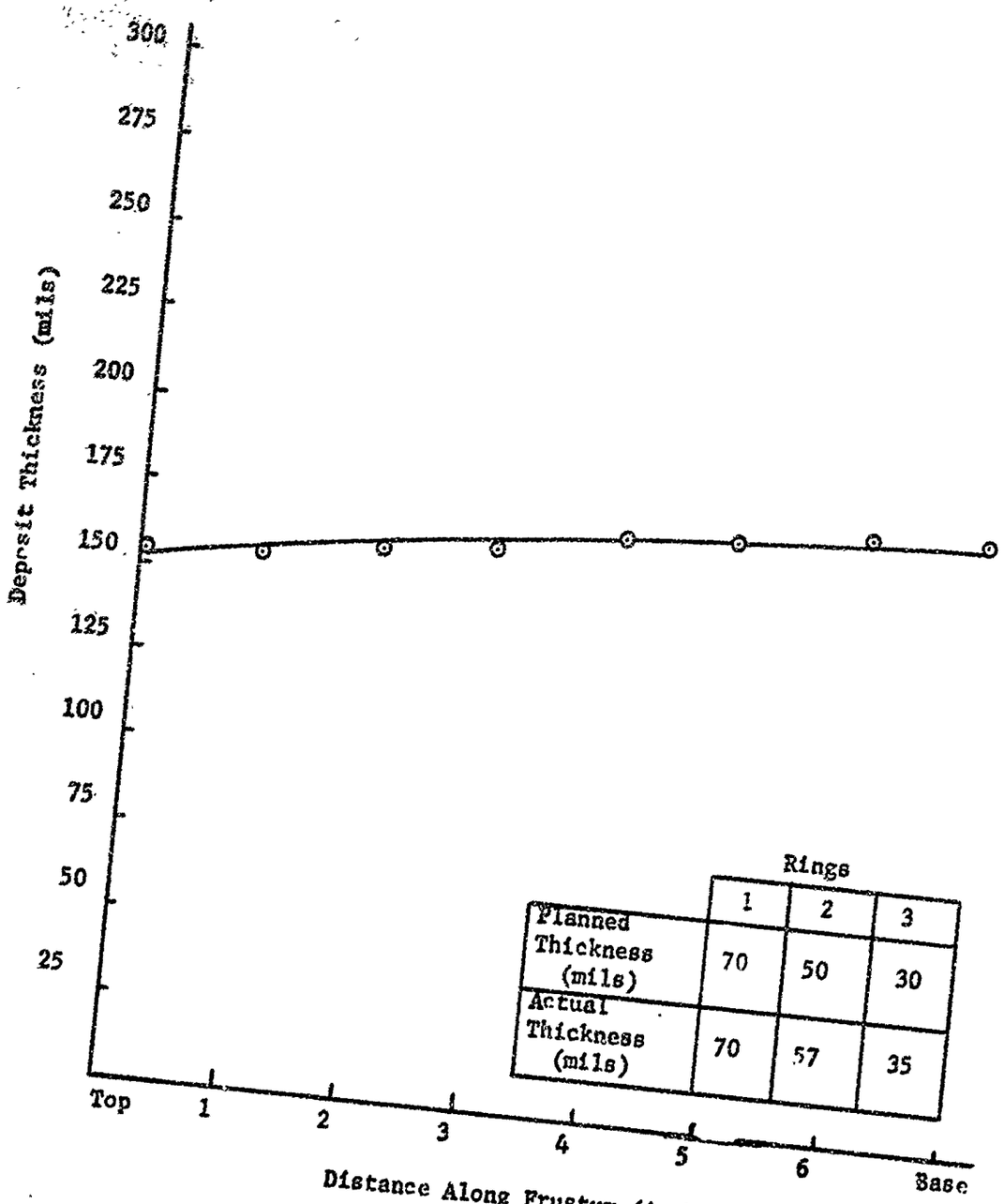
Illustrating excellent and complete separation between the three concentric frustum shells.



Material through deposit thickness at large end of frustum - Again there were no random delaminations or interdelamination cracks.

Photographs of Fabricated Part No. 2-105

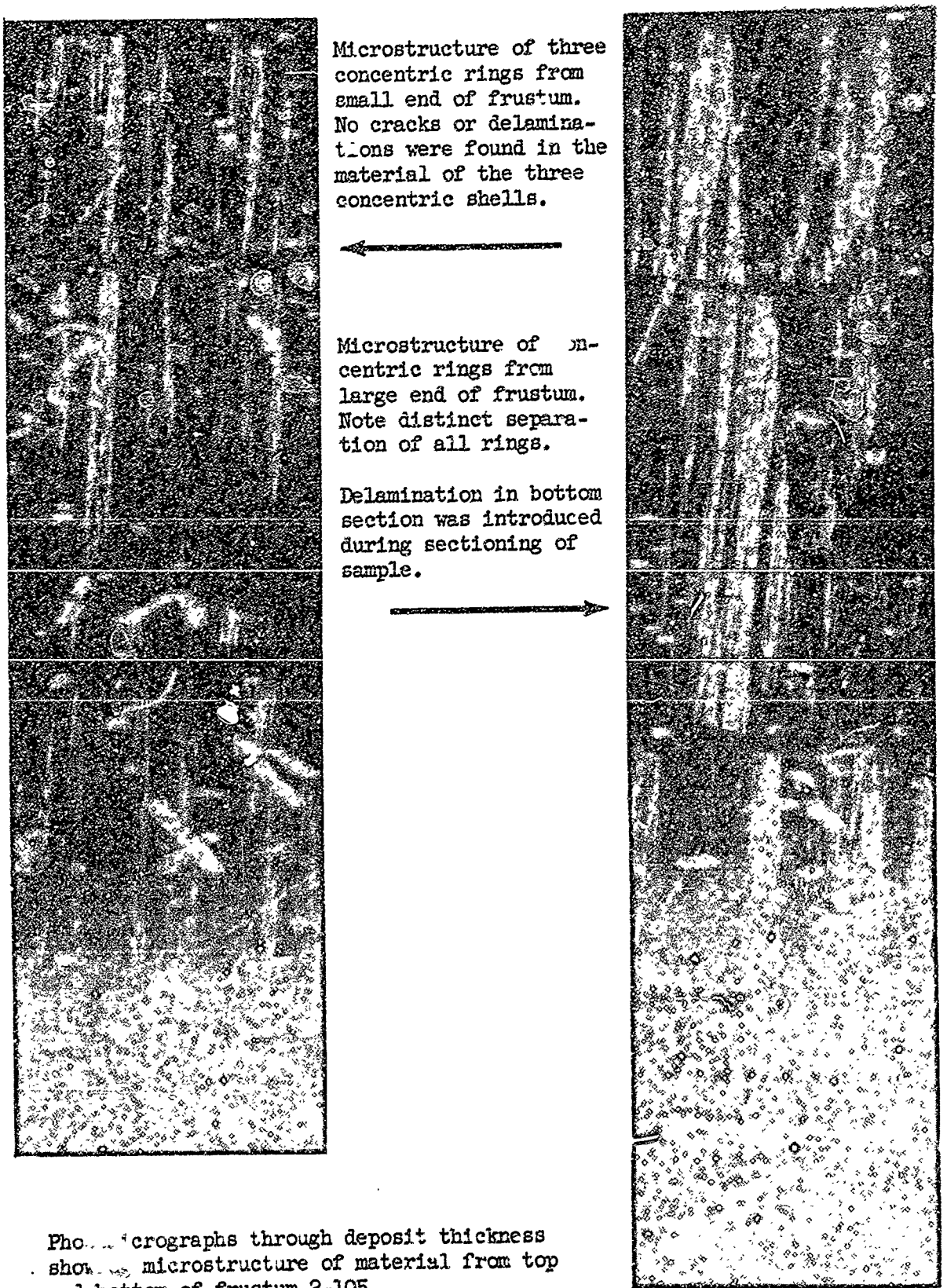
Figure 230



	Rings		
	1	2	3
Planned Thickness (mils)	70	50	30
Actual Thickness (mils)	70	57	35

Deposit Thickness Profile For Frustum No. 2-105

Figure 231



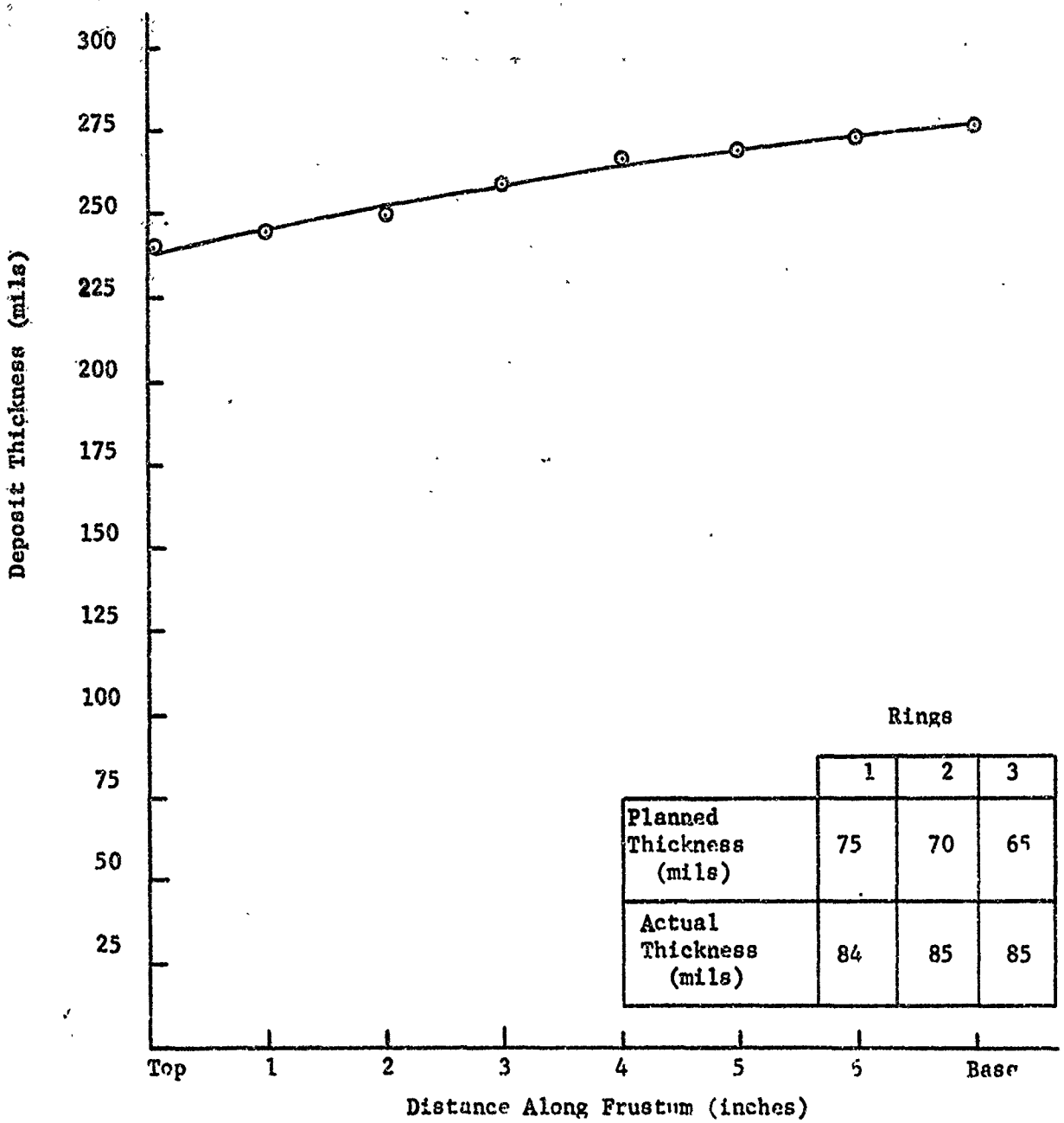
Microstructure of three concentric rings from small end of frustum. No cracks or delaminations were found in the material of the three concentric shells.

Microstructure of concentric rings from large end of frustum. Note distinct separation of all rings.

Delamination in bottom section was introduced during sectioning of sample.

Photomicrographs through deposit thickness showing microstructure of material from top and bottom of frustum 2-105.

Figure 232

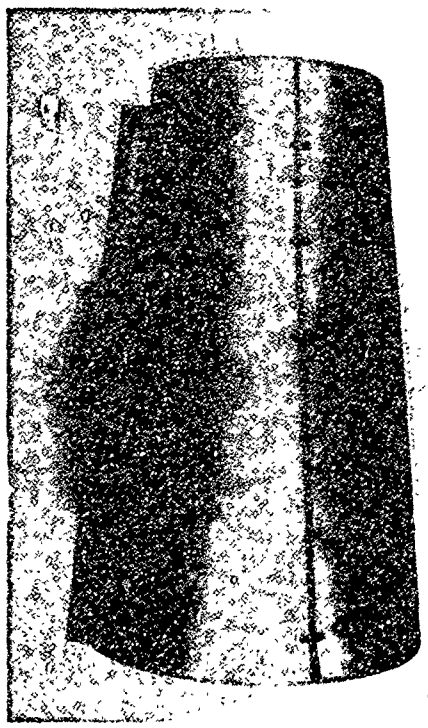


Rings

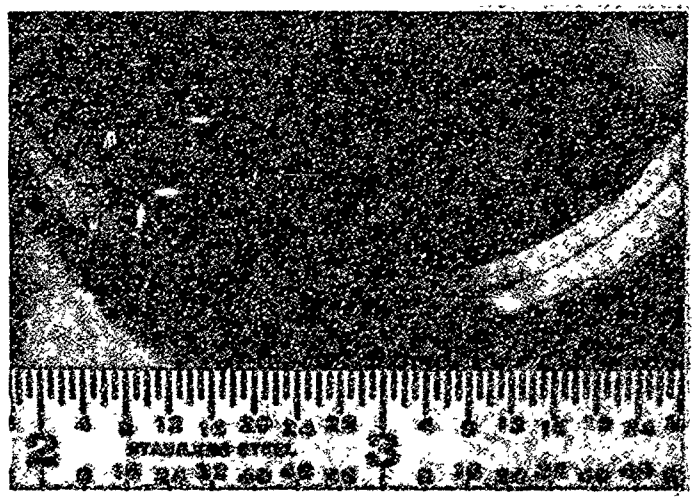
	1	2	3
Planned Thickness (mils)	75	70	65
Actual Thickness (mils)	84	85	85

Deposit Thickness Profile for Frustum No. 2-108

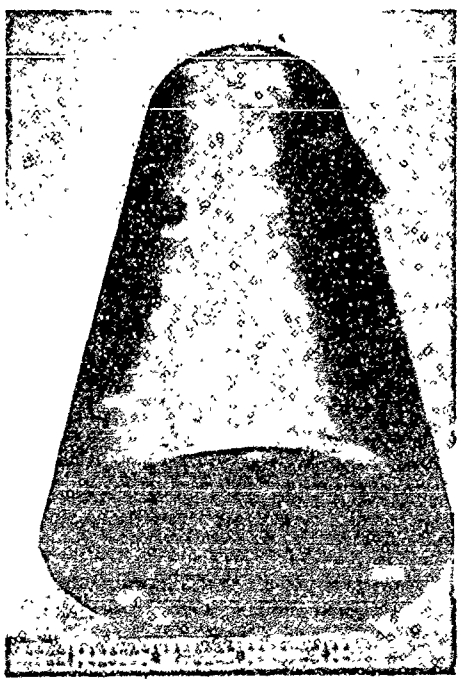
Figure 233



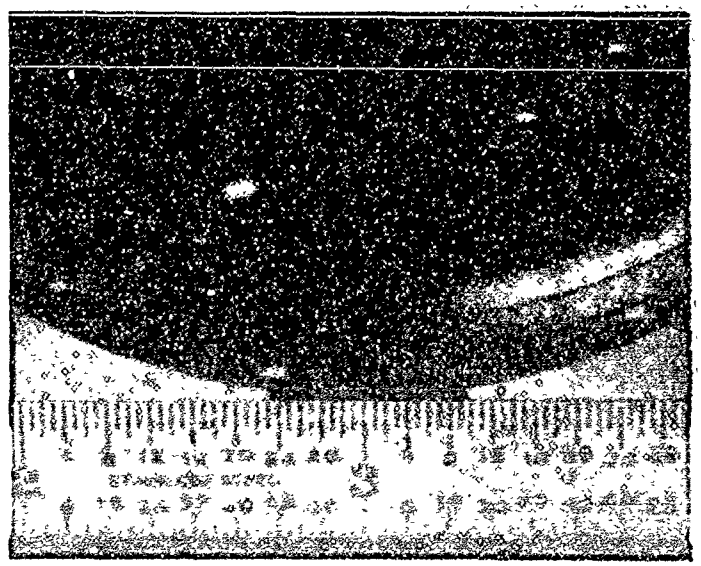
Outer Surface of Frustum



Good Separation between Concentric Frustums in Localized Areas.



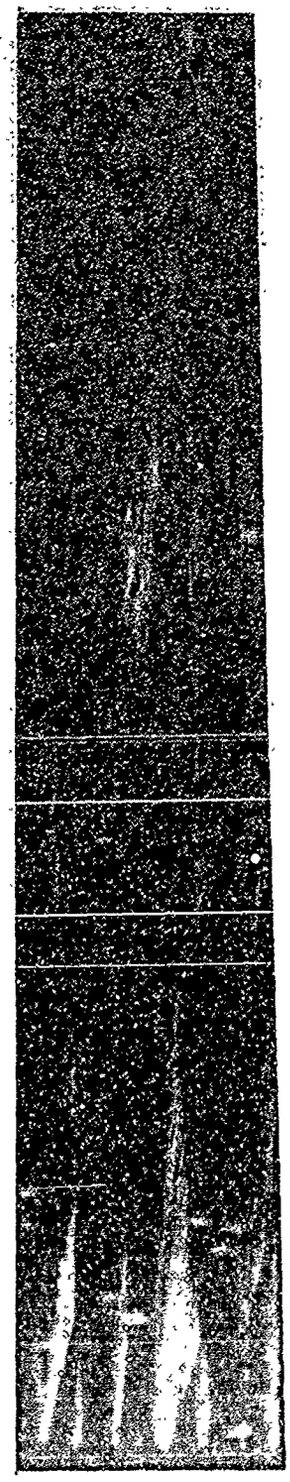
Part Developed Two Axial Cracks 180° Apart during Furnace Cool-down



Random Delaminations and Interdelamination Cracks were Present in Part.

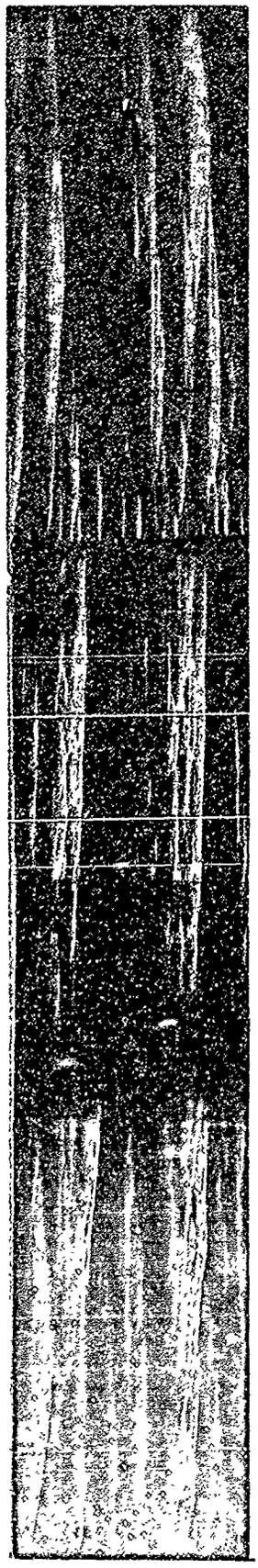
Photographs of Fabricated Part No. 2-108

Figure 234



Microstructure of three concentric rings from small end of frustum.

Microctructure of three concentric rings from large end of frustum.



Photomicrographs Through the Deposit Thickness Showing Microstructure of Material from Top and Bottom of Frustum No. 2-108

Figure 235

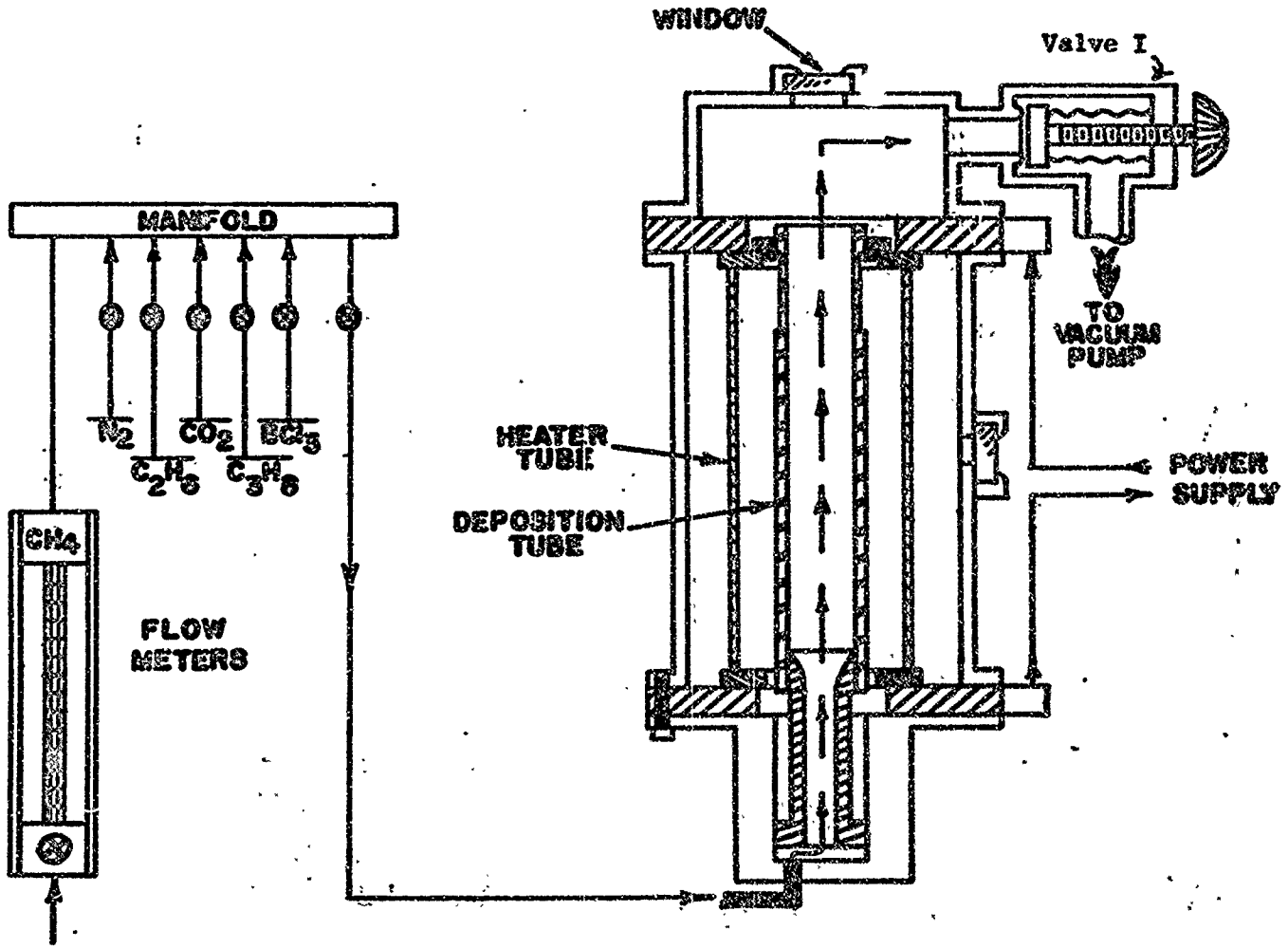
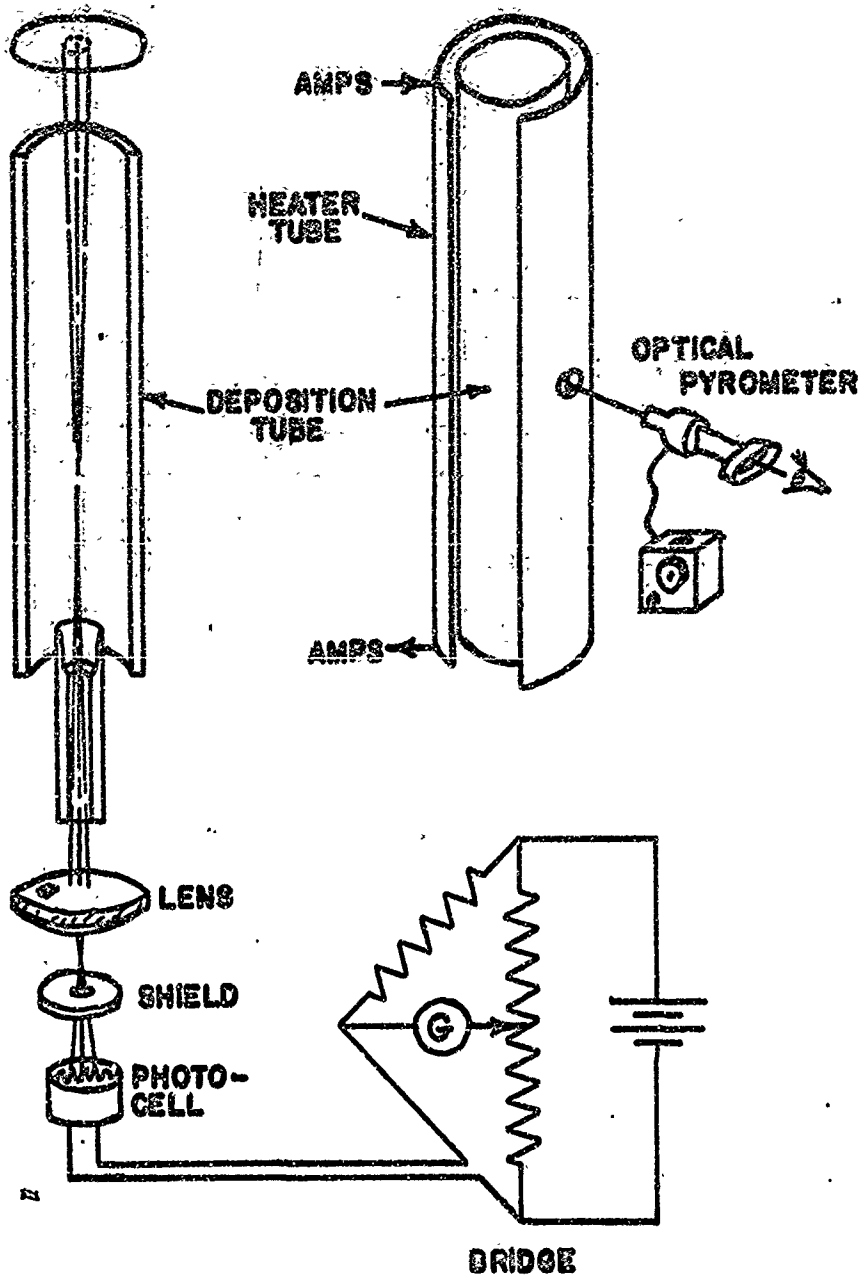
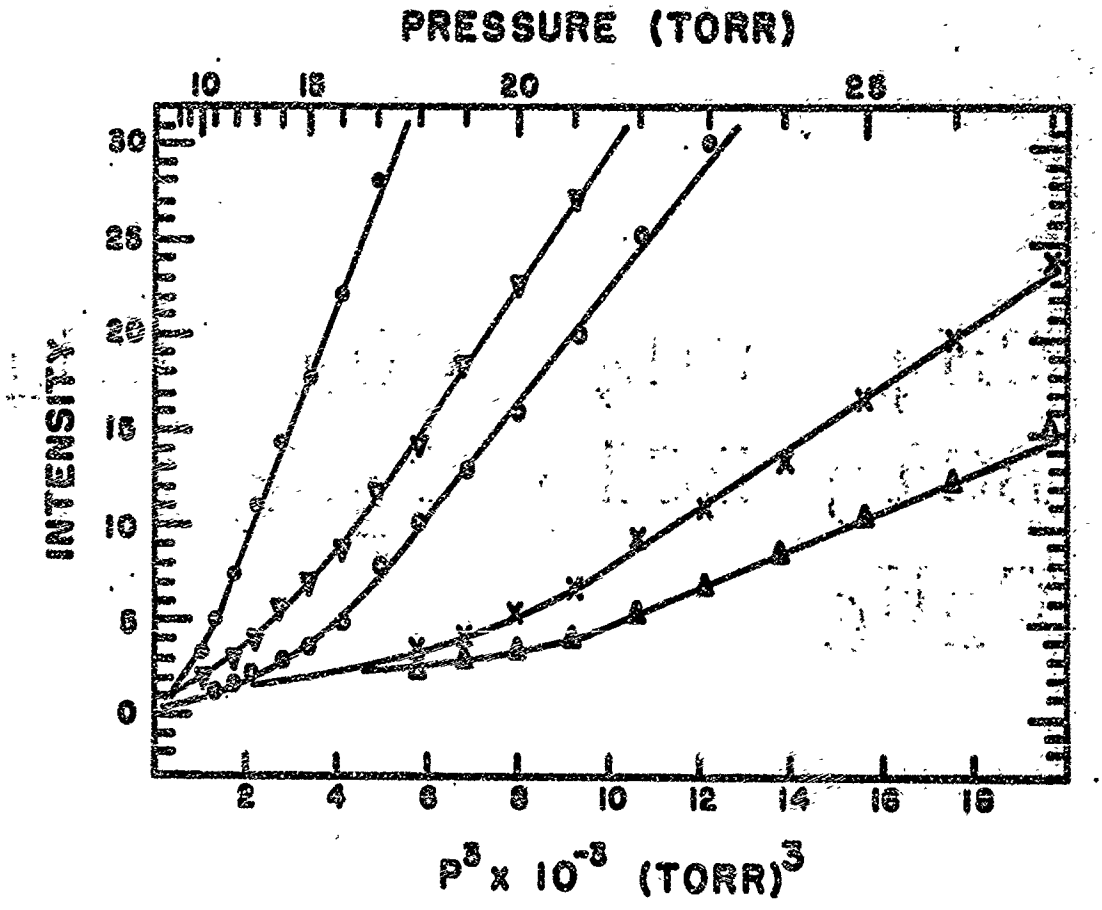

WINDOW
Valve I
MANIFOLD
N_2
CO_2
BCl_3
C_2H_6
C_3H_6
CH_4
FLOW METERS
HEATER TUBE
DEPOSITION TUBE
TO VACUUM PUMP
POWER SUPPLY
DEPOSITION FURNACE

Figure 236



OPTICAL SYSTEMS

Figure 237

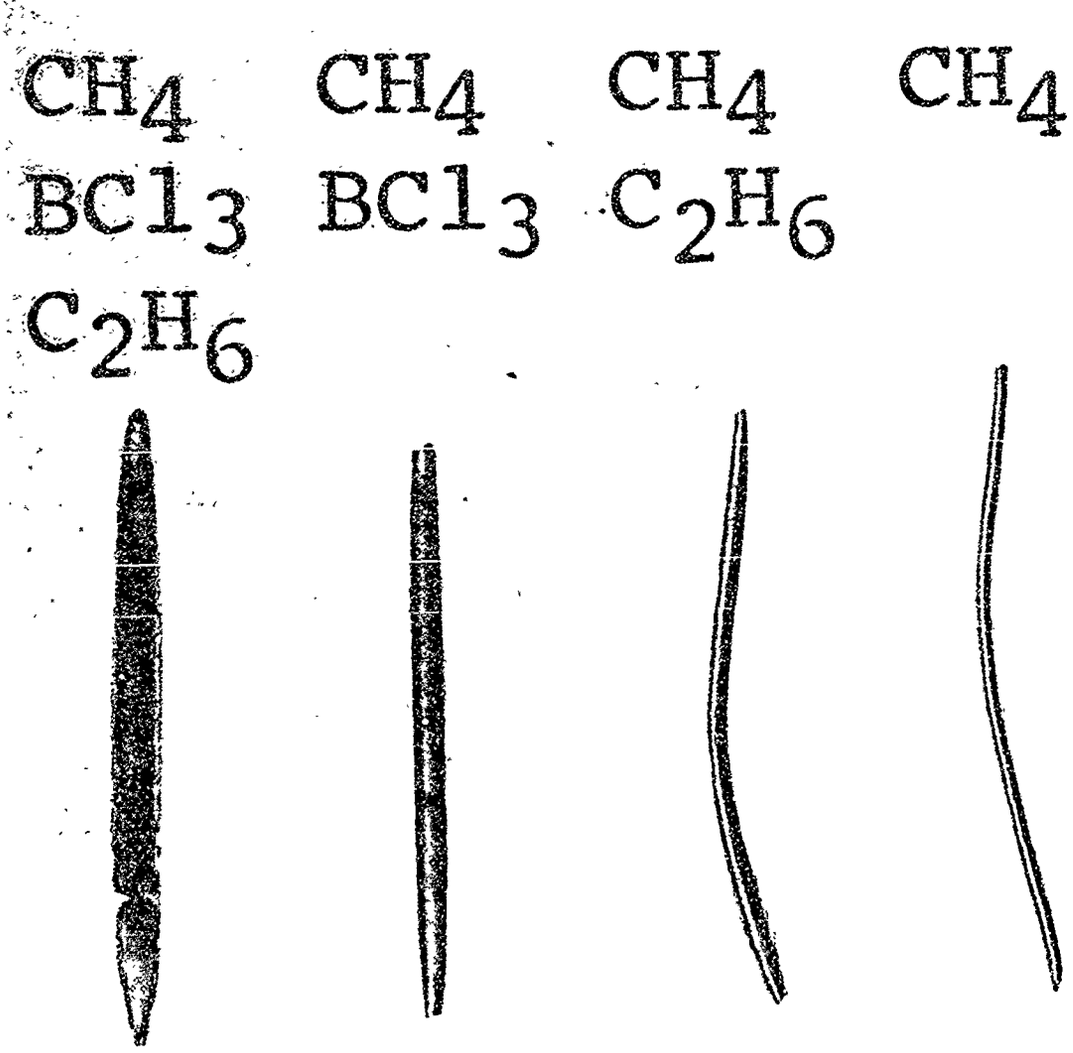


VOLUME PERCENT

	CH_4	C_2H_6	BCl_3	CO_2	H_2
•	70.02%	5.78%	1.05%	2.10%	21.05%
▽	98.95%		1.05%		
○	94.22%	5.78%			
△	78.95%				21.05%
×	99.95%				

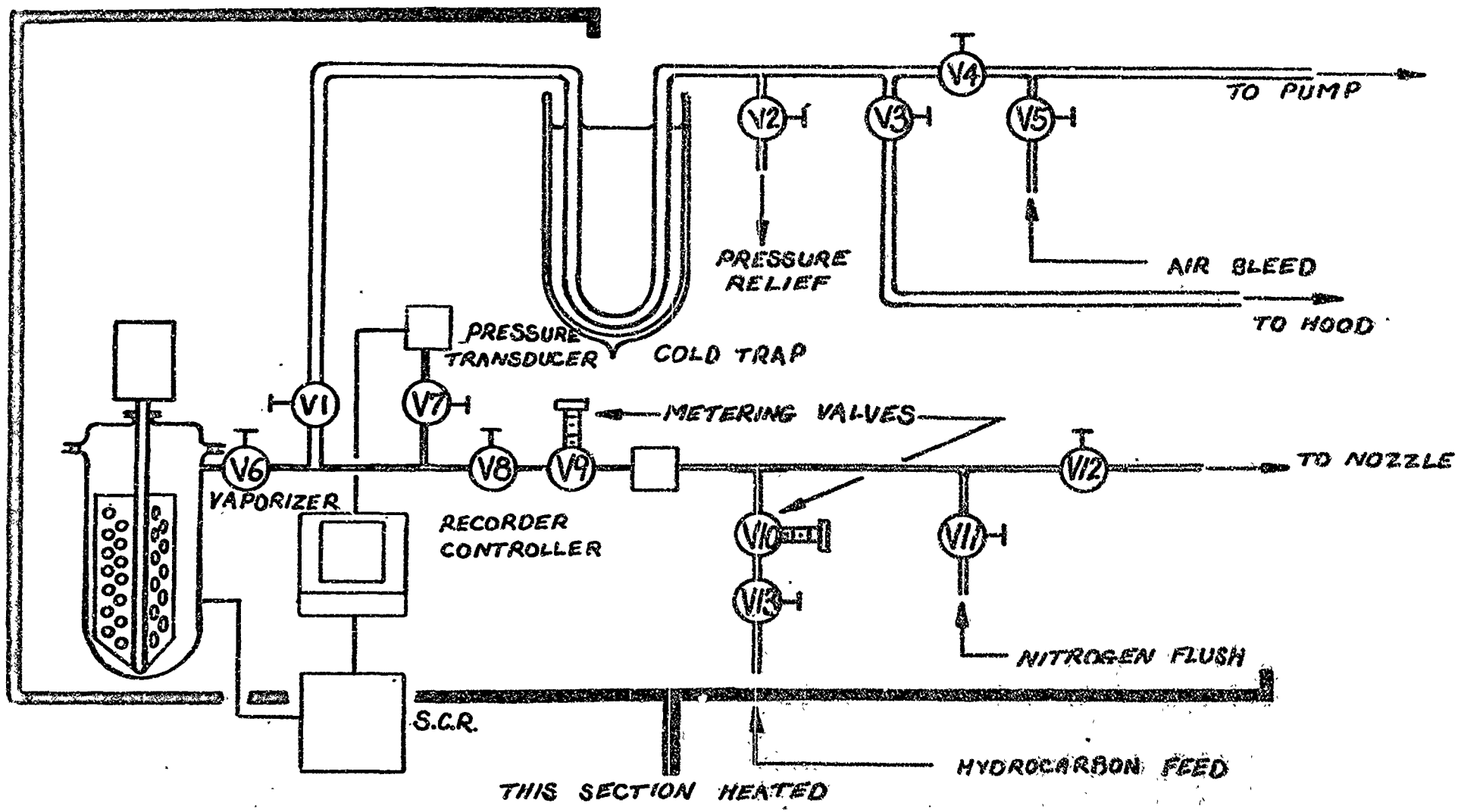
IMPURITY EFFECTS ON PURE CH_4
AT 1500 °C

Figure 238



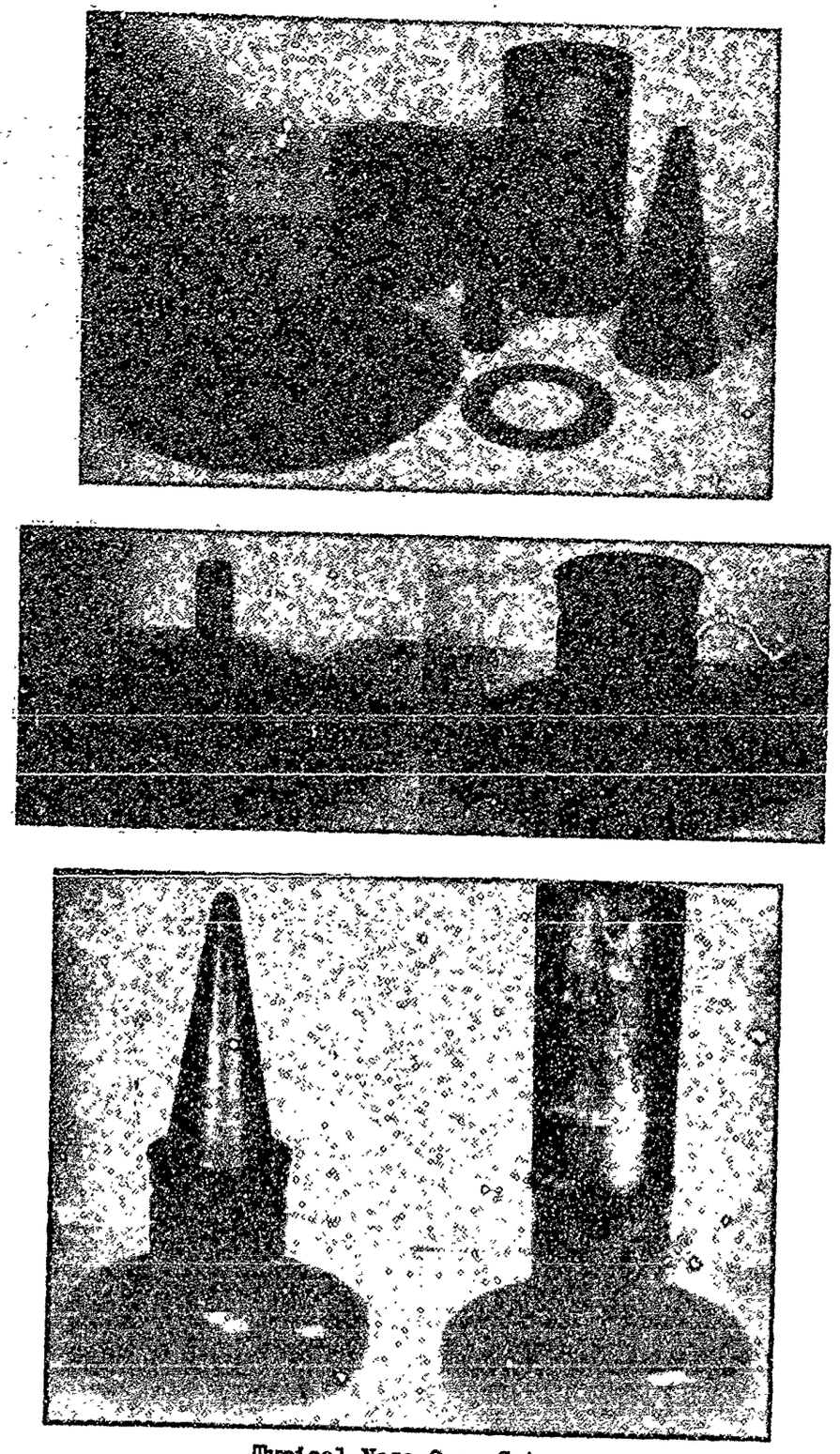
Deposit on Filaments Near Tops of Tubes
Gas Composition as Shown

Figure 239



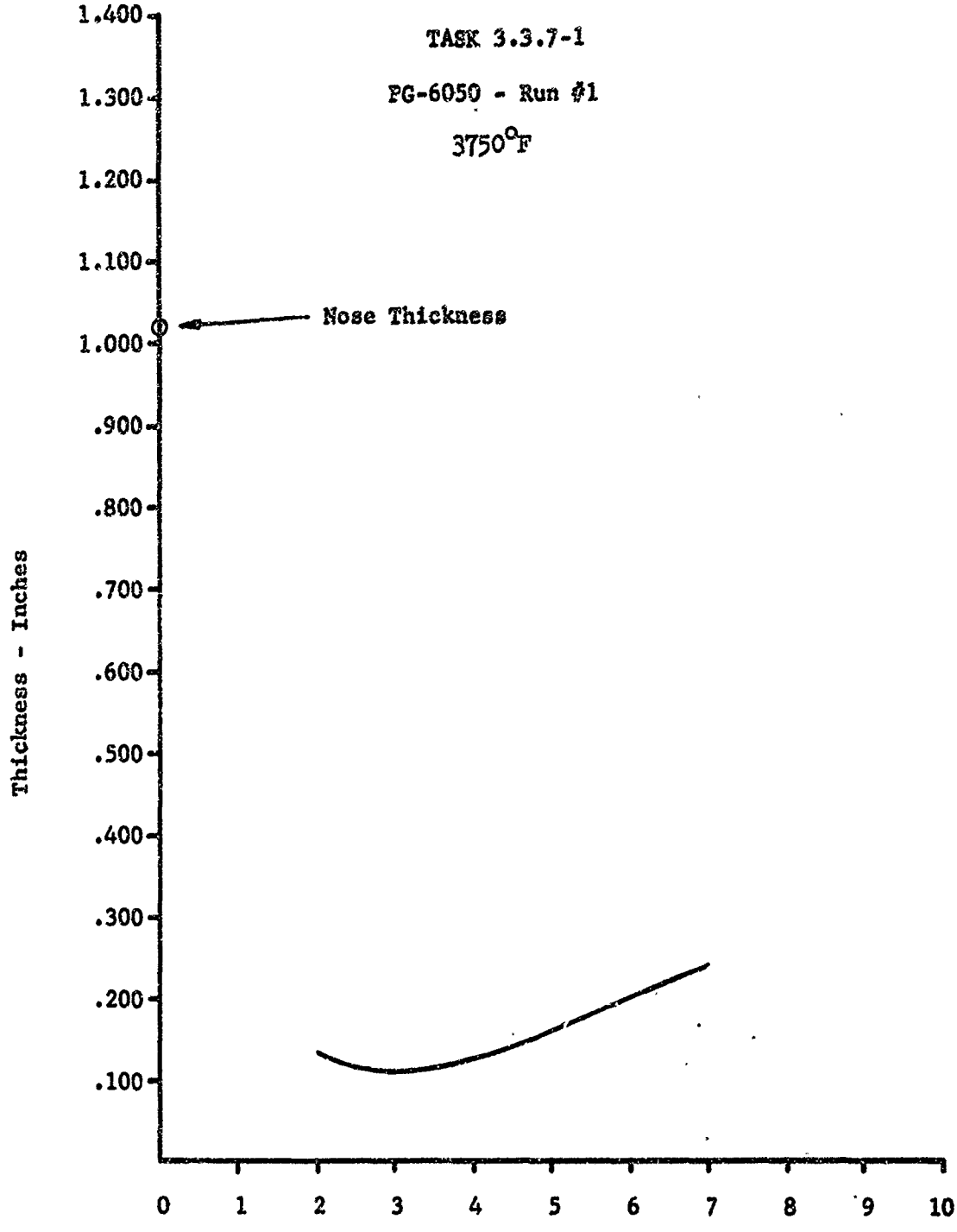
HAFNIUM FEED SYSTEM SCHEMATIC

Figure 2b0



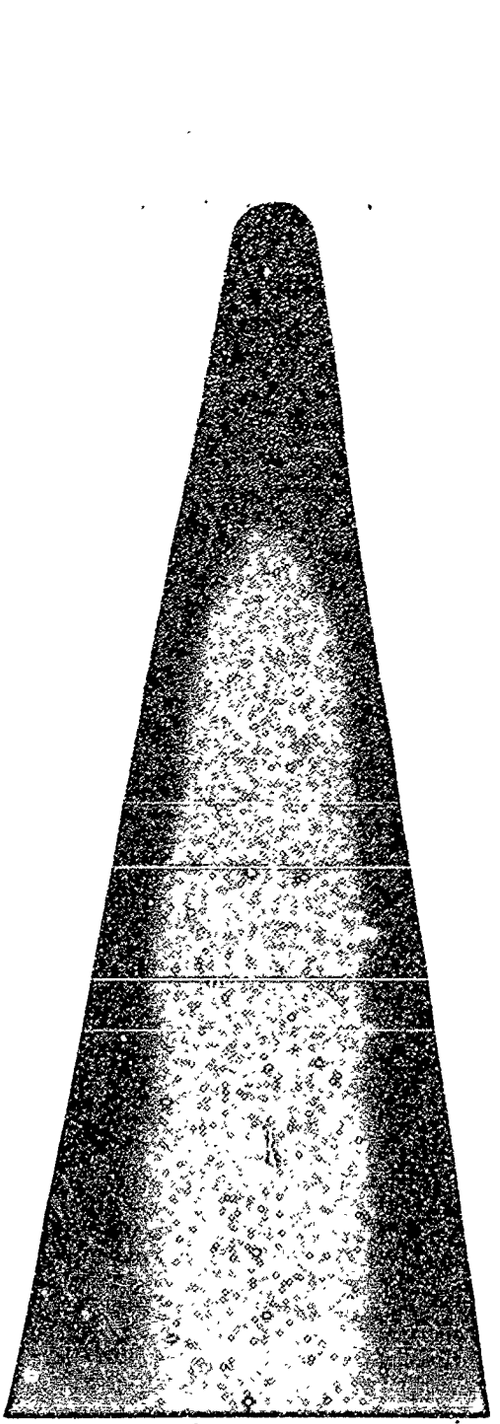
Typical Nose Cone Setup

Figure 241



Deposition Thickness Profile

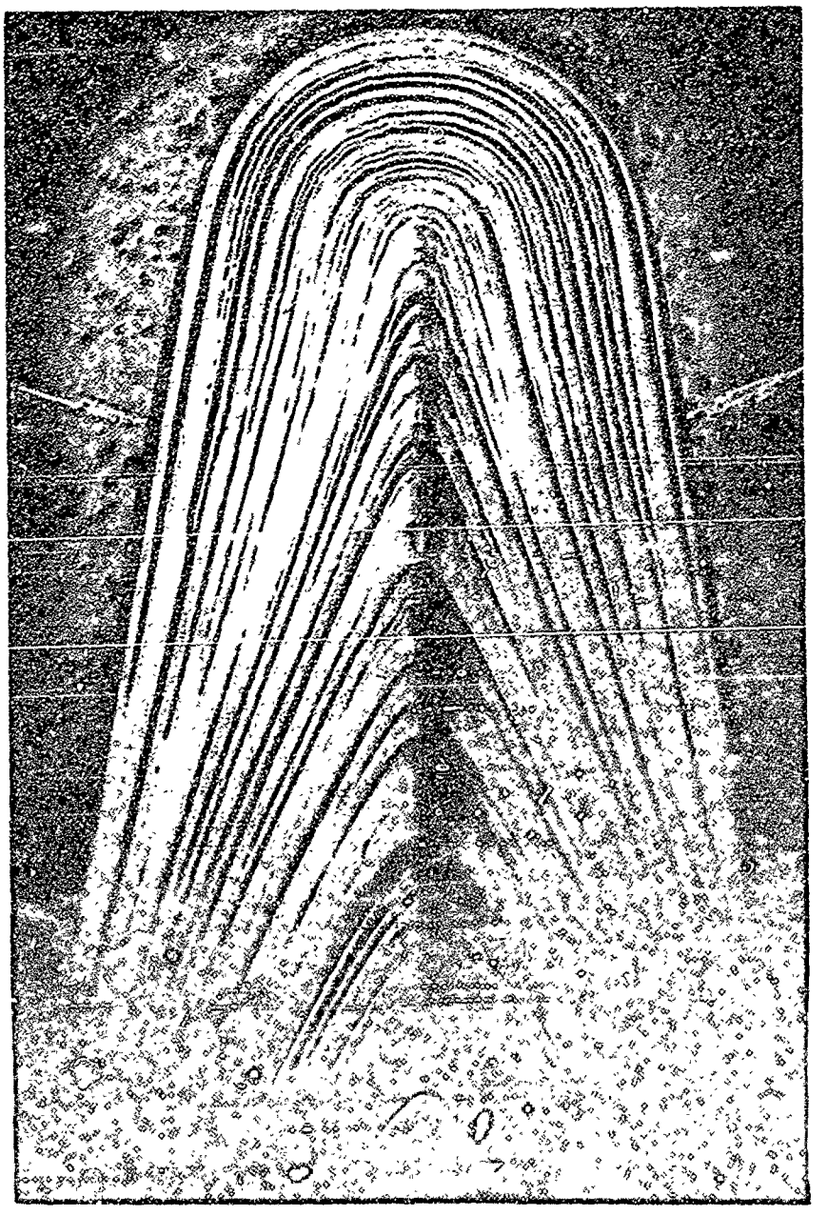
Figure 242



Task 3.3.7-1

Radiograph of 6050

Figure 243



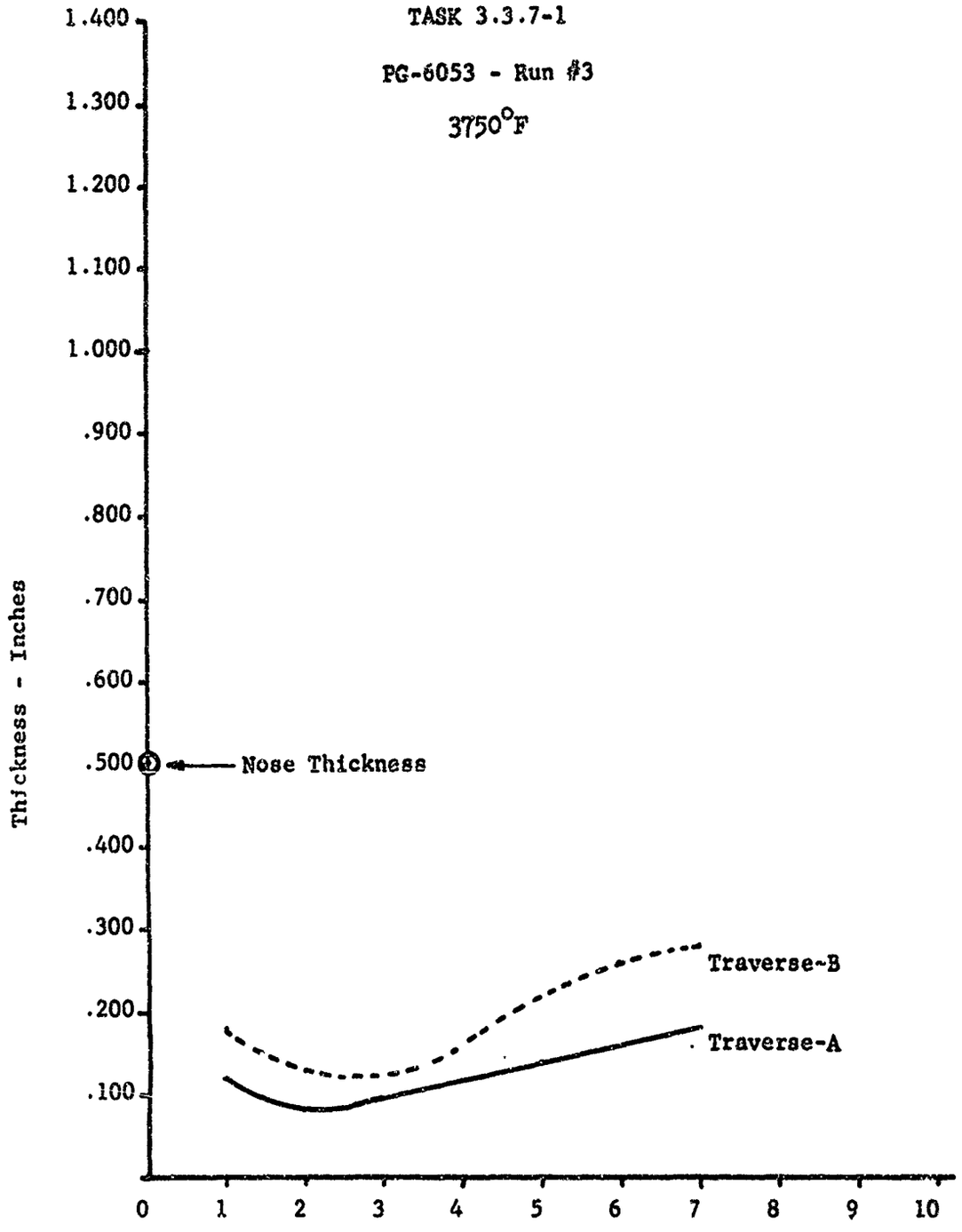
Run 6050 - Nose Region Cross Section - 5X

Figure 244



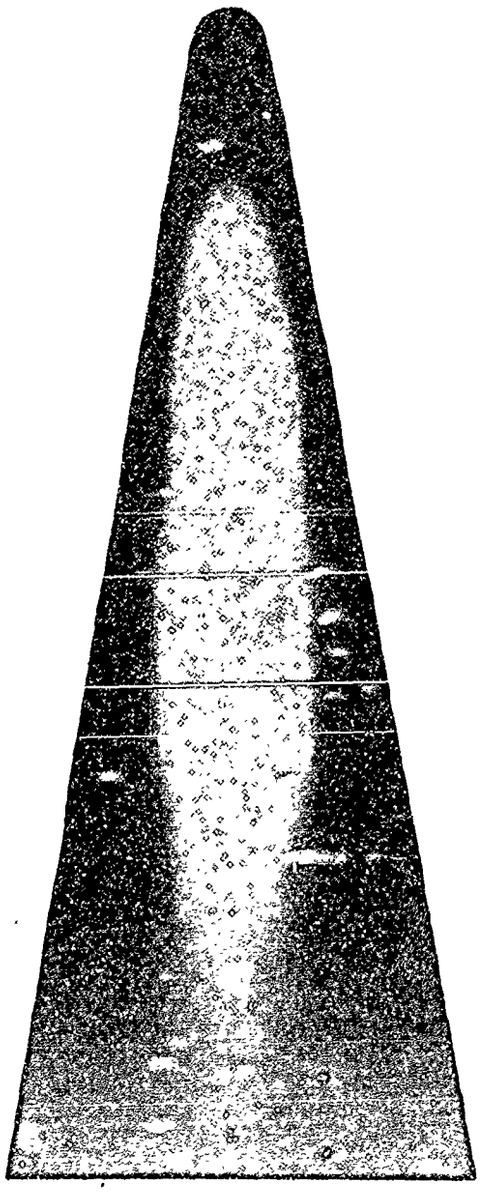
Run 4063 - Nozzle Growth

Figure 245



Deposition Thickness Profile

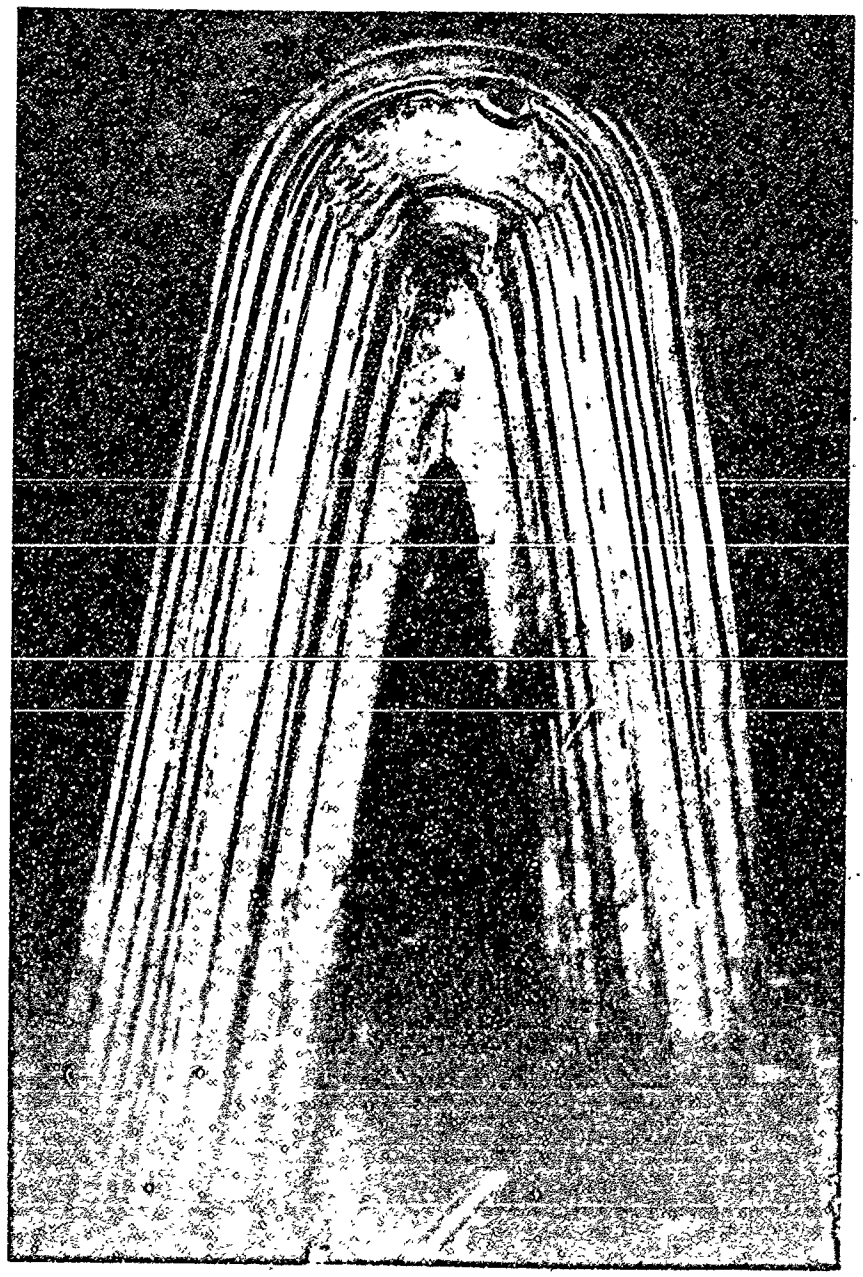
Figure 246



Task 3.3.7-1

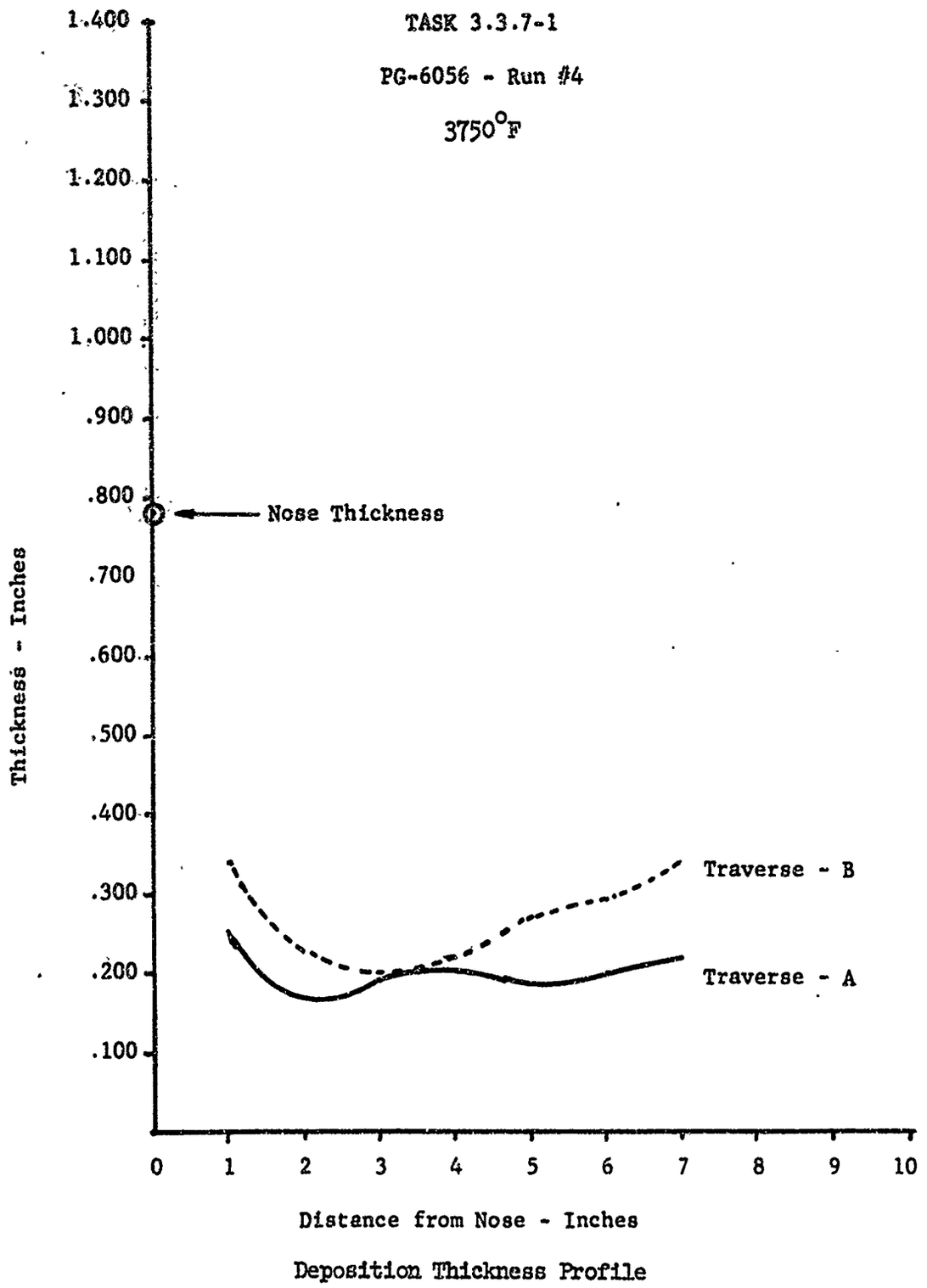
Radiograph of 6053

Figure 247



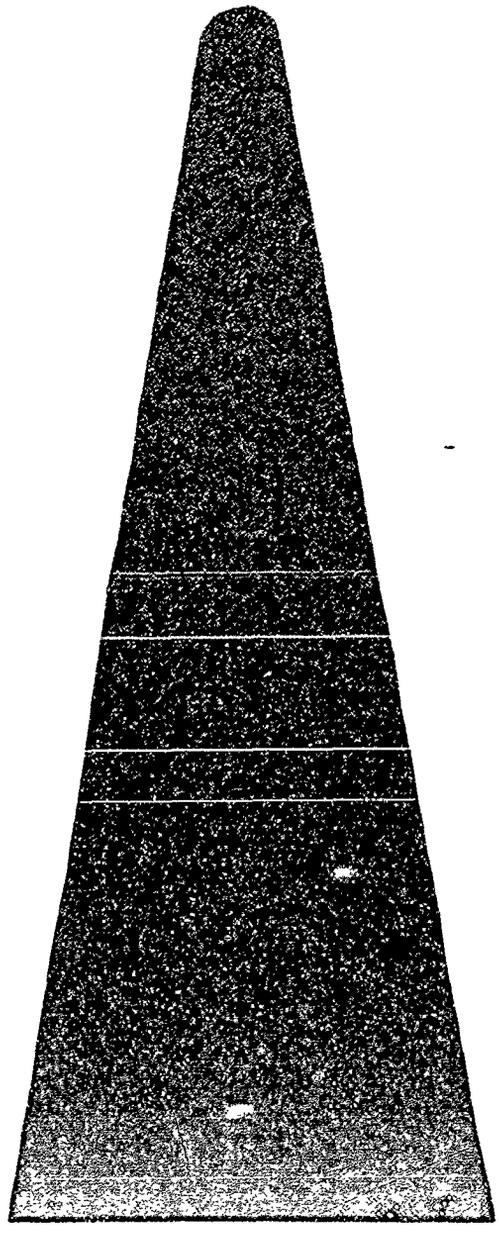
Run 6053 - Nose Region Cross Section - 5X

Figure 248



Deposition Thickness Profile

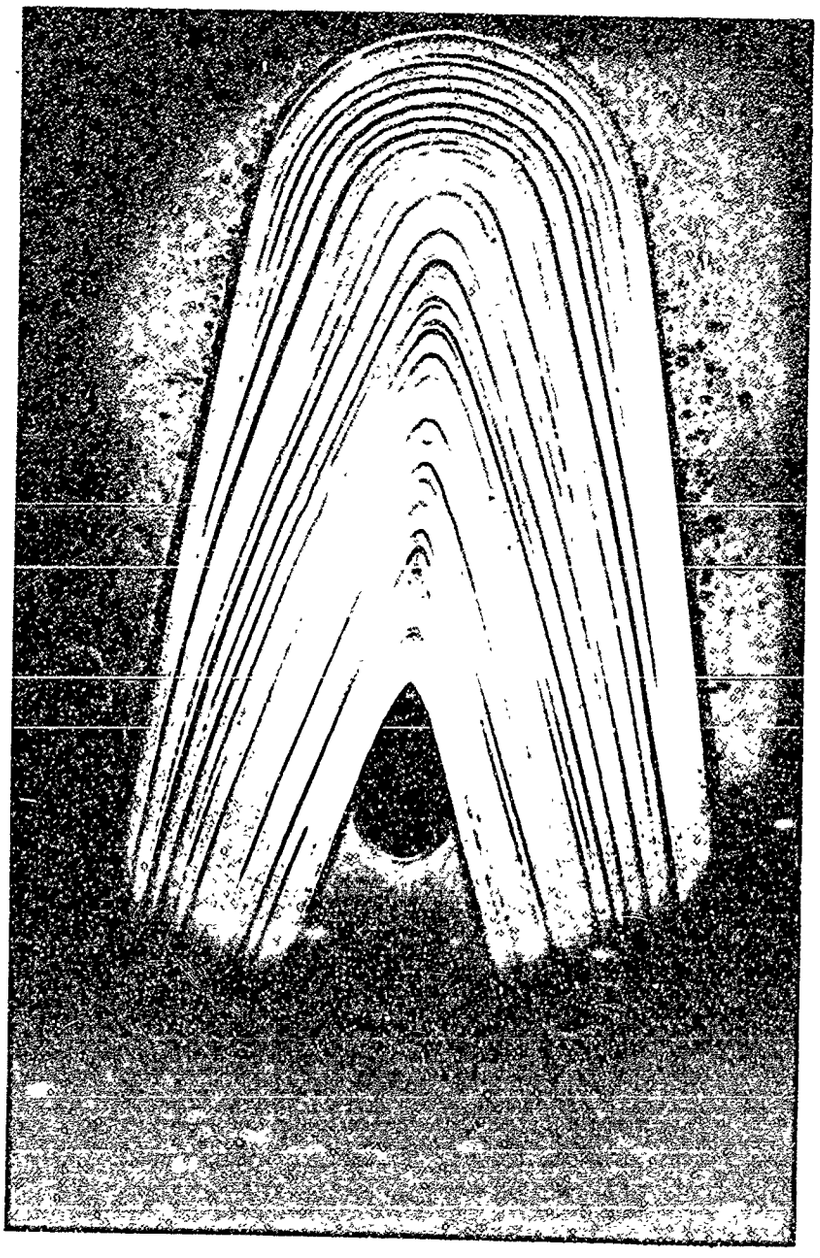
Figure 249



Task 3.3.7-1

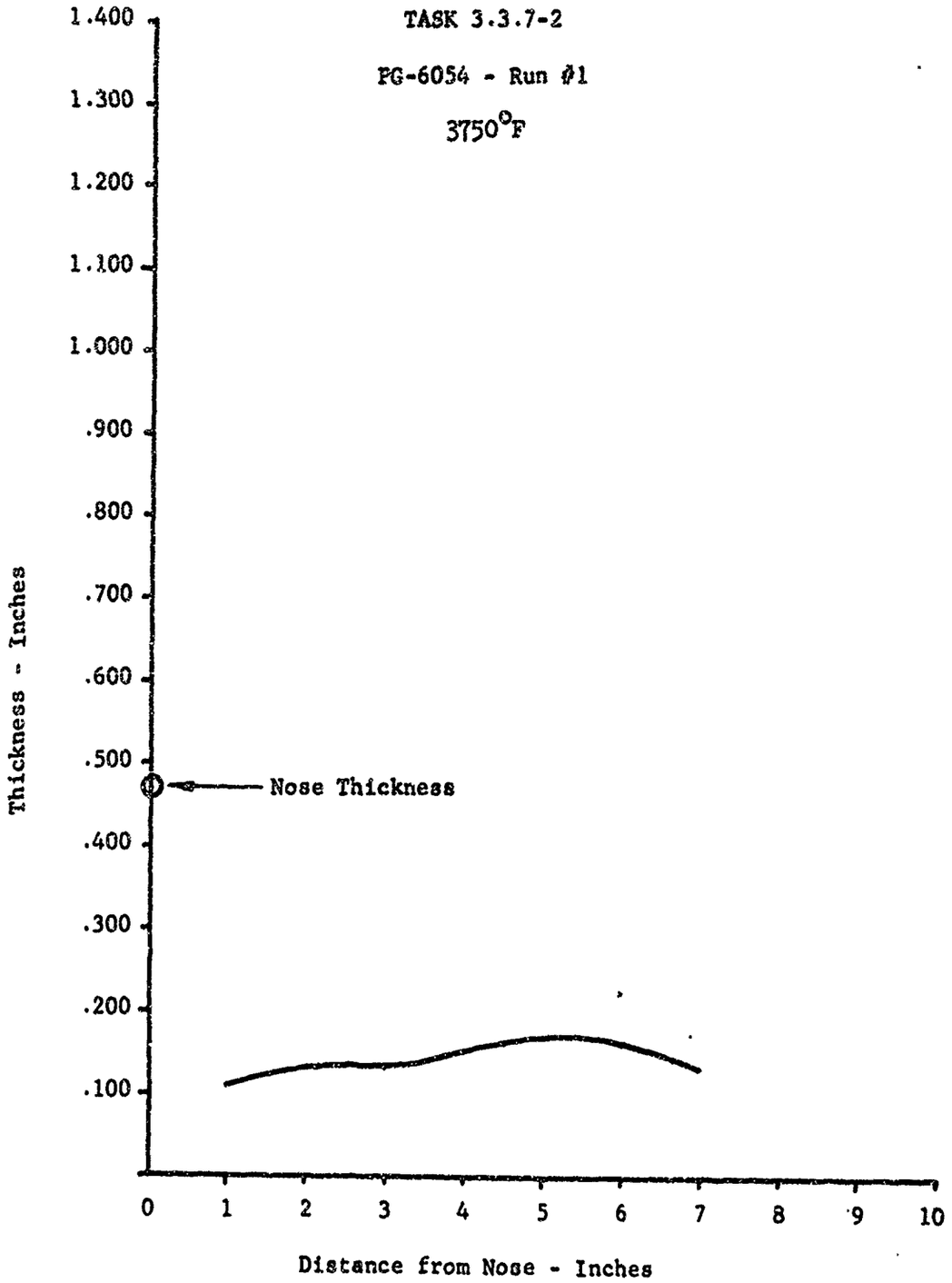
Radiograph of 6056

Figure 250

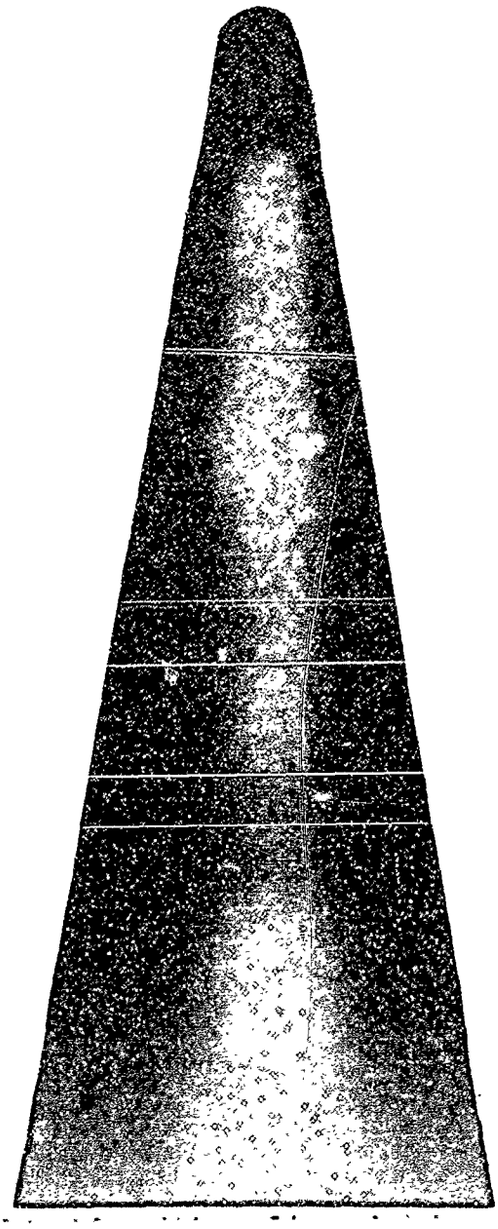


Run 6056 - Nose Region Cross Section - 5X

Figure 251



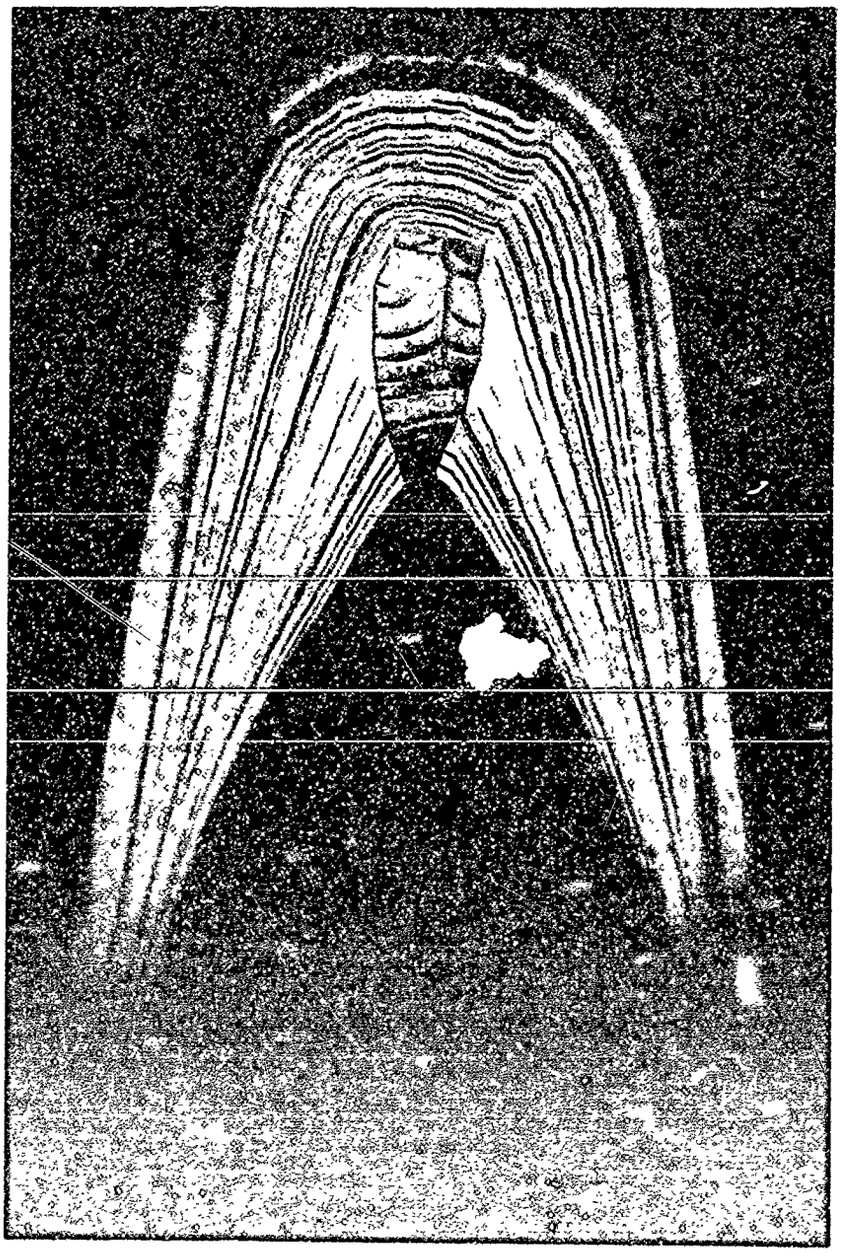
Deposition Thickness Profile
Figure 252



Task 3.3.7-2

Radiograph of 6054

Figure 253



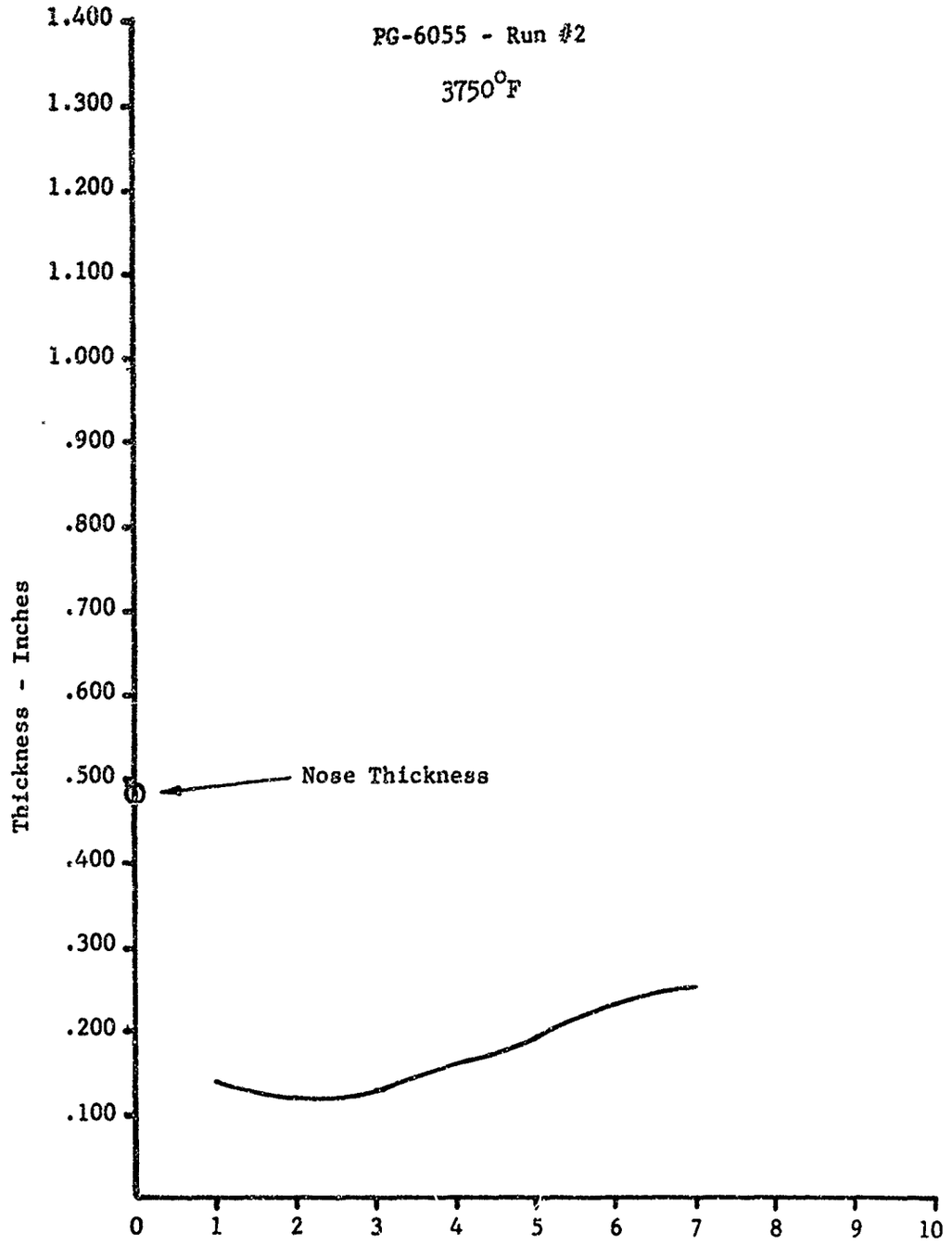
Run 6054 - Nose Region Cross Section - 5X

Figure 254

TASK 3.3.7-2

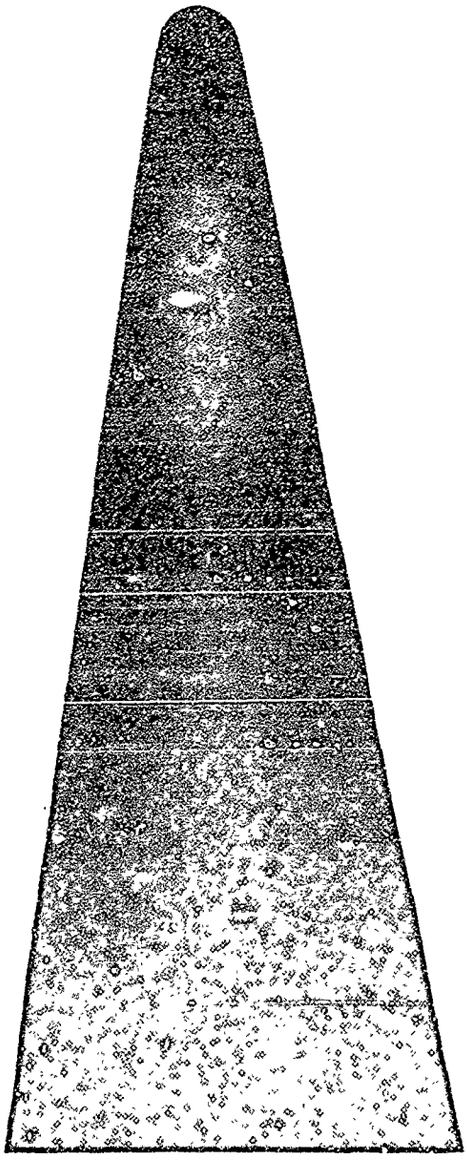
PG-6055 - Run #2

3750°F



Deposition Thickness Profile

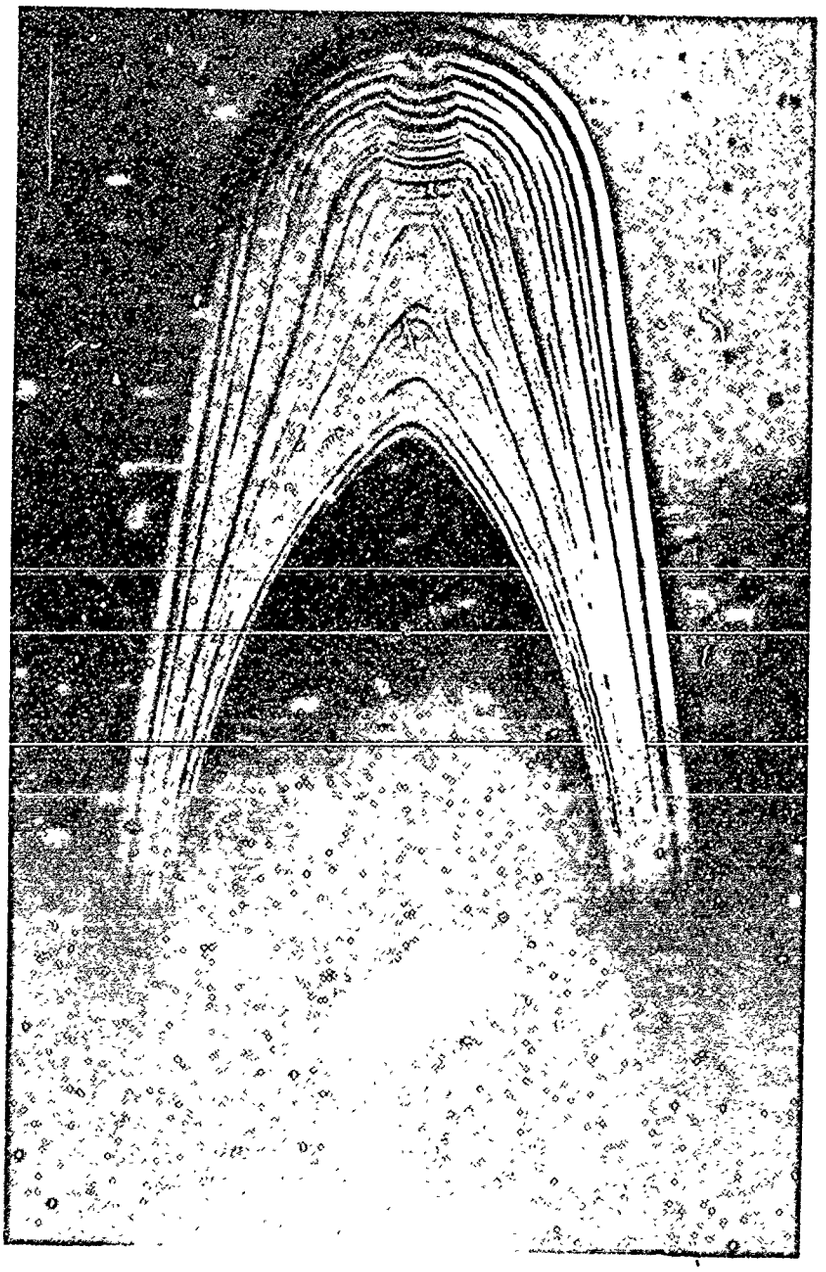
Figure 255



Task 3.3.7-2

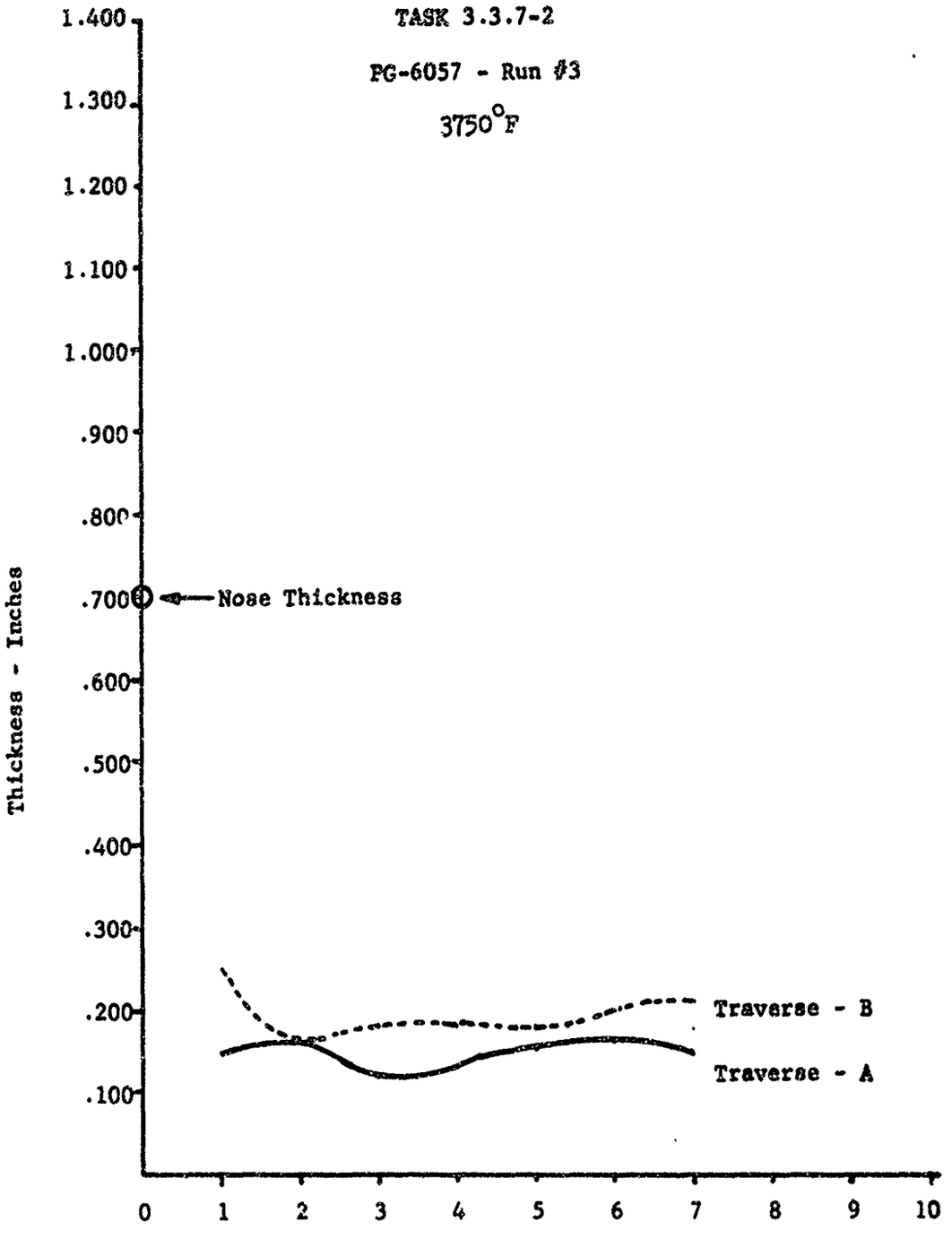
Radiograph of 6055

Figure 256



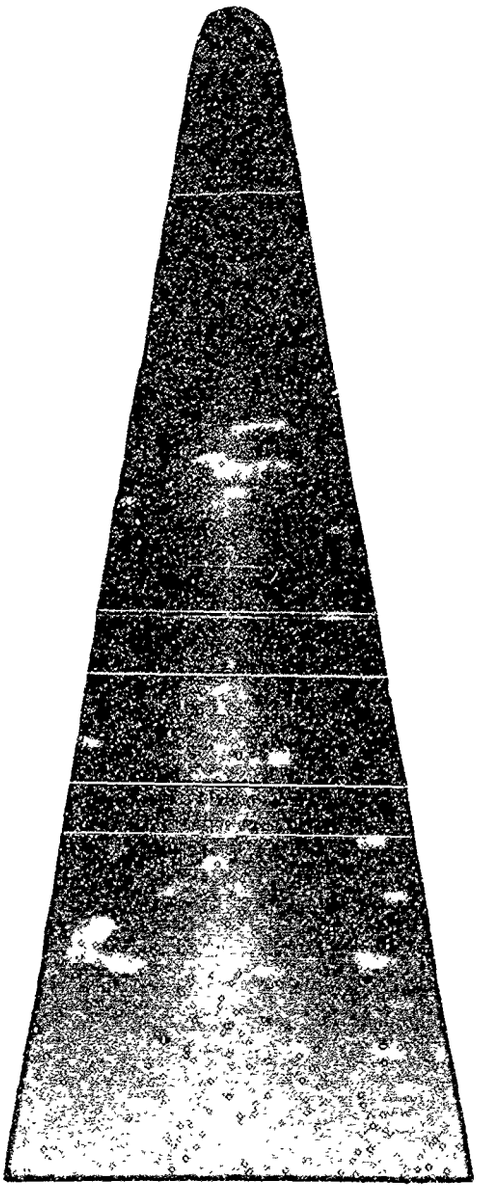
Run 6055 - Nose Region Cross Section - 5X

Figure 257



Deposition Thickness Profile

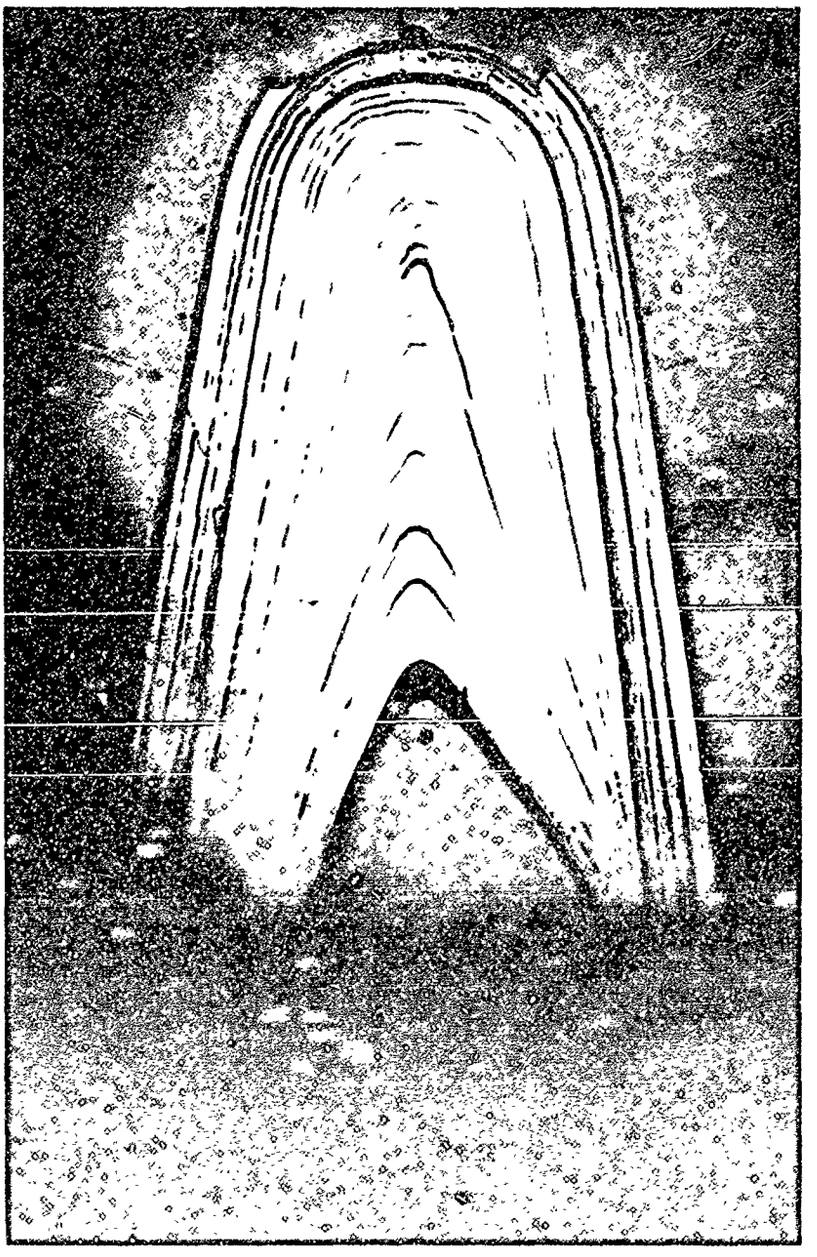
Figure 258



Task 3.3.7-2

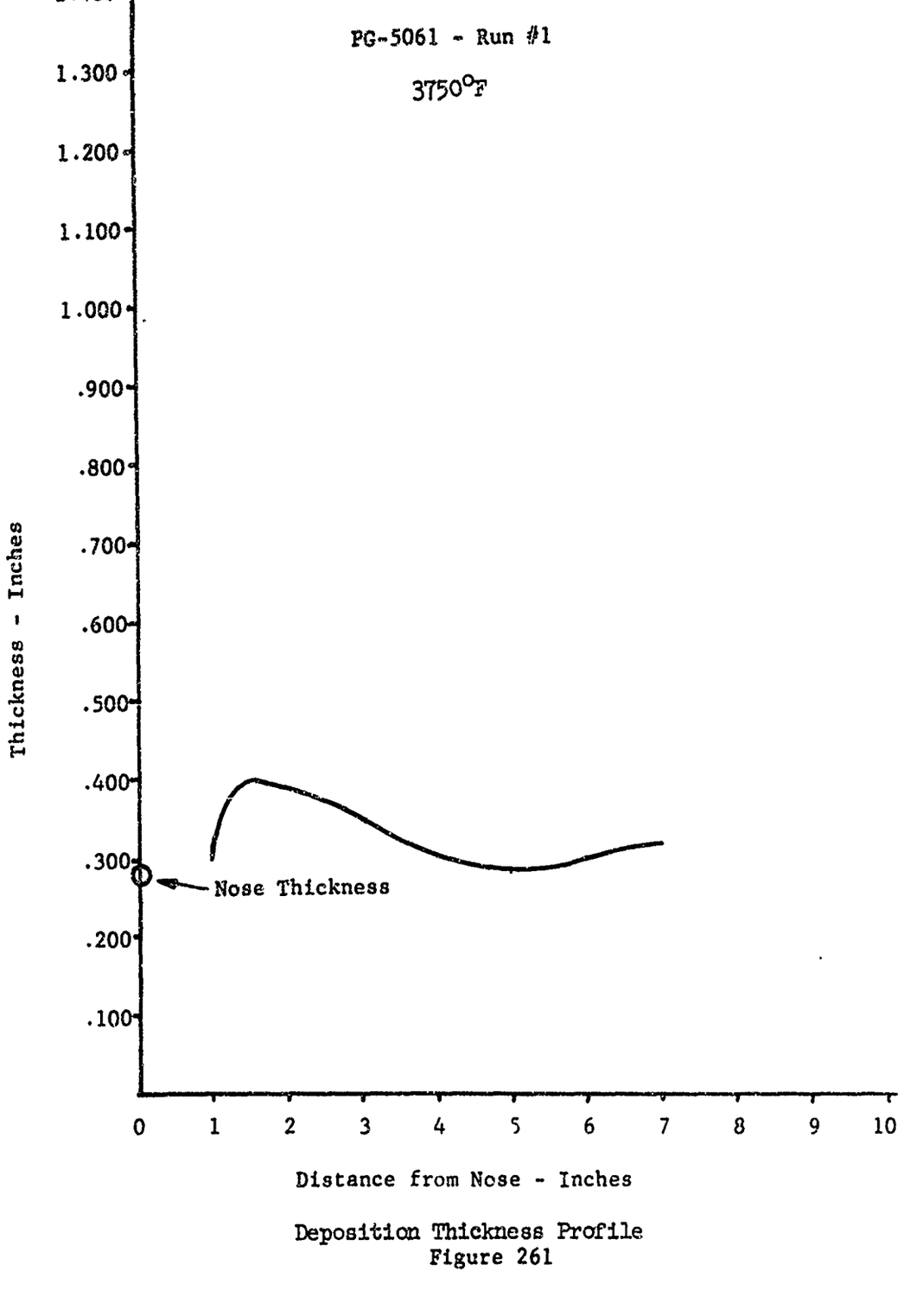
Radiograph of 6057

Figure 259

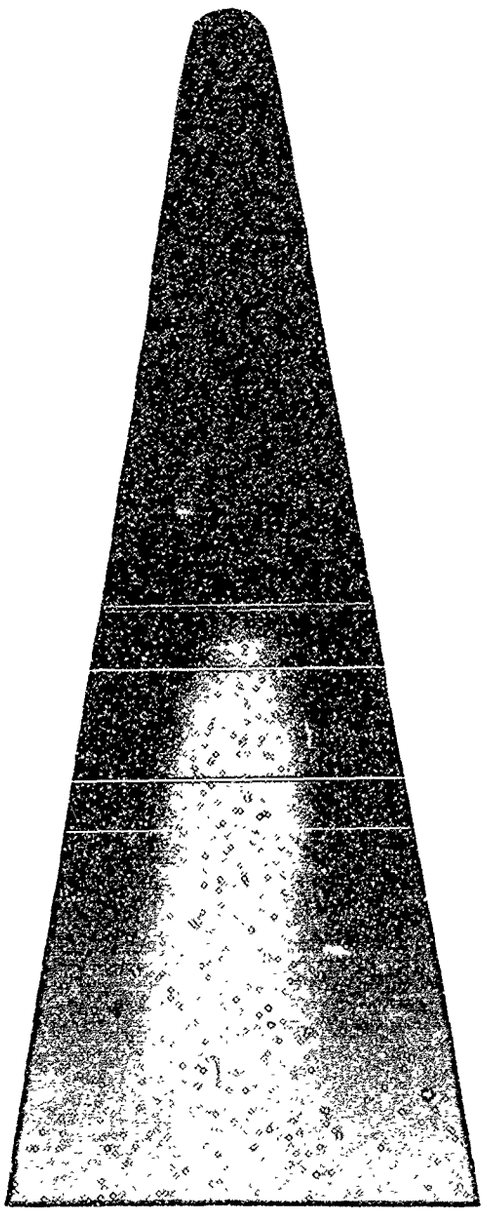


Run 6057 - Nose Region Cross Section - 5X

Figure 260



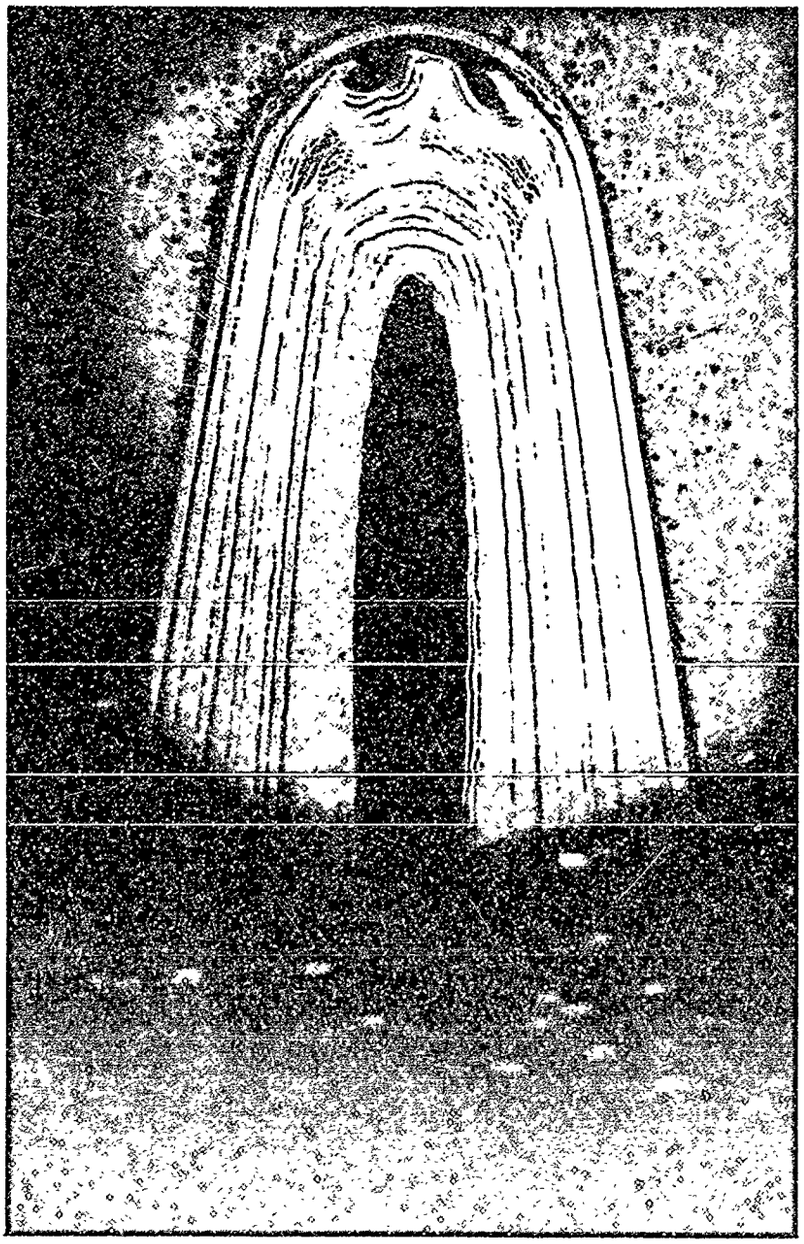
Deposition Thickness Profile
Figure 261



Task 3.3.7-3

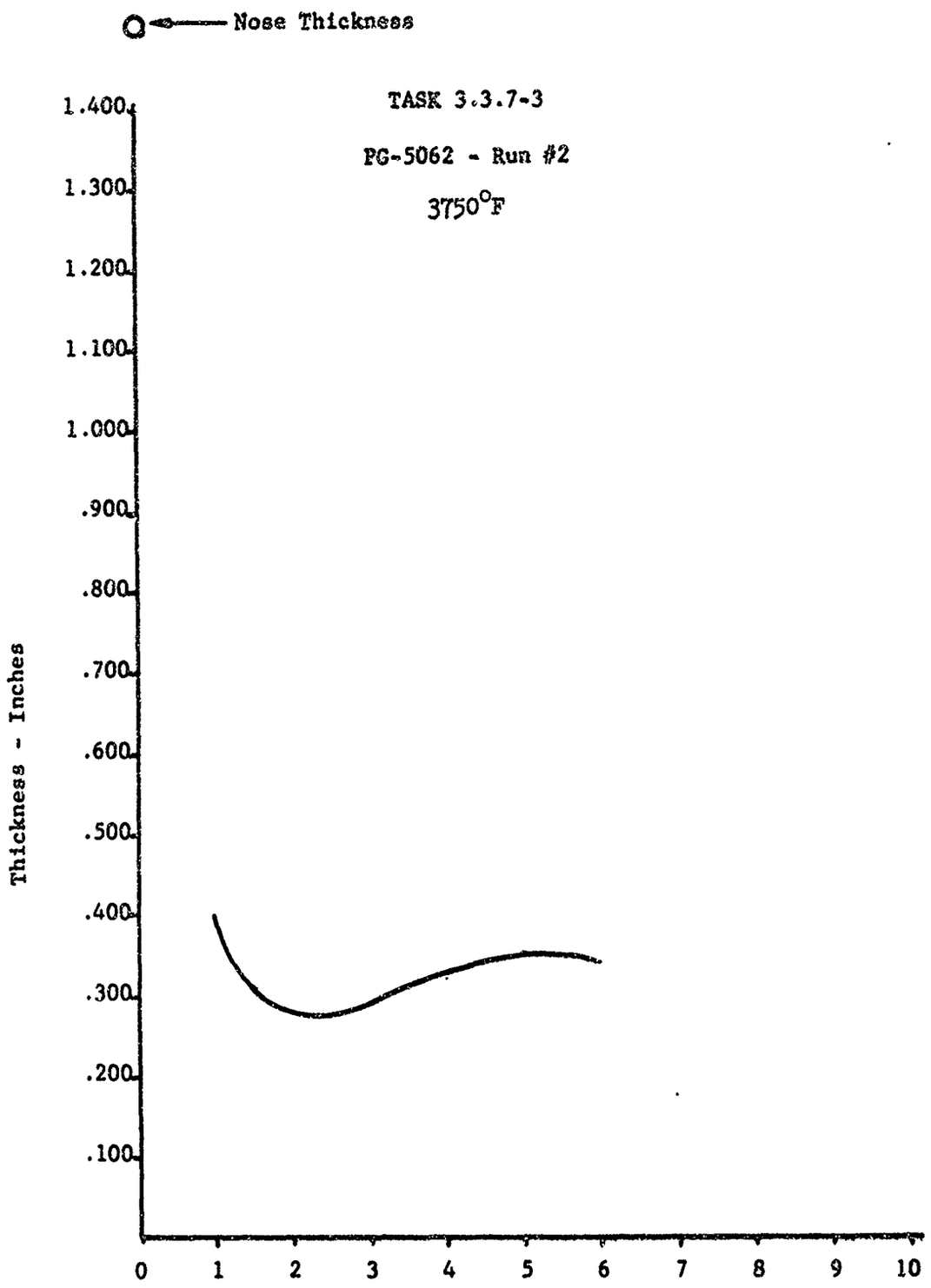
Radiograph of 5061

Figure 262



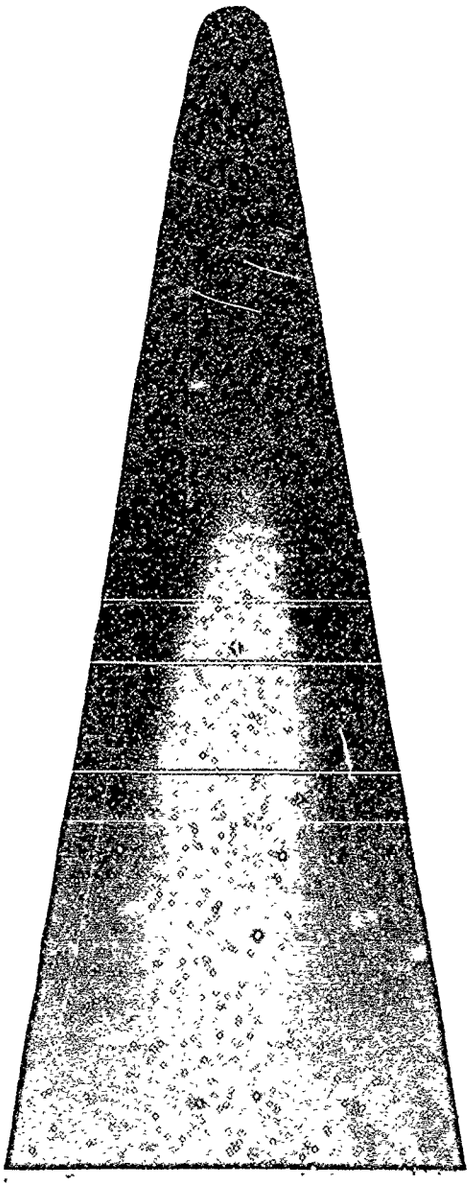
Run 5061 - Nose Region Cross Section - 5X

Figure 263



Deposition Thickness Profile

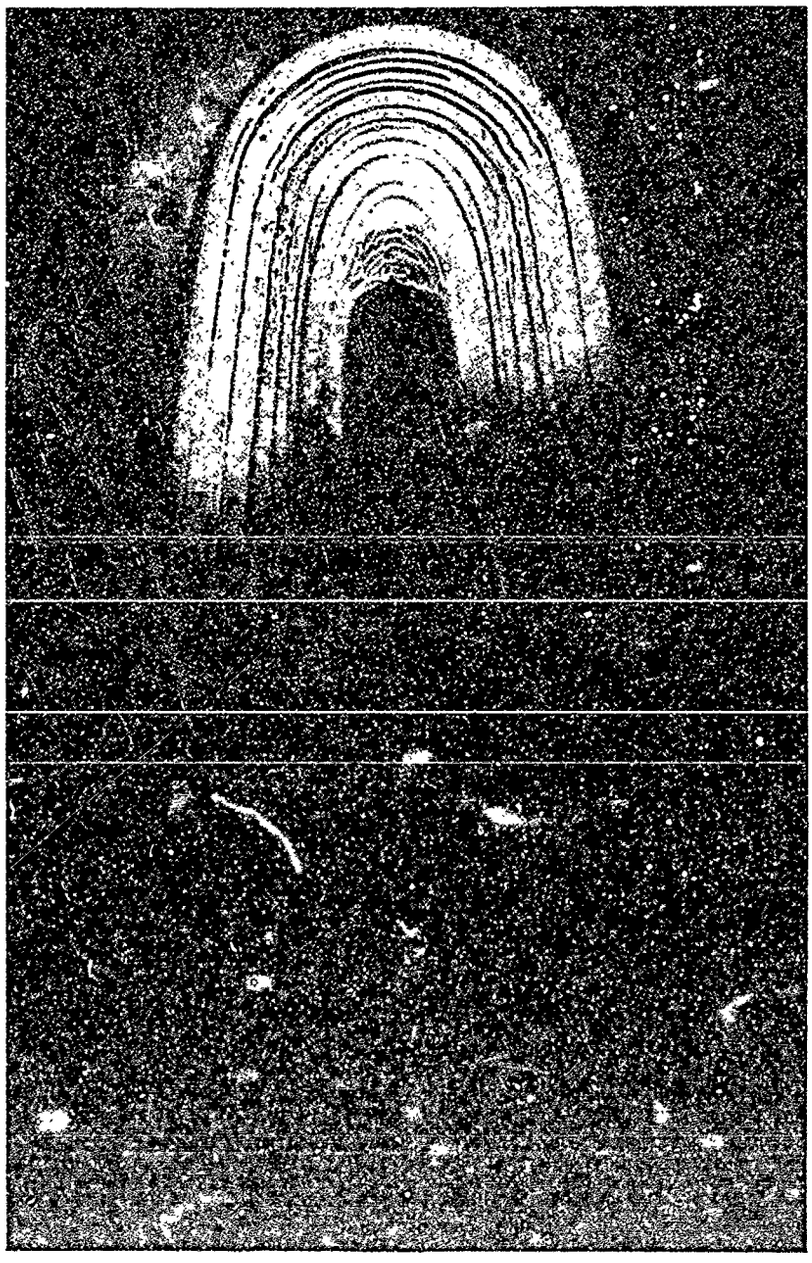
Figure 264



Task 3.3.7-3

Radiograph of 5062

Figure 265



Run 5062 - Nose Region Cross Section - 5X

Figure 266

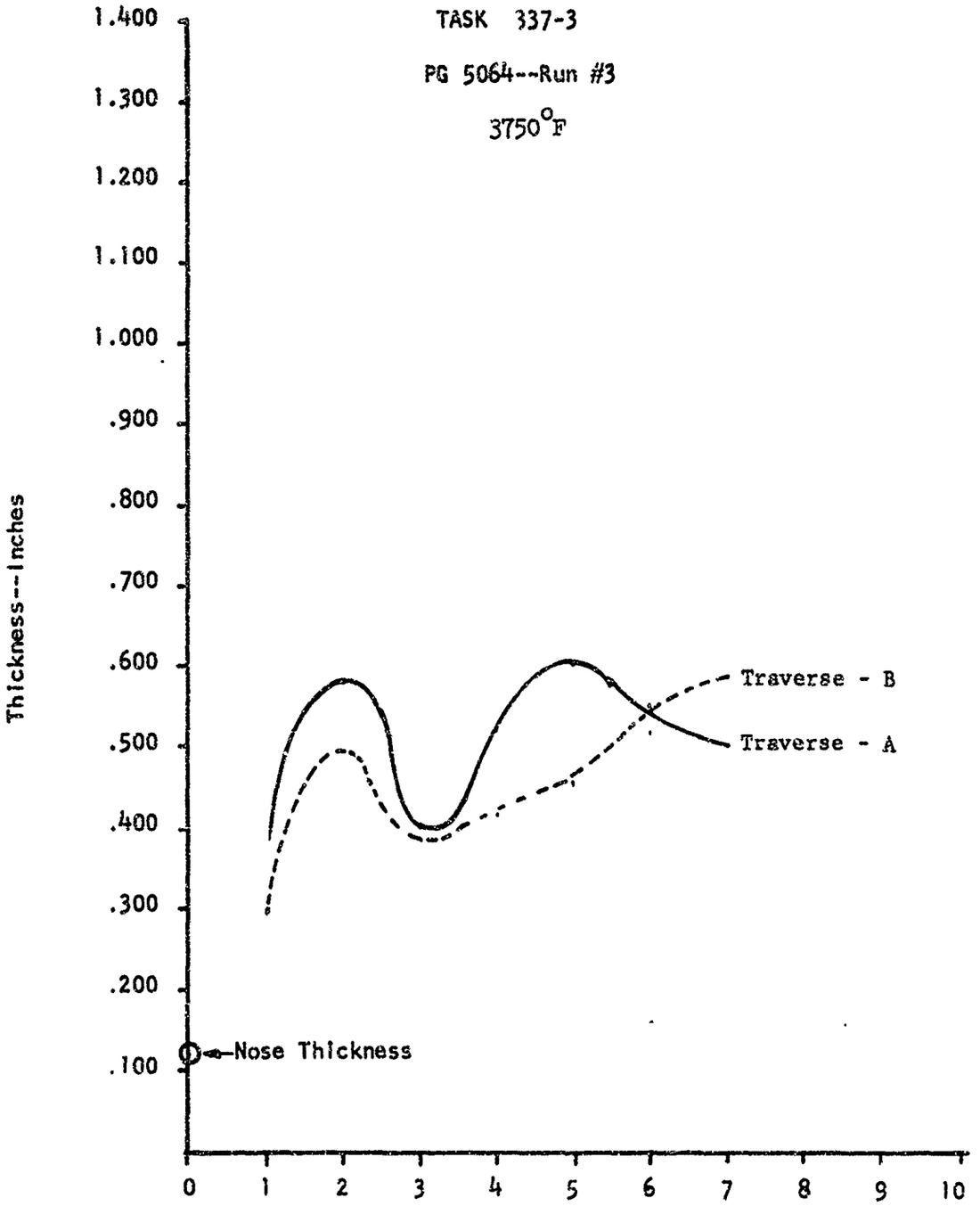
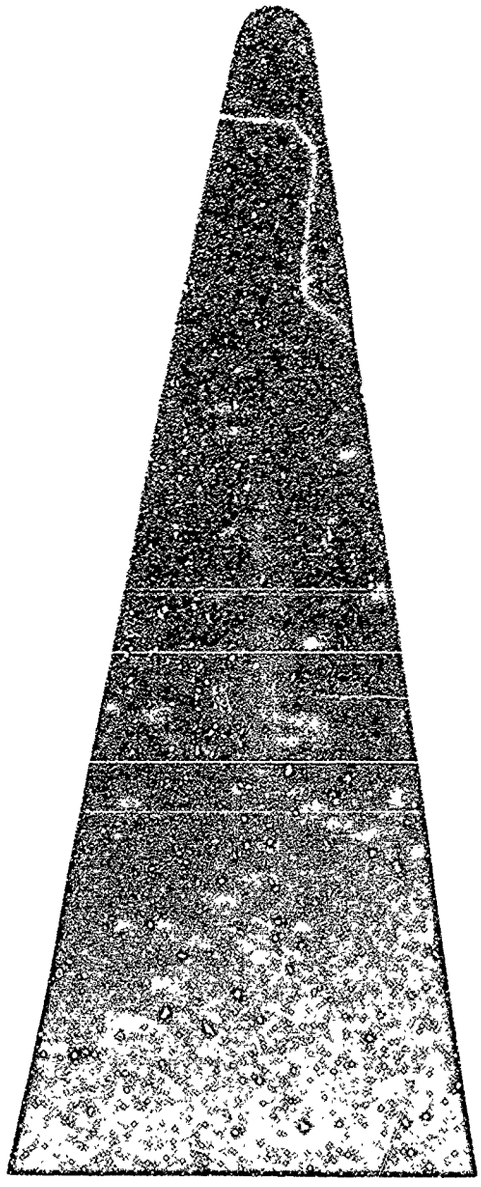

TASK 337-3
PG 5064--Run #3
3750°F
1.400
1.300
1.200
1.100
1.000
.900
.800
.700
.600
.500
.400
.300
.200
.100
Thickness--Inches
Traverse - B
Traverse - A
Nose Thickness
0
1
2
3
4
5
6
7
8
9
10
Distance from Nose
Deposition Thickness

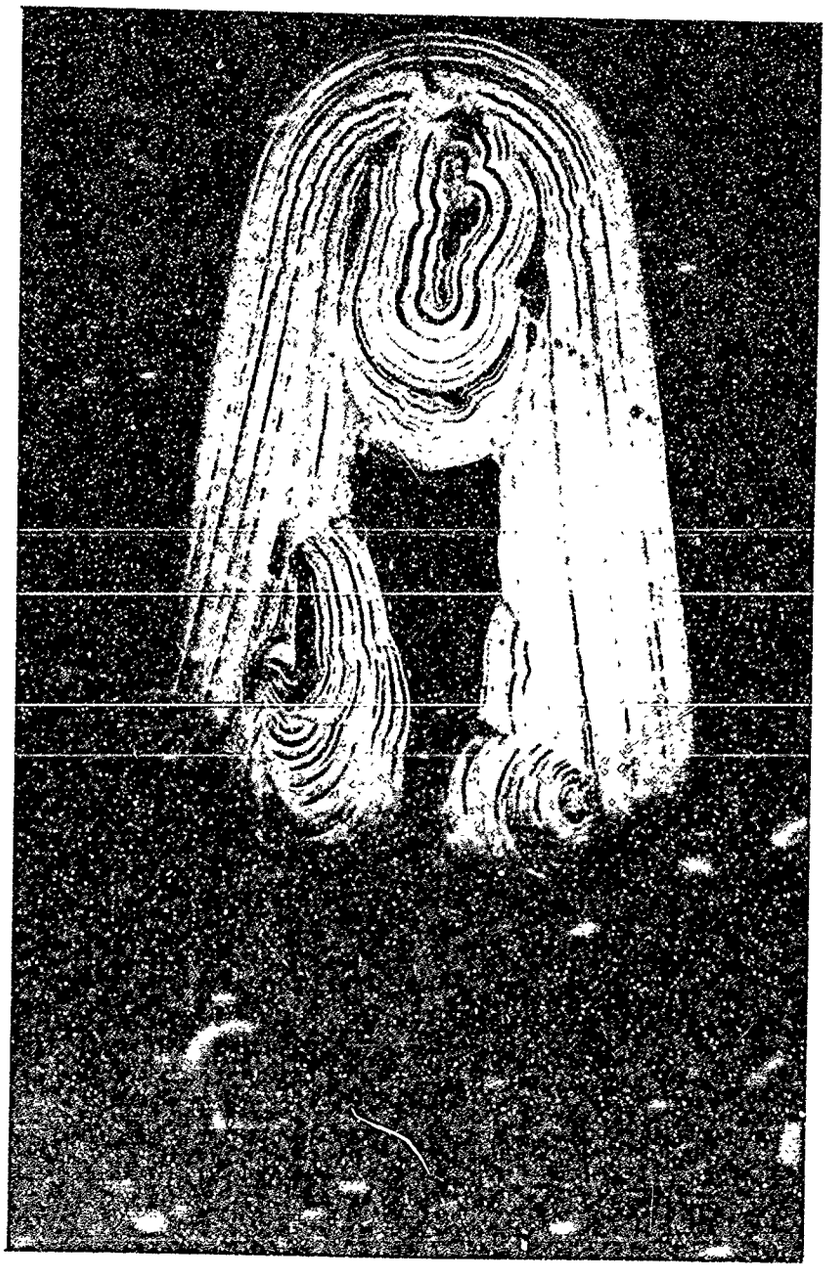
Figure 267



Task 3.3.7-3

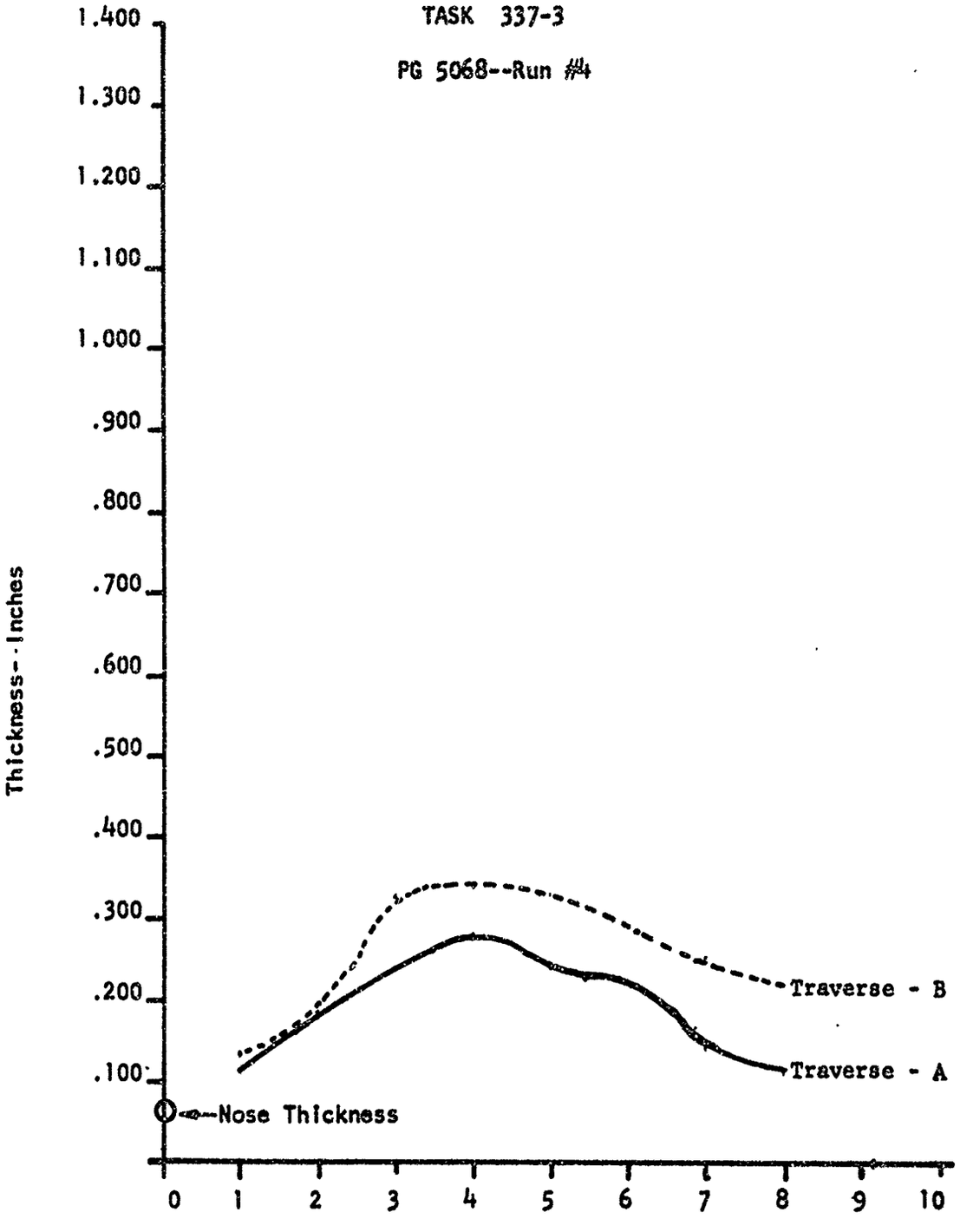
Radiograph of 5064

Figure 268

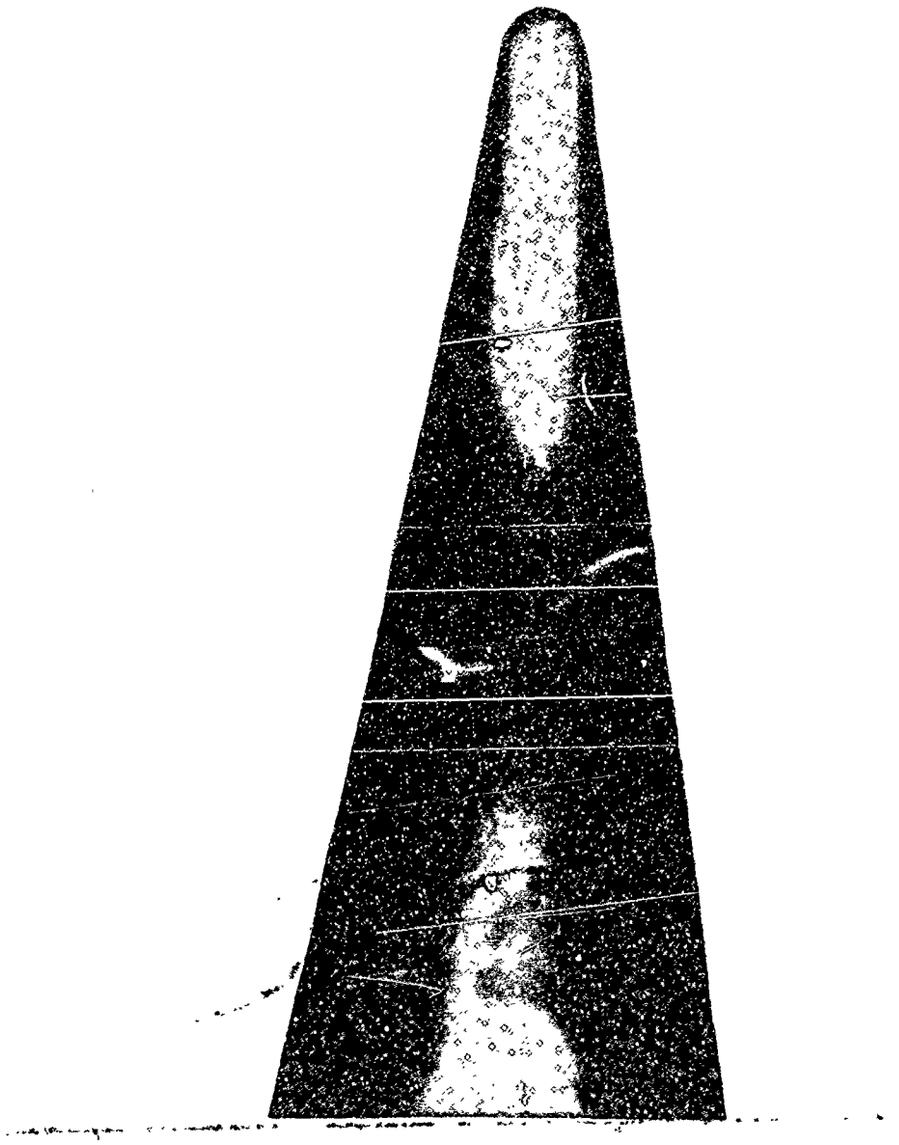


Run 5064 - Nose Region Cross Section - 5X

Figure 269



Deposition Thickness Profile
Figure 270



Task 3.3.7-3

Radiograph of 5068

Figure 271



Run 5068 - Nose Region Cross Section - 5X

Figure 272

51.6 •

TASK 3.3.7-3

SUMMARY OF DEPOSITION THICKNESS PROFILES

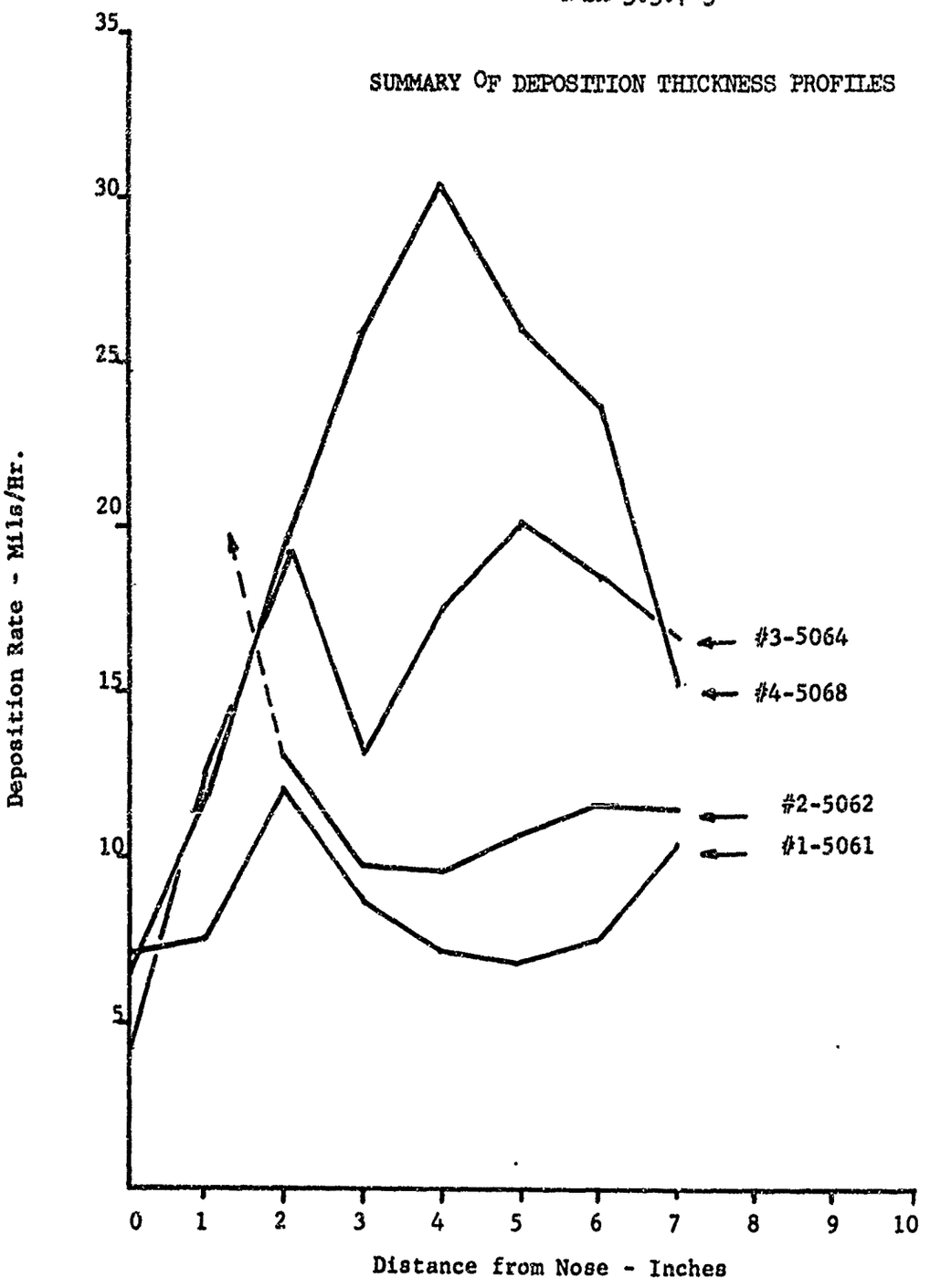
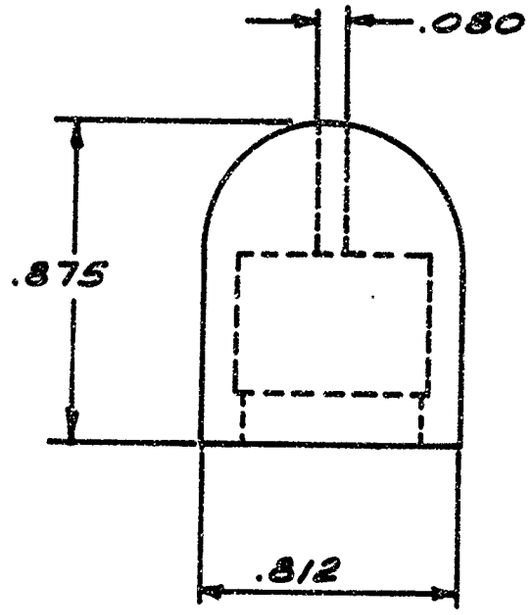


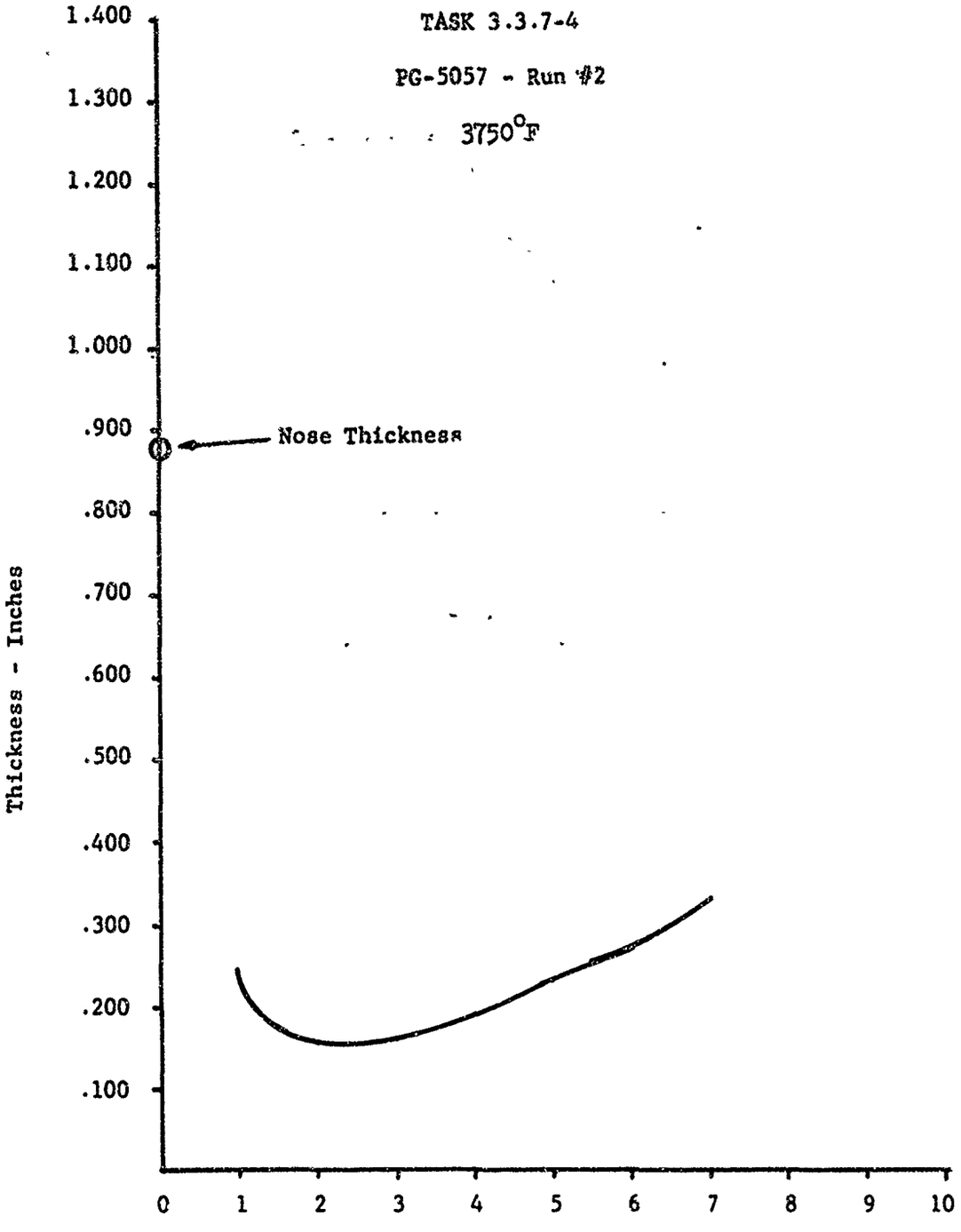
Figure 273



MATERIAL:
GRAPHITE

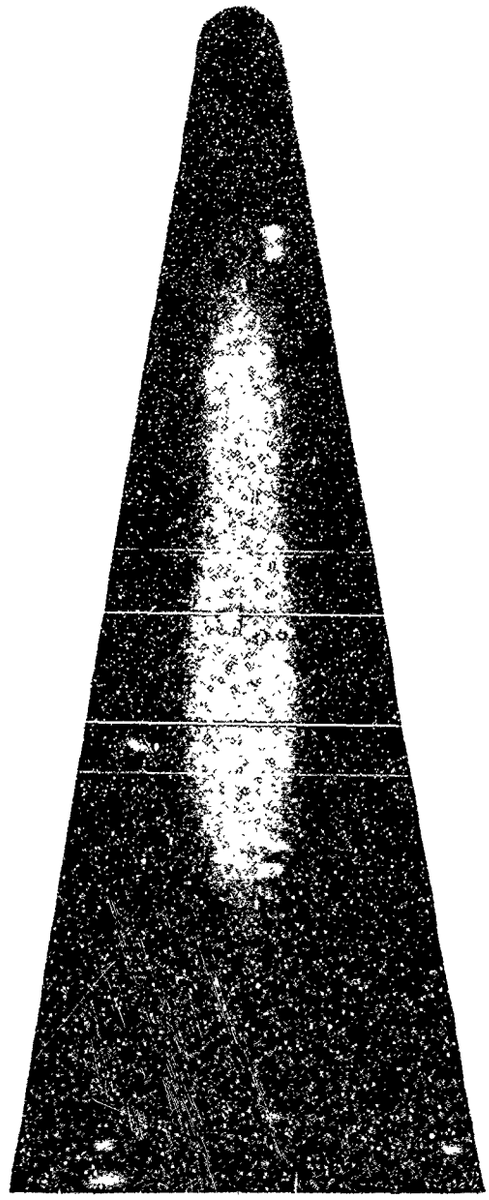
304014
NOZZLE CAP

Figure 274



Deposition Thickness Profile

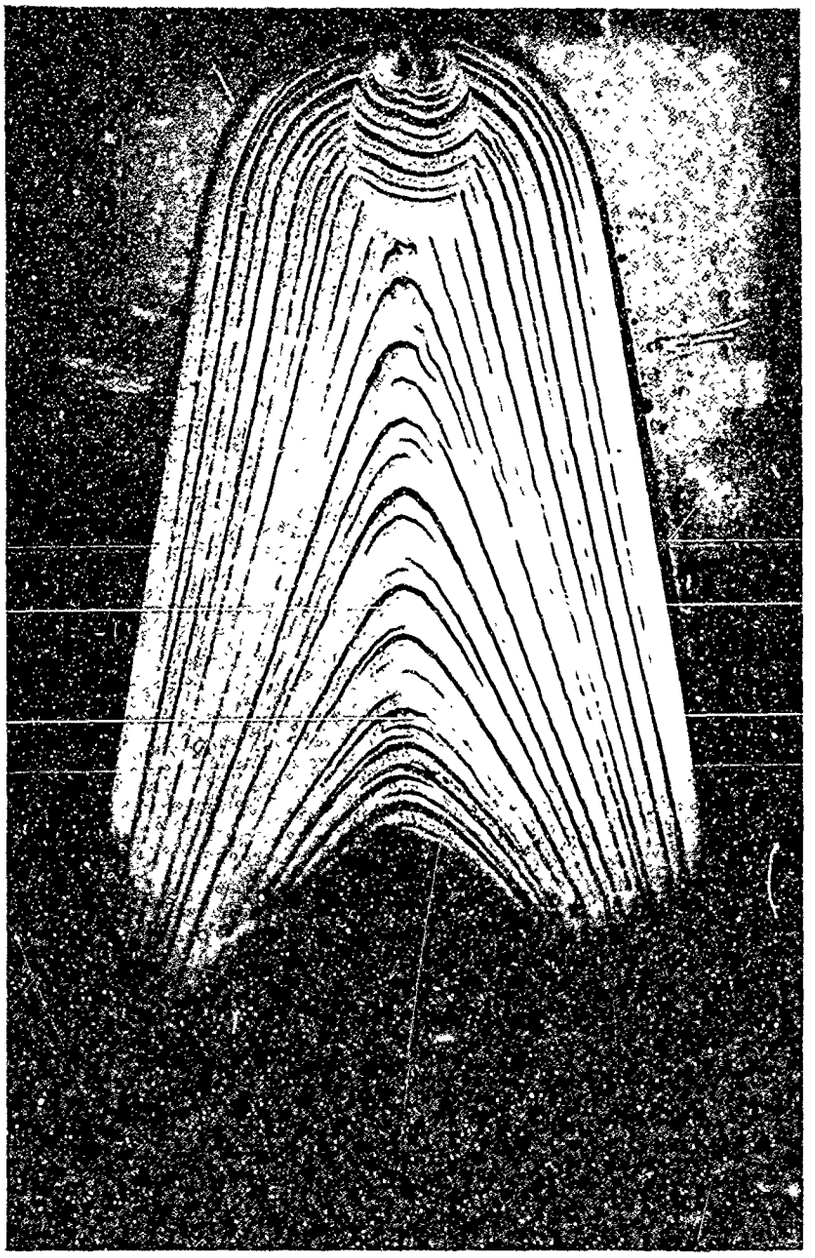
Figure 275



Task 3.3.7-4

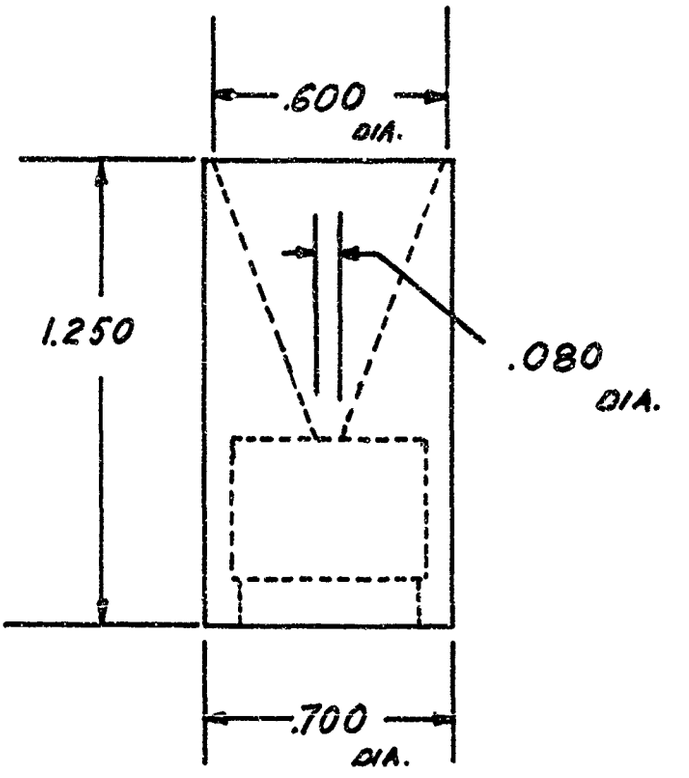
Radiograph of 5057

Figure 276



Run 5057 - Nose Region Cross Section - 5X

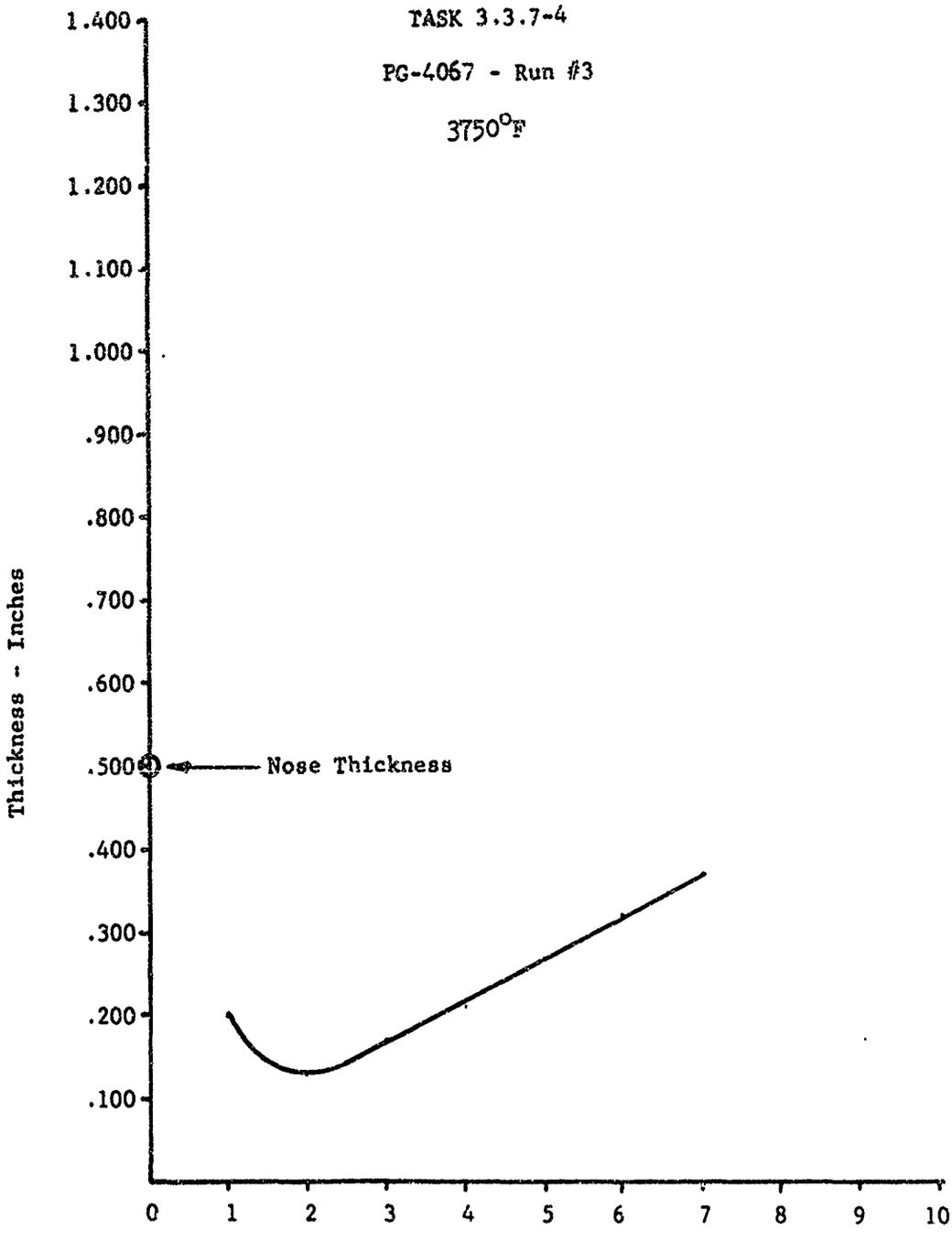
Figure 277



MATERIAL :
GRAPHITE

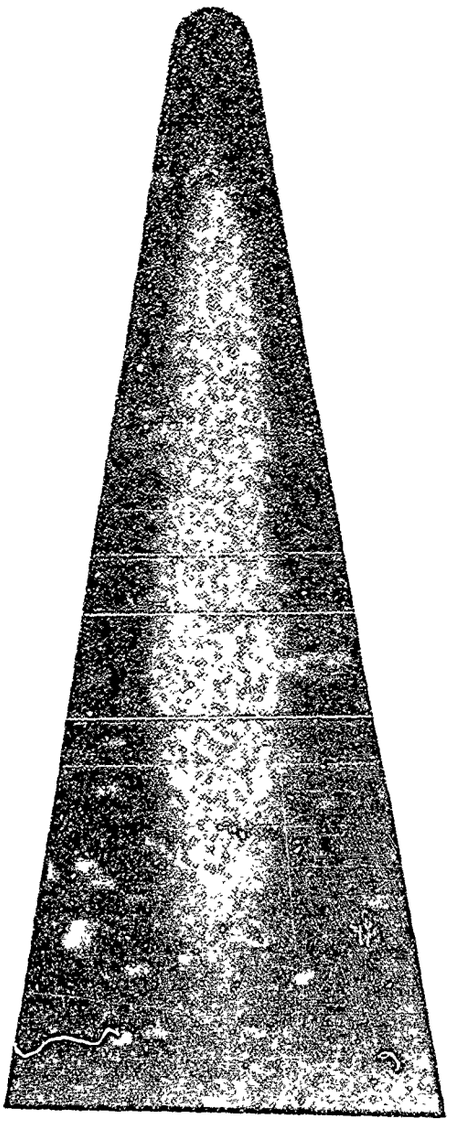
304016
NOZZLE CAP

Figure 278



Deposition Thickness Profile

Figure 279



Task 3.3.7-4

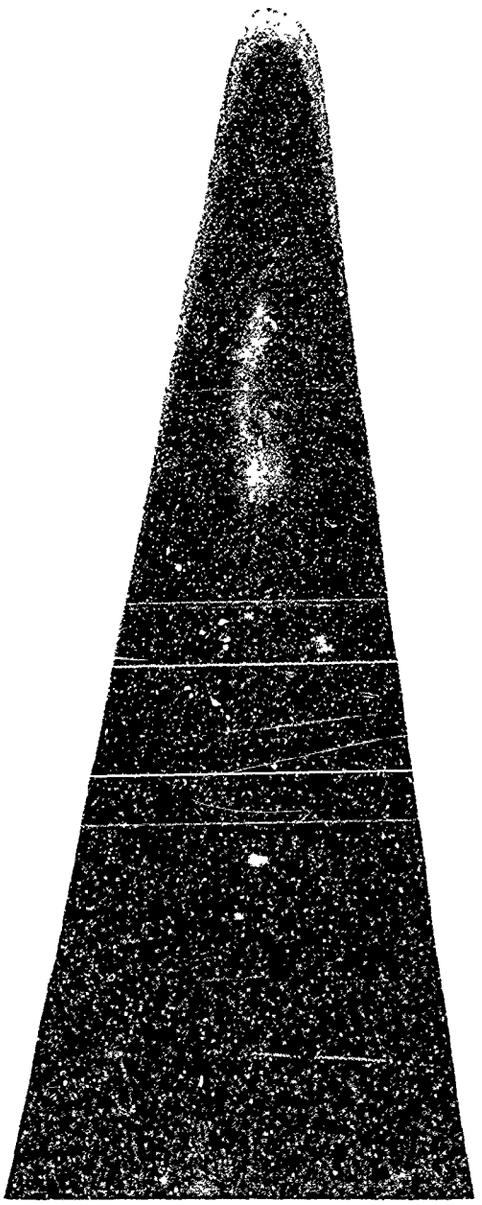
Radiograph of 4067

Figure 280



Run 4067 - Nose Region Cross Section - 5X

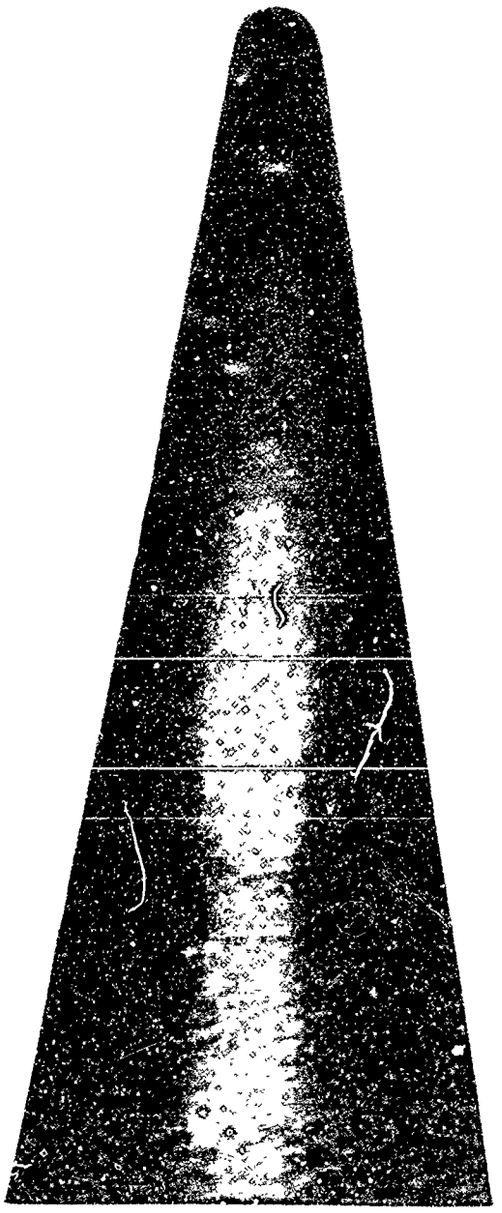
Figure 281



Task 3.3.7-5

Radiograph of 5065

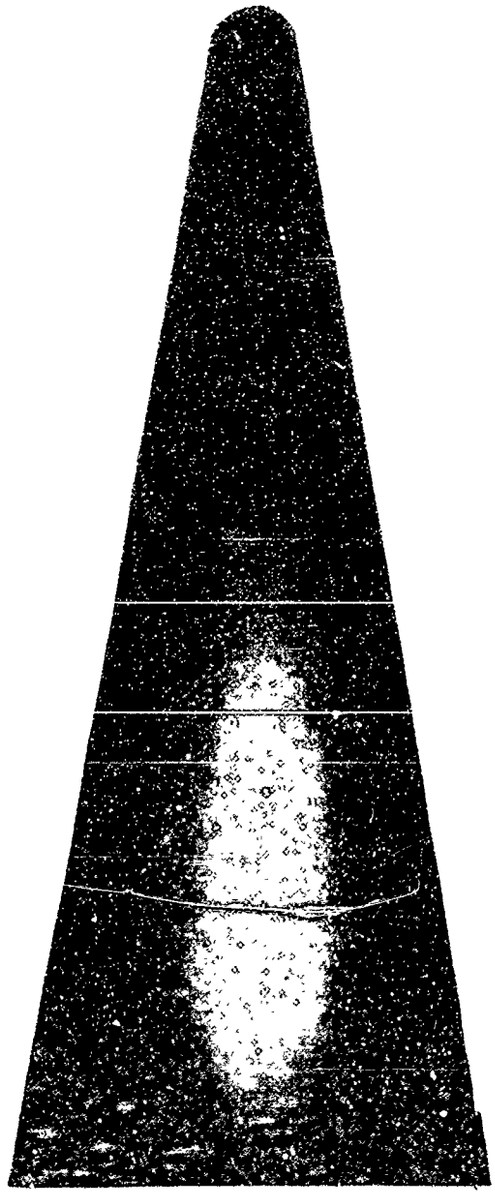
Figure 282



Task 3.3.7-5

Radiograph of 4071

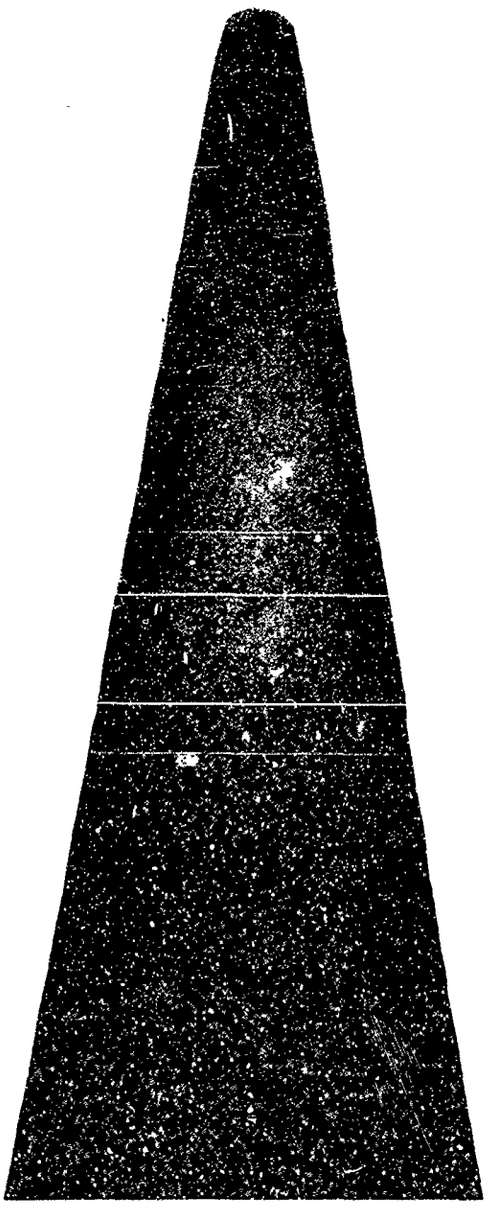
Figure 283



Task 3.3.7-5

Radiograph of 6060

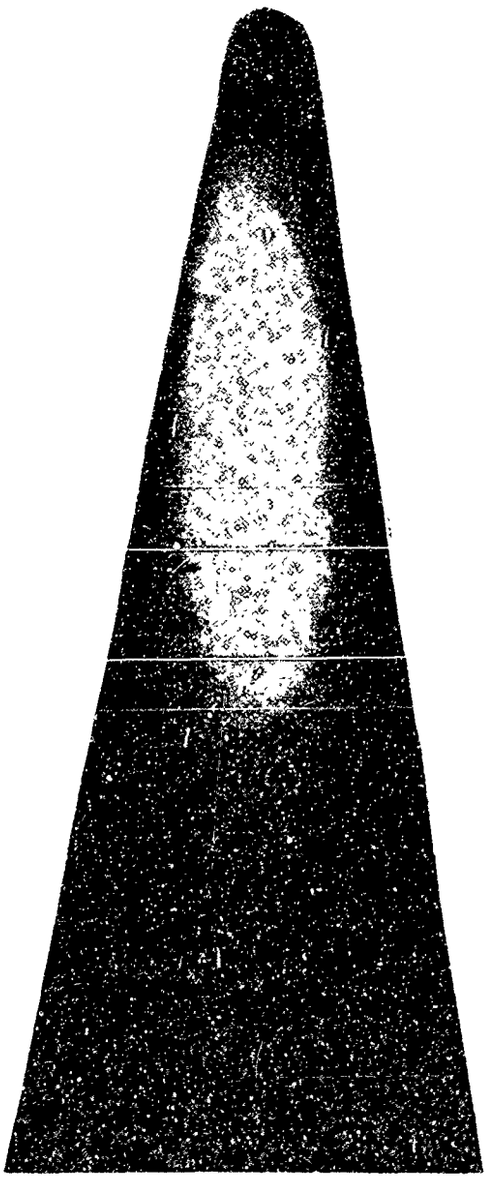
Figure 28



Task 3.3.7-5

Radiograph of 5066

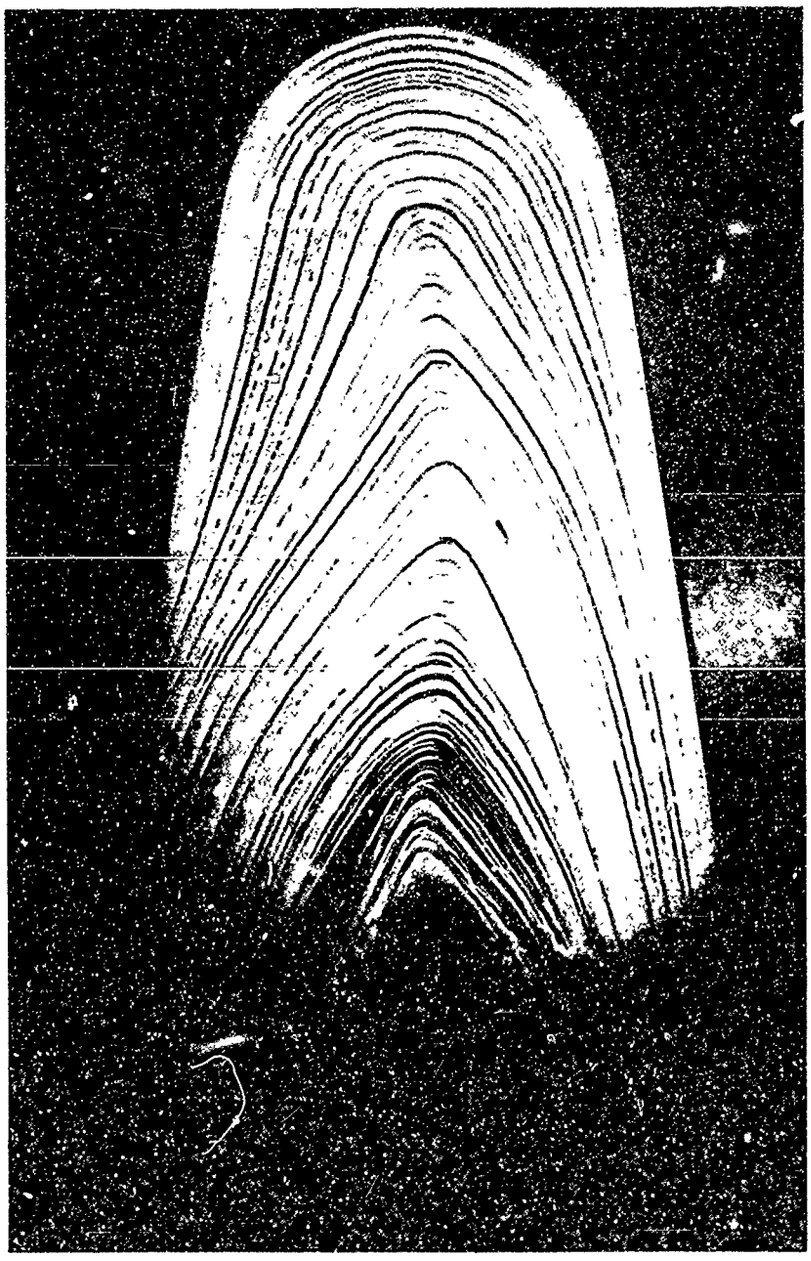
Figure 285



Task 3.3.7-5

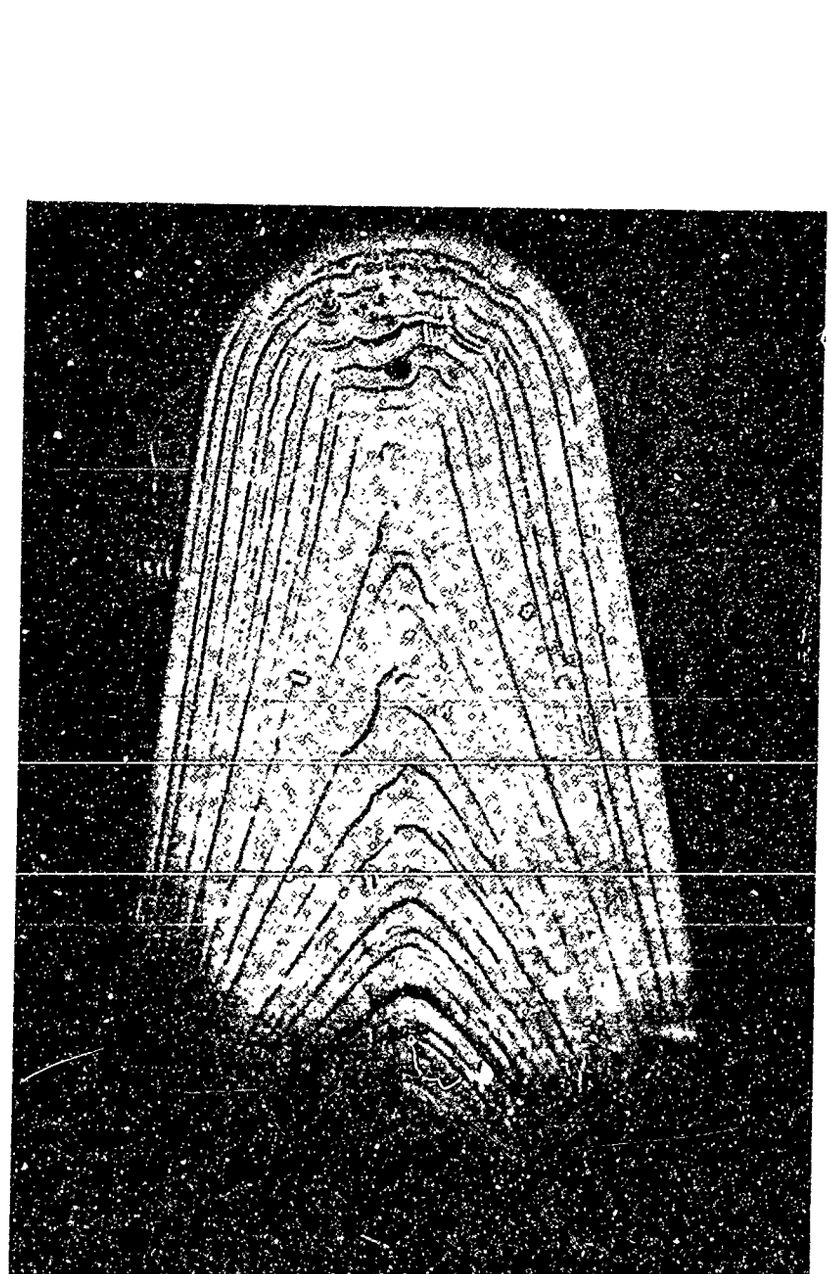
Radiograph of 5071

Figure 286



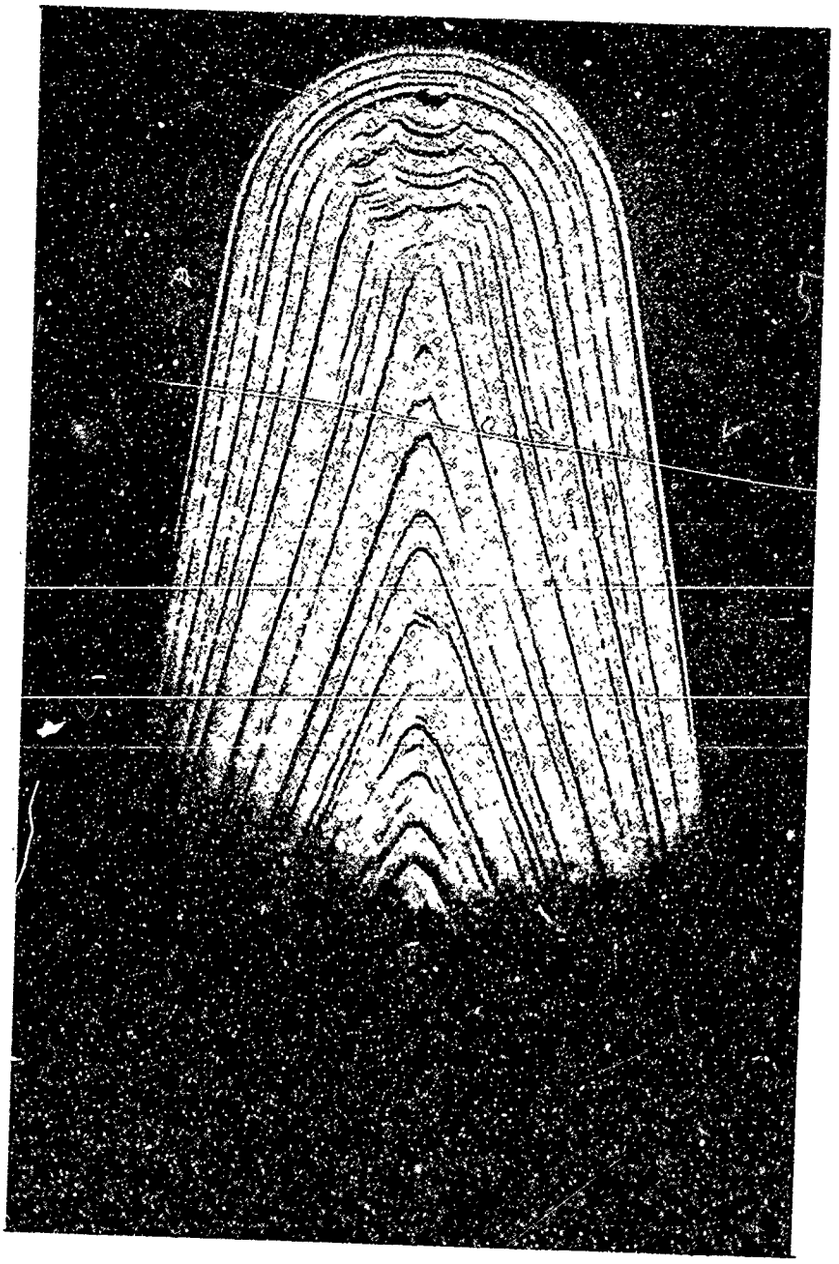
Run 5065 - Nose Region Cross Section - 5X

Figure 287



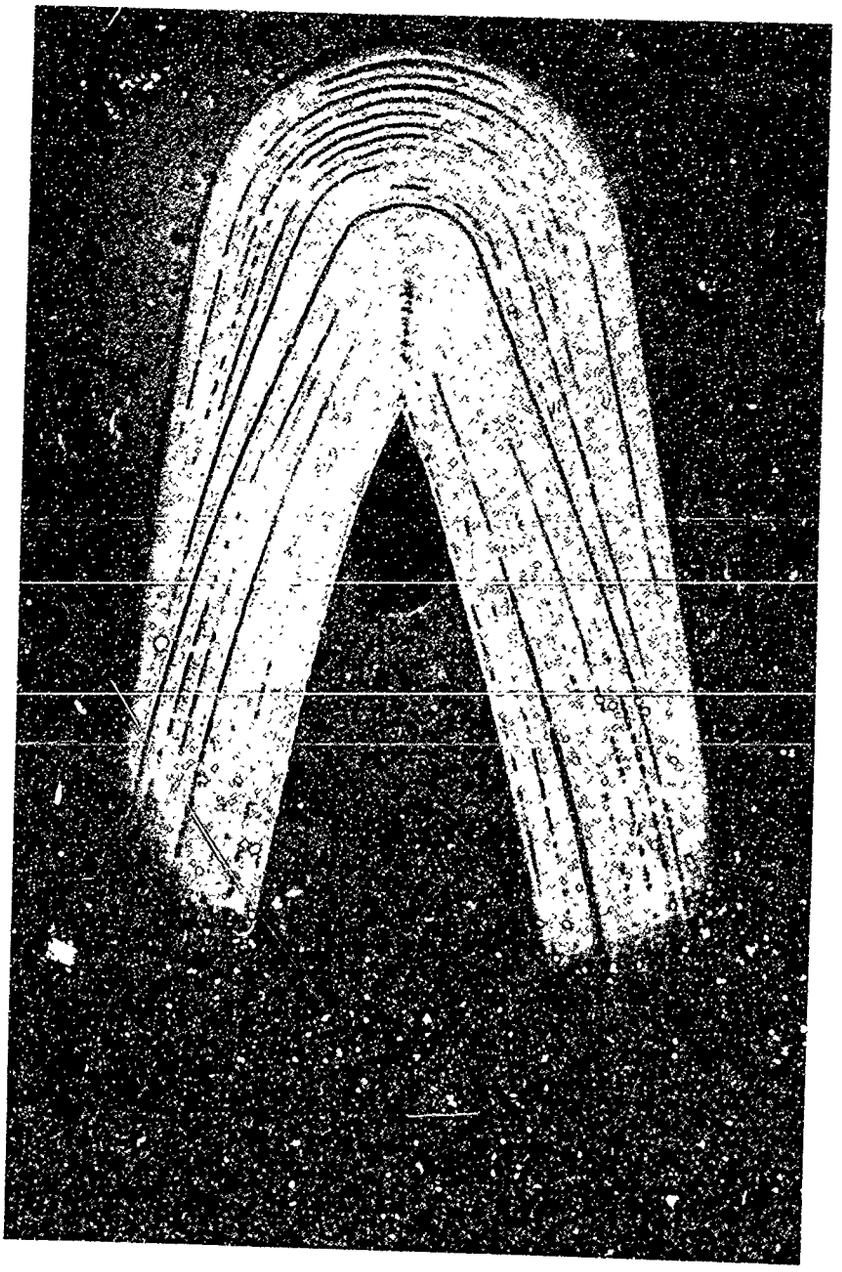
Run 4071 - Nose Region Cross Section - 5X

Figure 288



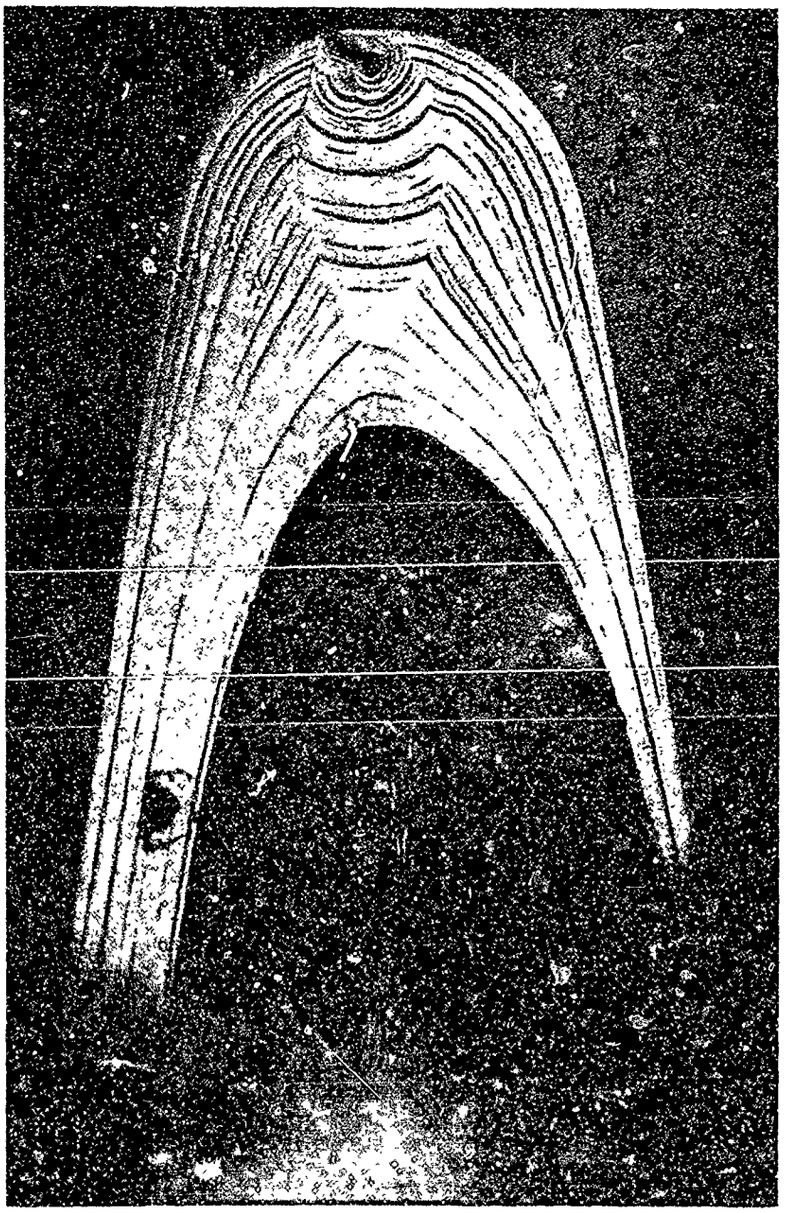
Run 6060 - Nose Region Cross Section - 5X

Figure 289



Run 5066 - Nose Region Cross Section - 5X

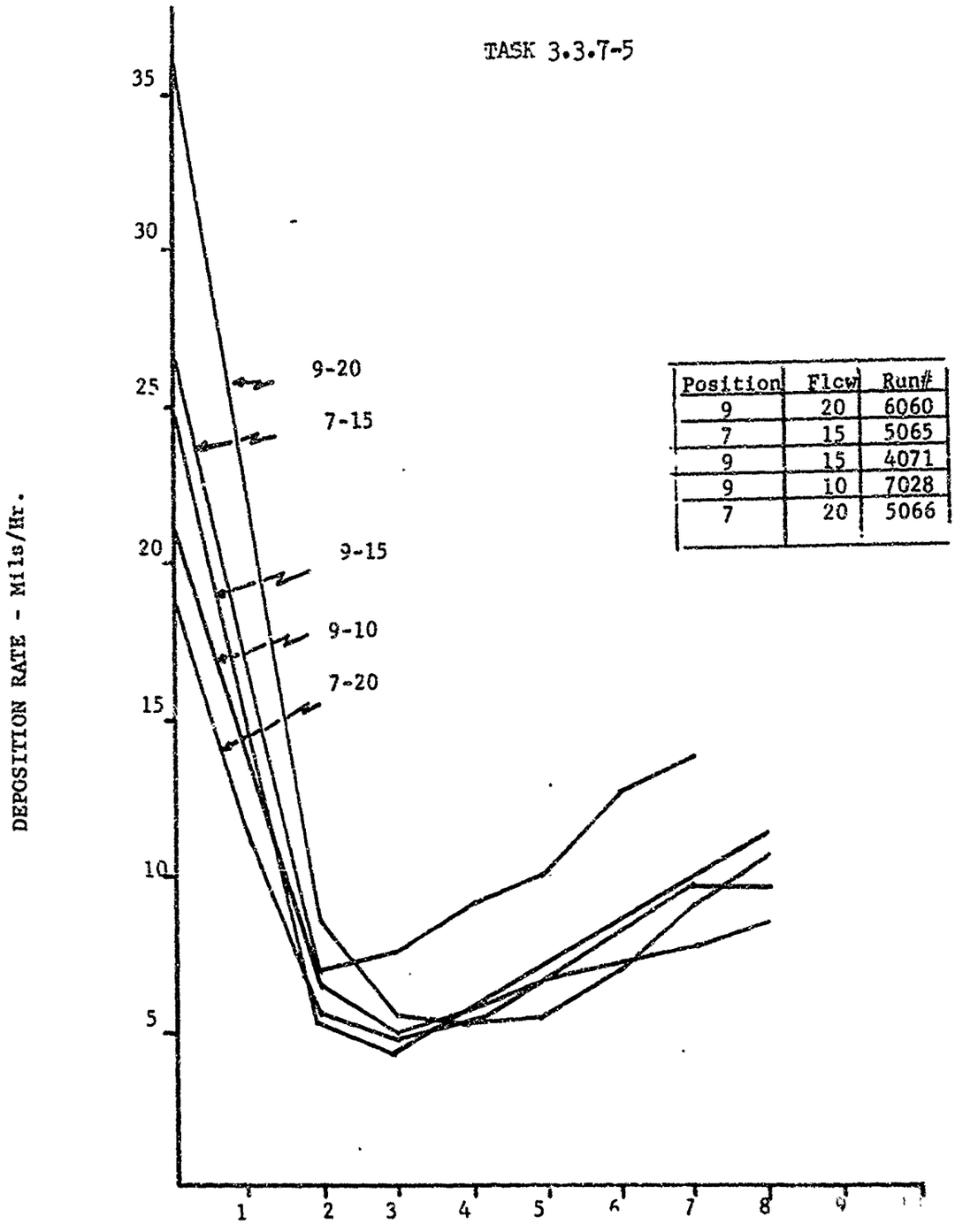
Figure 290



Run 5071 - Nose Region Cross Section - 5X

Figure 291

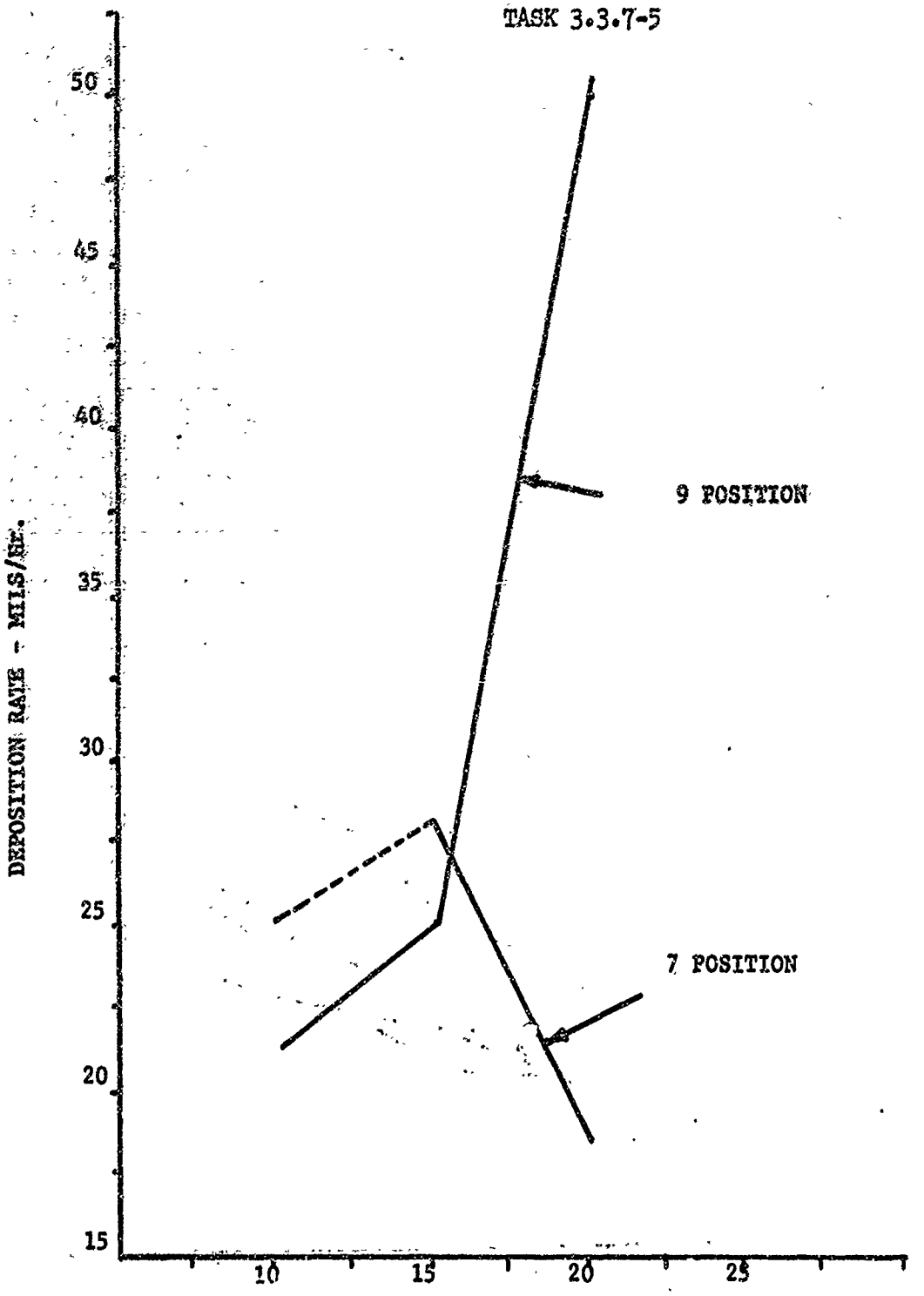
TASK 3.3.7-5



Position	Flow	Run#
9	20	6060
7	15	5065
9	15	4071
9	10	7028
7	20	5066

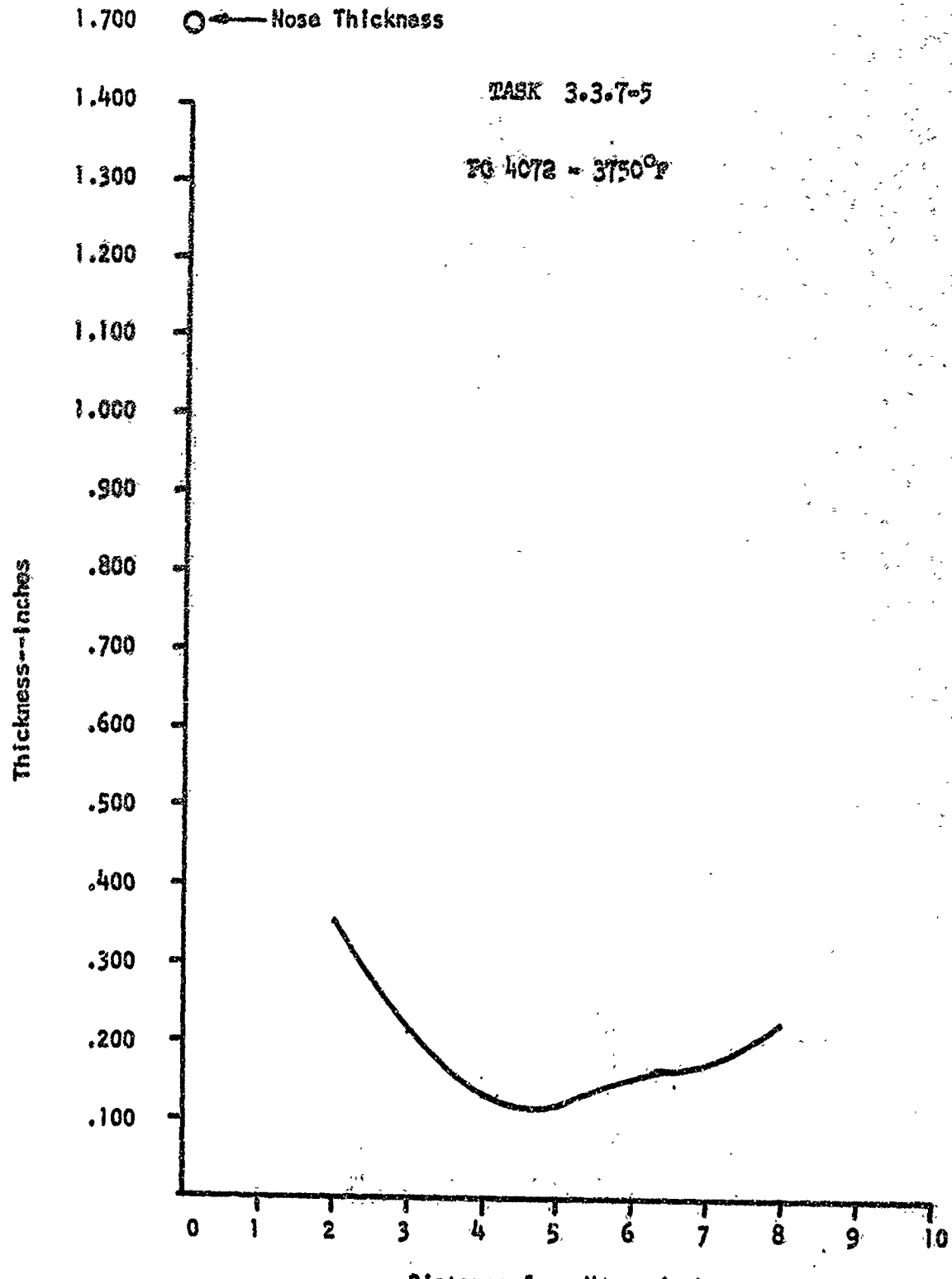
Profile Summary

Figure 292



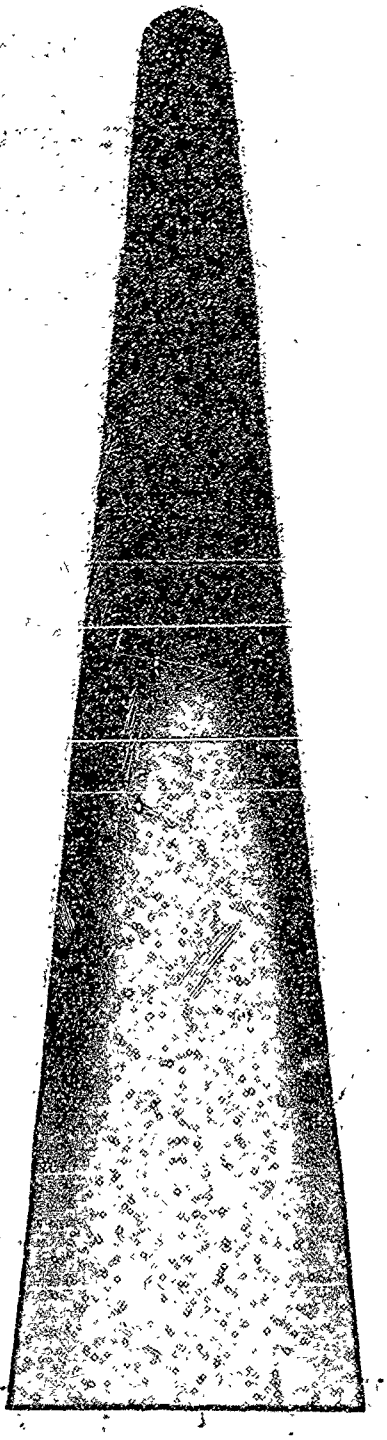
Nose Deposition Rate

Figure 293



Deposition Thickness Profile.

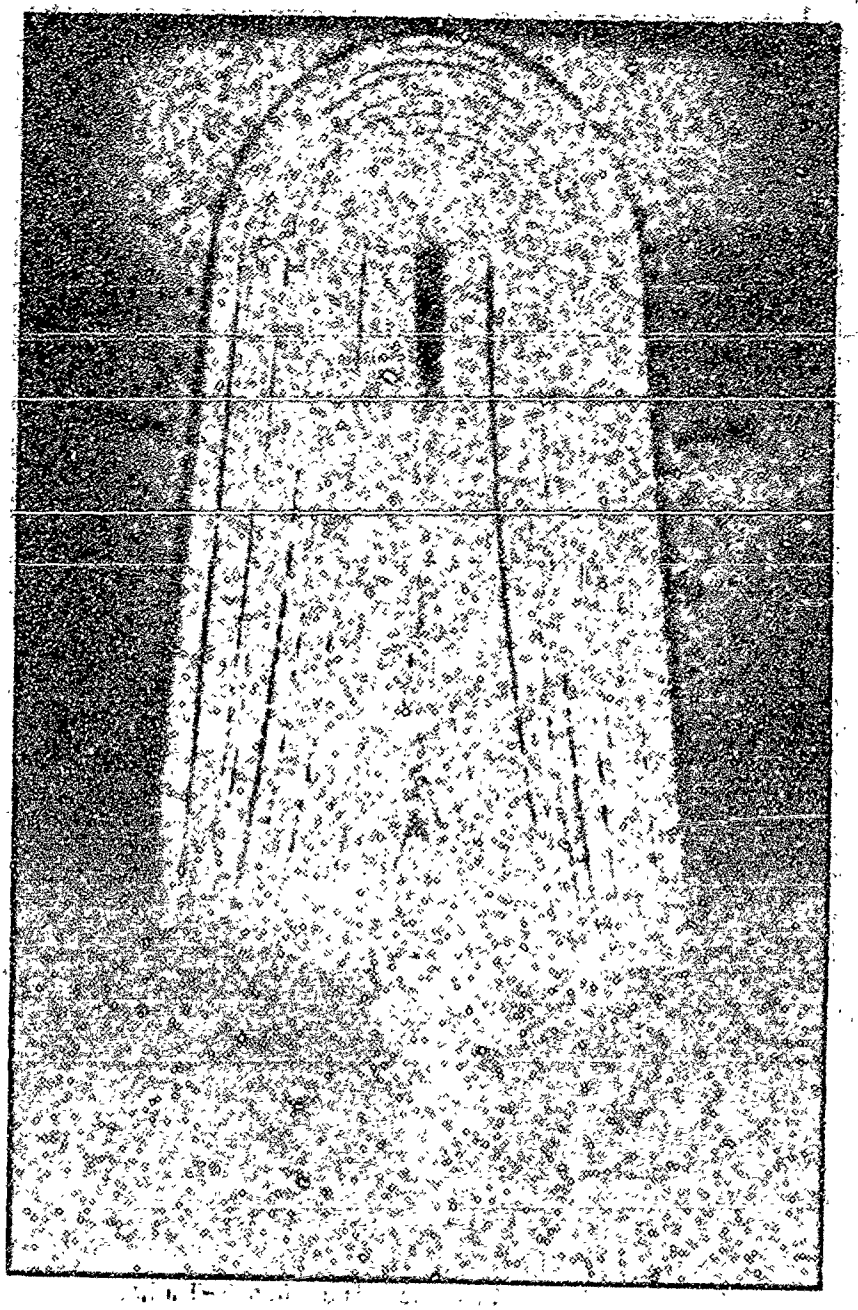
Figure 294



Task 3.3.7-5

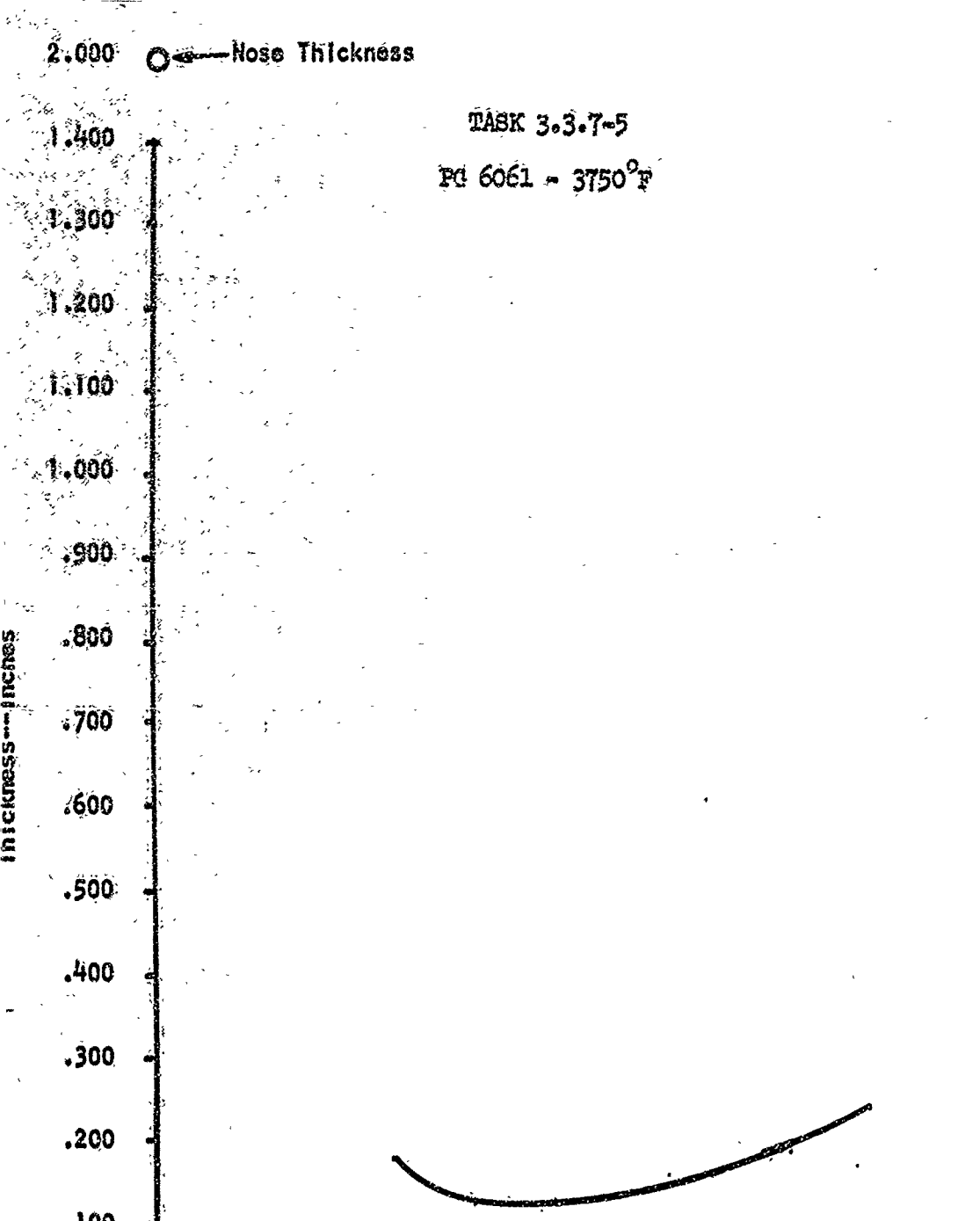
Radiograph of 4072

Figure 295



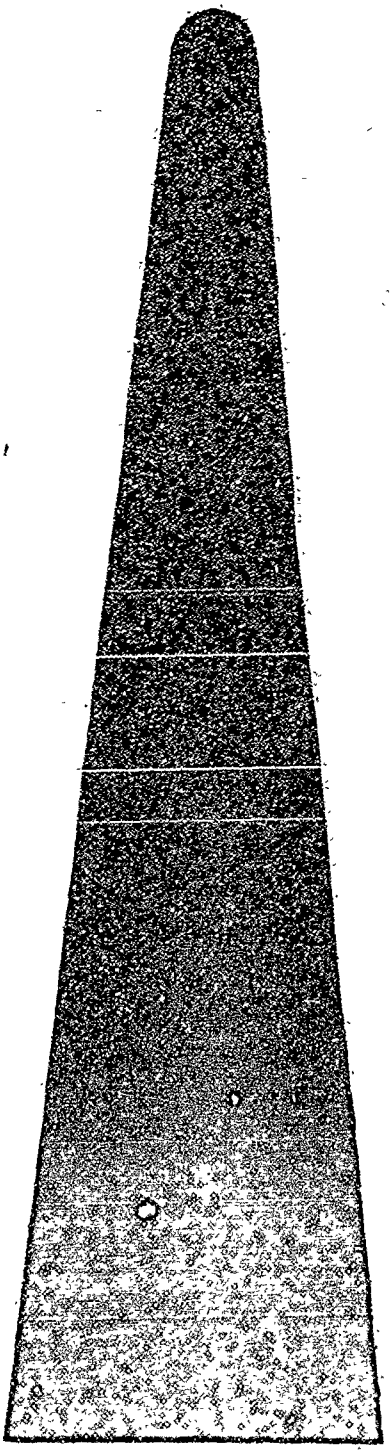
Run 4072 - Nose Region Cross Section - 5X

Figure 296



Deposition Thickness Profile

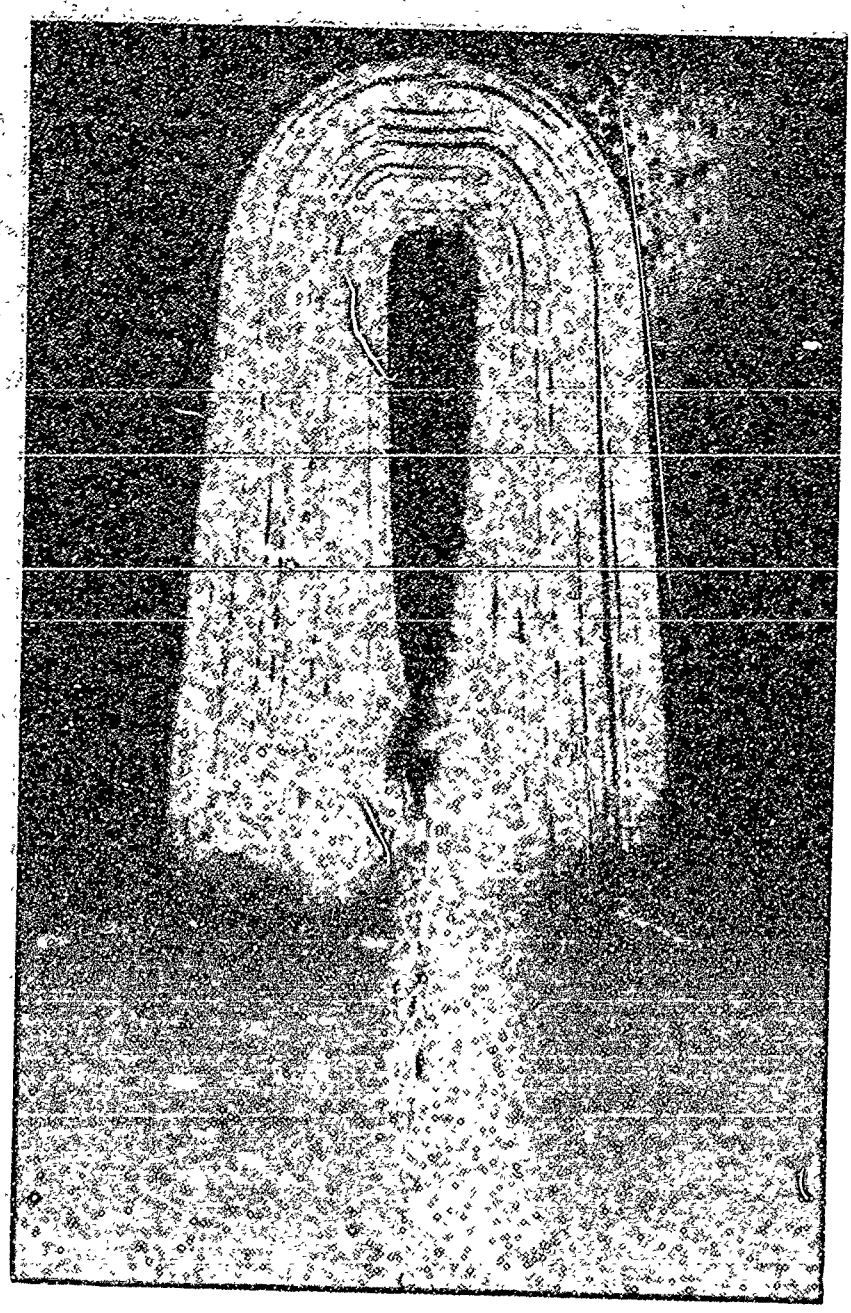
Figure 297



Task 3.3.7-5

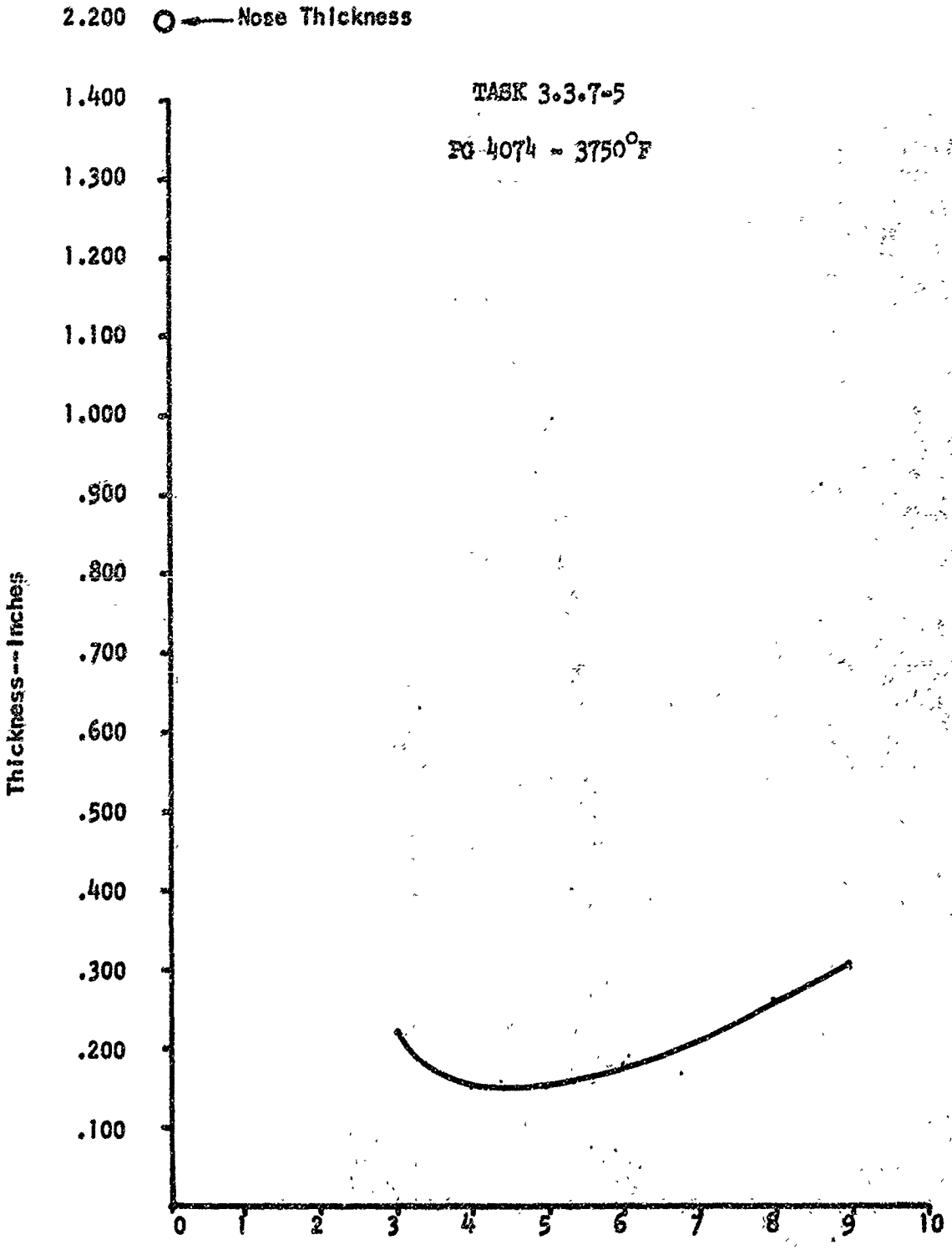
Radiograph of 6061

Figure 298



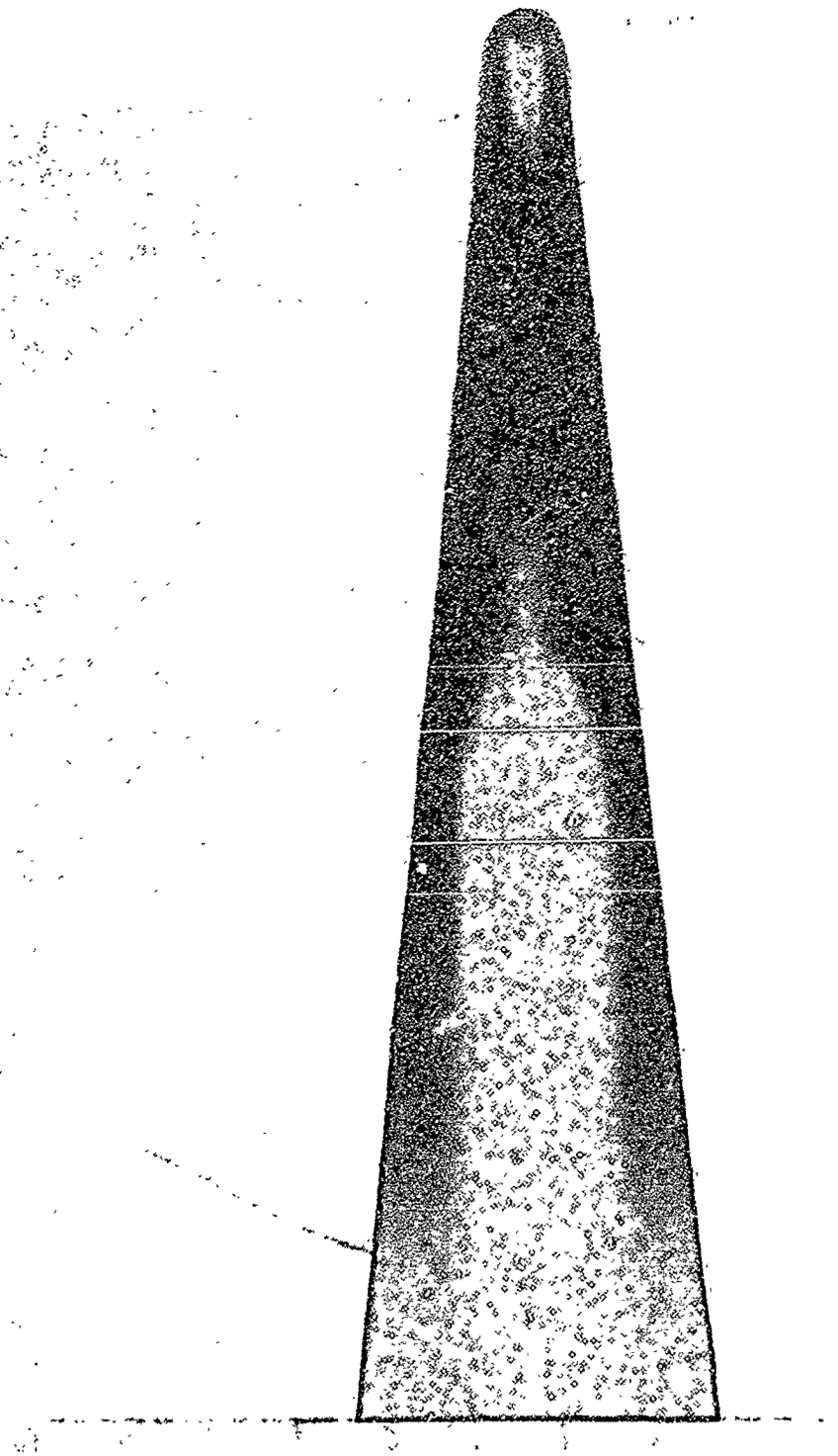
Run 6061 - Nose Region Cross Section - 5X

Figure 299



Deposition Thickness Profile

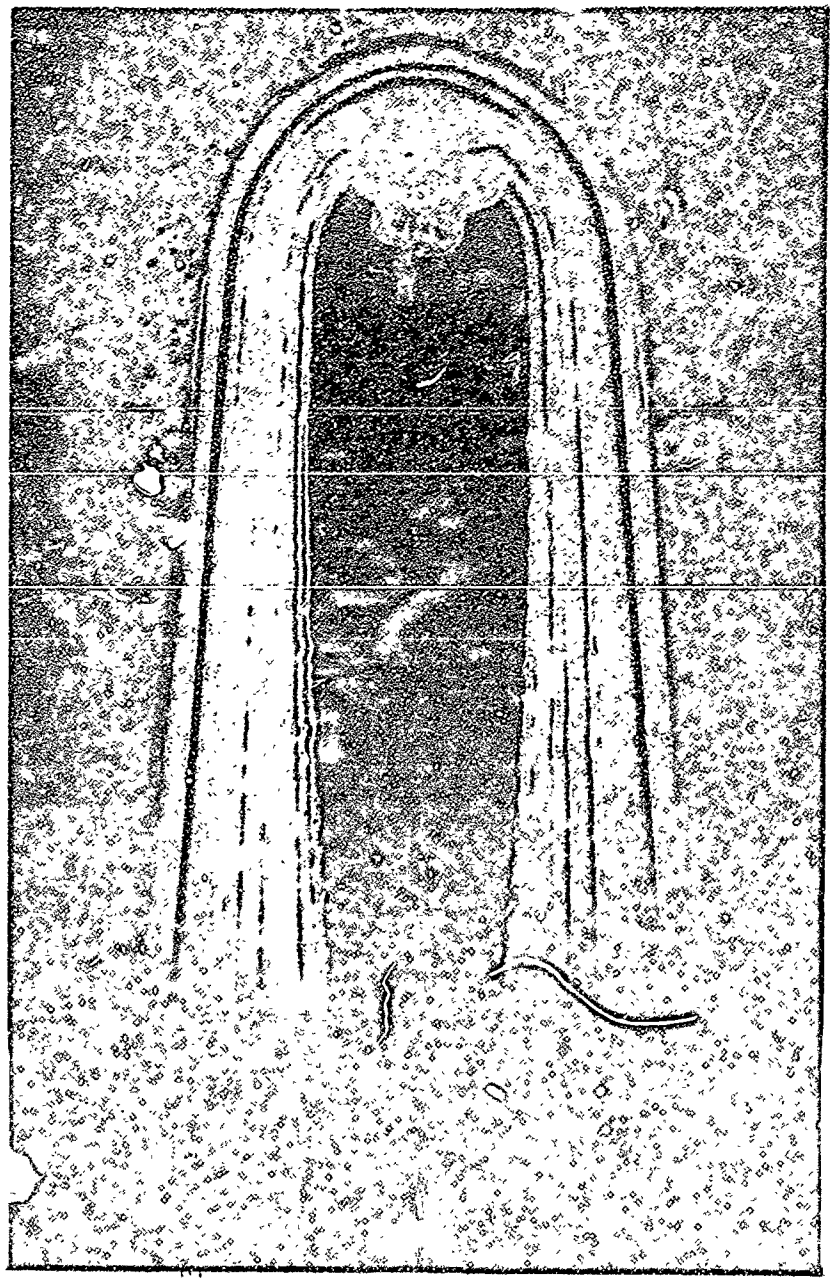
Figure 300



Task 3.3.7-5

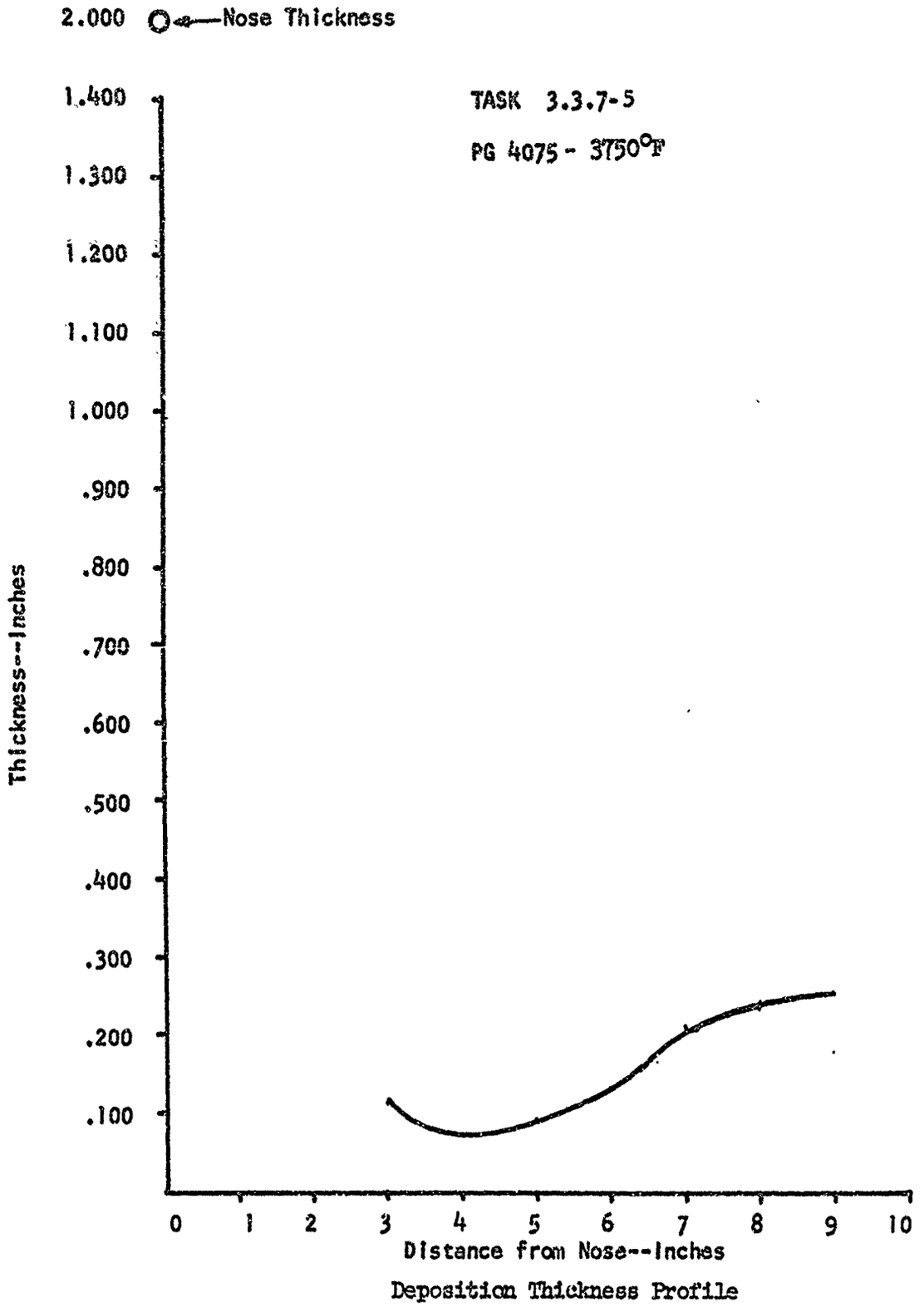
Radiograph of 4074

Figure 301



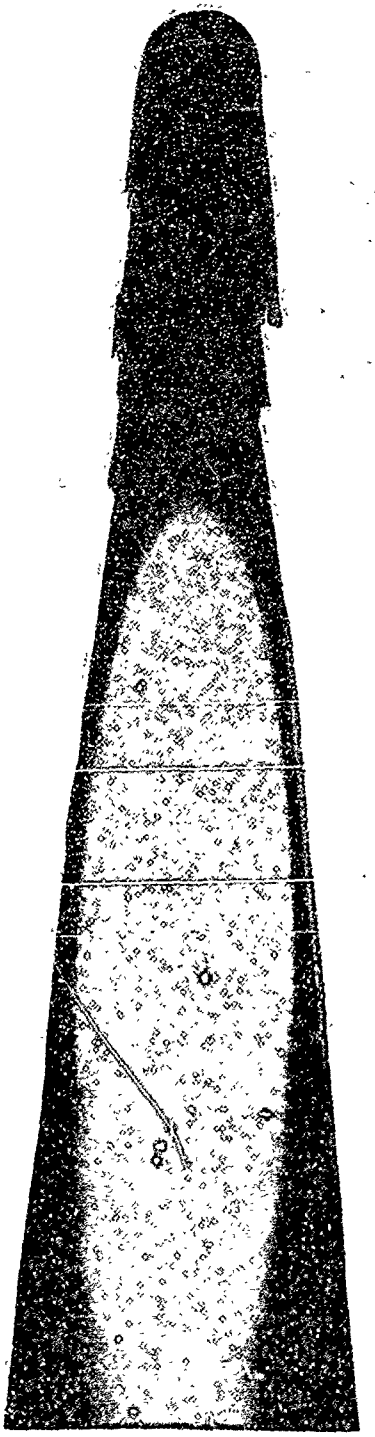
Run 4074 - Nose Region Cross Section - 5X

Figure 302



Deposition Thickness Profile

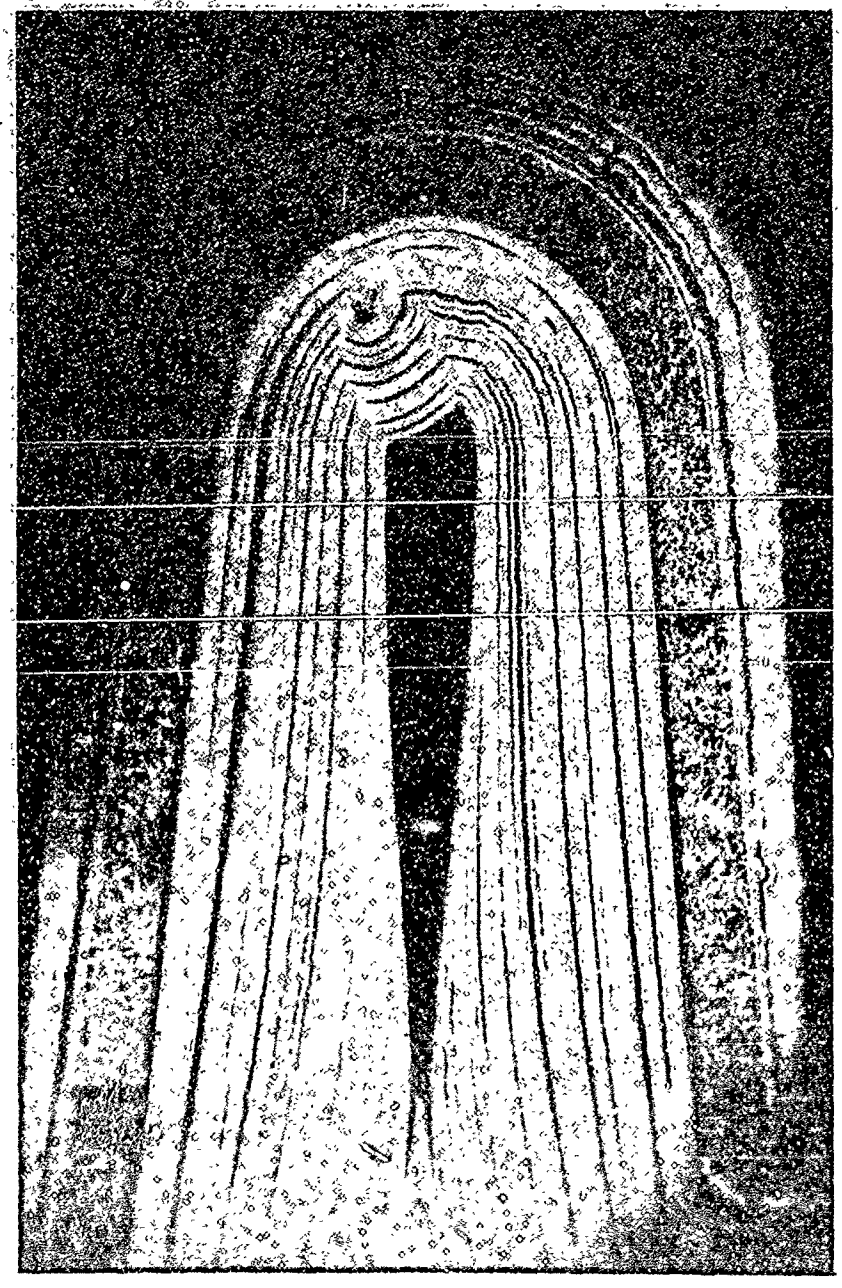
Figure 303



Task 3.3.7-5

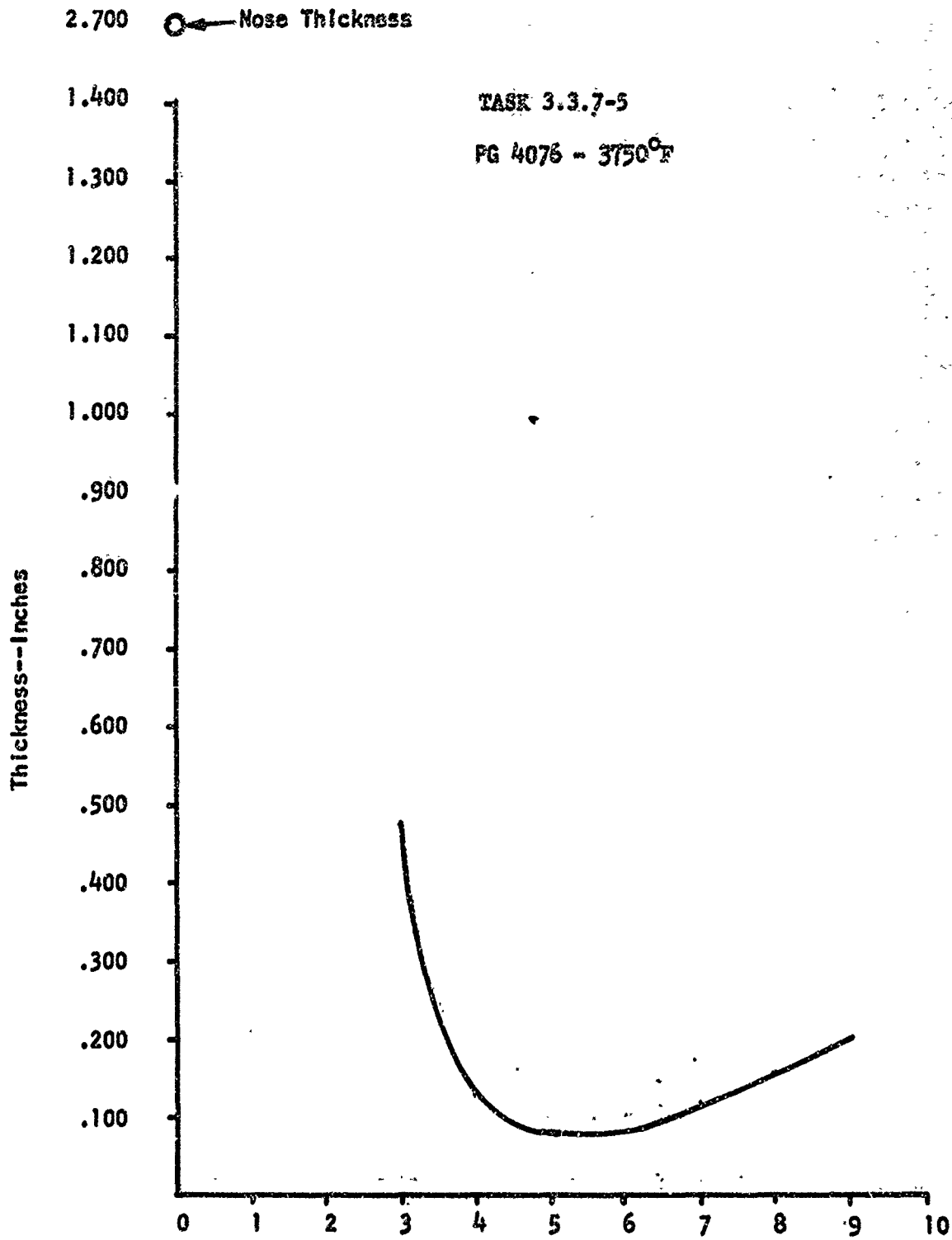
Radiograph of 4075

Figure 304



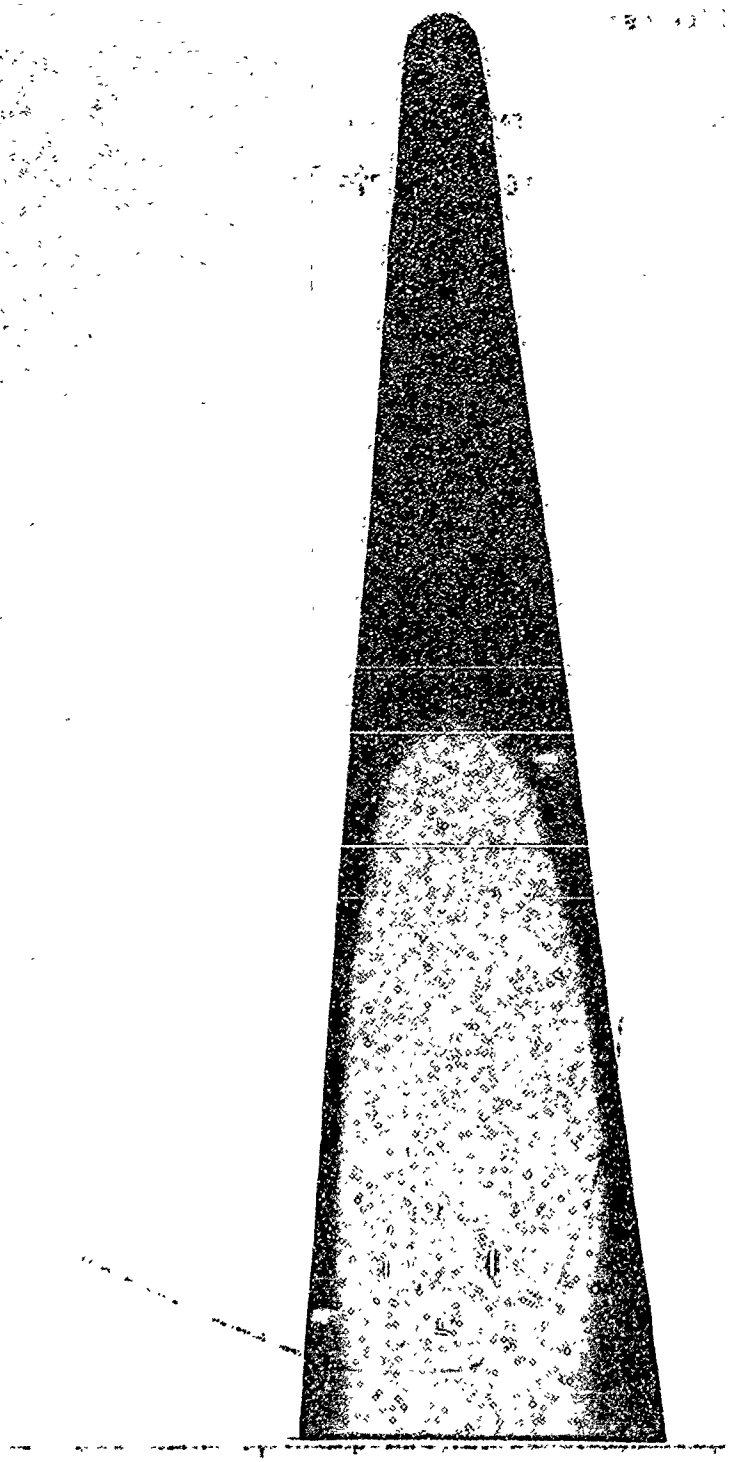
Run 4075 - Nose Region Cross Section - 5X

Figure 305



Deposition Thickness Profile

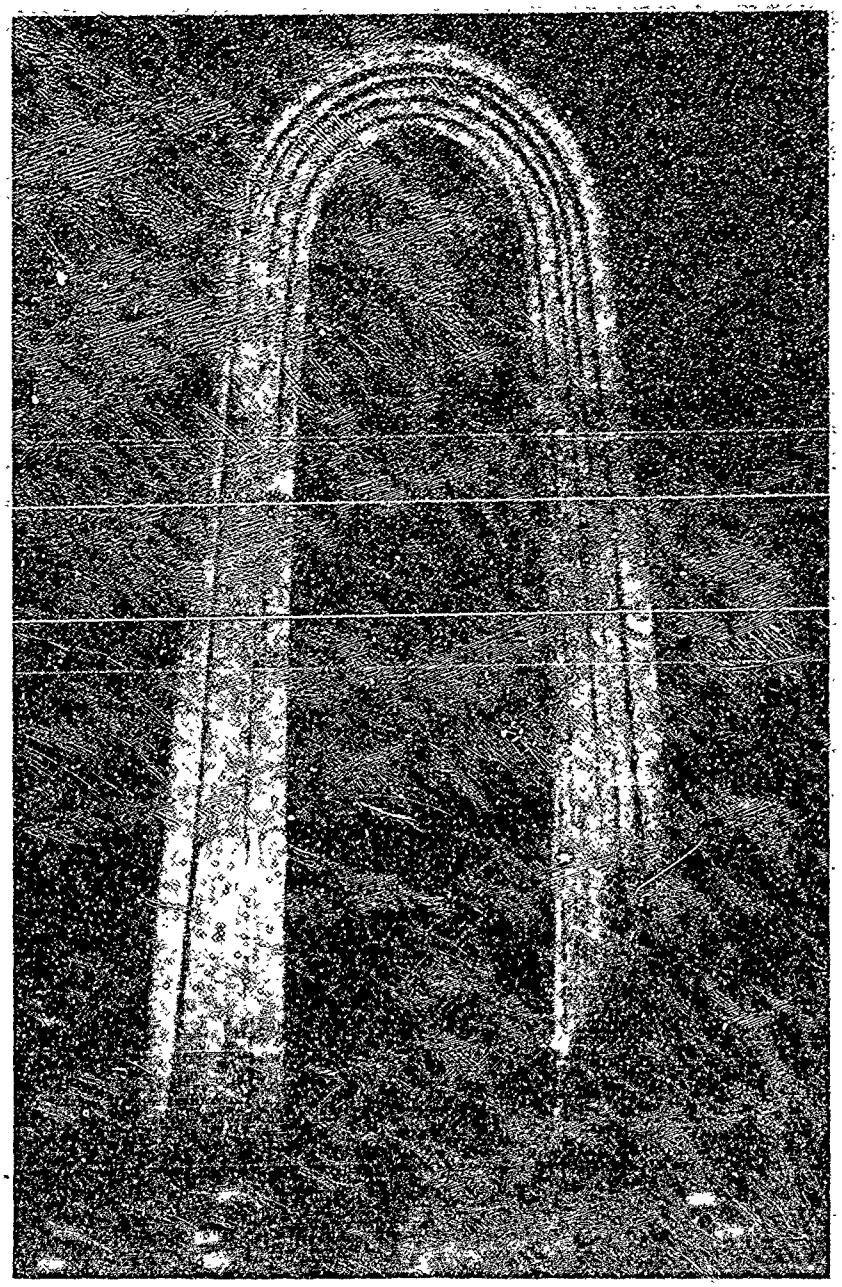
Figure 306



Task 3.3.7-5

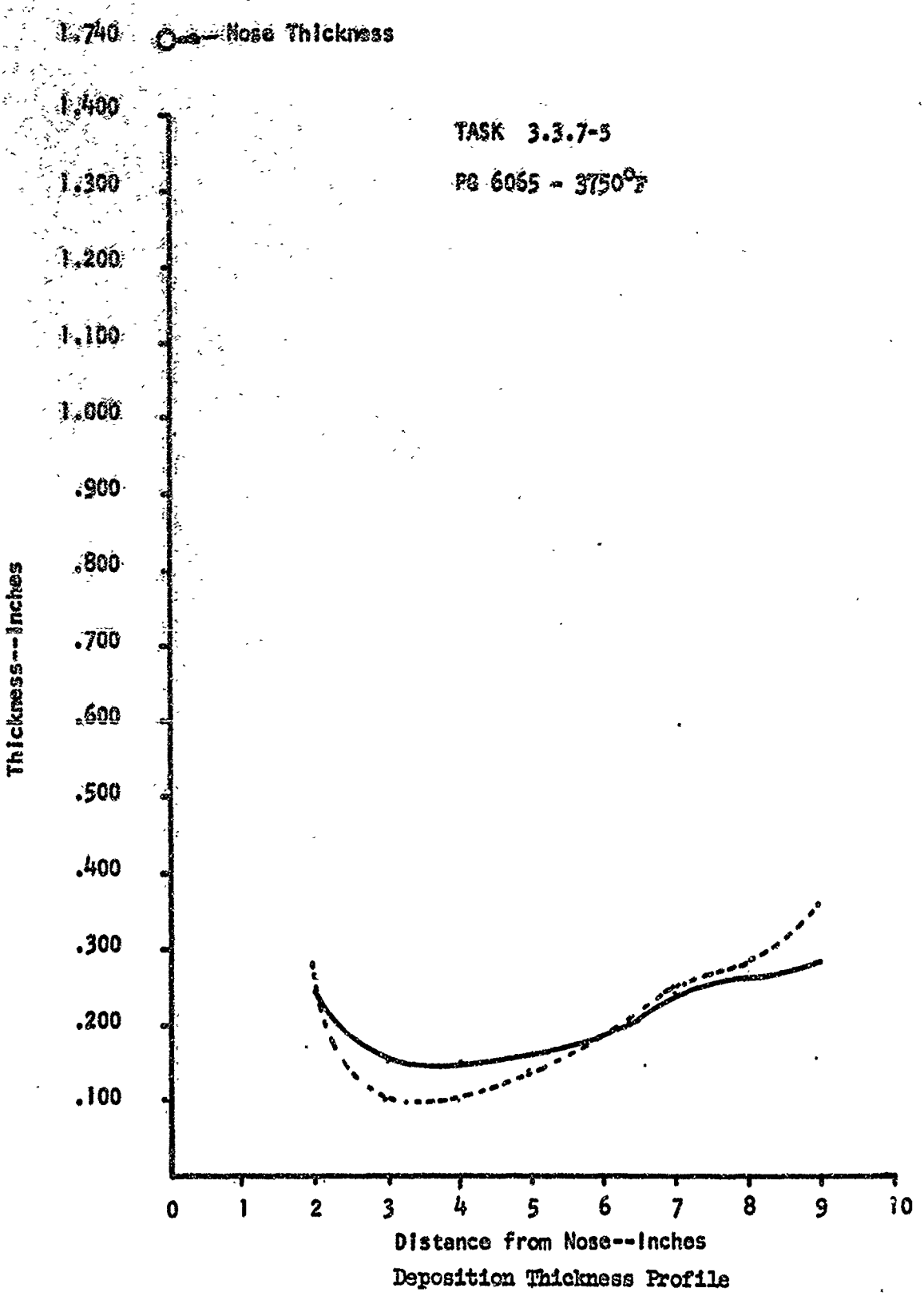
Radiograph of 4076

Figure 307



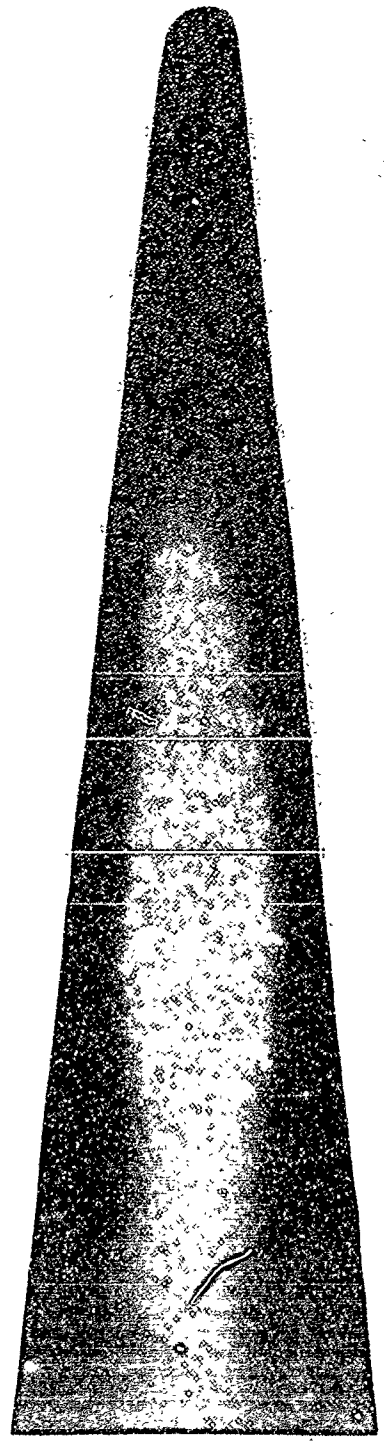
Run 4076 - Nose Region Cross Section - 5X

Figure 308



Deposition Thickness Profile

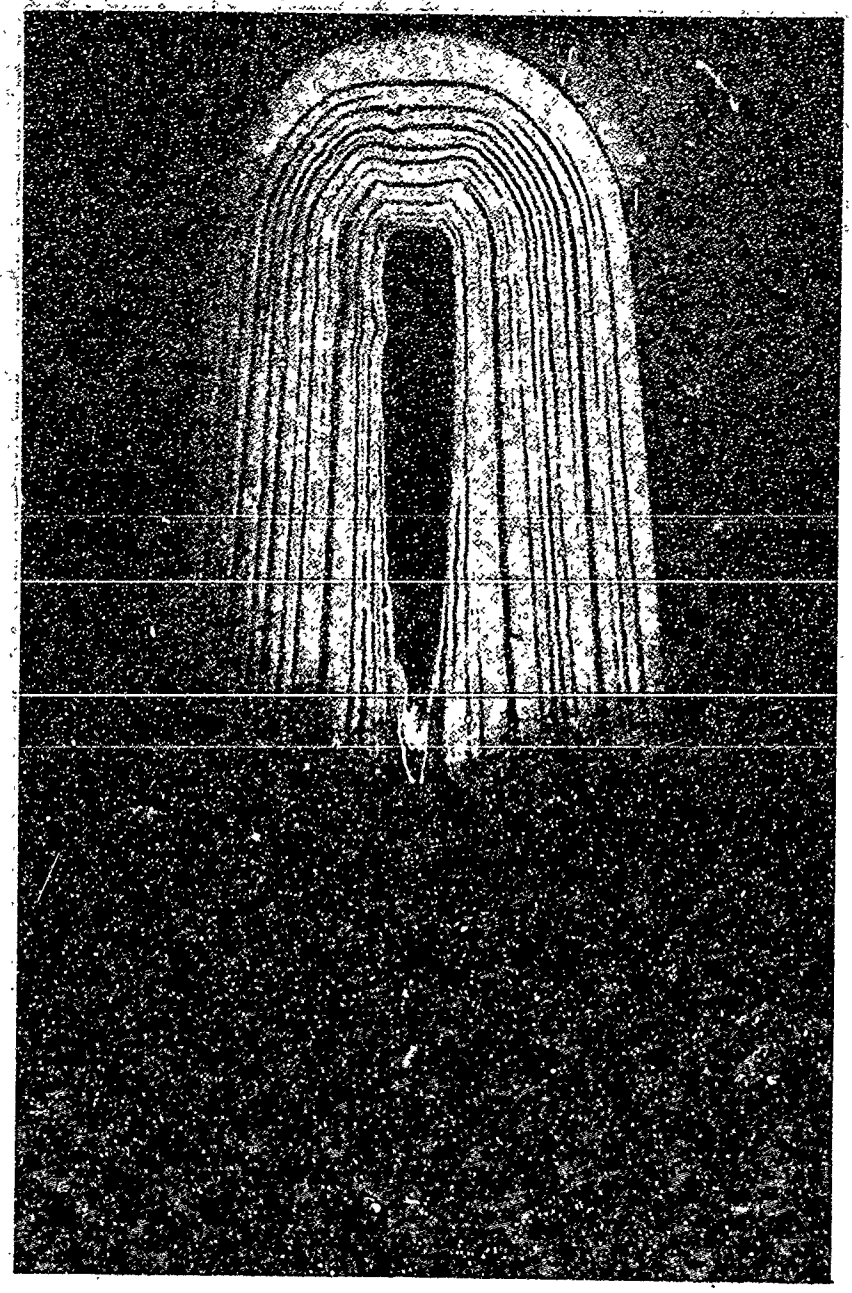
Figure 309



Task 3.3.7-5

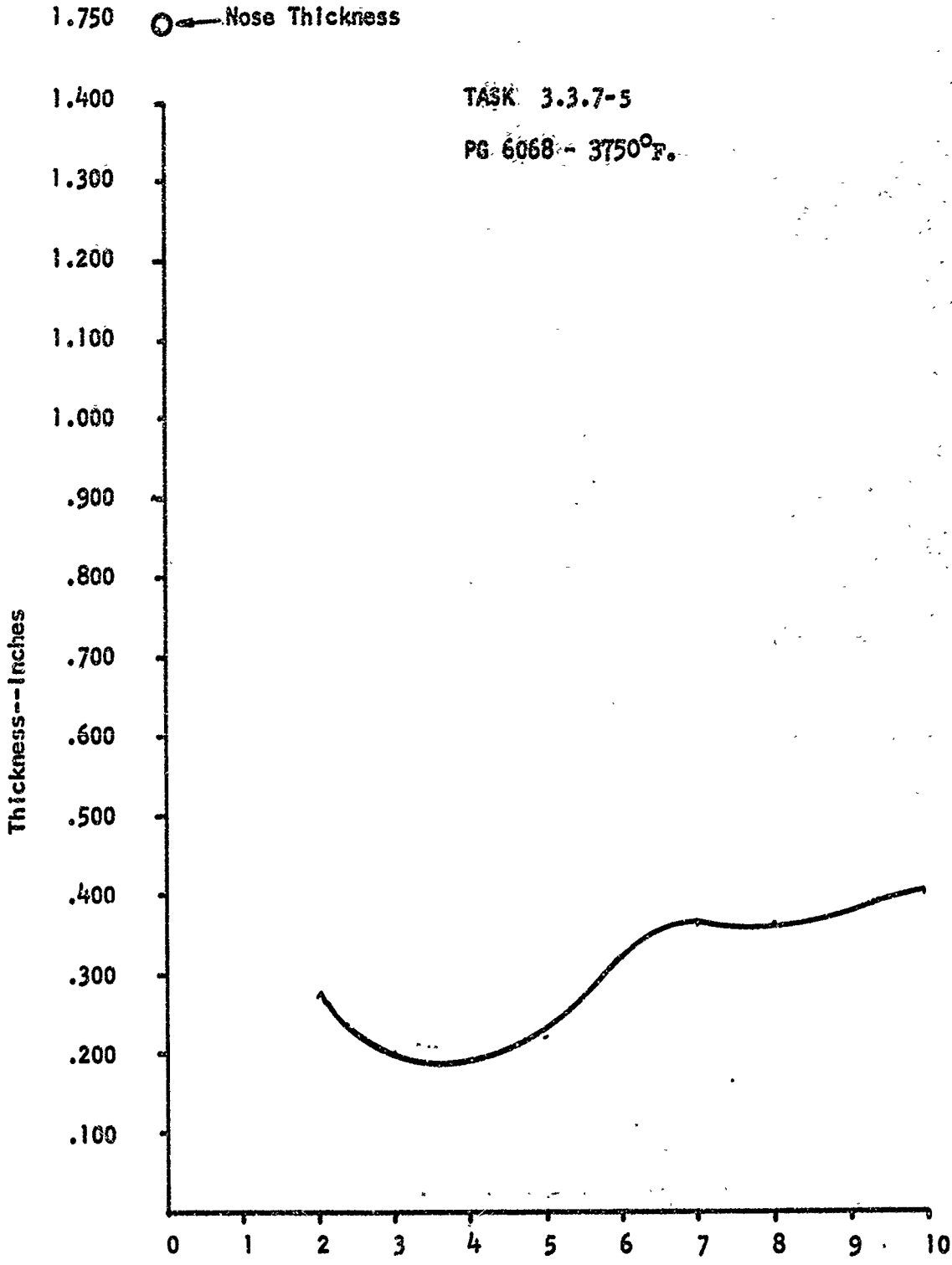
Radiograph of 6065

Figure 310



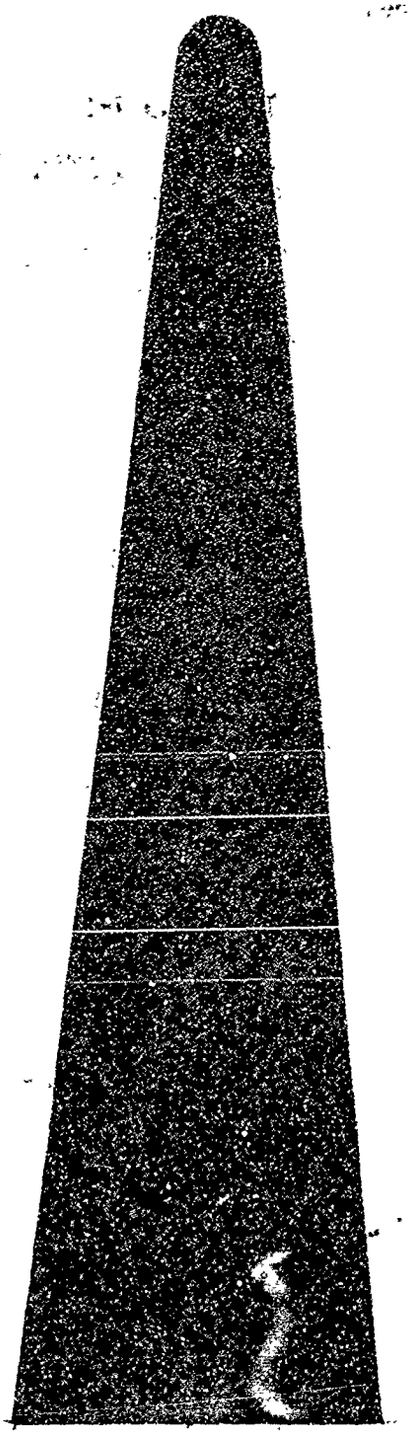
Run 6065 - Nose Region Cross Section - 5X

Figure 311



Deposition Thickness Profile

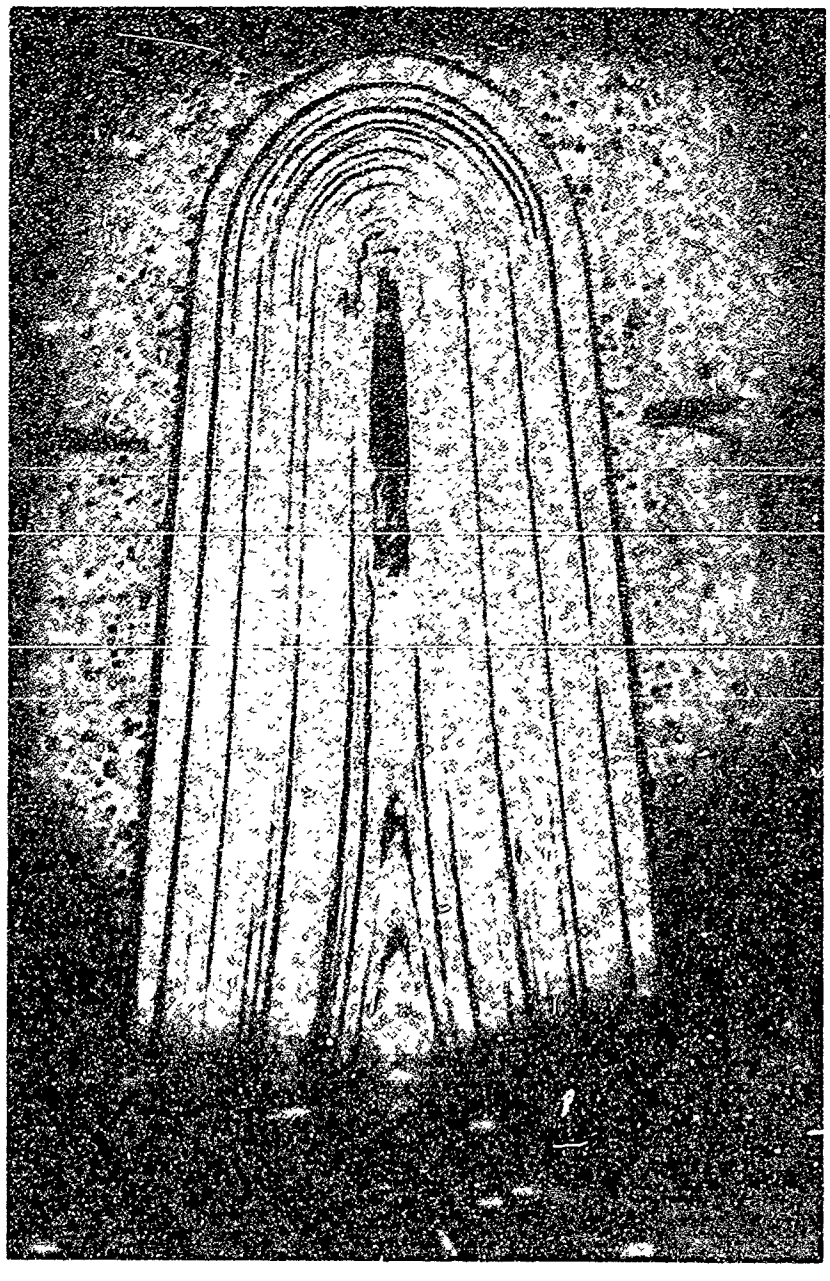
Figure 312



Task 3.3.7- 5

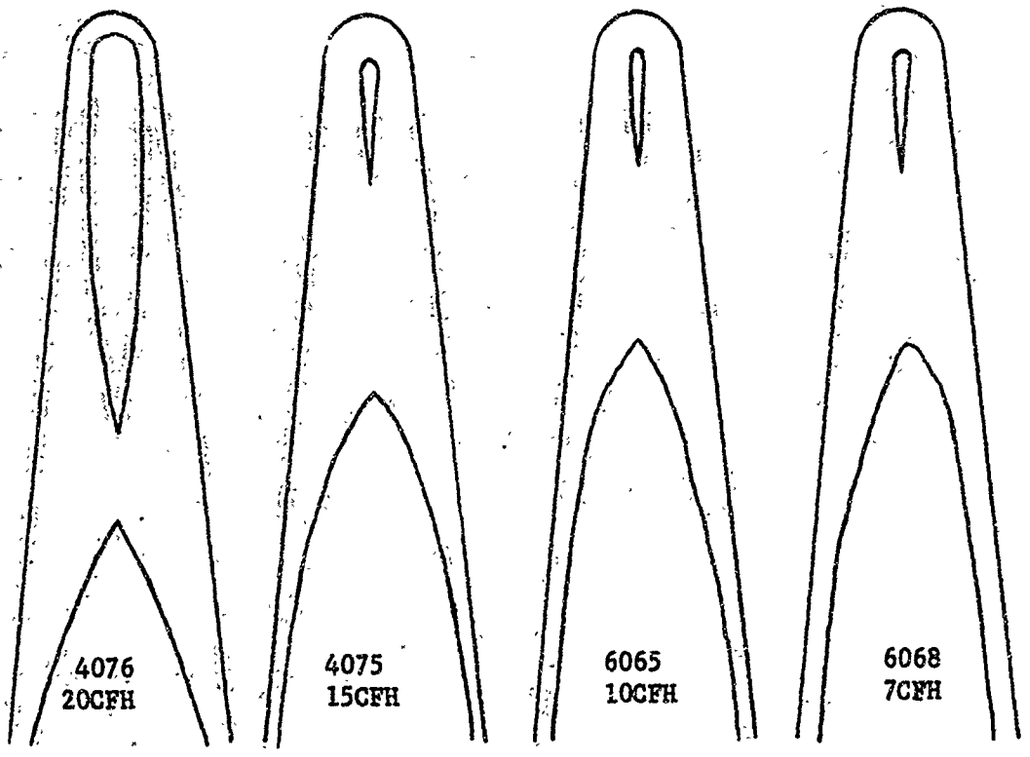
Radiograph of 6068

Figure 313

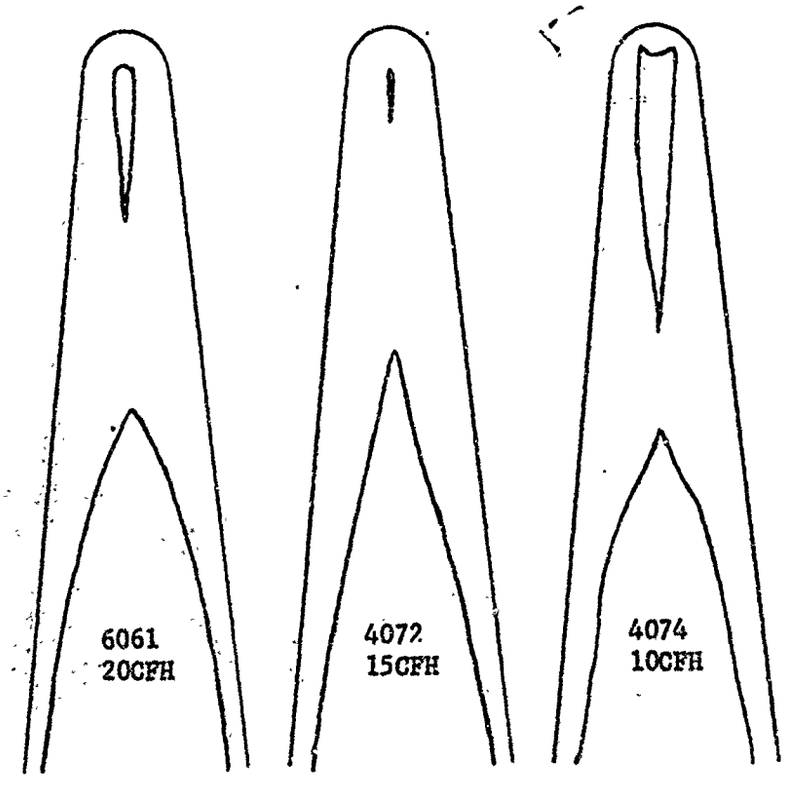


Run 6068 - Nose Region Cross Section - 5X

Figure 314



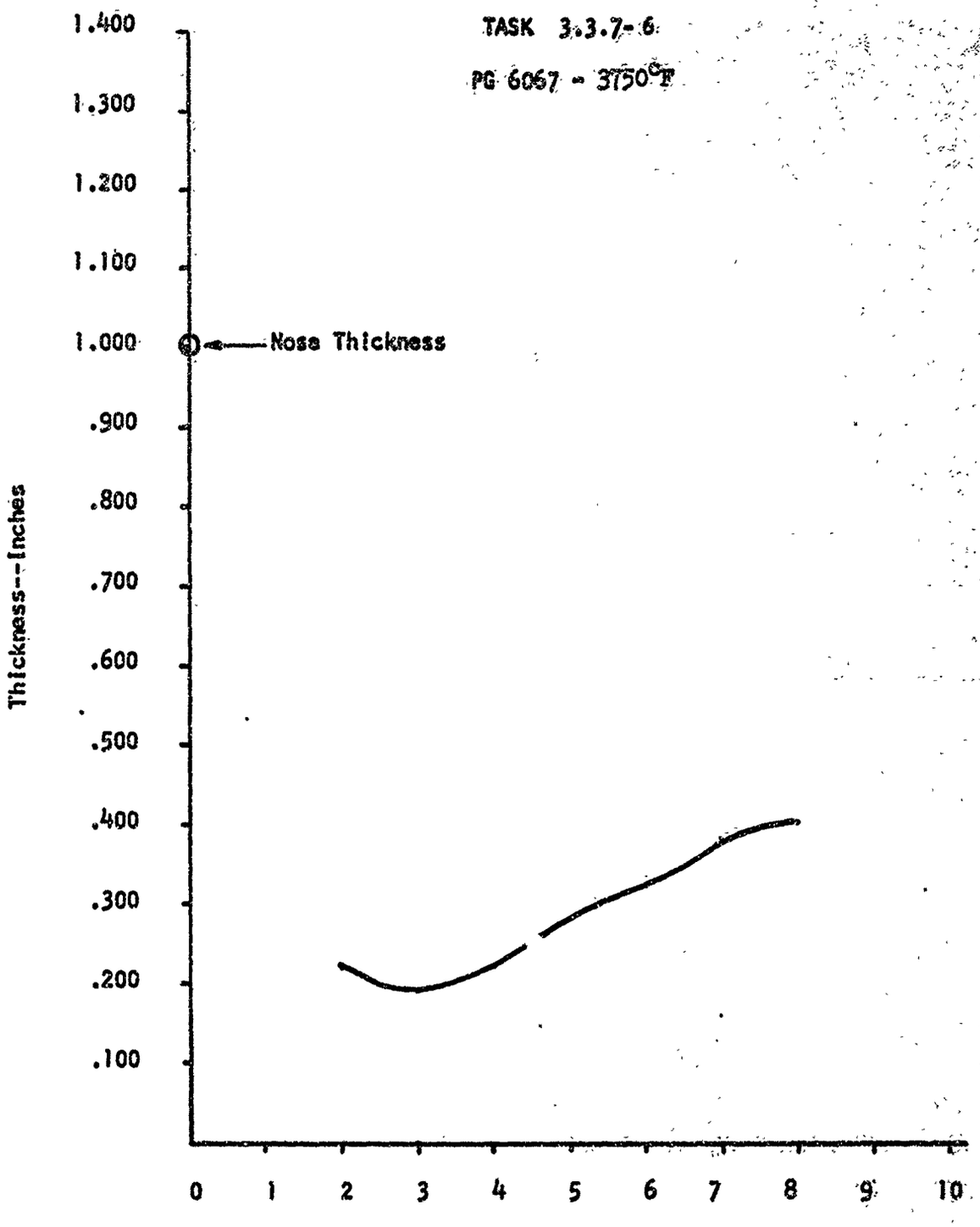
7" - Nozzle Distance from Nose



9" - Nozzle Distance from Nose

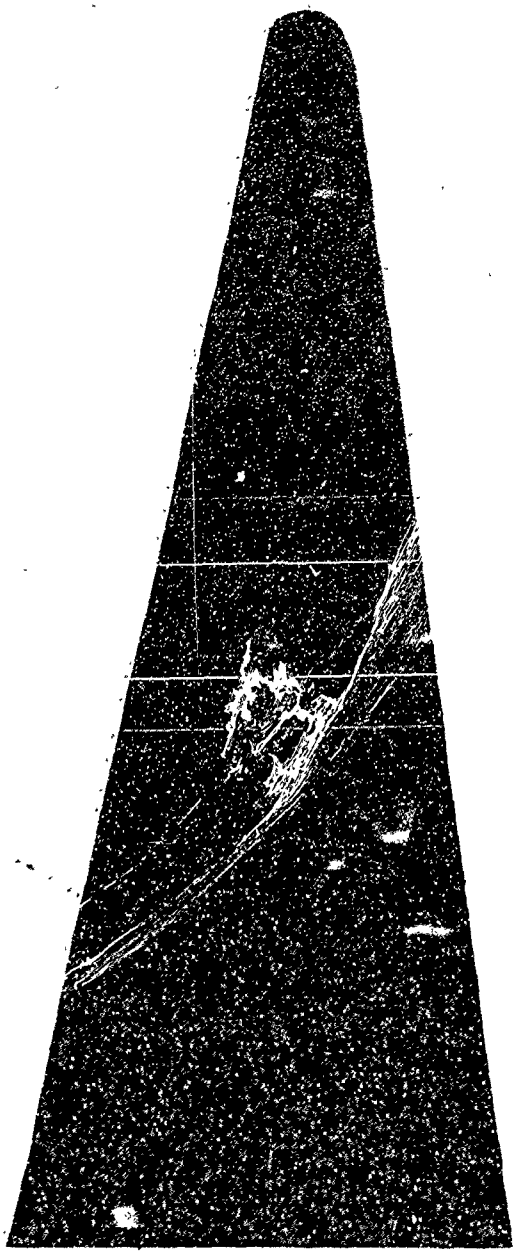
Nose Region Thickness Patterns

Figure 315



Deposition Thickness Profile

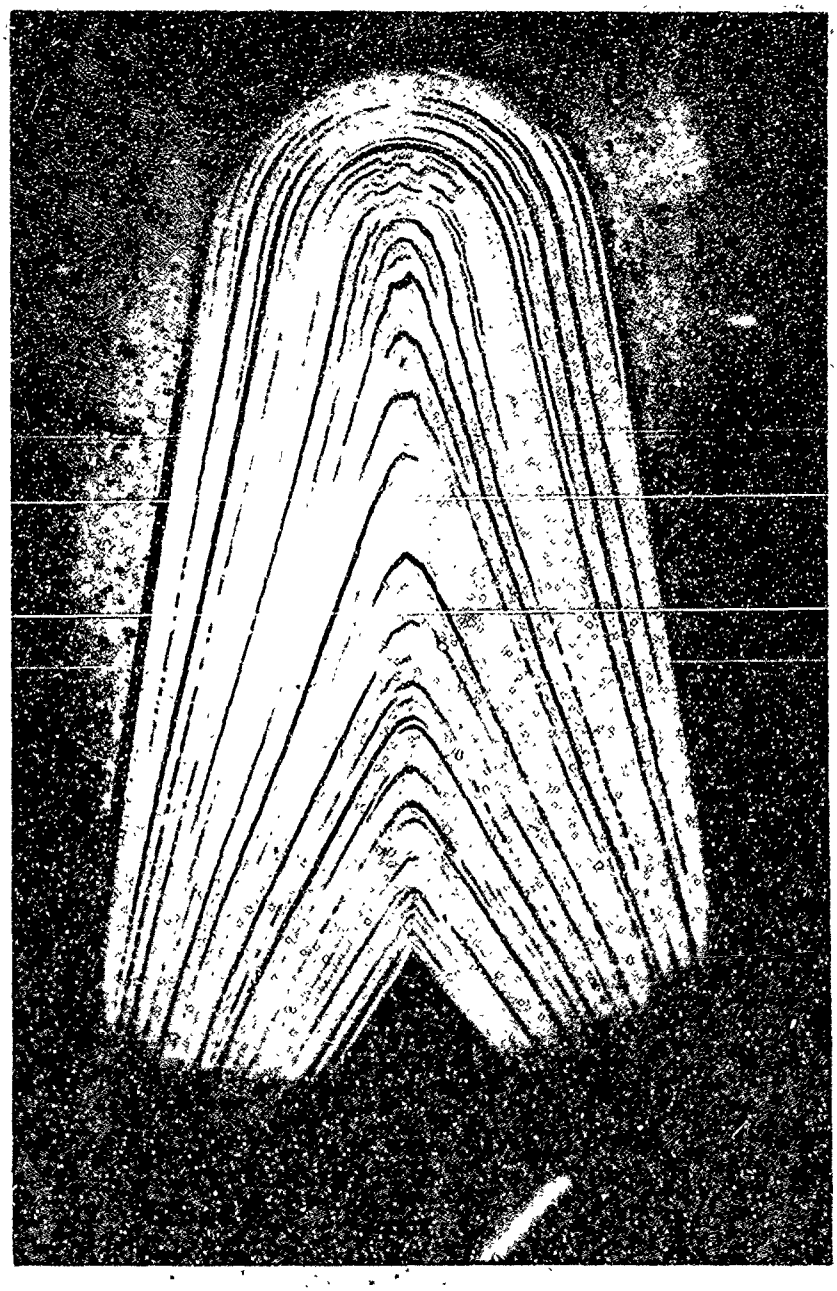
Figure 316



Task 3.3.7-6

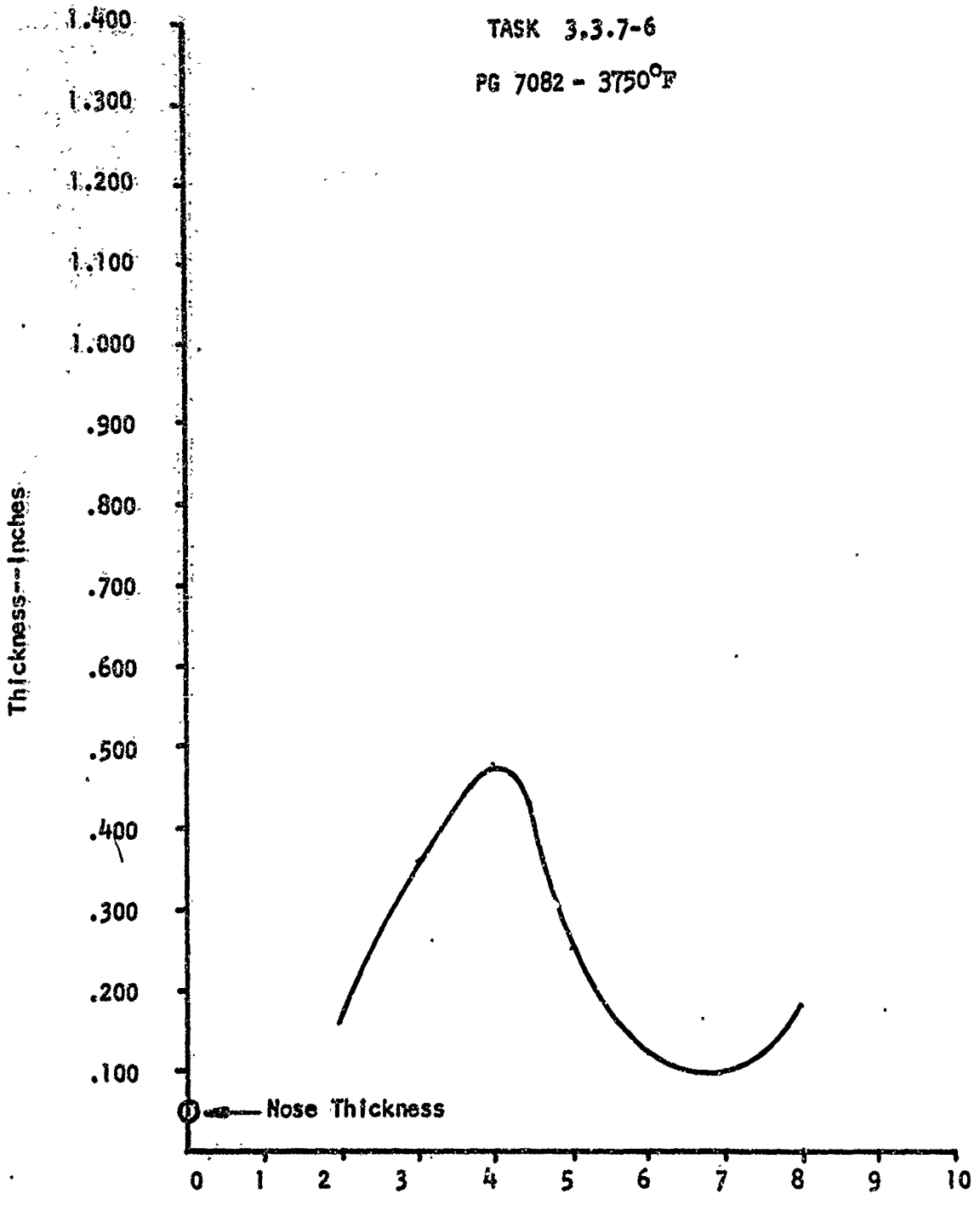
Radiograph of 6067

Figure 317



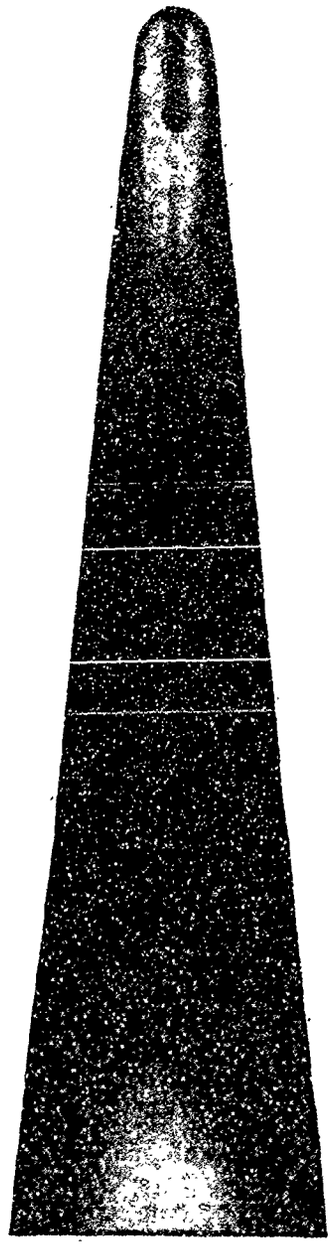
Run 6067 - Nose Region Cross Section - 5X

Figure 318



Deposition Thickness Profile

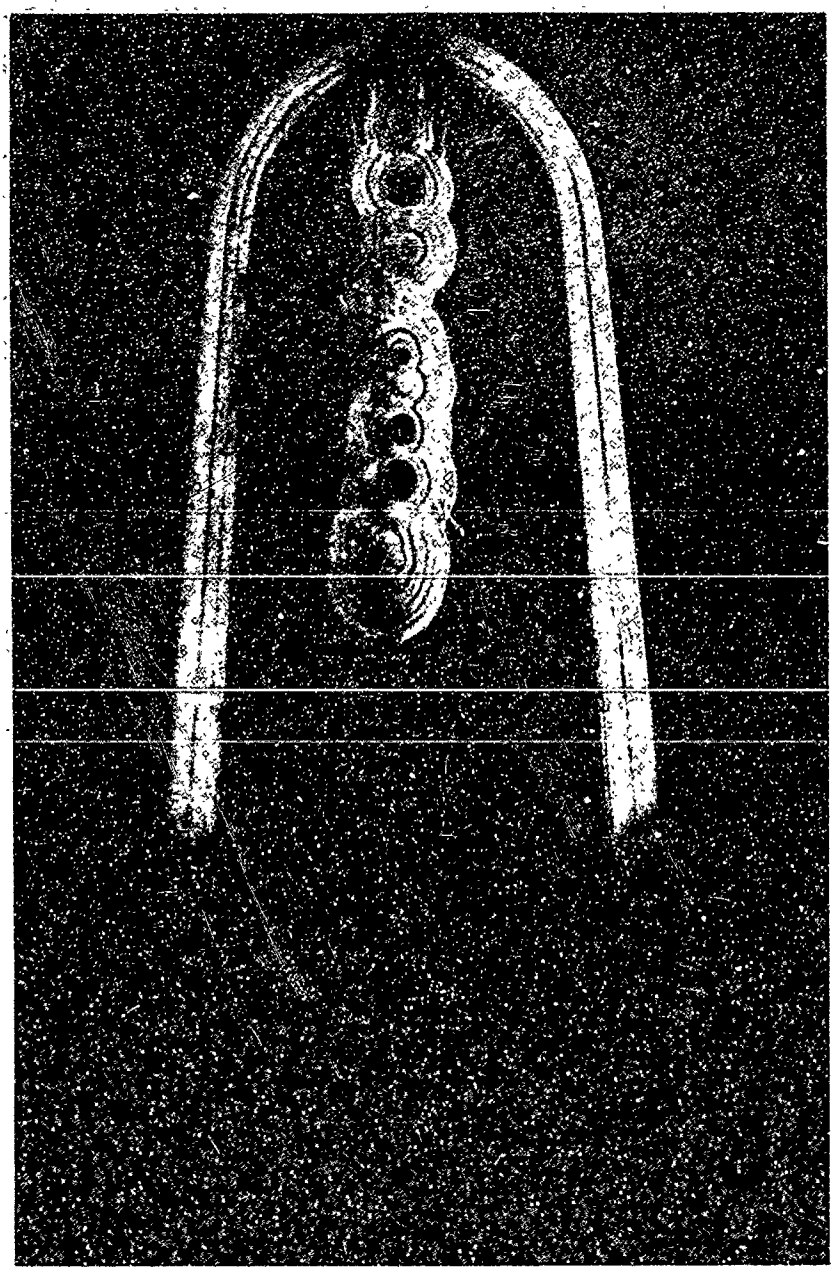
Figure 319



Task 3.3.7-6

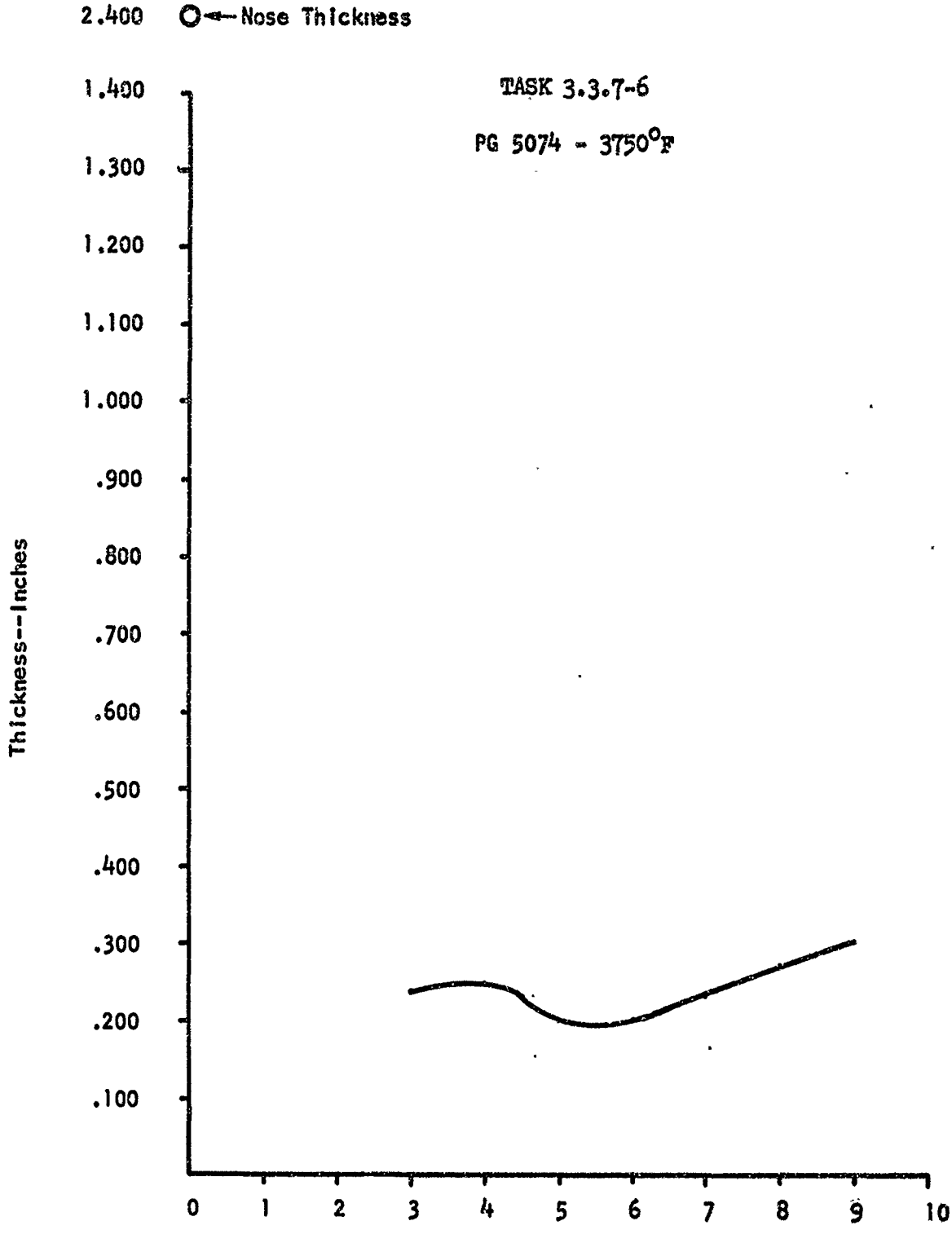
Radiograph of 7082

Figure 320



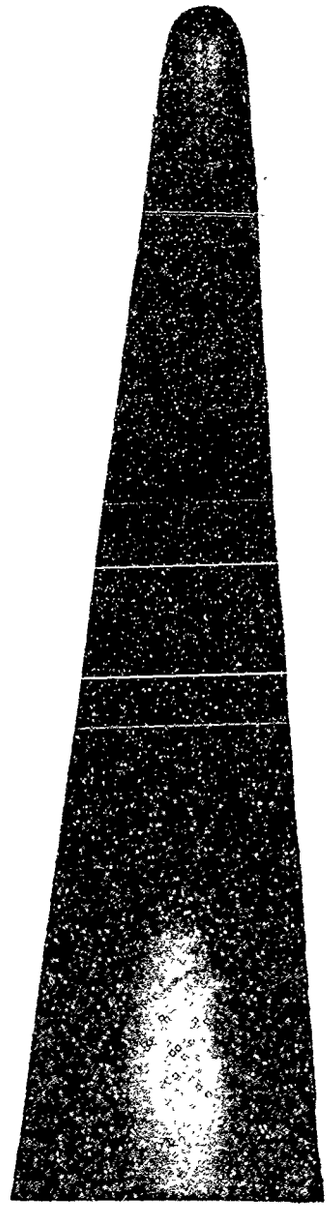
Run 7082 - Nose Region Cross Section - 5X

Figure 321



Deposition Thickness Profile

Figure 322



Task 3.3.7-6

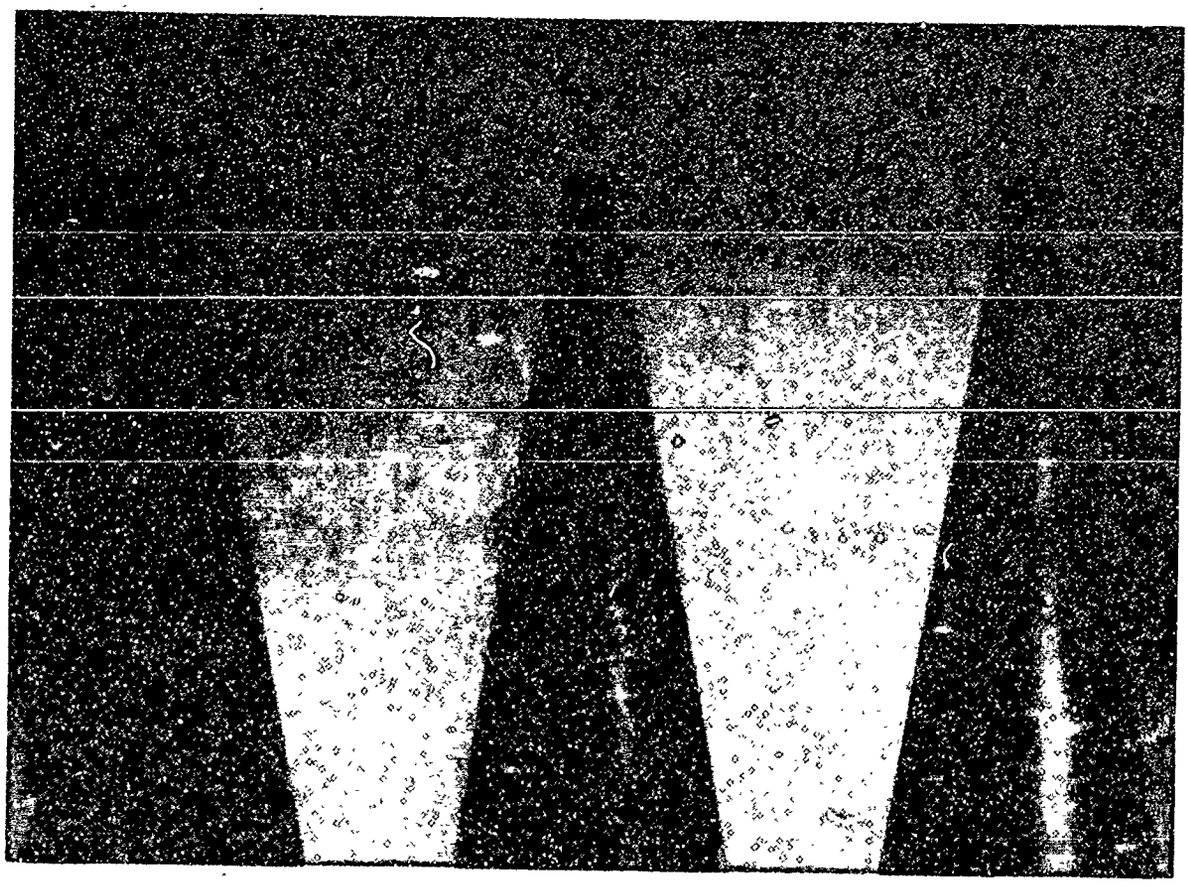
Radiograph of 5074

Figure 323



Run 5074 - Nose Region Cross Section - 5X

Figure 324



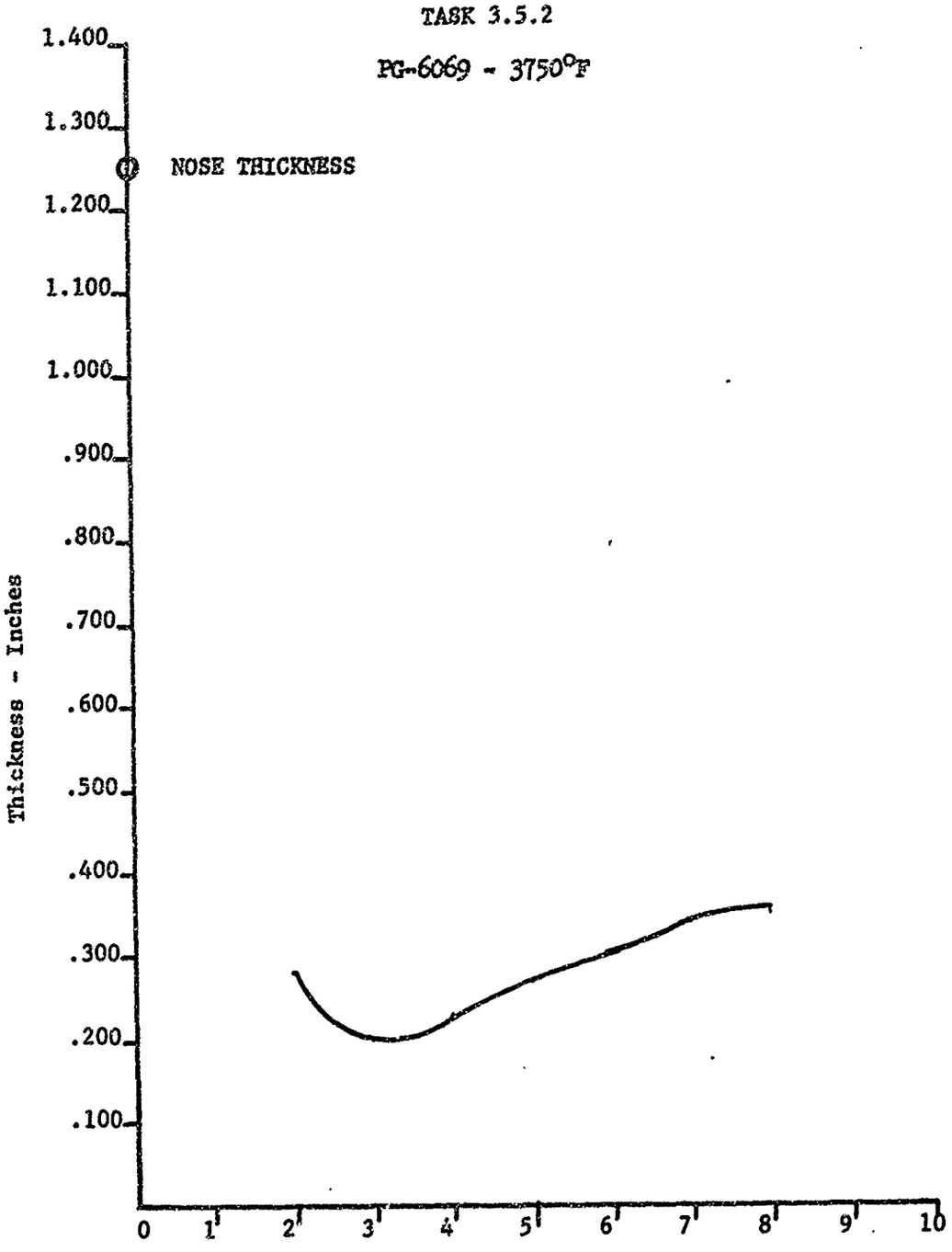
Task 3.5.2

Specification Deposits

Figure 325

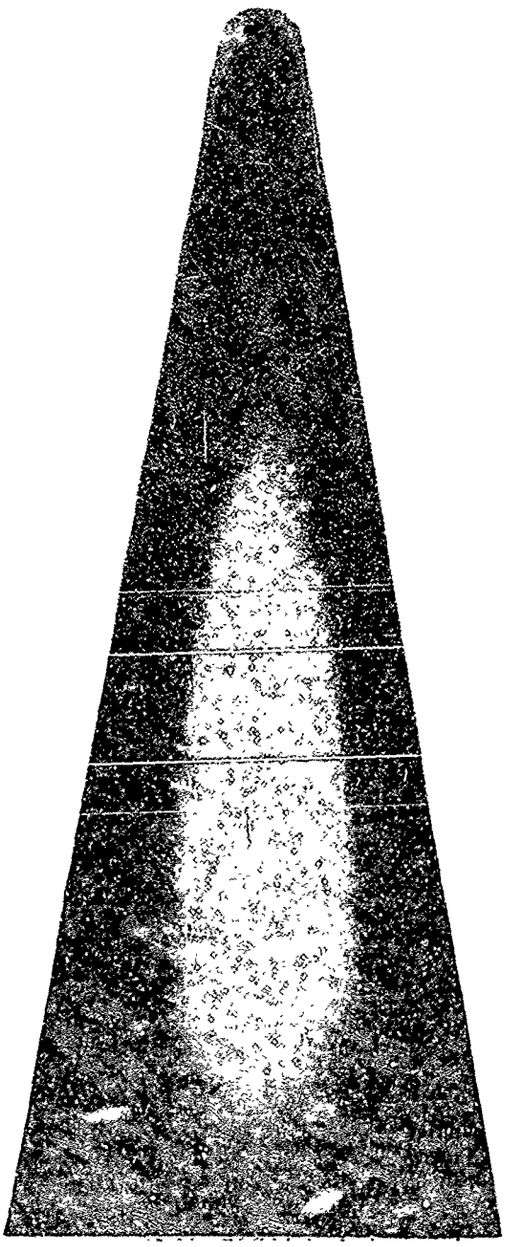
TASK 3.5.2

PG-6069 - 3750°F



Deposition Thickness Profile

Figure 326



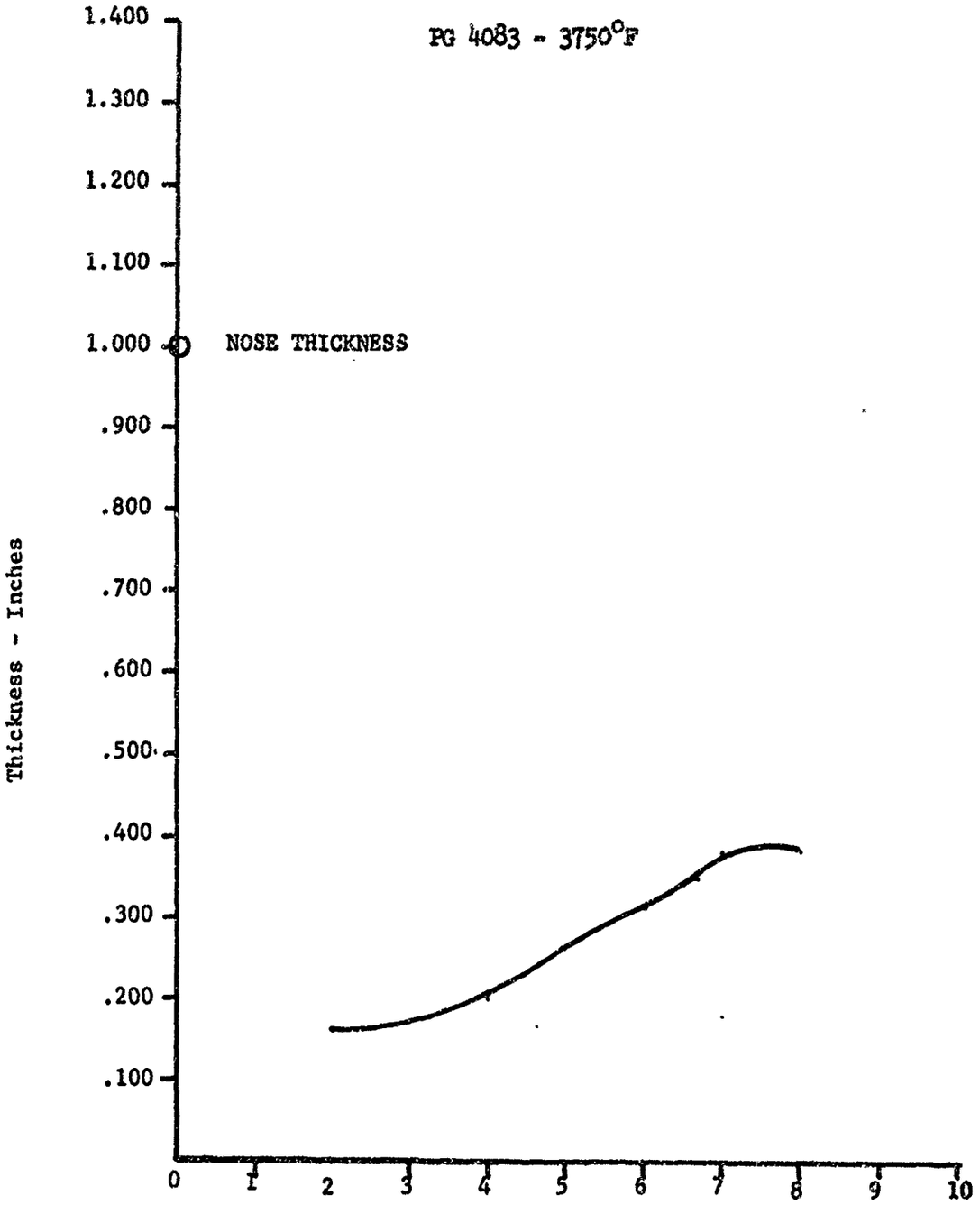
Task 3.5.2

Radiograph of 6069

Figure 327

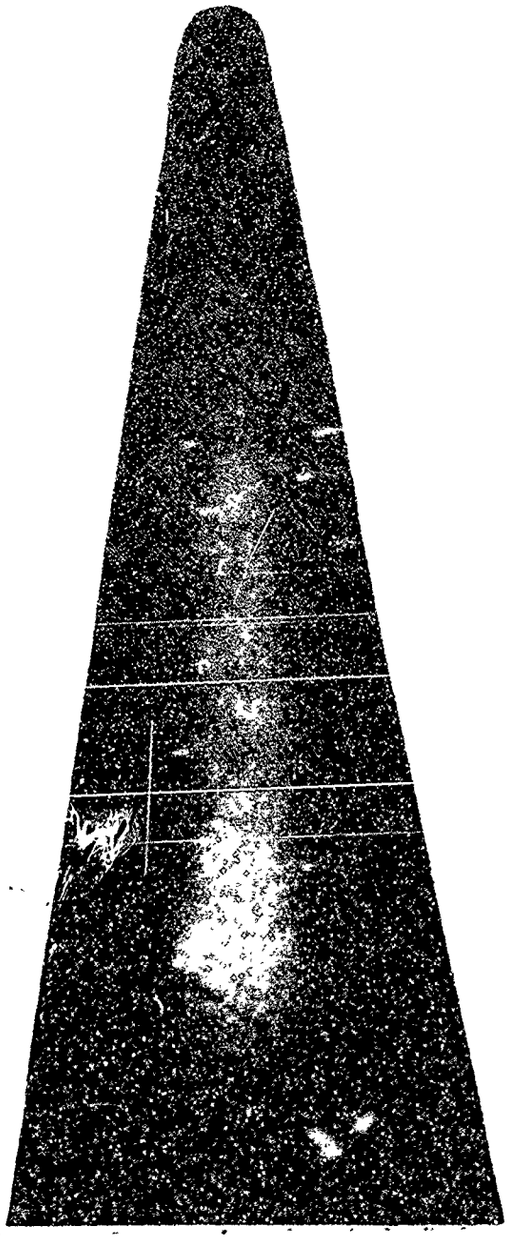
TASK 3.5.2

PG 4083 - 3750°F



Deposition Thickness Profile

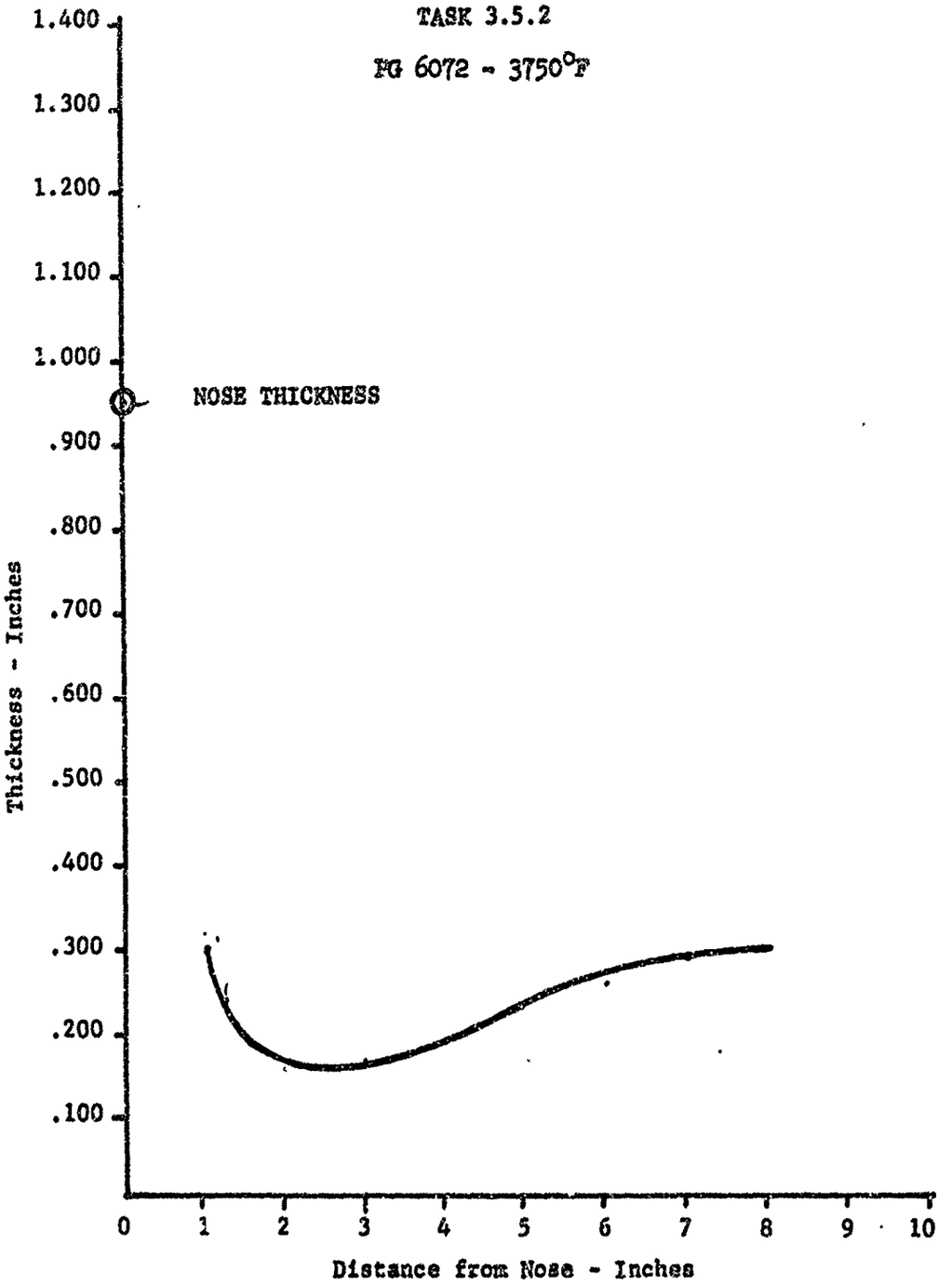
Figure 328



Task 3.5.2

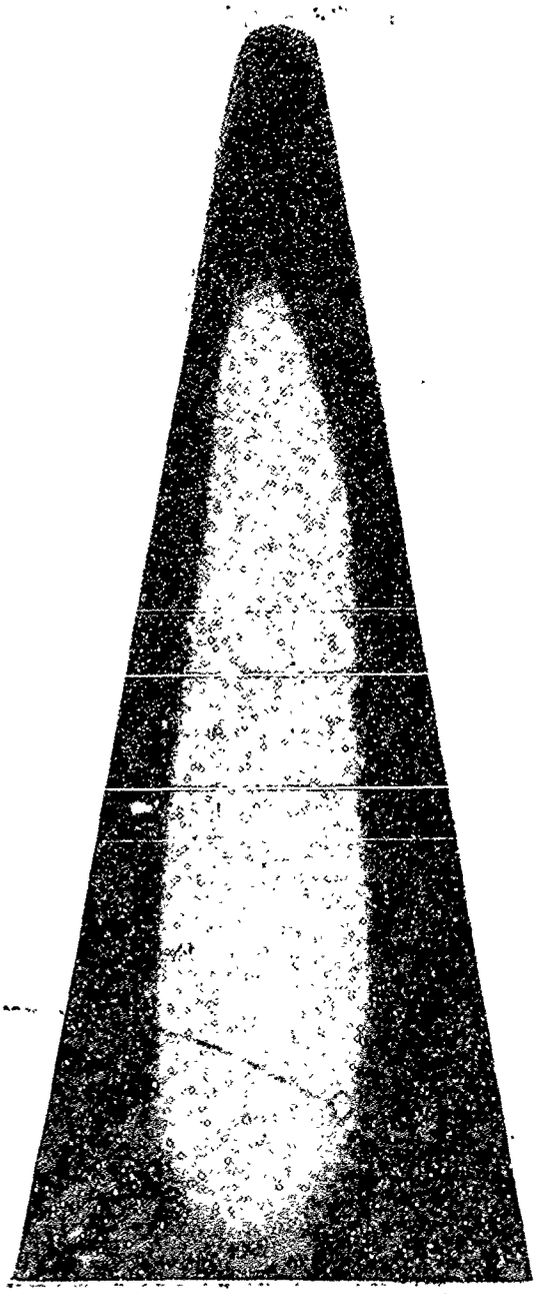
Radiograph of 4083

Figure 329



Deposition Thickness Profile

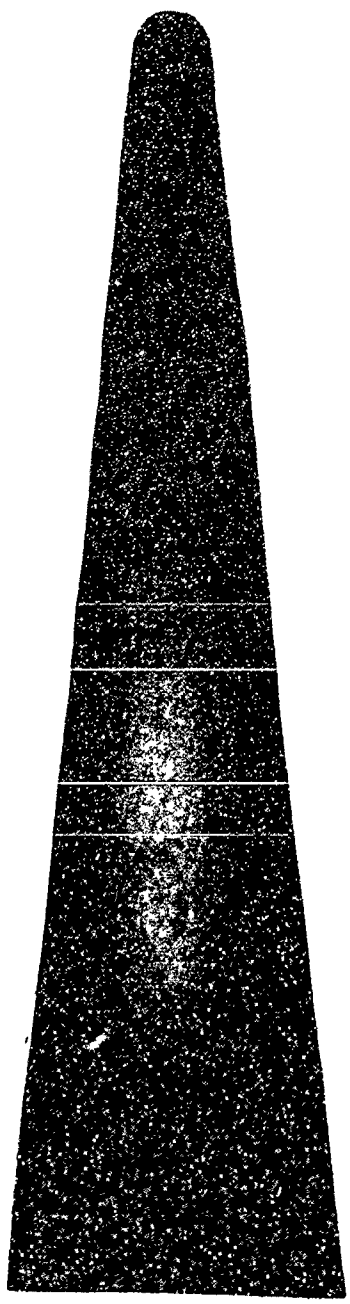
Figure 330



Task 3.5.2

Radiograph of 6072

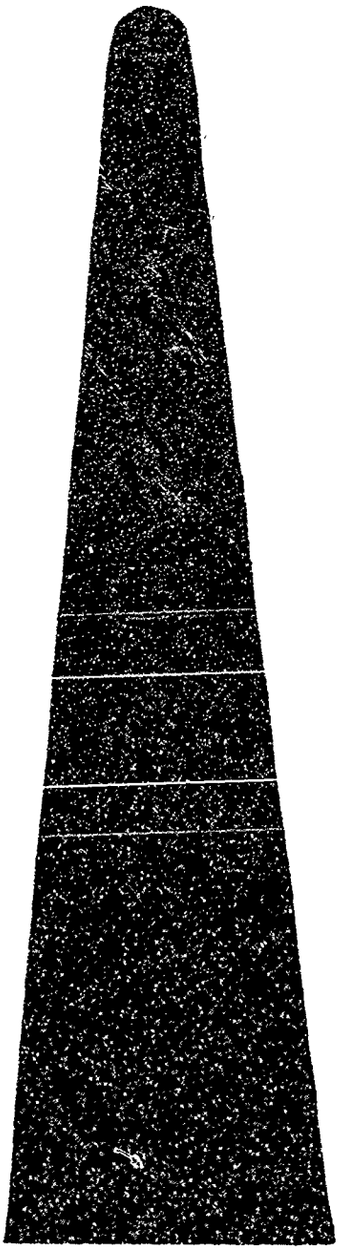
Figure 331



Task 3.5.2

Radiograph of 6070

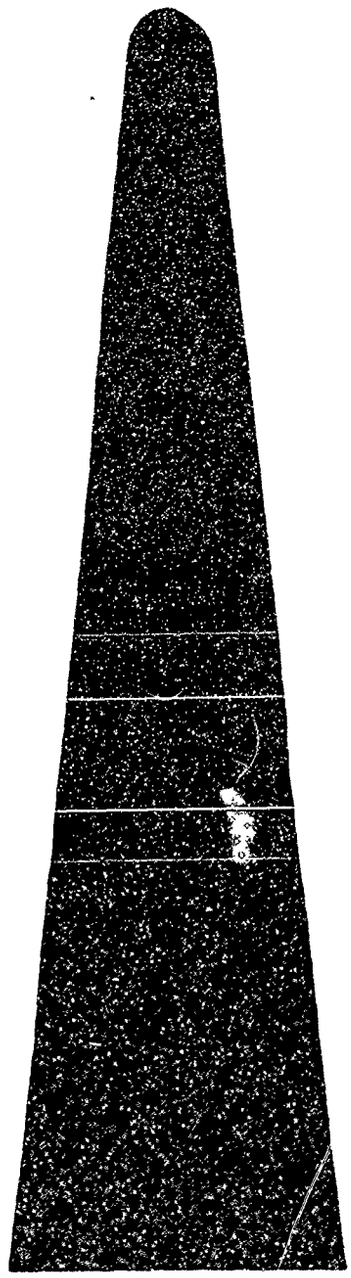
Figure 332



Task 3.5.2

Radiograph of 4084

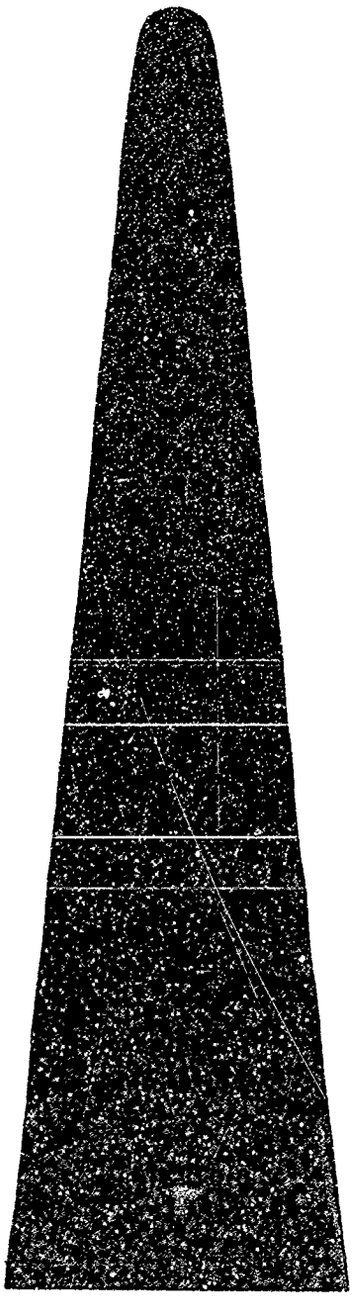
Figure 333



Task 3.5.2

Radiograph of 6071

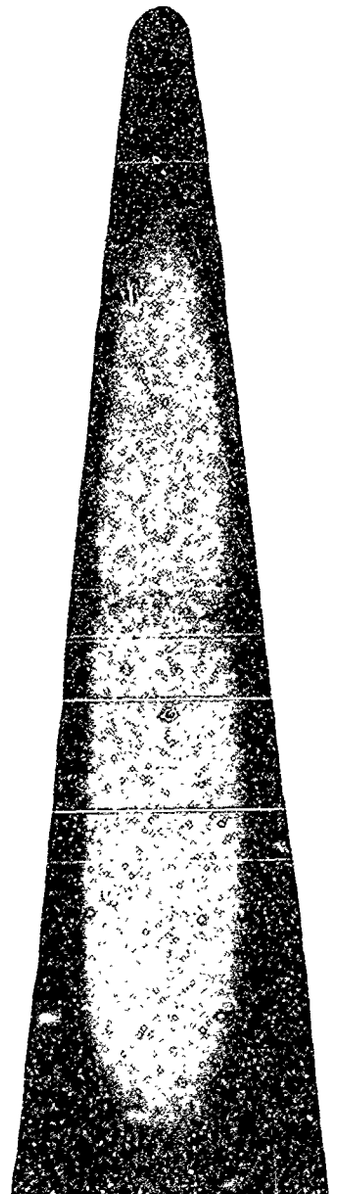
Figure 334



Task 3.5.2

Radiograph of 5078

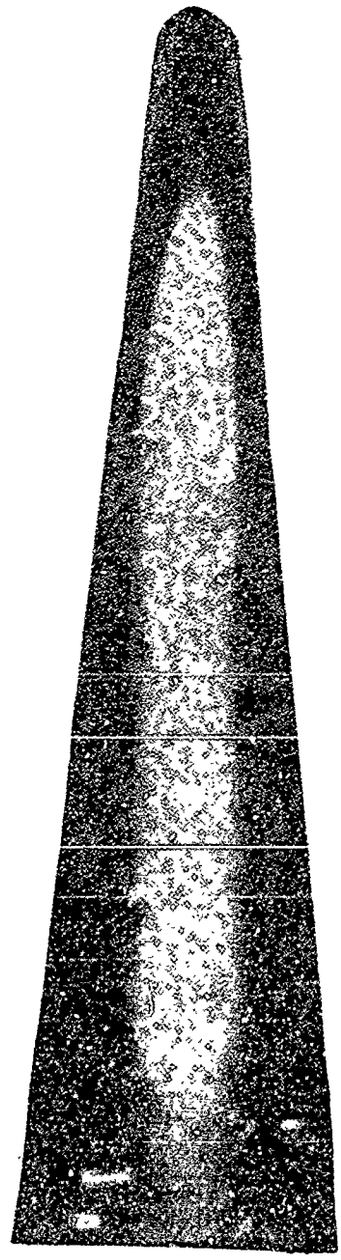
Figure 335



Task 3.5.2

Radiograph of 4085

Figure 336



Task 3.5.2

Radiograph of 5079

Figure 337

APPENDIX I

MATERIAL SPECIFICATION

AF 33(615)-3136

1.0 SCOPE

1.1 This specification covers as deposited boron alloyed pyrolytic graphite cones and related shapes and defines the engineering requirements for this material.

2.0 APPLICABLE DOCUMENTS

2.1 MIL-STD-453	Inspection, Radiographic
MIL-T6866	Inspection, Penetrant
ASTM-D-792	Method of Tests for Specific Gravity and Density of Plastics

3.0 REQUIREMENTS

3.1 Vendor Approval - Vendors must meet the requirements of this specification to be considered engineering approved sources.

3.2 Material Type - The material shall be regenerative boron alloyed pyrolytic graphite.

3.3 Material Properties

3.3.1 Basic Process - Parts shall be formed by pyrolytic decomposition of appropriate carbon and boron bearing gases on the internal form of a high quality graphite mandrel at temperatures in excess of 2000°C but less than 2400°C.

3.3.2 Boron Alloying - The ratio of carbon bearing gases to boron trichloride gas shall be a maximum of 90 to 1 and a minimum of 160 to 1 during the entire deposition cycle.

3.3.3 Specific Gravity - The specific gravity of the material shall be 2.180 minimum.

3.3.4 Residual Stress - The residual stress of each part shall not exceed 8000 psi.

3.3.5 Nodule Size and Frequency

3.3.5.1 The diameter of any nodule or cluster of nodules on the surface shall not exceed 0.6 of the material thickness.

3.3.5.2 Nodule distribution shall be such that not more than two nodules of acceptable size shall be closer than one inch apart.

3.3.6 Delaminations

3.3.6.1 Delaminations as determined from radiographic analysis or visual inspection of machined edges are cause for rejection in parts with a maximum t/r of 0.08.

3.3.6.2 Delaminations in parts with a t/r greater than 0.08 are only acceptable as defined in paragraphs 3.3.6.2.1 through 3.3.6.2.3.

3.3.6.2.1 Maximum Material Separation - The maximum material separation as determined from radiographic films with low magnification (2 to 10X) for an acceptable delamination is .005 inches.

3.3.6.2.2 Delamination Pattern - An acceptable delamination shall be parallel to the outside contour of the part except in the nose tip and 1-1/2 inches beyond the required stagnation thickness. (See Figure 1)

3.3.6.2.3 Continuous Delaminations - Any delamination that can be traced for more than 75% of the length (both sides) of a part on the radiographic film in any of the four views required shall be cause for rejection.

3.3.7 Deposition Symmetry - The material thickness at any station along the length of an "as-deposited" part shall not vary more than .040 inches from the minimum material thickness to the maximum material thickness.

3.3.8 Dimensions and Finish - Unless otherwise specified in the contract or purchase order, dimensions and finish shall be as specified on the Design Drawing.

3.3.9 Workmanship - The pyrolytic graphite forms procured under this specification shall be uniform in quality and condition, free from surface defects such as porosity, pits, cracks, and chips and internal defects such as voids, cracks and inclusions.

3.4 Process History

3.4.1 The vendor shall supply with each piece submitted a complete process history.

4.0 QUALITY ASSURANCE PROVISIONS

4.1 Inspection - The vendor shall be responsible for the performance of all inspection requirements as specified herein. The vendor shall also maintain complete inspection records of all examinations and tests as specified on each piece submitted for acceptance.

4.2 A lot shall consist of the material fabricated in one furnace run.

4.3 Each part fabricated shall have sufficient length to allow for the removal of two test rings one inch long. These test rings shall be removed from the same end of the part. One test ring shall be tested by the vendor to the requirements of this specification. The other test ring will be shipped with the part for verification testing at General Electric. The tests outlined in Paragraphs 4.4.2, 4.4.4, 4.4.5 and 4.4.6 shall be performed on the test ring.

4.4 Acceptance Test - The following destructive and non-destructive tests shall be performed on each piece. Failure of the material to conform to any requirement of this specification shall be cause for rejection.

4.4.1 Visual Examination - Each part shall be visually inspected for defects such as porosity, pits, cracks and chips. Porosity, pits, cracks, and chips are cause for rejection.

4.4.2 Gross Residual Stress - Residual stress measurements shall be determined utilizing a split ring technique. The following formula will be used to calculate gross residual stress.

$$\sigma \text{ test} = \frac{E_A \, t \, \Delta \, s}{4\pi r^2 - 2r \Delta s}$$

where: E_A = Elastic Modulus (Assume 4.5×10^6 psi).

t = Material Thickness

s = The distance the test ring opens or closes as a section is removed.

r = Inside radius of the part.

4.4.3 Deposition Symmetry - The deposition symmetry as required in Paragraphs 3.3.7 of the specification shall be determined from radiographs of the "as-deposited" cone. Two radiographs at a 90° interval shall be submitted with each part for verification to the requirements of Paragraph 3.3.7.

4.4.4 Specific Gravity - The specific gravity shall be determined in accordance with method A of ASTM D-792, using carbon tetrachloride as the immersion fluid. Each piece tested for specific gravity shall be free of cracks and delaminations as determined by visual inspection and/or dye penetrant inspection.

4.4.5 Boron Analysis - The boron content shall be determined using spectrographic techniques. The average boron content shall be not less than 0.2 or exceed 1.6 weight percent.

4.4.6 Structure - A photomicrograph shall be made on each piece of material submitted for acceptance. Sample location shall be from the trim ring unless otherwise specified on the engineering drawing.. This photomicrograph shall be approximately 50X under polarized light.

4.4.7 Radiographic Inspection - All parts shall be radiographically inspected. Four radiographs shall be taken at 45° intervals perpendicular to the longitudinal axis of the part. Any internal cracks, inclusions or voids are cause for rejection of the part. Delaminations are acceptable only as defined in Paragraph 3.3.6 of this specification.

4.4.8 Process History - The vendor shall submit with each piece offered for acceptance the following process information.

4.4.8.1 Deposition temperature taken at least every 30 minutes.

4.4.8.2 Ratio of boron bearing gases to carbon bearing gases throughout the deposition cycle.

4.4.8.3 Any interruptions in the deposition cycle.

4.4.9 Packaging and Marking

4.4.9.1 Each part and its associated trim ring shall be marked in accordance with the applicable engineering drawing. Each part shall be

indexed at 0° and 90° by a solvent soluble ink. Inspection reports shall reference these indices for location of defects.

4.4.9.2 Each part and its associated trim ring shall be packaged in a foamed container with the parting line running in the axial direction so that each half of the container will form a cradle for the part.

5.0 NOTES

5.1 Definitions - To insure uniformity of interpretations the following items are defines.

5.1.1 Nodules - A single grain growth significantly larger in size than the surrounding matrix, appearing as a blister on the deposited surface.

5.1.2 Delaminations - A material separation parallel to the plane of deposition that is discernible at low magnification from radiographic film.

5.1.3 t/r Ratio - The t/r ratio is the ratio of material thickness at a point to the radius of curvature at that point.

5.1.4 Cracks - Any material separation other than a delamination.

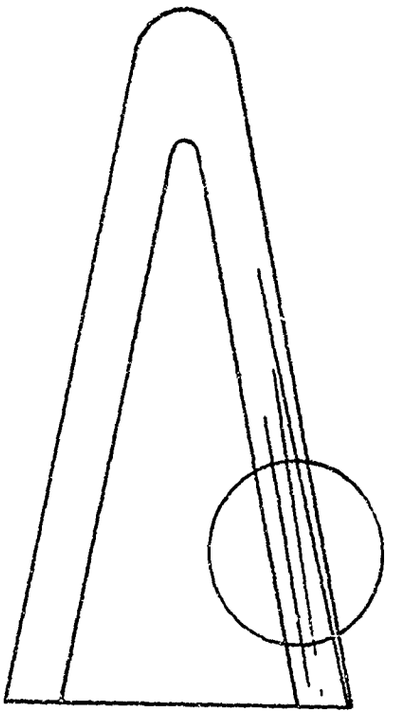
5.1.5 Clusters - Two or more nodules in contact.

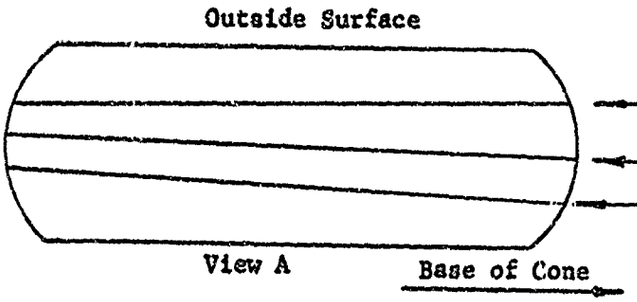
5.1.6 "As-Deposited" - The "as-deposited" condition refers to the condition of the part after it has been removed from the furnace and the mandrel has been removed from the part but prior to any internal machining.

5.1.7 Station - Station as used in this specification refers to any axial location in inches measured from the small end of cones and frustums and from a reference end on cylinders.

5.1.8 Document Precedence - In case of discrepancy between Engineering Drawing and this specification, the requirements of the drawing shall prevail.

Figure 1.





1 - Delamination running toward outside surface at base of cone.

2 - Delamination parallel to outside surface.

3. Delamination running toward inside surface at base of cone.

APPENDIX II

PROCESS SPECIFICATION FOR

BORON ALLOYED PYROLYTIC GRAPHITE NOSE CONES

AF 33(615)-3136

1.0 Introduction

1.1 Purpose

The purpose of this Process Specification is to outline the procedures by which manufacturers skilled in the art can produce boron alloyed pyrolytic graphite nose cones.

1.2 Scope

This specification covers the basic design and process parameters for a nose cone with a 1/4 inch nose radius, half-angle of 10° and a ratio of the nose tip thickness to skirt thickness of 5 to 1.

2.0 Process Requirements

2.1 Temperature

The nominal temperature specified in Section 4 shall be used with allowable variations of ± 20°F. The temperature shall be measured on the mandrel container lid located approximately 1/2" above the mandrel tip.

2.2. Pressure

The nominal pressure specified in Section 3 shall be used for deposition with allowable variation of ± 0.2 mm Hg. The pressure shall be measured in the main furnace tank outside the deposition chamber.

2.3 Flow Rate and Gas Composition

The hydrocarbon gas shall be supplied to the furnace in the form of natural gas or from cylinders of purified gas. The boron trichloride shall be supplied from cylinders of technical grade quality or better. The supply of all reactants must be sufficient so that no interruption in flow is required during the deposition. The flow rates required are quoted as standard cubic feet and should be maintained at ± 5% or better.

2.4 Nozzle Geometry

The nozzle shall be water cooled, with an outside diameter of approximately 13/16 inches and with a discharge orifice of 0.069 inches in diameter. The nozzle must be capable of being raised or lowered smoothly over an accurately measurable range.

2.5 Mandrel Design and Material

The nose cone shall be deposited in a female mandrel fabricated from an acceptable grade of graphite; such as,* grade A,C, or B. The mandrel thickness shall be not less than 1/3 and not greater than 1-1/2 times the intended wall thickness of the deposit. The most preferred form is to taper the mandrel wall thickness from the maximum recommended thickness at the base to the minimum recommended thickness at the nose.

The machined finish on the mandrel shall be equivalent to the finish obtained with 600 grit paper.

2.6 Related Parts Design and Material

The related supporting parts for the nose cone mandrel as shown in Figure A shall be fabricated from an acceptable grade of graphite, such as the mandrel grades above or other graphites with similar chemical purity. The design shall be consistent with good practice and in addition meet the following special requirements:

A. The I.D. of the support cylinder shall be larger than the mandrel I.D. by at least four times the intended thickness of the deposit.

B. The nozzle shield shall be cut off flush with the nozzle at its lowest position during the deposition cycle.

C. For an intended wall thickness deposit of 250 mils the exhaust path in the mandrel support will be three 7/8" holes.

2.7 Mandrel and Related Parts Preparation

The mandrel and related graphite parts shall be thoroughly vacuumed and all surfaces exposed to the gas flow shall be cleaned with a thermally degradable organic solvent and wiped clean with lintless wipers.

*For graphite identification, contact MATC, Air Force Materials Laboratory, WPAFB.

3.0 Process Procedure for Cone with .200 Minimum Wall Thickness

3.1 Loading

Thoroughly clean mandrel and related parts and assemble per Figure A. The nozzle is to be positioned 12 inches from the nose at assembly. The details of assembly not shown in Figure A are peculiar to each furnace design and should not influence the deposit.

3.2 Furnace Evacuation and Heat-up

These factors are for the most part a function of equipment design and standard shop practices. The evacuation and heat-up procedures shall insure that the furnace and associated equipment is vacuum tight and in sufficiently adequate operating condition to complete the process cycle uninterrupted. The deposition assembly shall be heated to 3750°.

3.3 Precoat

Turn methane on to 10 cfh and hold for 5 minutes. Turn off methane and purge with hydrogen for 1/2 hour at 2.5 cfh. Turn off hydrogen.

3.4 Deposition Cycle

Turn on methane and boron trichloride and adjust pressure and nozzle position according to the following schedule:

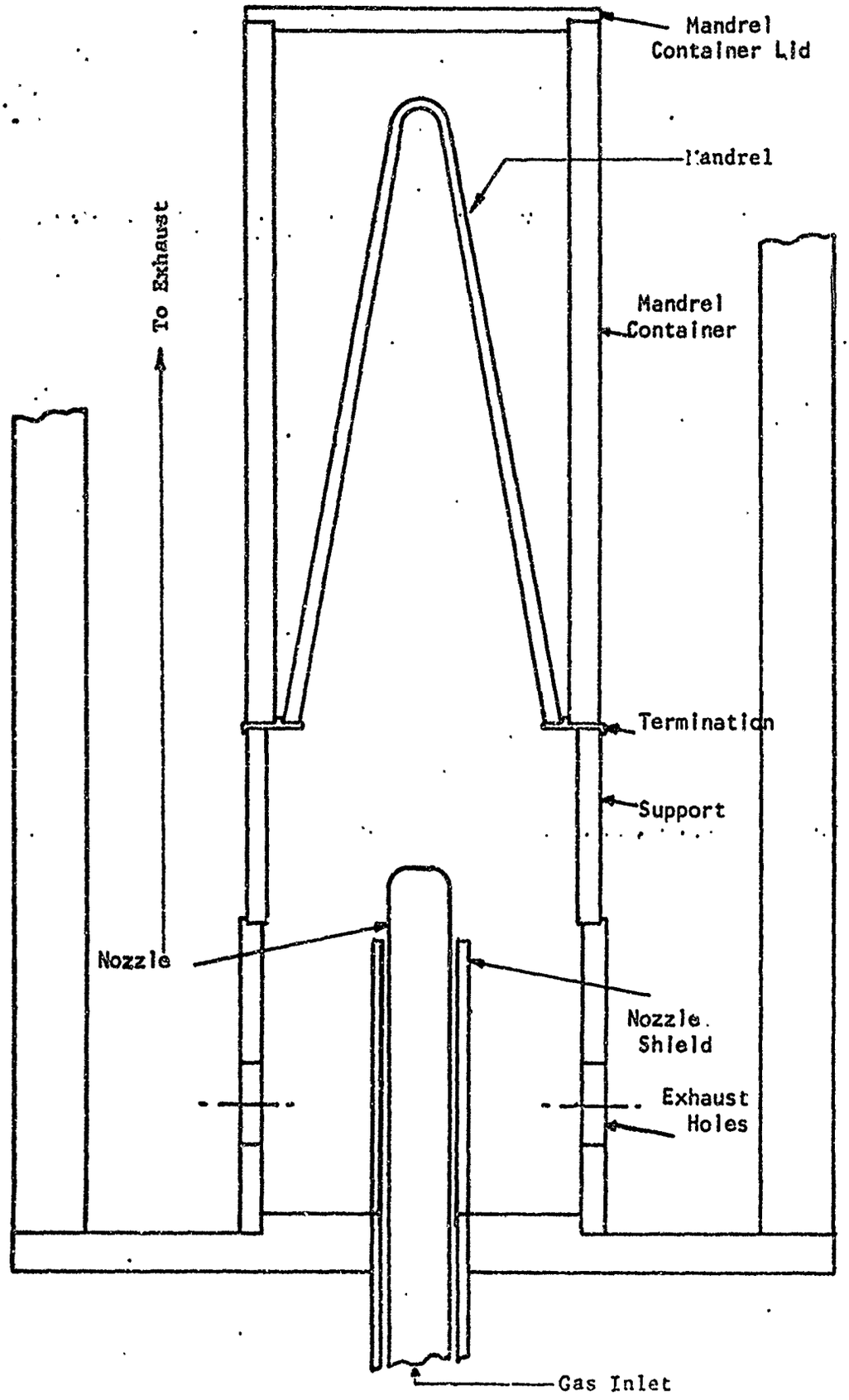
Nozzle Position	Time	BC_3 (CFH)	Methane (CFH	Pressure (mm Hg)
12"	0-12 Hours	.028	4 (+10 CFH H_2)	2
7 1/2"	12-22	.109	10	2
7 5/8"	22-27	.092	10	2
7 3/4"	27-32	.076	10	2
7 7/8"	32-37	.061	10	2
8"	37-42	.046	10	2
8 1/8"	42-47	.034	10	2
8 1/4"	47-52	.028	10	2
8 3/8"	52-57	.023	10	2
8 1/2"	57-62	.015	10	2

3.5 Cooling and Unloading

The furnace shall be cooled and disassembled according to standard shop practices.

FIGURE A

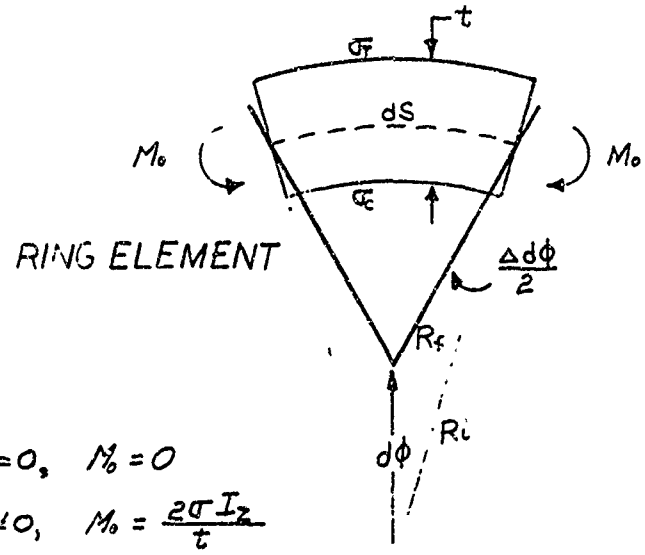
APPENDIX II



Deposition Assembly for Nose Cones

APPENDIX III

STRESS EQUATION FOR
CUT RINGS



when $\sigma = 0$, $M_o = 0$

when $\sigma \neq 0$, $M_o = \frac{2\sigma I_z}{t}$

$R_i = \frac{dS}{d\phi}$

$R_f = \frac{dS}{d\phi + \Delta d\phi}$

$\Delta d\phi = \frac{dS}{R_f} - d\phi$

$\Delta d\phi = \frac{dS}{R_f} - \frac{dS}{R_i}$

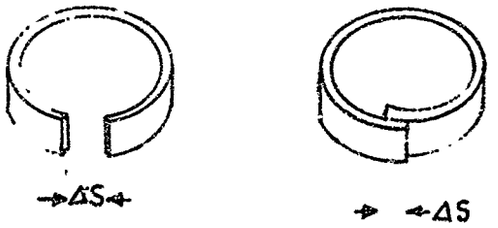
$\frac{\Delta d\phi}{dS} = \frac{M_o}{EI_z}$

$$\frac{dS\left(\frac{1}{R_f} - \frac{1}{R_i}\right)}{dS} = \frac{M_o}{EI_z} = \frac{2\sigma I_z}{EI_z t}$$

$$\frac{Et(R_i - R_f)}{2(R_f R_i)} = \sigma$$

$$\sigma = \frac{Et\,\Delta R}{2(R_f R_i)}$$

If ΔR is Small



$$\Delta R = \frac{\Delta S}{2\pi}$$

$$\sigma = \frac{Et\,\Delta R}{2(R_f R_i)} = \frac{Et\,\Delta S}{4\pi\left[R_i\left(R_i - \frac{\Delta S}{2\pi}\right)\right]}$$

$$\sigma = -\frac{Et\,\Delta S}{4\pi R_i^2 - 2R_i\Delta S}$$

APPENDIX IV

RESIDUAL STRESS PREDICTIONS (TASK 3.4.4)

AF 33(615) -3136

In order to provide means of extrapolating the use of the toroidal mandrel separator developed in Tasks 3.3.1 and 3.3.2 to other sizes, an investigation of the residual stresses in the separator was performed. The geometry of this separator is illustrated in Figure VIII-1.

The residual stresses in the part were estimated on the basis of "cool-down" phenomena only - using the following properties:

$$E = 3.5 \times 10^6 \text{ psi}$$
$$\nu = .22$$
$$\alpha \Delta T = .044 \quad \text{for } T = 4000^\circ F.$$
$$\alpha \Delta T = .055$$

In the analysis of the residual stresses only half of the part was considered; because of symmetry, the stresses in the other half are identical. Two problems were studied - the only difference being the boundary conditions at $s = 0$. The stresses presented on Figures VIII-2 through VIII-4 are for "membrane" type boundary conditions (no edge rotation nor shear stress resultant), and those presented on Figures VIII-5 through VIII-7 are for "free" edges (no moment nor shear resultants).

As a matter of convenience the problems were studies in two steps - first the "membrane" solution (presented as solid lines on the Figures) and then the total solution including shell bending (presented as dashed lines). The difference between the two represents the stresses due to only shell bending and obviously is very important for this problem.

To consider the possibility of cracks developing in the piece due to "cool-down" it was appropriate to examine particularly the circumferential stress on Figure VIII-6 in the vicinity of $s = 0$. Notice that the total stress in that region were significantly reduced below the membrane solution due to shell bending. But were this piece a cylindrical shell for its total length the bending at the free edge (machined edge away from the component being deposited) would tend to increase the tensile stress on the inner surface above its "membrane" value. It is this stress which causes cracks to start at machined edges. Therefore the tendency for cracks is much less in the toroidal mandrel separator than in a straight cylindrical end.

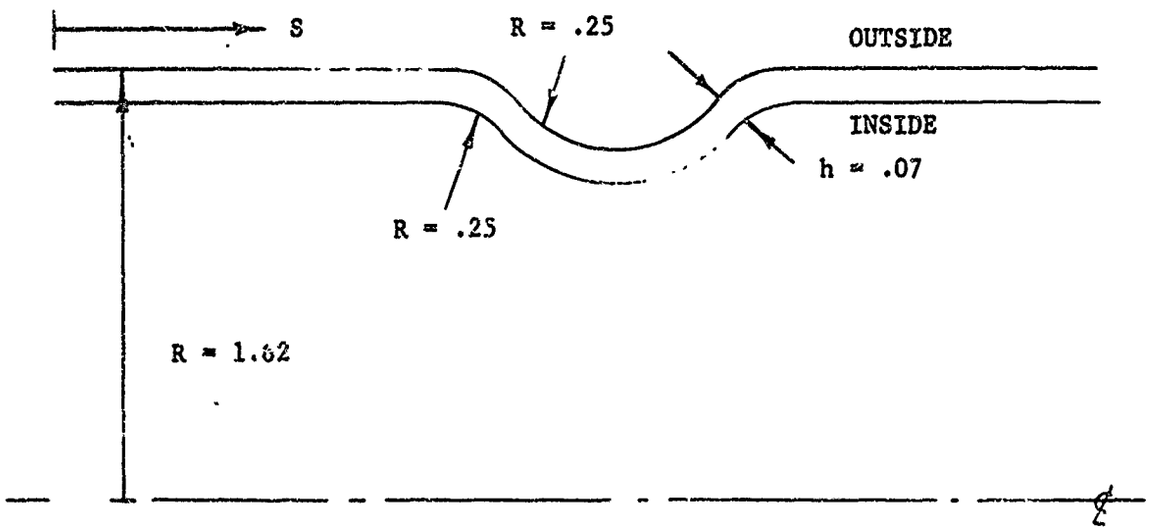


Figure VIII-1

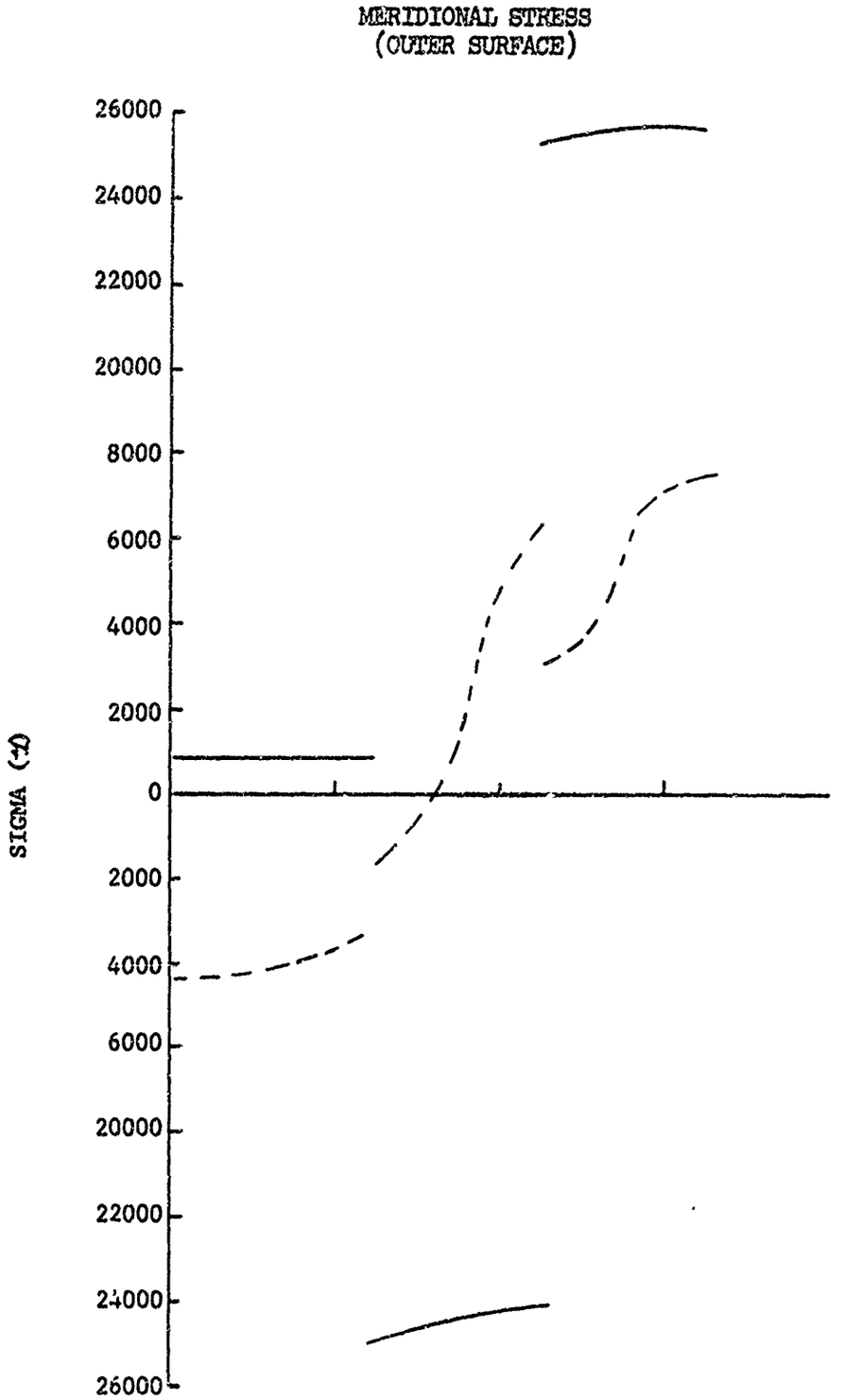


Figure VIII-2

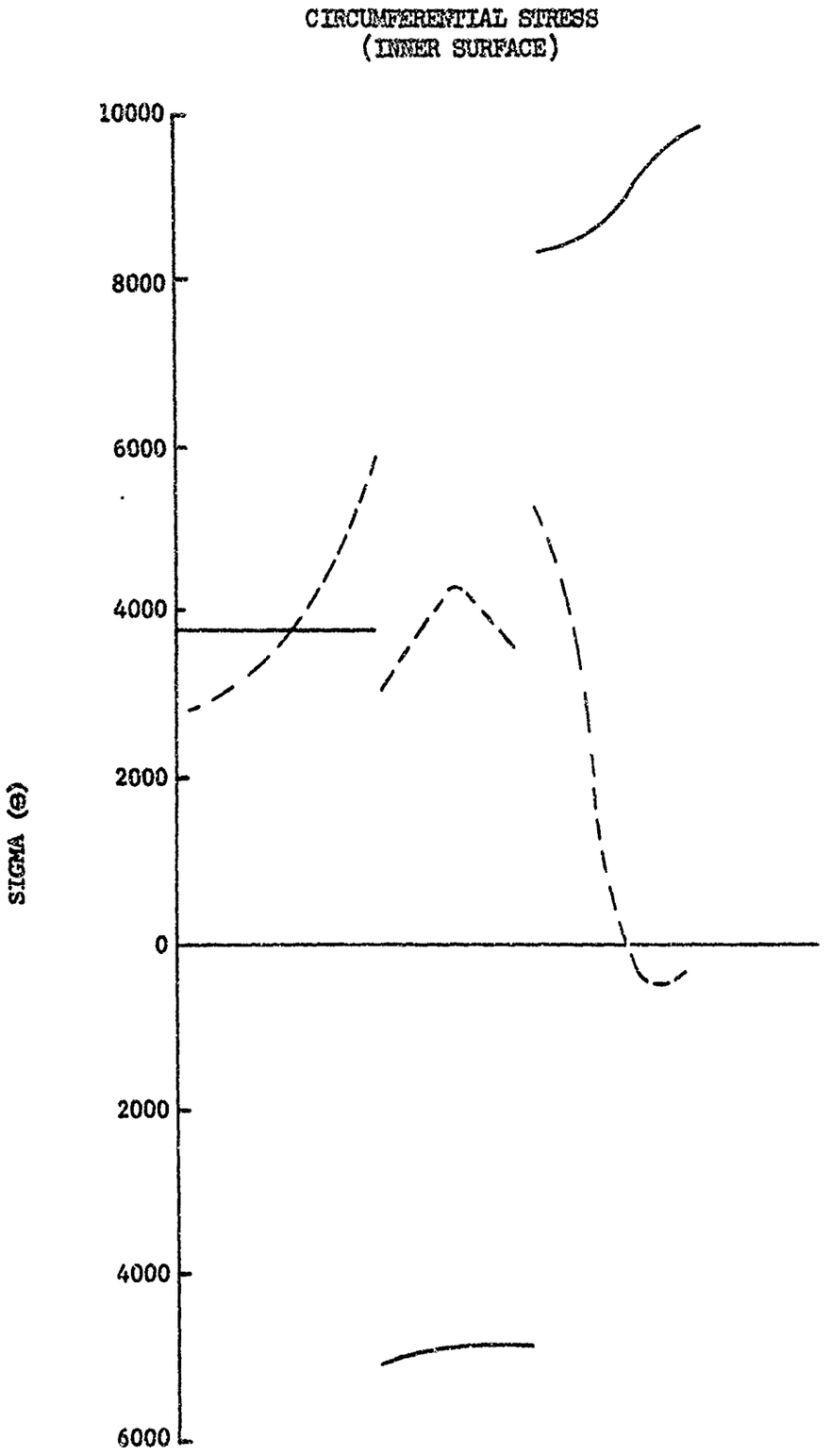
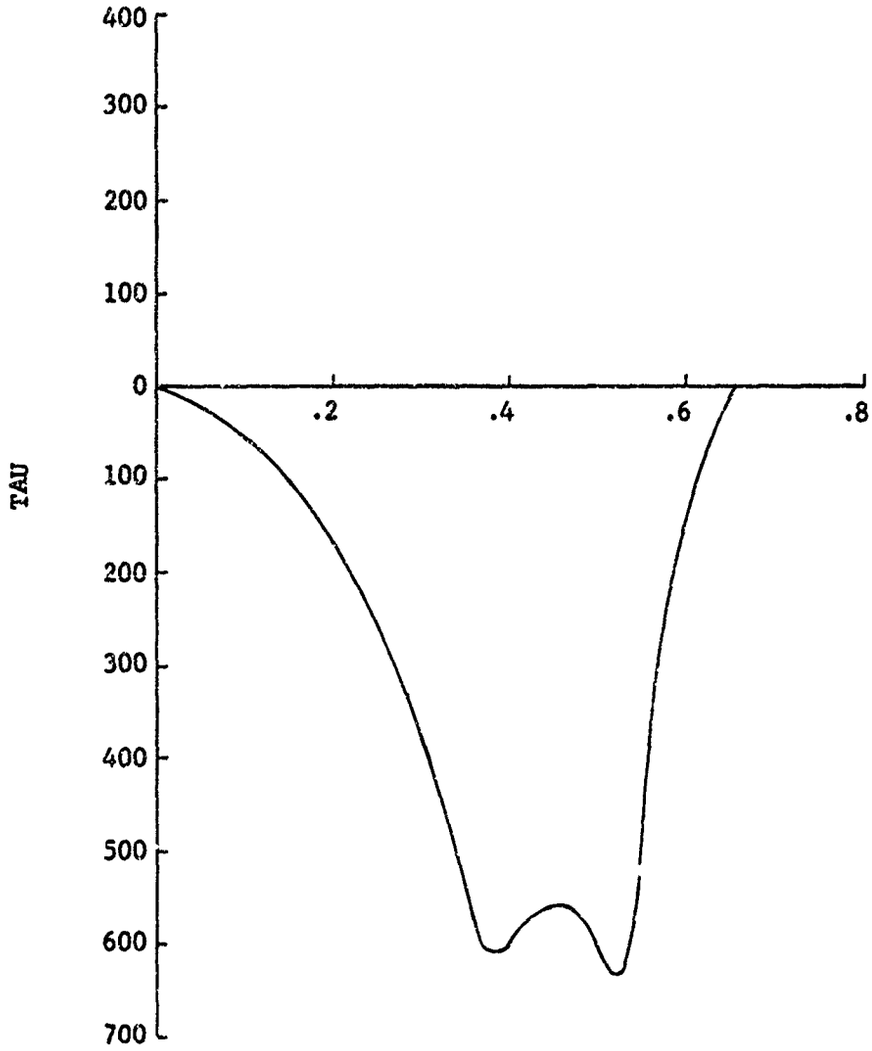


Figure VIII-3

SHEAR STRESS
(MIDDLE SURFACE)



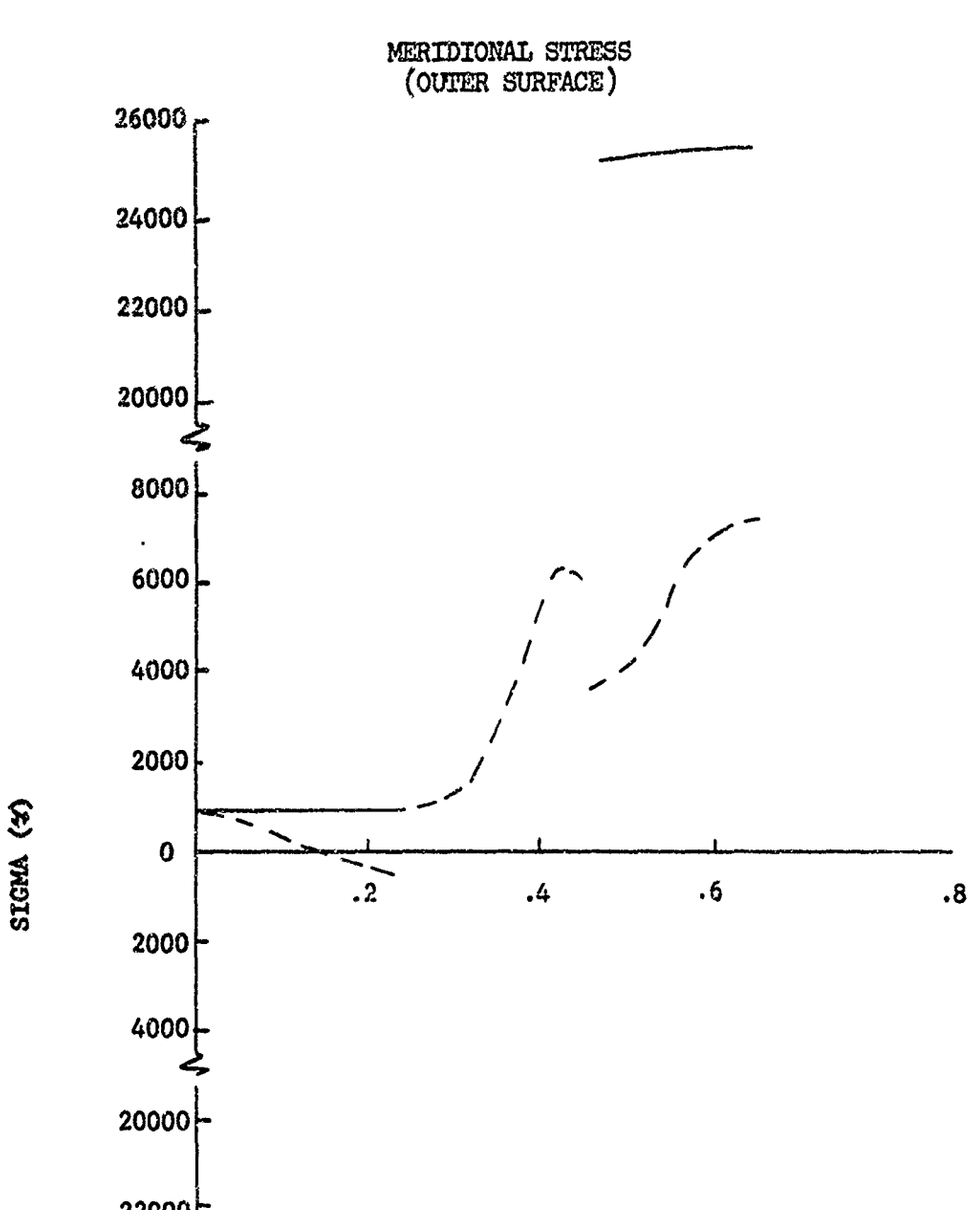


Figure VIII-5

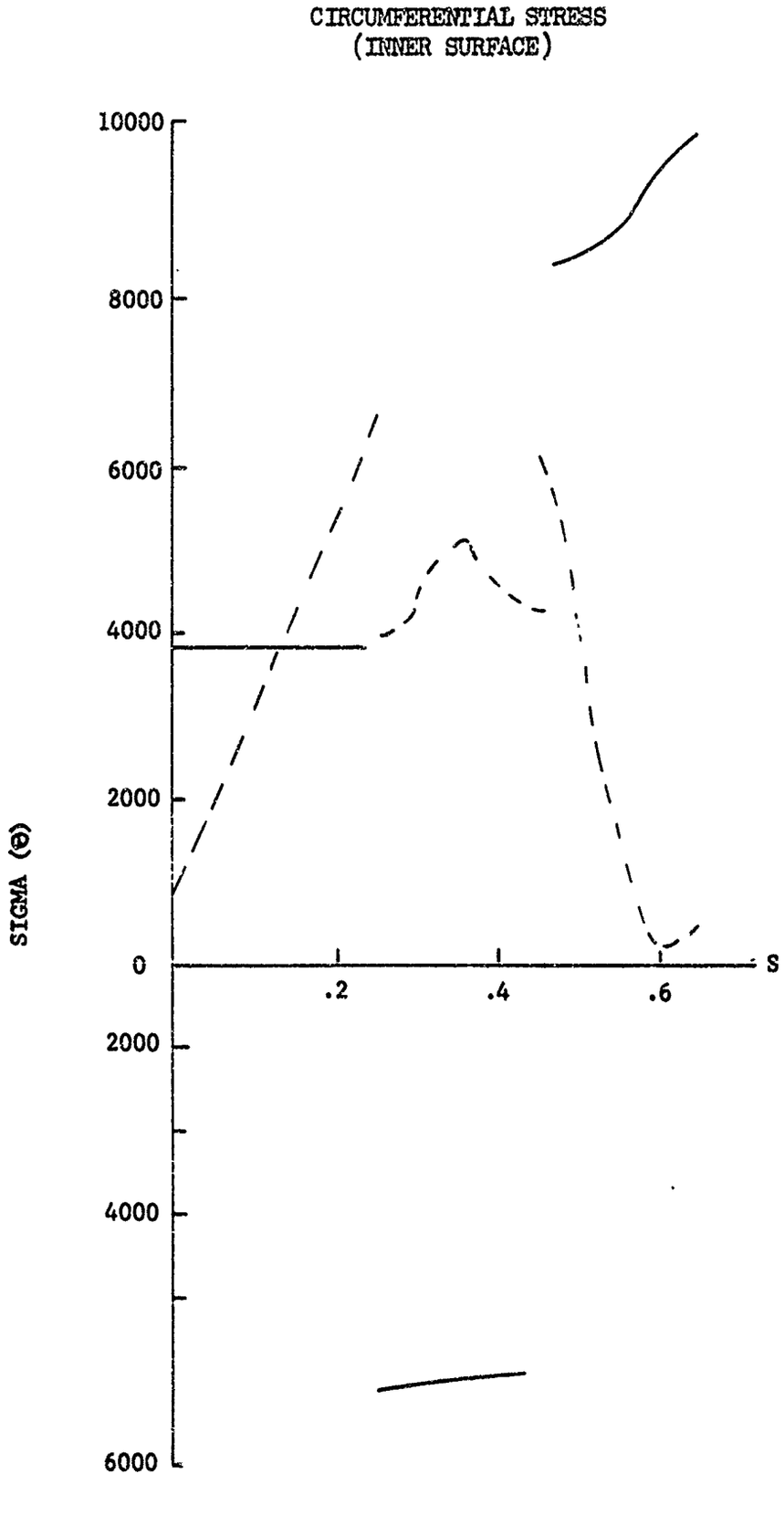


Figure VIII-6

SHEAR STRESS
(MIDDLE SURFACE)

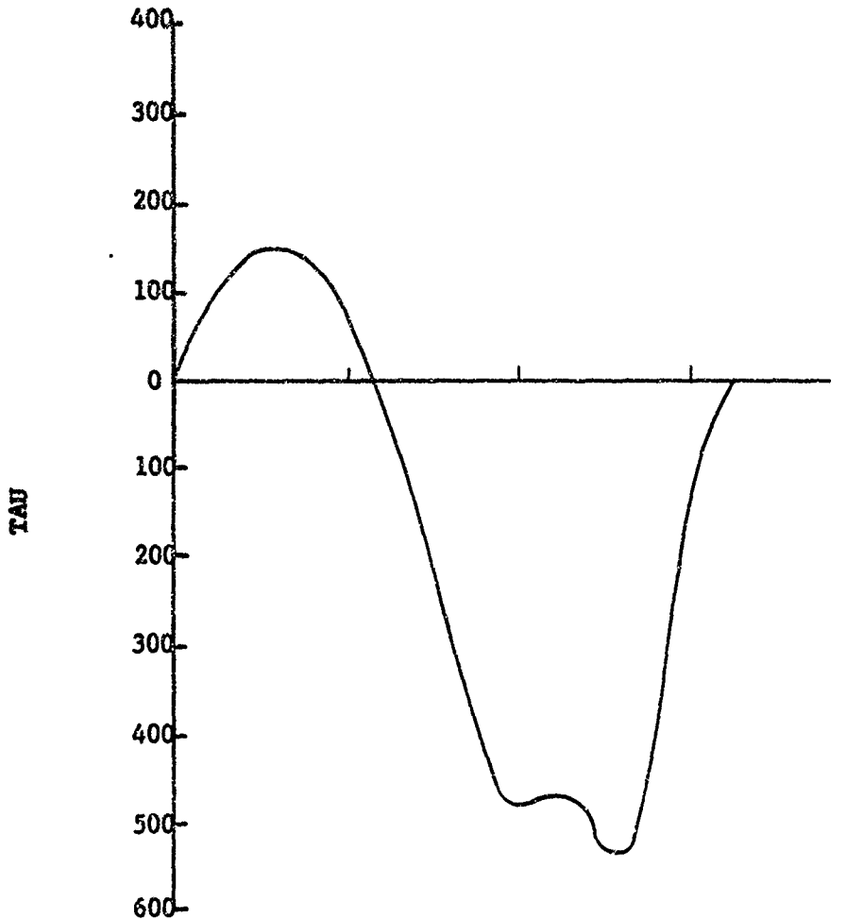


Figure VIII-7

Unclassified

Security Classification

DOCUMENT CONTROL DATA - R & D

(Security classification of title, body of abstract and indexing annotation must be entered when the overall report is classified)

1. ORIGINATING ACTIVITY (Corporate author)
General Electric Company
Metallurgical Products Department
Detroit, Michigan

2a. REPORT SECURITY CLASSIFICATION
Unclassified

2b. GROUP
---

3. REPORT TITLE
Development of Manufacturing Methods for Producing Pyrolytic Graphite in Various Shapes and Structures.

4. DESCRIPTIVE NOTES (Type of report and inclusive dates)
Final Report June 1965 - September 1967

5. AUTHOR(S) (First name, middle initial, last name)
Thomas J. Clark

6. REPORT DATE	7a. TOTAL NO. OF PAGES	7b. NO. OF REFS
September, 1967	590	80

8a. CONTRACT OR GRANT NO.	9a. ORIGINATOR'S REPORT NUMBER(S)
AF 33(615)-3136	AFML-TR-67-344
b. PROJECT NO. 8-349	
c. ----	9b. OTHER REPORT NO(S) (Any other numbers that may be assigned this report)
d.	----------

10. DISTRIBUTION STATEMENT
This document is subject to special export controls and each transmittal to foreign governments or foreign nationals may be made only with prior approval of the Air Force Materials Laboratory (MATC) Wright-Patterson Air Force Base, Ohio, 45433

11. SUPPLEMENTARY NOTES	12. SPONSORING MILITARY ACTIVITY
-------	Air Force Materials Laboratory Wright-Patterson AFB, Ohio 45433

13. ABSTRACT

The objective of ~~this~~ the program was the development of a manufacturing technology that will enable the prediction and specification of manufacturing process parameters for producing, with a high degree of reliability, pyrolytic graphites in specific sizes, shapes, and quality beyond the present state of the art and suitable for re-entry vehicles and rocket nozzles.

The investigations made during the course of this program were in the following areas; mandrel graphite selection and preparation for deposition, mandrel design, effects of gas composition, effects of process parameters (temperature, pressure, flow), boron analysis, delamination control in the deposits, and controlled graphitization of the pyrolytic graphites.

A complete process specification for producing 10° half angle, 1/4" nose radius, 1.00" stagnation thickness and 0.180" wall thickness nose cones is presented in this report.

DD FORM NO. 1473

Unclassified

Security Classification

Unclassified
Security Classification

14. KEY WORDS	LINK A		LINK B		LINK C	
	ROLE	WT	ROLE	WT	ROLE	WT
Pyrolytic Graphite						
Aerospace Materials						
Flight Hardware						
Manufacturing Technology						

Unclassified
Security Classification